



รายงานวิจัยฉบับสมบูรณ์

โครงการ
การทำแห้งผลิตภัณฑ์อาหารโดยใช้ไอน้ำร้อนยวดยิ่งที่สภาวะ
ความดันต่ำ (ระยะที่ 2)

โดย

รศ.ดร. สักกมน เทพหัสติน ณ อรุณา

มิถุนายน พ.ศ. 2551

รายงานวิจัยฉบับสมบูรณ์

โครงการ
การทำแห้งผลิตภัณฑ์อาหารโดยใช้ไอน้ำร้อนยวดยิ่งที่สภาวะ
ความดันต่ำ (ระยะที่ 2)

รศ.ดร. สักกมณ เทพหัสดิน ณ อยุธยา
ภาควิชาวิศวกรรมอาหาร คณะวิศวกรรมศาสตร์
มหาวิทยาลัยเทคโนโลยีพระจอมเกล้าธนบุรี

สนับสนุนโดยสำนักงานคณะกรรมการอุดมศึกษาและสำนักงานกองทุนสนับสนุนการวิจัย

(ความเห็นในรายงานนี้เป็นของผู้วิจัย สกอ. และ สกว. ไม่จำเป็นต้องเห็นด้วยเสมอไป)

Acknowledgements

The investigator expresses his sincere appreciation to the Commission on Higher Education (CHE) and the Thailand Research Fund (TRF) for supporting this study financially through the grant no. RMU4880001. Additional support from the International Foundation for Science (IFS), Sweden is also appreciated.

บทคัดย่อ

รหัสโครงการ: RMU4880001

ชื่อโครงการ: การทำแห้งผลิตภัณฑ์อาหารโดยใช้ไอน้ำร้อนยวดยิ่งที่สภาวะความดันต่ำ (ระยะที่ 2)

ชื่อนักวิจัย: รศ.ดร. สักกมน เทพหัตถิน ณ อุทยาน

E-mail Address: sakamon.dev@kmutt.ac.th

ระยะเวลาโครงการ: 3 ปี (1 มิถุนายน พ.ศ. 2548 – 31 พฤษภาคม พ.ศ. 2551)

โครงการวิจัยนี้เป็นโครงการต่อเนื่องจากโครงการวิจัยเรื่อง การทำแห้งผลิตภัณฑ์อาหารโดยใช้ไอน้ำร้อนยวดยิ่งที่สภาวะความดันต่ำ (TRG 4580099) โดยโครงการแบ่งออกเป็น 5 ส่วนย่อย แต่ละส่วนย่อยมุ่งศึกษาประเด็นต่างๆ ที่เกี่ยวกับการทำแห้งอาหารโดยใช้ไอน้ำร้อนยวดยิ่งที่สภาวะความดันต่ำ (LPSSD)

ส่วนแรกของโครงการวิจัยเป็นการมุ่งศึกษา LPSSD ในระดับพื้นฐาน โดยมีการพัฒนาแบบจำลองทางคณิตศาสตร์ ซึ่งสามารถใช้ทำนายการเปลี่ยนแปลงความชื้นและอุณหภูมิของอาหาร (หรือวัสดุชีวภาพ) ใดๆ ระหว่าง LPSSD นอกจากนี้ยังได้เสนอแนะการใช้การวิเคราะห์แฟรคทัล เพื่อเป็นเครื่องมือในการหาความสัมพันธ์ระหว่างข้อมูลการเปลี่ยนแปลงเชิงโครงสร้างและเชิงกายภาพ ซึ่งความสัมพันธ์ในลักษณะนี้จะนำไปสู่การพัฒนาตัวชี้วัดการเปลี่ยนแปลงเชิงกายภาพ/โครงสร้างของอาหารในระหว่างการอบแห้งได้ต่อไป

ในส่วนที่สองของโครงการวิจัย ได้ทำการทดลองเพื่อศึกษาผลของ LPSSD และกระบวนการอบแห้งแบบอื่นๆ ที่มีต่อคุณค่าทางโภชนาการของอาหารต่างชนิด ซึ่งรวมถึงการศึกษาจลนพลศาสตร์การเกิดไอโซเมอร์ไรเซชันและการเสื่อมสลายของเบต้าแคโรทีนในแครอท การศึกษาการเสื่อมสลายของกรดแอสคอร์บิกในมะขามป้อม และการศึกษาผลของวิธีการทำแห้งและอุณหภูมิที่ใช้ในการชงชาที่มีต่อปริมาณวิตามินซีในน้ำชามะขามป้อม ส่วนถัดมาของโครงการวิจัยเป็นการศึกษาการใช้ LPSSD และการเตรียมการก่อนการทำแห้งที่เหมาะสมในการผลิตขนมขบเคี้ยวสุขภาพ ซึ่งก็คือ มันฝรั่งแผ่นแบบไร้ไขมัน ซึ่งผลการศึกษาในส่วนนี้แสดงให้เห็นว่า LPSSD มีศักยภาพที่จะมาแทนที่กระบวนการทอดในการผลิตมันฝรั่งแผ่นได้

ส่วนที่สี่ของงานวิจัยเป็นการศึกษาวิธีการต่างๆ ซึ่งอาจนำมาใช้ในการเพิ่มประสิทธิภาพของ LPSSD โดยพิจารณาทั้งในแง่ของจลนพลศาสตร์การอบแห้งและคุณภาพของผลิตภัณฑ์ ในงานวิจัยส่วนนี้ได้มีการทดสอบการใช้การแผ่รังสีอินฟราเรดไกล เพื่อเป็นแหล่งพลังงานเสริมในการเร่งกระบวนการทำแห้งและช่วยเพิ่มการระเหยของความชื้นภายในผลิตภัณฑ์อันจะส่งผลให้เกิดโครงสร้างที่มีลักษณะเป็นรูพรุนมากขึ้น นอกจากนี้ยังได้ศึกษาการทำแห้งแบบเป็นช่วง ซึ่งพบว่าสามารถลดการใช้พลังงานในการอบแห้งลงได้ดี สำหรับส่วนสุดท้ายของงานวิจัยเป็นการประยุกต์ใช้ LPSSD ในการผลิตฟิล์มบริโอคได้สำหรับประยุกต์ใช้ในการพัฒนาบรรจุภัณฑ์แบบใหม่ จากผลการวิจัยพบว่า ฟิล์มบริโอคได้ซึ่งเตรียมโดย LPSSD มีสมบัติเชิงกลดีกว่าฟิล์มที่ได้จากการทำแห้งแบบอื่นๆ อย่างมีนัยสำคัญ

คำหลัก: การจำลองทางคณิตศาสตร์ การทำแห้ง การทำแห้งแบบเป็นช่วง การแผ่รังสีอินฟราเรดไกล การวิเคราะห์แฟรคทัล ขนมขบเคี้ยวสุขภาพ คุณค่าทางโภชนาการ ความสัมพันธ์ระหว่างโครงสร้าง-คุณภาพ วัสดุชีวภาพ สมบัติทางกายภาพ

Abstract

Project Code: RMU4880001

Project Title: Low-pressure Superheated Steam Drying of Food Products (Stage 2)

Investigator: Associate Professor Dr. Sakamon Devahastin

E-mail Address: sakamon.dev@kmutt.ac.th

Project Period: 3 years (June 1, 2005-May 31, 2008)

The present research project is a continuation of the project entitled “Low-pressure Superheated Steam Drying of Food Products” (TRG4580099). The project could be divided into 5 parts (groups), each focusing on different aspects of low-pressure superheated steam drying (LPSSD) of foods products.

The first part of the project focused on the fundamental study of LPSSD of food products. This included the development of a mathematical model, which allows prediction of evolutions of moisture and temperature of a food product (or, in fact, any biomaterial) undergoing LPSSD. The use of fractal analysis was also proposed as a means to correlate structural and various physical changes data, thus allowing one to obtain a more universal indicator of physical/structural changes of foods and biomaterials during drying.

In the second part of the study, experiments were performed to study the effects of LPSSD and other drying techniques on nutritive quality of foods. This included the study of β -carotene isomerization and degradation in carrot, ascorbic acid degradation in Indian gooseberry and the study of the effects of drying methods and tea preparation temperature on the vitamin C content in Indian gooseberry tea. The following part of the study involved the use of LPSSD and appropriate pretreatments to produce health snack viz. fat-free potato chip. The results illustrated feasibility of LPSSD as an alternative to deep-fat frying to produce potato chip.

The fourth part investigated various means to enhance LPSSD, both from the drying kinetics and product quality points of view. The use of far-infrared radiation (FIR) as an additional heat source to augment drying and to induce more vigorous vaporization of moisture within a food product, thus creating more porous structure within a dried product, was attempted and found to be successful. The use of intermittent drying was also investigated and was found helpful in conserving the energy for LPSSD. Finally, the use of LPSSD to produce edible films for active packaging applications was investigated. It was found that LPSSD could produce edible films with superior mechanical properties to films produced by other conventional drying methods.

Keywords: Biomaterials; Drying; Far-infrared radiation; Fractal analysis; Health snack; Intermittent drying; Mathematical modeling; Nutritive quality; Physical properties; Structure-quality relationships.

1. Introduction

The present research project is a continuation of the project entitled “Low-pressure Superheated Steam Drying of Food Products” (TRG4580099). The project continued to investigate detailed effects of various drying parameters and strategies on the drying kinetics as well as physical and chemical (nutritive) qualities of selected food products deemed important for both domestic and international markets. The project could be casually divided into 5 parts (groups), each focusing on different aspects of low-pressure superheated steam drying (LPSSD) of food products.

The first part of the project focused on the fundamental study of LPSSD of food products. This included the development of a three-dimensional liquid-diffusion based mathematical model, which allows prediction of evolutions of moisture and temperature of a food product (or, in fact, any biomaterial) undergoing LPSSD (Suvarnakuta et al., 2007). The model was validated with the available experimental data and it was found that the simulated and observed moisture and temperature evolutions agreed well with each other. The effect of product shrinkage on the model predictability was also investigated. It was noted that the model, which took into account the product shrinkage performed better than the one assuming no product shrinkage.

The use of combined fractal and image analysis was also proposed as a means to correlate structural and various physical changes data, thus allowing one to obtain a more universal indicator (in terms of the dimensionless change of fractal dimension of a microstructural image of a drying product) of physical/structural changes of foods and biomaterials during drying (Kerdpi boon et al., 2006; Kerdpi boon and Devahastin, 2007; Kerdpi boon et al., 2007). In addition, a means to monitor non-uniform product deformation was proposed and tested. It was found that the use of the so-called Heywood shape factor was effective in describing non-uniform product deformation (Panyawong and Devahastin, 2007). This indicator was also found to correlate well with the drying kinetics data, allowing indication of different changes during different periods of drying.

In the second part of the study, experiments were performed to study the effects of LPSSD and other drying techniques on nutritive quality of foods. This included the study of β -carotene isomerization (Hiranvarachat et al., 2008) and degradation (Suvarnakuta et al., 2005) in carrot, ascorbic acid degradation in Indian gooseberry (Methakhup et al., 2005) and the study of the effects of drying methods and tea preparation temperature on the vitamin C content in Indian gooseberry tea

(Kongsoontornkijkul et al., 2006). In almost all cases, LPSSD performed better than other competing technologies, i.e., hot air drying and vacuum drying, in preserving the nutritive quality of the products. This is due to the oxygen-free environment of LPSSD, which prevented oxidative degradation of active compounds during drying.

The following part of the study involved the use of LPSSD and appropriate physical or chemical pretreatment methods to produce health snack viz. fat-free potato chip (Leeratanarak et al., 2006; Pimpaporn et al., 2007; Kingcam et al., 2008). By blanching (to achieve starch gelatinization) and freezing (to achieve starch retrogradation) potato slices prior to LPSSD, it was possible to obtain potato chips that had only slightly inferior quality to commercially available fried chips. The results illustrated feasibility of LPSSD as an alternative to deep-fat frying to produce potato chip. Further work is underway to improve the quality of LPSSD chip.

The fourth part investigated various means to enhance LPSSD, both from the drying kinetics and product quality points of view. The use of far-infrared radiation (FIR) as an additional heat source to augment drying was attempted and found to be successful (Nimmol et al., 2007a). In addition to being able to speed up drying the use of FIR also induced more vigorous vaporization of moisture within a food product, thus creating more porous structure within the dried product. This helped improve the texture of the dried product (banana chips) significantly, especially in terms of the hardness and crispness (Nimmol et al., 2007b), which are two important parameters affecting the consumer preference of a snack product. The enhanced product porosity was also evident from the X-ray microtomographic results; both the average total porosity and the pore size distribution moved towards the directions of higher and larger sizes, respectively (Léonard et al., 2008).

The use of intermittent drying, i.e., supplying either energy or vacuum only intermittently instead of doing so continuously, was also investigated and was found helpful in conserving the energy for LPSSD. The quality of a heat- and oxygen-sensitive product viz. banana slice was found to be insignificantly different or, in some cases, even better than that obtained via the continuous drying process (Thomkapanish et al., 2007).

Finally, the use of LPSSD to produce edible films for active packaging applications was investigated. It was found that LPSSD could produce edible films with superior mechanical properties to films produced by other conventional drying methods (Mayachiew and Devahastin, 2008a). The effects of different drying methods on the

retention and release behavior of active compounds, i.e., galangal and Indian gooseberry extracts, which have been shown to have high antimicrobial and antioxidant activities, respectively (Mayachiew and Devahastin, 2008b), will also be investigated.

2. Materials and Methods

Please refer to appropriate papers in the Appendix for detailed Materials and Methods used in the project.

3. Results and Discussion

Please refer to appropriate papers in the Appendix for detailed Results and Discussion of the various studies mentioned earlier.

4. Conclusion

Please refer to appropriate papers in the Appendix for detailed Conclusion of the various studies mentioned earlier.

5. References

- Hiranvarachat, B., Suvarnakuta, P., Devahastin, S., 2008, "Isomerization Kinetics and Antioxidant Activities of β -Carotene in Carrots Undergoing Different Drying Techniques and Conditions," *Food Chemistry*, 107(4), pp. 1538-1546.
- Kerdpi boon, S., Kerr, W.L., Devahastin, S., 2006, "Neural Network Prediction of Physical Property Changes of Dried Carrot as a Function of Fractal Dimension and Moisture Content," *Food Research International*, 39(10), pp. 1110-1118.
- Kerdpi boon, S., Devahastin, S., 2007, "Fractal Characterization of Some Physical Properties of a Food Product under Various Drying Conditions," *Drying Technology*, 25(1), pp. 135-146.
- Kerdpi boon, S., Devahastin, S., Kerr, W.L., 2007, "Comparative Fractal Characterization of Physical Changes of Different Food Products during Drying," *Journal of Food Engineering*, 83(4), pp. 570-580.
- Kingcam, R., Devahastin, S., Chiewchan, N., 2008, "Effect of Starch Retrogradation on Texture of Potato Chips Produced by Low-Pressure Superheated Steam Drying," *Journal of Food Engineering*, 89(1), pp. 72-79.

- Kongsoontornkijkul, P., Ekwongsupasarn, P., Chiewchan, N., Devahastin, S., 2006, "Effects of Drying Methods and Tea Preparation Temperature on the Amount of Vitamin C in Indian Gooseberry Tea," *Drying Technology*, 24(11), pp. 1509-1513.
- Leeratanarak, N., Devahastin, S., Chiewchan, N., 2006, "Drying Kinetics and Quality of Potato Chips Undergoing Different Drying Techniques," *Journal of Food Engineering*, 77(3), pp. 635-643.
- Léonard, A., Blacher, S., Nimmol, C., Devahastin, S., 2008, "Effect of Far Infrared Radiation Assisted Drying on Microstructure of Banana Slices: An Illustrative Use of X-Ray Microtomography in Microstructural Evaluation of a Food Product," *Journal of Food Engineering*, 85(1), pp. 154-162.
- Mayachiew, P., Devahastin, S., 2008a, "Comparative Evaluation of Physical Properties of Edible Chitosan Films Prepared by Different Drying Methods," *Drying Technology*, 26(2), pp. 176-185.
- Mayachiew, P., Devahastin, S., 2008b, "Antimicrobial and Antioxidant Activities of Indian Gooseberry and Galangal Extracts," *LWT – Food Science and Technology*, 41(7), pp. 1153-1159.
- Methakhup, S., Chiewchan, N., Devahastin, S., 2005, "Effects of Drying Methods and Conditions on Drying Kinetics and Quality of Indian Gooseberry Flake," *LWT – Food Science and Technology*, 38(6), pp. 579-587.
- Nimmol, C., Devahastin, S., Swasdisevi, T., Soponronnarit, S., 2007a, "Drying and Heat Transfer Behavior of a Food Product Undergoing Combined Low-Pressure Superheated Steam and Far-Infrared Radiation Drying," *Applied Thermal Engineering*, 27(14&15), pp. 2483-2494.
- Nimmol, C., Devahastin, S., Swasdisevi, T., Soponronnarit, S., 2007b, "Drying of Banana Slices Using Combined Low-Pressure Superheated Steam and Far-Infrared Radiation," *Journal of Food Engineering*, 81(3), pp. 624-633.
- Panyawong, S., Devahastin, S., 2007, "Determination of Deformation of a Food Product Undergoing Different Drying Methods and Conditions via Evolution of a Shape Factor," *Journal of Food Engineering*, 78(1), pp. 151-161.
- Pimpaporn, P., Devahastin, S., Chiewchan, N., 2007, "Effects of Combined Pretreatments on Drying Kinetics and Quality of Potato Chips Undergoing Low-Pressure Superheated Steam Drying," *Journal of Food Engineering*, 81(2), pp. 318-329.

- Suvarnakuta, P., Devahastin, S., Mujumdar, A.S., 2007, "A Mathematical Model for Low-Pressure Superheated Steam Drying of a Biomaterial," *Chemical Engineering and Processing*, 46(7), pp. 675-683.
- Suvarnakuta, P., Devahastin, S., Mujumdar, A.S., 2005, "Drying Kinetics and β -Carotene Degradation in Carrot Undergoing Different Drying Processes," *Journal of Food Science*, 70(8), pp. S520-S526.
- Thomkapanish, O., Suvarnakuta, P., Devahastin, S., 2007, "Study of Intermittent Low-Pressure Superheated Steam and Vacuum Drying of a Heat-Sensitive Material," *Drying Technology*, 25(1), pp. 205-223.

Outputs of the Project

I. Refereed papers in international journals (18 papers)

Group I Fundamental study of LPSSD for food products

1. Suvarnakuta, P., Devahastin, S., Mujumdar, A.S., 2007, "A Mathematical Model for Low-Pressure Superheated Steam Drying of a Biomaterial," *Chemical Engineering and Processing*, 46(7), pp. 675-683 (IF = 1.129).
2. Kerdpi boon, S., Devahastin, S., 2007, "Fractal Characterization of Some Physical Properties of a Food Product under Various Drying Conditions," *Drying Technology*, 25(1), pp. 135-146 (IF = 1.100).
3. Kerdpi boon, S., Devahastin, S., Kerr, W.L., 2007, "Comparative Fractal Characterization of Physical Changes of Different Food Products during Drying," *Journal of Food Engineering*, 83(4), pp. 570-580 (IF = 1.696).
4. Panyawong, S., Devahastin, S., 2007, "Determination of Deformation of a Food Product Undergoing Different Drying Methods and Conditions via Evolution of a Shape Factor," *Journal of Food Engineering*, 78(1), pp. 151-161 (IF = 1.696).
5. Kerdpi boon, S., Kerr, W.L., Devahastin, S., 2006, "Neural Network Prediction of Physical Property Changes of Dried Carrot as a Function of Fractal Dimension and Moisture Content," *Food Research International*, 39(10), pp. 1110-1118 (IF = 1.652).

Group II Study of the effects of drying methods on quality of food products

1. Hiranvarachat, B., Suvarnakuta, P., Devahastin, S., 2008, "Isomerization Kinetics and Antioxidant Activities of β -Carotene in Carrots Undergoing Different Drying Techniques and Conditions," *Food Chemistry*, 107(4), pp. 1538-1546 (IF = 2.433).
2. Kongsoontornkijkul, P., Ekwongsupasarn, P., Chiewchan, N., Devahastin, S., 2006, "Effects of Drying Methods and Tea Preparation Temperature on the Amount of Vitamin C in Indian Gooseberry Tea," *Drying Technology*, 24(11), pp. 1509-1513 (IF = 1.100).
3. Suvarnakuta, P., Devahastin, S., Mujumdar, A.S., 2005, "Drying Kinetics and β -Carotene Degradation in Carrot Undergoing Different Drying Processes," *Journal of Food Science*, 70(8), pp. S520-S526 (IF = 1.004).
4. Methakhup, S., Chiewchan, N., Devahastin, S., 2005, "Effects of Drying Methods and Conditions on Drying Kinetics and Quality of Indian Gooseberry Flake," *LWT – Food Science and Technology*, 38(6), pp. 579-587 (IF = 1.299).

Group III Use of LPSSD and related technologies to produce health snacks

1. Kingcam, R., Devahastin, S., Chiewchan, N., 2008, "Effect of Starch Retrogradation on Texture of Potato Chips Produced by Low-Pressure Superheated Steam Drying," *Journal of Food Engineering*, 89(1), pp. 72-79 (IF = 1.696).
2. Pimpaporn, P. Devahastin, S., Chiewchan, N., 2007, "Effects of Combined Pretreatments on Drying Kinetics and Quality of Potato Chips Undergoing Low-Pressure Superheated Steam Drying," *Journal of Food Engineering*, 81(2), pp. 318-329 (IF = 1.696).
3. Leeratanarak, N., Devahastin, S., Chiewchan, N., 2006, "Drying Kinetics and Quality of Potato Chips Undergoing Different Drying Techniques," *Journal of Food Engineering*, 77(3), pp. 635-643 (IF = 1.696).

Group IV Enhancement of LPSSD

1. Nimmol, C., Devahastin, S., Swasdisevi, T., Soponronnarit, S., 2007, "Drying and Heat Transfer Behavior of a Food Product Undergoing Combined Low-Pressure Superheated Steam and Far-Infrared Radiation Drying," *Applied Thermal Engineering*, 27(14&15), pp. 2483-2494 (IF = 0.814).
2. Nimmol, C., Devahastin, S., Swasdisevi, T., Soponronnarit, S., 2007, "Drying of Banana Slices Using Combined Low-Pressure Superheated Steam and Far-Infrared Radiation," *Journal of Food Engineering*, 81(3), pp. 624-633 (IF = 1.696).
3. Thomkapanich, O., Suvarnakuta, P., Devahastin, S., 2007, "Study of Intermittent Low-Pressure Superheated Steam and Vacuum Drying of a Heat-Sensitive Material," *Drying Technology*, 25(1), pp. 205-223 (IF = 1.100).
4. Léonard, A., Blacher, S., Nimmol, C., Devahastin, S., 2008, "Effect of Far Infrared Radiation Assisted Drying on Microstructure of Banana Slices: An Illustrative Use of X-Ray Microtomography in Microstructural Evaluation of a Food Product," *Journal of Food Engineering*, 85(1), pp. 154-162 (IF = 1.696).

Group V Production of advanced material using LPSSD

1. Mayachiew, P., Devahastin, S., 2008, "Comparative Evaluation of Physical Properties of Edible Chitosan Films Prepared by Different Drying Methods," *Drying Technology*, 26(2), pp. 176-185 (IF = 1.100).
2. Mayachiew, P., Devahastin, S., 2008, "Antimicrobial and Antioxidant Activities of Indian Gooseberry and Galangal Extracts," *LWT – Food Science and Technology*, 41(7), pp. 1153-1159 (IF = 1.299).

II. Papers presented at international conferences (6 papers)

1. Jinorose, M., Devahastin, S., 2007, "Describing Deformation during Drying Using Indicators Calculated from External and Microstructural Changes of a Food Product," *Proceedings of the 5th Asia-Pacific Drying Conference*, Hong Kong, pp. 158-165.
2. Léonard, A., Blacher, S., Devahastin, S., 2007, "Characterization of Dried Banana Porous Structure by X-Ray Microtomography Coupled with Image Analysis," *Proceedings of the 5th Asia-Pacific Drying Conference*, Hong Kong, pp. 197-202.
3. Mayachiew, P., Devahastin, S., 2007, "Characterization of Edible Chitosan Films Prepared by Different Drying Methods," *Proceedings of the 5th Asia-Pacific Drying Conference*, Hong Kong, pp. 1011-1018.
4. Hiranvarachat, B., Suvarnakuta, P., Chiewchan, N., Devahastin, S., 2007, "Determination of Isomerization Kinetics of β -Carotene in Carrots Undergoing Different Drying Techniques and Conditions," *Proceedings of the 5th Asia-Pacific Drying Conference*, Hong Kong, pp. 1019-1024.
5. Kerdpi boon, S., Devahastin, S., 2006, "Use of Fractal Analysis to Monitor Physical Property Changes of Biomaterials under Various Drying Conditions," *Proceedings of the 15th International Drying Symposium*, Budapest, Hungary, pp. 547-553.
6. Mujumdar, A.S., Devahastin, S., 2005, "Recent Advances in Drying Technologies for Roots," *2nd International Symposium on Sweet Potato and Cassava*, Kuala Lumpur, Malaysia (invited).

II. Book chapters (2 chapters)

1. Jinorose, M., Devahastin, S., Blacher, S., Léonard, A., "Application of Image Analysis in Food Drying," in C. Ratti (Ed.) *Advances in Food Dehydration*, CRC Press, Boca Raton. (*In press*, to appear in 2008).
2. Devahastin, S., Suvarnakuta, P., "Low-Pressure Superheated Steam Drying of Food Products," in X.D. Chen and A.S. Mujumdar (Eds.) *Drying Technologies for Food Processing*, Wiley-Blackwell, Oxford. (*In press*, to appear in 2008).

Contents

Acknowledgements	i
Abstract	ii
บทคัดย่อ	iii
Contents	iv
1. Introduction	1
2. Materials and Methods	3
3. Results and Discussion	3
4. Conclusion	3
5. References	3
Outputs of the Project	6
Appendix	9
I. Refereed papers in international journals	
<u>Group I</u> Fundamental study of LPSSD of food products	
<u>Group II</u> Study of the effects of drying methods on quality of food products	
<u>Group III</u> Use of LPSSD and related technologies to produce health snacks	
<u>Group IV</u> Enhancement of LPSSD	
<u>Group V</u> Production of advanced material using LPSSD	
II. Papers presented at international conferences	
III. Book chapters	

Antimicrobial and antioxidant activities of Indian gooseberry and galangal extracts

Pornpimon Mayachiew, Sakamon Devahastin*

Department of Food Engineering, King Mongkut's University of Technology Thonburi, 126 Pracha u-tid Road, Bangkok 10140, Thailand

Received 19 June 2007; received in revised form 26 July 2007; accepted 26 July 2007

Abstract

The antimicrobial and antioxidant activities of Indian gooseberry (*Phyllanthus emblica* Linn.) and galangal (*Alpinia galanga*) extracts were investigated. Two different methods (disc diffusion and agar dilution methods) were employed to evaluate the antimicrobial activities of plant extracts against *Staphylococcus aureus*. The minimum inhibitory concentration (MIC) values of Indian gooseberry and galangal extracts were found to be 13.97 and 0.78 mg/ml and the minimum biocidal concentration (MBC) values were 13.97 and 2.34 mg/ml, respectively. The antioxidant activities of Indian gooseberry and galangal extracts, which were evaluated by the β -carotene bleaching method, were 86.4% and 70.3%, respectively. The total phenolic contents of Indian gooseberry and galangal extracts, as determined by the Folin–Ciocalteu method, were 290.4 ± 0.7 and 40.9 ± 0.2 mg/g plant extract (in GAE), respectively. The GC–MS analysis showed that the main compounds of galangal extract are 1,8-cineole (20.95%), β -bisabolene (13.16%), β -caryophyllene (17.95%) and β -selinene (10.56%). On the other hand, the use of high-performance liquid chromatography (HPLC) with UV detection indicated many compounds within the Indian gooseberry extract.

© 2007 Swiss Society of Food Science and Technology. Published by Elsevier Ltd. All rights reserved.

Keywords: GC–MS; Minimum inhibitory concentration; Natural antioxidants; *Staphylococcus aureus*; Total phenolic contents; UV–HPLC

1. Introduction

Herbs and spices are known for their antimicrobial and antioxidative properties. Due to an increasing demand for natural food additives, herbs and spices have emerged as popular ingredients and have a tendency of replacing synthetic antimicrobial and antioxidant agents. Generally, essential oils of spices possess strong antibacterial properties against foodborne pathogens and contain high concentrations of phenolic compounds (Burt, 2004; Delaquis, Stanich, Girard, & Mazza, 2002; Nevas, Korhonen, Lindström, Turkki, & Korkeala, 2004). These compounds exhibit a wide range of biological effects, including antioxidant properties.

Indian gooseberry (*Phyllanthus emblica* Linn.) or “Ma-khaam Pom” in Thai or “Amla” in Hindi is one of the most often used herbs and is widely available in most tropical and

subtropical countries. Its fruit is reputed to probably have the highest content of vitamin C compared with any other naturally occurring substances in nature. Active extracts of *P. emblica* have been shown to possess several pharmacological properties, e.g., analgesic, anti-inflammatory, antioxidant and chemoprotective activities (Khan et al., 2002).

Galangal (*Alpinia galanga*) or “Kha” in Thai has traditionally been used as spice in Thai foods. This spice is, like other spices, rich in phenolic compounds such as flavonoids and phenolic acids. In Thailand, galangal is used for medical purposes such as carminative, stomachic, antispasmodic, antiphlogistic and antibacterial drugs. Galangal is also readily available and inexpensive in Thailand. Among the predominant bacteria involved in food-borne diseases, *Staphylococcus aureus* is one of the leading causes of gastroenteritis resulting from the consumption of contaminated foods. Staphylococcal food poisoning is due to the absorption of staphylococcal enterotoxins in foods. *S. aureus* is an important pathogen due to a combination of toxin-mediated virulence,

*Corresponding author. Tel.: +66 2 470 9246; fax: +66 2 470 9240.

E-mail address: sakamon.dev@kmutt.ac.th (S. Devahastin).

invasiveness and antibiotic resistance (Jablonski & Bohach, 2001).

Since food processors and consumers have expressed a desire to reduce the use of synthetic chemicals in food preservation, common culinary herbs and spices that exhibit antimicrobial and antioxidant activities could be a source of natural alternatives. Although herbs and spices in Thailand, including Indian gooseberry and galangal, contain potent antimicrobials and antioxidants, they have not been sufficiently tested for their activities. The aims of the present investigation were therefore to assess the antimicrobial and antioxidant activities of Indian gooseberry and galangal, which are common plants of Thailand. From our preliminary study, it was found that Indian gooseberry and galangal juices exhibited very low antimicrobial and antioxidant activities, hence only the ethanolic extracts of these plants were investigated in the present study. The antimicrobial activities of the extracts were determined by the disc diffusion and agar dilution methods, while the antioxidant activities were determined by the β -carotene bleaching method. The chemical composition of the galangal extract and of its fractions was studied using gas chromatography–mass spectrometry (GC–MS). The composition of the Indian gooseberry extract was determined by the UV-high performance liquid chromatography (HPLC).

2. Materials and methods

2.1. Chemicals

Ascorbic acid was purchased from Riedel-de-Haën (Seelze, Germany). Linoleic acid, β -carotene and gallic acid were obtained from Fluka (Buchs, Switzerland). Folin–Ciocalteu reagent, orthophosphoric acid, sodium carbonate and absolute ethyl alcohol were purchased from Carlo Erba (Vigevano, Italy) while polyoxyethylene (20) sorbitan monolaurate (Tween 20) was obtained from BDH (Dorset, England). Methanol and acetonitrile were of HPLC grade and were purchased from Lab-Scan Analytical Sciences (Bangkok, Thailand). For antimicrobial tests Tryptic Soy Agar (TSA), Tryptic Soy Broth (TSB), Mueller Hinton agar (MHA) and buffer peptone water were purchased from Difco (Detroit, USA).

2.2. Materials

Indian gooseberry fruits (*P. emblica* Linn.) and galangal (*A. galanga*) rhizomes were purchased from a local market. The Indian gooseberry fruits were first washed thoroughly to remove impurities. After washing the fruits were cut into small pieces and dried overnight in a tray dryer at 40 °C. They were then ground with a blender (Waring, model HGB2WT, Torrington, CT) to make a powder. For preparation of galangal, the fresh rhizomes were cleaned, washed with water, cut into small pieces and dried in a tray

dryer at 40 °C, after which they were ground in a blender to make a powder.

2.3. Extraction procedures

To prepare Indian gooseberry extract, the dried Indian gooseberry powder (10 g dry basis) was extracted with 50 ml of 95% ethanol (Ahmad, Mehmood, & Mohammad, 1998). The extract was filtered through a filter paper (Ø110 mm, Cat. no. 1001 110, Schleicher and Schuell GmbH, Dassel, Germany); the filtrate was collected and concentrated in a rotary evaporator (Resona Technics, Labo Rota 300, Gossau, Switzerland) at 40 °C for 10 min and kept at 4 °C until its use.

The dried galangal powder (10 g dry matter) was extracted with 100 ml of 95% ethanol (Oonmetta-aree, Suzuki, Gasaluck, & Eumkeb, 2006) and left at room temperature overnight. The extract was filtered through a filter paper (Ø110 mm, Cat. no. 1001 110, Schleicher and Schuell GmbH, Dassel, Germany); the filtrate was collected and concentrated by the rotary evaporator at 40 °C for 15 min and kept at 4 °C until its use.

2.4. Antimicrobial activity evaluation

2.4.1. Microbial culture

S. aureus (ATCC 25923) was obtained from the Department of Medical Sciences, Ministry of Public Health, Thailand. The microorganism was maintained in TSA at 5 °C. Stock culture of *S. aureus* was grown in TSB at 37 °C for 18 h at 160 rpm (cell in early stationary phase). The maximum level of the microorganism was 10^{10} CFU/ml; the concentration was subsequently adjusted to 10^8 CFU/ml using buffer peptone water.

2.4.2. Disc diffusion method

The agar diffusion method was employed for screening of the antimicrobial activities of the extracts. Briefly, a suspension of the tested microorganism (0.1 ml of 10^8 CFU/ml) was spread on the MHA. Filter paper discs (6 mm in diameter) were soaked with 15 μ l of the extracts and placed on the inoculated plates (Vardar-Ünlü et al., 2003). After being kept at 4 °C for 2 h, the plates were incubated at 37 °C for 24 h. The diameters of the inhibition zones were then measured in millimeters. All experiments were performed in duplicate.

2.4.3. Agar dilution method

A series of two-fold dilutions of each extract, ranging from 20 to 0.1 ml/l, were prepared in MHA with 5 ml/l Tween 20. Plates were dried at 37 °C for 30 min prior to inoculation with 1–2 μ l spots containing approximately 10^4 CFU of microorganism (Hammer, Carson, & Riley, 1999). MHA, with 5 ml/l Tween 20 but with no extracts, was used as a positive growth control. Inoculated plates were incubated at 37 °C. The minimum inhibitory concentration (MIC) was determined as the lowest concentration

of each extract that completely inhibited growth of microorganism up to 24 h, whereas the minimum bactericidal concentration (MBC) was the lowest concentration at which no growth was observed after incubation up to 5 days. All experiments were performed in duplicate.

2.5. Antioxidant activity evaluation

2.5.1. β -Carotene bleaching method

The antioxidant activity of each extract was examined by the β -carotene bleaching method following a modification of the procedures described by Juntachote and Berghofer (2005). Two milligrams of β -carotene was dissolved in 20 ml of chloroform. A 3 ml aliquot of the solution was put into a 50 ml beaker; 40 mg of linoleic acid and 400 mg of Tween 20 were then added. Chloroform was removed by purging with nitrogen. One hundred milliliters of oxygenated distilled water, which was prepared by aerating air bubble into distilled water for 1 h, was added into the β -carotene emulsion and mixed well by using a vortex mixer (Scientific Industries, model G-560, Bohemia, NY). Three milliliters of aliquot of the oxygenated β -carotene emulsion and 0.12 ml of each ethanolic plant extract were placed in test tubes and mixed thoroughly. The tubes were immediately placed in a water bath and incubated at 50 °C. Oxidation of β -carotene emulsion was monitored spectrophotometrically by measuring the absorbance at 470 nm via a Shimadzu UV-2101 spectrophotometer (Shimadzu Scientific Instruments, model UV-2101 PC, Kyoto, Japan). Absorbance was measured at 0, 10, 20, 30 and 40 min. A control sample was prepared by using 0.12 ml of ethanol instead of the ethanolic extracts. Degradation rate of the extracts was calculated according to the first-order kinetics using:

$$\text{Sample degradation rate} = \ln \frac{a}{b} \times \frac{1}{t}, \quad (1)$$

where a is the initial absorbance (470 nm) at time zero; b is the absorbance (470 nm) at 40 min; t is time (min).

The antioxidant activity (AA) was expressed as % inhibition relative to the control using:

$$\text{AA} = \frac{\text{degradation rate of control} - \text{degradation rate of sample}}{\text{degradation rate of control}} \times 100. \quad (2)$$

All experiments were performed in duplicate.

2.6. Total phenolic contents

The total phenolic contents of each extract were determined using the Folin–Ciocalteu reagent (Zhou & Yu, 2006). The reaction mixture contained 50 μ l of Indian gooseberry or galangal extract, 250 μ l of the Folin–Ciocalteu reagent, 0.75 ml of 20 g/100 ml sodium carbonate and 3 ml of pure water. After 2 h of reaction at ambient temperature, the absorbance at 765 nm was measured and used to calculate the phenolic contents using gallic acid as a standard. The total phenolic contents were then expressed

as gallic acid equivalent (GAE), in mg/g dry sample. All experiments were performed in duplicate.

2.7. GC–MS analysis

The chemical compositions of the galangal extract were determined by the GC–MS analysis. The extract was dissolved in ethanol at the concentration of 10 mg/ml and the volume of the injected sample was 1 μ l. A Hewlett–Packard 6890 combined GC–MS (Hewlett–Packard Co., Wilmington, MA) was used for the analysis. The capillary column HP-5 (30 m \times 0.25 mm; phase thickness, 0.25 μ m) was used and the temperature was first held at 40 °C (2 min) and then raised to 250 °C (5 min) at a rate of 10 °C/min. The carrier gas was helium at a flow rate of 0.9 ml/min. The components of the extract were recognized by the retention time of the chromatogram peaks and by their mass spectra. The identities of the main component peaks were confirmed by comparison of their retention time with that of reference compounds using Wiley, NIST libraries as well as mass spectra databases (Nevás et al., 2004).

2.8. HPLC analysis

The HPLC analysis method that was used to isolate compounds of Indian gooseberry extract was described by Kumaran and Joel Karunakaran (2006). Indian gooseberry extract was dissolved in methanol (1 mg/ml) and filtered through a nylon syringe filter (0.45 μ m) (Filtrex Technology, Singapore) and 10 μ l aliquots of the filtrate were injected to HPLC. The standard solutions of ascorbic acid and gallic acid were prepared in methanol (1 mg/ml).

The components of Indian gooseberry extract were characterized by HPLC (Varian Chromatography Systems, model Pro Star, Walnut Creek, CA) with a Prevail™ reverse phase C₁₈ column (4.6 mm \times 250 mm; 5 μ m) (Alltech, Deerfield, IL). The HPLC system consists of a pump (ProStar, model 240, Walnut Creek, CA), a photodiode array detector (ProStar, model 335, Walnut Creek, CA) and an autosampler (ProStar, model 410, Walnut Creek, CA). A gradient elution at 1 ml/min with a gradient program was performed by varying the portion of solvent A to solvent B (0–6 min 5% B, 6–15 min 15% B, 15–35 min 20% B, 35–40 min 40% B). A 0.05% H₃PO₄ (concentrated, 85%) in water was used as solvent A and acetonitrile as solvent B in order to resolve peaks in the sample. UV detection was carried out at a wavelength of 220 nm. Injection volume was 10 μ l. Standard ascorbic acid and gallic acid were used for the identification of the components in the Indian gooseberry extract.

3. Results and discussion

3.1. Antimicrobial activities of extracts

The *in vitro* antimicrobial activities of Indian gooseberry and galangal extracts against *S. aureus* and their activity

potentials were qualitatively and quantitatively assessed by the presence or absence of inhibition zones, zone diameters, MIC and MBC values. The results given in Table 1 show that galangal extract had greater potential as an antimicrobial agent against *S. aureus* than did Indian gooseberry extract. The maximum inhibition zones, MIC and MBC values for *S. aureus* were 21.8 ± 0.6 mm, 13.97 mg/ml and 13.97 mg/ml for Indian gooseberry extract and 29 ± 0.6 mm, 0.78 mg/ml and 2.34 mg/ml for galangal extract, respectively.

The antimicrobial nature of the galangal extract is apparently related to the components shown in the GC–MS analysis as will be discussed in detail later. Several components of galangal probably acted as antimicrobial agents. 1,8-Cineole, the main component of galangal extract, has been previously reported to have an antibacterial activity against *S. aureus* (Gachkar et al., 2007).

As reported by Canillac and Mourey (2001), if the MBC/MIC ratio is found to be less than or equal to 4, the strain is considered to be susceptible; on the other hand, if this ratio is greater than 4, the strain is considered to be tolerant. From our results, MBC/MIC ratios of Indian gooseberry and galangal extracts were less than 4, so *S. aureus* was considered to be sensitive to these extracts.

3.2. Antioxidant activities of extracts

The antioxidant activity of the extracts was determined based on the coupled oxidation of β -carotene and linoleic acid. Antioxidant activity is expressed as percent inhibition relative to the control. As seen in Table 2, the antioxidant activities of Indian gooseberry and galangal extract were 86.4% and 70.3%, respectively. Indian gooseberry extract exhibited stronger antioxidant activity than did galangal extract. This is because of the different antioxidative compounds in the two extracts.

Phenolic compounds and some of their derivatives are very efficient in preventing auto-oxidation. The antioxidant

activities of phenolic compounds are mainly of redox properties, which include free radical scavenging, hydrogen donating and singlet oxygen quenching. Since Indian gooseberry is rich in tannins and phenolic compounds, these compounds acted effectively as the antioxidant agents. The better antioxidative results might also correlate to the higher total phenolic contents (see next section) in Indian gooseberry extract as well.

3.3. Total phenolic contents

The amounts of the total phenolic contents of Indian gooseberry and galangal extracts were 290.4 ± 0.7 and 40.9 ± 0.2 mg/g plant extract or 130.8 ± 0.34 and 4.7 ± 0.02 mg/g dry sample, respectively (Table 2). Indian gooseberry extract possessed much higher total phenolic contents than did galangal extract. The total phenolic contents of Indian gooseberry extract in this study are similar to the result of Kumaran and Joel Karunakaran (2007), who reported that the total phenols in *Phyllanthus* species are in the range of 171–380 mg/g plant extract (in GEA). However, the total phenolic contents data of galangal are not available elsewhere.

Phenolic compounds contribute to the overall antioxidant activities of herbs and spices. Generally, the mechanisms of phenolic compounds for antioxidant activity are inactivating lipid free radicals and preventing decomposition of hydroperoxides into free radicals. Kumar, Nayaka, Dharmesh, and Salimath (2006) found that gallic acid and tannic acid, in phenolic fraction, are major antioxidant compounds of *P. emblica*.

Antimicrobial and antioxidant activities of plant extracts correlated well with their phenolic fraction. Puupponen-Pimiä, Nohynek, Alakomi, and Oksman-Caldentey (2005) indeed reported that bioactive compounds such as phenolics and organic acids have antimicrobial activities against human pathogens, e.g., *Salmonella* and *Staphylococcus*.

3.4. Identification of galangal extract compounds

Through the use of the GC–MS, the main compounds of galangal extract were found to consist of 1,8-cineole (20.95%), β -caryophyllene (13.16%), β -bisabolene (17.95%) and β -selinene (10.56%), whereas α -selinene (9.67%), farnesene (7.47%), 1,2-benzenedicarboxylic acid (6.42%), germacrene B (6.10%) and pentadecane (2.70%) are the minor components (Table 3). Each component has different retention time; the characterization of individual components was performed with the mass spectrometry (Fig. 1). 1,8-Cineole is an oxygenated monoterpenes, while β -caryophyllene is a sesquiterpene. In addition, β -bisabolene and β -selinene are terpenes. Mallavarapu et al. (2002) also reported similar main compounds in galangal, i.e., 1,8-cineole, α -fenchyl acetate and camphor; they reported 1,8-cineole as the main component of galangal. However, the composition of galangal in this study differs from that described by other authors (Mallavarapu et al., 2002; Oonmetta-aree et al.,

Table 1
Antimicrobial activity of plant extracts against *S. aureus*

Type of plant	Inhibition zone (mm)	MIC (mg/ml)	MBC (mg/ml)
Indian gooseberry	21.8 ± 0.6	13.97	13.97
Galangal	29 ± 0.6	0.78	2.34

Table 2
Antioxidant activity and total phenolic contents of plant extracts

Type of plant	Antioxidant activity (%)	Total phenolic contents	
		mg/g extract	mg/g dry sample
Indian gooseberry	86.4 ± 1.1	290.4 ± 0.7	130.8 ± 0.34
Galangal	70.3 ± 0.8	40.9 ± 0.2	4.7 ± 0.02

Table 3
Chemical compositions of *Alpinia galanga* essential oil

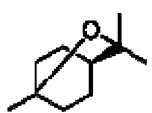
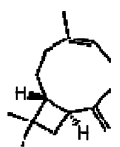


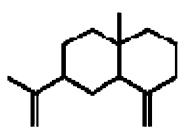

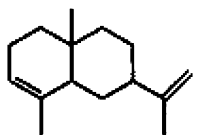
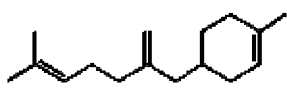
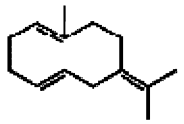
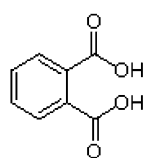
No.	Composition	% Composition	RT
1	1,8-cineole	20.95	8.81
2	 β-caryophyllene	13.16	16.68
3	 farnesene	7.47	17.19
4	 α-humulene	5.02	17.24
5	 β-selinene	10.56	17.77
6	 pentadecane	2.70	17.82
7	 α-selinene	9.67	17.90
8	 β-bisabolene	17.95	18.04
9	 germacrene B	6.10	18.86
			

Table 3 (continued)

No.	Composition	% Composition	RT
10	1,2-benzenedicarboxylic acid	6.42	19.24
			
	Total	100	

RT: retention time.

2006) because the composition of any plant essential oil is influenced by several factors such as planting, climatic, seasonal and experimental conditions (Daferera, Ziogas, & Polissiou, 2000).

The main components of galangal extract have a mechanism of action involving disruption of cytoplasmic membrane and coagulation of cell contents (Oonmetta-aree et al., 2006). 1,8-Cineole in the essential oil can inactivate against Gram-positive bacteria including *S. aureus* (Viljoen et al., 2003). Besides, the minor components might also have a critical part for action in antimicrobial activity, possibly by producing a synergistic effect between other components.

3.5. HPLC analysis of Indian gooseberry extract

The use of HPLC with UV detector at a wavelength of 220 nm along with a gradient elution program to identify compounds of the Indian gooseberry extract revealed many peaks in the chromatogram of the extract (Fig. 2). A comparison between the spectra of the sample peaks with those obtained from ascorbic acid and gallic acid standards confirmed that the retention time of ascorbic acid was 3.60 min (peak 1) while the retention time of gallic acid was 12.085 min (peak 4). The major peak (peak 3) and the second highest peak (peak 2) appeared at the retention time of 7.758 and 4.949 min, respectively. It is possible that these peaks belong to hydrolysable tannins because these compounds have high polarity due to the presence of hydroxyl group (Ghosal, Triethi, & Chauhan, 1996), which generally show as initial peaks of chromatograms.

Kumar et al. (2006) identified that gallic acid and tannic acid are the major phenolic acids of Indian gooseberry extract with 70% ethanol. Gallic acid was also found to be a major compound in the ethyl acetate extract of Indian gooseberry (Kumaran & Joel Karunakaran, 2006). These results do not agree with those of the present study, which shows that gallic acid is not the main compound of the extract, however.

In this study, it was found that the amount of ascorbic acid in Indian gooseberry extract was 11.21%, which is higher than the amount of ascorbic acid present in many Indian gooseberry products (dried fruits, processed fruits

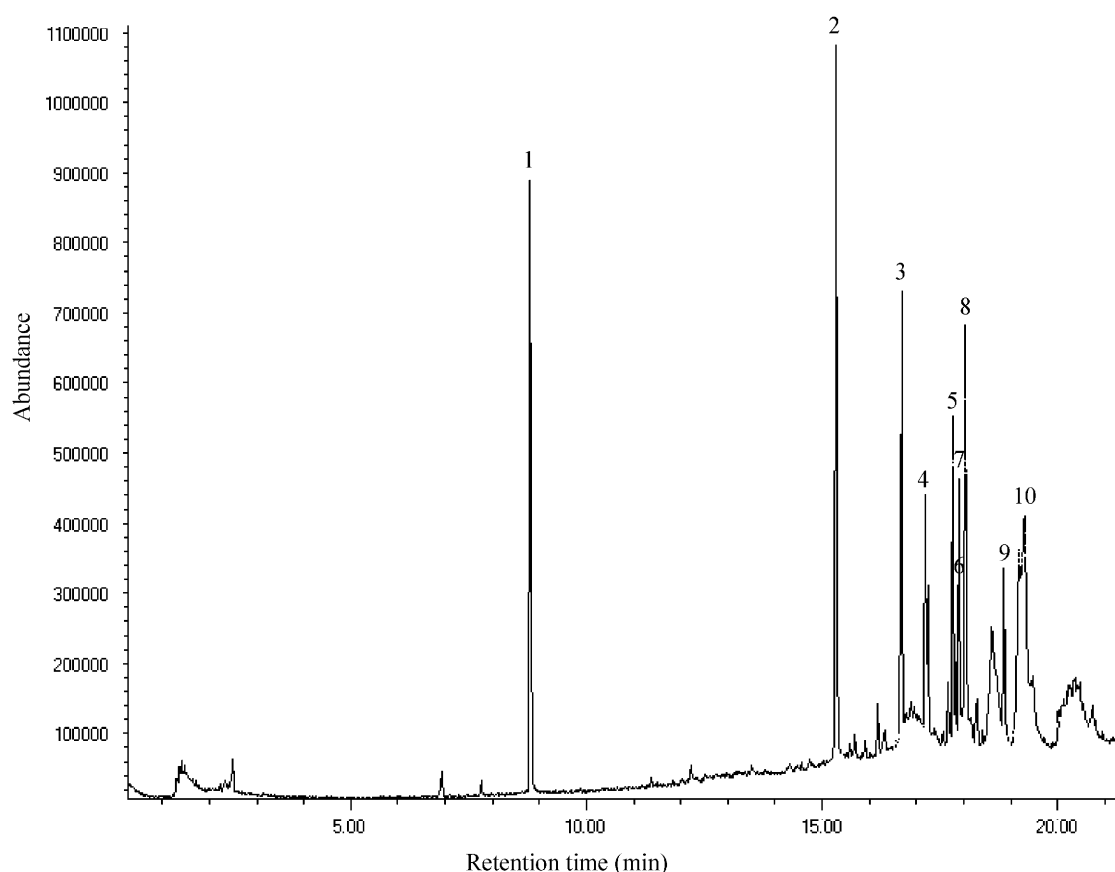


Fig. 1. Typical gas chromatograms of galangal extract: 1,8-cineole (1), β -caryophyllene (2), farnesene (3), α -humulene (4), β -selinene (5), pentadecane (6), α -selinene (7), β -bisabolene (8), germacrene B (9) and 1,2-benzenedicarboxylic acid (10).

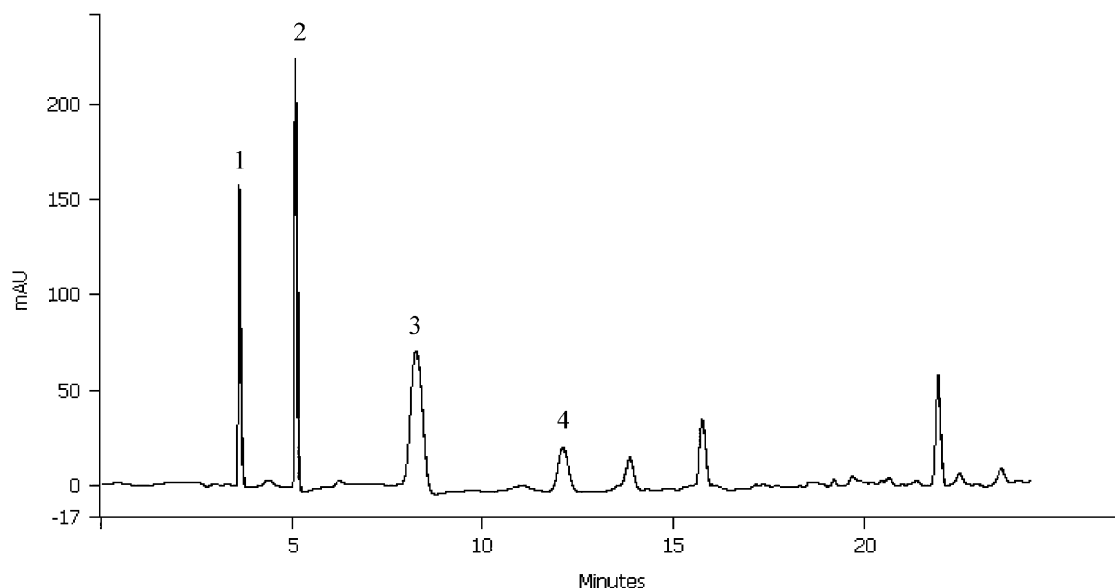


Fig. 2. HPLC chromatograms of Indian gooseberry extract at wavelength 220 nm: ascorbic acid (1), hydrolysable tannins (2, 3) and gallic acid (4).

and a commercial Merck extract); the amount of ascorbic acid is in the range of 0.37% in dried fruits to 2.0% in the Merck extract (Scartezzini, Antognoni, Raggi, Poli, & Sabbioni, 2006).

From the HPLC analysis results, it might be possible to conclude that ascorbic acid and other phenolic compounds contributed to the antioxidant activities of Indian gooseberry extract.

4. Conclusions

The antimicrobial and antioxidant activities of Indian gooseberry and galangal extracts were evaluated. These extracts showed good activity against the growth of food poisoning bacteria, *S. aureus*. In this study, both extracts were found to possess high antioxidant activities. However, Indian gooseberry extract was found to have higher total phenolic contents than did the galangal extract. The major compounds of galangal extract, which were identified by GC–MS, are 1,8-cineole, β -bisabolene, β -caryophyllene and β -selinene. Many phenolic compounds could be isolated from the Indian gooseberry extract through the use of UV-HPLC with C₁₈ column including ascorbic acid and gallic acid. The present study provides additional data for supporting the use of Indian gooseberry and galangal extracts as natural antimicrobial and antioxidant agents. Future work will be performed to encapsulate these extracts in edible films to prepare active packaging materials, which can release antimicrobial and antioxidant agents to extend the shelf life of foods.

Acknowledgments

The authors express their sincere appreciation to the Commission on Higher Education, the Thailand Research Fund (TRF) and the International Foundation for Science (IFS) in Sweden for their financial support.

References

- Ahmad, I., Mehmood, Z., & Mohammad, F. (1998). Screening of some Indian medical plants for their antimicrobial properties. *Journal of Ethnopharmacology*, 62, 183–193.
- Burt, S. (2004). Essential oils: Their antibacterial properties and potential applications in foods—A review. *International Journal of Food Microbiology*, 94, 223–253.
- Canillac, N., & Mourey, A. (2001). Antibacterial activity of the essential oil of *Picea excelsa* on *Listeria*, *Staphylococcus aureus* and coliform bacteria. *Food Microbiology*, 18, 261–268.
- Daferera, D. J., Ziogas, B. N., & Polissiou, M. G. (2000). GC–MS analysis of essential oils from Greek aromatic plants and their fungitoxicity on *Penicillium digitatum*. *Journal of Agricultural and Food Chemistry*, 48, 2576–2581.
- Delaquis, P. J., Stanich, K., Girard, S., & Mazza, G. (2002). Antimicrobial activity of individual and mixed fractions of dill, cilantro, coriander and eucalyptus essential oils. *International Journal of Food Microbiology*, 74, 101–109.
- Gachkar, L., Yadegari, D., Rezaei, M. B., Taghizadeh, M., Astaneh, S. A., & Rasooli, I. (2007). Chemical and biological characteristics of *Cuminum cyminum* and *Rosmarinus officinalis* essential oils. *Food Chemistry*, 102, 898–904.
- Ghosal, S., Triethi, V. K., & Chauhan, S. (1996). Active constituents of *Embolia officinalis*: Part 1—The chemistry and antioxidative effects of two new hydrolysable tannins, Emblicanin A and B. *Indian Journal of Chemistry*, 35, 941–948.
- Hammer, K. A., Carson, C. F., & Riley, T. V. (1999). Antimicrobial activity of essential oils and other plant extracts. *Journal of Applied Microbiology*, 86, 985–990.
- Jablonski, L. M., & Bohach, G. A. (2001). *Staphylococcus aureus*. In M. P. Doyle, L. R. Beuchat, & T. J. Montville (Eds.), *Food microbiology: Fundamentals and frontiers* (pp. 411–434). Washington, DC: ASM Press.
- Juntachote, T., & Berghofer, E. (2005). Antioxidative properties and stability of ethanolic extracts of Holy basil and Galangal. *Food Chemistry*, 92, 193–202.
- Khan, M. T. H., Lampronti, I., Martello, D., Bianchi, N., Jabbar, S., Choudhuri, M. S. K., et al. (2002). Identification of pyrogallol as an antiproliferative compound present in extracts from the medicinal plant *Embolia officinalis*: Effect on in vitro cell growth of human tumor cell lines. *International Journal of Oncology*, 20, 187–192.
- Kumar, G. S., Nayaka, H., Dharmesh, S. M., & Salimath, P. V. (2006). Free and bound phenolic antioxidants in amla (*Embolia officinalis*) and turmeric (*Curcuma longa*). *Journal of Food Composition and Analysis*, 19, 446–452.
- Kumaran, A., & Joel Karunakaran, R. (2006). Nitric oxide radical scavenging active components from *Phyllanthus emblica* L. *Plant Foods for Human Nutrition*, 61, 1–5.
- Kumaran, A., & Joel Karunakaran, R. (2007). In vitro antioxidant activities of methanol extracts of five *Phyllanthus* species from India. *Lebensmittel-Wissenschaft und-Technologie*, 40, 344–352.
- Mallavarapu, G. R., Rao, L., Ramesh, S., Dimri, B. P., Rao, B. R. R., Kaul, P. N., et al. (2002). Composition of the volatile oils of *Alpinia galanga* rhizomes and leaves from India. *Journal of Essential Oil Research*, 14, 397–399.
- Nevas, M., Korhonen, A.-R., Lindström, M., Turkki, P., & Korkeala, H. (2004). Antibacterial efficiency of Finnish spice essential oils against pathogenic and spoilage Bacteria. *Journal of Food Protection*, 67, 199–202.
- Oonmetta-aree, J., Suzuki, T., Gasaluck, P., & Eumkeb, G. (2006). Antimicrobial properties and action of galangal (*Alpinia galanga* Linn.) on *Staphylococcus aureus*. *Lebensmittel-Wissenschaft und-Technologie*, 39, 1214–1220.
- Puupponen-Pimiä, R., Nohynek, L., Alakomi, H.-L., & Oksman-Caldentey, K.-M. (2005). Bioactive berry compounds—Novel tools against human pathogens: Mini-review. *Applied Microbiology and Biotechnology*, 67, 8–18.
- Scartezzini, P., Antognoni, F., Raggi, M. A., Poli, F., & Sabbioni, C. (2006). Vitamin C content and antioxidant activity of the fruit and of the Ayurvedic preparation of *Embolia officinalis* Gaertn. *Journal of Ethnopharmacology*, 104, 113–118.
- Vardar-Ünlü, G., Candan, F., Sökmen, A., Daferera, D., Polissiou, M., Sökmen, M., et al. (2003). Antimicrobial and antioxidant activity of the essential oil and methanol extracts of *Thymus pectinatus* Fisch. et Mey. Var. *pectinatus* (Lamiaceae). *Journal of Agricultural and Food Chemistry*, 51, 63–67.
- Viljoen, A., van Vuuren, S., Ernst, E., Klepser, M., Demirci, B., Başer, H., et al. (2003). *Osmotis asteriscoides* (Asteraceae)—The antimicrobial activity and essential oil composition of a Cape-Dutch remedy. *Journal of Ethnopharmacology*, 88, 137–143.
- Zhou, K., & Yu, L. (2006). Total phenolic contents and antioxidant properties of commonly consumed vegetables grown in Colorado. *Lebensmittel-Wissenschaft und-Technologie*, 39, 1155–1162.

Fractal Characterization of Some Physical Properties of a Food Product under Various Drying Conditions

Soraya Kerdpi boon and Sakamon Devahastin

Department of Food Engineering, King Mongkut's University of Technology Thonburi, Bangkok, Thailand

The present work was aimed at monitoring and studying the relationship between microstructural changes of a food product and its physical property changes during two different types of drying; i.e., conventional hot air drying and low-pressure superheated steam drying, using fractal analysis. The external changes of a model food product, viz. carrot, which were represented in terms of the percentage of shrinkage and the rehydration behavior, correlated well with its microstructural changes, which were represented by the rate of change of the fractal dimension of the microstructural images. The changes of physical properties and microstructure of carrot could be divided into two periods, which are periods of uniform and nonuniform deformation. The microstructural changes of the samples undergoing different drying techniques were quite different, however. Fractal dimension of carrot undergoing drying increased with drying time for both hot air drying and low-pressure superheated steam drying cases. Fractal dimension was found to be a good indicator of the microstructural changes of a product undergoing different drying techniques and conditions.

Keywords Carrot; Fractal analysis; Hot air dryer; Low-pressure superheated steam dryer; Microstructure; Shrinkage; Structure-quality relationship

INTRODUCTION

During drying, physical properties of food change mainly because of the loss of its moisture. Attempts have been made to characterize these physical property changes in terms of such parameters as the changes in volume, area and shape.^[1–5] However, these external changes are caused by internal changes within the sample, which are directly related to the structure of the drying material.

Among many methods that could be used to describe the structural and physical changes of materials are illustrating and evaluating their microstructural changes using such optical instruments as light scanning microscope (LSM) and scanning electron microscope (SEM).^[6] These

microstructural images cannot be easily quantified without the use of other appropriate evaluation techniques, however. For example, Leonard et al.^[7] applied X-ray microtomography in combination with image analysis to evaluate the shrinkage and crack formation of a sample (wastewater sludge) during convective drying. They found a good relationship between the drying kinetics and crack development, which was caused by internal diffusion limitations leading to moisture gradients and mechanical stresses within the sample. Due to the usefulness of image analysis, some researchers have applied this technique in combination with the technique called fractals (or fractal analysis) to quantify property changes of different samples. Fractals have been used successfully to quantify, among others, the shapes of brain cells, gold colloids, sponge iron, etc.^[8,9]

Some researchers have used fractals to describe the microstructural changes and mechanical property changes of foods (via the description of the changes of images representing food surfaces) such as viscoelastic property changes of rice starch suspensions during gelatinization; stress cracks in grain kernel endosperm (corn kernel), which were caused by rapid drying at high temperatures; ruggedness of instant coffee after agglomeration; as well as ruggedness of restructured potato during deep fat frying, among others.^[10–13] Fractal dimension values are different depending on the dimension of images and equal to 1–2 if images are two-dimensional and 2–3 if images are three-dimensional.

Few attempts have been made so far in applying fractal analysis to describe or monitor the process of drying. Chanola et al.^[14] applied fractal analysis to the distributions of the surface temperature of a model food (a slab of a mixture of glucose syrup and agar gel) in order to monitor the drying kinetics of the sample. In addition, the evolution of the fractal dimension of the images of the sample surface was also monitored. Based on a fractal analysis of the surface temperature distributions, different periods of drying can be identified. It was also observed that the fractal dimension of the images of the sample surface increased with the drying time due to an increased

Correspondence: Sakamon Devahastin, Department of Food Engineering, King Mongkut's University of Technology Thonburi, 126 Pracha u-tid Road, Bangkok 10140, Thailand; E-mail: sakamon.dev@kmutt.ac.th

irregularity of the surface as drying proceeded. It was also noted that higher air temperatures and velocities led to higher values of fractal dimension of the surfaces. No attempt was made to use fractal analysis to monitor the change of physical properties of the sample, however.

This work investigated the use of fractal analysis to monitor changes of some properties; i.e., shrinkage and rehydration behavior of a food product undergoing different drying techniques, such as hot air drying and low-pressure superheated steam drying.^[15] A box counting method (BCM) was used to calculate the values of fractal dimension (FD) of microstructural images of a food product, viz. carrot. The values of FD were then related to shrinkage and rehydration behavior of carrot and to its drying kinetics. Correlations between the values of FD, in terms of the changes of FD after and before drying, and the two physical properties as well as the drying kinetics of the product were also assessed using Pearson's square correlation.

EXPERIMENTAL SETUP, MATERIALS AND METHODS

Experimental Setup

A schematic diagram of a hot air tray dryer (HAD) used in this study is presented in Fig. 1. It consists of a stainless steel drying chamber that is connected to an electric heater rated at 6.6 kW, which was used to heat up the air to the desired drying temperature. The heater was controlled by a PID temperature controller. Cubes of sample (carrot) were placed on a tray with dimensions of $30 \times 40 \text{ cm}^2$. Drying temperatures used were 60, 70, and 80°C and two air velocities of 0.5 and 1 m/s were used to dry the samples.

A schematic diagram of a low-pressure superheated steam dryer (LPSSD) and its accessories is shown in Fig. 2. The dryer consists of a stainless steel drying chamber with inner dimensions of $45 \times 45 \times 45 \text{ cm}^3$; a steam reservoir, which received the steam from the boiler and maintained its pressure at around 200 kPa (gauge); and a liquid ring vacuum pump (Nash, model ET32030, Trumbull, CT), which was used to maintain the vacuum in the drying chamber. A steam trap was installed to reduce the excess steam condensation in the reservoir. An electric

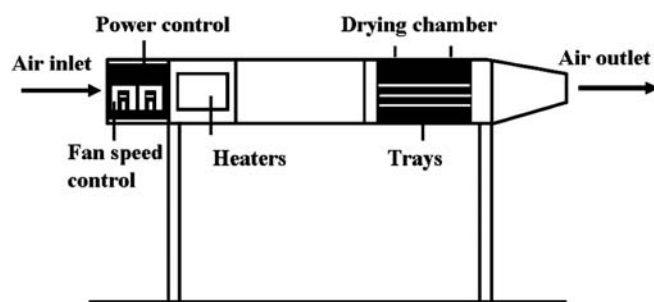


FIG. 1. A schematic diagram of a conventional hot air dryer.

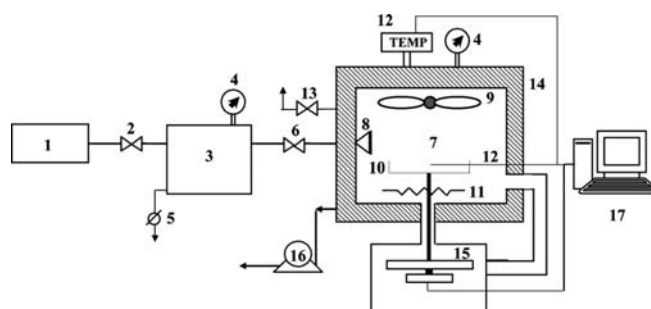


FIG. 2. A schematic diagram of low-pressure superheated steam dryer and associated units. 1, boiler; 2, steam valve; 3, steam reservoir; 4, pressure gauge; 5, steam trap; 6, steam regulator; 7, drying chamber; 8, steam inlet and distributor; 9, electric fan; 10, sample holder; 11, electric heater; 12, on-line temperature sensor and logger; 13, vacuum break-up valve; 14, insulator; 15, on-line weight indicator and logger; 16, vacuum pump; 17, PC with installed data acquisition card.

heater rated at 1.5 kW, which was controlled by a PID controller (Omron, model E5CN, Tokyo, Japan), was installed in the drying chamber to control the steam temperature and to minimize condensation of steam in the drying chamber during the start-up period. A variable-speed electric fan was used to disperse steam throughout the drying chamber. The sample holder was made of a stainless steel screen with dimensions of $12 \times 12 \text{ cm}^2$. The change of the mass of the sample was detected continuously (at 1-min intervals) using a load cell (Minebea, model Ucg-3kg, Nagano, Japan), which was installed in a smaller chamber connected to the drying chamber by a flexible hose (in order to maintain the same vacuum pressure as that in the drying chamber) and also to an indicator and recorder; A&D, model AD 4329, Tokyo, Japan). The temperatures of the steam and of the drying sample were measured continuously using type K thermocouples, which were connected to an expansion board (Omega Engineering, model no. EXP-32, Stamford, CT). Thermocouple signals were multiplexed to a data acquisition card (Omega Engineering, model no. CIO-DAS16JR., Stamford, CT) installed in a PC. Labtech Notebook software (Laboratory Technologies Corp. version 12.1, Andover, MA) was used to read and record the temperature data. Drying experiments were performed at an absolute pressure of 7 kPa and the drying temperatures of 60, 70, and 80°C .

Material

Fresh carrot (*Daucus carota* var. *sativa*) was obtained from a local supermarket and kept at 4°C . Prior to the start of each experiment, carrot was removed from the refrigerator to attain the room temperature. It was then peeled and sliced. In this work, samples were prepared using only the cortex tissues because different parts of carrot have different microstructures. The sliced carrot was diced into cubes with dimensions of $1 \times 1 \times 1 \text{ cm}^3$.

Methods

For each drying experiment, the drying process was carried out up to a predetermined sampling time; that particular experiment was terminated at that time. A new experimental run was then performed up to the next predetermined

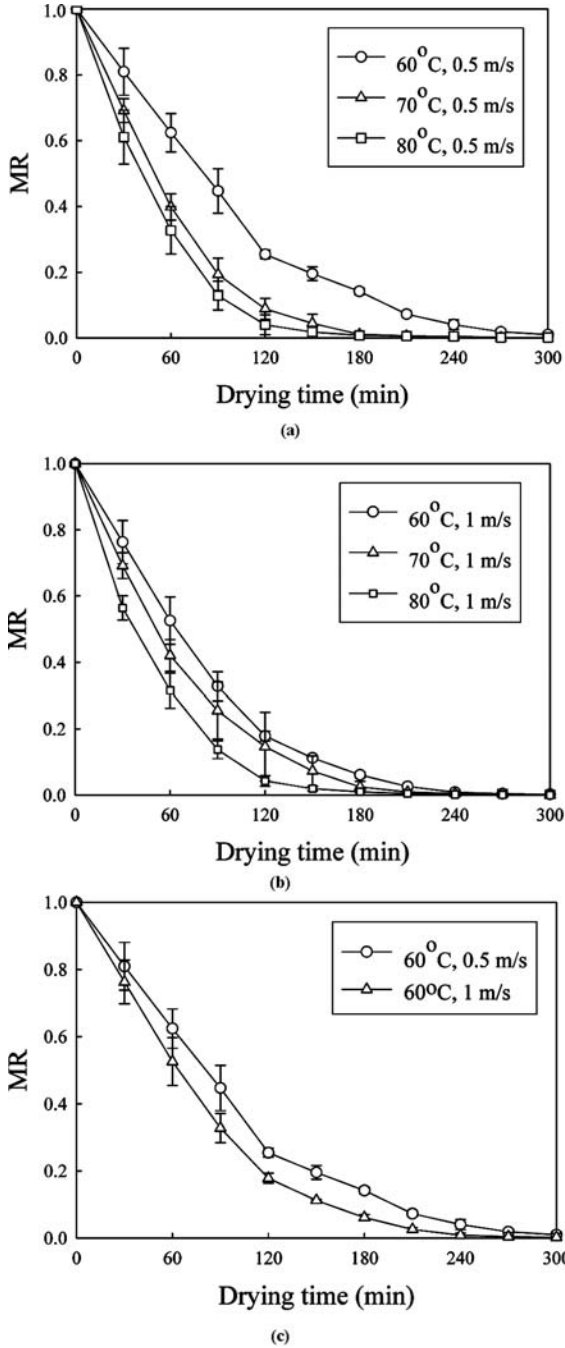


FIG. 3. Drying curves of carrot undergoing hot air drying at different drying conditions. $MR = (X - X_{eq}) / (X_i - X_{eq})$ where X = instantaneous moisture content (kg/kg, d.b.); X_{eq} and X_i are equilibrium and initial moisture contents (kg/kg, d.b.), respectively.

sampling time; these steps were repeated until the complete drying curves (down to the equilibrium moisture content at each condition) were obtained. At the end of each experimental run, the sample was taken out to determine the moisture content,^[16] percentage of shrinkage, rehydration ratio, and microstructural changes. Approximately 100 cubes of carrot (about 100 g) were used in each one of the hot air drying experiments while approximately 35 cubes of carrot (about 35 g) were used in each one of the LPSSD experiments.

Measurement of Shrinkage and Rehydration Behavior

To study the physical property changes of carrot cube during drying, the percentage of shrinkage and rehydration ratio of the sample were selected as representative properties and were calculated as follows.

Shrinkage

Five carrot cubes were used for each shrinkage measurement. Shrinkage is expressed in terms of the percentage change of the volume of the sample as compared with its original volume.

$$\% \text{ shrinkage} = \left(\frac{V_i - V}{V_i} \right) \times 100 \quad (1)$$

where V_i and V are, respectively, the volumes of carrot at the beginning and at the end of each drying run. The average values of the percentage of shrinkage of five cubes were reported. All measurements were performed in duplicate.

Rehydration Ratio

The rehydration ratio (R) of the dried sample was determined by immersing the dried carrot cube in hot water at 100°C for 10 min. The sample was then drained and its masses, both before and after immersion, were measured with an electronic balance (accurate to ± 0.0001 g). The rehydration ratio of

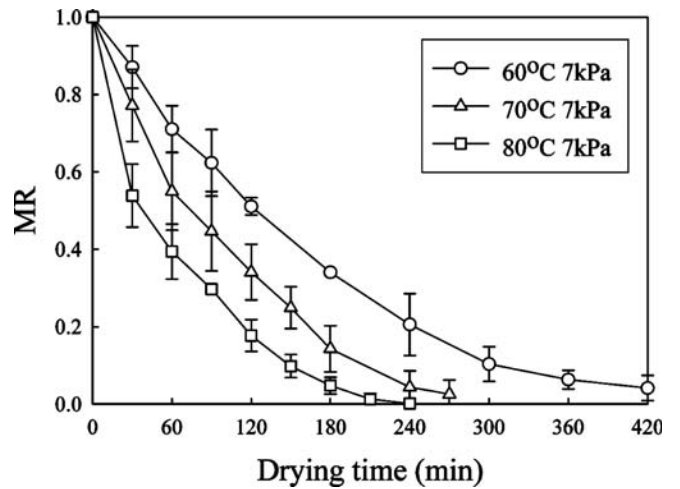


FIG. 4. Drying curves of carrot undergoing LPSSD at 7 kPa.

the dried carrot cube is calculated as:

$$R = \frac{M}{M_0} \quad (2)$$

where M_0 and M are, respectively, the masses of carrot before and after immersion in hot water. The average values of five cubes were reported and all measurements were performed in duplicate.

Measurement of Microstructural Changes and Image Processing

Microstructural Imaging

To obtain microstructural images of a drying sample the sample was taken from each type of dryer at every 30-min interval. The sample was preserved with 10% (V/V) formaldehyde prior to passing through the remaining steps. The sample was subsequently soaked with flowing distilled water for 20 min before removing the remaining moisture within the sample cells by flushing the sample with a series of isopropyl alcohol solutions of different concentrations, starting with 50, 70, 95, 95, 95, 100, 100, and 100% (V/V), respectively. The sample was flushed with isopropyl alcohol from lower to higher concentrations to prevent the damage of the cell structure, which might occur from the sudden loss of moisture. Isopropyl alcohol within the sample was then removed by flushing the sample with absolute xylene for two times. The time used for flushing the sample with each concentration of isopropyl alcohol and absolute

xylene was approximately 90 min per solution. Finally, the pores of the sample were replaced with paraffin by dipping the sample in melted paraffin at 60°C.^[17] Only the sample whose pores were fully replaced with paraffin could be sectioned by a microtome, however. If the pores of the sample were not fully replaced with paraffin, the sample must be dipped in melted paraffin at 60°C again.

Treated sample was then embedded in paraffin wax, which has a melting point in the range of 58–59°C. The steps for preparing an embedded sample started from pouring heated paraffin wax into a stainless steel box with dimensions of $30 \times 24 \times 5 \text{ mm}^3$ to about one third of the box. The sample was then placed at the middle of the stainless steel box and covered with a plastic embedded ring. Finally, liquid paraffin was poured to fully fill the box.

The embedded sample was sectioned by a microtome (Jung, model RM2025, Germany) into a 5- μm thick slice. The sliced sample was placed on a glass slide; 95% ethanol was dropped indirectly to the sliced sample to expand the cell tissue. Ethanol was then eliminated by floating the sliced sample in water at 42–43°C and removing the sliced sample immediately to the glass slide. The sliced sample was dried at room temperature and then fixed on a glass slide with the use of a hotplate set at temperature of 48–50°C for 8 h. The finished slide was dyed by haematoxylin and eosin to highlight the cell walls. Finally, the microstructural images were obtained using a light microscope (Olympus, model LH30RF200, Japan) at 10 \times magnification level.

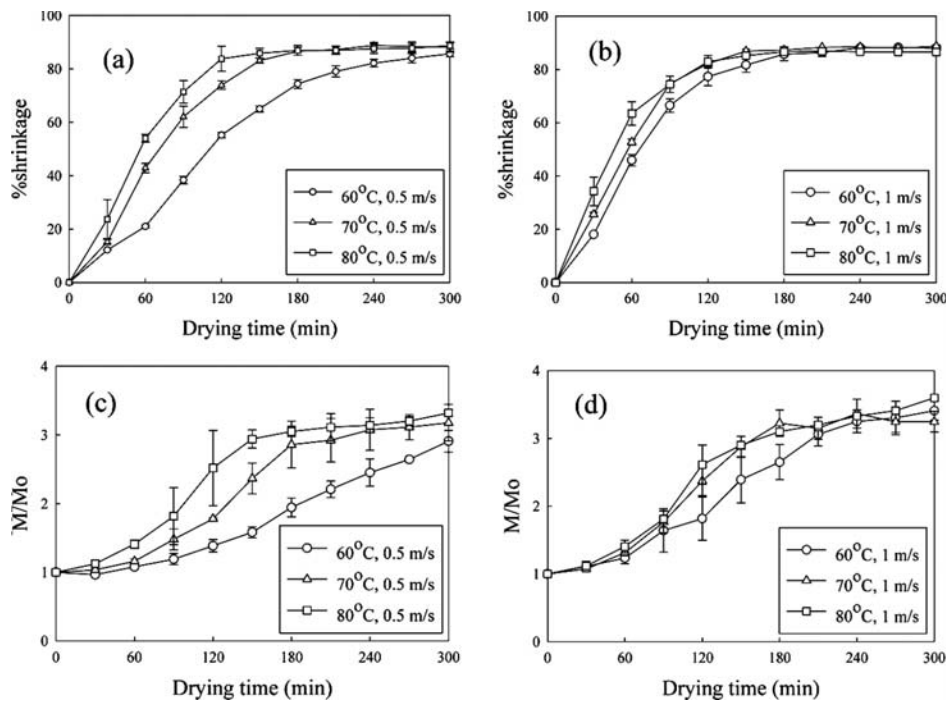


FIG. 5. Percentage of shrinkage ((a) and (b)) and rehydration ratio ((c) and (d)) of carrot undergoing conventional hot air drying.

Image Processing

A light microscopic image of the sample was captured by a Pixel View capture (Pixel View Program, Play TV/USBpro, Taiwan) at an image size of 520×520 pixels. The image was then transformed from an RGB format to a black-and-white format before a calculation of the fractal dimension (FD) was performed.

Fractal Dimension (FD) Calculation

The fractal dimension of a black-and-white image obtained as described in the previous section was calculated using the box counting method^[18] at the box sizes of 4, 5, 10, 13, 26, 65, 130, and 260 pixels and threshold values of 0.5–0.8 using Matlab[™] Software (version 6.5). The value of the threshold used for each image was chosen as the lowest value that could yield clearest the cell walls of

the sample. Ten light microscopic images were captured for one sample obtained at each sampling time.

To compare the changing values of FD of the sample undergoing drying, the normalized change of FD is reported as:

$$\Delta FD / FD_0 \quad (3)$$

$$\Delta FD = FD_t - FD_0 \quad (4)$$

where FD_0 and FD_t are, respectively, the fractal dimension of fresh sample and the fractal dimension of the sample at any instant during drying.

The correlations between FD and the drying kinetics and between FD and the physical property changes were determined by Pearson's correlation coefficient. Pearson's

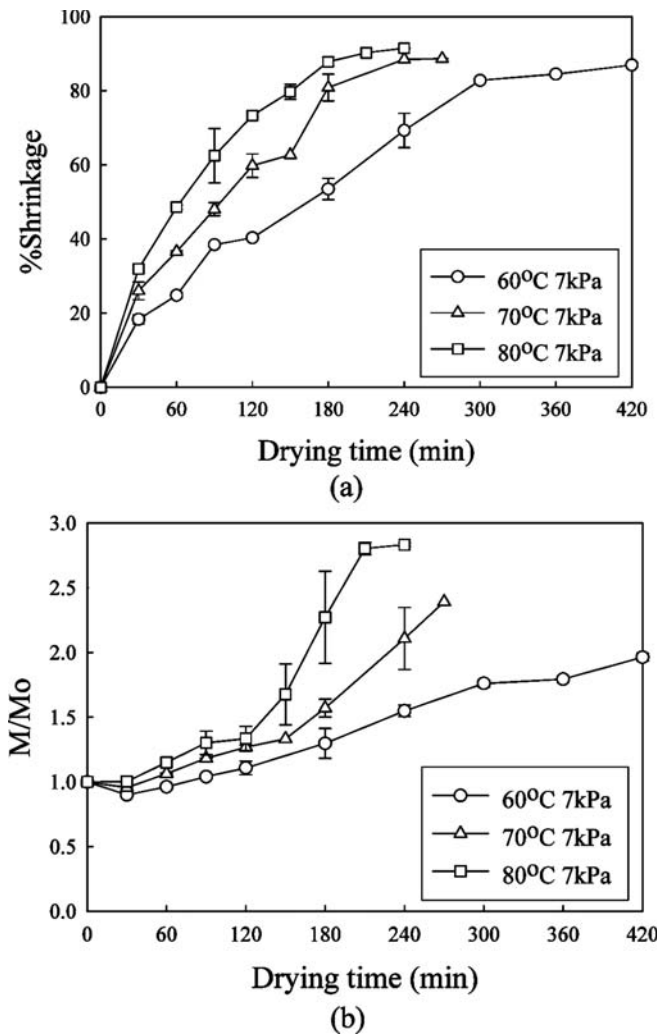


FIG. 6. Percentage of shrinkage (a) and rehydration ratio (b) of carrot undergoing LPSSD.

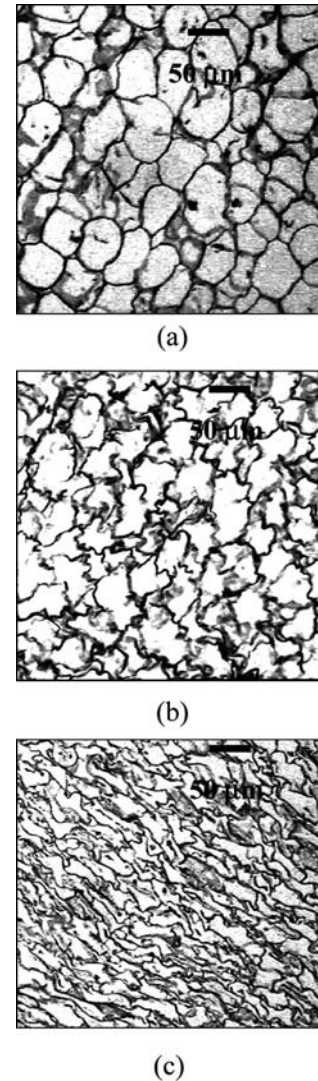


FIG. 7. Microstructure of carrot underwent hot air drying at 60°C, 0.5 m/s at 0 min (a), 150 min (b), and 300 min (c).

correlation coefficient (r) is a measure of the degree of linear relationship between two variables and the correlation coefficient may take on any values between plus and minus one; the sign of the correlation coefficient (+, -) is the direction of the relationship. A positive correlation coefficient means the values of both variables change in the same direction and vice versa. The absolute value of the coefficient illustrates the closeness of the relationship between the two variables.^[19]

RESULTS AND DISCUSSION

Drying Kinetics of Carrot Cube

Fresh carrot that had initial moisture content around 88–90% w.b. (or about 8.9–9 kg/kg d.b.) was dried until reaching its equilibrium moisture content of about 7%

w.b. (or about 0.07 kg/kg d.b.). The drying kinetics of carrot cube undergoing HAD are shown in Figs. 3a and 3b. It was found, as expected, that higher temperatures led to higher drying rates of the samples. The samples reached their equilibrium moisture contents after 300, 240, 210, 180, 180, and 150 min of drying for the cases when using drying air temperatures and velocities of 60°C, 0.5 m/s; 60°C, 1 m/s; 70°C, 0.5 m/s; 70°C, 1 m/s; 80°C, 0.5 m/s; and 80°C, 1 m/s, respectively. The effect of drying air velocity on the drying kinetics of carrot cubes is shown in Fig. 3c.

For all drying conditions tested, no constant rate period was observed; if a constant rate period existed it should be shorter than 30 min, since the first sample was taken only after 30 min. Moreover, moisture migration might be

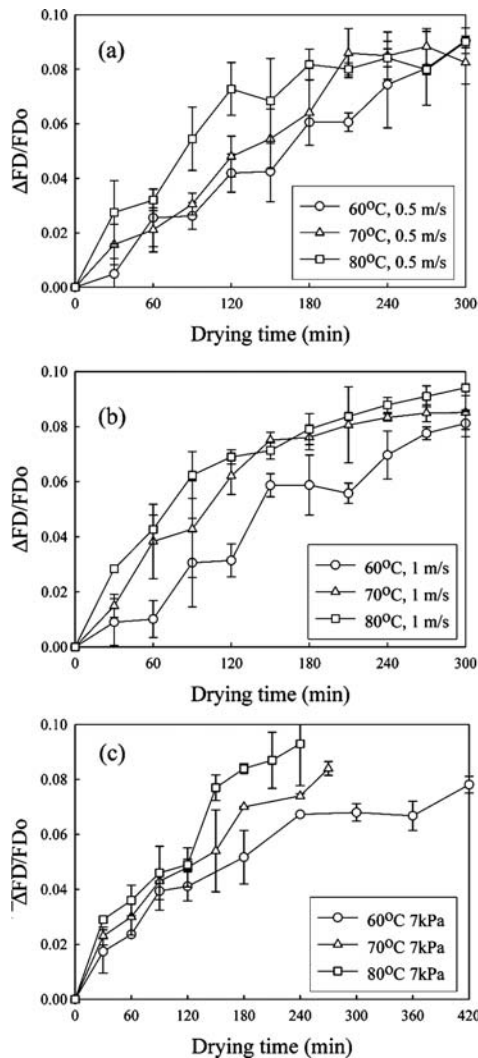


FIG. 8. $\Delta FD/FD_0$ of carrot cube undergoing hot air drying (velocity of 0.5 m/s (a) and 1 m/s (b)) and LPSSD at 7 kPa (c).

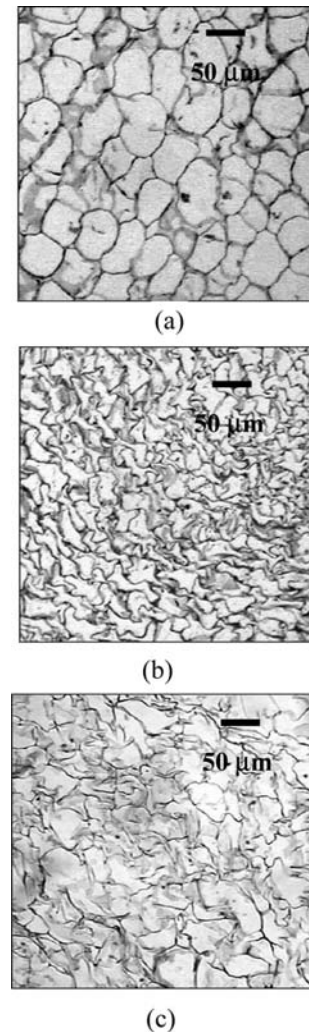


FIG. 9. Microstructure of fresh carrot (a) and of carrot dried until reaching equilibrium moisture content using hot air drying (b) and LPSSD (c).

resisted due to the collapse at the surface of the sample. Similar results were also reported by Doymaz^[20] and Prakash et al.^[21] In each case, there exist two falling rate periods. Initially, the moisture content decreased more rapidly because moisture gradients within the sample were still large and hence led to faster movement of moisture. For instance, carrot sample dried in an HAD at 60°C

and 0.5 m/s was in the first falling rate period until 120 min. Then it was in the second falling rate period until reaching equilibrium moisture content at 300 min (Fig. 3c).

Figure 4 illustrates the drying kinetics of carrot cube undergoing LPSSD. The trends of the results are the same as those of HAD; i.e., higher drying temperatures led to higher rates of drying. Carrots reached their equilibrium moisture contents after 450, 270, and 240 min when drying were performed at 60, 70, and 80°C at an absolute pressure of 7 kPa, respectively. It was found that the average drying rates over the whole period of drying in the case of LPSSD were lower than those of HAD at the same

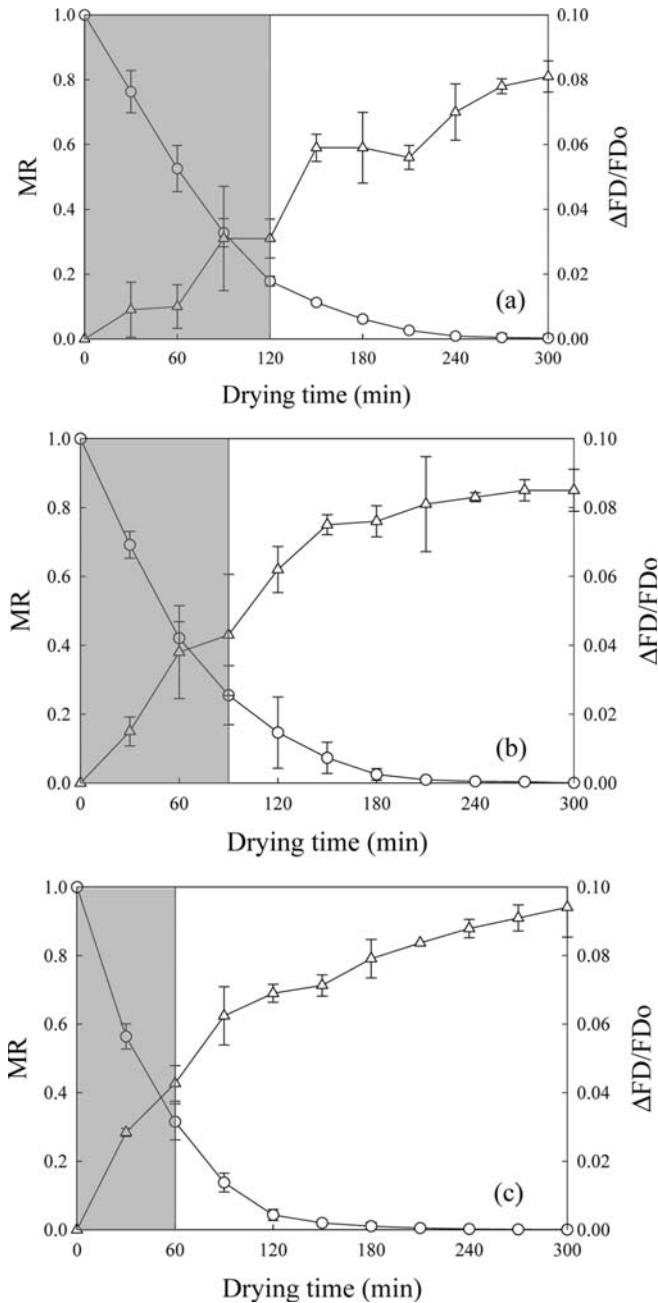


FIG. 10. Relationship between drying kinetics (o) and $\Delta FD/FD_0$ (Δ) of carrot undergoing hot air drying at velocity of 1 m/s and temperature of 60°C (a), 70°C (b), and 80°C (c).

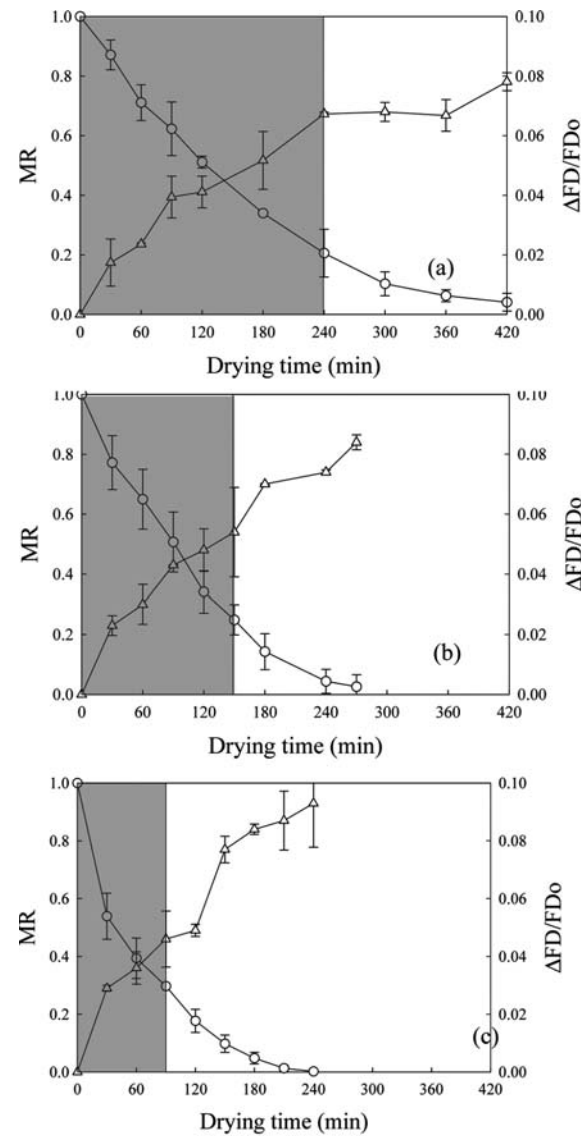


FIG. 11. Relationship between drying kinetics (o) and $\Delta FD/FD_0$ (Δ) of carrot undergoing LPSSD at temperature of 60°C (a), 70°C (b), and 80°C (c).

drying temperature. This is because the heat transfer driving forces were higher in the case of HAD than in the case of LPSSD over the range of drying temperatures investigated. The chamber of an LPSSD might also be more humid than that of an HAD and hence led to lower driving forces for mass transfer as well.

Physical Property Changes of Carrot Cube

Percentage of shrinkage and rehydration ratio of carrot cube undergoing HAD are shown in Fig. 5. As for shrinkage (Figs. 5a and 5b), it increased with the drying time. Moreover, at the same sampling time, samples undergoing drying at higher temperatures suffered more shrinkage than those undergoing drying at lower temperatures. This is because the drying temperature directly affected the shrinkage property of the product; larger moisture gradients within the sample developed when using higher drying temperatures and these larger gradients led to larger

internal stresses that in turn led to larger degrees of shrinkage.^[15] Moreover, the shape of dried carrot samples was not uniform, indicating that the deformation of the sample was not uniform.^[5]

It was observed that initially the percentage of shrinkage increased rapidly and then increased slowly until reaching the final values at the time corresponding to the point where the samples reached their equilibrium moisture contents. This trend applied to both drying techniques (Figs. 5a and 5b for HAD and Fig. 6a for LPSSD). The drying time that divided the period of shrinkage into the rapid increase and slow increase (and then constant) was the same as the time that divided the drying curves into the first falling and second falling rate periods (Figs. 3 and 4). Toward the end of drying, case-hardened skin developed and this inhibited further shrinkage of the sample.

It can be seen in Fig. 5 that the samples undergoing HAD at higher temperatures had higher rates of shrinkage

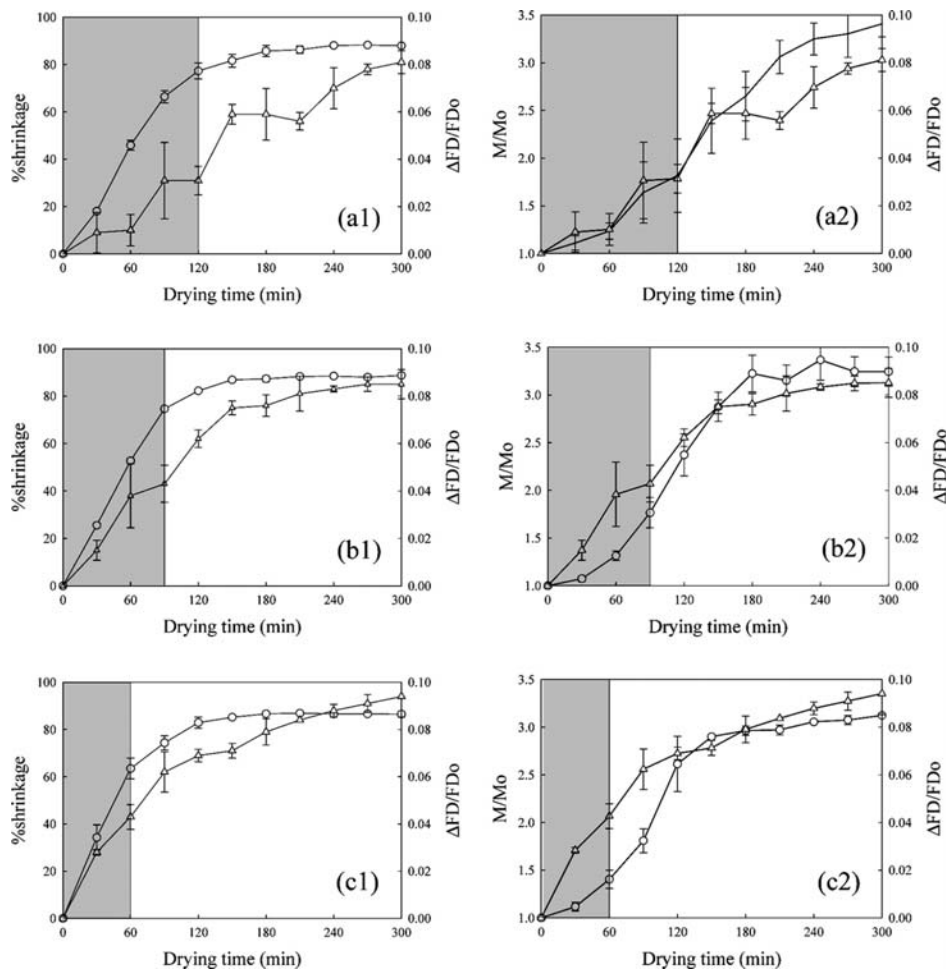


FIG. 12. Relationship between % shrinkage (o) and $\Delta FD/FD_o$ (Δ); rehydration ratio (o) and $\Delta FD/FD_o$ (Δ) of carrot undergoing hot air drying at velocity of 1 m/s temperature of 60°C (a), 70°C (b), and 80°C (c).

than those of samples undergoing drying at lower temperatures. This is because the results were compared at the same sampling periods, not at the same moisture contents. The trends of the results of LPSSD (Fig. 6a) were also the same as those of HAD.

Comparing the two drying techniques, it was found that carrot cubes dried using LPSSD had lower percentage of shrinkage than that of HAD. This is because superheated steam drying is known to have a potential to reduce the degree of shrinkage of the drying product due to evolution of water vapor inside the product that expands into cells, leading to a normally porous dried product.^[15,22,23]

As for the rehydration ratio, higher drying temperatures led to products with higher rehydration ratios. Higher rehydration ratios were observed in carrot cubes dried using either HAD or LPSSD at 80°C than those dried at lower temperatures (Figs. 5c and 5d for HAD and Fig. 6b for LPSSD). This is because the samples that were dried at lower temperatures needed a longer time to achieve their equilibrium moisture contents than those dried at higher

temperatures; the samples therefore suffered more structural damage (e.g., collapse of porous structure) than when drying at lower temperatures. The capability to reconstitute samples that underwent high-temperature drying was therefore higher than those that underwent low-temperature drying.

Microstructural Changes of Carrot Cube

The images used for microstructural analysis were observed from a light microscope at 10× magnification. After capturing the images from the light microscope, the images were used for fractal dimension calculation.

The fractal dimension of fresh carrot (Fig. 7a) was about 1.75, whereas the fractal dimension of the samples increased upon drying. Initially, the cell walls of carrot were of round shape. After some period of time, however, moisture within the cells started to migrate to the surface. Moisture gradients thus started to develop and these led to internal stresses and shrinkage of the cells (Figs. 7b

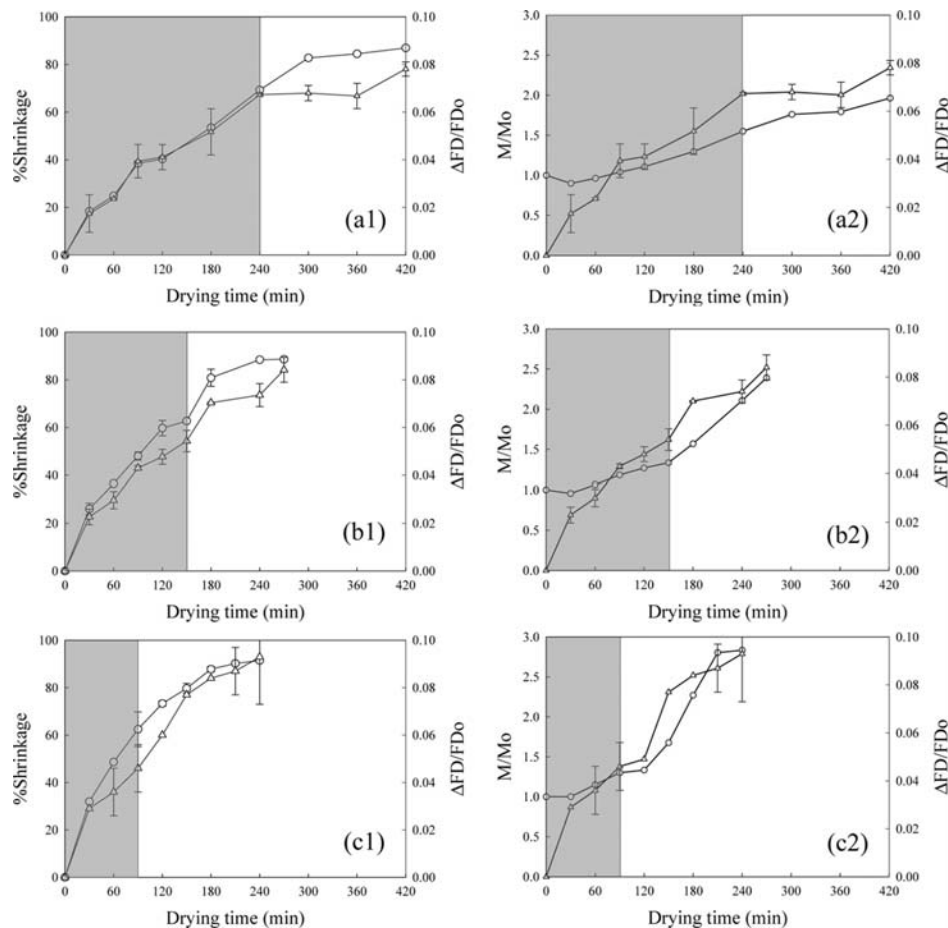
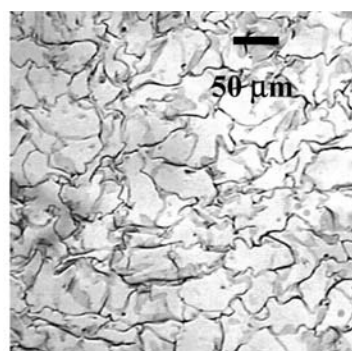


FIG. 13. Relationship between % shrinkage (o) and $\Delta FD/FD_0$ (Δ); rehydration ratio (o) and $\Delta FD/FD_0$ (Δ) of carrot undergoing LPSSD at temperature of 60°C (a), 70°C (b), and 80°C (c).

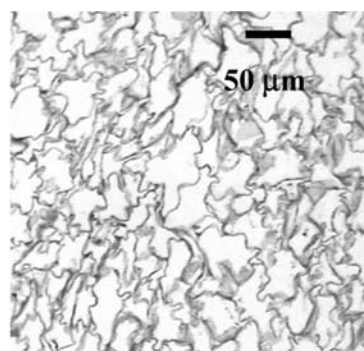
and 7c). The ruggedness of cell walls increased the fractal dimension of cell walls, as expected.

The microstructural changes of carrot cube undergoing drying are illustrated in terms of $\Delta FD/FD_0$ because this ratio represents the rate of change of fractal dimension of the sample undergoing each drying technique and hence could be used when comparing results of different drying processes and conditions.

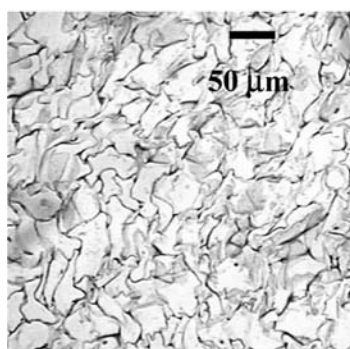
The rates of change of fractal dimension of carrot samples undergoing HAD (Figs. 8a and 8b) and LPSSD (Figure 8c) were monitored. It was found that the rates of change of the fractal dimension could be divided roughly into two periods; one is linear and the other nonlinear. The rates of fractal dimension change of carrot cubes undergoing HAD and LPSSD increased linearly during the first period of drying and increased slowly until reaching the



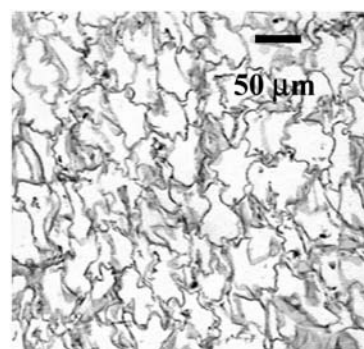
LPSSD, 60°C, 210 min



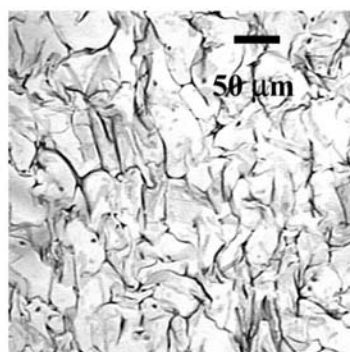
HAD, 60°C, 1 m/s, 150 min



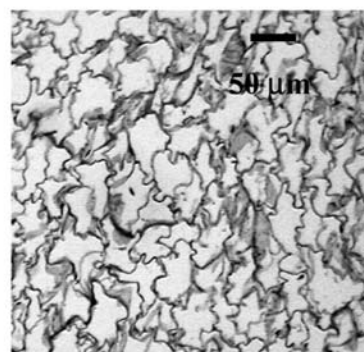
LPSSD, 70°C, 150 min



HAD, 70°C, 1m/s, 120 min



LPSSD, 80°C, 120 min



HAD, 80°C, 1m/s, 90 min

FIG. 14. Images of carrot at $\Delta FD/FD_0 = 0.06$.

constant rates of change. The drying time that identified the end point of the period where the rates of fractal dimension changed in a linear fashion was also the same as the drying time that divided the drying curves into the first and second falling rate periods and that divided the property changes (in terms of the percentage of shrinkage and rehydration ratio) into rapid increase and slow increase periods, respectively.

The microstructural changes of cell walls of carrot undergoing different drying techniques and conditions are quite different (Fig. 9). Carrots that were dried using HAD suffered more deformation of cell structure than in the case of LPSSD. This is because in HAD, cell structure was damaged directly from the hot air, whereas in LPSSD there was an evolution of vapor inside the cell structure that expanded into cells, leading to a porous dried product.^[14,15]

Relationship between FD and Physical Property Changes of Carrot Cube

As mentioned earlier, the rates of change of fractal dimension could be divided into two periods. During the first falling rate period, although the rate of moisture migration from the internal cells to the surface was not equal to the rate of moisture evaporation from the surface to the surrounding, these rates might not be much different to cause significant gradients within the sample; therefore, linear changes of fractal dimension were observed. When samples were dried further, the migration of moisture from the cells to the surface was slower than from the surface to the surrounding and this led to larger gradients, which in turn led to microstructural changes and deformation.

Drying time (Figs. 10 and 11) that divided the rates of change of fractal dimension into linear periods and nonlinear periods correlated well with the changes of physical properties, especially the percentage of shrinkage (Figs. 12 and 13). The time that the rates of change of

fractal dimension switched from the linear to nonlinear periods was the same as the point where the drying curves changed from the first falling rate period to the second falling rate period. Moreover, it was the same point where the percentage of shrinkage started to vary nonlinearly as well. The percentage of shrinkage, which represents the external changes of the samples, correlated well with the rates of change of fractal dimension, which represents the microstructural (or internal) changes of the samples.

The normalized change of fractal dimension could be used to monitor the physical property changes of carrot during drying. For example, at $\Delta FD/FD_0$ of around 0.06, the percentage of shrinkage was around 60% in all HAD and LPSSD cases (Figs. 12 and 13). This kind of relationship was also observed at other $\Delta FD/FD_0$ and percentage of shrinkage values. These results are supported by results presented in Fig. 14, which illustrates the microstructure of the samples at $\Delta FD/FD_0$ of 0.06 when drying with HAD at 60°C, 1 m/s, 150 min; 70°C, 1 m/s, 120 min; 80°C, 1 m/s, 90 min, and LPSSD at 60°C, 7 kPa, 210 min; 70°C, 7 kPa, 150 min; 80°C, 7 kPa, 90 min. All of the samples had similar levels of shrinkage although they had different microstructure. However, they all had the same $\Delta FD/FD_0$ values.

On the other hand, values of the rehydration ratio at the same $\Delta FD/FD_0$ were quite different. For instance, at $\Delta FD/FD_0$ of around 0.06, the rehydration ratio was around 2.50 at all conditions of HAD while the rehydration ratio was around 1.75 at all conditions of LPSSD (Figs. 12 and 13). However, $\Delta FD/FD_0$ could be used to correlate the rehydration behavior of samples dried using the same type of dryer.

The simple correlations between the rates of change of fractal dimension and the drying kinetics and physical property changes of carrot cube undergoing different drying techniques and conditions are shown in Table 1. The symbols (+, -) represent the direction of the relationship. It is

TABLE 1

Pearson's square correlation between $\Delta FD/FD_0$ and drying kinetics and $\Delta FD/FD_0$ and physical properties of carrot undergoing different drying techniques and conditions

Drying technique	Conditions	Parameter of interest		
		Drying kinetics	% Shrinkage	Rehydration ratio
Hot air drying	60°C, 0.5 m/s	-0.941	0.961	0.954
	60°C, 1 m/s	-0.883	0.872	0.964
	70°C, 0.5 m/s	-0.844	0.913	0.966
	70°C, 1 m/s	-0.981	0.955	0.972
	80°C, 0.5 m/s	-0.979	0.964	0.954
	80°C, 1 m/s	-0.962	0.959	0.945
LPSSD	60°C, 7 kPa	-0.970	0.976	0.885
	70°C, 7 kPa	-0.984	0.985	0.859
	80°C, 7 kPa	-0.947	0.947	0.901

seen from the table that the changes of the fractal dimension correlated well with the drying kinetics and the changes of physical properties during drying. The Pearson's square correlation coefficients between the fractal dimension and the physical property changes were between 0.86 and 0.99 depending on the tested conditions and techniques of drying. These close-to-unity coefficients imply that $\Delta FD/FD_0$ and other observed variables correlated well with each other.

CONCLUSION

Fractal dimension was used to relate the physical property changes to the microstructural changes of carrot undergoing two different types of drying at various conditions. The external changes of carrot, which were represented in terms of percentage of shrinkage, correlated well with the changes of fractal dimension, which were used to represent the microstructural changes. Fractal dimension was proved to be capable of being a structure-quality index of food undergoing drying. Further work is now underway to develop an approach (via the use of neural network simulation) to predict the physical properties of products when the values of fractal dimension are given.

ACKNOWLEDGEMENTS

The authors express their sincere appreciation to the Commission on Higher Education, the Thailand Research Fund (TRF), the National Research Council of Thailand, and the International Foundation for Science (IFS), Sweden, for financial support. Our appreciation also goes to the Faculty of Fishery, Kasetsart University, for their help with the microstructural imaging of the samples.

REFERENCES

1. Ratti, C. Shrinkage during drying of foodstuffs. *Journal of Food Engineering* **1994**, *23*, 91–105.
2. Khraisheh, M.A.M.; Cooper, T.J.R.; Magee, T.R.A. Shrinkage characteristics of potatoes dehydrated under combined microwave and convective air conditions. *Drying Technology* **1997**, *15*, 1003–1022.
3. Ochoa, M.R.; Kessler, A.G.; Pirone, B.N.; Marquez, C.A.; De Michelis, A. Volume and area shrinkage of whole sour cherry fruits (*Prunus cerasus*) during dehydration. *Drying Technology* **2002**, *20*, 147–156.
4. Madamba, P.S. Physical changes in bamboo (*Bambusa phyllostachys*) shoot during hot air drying: Shrinkage, density, and porosity. *Drying Technology* **2003**, *21*, 555–568.
5. Panyawong, S.; Devahastin, S. Determination of deformation of a food product undergoing different drying methods and conditions via evolution of a shape factor. *Journal of Food Engineering* **2007**, *78*, 151–161.
6. Aguilera, J.M.; Stanley, D.W. *Microstructural Principles of Food Processing and Engineering*; 2nd edition, Aspen Publishers: Gaithersburg, 1999.
7. Leonard, A.; Blacher, S.; Marchot, P.; Pirard, J.P.; Crine, M. Measurement of shrinkage and cracks associated to convective drying of soft materials by X-ray microtomography. *Drying Technology* **2004**, *22*, 1695–1708.
8. Graf, J.C. The importance of resolution limits to the interpretation of fractal descriptions of fine particles. *Powder Technology* **1991**, *67*, 83–85.
9. Mandelbrot, B.M. *The Fractal Geometry of Nature*; Freeman Press: New York, 1983.
10. Hsu, S.; Lu, S.; Huang, C. Viscoelastic changes of rice starch suspensions during gelatinization. *Journal of Food Science* **2000**, *65*, 215–220.
11. Peleg, M.; Normand, M.D. Characterization of the ruggedness of instant coffee particle shape by natural fractals. *Journal of Food Science* **1985**, *50*, 829–831.
12. Zhu, W.; Dong, T.; Cao, C.; Li, D. Fractal modeling and simulation of the developing process of stress cracks in corn kernel. *Drying Technology* **2004**, *22*, 59–69.
13. Rubnov, M.; Saguy, I.S. Fractal analysis and crust water diffusivity of a restructured potato product during deep-fat frying. *Journal of Food Science* **1997**, *62*, 135–154.
14. Chanola, P.J.J.; Alamilla, B.L.; Farrera, R.R.R.; Quevedo, R.; Aguilera, J.M.; Gutierrez, L.G.F. Description of the convective air-drying of a food model by means of the fractal theory. *Food Science and Technology International* **2003**, *9*, 207–213.
15. Devahastin, S.; Suvarnakuta, P.; Soponronnarit, S.; Mujumdar, A.S. A comparative study of low-pressure superheated steam and vacuum drying of a heat-sensitive material. *Drying Technology* **2004**, *22*, 1854–1867.
16. Association of Official Analytical Chemists. *Official Methods of Analysis*, 14th Ed.; AOAC: Washington, DC, 1984.
17. Humason, G.L. *Animal Tissue Techniques*, 4th Ed.; W.H. Freeman and Company: San Francisco, 1979.
18. Quevedo, R.; Calos, L.G.; Aguilera, J.M.; Cadoche, L. Description of food surfaces and microstructural changes using fractal image texture analysis. *Journal of Food Engineering* **2002**, *53*, 361–371.
19. Downie, N.M.; Health, R.W. *Basic Statistical Methods*, 4th Ed.; Harper & Row Publishers: New York, 1974.
20. Doymaz, I. Convective air drying characteristics of thin layer carrots. *Journal of Food Engineering* **2004**, *61*, 359–364.
21. Prakash, S.; Jha, S.K.; Datta, N. Performance evaluation of blanched carrot dried by three different driers. *Journal of Food Engineering* **2004**, *62*, 305–313.
22. Elustondo, D.M.; Mujumdar, A.S.; Urbicain, M.J. Optimum operating conditions in drying foodstuffs with superheated steam. *Drying Technology* **2002**, *20*, 381–402.
23. Moreira, R.G. Impingement drying of foods using hot air and superheated steam. *Journal of Food Engineering* **2001**, *49*, 291–295.

Comparative fractal characterization of physical changes of different food products during drying

Soraya Kerdpi boon^a, Sakamon Devahastin^{a,*}, William L. Kerr^b

^a Department of Food Engineering, King Mongkut's University of Technology Thonburi, 126 Pracha u-tid Road, Bangkok 10140, Thailand

^b Department of Food Science and Technology, University of Georgia, Athens, GA, USA

Received 12 February 2007; received in revised form 12 March 2007; accepted 30 March 2007

Available online 14 April 2007

Abstract

The development of a relationship between microstructural changes of model food products (carrot and potato cubes) and their physical changes during conventional hot air drying (HAD) using combined fractal and image analysis was performed in this study. Dried carrot and potato sections were examined by light microscopy and the fractal dimension (FD) of the microscopic images was determined using a box counting technique. The apparent physical changes of the samples undergoing HAD were represented in terms of the percentage of shrinkage and rehydration ratio. These apparent changes correlated well with their microstructural changes represented by the normalized changes of fractal dimension ($\Delta FD/FD_0$) of the microstructural images. Although the microstructural changes of the samples undergoing HAD were quite different, the changes of $\Delta FD/FD_0$ of the samples undergoing drying were in the same trend. FD has thus proved to be a good indicator of microstructural changes of products undergoing drying.

© 2007 Elsevier Ltd. All rights reserved.

Keywords: Carrot; Conventional hot air drying; Deformation; Fractal analysis; Physical properties; Potato; Structure-quality relationship

1. Introduction

Physical properties are those properties that provide descriptive quantification of foods by physical rather than chemical means. During drying physical properties of foods change primarily due to the loss of moisture from the interior regions to the surfaces and surrounding air. Numerous studies have attempted to characterize these physical changes in terms of such parameters as changes in volume, area, size and shape (Khraisheh, Cooper, & Magee, 1997; Madamba, 2003; Ochoa, Kessler, Pirone, Marquez, & De Michelis, 2002; Panyawong & Devahastin, 2007; Ratti, 1994). However, these external or apparent changes are primarily caused by internal changes, which are directly related to the microstructure of drying materials.

Structural changes of drying materials can be observed using microscopy. However, it is not easy to describe changes

of these microstructural images quantitatively. One technique, called fractal analysis, could be used to quantify these microstructural images. Fractal analysis has been applied successfully to quantify irregular fragments or complex particles such as shorelines, clouds, plants, brain cells, gold colloids and sponge iron (Graf, 1991; Mandelbrot, 1983). Fractal analysis has also been used to study surface and morphology of food materials after processing. Barletta and Canovas (1993) characterized the ruggedness of food powders, which were commercial instant coffee and instant skim milk, exposing to attrition in a tap density tester. It was shown that the calculated fractal dimension (FD) was sensitive enough to detect the ruggedness of the agglomerates when exposing to small amount of tapping. FD can also be used to describe the surface and morphology of food products such as chocolate, bread, and potato, among others (Pedreschi & Aguilera, 2000; Quevedo, Carlos, Aguilera, & Cadoche, 2002).

Recently, Kerdpi boon and Devahastin (2007) developed a relationship between microstructural changes of carrot

* Corresponding author. Tel.: +66 2 470 9246; fax: +66 2 470 9240.
E-mail address: sakamon.dev@kmutt.ac.th (S. Devahastin).

cubes and their physical changes during conventional hot air drying (HAD) and low-pressure superheated steam drying (LPSSD) using combined fractal and image analysis. The apparent changes of carrot cubes, which were represented in terms of the percentage of shrinkage and rehydration behavior, correlated well with their microstructural changes, which were represented by the normalized changes of fractal dimension ($\Delta FD/FD_0$) of the microstructural images. In addition, the use of artificial neural networks (ANN) to predict the percentage of shrinkage and rehydration ratio of dried carrots based on the inputs of moisture content and $\Delta FD/FD_0$ of the cell structure was implemented (Kerdpiroon, Kerr, & Devahastin, 2006). ANN models were developed and the measured values of the percentage of shrinkage and rehydration ratio were predicted with $R^2 > 0.95$ in all cases.

To investigate if the above correlations can also be extended to other products the application of fractal analysis to monitor physical changes of various kinds of foods during drying is of interest. This work aimed at studying apparent physical changes (in terms of shrinkage and rehydration ratio) of food products (which are carrot and potato cubes) during conventional hot air drying. The normalized changes of fractal dimension of different microstructural images of carrot and potato cubes undergoing drying were compared. Simple correlations between apparent and microstructural changes of samples were also calculated.

2. Materials and methods

2.1. Experimental set-up

A schematic diagram of the hot air tray dryer (HAD) used in this study is presented in Fig. 1. The HAD consists of a stainless steel drying chamber that is connected to an electric heater rated at 6.6 kW, which was used to heat up the air to the desired drying temperature. The heater was controlled by a PID temperature controller. The cubes of sample were placed on trays with dimensions of $30 \times 40 \text{ cm}^2$.

2.2. Materials

Fresh carrots (*Daucus carota* var. *sativa*) and potatoes (*Solanum tuberosum* Linn.) were obtained from a local supermarket and stored at 4°C . Prior to the start of each

experiment the samples were removed from the refrigerator to attain room temperature. The carrots and potatoes were then peeled and sliced. In this study, carrots were prepared using only the cortex tissues since different parts of carrots may have different microstructures. Moreover, the samples were used immediately after preparation, especially in the case of potatoes, which could suffer browning reactions on their surfaces. The sliced carrots and potatoes were then diced into cubes with dimensions of $1 \times 1 \times 1 \text{ cm}^3$.

2.3. Methods

2.3.1. Drying experiments

The samples were dried using HAD at drying temperatures of 60 , 70 and 80°C and two air velocities of 0.5 and 1 m/s in the case of carrot cubes and one air velocity of 1 m/s in the case of potato cubes. Carrot and potato cubes were dried by HAD to compare the differences in their physical and microstructural changes.

Approximately 100 cubes of sample (about 100 g) were used in each HAD experiment. In each drying experiment the drying process was carried out up to a predetermined sampling time and ended at that time. A new experimental run was then performed up to the next predetermined sampling time. These steps were repeated until a complete drying curve (down to the equilibrium moisture content at each condition) was obtained. At the end of each experimental run the samples were taken out to determine the moisture content (AOAC, 1984), percentage of shrinkage, rehydration ratio and microstructural changes.

2.3.2. Measurement of shrinkage and rehydration ratio

To study the physical changes of carrot cubes and potato cubes during drying the percentage of shrinkage and rehydration ratio of the samples were selected as representative properties and were calculated as follows.

2.3.2.1. Percentage of shrinkage. Five sample cubes were used for each shrinkage measurement. Shrinkage is expressed in terms of the percentage change of the volume of the sample as compared with its original volume.

$$\%S = \left(\frac{V_i - V}{V_i} \right) \times 100, \quad (1)$$

where V_i and V are the volumes of the sample at the beginning and at the end of each drying run, respectively. The average values of the percentage of shrinkage of five samples were reported. All measurements were performed in triplicate.

2.3.2.2. Rehydration ratio. The rehydration ratio (R) of the dried sample was determined by immersing the dried sample in hot water at 100°C for 10 min. The sample was then drained and its mass, both before and after immersion, was measured by using an electronic balance (accurate to 0.001 g). The rehydration ratio of the sample was calculated by

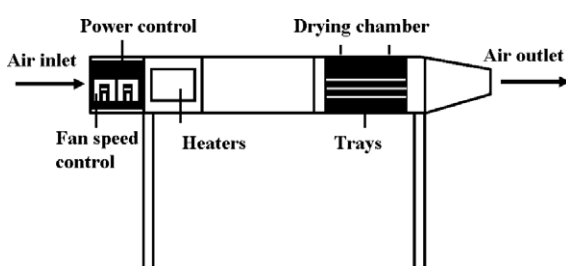


Fig. 1. Conventional hot air dryer.

$$R = \frac{M}{M_0} \quad (2)$$

where M_0 and M are the masses of sample before and after immersion in hot water, respectively. The average values of five samples were reported and all measurements were performed in duplicate.

2.3.3. Microstructural analysis

2.3.3.1. Microstructural imaging. The process of microstructural imaging consists of fixation, in which the sample was preserved with 10% (V/V) formaldehyde prior to passing through the remaining steps. The objective of the fixation step is to immobilize cellular components in order to ensure that the structure and tissue shown in the microstructural images reflect as closely as possible the living state of the sample. After fixation the sample was soaked with flowing distilled water for 20 min before removing the remaining moisture within the sample cells by flushing the sample with a series of isopropyl alcohol solutions at different concentrations starting with 50%, 70%, 95%, 95%, 95%, 100%, 100% and 100% (V/V), respectively. The sample was flushed with isopropyl alcohol from the lower to higher concentrations to prevent the damage of the cell structure, which might occur from the sudden loss of moisture. Isopropyl alcohol within the sample was subsequently removed by flushing the sample with absolute xylene for two times. The time used for flushing the sample with each concentration of isopropyl alcohol and absolute xylene was approximately 90 min per solution. Finally, the pores of the sample were replaced with paraffin by dipping the sample in melted paraffin at 60 °C (Humason, 1979; Aguilera & Stanley, 1999).

The treated sample was embedded in paraffin wax, which has a melting point in the range of 58–59 °C. The steps for preparing an embedded sample started from pouring heated paraffin wax into a stainless steel box with dimensions of $30 \times 24 \times 5 \text{ mm}^3$ to cover approximately one-third of the depth of the box. The sample was then placed at the middle of the stainless steel box and covered with a plastic embedded ring. Finally, additional liquid paraffin was poured to fully fill the box. The paraffin within the embedded sample could be set at room temperature and kept in a refrigerator at 4 °C. The cool embedded sample was easier to be sectioned than the sample at room temperature.

Each embedded sample was sectioned by a microtome (Jung, model RM2025, Germany) into a 5 µm thick slice. As the deformation of the sample occurred from the outside to inside, the samples were sliced at their center. For example, fresh sample was sectioned at $0.5 \text{ cm} \pm 2.5 \text{ µm}$. Sliced sample was placed on a glass slide and 95% ethanol was dropped indirectly to the sliced sample to expand the cell tissue. Ethanol was then eliminated by floating the sliced sample in water at 42–43 °C and removing the sliced sample immediately to the glass slide. The sliced sample was dried by placing at room temperature and then fixed

on the glass slide with the use of a hotplate set at temperature of 48–50 °C for 8 h. The finished slide was then dyed using haematoxylin and eosin to highlight the cell walls. Finally, the microstructural images were obtained using a light microscope (Olympus, model LH30RF200, Japan) at a 10× magnification level.

Although the microstructure of sample cells might change during the fixation step, the normalized fractal dimension of a sample undergoing drying was determined from the difference between the fractal dimension of the fresh sample and of the sample undergoing drying. All of the samples were fixed with paraffin and sectioned with a microtome in the same fashion. Therefore, the sample characteristic change was expected to be similar.

2.3.3.2. Image analysis. A light microscopic image of the sample was captured by a Pixel View capture (Pixel View Program, Play TV/USBpro, Taiwan) at an image size of 520×520 pixels (one pixel has the resolution of 0.71 µm). The image was then transformed from an RGB format to a black and white format before a calculation of the fractal dimension (FD) was performed.

2.3.4. Fractal dimension (FD) calculation

The fractal dimension of a black and white image obtained as described in the previous section was calculated using the box counting method (Quevedo et al., 2002). Cubic boxes with different sizes (r) were mounted into the images. The number of boxes (N_r), which were formed on the image was then counted. Fractal dimension was calculated by

$$\text{FD} = \frac{\log(N_r)}{\log(1/r)} \quad (3)$$

The sizes of boxes are composed of 4, 5, 10, 13, 26, 65, 130 and 260 pixels and the threshold values used were between 0.5 and 0.8. Fractal dimension calculation was performed using Matlab™ Software (version 6.5). Ten light microscopic images were captured for each sample obtained at each sampling time.

To compare the changing values of FD of the sample undergoing drying the normalized changes of FD is reported as

$$\frac{\Delta \text{FD}}{\text{FD}_0}, \quad (4)$$

$$\Delta \text{FD} = \text{FD}_t - \text{FD}_0, \quad (5)$$

where FD_0 and FD_t are the fractal dimensions of fresh sample and of the sample at any instant during drying, respectively.

2.4. Structure-quality relationship determination

The correlations between normalized changes of FD and the drying kinetics as well as between normalized changes of FD and the physical changes were determined by the

Pearson's correlation coefficient. Pearson's correlation coefficient (r) is a measure of the degree of the linear relationship between two variables and the correlation coefficient may take on any values between plus and minus one. The sign of this correlation coefficient (+, −) represents the direction of the relationship. A positive correlation coefficient indicates that the values of both variables change in the same direction and a negative r indicates that the values change in opposite directions. The absolute value of the coefficient illustrates the closeness of the relationship between the two variables.

Pearson's correlation coefficient was calculated by Eq. (6).

$$r = \frac{\sum XY - \frac{\sum X \sum Y}{N}}{\sqrt{\left(\sum X^2 - \frac{(\sum X)^2}{N}\right) \left(\sum Y^2 - \frac{(\sum Y)^2}{N}\right)}}, \quad (6)$$

where X , Y and N represent the data of variables X , Y and the number of data X and Y , respectively.

3. Results and discussion

3.1. Drying kinetics of carrot and potato cubes

Fresh carrots with an initial moisture content around 88–90% (w.b.) (or about 8.8–9 kg/kg (d.b.)) were dried until reaching an equilibrium moisture content of approximately 7% (w.b.) (or about 0.075 kg/kg (d.b.)). The drying kinetics of carrot cubes undergoing HAD are shown in Fig. 2. As expected, higher temperatures led to higher drying rates of the samples. Carrot cubes reached their equilibrium moisture contents after 300, 240, 210, 180, 180 and 150 min of drying with air temperatures and air velocities of 60 °C, 0.5 m/s; 60 °C, 1 m/s; 70 °C, 0.5 m/s; 70 °C, 1 m/s; 80 °C, 0.5 m/s and 80 °C, 1 m/s, respectively. The effect of drying air velocity on the drying kinetics of carrot cubes is shown in Fig. 2c.

For all drying conditions tested no constant rate period was observed; a constant rate period might be shorter than 30 min, which was the first sampling time. Moreover, moisture migration might be resisted due to the collapse at the surface of the sample. Similar results were also reported by Doymaz (2004). In each case, two falling rate periods were noted. Initially, the moisture content decreased more rapidly due to large moisture gradients within the sample, leading to faster movement of moisture. For example, carrot dried in an HAD at 60 °C and 0.5 m/s remained in the first falling rate period for 120 min. It was subsequently in the second falling rate period until reaching an equilibrium moisture content at 300 min (Fig. 2c).

The drying kinetics of potato cubes undergoing HAD at temperatures of 60, 70 and 80 °C and air velocity of 1 m/s are shown in Fig. 3. Potato cubes were dried until reaching an equilibrium moisture content of 8–9% (w.b.) (or about 0.087–0.099 kg/kg (d.b.)). Potato cubes reached their equi-

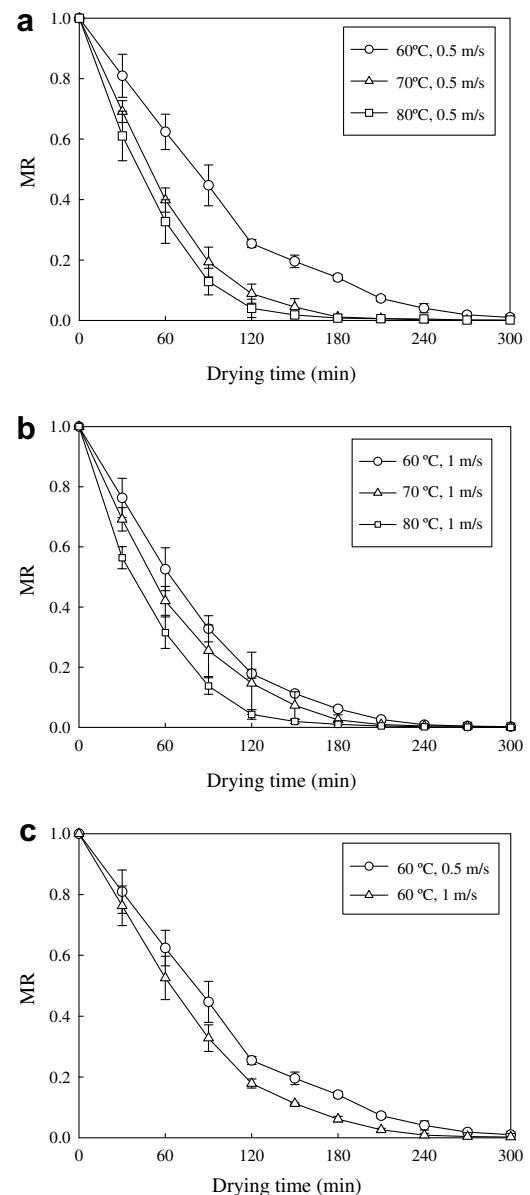


Fig. 2. Drying kinetics of carrot cubes undergoing hot air drying at different drying conditions. $MR = (X - X_{eq}) / (X_i - X_{eq})$, where X = instantaneous moisture content (kg/kg, d.b.); X_{eq} and X_i are equilibrium and initial moisture contents (kg/kg, d.b.), respectively.

librium moisture contents after 420, 390 and 300 minutes of drying at air temperatures of 60, 70 and 80 °C, respectively. Similar results were found for both potato and carrot cubes; there was no constant rate period at all conditions tested.

3.2. Physical changes of carrot and potato cubes

Physical changes of carrot cubes and potato cubes undergoing HAD are shown in Figs. 4 and 5, respectively. As for shrinkage (Fig. 4a and b for carrot cubes and Fig. 5a for potato cubes), it increased with the drying time. In addition, at the same sampling time, samples undergoing

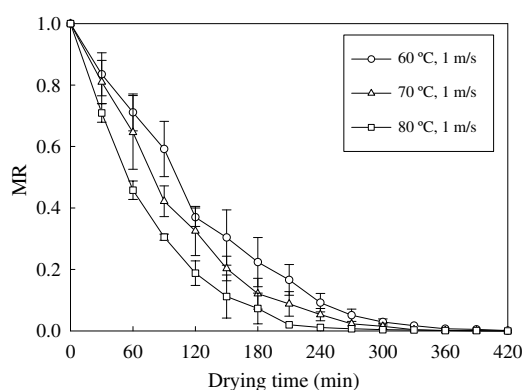


Fig. 3. Drying kinetics of potato cubes undergoing hot air drying at different drying conditions.

drying at an air velocity of 0.5 m/s and higher temperatures suffered more shrinkage than those undergoing drying at lower temperatures. This is because the drying temperature directly affected shrinkage (or deformation) of the product; larger moisture gradients within the samples developed when using higher drying temperatures and these larger gradients led to increased internal stresses, which in turn led to larger degrees of shrinkage (Devahastin, Suvarnaku-ta, Soponronnarit, & Mujumdar, 2004). Moreover, the shape of the drying samples was not uniform indicating that deformation of the samples was not symmetrical

(Panyawong & Devahastin, 2007). However, the samples undergoing drying at an air velocity of 1 m/s at different temperatures (Fig. 4b) were not much different in terms of the percentage of shrinkage. This is because case-hardening occurred more at the surface and limited shrinkage of the samples.

Initially, the percentage of shrinkage increased rapidly. This was followed by a period of slow increase until reaching the final values at the time corresponding to the points where the samples reached their equilibrium moisture contents. The drying time that divided the periods of shrinkage into the rapid increase and slow increase (followed by constant) periods was the same as the time that divided the drying curves into the first falling and second falling rate periods (Figs. 2 and 4 for carrot cubes and Figs. 3 and 5 for potato cubes). Towards the end of drying case hardened skin developed, which inhibited further shrinkage of the samples. It can be seen in Figs. 4 and 5 that the samples undergoing HAD at higher temperatures possessed higher rates of shrinkage than those of samples undergoing drying at lower temperatures. This is because the results were compared at the same sampling periods rather than at the same moisture contents.

Higher drying temperatures led to products with higher rehydration ratios. Higher rehydration ratios were observed with both carrot and potato cubes dried using HAD at 80 °C as compared to those dried at lower temperatures (Fig. 4c

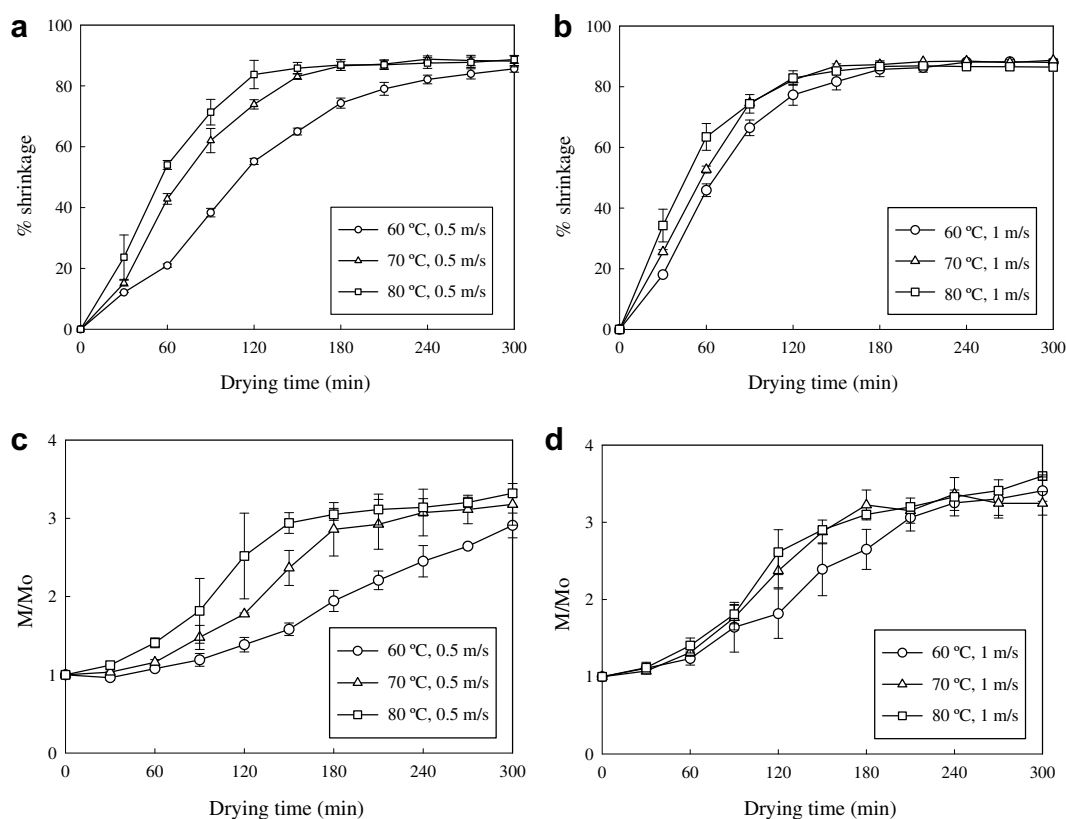


Fig. 4. Percentage of shrinkage ((a) and (b)) and rehydration ratio ((c) and (d)) of carrot cubes undergoing hot air drying.

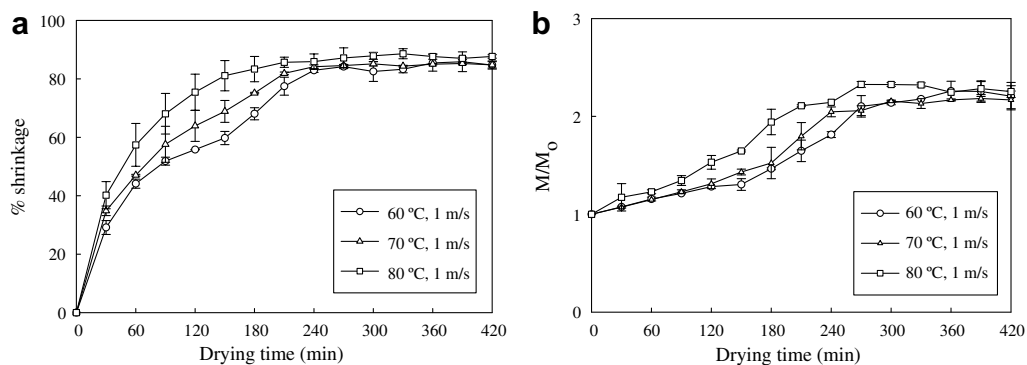


Fig. 5. Percentage of shrinkage (a) and rehydration ratio (b) of potato cubes undergoing hot air drying.

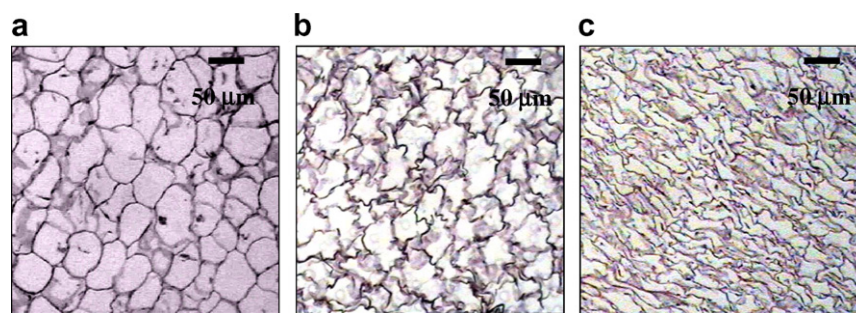


Fig. 6. Microstructure of carrot cubes undergoing hot air drying at 60 °C, 0.5 m/s after 0 min (a), 150 min (b) and 300 min (c).

and d for HAD carrot and Fig. 5b for HAD potato). This is because the samples, which were dried at lower temperatures, needed more time to achieve their equilibrium moisture contents than those dried at higher temperatures; the samples therefore suffered more structural damage (e.g., collapse of porous structure) than when drying at lower temperatures. As a result, the reconstitution capability of the sample undergoing high-temperature drying was higher than those undergoing low-temperature drying.

3.3. Microstructural changes of carrot and potato cubes

The images for microstructural analysis were observed with a light microscope at 10× magnification. After capturing the images these images were used for fractal dimension calculation.

The fractal dimension of fresh carrot (Fig. 6a) was approximately 1.75 whereas the fractal dimension of the samples increased upon drying. Initially, the cell walls of carrots were of round shape. After some period of time, however, moisture within the cells started to migrate to the surface. As a result, moisture gradients started to develop, which led to internal stresses and shrinkage of the cells (Fig. 6b and c). The ruggedness of cell walls increased leading to an increase in the fractal dimension of the cells, as expected.

The microstructural changes of carrot cubes undergoing drying are illustrated in terms of $\Delta FD/FD_0$ because this ratio represents the rates of change of fractal dimension

of the samples and hence could be used to compare the results of different drying conditions.

The rates of change of fractal dimension of carrot cubes undergoing HAD (Fig. 7) were monitored. The rates of change of fractal dimension were observed to be divided roughly into two periods, consisting of linear and non-linear rates of change. The drying time that identified the end point of the period where the rates of change of fractal dimension were linear was the same as the time that divided the drying curves into the first and second falling rate periods and that divided the physical changes (in terms of the percentage of shrinkage and rehydration ratio) into rapid increase and slow increase periods, respectively.

The light microscopic images of potato were also captured at 10× magnification. Each image represents both cell walls and starch granules. However, it was not easy to describe the changes of starch granules using a light microscope. The starch granules were therefore eliminated from every image. Thus, only cell walls of potato are displayed within the images. Fig. 8 represents the steps in processing the images starting from an original image (Fig. 8a), deleting the starch granules via the use of Matlab™ (version 6.5) (Fig. 8b) and converting the image without starch granules into a black and white format (Fig. 8c). Some starch granules that could not be deleted via the use of the program could be deleted manually to allow better analysis of the image (Aguilera & Stanley, 1999). In this research, starch granules were deleted manually using Adobe Photoshop™ (version 6.0).

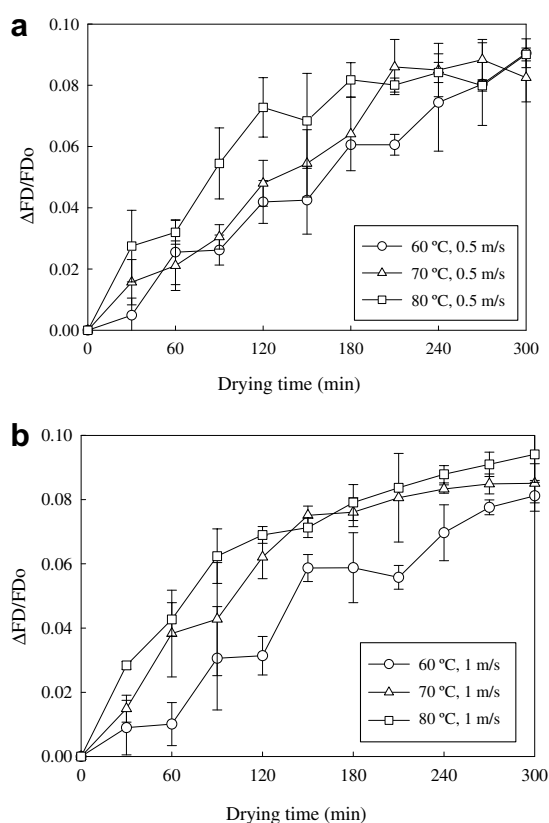


Fig. 7. $\Delta FD/FD_0$ of carrot cubes undergoing hot air drying (velocities of 0.5 m/s (a) and 1 m/s (b)).

Fractal dimension (FD) of fresh potato (Fig. 9a) was approximately 1.61. Again, FD of potato increased as drying time increased. For example, FD of potato cubes undergoing drying at an air temperature of 60 °C and air velocity of 1 m/s was approximately 1.70 (Fig. 9b) and 1.73 (Fig. 9c) at 180 and 240 min, respectively. However, fractal dimension of potato cubes did not change much comparing with that of carrot cubes undergoing hot air drying at the same condition; for carrot FD varied between 1.75 and 1.91. This is because the structures of potatoes and carrots are quite different. Carrot structure is composed mainly of cellulose and water. When carrots were dried water migrate from inside to the outside of cell walls. In contrast, potato structure consists mainly of cell walls, water and starch granules, which might have limited changes during drying. Moreover, initial moisture content of carrot (89–90% (w.b.)) was higher than that of potato (85–86% (w.b.)). This led carrots to have higher moisture gradients and larger changes in their structure during drying than potatoes.

Fractal dimension changes of potatoes were again presented in terms of the normalized changes of fractal dimension ($\Delta FD/FD_0$). It was found that $\Delta FD/FD_0$ increased with the drying time (Fig. 10). The results were in the same trend as those of carrots undergoing HAD.

3.4. Structure-quality relationship of carrot and potato cubes

As mentioned earlier, the rates of change of the fractal dimension could be divided into two periods, consisting

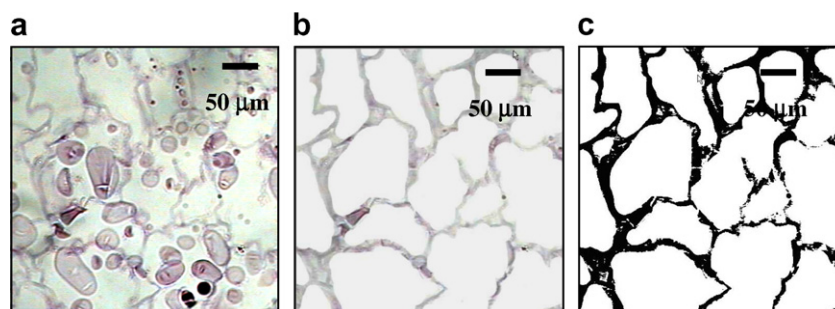


Fig. 8. Image processing of potato cubes; original image (a), image after deleting of starch granules (b) and black and white image (c).

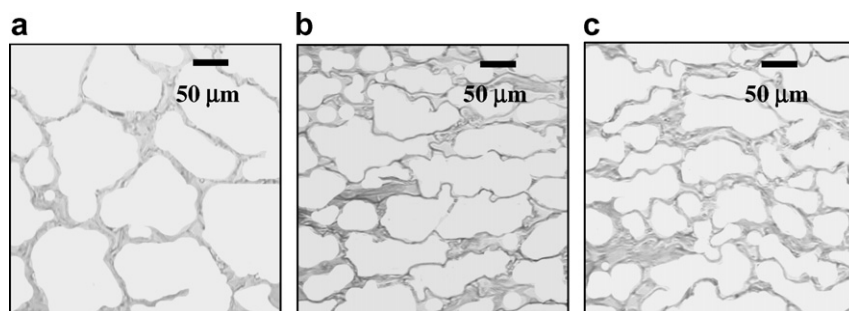


Fig. 9. Microstructure of potato cubes undergoing hot air drying at 60 °C, 1 m/s after 0 min (a), 150 min (b) and 300 min (c).

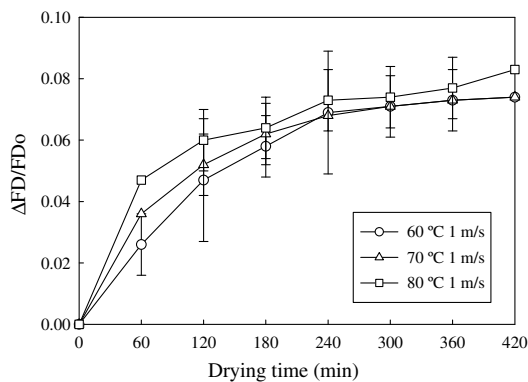


Fig. 10. $\Delta FD/FD_0$ of potato cubes undergoing hot air drying.

of periods of linear and non-linear changes. During the first falling rate period, although the rate of moisture migration from the internal cells to the surface was not equal to the rate of moisture evaporation from the surface to the surrounding, these rates might not be much different to cause large gradients within the sample and therefore linear changes of fractal dimension were observed. When samples were further dried the migration of moisture from the cells to the surface was slower than from the surface to the surroundings leading to larger gradients, which in turn led to more severe microstructural changes and deformation.

The drying time (Fig. 11) that divided the rates of change of the fractal dimension into linear period and non-linear period correlated well with the physical changes, especially the percentage of shrinkage (Fig. 12). The time at which the rates of change of fractal dimension switched from the linear to non-linear periods was the same as the point where the drying curves changed from the first falling rate period to the second falling rate period. Moreover, these were the same points where the percentage of shrinkage started to vary non-linearly as well. The percentage of shrinkage, which represents the apparent changes of the samples, correlated well with the normalized changes of fractal dimension, which represents the microstructural changes of the samples.

The normalized changes of fractal dimension could be used to monitor the physical changes of carrot and potato during drying (Figs. 12 and 13). For example, at $\Delta FD/FD_0$ of approximately 0.06 the percentage of shrinkage of carrot and potato cubes was around 70–80% in all cases. This type of relationship was also observed at other $\Delta FD/FD_0$ and percentage of shrinkage values. This has therefore proved that $\Delta FD/FD_0$ could be used to monitor shrinkage (deformation) of both potatoes and carrots undergoing HAD and thus has the potential of being an indicator for describing deformation of other products undergoing drying as well. Further investigation is certainly needed to confirm this hypothesis.

The ability to predict the percentage of shrinkage was better than that for rehydration ratio. This is likely due to the fact that shrinkage is more dependent on cellular changes throughout the volume of the dried samples and

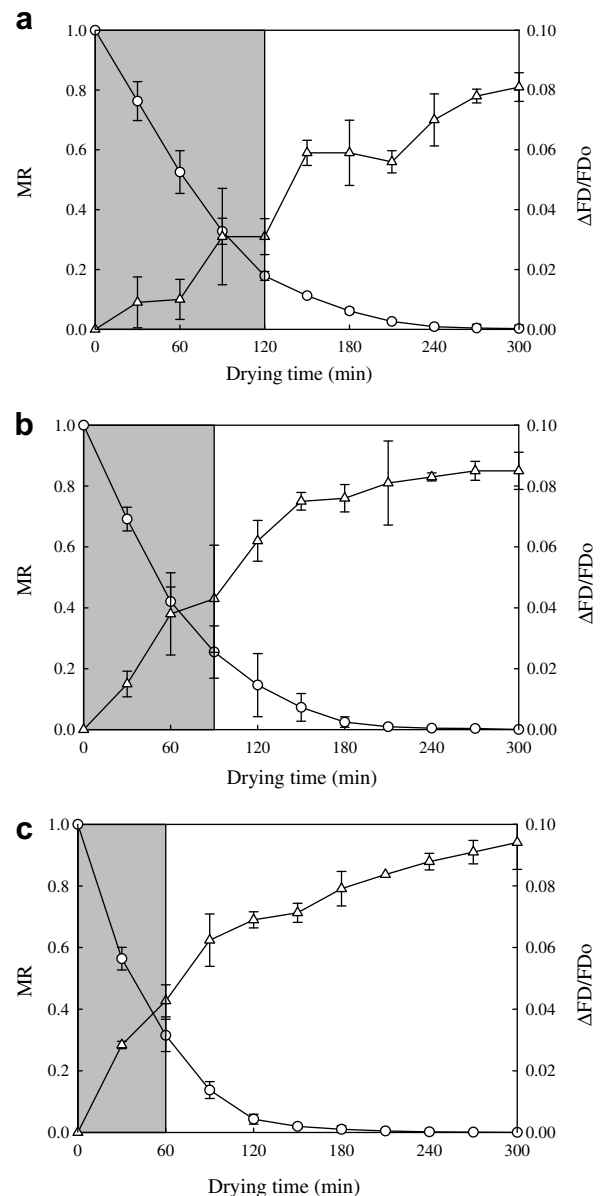


Fig. 11. Relationship between drying kinetics (○) and $\Delta FD/FD_0$ (Δ) of carrot cubes undergoing hot air drying at velocity of 1 m/s and temperature of 60 °C (a), 70 °C (b) and 80 °C (c).

these are well-characterized by the changes in the normalized fractal dimension. While rehydration is also dependent on internal structural changes and the ability for water to diffuse within the sample matrix, it may also depend on limiting factors at the surface such as case-hardening as well as the presence of some chemical constituents such as pectin, as in the case of carrot.

The relationship between the normalized changes of fractal dimension and rehydration ratio of carrots and potatoes undergoing HAD at different conditions are shown in Figs. 12 and 14, respectively. $\Delta FD/FD_0$ could somehow be used to monitor the changes in rehydration ratio. For example, $\Delta FD/FD_0$ of approximately 0.06 referred to the rehydration ratio of potato of around 1.50

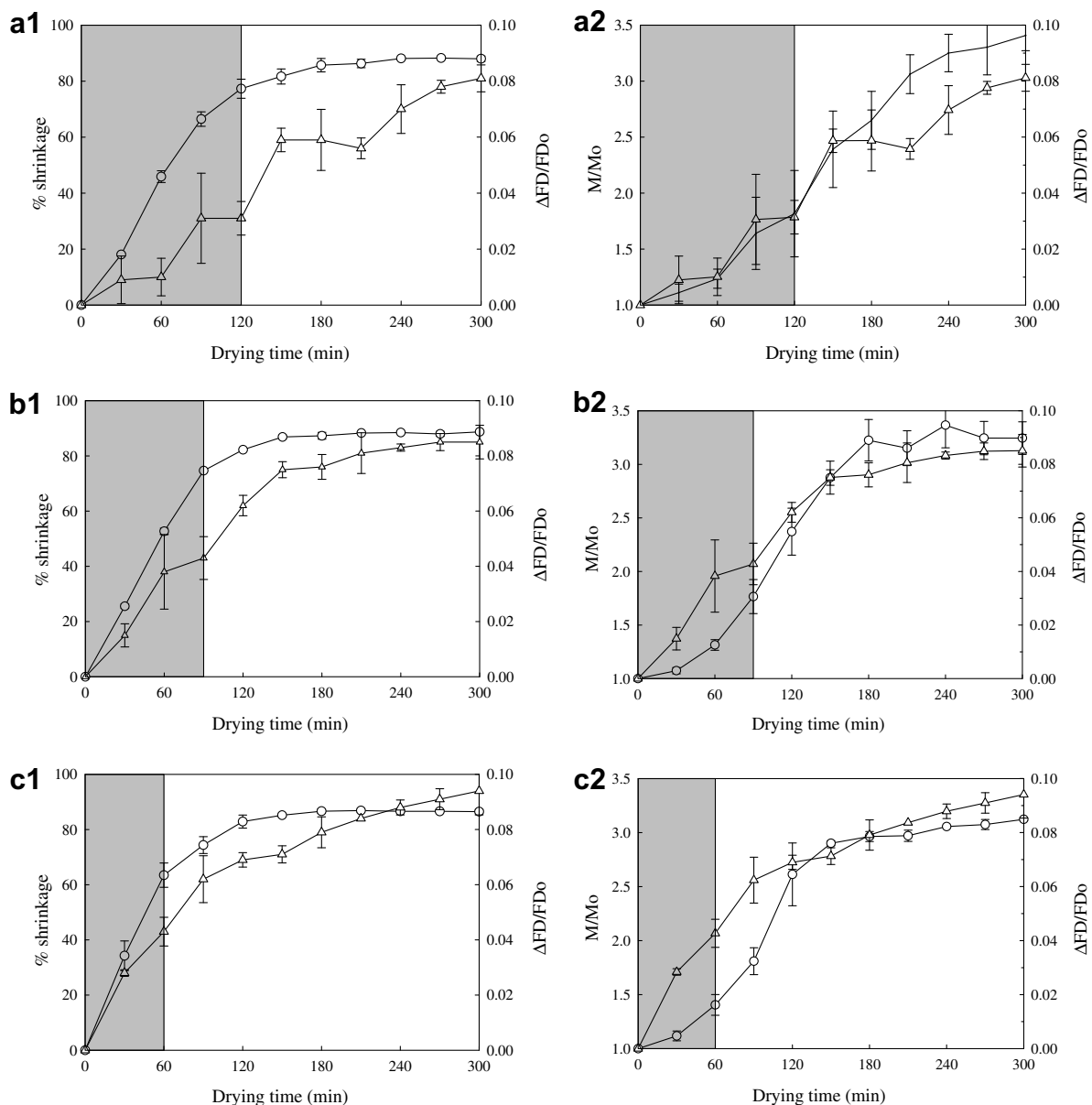


Fig. 12. Relationship between % shrinkage (\circ) and $\Delta FD/FD_0$ (Δ); rehydration ratio (\circ) and $\Delta FD/FD_0$ (Δ) of carrot cubes undergoing hot air drying at velocity of 1 m/s and temperatures of 60 °C (a), 70 °C (b) and 80 °C (c).

at all conditions tested. However, the same value of $\Delta FD/FD_0$ of carrot cubes undergoing HAD referred to the rehydration ratio of around 2.0–3.0.

The simple correlations between the rates of change of fractal dimension and the drying kinetics and physical changes of carrot and potato cubes undergoing different drying techniques and conditions are shown in Table 1. The results illustrated that the changes of fractal dimension correlated well with both the drying kinetics and physical changes. The Pearson's correlation coefficients representing the fractal dimension and the physical changes were between 0.86 and 0.99, depending on the tested conditions. These close-to-unity coefficients imply that $\Delta FD/FD_0$ and other observed variables correlated well with each other. However, the normalized changes of fractal dimension cor-

related better with shrinkage compared to the correlations with the rehydration ratio.

4. Conclusions

Fractal dimension was used in the present study to relate the apparent physical changes to the microstructural changes of food products (carrot and potato cubes) undergoing conventional hot air drying at various conditions. The apparent changes of the foods, which were represented in terms of the percentage of shrinkage correlated well with the normalized changes of fractal dimension, which were used to represent the microstructural changes. Fractal dimension (or more exactly, the normalized changes of fractal dimension) was thus proved to be capable of being

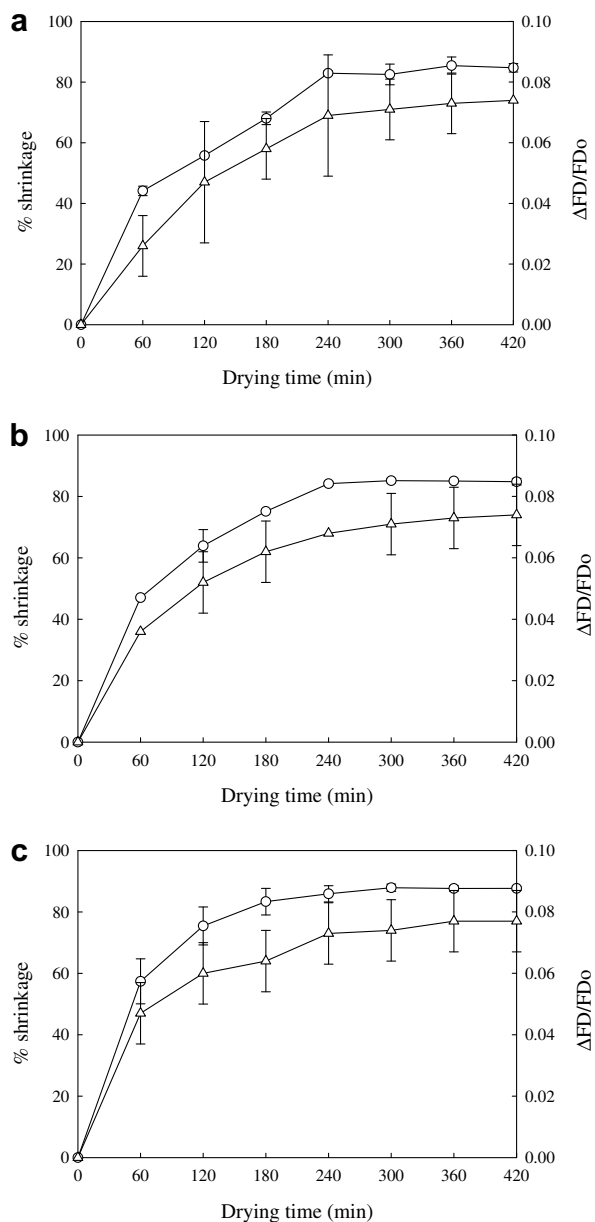


Fig. 13. $\Delta FD/FD_0$ (Δ) and % shrinkage (\circ) of potato cubes undergoing hot air drying at 60 °C, 1 m/s (a), 70 °C, 1 m/s (b) and 80 °C, 1 m/s (c).

Table 1

Pearson's correlation coefficients between $\Delta FD/FD_0$ and drying kinetics as well as between $\Delta FD/FD_0$ and physical changes of samples undergoing hot air drying

Sample	HAD conditions	Parameter of interest		
		Drying kinetics	% Shrinkage	Rehydration ratio
Carrot cubes	60 °C, 0.5 m/s	−0.941	0.961	0.954
	60 °C, 1 m/s	−0.883	0.872	0.964
	70 °C, 0.5 m/s	−0.844	0.913	0.966
	70 °C, 1 m/s	−0.981	0.955	0.972
	80 °C, 0.5 m/s	−0.979	0.964	0.954
	80 °C, 1 m/s	−0.962	0.959	0.945
Potato cubes	60 °C, 1 m/s	−0.998	0.988	0.894
	70 °C, 1 m/s	−0.990	0.997	0.876
	80 °C, 1 m/s	−0.992	0.993	0.893

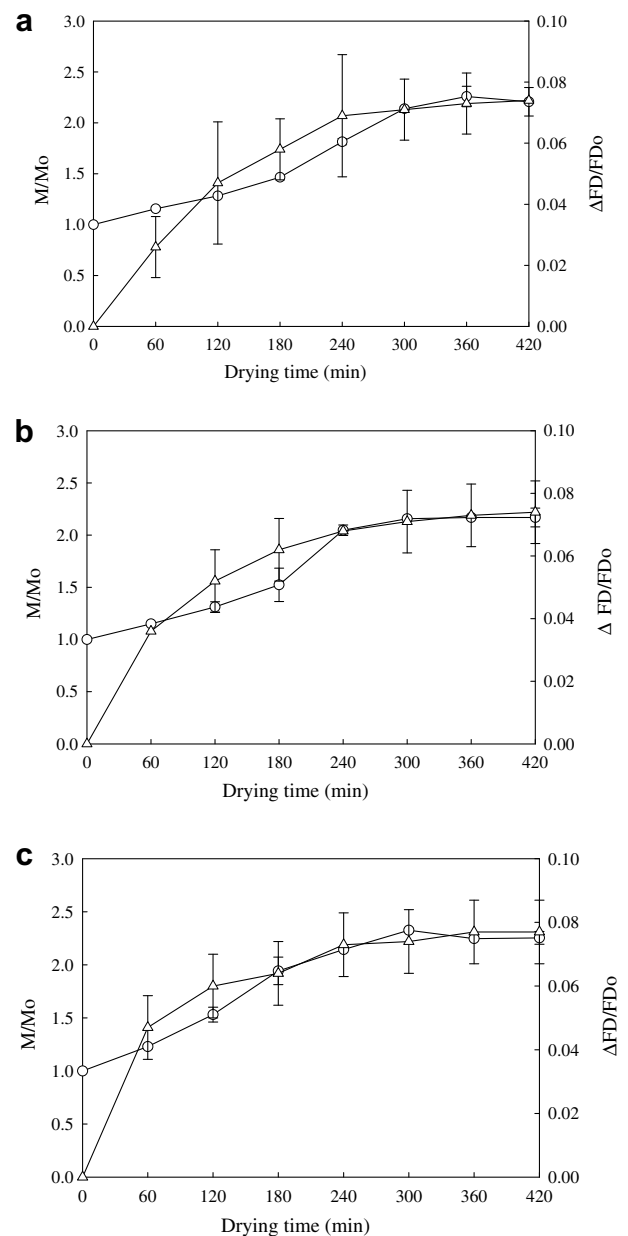


Fig. 14. $\Delta FD/FD_0$ (Δ) and rehydration ratio (\circ) of potato cubes undergoing hot air drying at 60 °C, 1 m/s (a), 70 °C, 1 m/s (b) and 80 °C, 1 m/s (c).

a generalized structure-quality index of foods undergoing drying. A comparison between the use of microstructural and apparent changes to monitor and/or evaluate physical properties of a sample should be made. This would allow the selection of an appropriate technique for an industrial use.

Acknowledgements

The authors express their sincere appreciation to the Commission on Higher Education, the Thailand Research Fund (TRF) and the International Foundation for Science (IFS), Sweden for financial support. Our appreciation also

goes to the Faculty of Fishery, Kasetsart University, Bangkok, Thailand for their help with the microstructural imaging of the samples.

References

- Aguilera, J. M., & Stanley, D. W. (1999). *Microstructural principles of food processing and engineering* (2nd ed.). Gaithersburg: Aspen Publishers.
- AOAC (1984). *Official methods of analysis* (14th ed.). Washington, DC: Association of Official Analytical Chemists.
- Barletta, B. J., & Canovas, V. B. (1993). An attrition index to assess fines formation and particle size reduction in tapped agglomerated food powders. *Powder Technology*, 77, 89–93.
- Devahastin, S., Suvarnakuta, P., Soponronnarit, S., & Mujumdar, A. S. (2004). A comparative study of low-pressure superheated steam and vacuum drying of a heat-sensitive material. *Drying Technology*, 22, 1845–1867.
- Doymaz, I. (2004). Convective air drying characteristics of thin layer carrots. *Journal of Food Engineering*, 61, 359–364.
- Graf, J. C. (1991). The importance of resolution limits to the interpretation of fractal descriptions of fine particles. *Powder Technology*, 67, 83–85.
- Humason, G. L. (1979). *Animal tissue techniques*. San Francisco: Freeman Press.
- Kerdpiiboon, S., & Devahastin, S. (2007). Fractal characterization of some physical properties of a food product under various drying conditions. *Drying Technology*, 25, 135–146.
- Kerdpiiboon, S., Kerr, W. L., & Devahastin, S. (2006). Neural network prediction of physical property changes of dried carrot as a function of fractal dimension and moisture content. *Food Research International*, 39, 1110–1118.
- Khraisheh, M. A. M., Cooper, T. J. R., & Magee, T. R. A. (1997). Shrinkage characteristics of potatoes dehydrated under combined microwave and convective air conditions. *Drying Technology*, 15, 1003–1022.
- Madamba, P. S. (2003). Physical changes in bamboo (*Bambusa Phyllostachys*) shoot during hot air drying: shrinkage, density, and porosity. *Drying Technology*, 21, 555–568.
- Mandelbrot, B. M. (1983). *The fractal geometry of nature*. New York: Freeman Press.
- Ochoa, M. R., Kessler, A. G., Pirone, B. N., Marquez, C. A., & De Michelis, A. (2002). Volume and area shrinkage of whole sour cherry fruits (*Prunus cerasus*) during dehydration. *Drying Technology*, 20, 147–156.
- Panyawong, S., & Devahastin, S. (2007). Determination of deformation of a food product undergoing different drying methods and conditions via evolution of a shape factor. *Journal of Food Engineering*, 78, 151–161.
- Pedreschi, F., & Aguilera, J. M. (2000). Characterization of food surfaces using scale-sensitive fractal analysis. *Journal of Food Process Engineering*, 23, 127–143.
- Quevedo, R., Carlos, L. G., Aguilera, J. M., & Cadoche, L. (2002). Description of food surfaces and microstructural changes using fractal image texture analysis. *Journal of Food Engineering*, 53, 361–371.
- Ratti, C. (1994). Shrinkage during drying of foodstuffs. *Journal of Food Engineering*, 23, 91–105.

Determination of deformation of a food product undergoing different drying methods and conditions via evolution of a shape factor

Sawitree Panyawong, Sakamon Devahastin *

Department of Food Engineering, King Mongkut's University of Technology Thonburi, 91 Pracha u-tid Road, Bangkok 10140, Thailand

Received 5 August 2005; accepted 14 September 2005

Available online 2 November 2005

Abstract

Shrinkage is a phenomenon that is common during drying of foods and other bio-products. Attempts have been made to describe shrinkage of different products undergoing different drying processes and conditions. However, most works describe shrinkage only in terms of its magnitude but fail to describe it in terms of pattern or, in other words, of how the drying material deforms during drying. Although the degree of shrinkage of a product undergoing different drying processes and conditions may not be significantly different, the shrinkage pattern may not be the same. Using only the degree of shrinkage to describe shrinkage (and deformation) is therefore not adequate. The present study proposed and investigated the use of a shape factor viz. Heywood shape factor to describe the deformation of a food product (carrot cube) undergoing different drying techniques viz. low-pressure superheated steam drying and vacuum drying at different conditions. It was found that the evolution of Heywood shape factor agreed reasonably well with the deformation kinetics of carrot cube as observed visually. It was possible, to some extent, to use this shape factor to describe the effects of drying methods and conditions on the deformation of carrot cube.

© 2005 Elsevier Ltd. All rights reserved.

Keywords: Carrot; Drying kinetics; Low-pressure superheated steam drying; Heywood shape factor; Shrinkage; Shrinkage pattern; Vacuum drying

1. Introduction

During drying water migrates from the inner cells of food via the cell membrane and the surrounding wall and then across the porous structure to the environment. Moisture gradients within the product induce microstructural stresses leading to shrinkage of the product, which in turn reflects the amount of water removed. Shrinkage may occur due to two reasons. Firstly, the tissue is unable to hold its structural network when the space taken by water is continuously emptied and air-filled. Secondly, the outside skin structure collapses and leads to shrinkage. In this case, case hardening at the skin surface also influences the shrinkage properties of the product as well (Achanta & Okos, 2000). Mostly, shrinkage of a food product is reported as a func-

tion of its moisture content. Shrinkage is generally quantified in terms of a shrinkage ratio, V/V_0 , i.e., the ratio of the volume of the product at any instant to its initial volume. However, drying does not cause only the volume change but also the change of the shape of the product. Therefore, expressing deformation of the product by indicating only the change of volume is inadequate.

It is well known that different drying methods and conditions affect the quality of the drying product, including volume and shape changes, differently. Ratti (1994) proposed the shrinkage characteristics as a function of water content for potato, apple and carrot of different geometries and under various drying conditions. Volumetric shrinkage of individual samples was affected mainly by air velocity; other drying variables had negligible effects. Changes in the ratio of the surface area to the volume with water content were practically independent of drying conditions but dependent on the sample geometry and the type of foodstuff. Khraisheh, Cooper, and Magee (1997) studied

* Corresponding author. Tel.: +66 2 470 9246; fax: +66 2 470 9240.
E-mail address: sakamon.dev@kmutt.ac.th (S. Devahastin).

the physical structure of potato during microwave and hot air drying and found that the shrinkage of potato undergoing both drying techniques was a linear function of the moisture content level. Shrinkage was reduced by the use of microwave drying but was rather independent on the sample geometry and air temperature. Ochoa, Kessler, Pirone, Marquez, and De Michelis (2002) investigated the volume and area shrinkage of whole sour cherry fruits during drying. It was observed that volume and area changes did not depend on the drying parameters. The linear relationship was again found between the dimensionless volume change and the dimensionless moisture content of the dehydrated fruits. Similar results were also reported for carrot drying in a mechanically agitated fluidized bed dryer (Reyes, Alvarez, & Marquardt, 2002).

On the other hand, Devahastin, Suvarnakuta, Soponronnarit, and Mujumdar (2004) reported that although the degrees of shrinkage of carrot cube underwent vacuum drying and low-pressure superheated steam drying (LPSSD) were similar, the changes of shape of carrot cube underwent these two drying processes were much different. Madamba (2003) also reported that although a linear relationship between the dimensionless volume change and the dimensionless moisture content was observed during hot air drying of bamboo shoot, shrinkage of bamboo shoot parallel to its fibers was different from that occurring perpendicular to its fibers. Thus, expressing the deformation of the drying material using only the degree of shrinkage (or volume shrinkage ratio) is not adequate.

Since experimental shrinkage results are product-specific and limited to the operating conditions tested, the use of a mathematical model to predict shrinkage as well as deformation and their effects on the rates of heat and mass transfer and drying kinetics of the drying material is desirable. Such models have indeed been proposed and tested with various products (Chemkhi, Zagrouba, & Bellagi, 2004; Mihoubi, Zagrouba, Vaxelaire, Bellagi, & Roques, 2004; Yang, Sakai, & Watanabe, 2001). Although these models

could predict the deformation of shrinkable materials to some extents, they are rather sophisticated and contain many parameters that must be known prior to the simulation. In addition, the need for a rapid and simple identification of deformation still exists.

The objective of the present study was to find a simple way to describe the deformation of a food product undergoing drying more precisely. Vacuum drying and LPSSD were chosen as the representative drying techniques and carrot cube was chosen as the representative product. The so-called Heywood shape factor, or the volume shape factor, was chosen to represent the shape of the drying product in this study.

2. Experimental set-up, material and methods

2.1. Experimental set-up

A schematic diagram of the low-pressure superheated steam dryer and its accessories is shown in Fig. 1. The dryer consists of a stainless steel drying chamber, insulated carefully with rock wool, with an inner dimension of $45 \times 45 \times 45 \text{ cm}^3$; a steam reservoir, which received the steam from the boiler and maintained its pressure at around 200 kPa (gauge); and a liquid ring vacuum pump (model ET32030, Nash, Trumbull, CT), which was used to maintain the vacuum in the drying chamber. Steam trap was installed to reduce the excess steam condensation in the reservoir. An electric heater, rated at 1.5 kW, which was controlled by a proportional-integral-derivative controller (model E5CN, Omron, Tokyo, Japan) was installed in the drying chamber to control the steam temperature and to minimize the condensation of steam in the drying chamber during the start-up period. A variable-speed electric fan was used to disperse steam throughout the drying chamber. The steam inlet was made into a conical shape and was covered with a screen to also help distributing steam in the chamber. The sample holder was made of

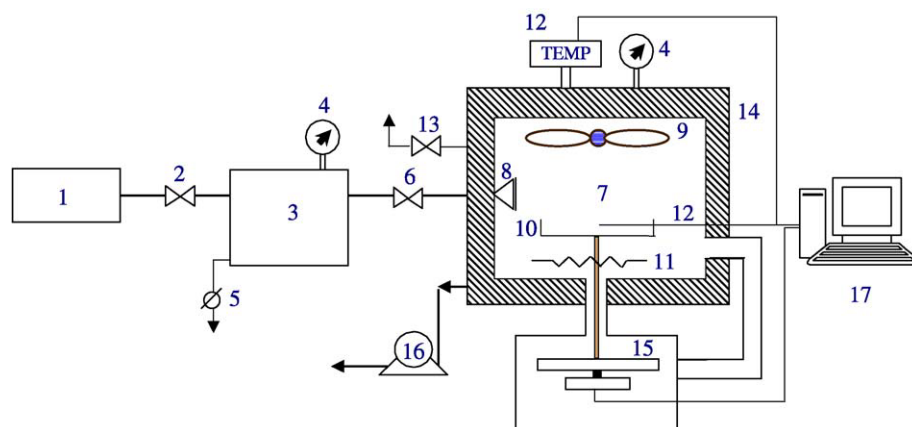


Fig. 1. A schematic diagram of low-pressure superheated steam dryer and associated units. (1) Boiler; (2) steam valve; (3) steam reservoir; (4) pressure gauge; (5) steam trap; (6) steam regulator; (7) drying chamber; (8) steam inlet and distributor; (9) electric fan; (10) sample holder; (11) electric heater; (12) on-line temperature sensor and logger; (13) vacuum break-up valve; (14) insulator; (15) on-line weight indicator and logger; (16) vacuum pump; (17) PC with installed data acquisition card.

stainless steel with a dimension of $12 \times 12 \text{ cm}^2$. The change of the mass of the sample was detected continuously (at 30 s interval) using a load cell (model Ucg-3 kg, Minebea, Nagano, Japan), which was installed in a smaller chamber connected to the drying chamber by a flexible hose (in order to maintain the same vacuum pressure as that in the drying chamber), and also to an indicator and recorder (model AD 4329, A&D Co., Tokyo, Japan). The temperatures of the steam and of the drying sample were measured continuously using type K thermocouples, which were connected to an expansion board (model no. EXP-32, Omega Engineering, Stamford, CT). Thermocouple signals were multiplexed to a data acquisition card (model no. CIO-DAS16Jr, Omega Engineering, Stamford, CT) installed in a PC. LABTECH NOTEBOOK software (version 12.1, Laboratory Technologies Corp., MA) was used to read and record the temperature data. For vacuum drying experiments the same experimental set-up was used but without an application of steam to the drying chamber.

2.2. Material

Fresh carrot was purchased from a local supermarket and stored in a refrigerator at 4°C . Prior to the start of each experiment carrot was removed from the refrigerator to attain the room temperature. It was then peeled and sliced. In this work, samples were prepared using only the cortex tissues because different microstructure of material may affect the degree and pattern of shrinkage. The sliced carrot was cut into cubes with the dimension of $1 \times 1 \times 1 \text{ cm}^3$.

2.3. Methods

To perform a drying experiment approximately 30 cubes of carrot (about 30 g) were placed in the sample holder. Each drying experiment was carried out up to a pre-determined sampling time; that particular experiment was ended at that time. The moisture content (AOAC, 1984), volume and area of the dried product were then measured. These properties were used to calculate the degree and pattern of shrinkage of carrot cube undergoing each drying condition. A new experiment was then performed until the next pre-determined sampling time was reached.

2.4. Measurement of degree of shrinkage

Five carrot cubes taken at any sampling time were used to determine the degree of shrinkage in terms of the volume change ratio. The degree of shrinkage was calculated using the volume of the sample at any sampling time along with its initial volume as shown in Eq. (1). The average values of five samples were then reported.

$$\text{Degree of shrinkage} = \frac{V}{V_0} \quad (1)$$

where V is the volume of carrot cube after drying (m^3); V_0 is the volume of carrot cube before drying (m^3). The sample

volume (V) was determined by n -heptane displacement. The weight of the sample displaced in n -heptane was measured using a digital balance (model RC 250S, Sartorius, Goettingen, Germany).

2.5. Measurement of shrinkage pattern

Many attempts have been made in the field of powder and particle technology to define the particle shape using one single parameter. Among many proposed parameters is the Heywood shape factor (k), which uses measurements of surface area and volume to characterize the shape of material. In the present study the shrinkage pattern of carrot cube was determined in terms of this shape factor, which is calculated as follows (Yang, 2003):

$$k = \frac{V_p}{d_a^3} \quad (2)$$

where V_p is the volume of the cube (m^3); A_p is the projected area of the cube (m^2); and d_a is the equivalent projected-area diameter of the cube (m), $d_a = \sqrt{4A_p/\pi}$.

The volume of each carrot cube was measured by n -heptane displacement. The projected area of six sides of the cube was determined by a planimeter (model X-plan360dII, Ushikata Manufacturing, Tokyo, Japan). The maximum projected area of the cube was then selected to calculate the equivalent diameter of the cube. This is because the equivalent diameter is defined as the diameter of a sphere having the same projected area as the cube viewed in a direction perpendicular to the plane of the greatest stability of the cube (Seville, Tüzün, & Clift, 1997).

The effects of two factors, i.e., drying method and temperature, on the deformation kinetics of carrot cube were investigated in this study. Drying was conducted at three levels of temperature, i.e., 60, 70 and 80°C ; the chamber pressure was maintained at 7 kPa. The drying samples were taken out at 0.5-h interval during the first 2.5 h and then at 1 h interval until the sample achieved the final moisture content of 0.07 kg/kg (d.b.).

2.6. Statistical analysis

The experiments were designed in complete random. The data were analyzed and presented as mean values with standard deviations. Differences between mean values were established using Tukey's HSD comparisons. Values were considered at 95% confidence level ($p < 0.05$). All experiments were performed in duplicate.

3. Results and discussion

3.1. Drying kinetics of carrot cube

Carrot cube that had an initial moisture content of about 9.2 kg/kg (d.b.) (or about 90% w.b.) was dried and sampled out at every 0.5 h interval during the first 2.5 h

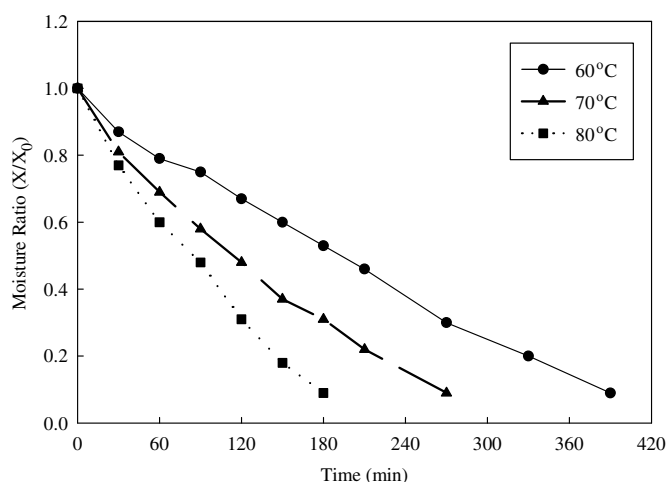


Fig. 2. Drying curves of carrot cube undergoing LPSSD.

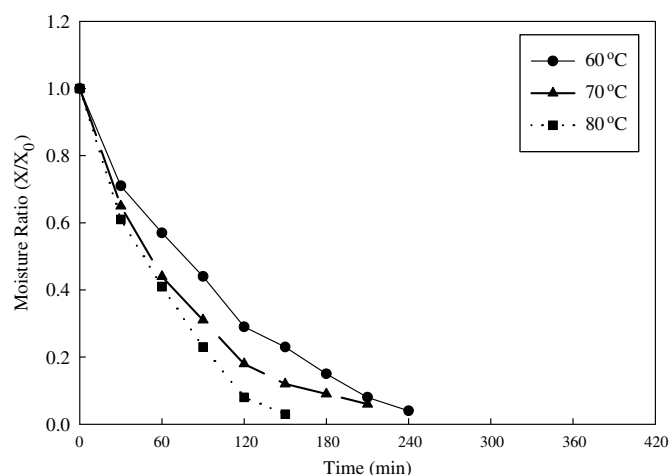


Fig. 3. Drying curves of carrot cube undergoing vacuum drying.

and every 1 h afterwards until the final moisture content of 0.07 kg/kg (d.b.) was reached in LPSSD and vacuum dryer. Figs. 2 and 3 show the drying curves of carrot cube undergoing LPSSD and vacuum drying, respectively. As

expected, higher drying temperatures led to higher rates of moisture removal due to higher temperature differences between the sample and the drying medium at higher drying temperatures. Moisture diffusivity is also higher at a

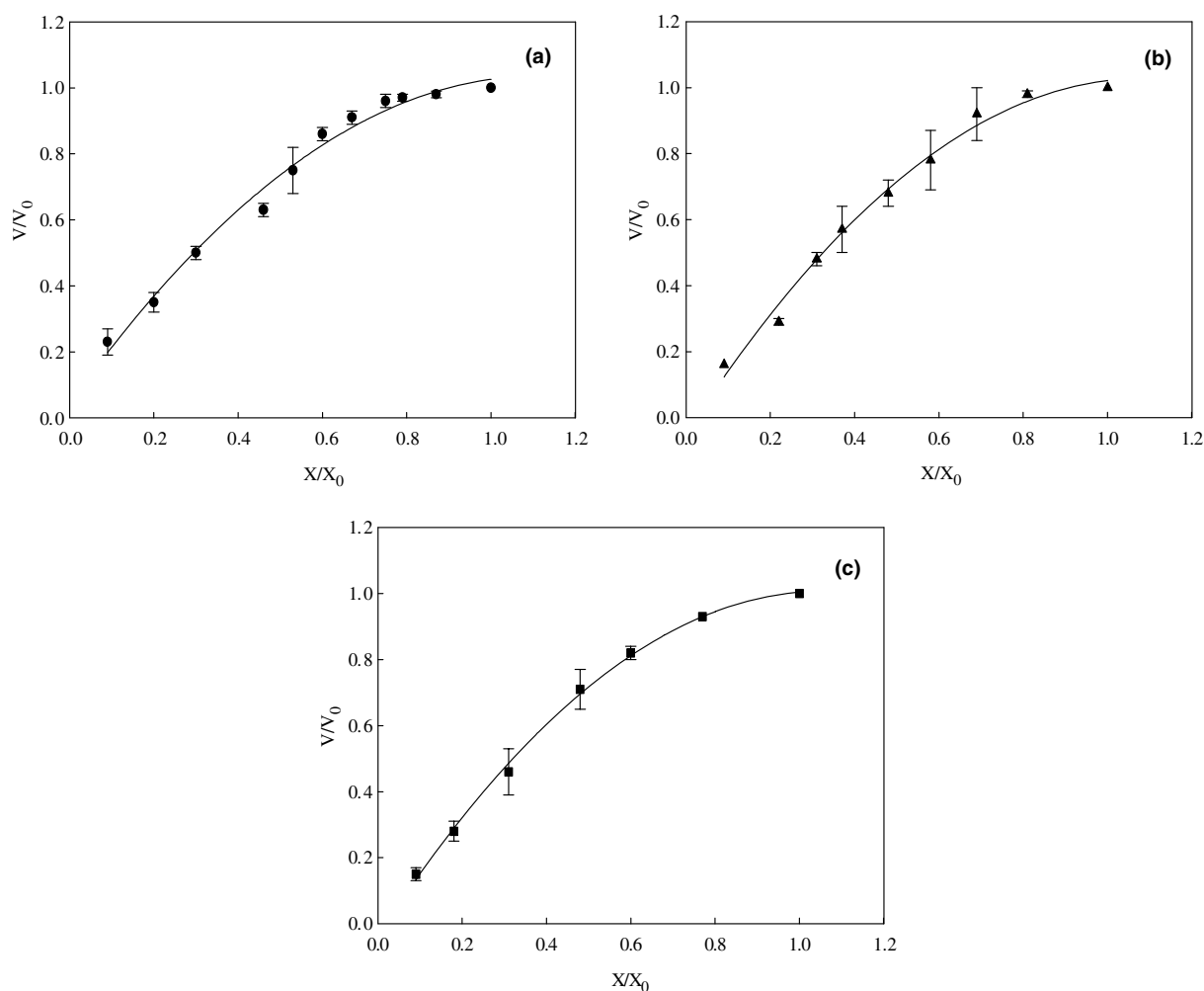


Fig. 4. Shrinkage of carrot cube during LPSSD as a function of moisture ratio at temperature: (a) 60 °C, (●) experimental data, (—) model (b) 70 °C, (▲) experimental data, (—) model (c) 80 °C, (■) experimental data, (—) model.

higher drying temperature leading to a greater mobility of water through the drying product.

Comparison between the two drying methods revealed that the drying time of vacuum drying was shorter than that of LPSSD at the same drying temperature. This is probably due to the fact that the electric heater was used more often during vacuum drying since it was the only source of energy for drying. This might increase the amount of radiation absorbed by the carrot surfaces, thus explaining the higher drying rate during vacuum drying (Devahastin et al., 2004). In addition, the chamber of the vacuum dryer was less humid and hence led to larger moisture gradients between the product and the surrounding, which facilitated drying. The driving force for heat transfer in the case of vacuum dryer might also be higher in this tested range of drying temperatures as well (Suvarnakuta, Devahastin, Soponronnarit, & Mujumdar, 2005).

3.2. Degree of shrinkage of carrot cube

Fig. 4 shows the degree of shrinkage (V/V_0) of carrot cube during LPSSD at 60, 70 and 80 °C as a function of

the moisture ratio. Generally, the literature reports the shrinkage of a food product as a linear function of moisture ratio (Corzo & Bracho, 2004; Ochoa et al., 2002; Raghavan & Silveira, 2001; Ratti, 1994). However, in this work, it was found that the relation between the volume ratio and the moisture ratio was almost second-order. However, if the data during the first period of drying were neglected, the trend of the volume ratio and the moisture ratio would be almost linear as reported by other researchers.

The degree of shrinkage of carrot cube during vacuum drying as a function of moisture ratio at 60, 70 and 80 °C is shown in Fig. 5. The result is similar to that of LPSSD, i.e., the relationship between the volume ratio and the moisture ratio is almost second-order in nature. The following equation may thus be used to represent the relationship between the volume ratio and the moisture ratio of carrot cube undergoing both LPSSD and vacuum drying

$$\frac{V}{V_0} = a \left(\frac{X}{X_0} \right)^2 + b \left(\frac{X}{X_0} \right) + c \quad (3)$$

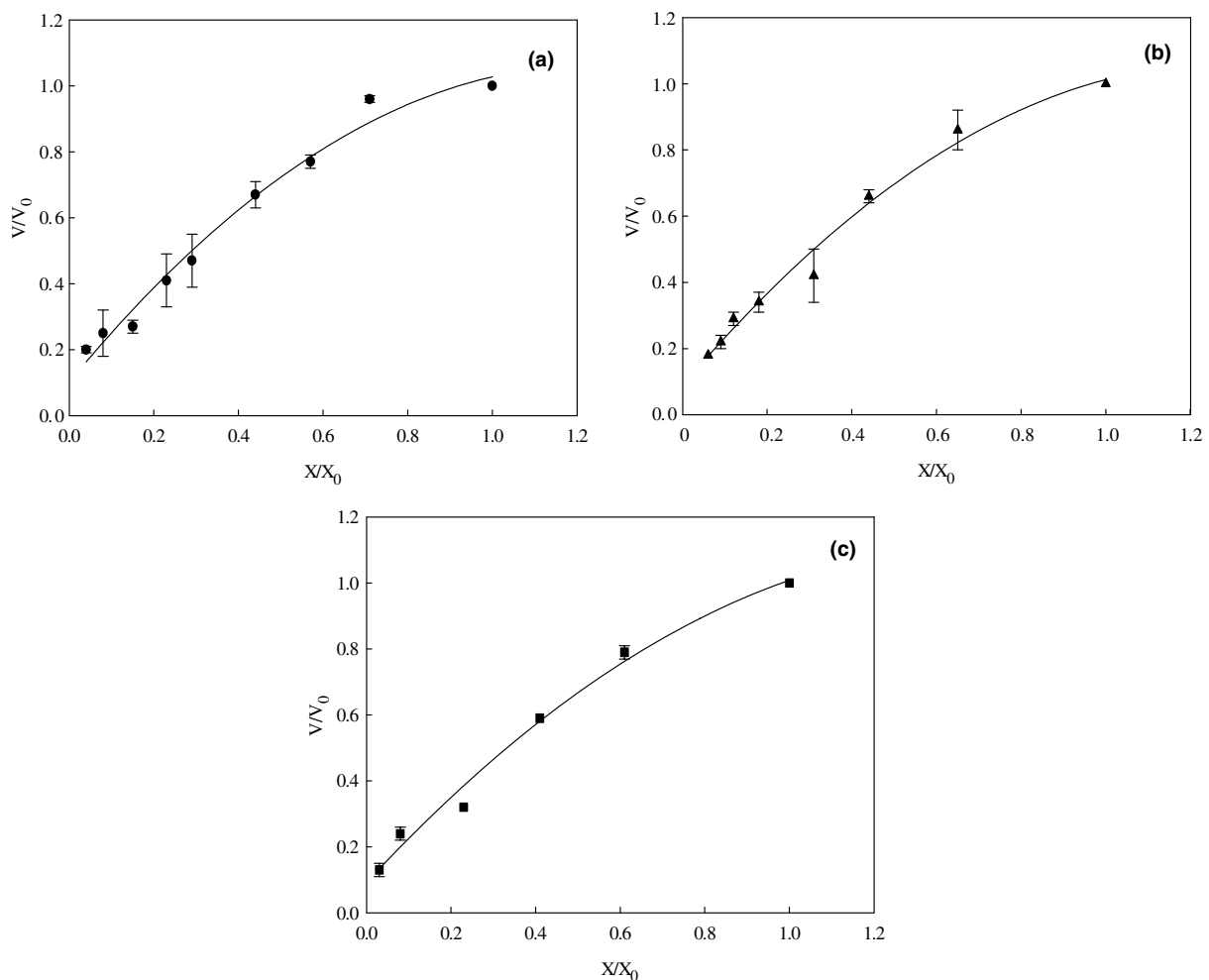


Fig. 5. Shrinkage of carrot cube during vacuum drying as a function of moisture ratio at temperature: (a) 60 °C, (●) experimental data, (—) model; (b) 70 °C, (▲) experimental data, (—) model; (c) 80 °C, (■) experimental data; (—) model.

a, *b* and *c* are constants obtained by fitting the equation to the experimental results at various drying conditions; the values of these constants are listed in Table 1. It can be observed nevertheless that the relationship between the volume ratio and the moisture ratio in the case of vacuum drying is slightly more linear than that of LPSSD due probably to its higher rate of water removal.

The comparison of the degree of shrinkage of carrot cube undergoing LPSSD and vacuum drying at various temperatures is shown in Fig. 6. During an early stage of drying shrinkage of carrot undergoing LPSSD was less than that of vacuum drying due probably to the steam

evolution and less moisture gradient induced stresses within carrot cube. However, towards the end of drying, at moisture ratios of less than 0.4, the results were opposite. Towards the end carrot cube undergoing vacuum drying shrank less than carrot cube undergoing LPSSD. This is because at this point the surface of vacuum dried carrot was much drier and some case hardening occurred; this case hardened skin acted to preserve the final size of carrot cube better than in the case of LPSSD dried carrot, which had much less case hardened skin. However, the differences of the results of the two drying methods were not significantly different at 95% confidence level.

Table 1
The *a*, *b* and *c* values at different drying methods and drying conditions

Drying method	Temperature (°C)	<i>a</i>	<i>b</i>	<i>c</i>	<i>R</i> ²	AME ^a
LPSSD	60	−0.8288	1.8170	0.0366	0.9864	0.0257
	70	−0.9026	1.9663	−0.0433	0.9916	0.0230
	80	−0.9492	1.9938	−0.0421	0.9971	0.0110
Vacuum drying	60	−0.7465	1.7048	0.0628	0.9850	0.0312
	70	−0.5871	1.5062	0.0882	0.9835	0.0233
	80	−0.4679	1.3828	0.0933	0.9877	0.0257

^a AME = absolute mean error.

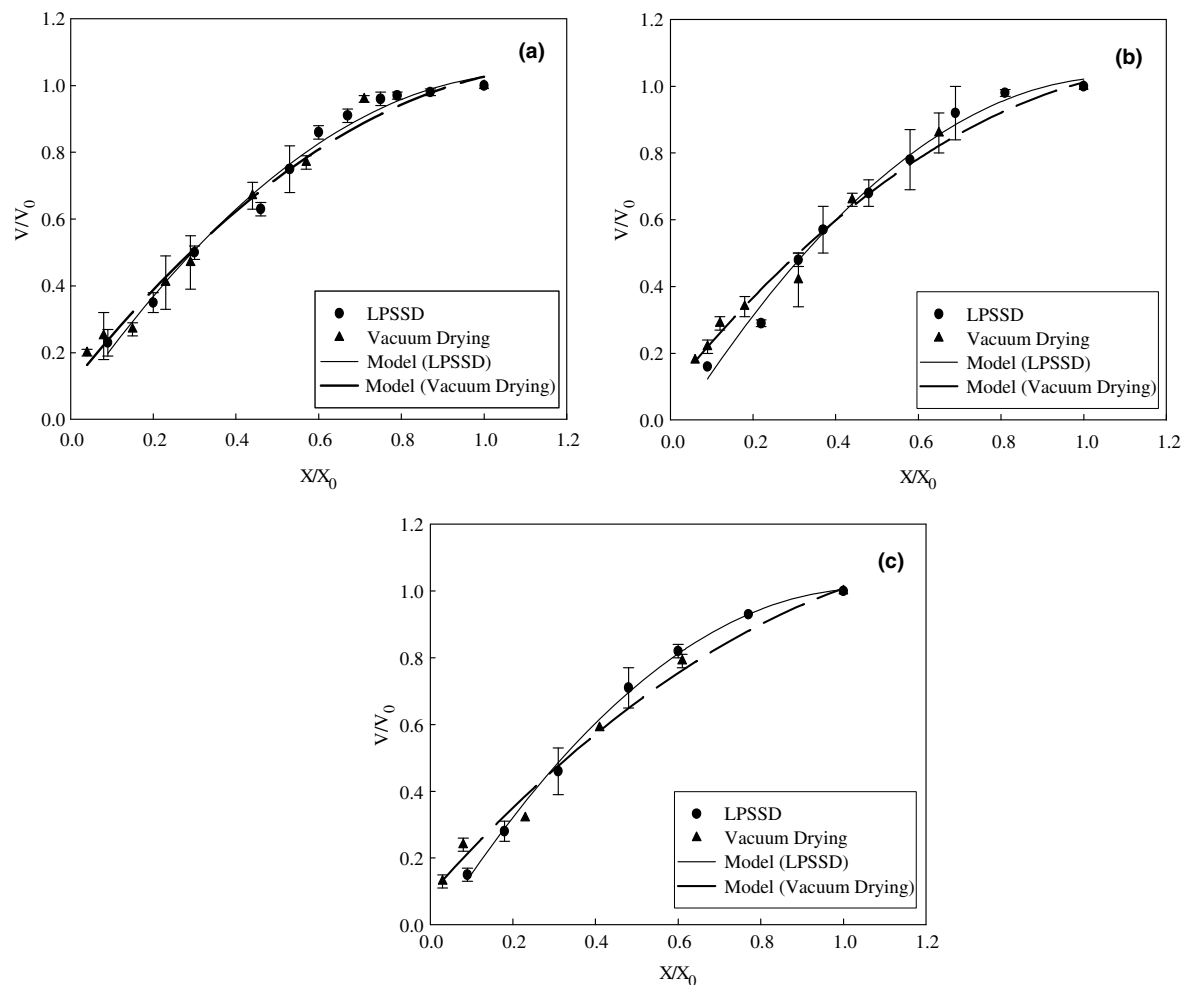


Fig. 6. Comparison of shrinkage of carrot cube undergoing LPSSD and vacuum drying at temperature: (a) 60 °C, (b) 70 °C and (c) 80 °C.

The comparison of the degree of shrinkage of carrot cube undergoing LPSSD at various drying temperatures is shown in Fig. 7a and b for vacuum drying. From these figures it is seen that the trends of shrinkage of carrot cube

at different temperatures were similar. However, small differences could be noticed from the results when using different drying temperatures. The degree of shrinkage at 60 °C was significantly different ($p < 0.05$) from those at

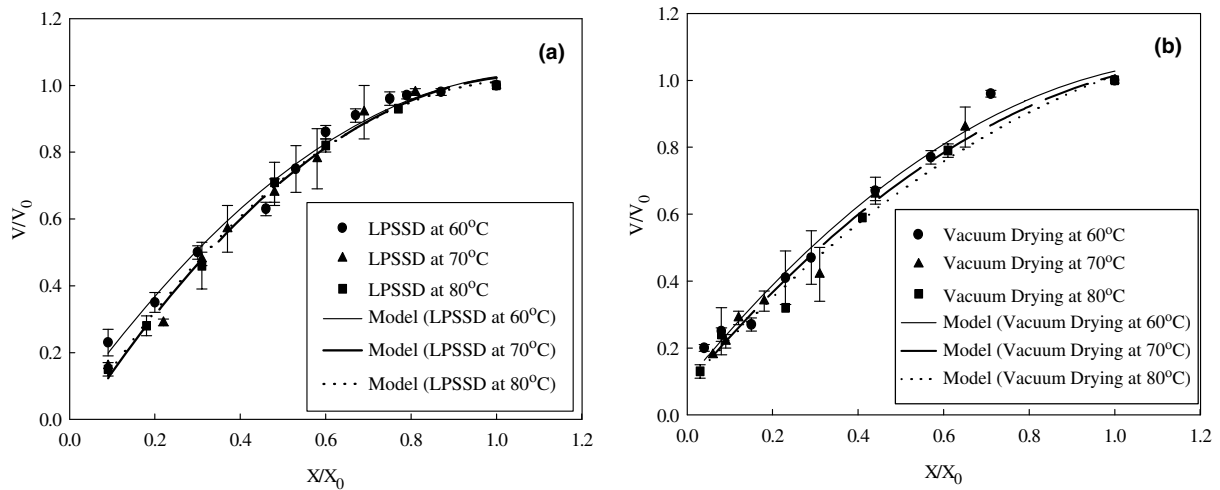


Fig. 7. Comparison of shrinkage of carrot cube at various temperatures undergoing: (a) LPSSD and (b) vacuum drying.

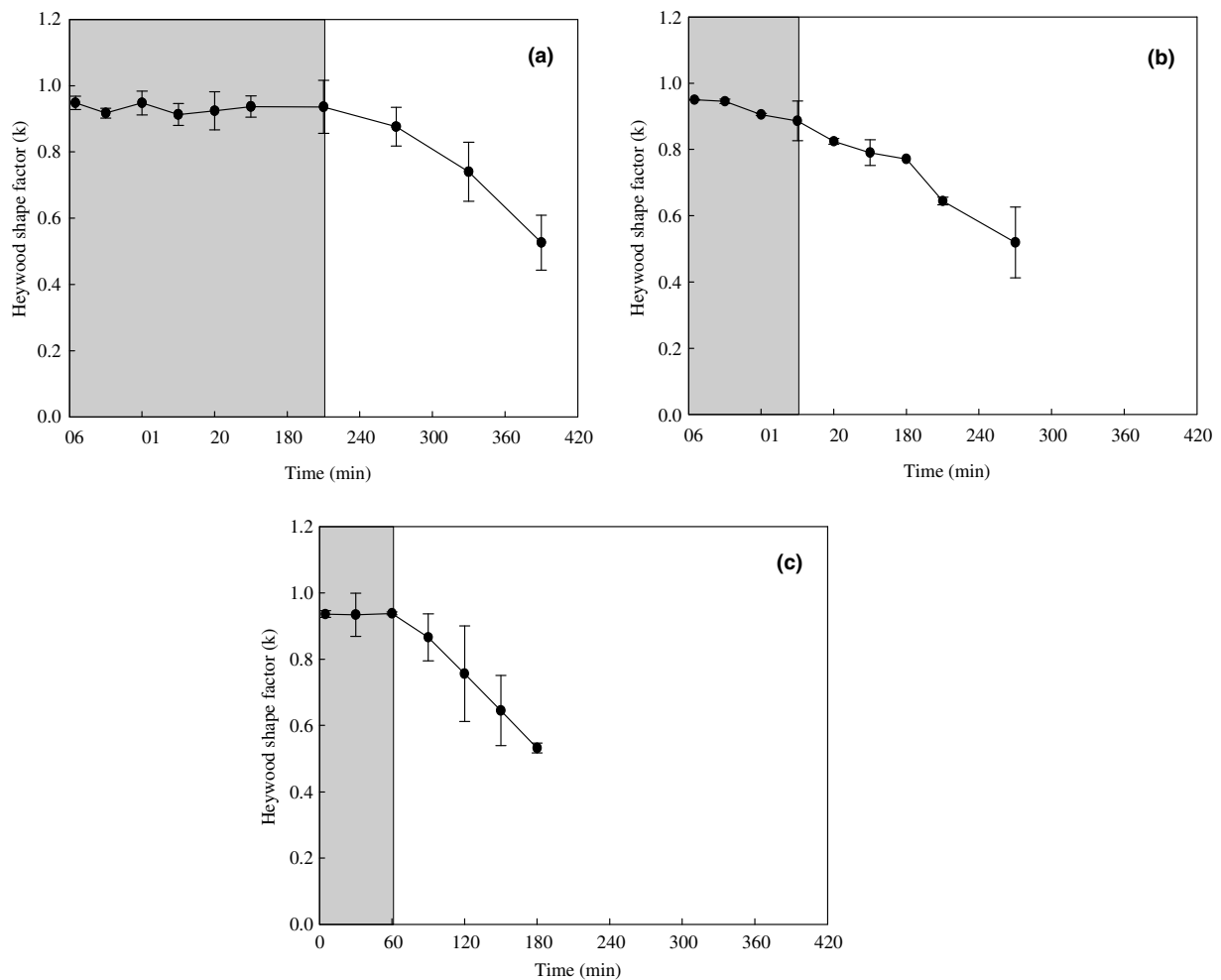


Fig. 8. Heywood shape factor of carrot cube during LPSSD at temperature: (a) 60 °C; (b) 70 °C and (c) 80 °C.

70 and 80 °C. This may be due to lower levels of temperature and moisture gradient induced stresses at lower drying temperatures. A result by Ochoa et al. (2002) was different, however. In their work it was observed that volume and area changes did not depend on drying conditions. The degree of shrinkage of carrot cube at the drying temperature of 70 °C was insignificantly different ($p > 0.05$) from that at 80 °C. This is probably due to the fact that the two drying temperatures might not be much different to cause any significant differences in the degree of shrinkage.

3.3. Pattern of shrinkage of carrot cube

Fig. 8 shows the evolution of Heywood shape factor of carrot cube during LPSSD at 60, 70 and 80 °C. It is seen that the results could be divided roughly into two portions. During an early stage of drying the Heywood shape factor remained almost constant, which implied that more or less uniform deformation occurred. During an early stage of drying the properties of the surface layers of the drying material might not differ much from those

of the center (Mujumdar, 1995). The duration of the uniform deformation periods was different at different drying temperatures, however. The duration of the uniform deformation period of LPSSD at 60, 70 and 80 °C was 210, 90 and 60 min, respectively. At the drying temperature of 60 °C the uniform deformation period was the longest because of the lowest temperature difference between the product and the heating medium leading to a lower water removal rate and hence smaller moisture and temperature gradient induced stresses. Towards the end of drying the Heywood shape factor decreased with drying time, which implied a non-uniform deformation during this later stage of drying. The deformation rates during this later stage were also different at different drying temperatures.

The shrinkage pattern of carrot cube undergoing vacuum drying (Fig. 9) was similar to that of LPSSD. The pattern could again be divided into two portions, uniform and non-uniform deformation periods. The uniform deformation period at 60 °C (150 min) was longer than that at 70 °C (60 min) for the same reason mentioned earlier for LPSSD. At 80 °C this period of uniform deformation did

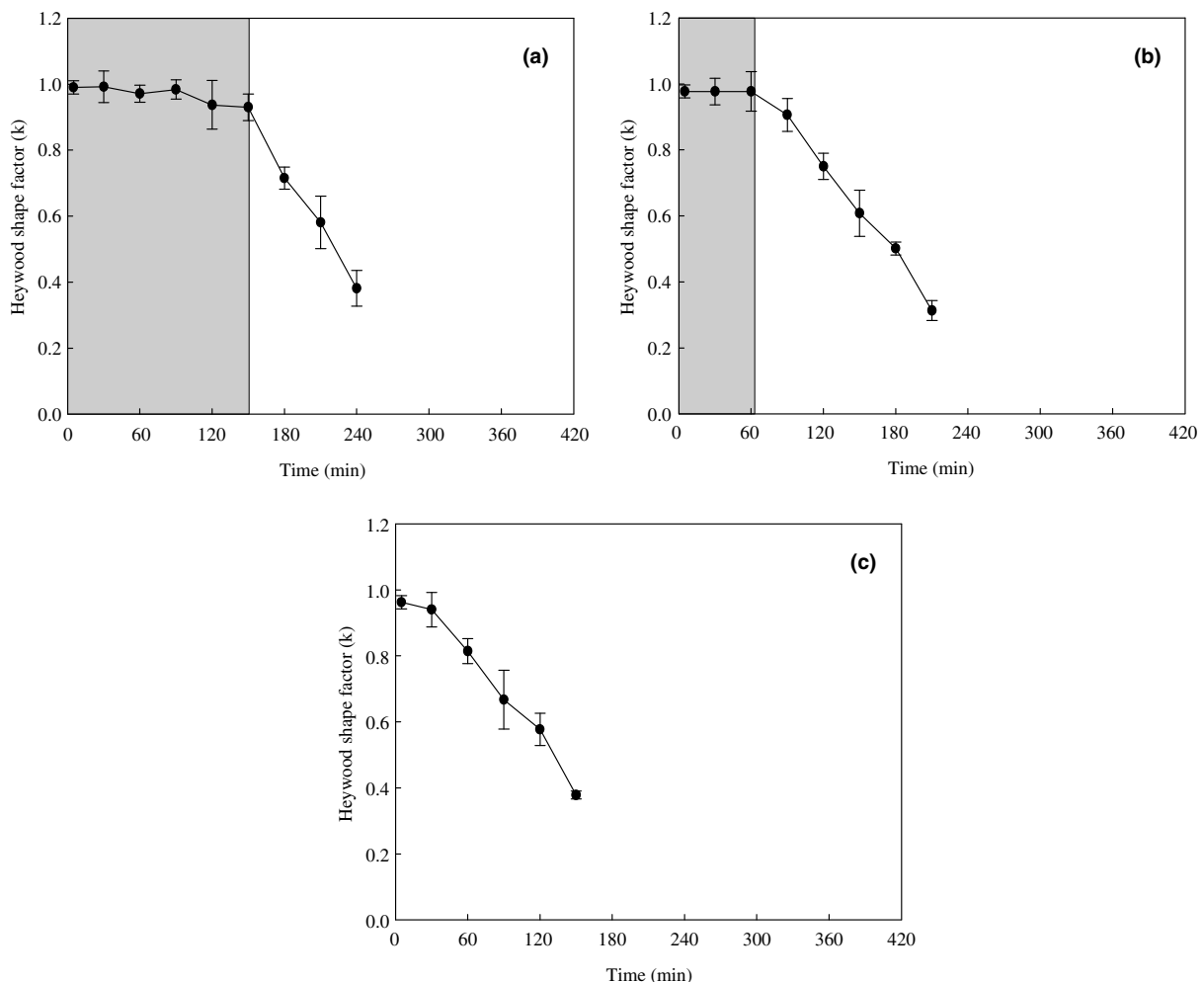


Fig. 9. Heywood shape factor of carrot cube during vacuum drying at temperature: (a) 60 °C, (b) 70 °C and (c) 80 °C.

not exist, however, since carrot cube deformed rapidly at this temperature. At higher temperature higher moisture gradients could be expected in the material and therefore higher internal stresses. In addition, the extent of damage

is a function of the drying temperature as well (Khraisheh et al., 1997).

The effect of drying temperature on the evolution of Heywood shape factor of carrot cube undergoing LPSSD

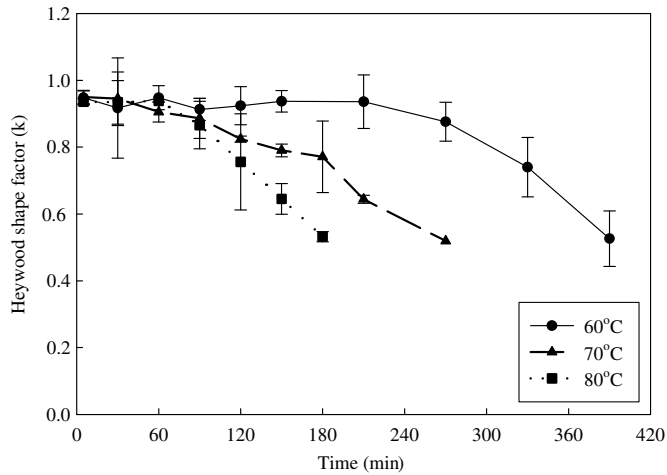


Fig. 10. Comparison of Heywood shape factor of carrot cube undergoing LPSSD at various temperatures.

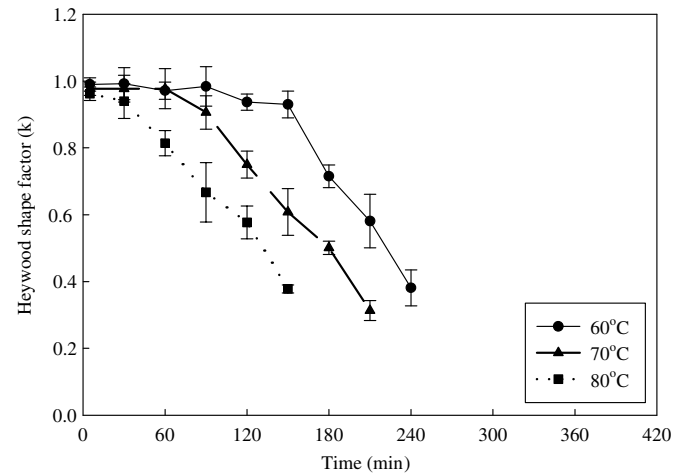


Fig. 11. Comparison of Heywood shape factor of carrot cube undergoing vacuum drying at various temperatures.

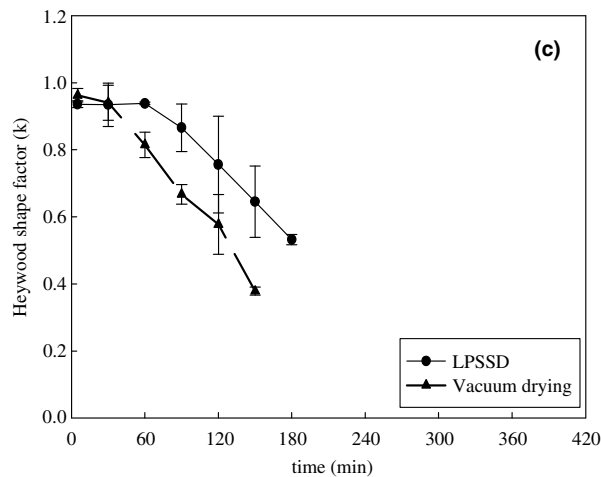
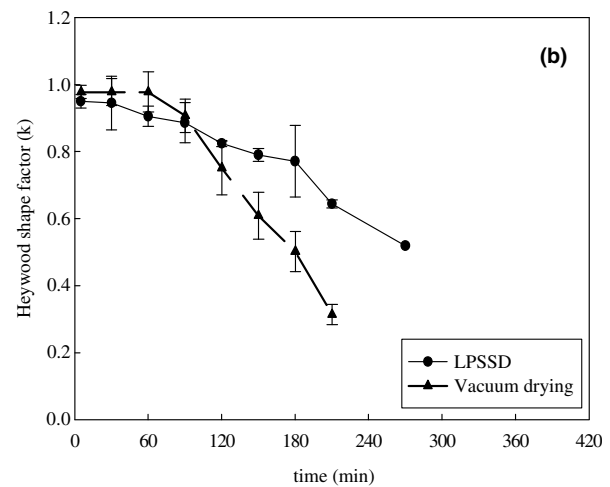
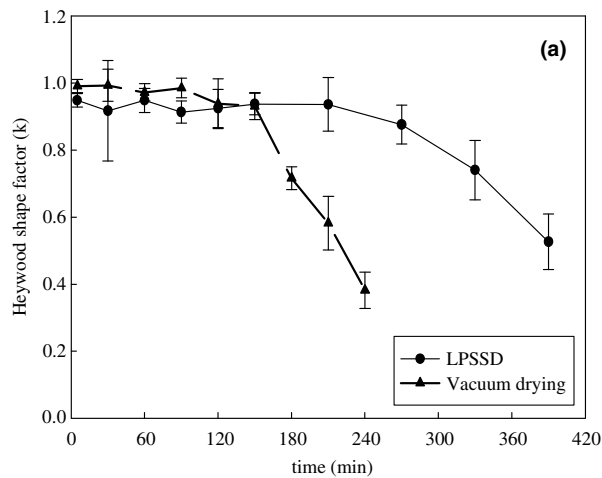


Fig. 12. Comparison of Heywood shape factor of carrot cube during LPSSD and vacuum drying at temperature: (a) 60 °C; (b) 70 °C and (c) 80 °C.

is shown in Fig. 10. As observed earlier, the pattern of shrinkage composed of two portions, uniform and non-uniform deformation periods. The uniform deformation periods varied with the drying temperature; this period was shorter at higher drying temperatures. So, it might be able to conclude that drying product at a lower temperature could maintain the shape of the product longer (or better) than drying at a higher temperature.

Consider then the non-uniform deformation period. The slope of the plot in this period could be used to represent the rate of deformation of the drying material. The slopes of the plots at 60, 70 and 80 °C were -0.0023 , -0.0027 and -0.0034 min^{-1} , respectively; the slope increased with the drying temperature. This again implies that drying the product at higher temperatures leads to a more rapid deformation of the product than doing so at lower temperatures.

Fig. 11 illustrates the shrinkage pattern of carrot cube undergoing vacuum drying. The period of uniform deformation was quite short compared with that of LPSSD. Considering the non-uniform deformation period the slopes of the plots at 60, 70 and 80 °C were -0.0044 ,

-0.0045 and -0.0045 min^{-1} , respectively. In this case, the slopes of all plots were almost the same indicating that the rates of non-uniform deformation were not much different at different drying conditions. This may be due to the fact that the properties of air are not as much dependent on the temperature as those of superheated steam, especially over a narrow range as that used in this work.

As mentioned earlier, the degrees of shrinkage of carrot cube undergoing two different drying methods were not significantly different. Fig. 12, on the other hand, shows the patterns of shrinkage of carrot cube during LPSSD

Table 2
Comparison of the deformation rates of carrot cube undergoing LPSSD and vacuum drying at various temperatures

Temperature (°C)	Rate of deformation (min^{-1})	
	LPSSD	Vacuum drying
60	-0.0023	-0.0044
70	-0.0027	-0.0045
80	-0.0034	-0.0045

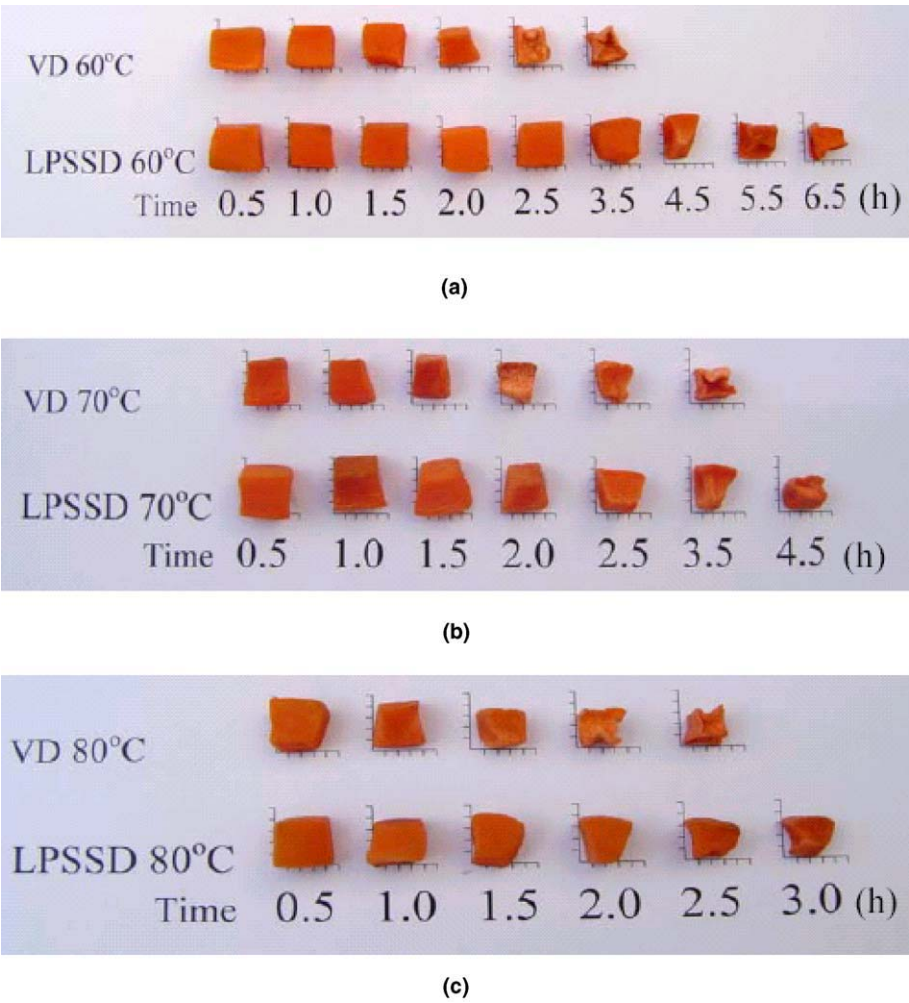


Fig. 13. Dried carrot undergoing vacuum drying and LPSSD at temperature: (a) 60 °C; (b) 70 °C and (c) 80 °C.

and vacuum drying at the same drying temperature. By comparing LPSSD and vacuum drying it is seen from this figure that the uniform deformation period of carrot cube undergoing LPSSD was longer than in the case of vacuum drying at every tested condition. This is because LPSSD yielded a slower drying rate than that in the case of vacuum drying at the same drying temperature. Slow drying product shrinks more uniformly into a solid core since the magnitude of internal stresses is lower (Mujumdar, 1995).

For the non-uniform deformation period the comparison of the deformation rates of LPSSD and vacuum drying, which were calculated from the slopes of the plots of the Heywood shape factor versus the drying time during the non-uniform deformation period, is shown in Table 2. It is seen that carrot undergoing vacuum drying deformed more rapidly and indeed less uniformly than that undergoing LPSSD at every drying condition tested. The final values of Heywood shape factor of carrot cube undergoing LPSSD stayed between 0.519 and 0.532 while they stayed between 0.313 and 0.381 in the case of vacuum drying. These results are consistent with the photographic results of Fig. 13, which shows the shapes of carrot cubes undergoing both LPSSD and vacuum drying at different conditions. Vacuum dried carrot deformed much more than LPSSD dried carrot although the two samples had similar degrees of shrinkage.

4. Conclusion

The drying kinetics as well as the degree and pattern of shrinkage of carrot cube undergoing LPSSD and vacuum drying at various temperatures were examined. In terms of drying kinetics the drying temperature affected in a normal fashion the moisture reduction rate of samples dried both by LPSSD and vacuum drying. The relationship between the degree of shrinkage and the moisture ratio was found to be almost second-order in nature at every tested condition. The degree of shrinkage of carrot cube undergoing LPSSD was not significantly different from that undergoing vacuum drying. However, the shrinkage pattern was found to depend both on the drying methods and drying conditions. Using only the degree of shrinkage to describe the shrinkage (and deformation) is therefore not enough. Further study should be done on refining the technique for evaluating the projected area of the drying sample; such technique as image analysis could be found useful as a more accurate result might be obtained. It should be noted also that there is obviously a limit to how well a single parameter can characterize the particle shape.

Acknowledgements

The authors express their sincere appreciation to the Commission on Higher Education, the Thailand Research Fund (TRF), as well as the International Foundation for Science (IFS), Sweden for supporting this study financially.

References

- Achanta, S., & Okos, M. (2000). Quality changes during drying of food polymers. In A. S. Mujumdar (Ed.), *Drying technology in agriculture and food sciences* (pp. 133–147). Enfield: Science Publishers.
- AOAC (1984). *Official methods of analysis* (14th ed.). Washington, DC: Association of Official Agricultural Chemists.
- Chemkhi, S., Zagrouba, F., & Bellagi, A. (2004). Mathematical modeling for drying of highly shrinkable media. *Drying Technology*, 22, 1023–1039.
- Corzo, O., & Bracho, N. (2004). Shrinkage of osmotically dehydrated sardine sheets at changing moisture contents. *Journal of Food Engineering*, 65, 333–339.
- Devahastin, S., Suvarnakuta, P., Soponronnarit, S., & Mujumdar, A. S. (2004). A comparative study of low-pressure superheated steam and vacuum drying of a heat sensitive material. *Drying Technology*, 22, 1845–1867.
- Khraisheh, M. A. M., Cooper, T. J. R., & Magee, T. R. A. (1997). Shrinkage characteristics of potatoes dehydrated under combined microwave and convective air conditions. *Drying Technology*, 15, 1003–1022.
- Madamba, P. S. (2003). Physical changes in bamboo (*Bambusa phyllostachys*) shoot during hot air drying: Shrinkage, density, and porosity. *Drying Technology*, 21, 555–568.
- Mihoubi, D., Zagrouba, F., Vaxelaire, J., Bellagi, A., & Roques, M. (2004). Transfer phenomena during the drying of a shrinkable product: Modeling and simulation. *Drying Technology*, 22, 91–109.
- Mujumdar, A. S. (1995). Superheated steam drying (2nd ed.). In A. S. Mujumdar (Ed.), *Handbook of industrial drying* (vol. 2, pp. 1071–1086). New York: Marcel Dekker.
- Ochoa, M. R., Kessler, A. G., Pirone, B. N., Marquez, C. A., & De Michelis, A. (2002). Volume and area shrinkage of whole sour cherry fruits (*Prunus cerasus*) during dehydration. *Drying Technology*, 20, 147–156.
- Raghavan, G. S. V., & Silveira, A. M. (2001). Shrinkage characteristics of strawberries osmotically dehydrated in combination with microwave drying. *Drying Technology*, 19, 405–414.
- Ratti, C. (1994). Shrinkage during drying of foodstuffs. *Journal of Food Engineering*, 23, 91–105.
- Reyes, A., Alvarez, P. I., & Marquardt, F. H. (2002). Drying of carrot in a fluidized bed. I. Effects of drying conditions and modelling. *Drying Technology*, 20, 1463–1483.
- Seville, J. P. K., Tüzün, U., & Clift, R. (1997). *Processing of particulate solids*. London: Blackie Academic & Professional.
- Suvarnakuta, P., Devahastin, S., Soponronnarit, S., & Mujumdar, A. S. (2005). Drying kinetics and inversion temperature in a low-pressure superheated steam-drying system. *Industrial & Engineering Chemistry Research*, 44, 1934–1941.
- Yang, H., Sakai, N., & Watanabe, M. (2001). Drying model with non-isotropic shrinkage deformation undergoing simultaneous heat and mass transfer. *Drying Technology*, 19, 1441–1460.
- Yang, W.-C. (2003). Particle characterization and dynamics. In W.-C. Yang (Ed.), *Handbook of fluidization and fluid-particle system* (pp. 1–24). New York: Marcel Dekker.

Neural network prediction of physical property changes of dried carrot as a function of fractal dimension and moisture content

Soraya Kerdpiboon ^a, William L. Kerr ^{b,*}, Sakamon Devahastin ^a

^a Department of Food Engineering, King Mongkut's University of Technology, Thonburi, 126 Pracha u-tid Road, Bangkok 10140, Thailand

^b Department of Food Science and Technology, University of Georgia, Athens, GA, USA

Received 22 May 2006; accepted 30 July 2006

Abstract

The relationship between microstructural and physical properties of dried foods is difficult to quantify. This study uses artificial neural network analysis (ANN) to predict shrinkage and rehydration of dried carrots, based on inputs of moisture content and normalized fractal dimension analysis ($\Delta D/D_0$) of the cell wall structure. Several drying techniques were used including conventional hot air (HAD), low pressure superheated steam (LPSSD), and freeze drying (FD). Dried carrot sections were examined by light microscopy and the fractal dimension (D) determined using a box counting technique. Optimized ANN models were developed for HAD, LPSSD, HAD + LPSSD, and HAD + LPSSD + FD, based on 1–10 hidden layers and neurons per hidden layer. ANN models were then tested against an independent dataset. Measured values of shrinkage and rehydration were predicted with an $R^2 > 0.95$ in all cases.

© 2006 Elsevier Ltd. All rights reserved.

Keywords: Artificial neural network; Carrot; Drying; Fractal analysis; Rehydration ratio; Shrinkage

1. Introduction

During food drying, moisture migrates from interior regions of the product to the surface and on into the surrounding air, resulting in changes in physical properties and structure of the product. Many studies have focused on changes of external properties of foods during drying, such as alterations in volume, area, and shape (Mayor & Sereno, 2004; Ochoa, Kessler, Pirone, Marquez, & De Michelis, 2002; Ratti, 1994). However, changes in these outward properties are primarily caused by internal changes, which are directly related to structural changes of the drying materials.

Structural changes in dried products can be viewed using light or electron microscopy. However, apparent differences in structural features caused by processing can be

difficult to quantify. Various techniques such as Fourier analysis, particle size distribution, or intensity measurements might be used depending on the structural feature of interest. Many foods, particularly those of a cellular nature, experience shrinkage, and convolution of the cell wall or membrane during drying. One approach then is to use fractal analysis to quantify structural changes in the microstructural features of dried products.

Fractals have been used to describe and quantify irregular fragments or complex shapes of materials such as shorelines, clouds, plants, brain cells, gold colloids, and sponge iron (Graf, 1991; Mandelbrot, 1982). Fractal analysis has also been used to study structural and mechanical attributes of some food products. From the particle contours seen in SEM images, Peleg and Normand (1985) characterized the ruggedness of instant coffee after agglomeration. Barletta and Barbosa-Canovas (1993) used machine-vision CCD technology to determine the contours of instant coffee and skim milk particles, and compared three methods for computing fractal values to describe ruggedness. Hsu, Lu, and Huang (2000) suggested that changes in the

* Corresponding author. Tel.: +1 706 542 1085; fax: +1 706 542 1050.
E-mail address: wkerr@uga.edu (W.L. Kerr).

Nomenclature

ANN	artificial neural network
D	fractal dimension
$\Delta D/D_0$	normalized fractal dimension
FD	freeze drying

HAD	hot air drying
LPSSD	low pressure superheated steam drying

viscoelastic properties of rice starch and soy protein suspensions during gelatinization could be related to fractal dimension descriptions of the gel networks. Rubnov and Saguy (1997) determined fractal dimensions from SEM images of restructured potato products and found that fractal dimension correlated with oil uptake during frying. Chanona et al. (2003) applied fractal analysis to the changing surface temperature of drying agar gel slabs, showing that there were three stages of drying. Few studies have demonstrated the correlation between physical property changes and product structure during processing. Such correlations could aid in understanding and predicting the property changes of foods undergoing drying.

There are several methods for constructing a relationship between the physical properties and structure of dried foods, such as models based on theoretical constructs, regression analysis, or principal component analysis. The properties of dried foods vary substantially depending on the type of product, moisture content, drying type, and drying conditions. Thus, a promising approach is to use artificial neural network (ANN) analysis, which can be trained to consider and weight various inputs. The ANN is made up of a group of interconnected artificial neurons. Each neuron transforms an input and sends its output to other neurons to which it is connected. The receiving neuron determines a weighted sum of the inputs. Each artificial neuron transforms its input through a system of linear equations, which may include logarithmic or hyperbolic tangent functions. The network is trained with a subset of observations and optimized based on its ability to predict a set of known outcomes.

Neural networks are effective for modeling, optimization, and process control of complex problems (Goncalves, Minim, Coimbra, & Minim, 2005). ANN has been used to predict thermal conductivity of food as a function of moisture content, temperature, and apparent porosity (Sablani & Rahman, 2003); to predict thermal inactivation of bacteria (Lou & Nakai, 2001); and to design and optimize high-pressure processes in the food industry (Torrecilla, Otero, & Sanz, 2005).

The objective of this work was to develop models for predicting properties of dried carrot based on composition, drying technique, and microstructural features, in which these microstructural features were characterized in terms of normalized fractal dimension. The two key physical properties considered for dried carrot were %shrinkage and rehydration ratio.

2. Methodology

2.1. Drying techniques

Fresh carrots (*Daucus carota* var. *sativa*) were obtained from a local supermarket and kept at 4 °C. Prior to the start of each experiment, carrots were removed from refrigerated storage and allowed to reach room temperature (~24 °C). The carrots were then peeled and sliced. In this study, samples were prepared using only the cortex tissue to limit structural variations in samples. Samples were diced into 1 × 1 × 1 cm³ cubes. Carrots were dried using three different drying techniques, namely conventional hot air drying (HAD), low pressure superheated steam drying (LPSSD), and freeze drying (FD). Cubed samples were dried in a hot air tray dryer constructed from stainless steel, with air heated by a 6.6 kW heater, and the temperature controlled to within 0.1 °C with a PID controller (Kerdpi-boon & Devahastin, in press). Samples were dried at 60, 70 and 80 °C and air velocities of 0.5 and 1 m/s. LPSSD drying was accomplished in a unit with a 0.45 m × 0.45 m × 0.45 m drying chamber, as described by Devahastin, Suvar-nakuta, Soponronnarit, and Mujumdar (2004). Steam was produced in a boiler, passed through a steam reservoir and steam trap, then introduced into the chamber and maintained at 7 kPa, with a variable-speed electric fan used to distribute steam throughout the chamber. A vacuum pump (Model ET32030, Nash Engineering Co., Trumbull, CT) was used to help maintain vacuum in the drying chamber. The temperature of steam in the chamber was kept constant with a 1.5 kW electrical heater, controlled by a PID controller. As with HAD, LPSSD samples were dried at 60, 70 and 80 °C. A Labconco 77550 freeze dryer (Labconco, Kansas City, MS) was used for FD samples. Samples were frozen to −25 °C by a plate contact freezer, with a freezing rate on the order of 0.2 °C/min, and held at that temperature for 3 h. The freeze dryer was operated with a condenser temperature of −51 °C, and a temperature program rate of 0.2 °C/min. In separate runs, samples were removed for analysis at 0, 4, 8, 12 and 16 h.

2.2. Structure and property measurements

At regular intervals, samples were removed to determine moisture content, percent shrinkage, rehydration ratio and microstructural changes. Moisture content was determined by AOAC Method 7.003 (AOAC, 1984).

Shrinkage was determined from the change in volume of five pieces. Volumes were determined by displacement of a known volume of *n*-hexane in a graduated cylinder. Percent shrinkage was expressed as:

$$\% \text{Shrinkage} = \left(\frac{V_i - V}{V_i} \right) \times 100 \quad (1)$$

where V_i is the initial volume (prior to drying) and V is the volume after drying.

Rehydration properties were determined by immersing dried samples in boiling water (100 °C) for 10 min. The wetted sample was drained and the mass determined to the nearest 0.0001 g. The rehydration ratio was calculated as:

$$R = \frac{m}{m_0} \quad (2)$$

where m_0 is the mass of the dried and m is the mass of rehydrated sample.

Samples for microstructural analysis were prepared as described by Kerdpi boon and Devahastin (in press). Each sample was fixed in 10% formaldehyde, washed, and then dehydrated in a series of isopropyl alcohol solutions. Samples were then embedded with melted paraffin at 60 °C, cooled, and sectioned by Leica Jung RM2025 microtome (Leica Microsystems, Wetzlar, Germany) into 5 µm slices. Cell wall materials were dyed with haematoxylin and eosin, and then examined by light microscopy (Olympus Model LH30RF200, Tokyo, Japan). Images were collected with a CCD digital camera system using the PixelView Geo-Force 7300 multimedia card and capture software (Pro-Link Computer, City of Industry, CA).

2.3. Fractal analysis

Digital images of the carrot sections were attained from the microscope at a 520 × 520 pixel resolution, and viewed at approximately 500× total magnification. Images of a micrometer scale at the same conditions show that this corresponds to an image resolution of 0.71 µm/pixel. Images were grayscale, then thresholded to provide clear contrast between the cell wall and background.

Fractal dimension was calculated using a box counting method (Quevedo, Calos, Aguilera, & Cadoche, 2002). Square boxes with a specified size (r) were overlayed onto the image. The number of boxes ($N(r)$) which contained cell wall were counted. This was repeated for box sizes of 4, 5, 10, 13, 26, 65, 130, and 260 pixels. Fractal dimension is calculated as

$$D = \lim_{r \rightarrow 0} \frac{\log(N(r))}{\log(1/r)} \quad (3)$$

The fractal dimension was calculated using Matlab software (version 6.5) as detailed in Kerdpi boon and Devahastin (in press). Normalized fractal dimensions were reported as:

$$\Delta D/D_0 = \frac{D - D_0}{D_0} \quad (4)$$

where D_0 and D are the fractal dimensions of fresh and dried samples, respectively.

2.4. Artificial neural network training

Artificial neural networks were developed using Matlab 7 software, with the Neural Network Toolbox 4 (The Mathworks, Inc., Natick, MA, USA). The networks were simulated based on a multilayer feed forward neural network. This type of network is very powerful in function optimization modeling (Lou & Nakai, 2001). The input layer, hidden layers, and output layer structures are shown in Fig. 1. A back-propagation algorithm was used to implement supervised training of the network. During training, weighting functions for the inputs to each ANN were determined, such that the predicted output best matched the actual output from the data set. Weights were randomly assigned at the beginning of the training phase, according to the back-propagation algorithm. A hyperbolic tangent was used as the transfer function in each hidden layer, and a linear transfer function was used in the output layer. Minimization of error was accomplished using the Levenberg–Marquardt (LM) algorithm. Training was finished when the mean square error (MSE) converged and was less than 0.001. If the MSE did not go below 0.001, training was completed after 1,000,000 epochs, where an epoch represents one complete sweep through all the data in the training set.

The inputs included the normalized fractal dimension ($\Delta D/D_0$), moisture content (mc; kg water/kg), and drying method. The output layer consisted of %shrinkage and rehydration ratio. The number of hidden layers and number of neurons in each hidden layer were varied from 1 to 10 (1, 2, 4, 6, 8, or 10). Training was done for thirty trial configurations in each hidden layer/neuron combination, in order to find the combination of hidden layers and neurons that produced the minimum error.

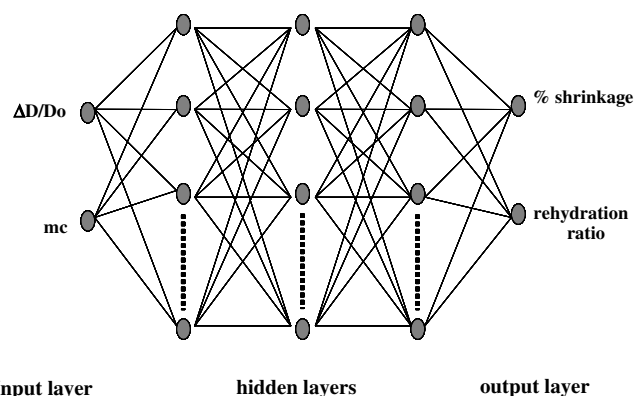


Fig. 1. Schematic diagram of multilayer neural network for prediction of physical properties used in this study.

2.5. Selection of optimal ANN configuration

The optimized configurations from training for each neuron were selected from thirty trial configurations based on neural network performance, which gave the minimum error from the training process. The average mean square error (MAE), standard deviation of MAE (STD_A), percentage of relative mean square error (%MRE), and standard deviation of %MRE (STD_R) were used to compare the performances of various ANN models, and were calculated as:

$$MAE = \frac{1}{N} \sum_{i=1}^N \Delta P_A \quad (5)$$

$$STD_A = \sqrt{\frac{\sum_{i=1}^N (\Delta P_A - \overline{\Delta P_A})^2}{N-1}} \quad (6)$$

$$\%MRE = \left(\frac{1}{N} \sum_{i=1}^N \Delta P_R \right) \times 100 \quad (7)$$

$$STD_R = \sqrt{\frac{\sum_{i=1}^N (\Delta P_R - \overline{\Delta P_R})^2}{N-1}} \quad (8)$$

where $\Delta P_A = |P_P - P_E|$, $\Delta P_R = |(P_P - P_E)/P_E|$, P_P is the predicted output (%shrinkage, rehydration ratio), and P_E the experimentally measured outputs.

3. Results and discussion

Typical light microscopy images are shown in Fig. 2 for HAD carrots. Visual inspection showed that longer drying times resulted in more extensive shrinkage and ruggedness of the carrot cell structure. Fig. 2 also shows the calculated

fractal dimension for each image shown. In general, fractal dimension increased with drying time corresponding to less orderly cell structures. A fractal dimension of 1 corresponds to a straight line, which exhibits self-similarity in 1 direction. A fractal dimension of 2 corresponds to a completely covered plane, which is self-similar in two independent directions. The two-dimensional images of the cell do not fall on a straight line, nor do they completely cover the image space, thus are expected to have a fractal dimension between 1 and 2. Due to the large number of data, the results are summarized in Table 1, which shows the range of normalized fractal dimension ($\Delta D/D_0$) for each of the drying methods. ($\Delta D/D_0$) varied from 0 to 0.094 for HAD, 0 to 0.092 for LPSSD, and 0 to 0.031 for FD. Table 1 also shows the range of moisture contents, the other major input for the ANN model.

The properties to be predicted included %shrinkage and rehydration ratio. The ranges of measured values are shown in Table 1. %Shrinkage varied from 0 to 88.7 for HAD, 0 to 91.4 for LPSSD, and 0 to 40.6 for FD. As expected, freeze drying resulted in the least changes in product volume. Rehydration ratio varied from 1 to 3.41 for HAD, 1 to 3.83 for LPSSD, and 1 to 4.34. It has been shown that LPSSD carrots are more readily rehydrated than HAD carrots, but not as well rehydrated as freeze dried carrots (Kerdpiiboon & Devahastin, in press).

The normalized fractal dimension ($\Delta D/D_0$) could be used to monitor the physical property changes of carrot during drying (Kerdpiiboon & Devahastin, in press). Both normalized fractal dimension and moisture content were used as inputs in the artificial neural network structure. The ANN optimization process was performed using a trial

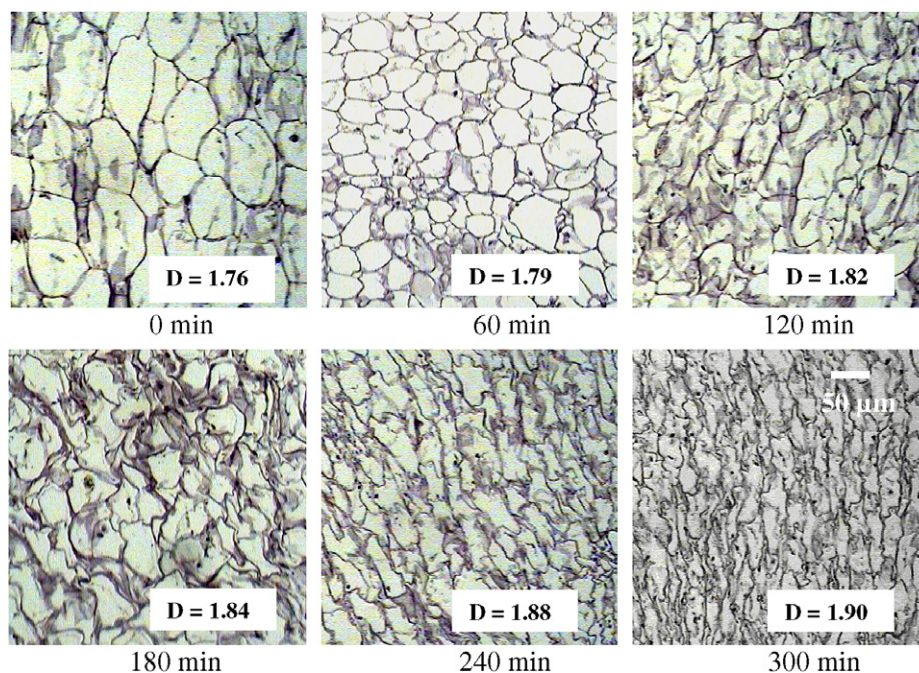


Fig. 2. LM micrographs for carrot undergoing hot-air drying at 60 °C. Inset shows the calculated fractal dimension for each image. Bar corresponds to 50 µm, with image resolution of 0.71 µm.

Table 1

Range of normalized fractal dimension and physical properties of carrot undergoing different drying techniques

Drying techniques	$\Delta D/D_0$	Moisture content (kg H ₂ O/100 kg)	%Shrinkage	Rehydration ratio (m/m_0)
HAD	0–0.094	12.3–0.15	0–88.7	1–3.41
LPSSD	0–0.092	12.2–0.21	0–91.4	1–3.83
Freeze dryer	0–0.031	12.0–0.09	0–40.6	1–4.34

and error technique. Data sets of inputs and outputs used to train the ANN consisted of HAD (66 cases), LPSSD (29 cases), HAD + LPSSD (95 cases), and HAD + LPSSD + freeze dryer (101 cases). Datasets for freeze drying were not considered separately as there were too few for successful training. Each dataset was divided into two groups, consisting of 75% for training/testing and 25% for validation.

During training, the datasets were used to determine the optimum number of hidden layers, and neurons per hidden layer, that gave the best predictive power. ANNs with between 1 and 10 hidden layers were tested (1, 2, 4, 6, 8, 10), and with 1–10 neurons per hidden layer. Each combination of hidden layers and neurons per hidden layer was trained for thirty trial configurations, with each trial start-

ing with a different set of randomized weights, and with the model error determined after each simulation. The results showed that the number of hidden layers, and neurons per hidden layer, that yielded minimum error was different for each drying technique (Table 2), and to a lesser extent the property being predicted. The minimum MRE for HAD was found with two hidden layers and four neurons per layer for shrinkage, and one hidden layer and 10 neurons for rehydration. For LPSSD (Table 3), the lowest MRE for both shrinkage and rehydration was found with two hidden layers and six neurons. A large number of hidden layers does not necessarily lower the error if there are enough numbers of neurons in each hidden layer (Torrecilla et al., 2005). The best prediction in most of the data sets contained two hidden layers.

Table 2

Errors in the prediction of physical properties with different number of hidden layers and neurons per layer for carrot undergoing HAD

No. of hidden	No. of neurons	%Shrinkage				Rehydration ratio (m/m_0)			
		MAE	STD _A	%MRE	STD _R	MAE	STD _A	%MRE	STD _R
1	1	5.70	4.58	8.76	8.92	0.23	0.15	12.7	10.6
	2	2.28	2.22	4.17	5.51	0.13	0.12	5.72	5.05
	4	1.95	2.18	3.86	5.54	0.12	0.11	5.42	4.65
	6	1.92	2.08	4.04	7.45	0.12	0.12	5.49	5.00
	8	1.94	2.15	4.13	5.87	0.13	0.12	5.69	4.90
	10	2.10	2.74	4.74	8.60	0.11	0.13	5.20	6.15
2	1	5.78	4.56	8.96	8.75	0.23	0.15	12.6	10.6
	2	2.15	2.19	4.21	5.68	0.12	0.12	5.54	5.20
	4	2.05	2.16	3.63	4.51	0.12	0.12	5.66	4.99
	6	2.12	2.12	4.33	5.97	0.12	1.35	5.38	5.01
	8	2.04	2.24	3.87	4.67	0.12	0.94	5.53	4.95
	10	2.25	2.40	4.75	7.52	0.12	0.12	5.70	5.76

Table 3

Errors in the prediction of physical properties with different number of hidden layers and neurons per layer for carrot undergoing LPSSD

No. of hidden	No. of neurons	%Shrinkage				Rehydration ratio (m/m_0)			
		MAE	STD _A	%MRE	STD _R	MAE	STD _A	%MRE	STD _R
1	1	6.78	4.90	9.68	7.30	0.15	0.12	9.93	6.69
	2	2.41	2.21	6.31	9.41	0.07	0.08	4.27	4.56
	4	1.59	3.31	3.57	4.44	0.06	0.08	3.75	4.29
	6	1.46	1.32	3.15	3.31	0.06	0.08	3.15	4.43
	8	1.47	1.33	3.52	3.82	0.07	0.08	4.18	4.54
	10	1.41	2.00	3.54	5.88	0.06	0.06	3.83	4.73
2	1	6.83	4.90	9.74	6.82	0.15	0.11	9.83	6.70
	2	2.23	1.67	4.47	3.25	0.06	0.06	4.17	3.34
	4	1.61	1.52	3.73	4.21	0.06	0.09	3.66	4.84
	6	1.30	1.79	2.82	3.57	0.04	0.06	2.66	3.67
	8	1.67	2.09	3.73	5.29	0.06	0.09	3.36	4.29
	10	2.51	3.50	5.59	9.50	0.08	0.09	4.77	5.63

Table 4

Errors in the prediction of physical properties with different number of hidden layers and neurons per layer for carrot undergoing HAD, LPSSD, HAD + LPSSD, and HAD + LPSSD + FD

Data from drying technique	%Shrinkage				Rehydration ratio (m/m_0)			
	MAE	STD _A	%MRE	STD _R	MAE	STD _A	%MRE	STD _R
HAD	2.05	2.16	3.63	4.51	0.12	0.12	5.66	4.99
LPSSD	1.30	1.79	2.82	3.57	0.04	0.06	2.66	3.67
HAD + LPSSD	2.56	2.56	5.28	7.62	0.14	0.14	6.67	6.23
HAD + LPSSD + FD	2.47	4.13	5.40	10.3	0.13	0.14	6.34	6.02

The ANN developed using combined HAD + LPSSD data had a minimum MRE with two hidden layers and eight neurons per hidden layer; that using combined HAD + LPSSD + FD data had minimum MRE with two hidden layers and six neurons per hidden layer. A comparison of errors associated with ANNs for each drying technique, as well as combinations of drying techniques, is shown in Table 4. LPSSD data had the least error during training (MRE = 2.82 and 2.66 for shrinkage and rehydration ratio, respectively), while that for HAD was somewhat higher (MRE = 3.63 and 5.20, respectively). ANNs developed for combined drying techniques had slightly higher errors than those developed for each drying technique individually. The MRE for HAD + LPSSD were 5.28 for shrinkage and 6.67 for rehydration, while those for HAD + LPSSD + FD were 5.40 and 6.34, respectively.

The system of equations representing the ANN for predicting %shrinkage and rehydration are shown in the Appendix. The equations show the inputs, transfer functions, and relative weight for each node. The equations

can be used in a computer program or spreadsheet to predict the physical properties of the dried carrots. These were implemented in a feed-forward algorithm to predict physical properties and compared with the independent validation sets of data. Plots of experimentally determined %shrinkage or rehydration ratio versus ANN predicted values are shown in Figs. 3–5. The correlation coefficients were greater than 0.95 in all cases. For HAD, $R^2 = 0.993$ for predicted shrinkage and 0.969 for rehydration. For LPSSD, $R^2 = 0.998$ and 0.993 for shrinkage and rehydration, respectively. When all drying methods were combined (HAD + LPSSD + FD), $R^2 = 0.987$ for predicted shrinkage and 0.956 for rehydration ratio.

The ability to predict shrinkage was slightly better than that for predicting rehydration ratio, as evidenced by the greater R^2 values for shrinkage. This is likely due to the fact that shrinkage is more highly interrelated with cellular changes throughout the volume of the dried carrot, and these are well-characterized by changes in the normalized fractal dimension. While rehydration is also dependent upon

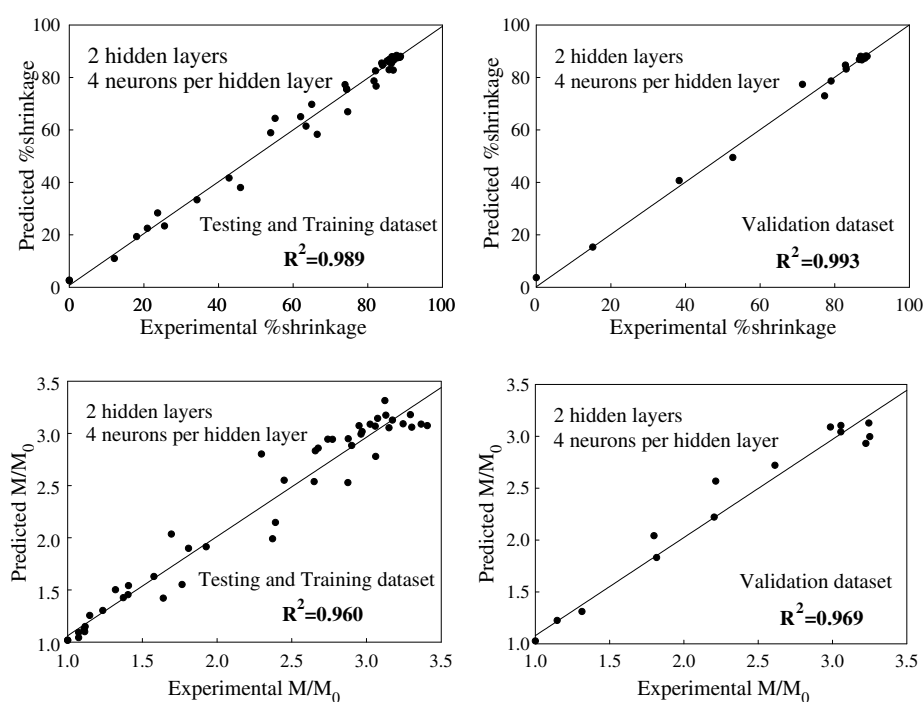


Fig. 3. Correlation of experimental and predicted physical properties with testing and training data sets, as well as validation data set for carrot undergoing HAD using the optimal ANN.

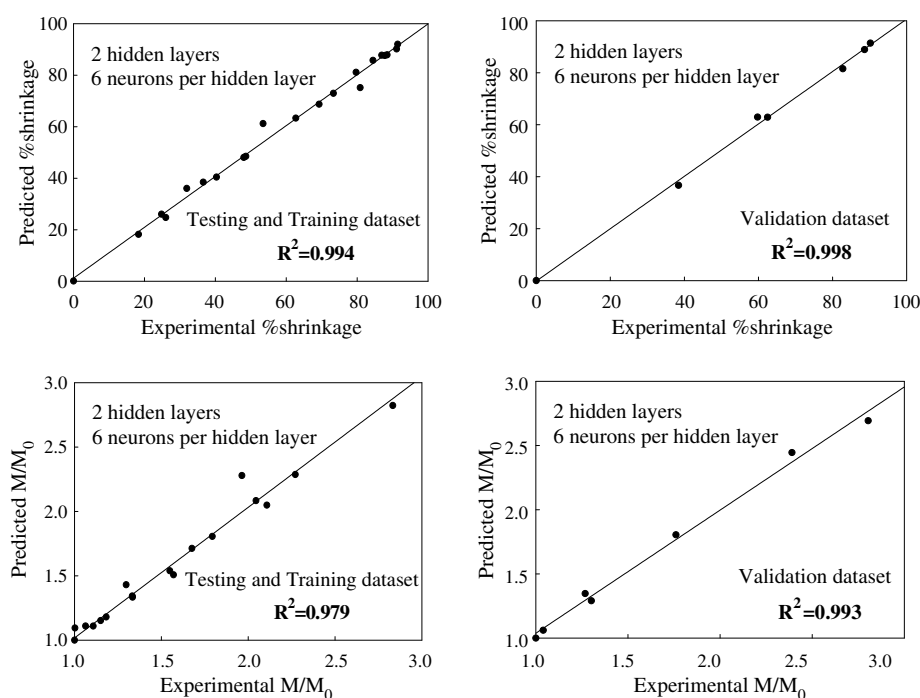


Fig. 4. Correlation of experimental and predicted physical properties with testing and training data sets, as well as validation data set for carrot undergoing LPSSD using the optimal ANN.

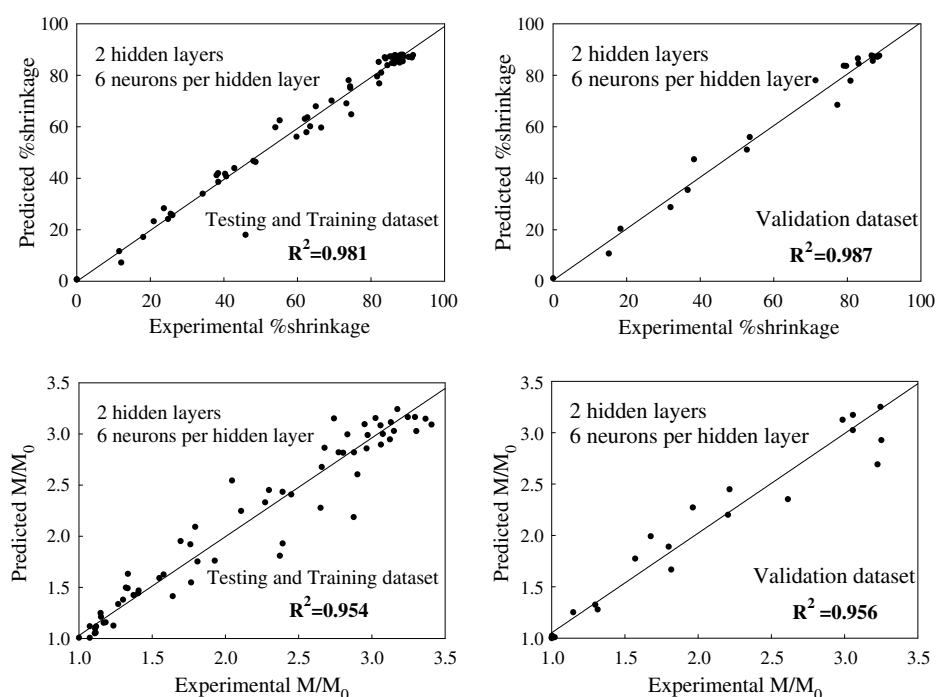


Fig. 5. Correlation of experimental and predicted physical properties with testing and training data sets, as well as validation data set for carrot using combined HAD + LPSSD + FD using the optimal ANN.

internal structural changes and the ability for water to diffuse within the carrot matrix, it may also depend upon limiting factors at the surface, such as case-hardening. These surface factors are more apparent with hot-air drying, and indeed we

found that rehydration for LPSSD was better predicted than for HAD ($R^2 = 0.993$ for LPSSD and 0.969 for HAD).

Artificial neural networks do have advantages and disadvantages. Network development can be computationally

expensive and time-consuming. Once developed, however, its use is straight-forward and can be easily implemented in programs, spreadsheets, calculators, or hardware devices. While predictive value can be very high, there are no particular mechanistic secrets to be learned from the system of equations representing the network. In our work, the ability to predict shrinkage and rehydration were very good. Studies using traditional regression techniques (Kerdpiboon & Devahastin, *in press*) showed R^2 values ranging from 0.844 to 0.984. While this is perhaps reasonable predictive power, the implementation of the ANN provided even better prediction capability.

4. Conclusion

Artificial neural networks can be used to predict the shrinkage and rehydration ratios of carrot undergoing different drying techniques in terms of normalized fractal dimension and moisture content. The optimal models from all the data sets had two hidden layers and 4–8 neurons in each hidden layer, depending on the complexity of each data set. Moreover, the optimal models can predict the %shrinkage and rehydration ratio with R^2 values greater than 0.969 in all cases, offering better predictive performance than with traditional regression techniques.

Fractal dimension was found to be a good measure of cell wall rugosity. Fractal dimensions have been used in many areas, including food science, to study morphological features. That does not mean that there are not other approaches, but this one is quite adequate. For example, for physical measurements of crispness/crunchiness of foods, there are several ways to analyze the jagged force/deformation curves. One might determine the total linear distance of the curve. Another approach is to determine the deviation about some model equation fit to the curve. Yet another approach is to use auto-correlation functions. And yet another approach is to use fractal dimensions to study the degree of jaggedness.

In this study, models based on fractal dimension and moisture content were found to have very good predictive value for the properties of dried carrots. As such, there is little incentive to find alternative parameters for quantifying morphological features.

Acknowledgments

We express appreciation to the Commission on Higher Education, the Thailand Research Fund and the International Foundation for Science in Sweden for financial support.

Appendix

HAD: two hidden layers/four neurons

x = moisture content

f = normalized fractal dimension

$$x1 = (x - (2.9173)) / (3.6868)$$

$$x2 = (f - (0.0544)) / (0.0298)$$

$$x3 = \tanh((-3.6532) * x1 + (0.3011) * x2 + (-1.5851))$$

$$x4 = \tanh((0.8610) * x1 + (0.0560) * x2 + (-0.6467))$$

$$x5 = \tanh((1.1348) * x1 + (-0.1271) * x2 + (1.1862))$$

$$x6 = \tanh((1.3475) * x1 + (0.2816) * x2 + (4.1462))$$

$$x7 = \tanh((-1.3689) * x3 + (1.6391) * x4 + (0.3131) * x5 + (-0.5434) * x6 + (1.4410))$$

$$x8 = \tanh((4.9423) * x3 + (1.2495) * x4 + (-2.2659) * x5 + (-1.3443) * x6 + (-2.2694))$$

$$x9 = \tanh((0.3076) * x3 + (-0.7299) * x4 + (0.6819) * x5 + (-0.1075) * x6 + (-0.7226))$$

$$x10 = \tanh((1.4197) * x3 + (-1.0404) * x4 + (1.6506) * x5 + (-1.1941) * x6 + (1.3532))$$

$$x11 = \text{purelin}((0.0469) * x7 + (0.4000) * x8 + (1.3336) * x9 + (1.0066) * x10 + (-0.2687))$$

$$x12 = \text{purelin}((-0.4735) * x7 + (1.5918) * x8 + (1.7325) * x9 + (-0.5560) * x10 + (1.8131))$$

$$\text{shrinkage} = ((29.9) * x11 + (65.6))$$

$$\text{rehydration} = ((0.87) * x12 + (2.21))$$

HAD + LPSSD + FD: two hidden layers/six neurons

x = moisture content

f = normalized fractal dimension

(continued on next page)

Appendix (continued)

$$x1 = (x - (3.4217)) / (3.8732)$$

$$x2 = (f - (0.0512)) / (0.0292)$$

$$x3 = \tanh((1.4735) * x1 + (-1.4626) * x2 + (-4.9553))$$

$$x4 = \tanh((1.7902) * x1 + (-2.5996) * x2 + (-3.1740))$$

$$x5 = \tanh((1.9172) * x1 + (0.4946) * x2 + (-0.8119))$$

$$x6 = \tanh((-3.0160) * x1 + (-0.2788) * x2 + (-2.2864))$$

$$x7 = \tanh((1.0300) * x1 + (-0.9892) * x2 + (-3.7330))$$

$$x8 = \tanh((-1.7226) * x1 + (1.0193) * x2 + (-1.8109))$$

$$x9 = \tanh((-1.5071) * x3 + (0.3235) * x4 + (-0.1621) * x5 + (-0.3690) * x6 + (-1.3489) * x7 + (-0.4828) * x8 + (2.3965))$$

$$x10 = \tanh((0.5054) * x3 + (-1.3033) * x4 + (-1.6142) * x5 + (1.9190) * x6 + (1.7592) * x7 + (-0.0554) * x8 + (-1.1052))$$

$$x11 = \tanh((-0.9494) * x3 + (-1.1667) * x4 + (0.2751) * x5 + (-1.8012) * x6 + (0.6882) * x7 + (1.2968) * x8 + (0.5427))$$

$$x12 = \tanh((-0.3766) * x3 + (-0.6707) * x4 + (0.3969) * x5 + (-1.1287) * x6 + (-0.4158) * x7 + (-1.0720) * x8 + (0.0877))$$

$$x13 = \tanh((0.2027) * x3 + (0.6496) * x4 + (1.0186) * x5 + (-0.7509) * x6 + (1.2507) * x7 + (-1.2624) * x8 + (1.0449))$$

$$x14 = \tanh((-0.3770) * x3 + (-1.0296) * x4 + (-1.0920) * x5 + (0.2778) * x6 + (0.2944) * x7 + (-1.2120) * x8 + (2.0312))$$

$$x15 = \text{purelin}((-1.2049) * x9 + (0.1499) * x10 + (1.3347) * x11 + (0.0638) * x12 + (-0.7283) * x13 + (-0.7560) * x14 + (0.8697))$$

$$x16 = \text{purelin}((0.9715) * x9 + (1.4665) * x10 + (-0.1211) * x11 + (-1.3050) * x12 + (-0.5546) * x13 + (0.6424) * x14 + (0.7259))$$

$$\text{shrinkage} = (30.6) * x15 + (60.8)$$

$$\text{rehydration} = (0.93) * x16 + (2.06)$$

References

- Association of Official Agricultural Chemists (AOAC) (1984). *Official method of analysis* (14th ed.). Washington DC: Association of Official Agricultural Chemists.
- Barletta, B. J., & Barbosa-Canovas, G. V. (1993). Fractal analysis to characterize ruggedness changes in tapped agglomerated food powders. *Journal of Food Science*, 58(5), 1030–1046.
- Chanona, P. J. J., Alamilla, B. L., Farrera, R. R. R., Quevedo, R., Aguilera, J. M., & Gutierrez, L. G. F. (2003). Description of the convective air-drying of a food model by means of the fractal theory. *Food Science and Technology International*, 9(3), 207–213.
- Devahastin, S., Suvarnakuta, P., Soponronnarit, S., & Mujumdar, A. S. (2004). A comparative study of low-pressure superheated steam and vacuum drying of a heat-sensitive material. *Drying Technology*, 22(8), 1845–1867.
- Goncalves, E. C., Minim, L. A., Coimbra, J. S. R., & Minim, V. P. R. (2005). Modeling sterilization process of canned foods using artificial neural networks. *Chemical Engineering and Processing*, 44(12), 1269–1276.
- Graf, J. C. (1991). The importance of resolution limits to the interpretation of fractal descriptions of fine particles. *Powder Technology*, 67(1), 83–85.
- Hsu, S., Lu, S., & Huang, C. (2000). Viscoelastic changes of rice starch suspensions during gelatinization. *Journal of Food Science*, 65(2), 215–220.
- Kerdpiiboon, S., & Devahastin, S. (in press). Fractal characterization of some physical properties of a food product under various drying conditions. *Drying Technology*.
- Lou, W., & Nakai, S. (2001). Application of artificial neural networks for predicting the thermal inactivation of bacteria: a combined effect of temperature, pH and water activity. *Food Research International*, 34(7), 573–579.
- Mandelbrot, B. B. (1982). *The fractal geometry of nature*. San Francisco: W. H. Freeman (pp. 1–65).
- Mayor, L., & Sereno, A. M. (2004). Modelling shrinkage during convective drying of food materials: a review. *Journal of Food Engineering*, 61(3), 373–386.
- Ochoa, M. R., Kesseler, A. G., Pirone, B. N., Marquez, C. A., & De Michelis, A. (2002). Volume and area shrinkage of whole sour cherry fruits (*Prunus cerasus*) during dehydration. *Drying Technology*, 20(1), 147–156.
- Peleg, M., & Normand, M. D. (1985). Characterization of the ruggedness of instant coffee particle shape by natural fractals. *Journal of Food Science*, 50, 829–831.
- Quevedo, R., Calos, L. G., Aguilera, J. M., & Cadoche, L. (2002). Description of food surfaces and microstructural changes using fractal image texture analysis. *Journal of Food Engineering*, 53(4), 361–371.
- Ratti, C. (1994). Shrinkage during drying of foodstuffs. *Journal of Food Engineering*, 23(1), 91–105.
- Rubnov, M., & Saguy, I. S. (1997). Fractal analysis and crust water diffusivity of a restructured potato product during deep-fat frying. *Journal of Food Science*, 62(1), 135–137, 154.
- Sablani, S. S., & Rahman, M. S. (2003). Using neural networks to predict thermal conductivity of food as a function of moisture content, temperature and apparent porosity. *Food Research International*, 36(6), 617–623.
- Torrecilla, J. S., Otero, L., & Sanz, P. D. (2005). Artificial neural networks: a promising tool to design and optimize high-pressure food processes. *Journal of Food Engineering*, 69(3), 299–306.



Volume 107, issue 4, 15 April 2008

ISSN: 0308-8146

FOOD CHEMISTRY

Managing Editor

G.G. Birch

Editors

P.M. Finglas

J.P. Roozen

F. Shahidi

Available online at

ScienceDirect
www.sciencedirect.com

This article was published in an Elsevier journal. The attached copy is furnished to the author for non-commercial research and education use, including for instruction at the author's institution, sharing with colleagues and providing to institution administration.

Other uses, including reproduction and distribution, or selling or licensing copies, or posting to personal, institutional or third party websites are prohibited.

In most cases authors are permitted to post their version of the article (e.g. in Word or Tex form) to their personal website or institutional repository. Authors requiring further information regarding Elsevier's archiving and manuscript policies are encouraged to visit:

<http://www.elsevier.com/copyright>



Isomerisation kinetics and antioxidant activities of β -carotene in carrots undergoing different drying techniques and conditions

Bhudsawan Hiranvarachai^a, Peamsuk Suvarnakuta^b, Sakamon Devahastin^{a,*}

^a Department of Food Engineering, King Mongkut's University of Technology Thonburi, 126 Pracha u-tid Road, Bangkok 10140, Thailand

^b Department of Food Science and Technology, Thammasat University, Paholyothin Road, Pathum Thani 12121, Thailand

Received 18 June 2007; received in revised form 23 July 2007; accepted 4 October 2007

Abstract

Carrots are known as a natural source of β -carotene. In order to preserve the latter, carrots must generally be processed, and drying is one of the most common methods for processing carrots. During drying β -carotene in carrots suffers degradation. β -Carotene degradation is generally due to thermal degradation and isomerisation. In this work, the drying kinetics as well as the isomerisation kinetics and antioxidant activities of β -carotene in carrots undergoing hot air drying, vacuum drying and low-pressure superheated steam drying (LPSSD) were determined within the temperature range of 60–80 °C and, in the case of vacuum drying and LPSSD, at a pressure of 7 kPa. A high performance liquid chromatography (HPLC) method was used to determine the β -carotene contents and its isomerisation kinetics, while the antioxidant activities of various combinations of all-*trans*- and *cis*-forms of β -carotene in carrots were evaluated using the Trolox equivalent antioxidant capacity (TEAC) assay.

© 2007 Elsevier Ltd. All rights reserved.

Keywords: Antioxidant activity; Degradation; Hot air drying; Low-pressure superheated steam drying; *cis/trans*-Isomerisation; Vacuum drying

1. Introduction

β -Carotene is one of the common carotenoid hydrocarbons that contain specific end groups or two-beta rings. It acts as provitamin A, which is converted by humans to vitamin A (Retinol) (Sergio & Russell, 1999; Patrick, 2000). Moreover, β -carotene has high antioxidant activity, by scavenging peroxyl radicals, which occur as a result of oxidation reactions, especially at low oxygen tension (Larson, 1988). Since carotene stereoisomers display different chemical properties and antioxidant activities, the knowledge of various factors affecting formation of all-*trans*- and *cis*-isomers of β -carotene in foods is of interest (Marx, Stuparic, Schieber, & Carle, 2003).

Carrots (*Daucus carota* var. *sativa*) are one of the most important root crops. The consumption of carrots and

their related products has increased steadily, partly due to the antioxidant activity of β -carotene in carrots (Rubatzky, Quiros, & Simon, 1999). However, in the food industry, carrots must generally be processed prior to their use and drying is one of the most frequently used processes. Many techniques have been developed to dry carrots, with the goal of maintaining their nutritional value, especially β -carotene, as much as possible.

Different drying techniques and conditions are known to affect the quality of a food product, either in terms of its physical properties, chemical properties or biochemical properties. In the food industry, hot air drying is widely used, although it often leads to much quality degradation, especially in terms of the nutritional properties. Several other drying techniques have therefore been proposed and studied (Devahastin, Suvarnakuta, Soponronnarit, & Mujumdar, 2004). Although there are some works that report the study of β -carotene degradation in carrots undergoing different drying techniques and conditions

* Corresponding author. Tel.: +66 2 470 9246; fax: +66 2 470 9240.
E-mail address: sakamon.dev@kmutt.ac.th (S. Devahastin).

(Suvarnakuta, Devahastin, & Mujumdar, 2005), no information is so far available on the effect of drying on the *cis/trans*-isomerisation of β -carotene in carrots.

Naturally, β -carotene exists in the all-*trans* form. After processing, however, some all-*trans* form is converted into its different *cis*-isomers (Aman, Schieber, & Carle, 2005). Heat, light and the presence of sensitizers promote isomerisation of *trans*-carotenoids to their *cis*-form (Dutta, Chaudhuri, & Chakraborty, 2005).

Lessin, Catigani, and Schwartz (1997) studied the quantification of *cis/trans*-isomers of carotenoids in canned carrots and other vegetables. They found that all-*trans*- β -carotene was lower in all processed samples, as compared to the fresh samples. Only all-*trans*- β -carotene was found in fresh carrots while 9-*cis*- β -carotene and 13-*cis*- β -carotene occurred after canning. Canning caused a 33% increase in total *cis*-isomers. This change in isomeric compositions was due to *cis/trans*-isomerisation, which occurred as a direct result of the thermal processing.

Chen, Peng, and Chen (1995) studied the thermal degradation of canned carrot juices. They found that canning of carrot juices at 121 °C led to the formation of 13-*cis*-isomer, which was the predominant isomer in that study. This result was consistent with that of Marx et al. (2003), who studied the effects of pasteurisation and sterilisation on *cis/trans*-isomerisation of β -carotene in carrot juices. They found that in the case of pasteurisation, only 13-*cis*- β -carotene occurred. On the other hand, in the case of sterilisation, 9-*cis*- β -carotene and 13-*cis*- β -carotene occurred. 9-*cis*- β -carotene was found at temperatures higher than 90 °C for processing times longer than 60 min.

As mentioned earlier, β -carotene has high antioxidant activity. Many investigators have thus studied the antioxidant activities of various isomers of β -carotene in different products undergoing processing. Bohm, Puspitasari-Nienaber, Ferruzzi, and Schwartz (2002), for example, studied the antioxidant activities of different geometrical isomers

of β -carotene and other carotenoids using TEAC assay. They reported that all-*trans*- β -carotene had higher antioxidant activity than 13-*cis*- β -carotene.

The objectives of this study were to investigate the effects of selected drying techniques, i.e., hot air drying, vacuum drying and low-pressure superheated steam drying (LPSSD), on the isomerisation kinetics and antioxidant activities of β -carotene in carrots at different conditions. The relationship between the amount of different isomers of β -carotene, as well as their antioxidant activities, and carrot moisture content were also investigated.

2. Materials and methods

2.1. Materials

Fresh carrots (*D. carota* var. *sativa*) were purchased from a local market and stored at 4 °C. Before starting each drying experiment, carrots were peeled and diced (only the cortex part was used) into 1 cm³ cubes. The moisture content of fresh carrots was determined by drying the samples at 105 °C for 24 h in a hot air oven (Memmert, model 800, Schwabach, Germany).

2.2. Experimental set-up

2.2.1. Low-pressure superheated steam dryer

A schematic diagram of the low-pressure superheated steam dryer and its accessories is shown in Fig. 1. The dryer consists of a stainless steel drying chamber with inner dimensions of 45 × 45 × 45 cm³; a steam reservoir, which received steam from a boiler and maintained its pressure at around 200 kPa; and a liquid ring vacuum pump (Nash, model ET32030, Trumbull, CT), which was used to maintain the vacuum in the drying chamber (fixed at 7 kPa in this study). An electric heater, rated at 1.5 kW, which was controlled by a PID controller (Omron, model

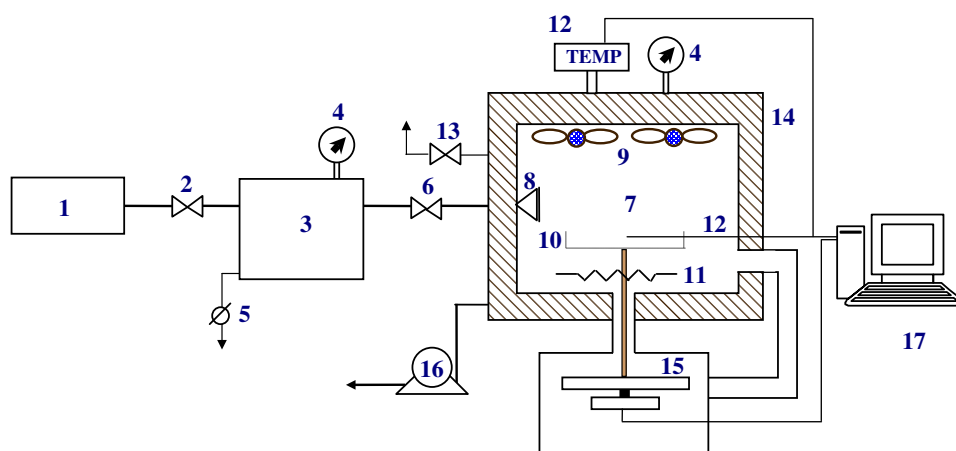


Fig. 1. A schematic diagram of the low-pressure superheated steam dryer and associated units. 1, boiler; 2, steam valve; 3, steam reservoir; 4, pressure gauge; 5, steam trap; 6, steam regulator; 7, drying chamber; 8, steam inlet and distributor; 9, electric fans; 10, sample holder; 11, electric heater; 12, on-line temperature sensor and logger; 13, vacuum purge valve; 14, insulator; 15, on-line weight indicator and logger; 16, vacuum pump; 17, PC with installed data acquisition card.

E5CN, Tokyo, Japan) was installed in the drying chamber to control the steam temperature and to minimise the condensation of steam in the drying chamber during the start-up period. Two variable-speed electric fans were used to disperse steam throughout the drying chamber. The sample holder was made of a stainless steel screen with dimensions of $16.5 \times 16.5 \text{ cm}^2$. The change of the mass of the sample was detected continuously (at 60 s intervals) using a load cell (Minebea, model UCG-3 kg, Nagano, Japan). The temperatures of the steam and of the drying sample were also measured continuously using type-K thermocouples, which were connected to an expansion board (Omega Engineering, model no. EXP-32, Stamford, CT). Thermocouple signals were multiplexed to a data acquisition card (Omega Engineering, model no. CIO-DAS16Jr.) installed in a PC. Labtech Notebook software (version 12.1, Laboratory Technologies Corp., Andover, MA) was then used to read and record the temperature data.

2.2.2. Vacuum dryer

For vacuum drying experiments the same experimental set-up was used as for the LPSSD experiments without the application of steam to the drying chamber.

2.2.3. Hot air dryer

A schematic diagram of the hot air dryer used is illustrated in Fig. 2. It consists of a stainless steel drying chamber ($45 \times 45 \text{ cm}^2$), in which the sample was placed. The inlet air that was used to dry the sample was heated up to the desired temperature by an electric heater rated at 9 kW. The sample was placed on a tray made of a stainless steel screen. The air velocity over the drying tray was fixed at 0.8 m/s.

2.3. β -Carotene analysis

Analysis of the total amount of β -carotene was performed using the methods described by [Suvarnakuta et al. \(2005\)](#). A sample of 5–8 g of dried carrots was ground for 2 min using a stainless steel pulveriser (Waring, model SS110, Torrington, CT). The ground sample was then placed in a flask filled with 40 ml of ethanol. 2 N potassium hydroxide (40 ml) was added, to saponify the solution, at 70°C for 30 min. The extract was then cooled down immediately to 0°C . β -Carotene was then extracted three times

with 5 ml of diisopropyl ether and the aqueous layer was discarded. The extracted solution was filtered through a 0.45 μm filter before being injected into a liquid chromatograph column.

A symmetry[®] C₃₀ 5 μm (4.6 mm \times 250 mm) HPLC column (YMC, Kyoto, Japan) was used for the analysis of different isomers of β -carotene. The HPLC system consisted of a pump and a controller (Waters, model 600, Milford, MA), a tunable absorbance detector (Waters, model 486). A sample of 75% methanol and 25% methyl tert-butyl ether (MTBE) was used as the mobile phase and its flow rate was set at 2 ml/min. A UV detector, at 450 nm, was used for detecting β -carotene. The mobile phase was degassed using an ultrasonic generator.

From the preliminary experiments, it was found that only 13-*cis*- β -carotene formed as a result of isomerisation; only this *cis*-isomer was then tested for in the subsequent study. A standard of all-*trans*- β -carotene was purchased from Fluka (Buchs, Switzerland). 13-*cis*- β -Carotene was obtained by iodine-catalysed photoisomerisation of all-*trans*- β -carotene as previously described by [Aman et al. \(2005\)](#). Briefly, all-*trans*- β -carotene was dissolved in diisopropyl ether containing two drops of 1% iodine. The solution was then exposed to ambient light for 30 min.

A typical chromatogram of β -carotene isomers of interest is shown in Fig. 3. The concentration of all-*trans*- β -carotene was calculated from the peak area of its chromatogram while the *cis*-isomer proportion was calculated from the relative peak area of the *cis*- β -carotene divided by the peak area of the *trans*- β -carotene in each sample.

Quantification of β -carotene was carried out based on a β -carotene standard curve. The standard curve was prepared daily by injecting solutions of HPLC β -carotene standard in diisopropyl ether at six concentrations (0, 2, 4, 6, 8 and 10 g/ml). All standard curves showed good linearity ($r^2 > 0.99$).

The measured all-*trans*- β -carotene content is expressed in terms of the β -carotene retention ratio, while the *cis*-proportion is reported in terms of the *cis/trans* ratio:

$$\beta\text{-Carotene retention ratio} = \frac{\beta_t}{\beta_i} \quad (1)$$

$$\text{cis-Proportion} = \frac{\beta_{cis}}{\beta_{trans}} \quad (2)$$

where β_i and β_t are the β -carotene contents of fresh and dried carrots (mg/100 g solids), respectively. β_{cis} and β_{trans} refer to the peak area of *cis*- β -carotene and the peak area of *trans*- β -carotene, respectively. All *trans*- and *cis*- β -carotene measurements were performed in duplicate and the data presented are an average of the two measurements.

2.4. Antioxidant activities measurement

Antioxidant activities of various combinations (or proportions) of isomers of β -carotene in carrots were determined following the TEAC procedure similar to that of

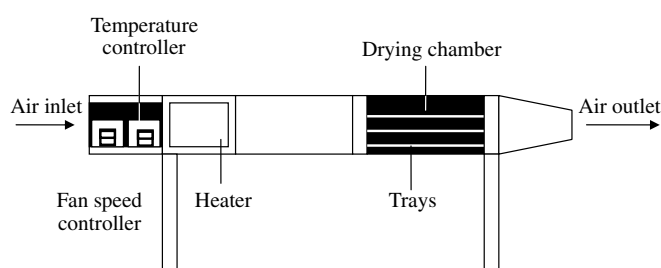


Fig. 2. A schematic diagram of hot air dryer and associated units.

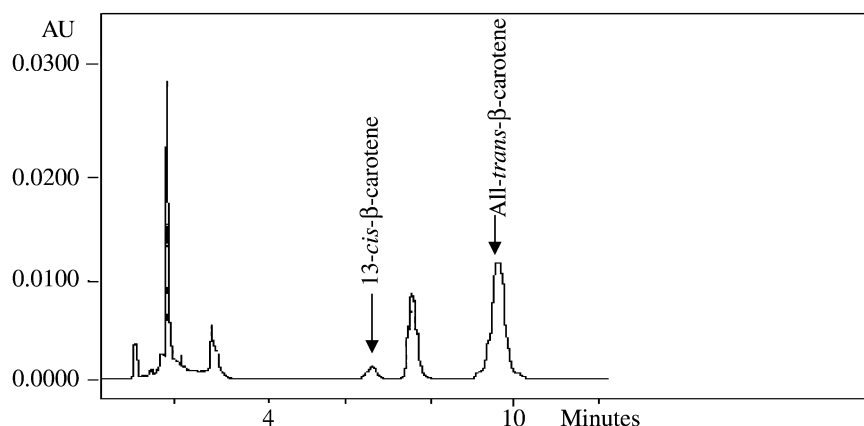


Fig. 3. Typical chromatogram of β -carotene in carrots at a wavelength of 450 nm.

Miller, Sampson, Candxias, Bramly, and Rice-Evans (1996) with some modifications. $\text{ABTS}^{\cdot+}$ radical cation was prepared by passing a 5 mM aqueous stock solution of ABTS (2,2'-azino-bis(3-ethylbenzothiazoline-6-sulphonic acid)) through manganese dioxide on a Whatman No. 5 filter paper. Excess manganese dioxide was removed twice from the filtrate by passing it through a 0.45 μm syringe filter. This solution was then diluted with ethanol to an absorbance of 0.70 (0.02) at 734 nm and pre-incubated at ambient temperature for 1 h prior to its use. Trolox (6-hydroxy-2,5,7,8-tetramethylchroman-2-carboxylic acid) was used as an antioxidant standard. 2.5 mM Trolox was prepared in phosphate buffer saline (PBS) at pH 7.4 for use as a stock solution. $\text{ABTS}^{\cdot+}$ solution (1 ml) and 200 μl of Trolox solution were well mixed using a vortex mixer (Scientific Industries Inc., model G-560E, Bohemia, NY) for 30 s.

UV–Vis scanning spectrophotometer (Shimadzu, model UV-2101PC, Nagoya, Japan) was used for the determination of antioxidant activity. The absorbance was taken at 734 nm exactly at 1 min after initiation of vortex mixing. A standard curve of Trolox was prepared by measuring solutions of Trolox standard in PBS at five concentrations (0, 25, 50, 75 and 100 μM). The standard curves showed good linearity ($r^2 > 0.99$).

To determine the antioxidant activities of various combinations of isomers of β -carotene, β -carotene was diluted in diisopropyl ether (1:9). $\text{ABTS}^{\cdot+}$ solution (1 ml) and 200 μl of the isomers solution were mixed for 30 s using the vortex mixer. The absorbance was then measured at the above wavelength.

The measured antioxidant activities of various combinations of all-*trans*-form and *cis*-form of β -carotene are expressed in terms of % relative inhibition:

$$\% \text{ Relative inhibition} = \frac{\% \text{ inhibition of dried carrots}}{\% \text{ inhibition of fresh carrots}} \quad (3)$$

where % inhibition of dried carrots and fresh carrots refer to the % inhibition of $\text{ABTS}^{\cdot+}$ by the combinations of various isomers of β -carotene in dried and fresh carrots,

respectively. To calculate % inhibition the following equation was used:

$$\% \text{ inhibition} = \frac{(A_{\text{solvent}} - A_{\beta\text{-carotene}}) \times 100}{A_{\text{solvent}}} \quad (4)$$

where A_{solvent} and $A_{\beta\text{-carotene}}$ are the absorbance of diisopropyl ether and the combinations of various isomers of all-*trans*-form and *cis*-form of β -carotene in carrots, respectively. All measurements were performed in duplicate and the data presented are an average of the two measurements.

2.5. Statistical analysis

The experiments were completely randomised. All data were analysed using the analysis of variance (ANOVA). Differences between mean values were established using Duncan multiple range test at a confidence level of 95% ($p = 0.05$). SPSS (version 13; SPSS Inc., Chicago, IL) was used to perform all statistical calculations.

3. Results and discussion

3.1. Drying kinetics of carrots

Since the results of the isomerisation of β -carotene in carrots undergoing different drying techniques and conditions were compared at the same moisture content, the drying curves of carrots undergoing different drying treatments and conditions were first constructed. Carrots that had an initial moisture content in the range of 9–11 kg/kg dry weight basis, (d.b.) were dried to a final moisture content of around 0.1 kg/kg (d.b.).

The drying curves and temperature profiles of carrots undergoing hot air drying, vacuum drying and LPSSD are shown in Figs. 4 and 5, respectively. Three different drying temperatures (60, 70 and 80 $^{\circ}\text{C}$) were employed in each set of experiments.

As can be seen in Fig. 4, although vacuum drying was a faster drying process than LPSSD and hot air drying, the differences between the drying times of LPSSD and vacuum drying were smaller at higher drying temperatures.

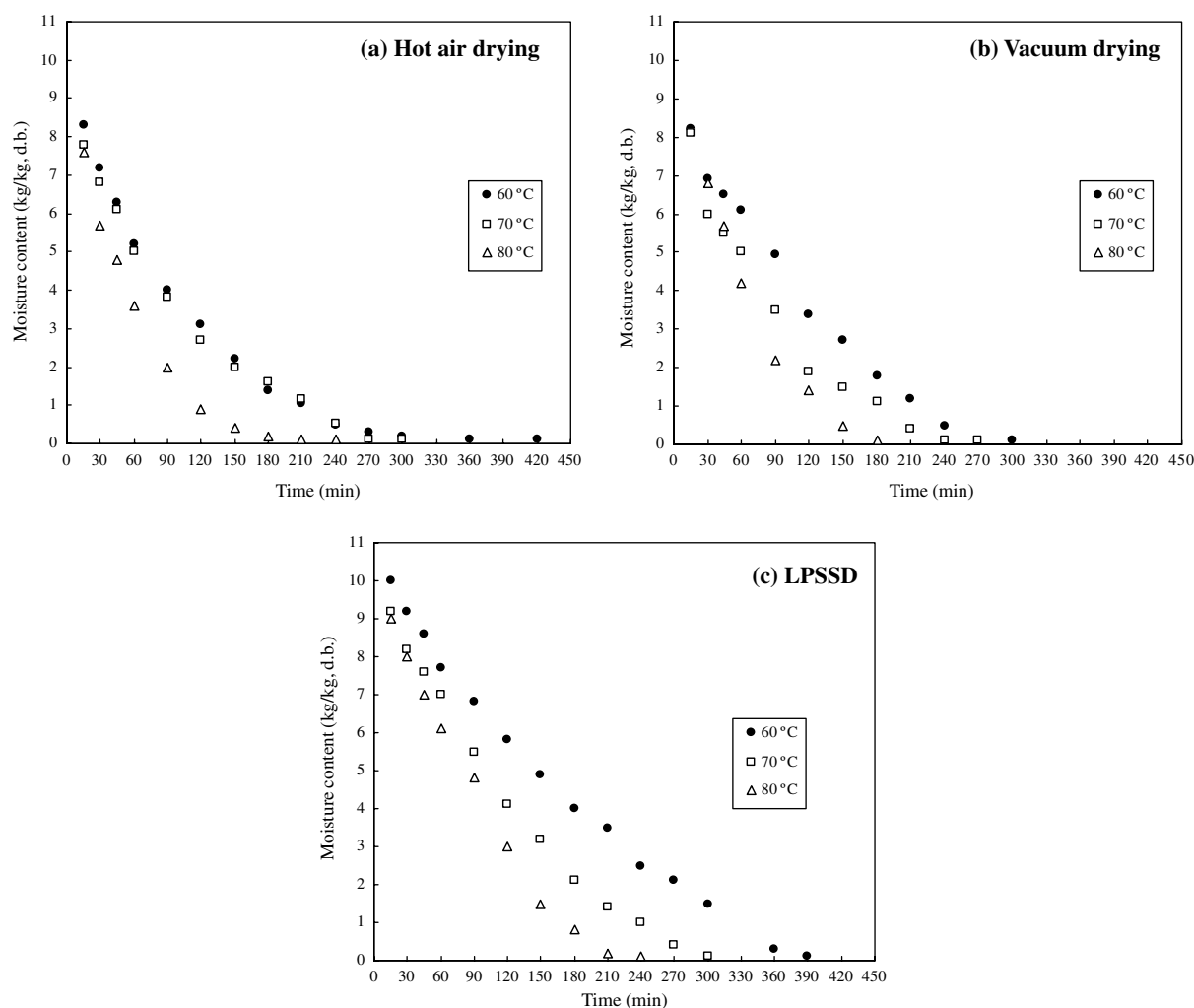


Fig. 4. Drying curves of carrots subjected to various drying treatments.

In the case of hot air drying, it took as much time to dry carrots to the final desired moisture content as did LPSSD. This is because the falling rate period of hot air drying was longer than that of LPSSD. The drying behaviour was characterised as follows: the drying rates increased with an increase in the drying temperature, due to an increased driving force for heat transfer, which is obviously related to mass transfer. Moisture diffusivities are also higher at higher temperatures.

3.2. Overall degradation kinetics of β -carotene

The β -carotene contents of fresh carrots varied slightly in the range of 68–76 mg/100 g (d.b.). The ratio of the β -carotene content of dried carrots to the fresh (β -carotene retention ratio) is therefore used to report the results in this study.

The β -carotene retention in carrots during hot air drying, vacuum drying and LPSSD is shown in Figs. 6–8, respectively. The β -carotene retention, in the case of hot air drying (Fig. 6), decreased continuously. It was observed, however, that the β -carotene retention at differ-

ent temperatures was only slightly different. The falling rate of β -carotene started at the moisture content around 5.5 kg/kg (d.b.), which corresponded to a carrot temperature of 45–60 °C (see also Figs. 4a and 5a). This is due to the fact that lipoxygenase, which is an aerobic catalyst of oxidation reactions, is activated at around 60 °C (Cui, Xu & Sun, 2004).

β -Carotene retention in the cases of vacuum drying and LPSSD (Figs. 7 and 8) was not significantly higher than that in the case of hot air drying. In the case of LPSSD, only slight changes, over the moisture content range of 3–8 kg/kg (d.b.), of β -carotene occurred due to the fact that the activities of lipoxygenase and peroxidase, which are responsible for the oxidative degradation of β -carotene, were reduced due to many effects, including the absence of oxygen in the drying chamber and the lower product temperature (Fig. 5a, b, c). At moisture contents below 3 kg/kg (d.b.), β -carotene content started to decrease continuously. This is because the temperature of the carrots started to rise again (Fig. 5c); thermal degradation thus started to be significant.

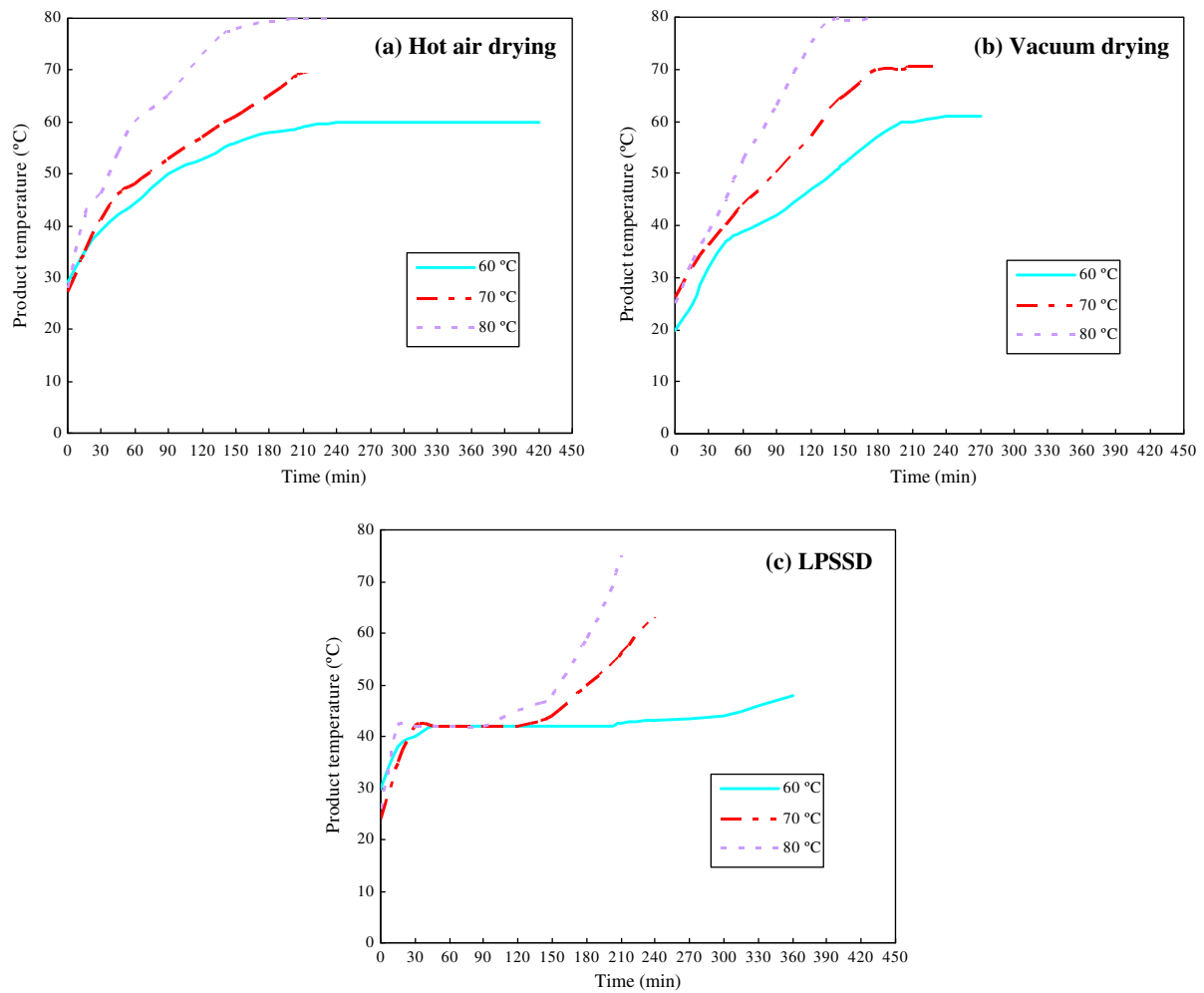


Fig. 5. Temperature profiles of carrots subjected to various drying treatments.

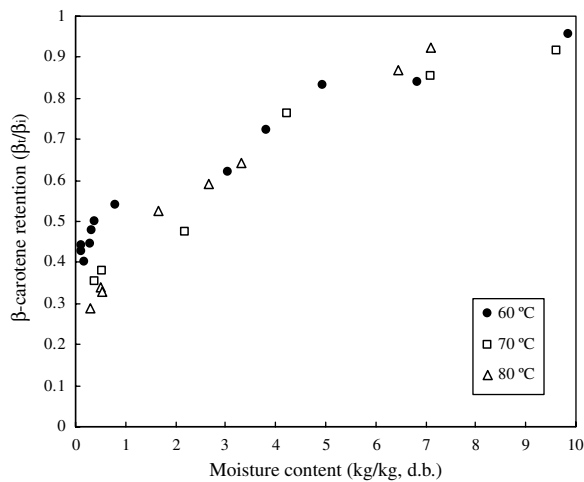


Fig. 6. Relationship between β -carotene retention and moisture content of carrots undergoing hot air drying.

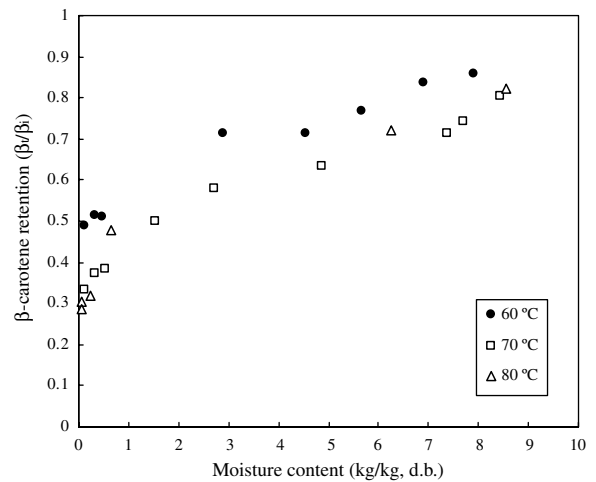


Fig. 7. Relationship between β -carotene retention and moisture content of carrots undergoing vacuum drying.

In the case of vacuum drying, the trend of β -carotene degradation was similar to that of LPSSD. However, because the level of vacuum pressure used in this study was not too low (7 kPa absolute), there still existed

some oxygen that could participate in oxidation reactions. Higher temperatures, in comparison with the case of LPSSD (Figs. 5b and c) also led to more degradation.

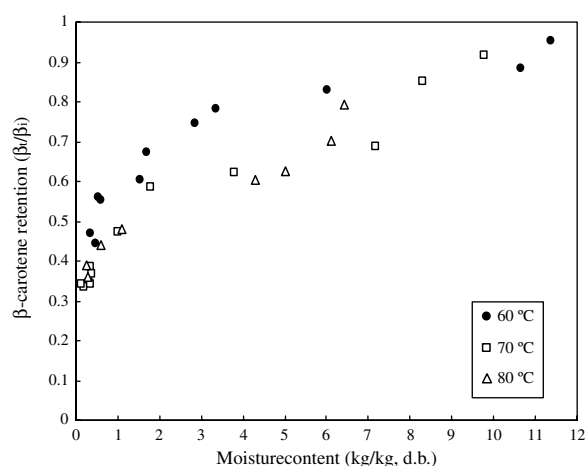


Fig. 8. Relationship between β -carotene retention and moisture content of carrots undergoing LPSSD.

3.3. Isomerisation kinetics of β -carotene

β -Carotene can be degraded either by thermal degradation or isomerisation degradation and it is known that thermal treatment promotes the formation of *cis*-isomers from all-*trans*- β -carotene in carrots (Sergio & Russell, 1999; Aman et al., 2005). In all dried (and drying) samples of this study, 13-*cis*- β -carotene was the only isomer detected by HPLC, as previously mentioned.

In the case of hot air drying (Table 1), 13-*cis*- β -carotene occurred when the product temperature, as seen in Fig. 5a, approached the drying air temperature, which was equal to or higher than 60 °C. Increased rates of isomerisation in this range of temperature are ascribed mainly to the elevated temperature, as also noted by Cui, Xu, and Sun (2004). However, the moisture contents of carrots when the formation of *cis*-isomer started were not much differ-

ent, i.e., 0.5, 0.4 and 0.5 kg/kg (d.b.) at 60, 70 and 80 °C, respectively. The *cis*-proportions were also not significantly different, in the range of 0.01–0.06.

For vacuum drying (Table 1), 13-*cis*- β -carotene occurred when the product temperature (Fig. 5b) was more than 50 °C. As can be seen from Table 1, the *cis*-isomer occurred at moisture contents lower than 1.8, 2.2 and 2.2 kg/kg (d.b.) at 60, 70 and 80 °C, respectively.

For LPSSD, the starting points of the formation of 13-*cis*-isomer are reported instead in terms of the elapsed drying time. As can be seen in Table 1 the formation of 13-*cis*-isomer started after 150, 120 and 60 min when drying was performed at 60, 70 and 80 °C, respectively. The formation of *cis*-isomer, in the case of LPSSD, started much earlier than in the case of hot air drying and vacuum drying. This is probably due to the fact that carrots were held at a constant temperature corresponding to the boiling point of water at 7 kPa (around 40 °C) for an extended period of time, compared with hot air drying and vacuum drying (Fig. 5c and Table 1). Normally, if the processing temperature is maintained for a long time (like in the case of pasteurisation or sterilisation), the formation of 13-*cis*- β -carotene increases (Marx et al., 2003).

The formation of 13-*cis*- β -carotene in the case of LPSSD started much earlier than in the cases of hot air drying and vacuum drying. However, as can be seen in Table 1, the proportions of 13-*cis*- β -carotene at various conditions were not significantly different, in the range of 0.01–0.1.

3.4. Antioxidant activities of β -carotene

The percent relative inhibition of β -carotene in carrots undergoing hot air drying, vacuum drying and LPSSD is shown in Table 2. Percent relative inhibition, in the case

Table 1
Formation of 13-*cis*- β -carotene during different drying conditions

Drying time (min)	<i>cis</i> -Proportion (<i>cis/trans</i>) ^a								
	Hot air drying			Vacuum drying			LPSSD		
	60 °C	70 °C	80 °C	60 °C	70 °C	80 °C	60 °C	70 °C	80 °C
60	n.d. ^b	n.d.	n.d.	n.d.	n.d.	n.d.	n.d.	n.d.	0.006 ± 0.003
90	n.d.	n.d.	n.d.	n.d.	n.d.	0.019	n.d.	n.d.	0.013 ± 0.001
120	n.d.	n.d.	n.d.	n.d.	0.017 ± 0.012	0.030 ± 0.028	n.d.	0.005	0.026 ± 0.003
150	n.d.	n.d.	0.03	0.016 ± 0.009	0.018 ± 0.005	0.017 ± 0.002	0.004	0.014	0.023 ± 0.004
180	n.d.	0.017 ± 0.004	0.067 ± 0.031	0.019 ± 0.002	0.035 ± 0.012	0.055 ± 0.015	0.006	0.007 ± 0.001	0.052 ± 0.037
210	n.d.	0.038 ± 0.029		0.014 ± 0.008	0.029 ± 0.003		0.009 ± 0.007	0.027	0.072 ± 0.036
240	n.d.	0.036 ± 0.024		0.015	0.031 ± 0.008		0.008 ± 0.002	0.016 ± 0.007	
270	n.d.	0.034 ± 0.004		0.019 ± 0.004	0.030		0.006 ± 0.002	0.024 ± 0.005	
300	0.049	0.049		0.021 ± 0.002			0.016 ± 0.002	0.032 ± 0.016	
330	0.047						0.01 ± 0.002	0.028 ± 0.005	
360	0.036						0.021 ± 0.001		
390	0.024 ± 0.021						0.023 ± 0.012		
420	0.026 ± 0.018						0.011 ± 0.001		
450	0.009								
480	0.016								

^a Mean ± SD of two replicates.

^b n.d. = not detectable; *cis*-isomers calculated as percentage of all-*trans*- β -carotene.

Table 2

Antioxidant activities of various combinations (or proportions) of isomers of β -carotene in carrots (during different drying conditions) in terms of % relative inhibition

Drying time (min)	% Relative inhibition ^a								
	Hot air drying			Vacuum drying			LPSSD		
	60 °C	70 °C	80 °C	60 °C	70 °C	80 °C	60 °C	70 °C	80 °C
15	0.896 ± 0.039	0.813 ± 0.139	0.806 ± 0.014	0.806 ± 0.101	0.715 ± 0.085	0.784 ± 0.098	0.938 ± 0.008	0.787 ± 0.074	0.798 ± 0.038
30	0.849 ± 0.018	0.842 ± 0.052	0.787 ± 0.054	0.718 ± 0.085	0.560 ± 0.045	0.639 ± 0.056	0.857 ± 0.158	0.908 ± 0.011	0.742 ± 0.153
45	0.853 ± 0.058	0.795 ± 0.027	0.547 ± 0.245	0.814 ± 0.105	0.643 ± 0.008	0.613 ± 0.070	0.869 ± 0.075	0.814 ± 0.079	0.719 ± 0.096
60	0.864 ± 0.011	0.852 ± 0.179	0.693 ± 0.062	0.739 ± 0.060	0.680 ± 0.183	0.606 ± 0.038	0.824 ± 0.175	0.930 ± 0.029	0.712 ± 0.167
90	0.775 ± 0.042	0.682 ± 0.266	0.489 ± 0.235	0.631 ± 0.008	0.450 ± 0.057	0.534 ± 0.152	0.789 ± 0.267	0.832 ± 0.084	0.678 ± 0.169
120	0.776 ± 0.032	0.685 ± 0.239	0.473 ± 0.039	0.698 ± 0.011	0.566 ± 0.195	0.589 ± 0.145	0.777 ± 0.109	0.757 ± 0.017	0.578 ± 0.253
150	0.723 ± 0.154	0.706 ± 0.277	0.735 ± 0.268	0.527 ± 0.080	0.501 ± 0.108	0.507 ± 0.162	0.766 ± 0.174	0.762 ± 0.045	0.597 ± 0.109
180	0.633 ± 0.142	0.643 ± 0.040	0.585 ± 0.100	0.544 ± 0.006	0.570 ± 0.100		0.779 ± 0.122	0.770 ± 0.070	0.539 ± 0.225
210	0.709 ± 0.214	0.580 ± 0.269	0.433 ± 0.146	0.561 ± 0.099	0.587 ± 0.197		0.683 ± 0.152	0.692 ± 0.191	0.562 ± 0.027
240	0.788 ± 0.113	0.494 ± 0.459		0.589 ± 0.109	0.509 ± 0.145		0.647 ± 0.203	0.642 ± 0.072	
270	0.725 ± 0.085	0.492 ± 0.116		0.556 ± 0.035			0.634 ± 0.138	0.647 ± 0.024	
300	0.630 ± 0.062	0.482 ± 0.398					0.654 ± 0.148	0.595 ± 0.154	
330	0.638 ± 0.157						0.684 ± 0.066	0.676 ± 0.036	
360	0.656 ± 0.097						0.621 ± 0.149		
390	0.685 ± 0.087						0.647 ± 0.131		
420	0.591 ± 0.011						0.621 ± 0.038		
450	0.587 ± 0.169								
480	0.323 ± 0.025								

^a Mean ± SD of two replicates.

of hot air drying, decreased continuously with decreasing moisture content. A significant drop in the % relative inhibition started at a moisture content around 1 kg/kg (d.b.), which corresponded to a β -carotene retention (Fig. 6) of about 55%. This early drop in antioxidant activities (as compared with the cases of vacuum drying and LPSSD, as will be discussed shortly) is due to the fact that the antioxidant activity of β -carotene depends on the oxygen tension presented in the system and hot air drying is the most obvious aerobic process in the present study (Burton & Ingold, 1984; Stahl & Sies, 2003).

For vacuum drying and LPSSD (Table 2), % relative inhibition remained almost constant over the moisture ranges of 1–10 and 2–12 kg/kg (d.b.), respectively. However, in the case of vacuum drying, a drop in the activities could be observed at moisture contents lower than 1 kg/kg (d.b.). As can be seen also from Fig. 7 over the moisture content range of 0.1–1 kg/kg (d.b.), a dropping period of % relative inhibition started when the β -carotene retention was around 30%. In the case of LPSSD (Table 2), a dropping period started when the moisture content was around 2 kg/kg (d.b.), which corresponded to a β -carotene retention of around 35% (Fig. 8).

In the case of vacuum drying and LPSSD (Table 2), the % relative inhibition at low moisture content was higher than in the case of hot air drying. At the final moisture content of 0.1 kg/kg (d.b.), the losses in the % relative inhibition were about 50% and 45% in the case of vacuum drying and LPSSD, respectively, while in the case of hot air drying the loss was about 70%. This is due to the low oxygen contents in the cases of vacuum drying and LPSSD.

Percent relative inhibition in the case of hot air drying implied lower antioxidant activities at the final moisture

content of 0.1 kg/kg (d.b.) than in the cases of vacuum drying and LPSSD. This result corresponded to the previously mentioned results of the isomerisation kinetics of β -carotene, in which LPSSD and vacuum drying could better preserve β -carotene than hot air drying by partially converting all-*trans*- β -carotene into 13-*cis*- β -carotene. In the present study, however, the formation of 13-*cis*- β -carotene in all cases did not much affect the antioxidant activities of various combinations of isomers of β -carotene. It can be seen from Table 1 that the relative amounts of 13-*cis*- β -carotene at various conditions were not significantly different, in the range of 0.01–0.1.

4. Conclusions

The isomerisation kinetics of β -carotene in carrots undergoing hot air drying, vacuum drying and LPSSD were investigated in this study. It was found that vacuum drying and LPSSD led to more conversion of all-*trans*- β -carotene to 13-*cis*- β -carotene, while total degradation, vacuum drying and LPSSD led to less total degradation of β -carotene than hot air drying.

Antioxidant activities of various combinations (or proportions) of isomers of β -carotene in carrots undergoing different drying techniques were determined using the TEAC assay. It was found that carrots undergoing LPSSD had higher antioxidant activity than those subjected to the other drying treatments. It could thus be concluded that, at the final moisture content of 0.1 kg/kg (d.b.), LPSSD at 60 °C was the best treatment to preserve β -carotene and antioxidant activities of carrots.

Since the drop in the total β -carotene retention at various drying conditions tended to occur more significantly

than the formation of 13-*cis*- β -carotene, the thermal degradation was noted to be more important than isomerisation degradation.

Acknowledgements

The authors express their sincere appreciation to the Commission on Higher Education, the Thailand Research Fund (TRF), and the International Foundation for Science (IFS) in Sweden for supporting this study financially.

References

- Aman, R., Schieber, A., & Carle, R. (2005). Effects of heating and illumination on *trans-cis* isomerization and degradation of β -carotene and lutein in isolated spinach chloroplasts. *Journal of Agricultural and Food Chemistry*, 53, 9512–9518.
- Bohm, V., Puspitasari-Nienaber, N., Ferruzzi, M. G., & Schwartz, S. J. (2002). Trolox equivalent antioxidant capacity of different geometrical isomers of α -carotene, β -carotene, lycopene and zeaxanthin. *Journal of Agricultural and Food Chemistry*, 50, 221–226.
- Burton, G. W., & Ingold, K. U. (1984). β -Carotene: An unusual type of lipid antioxidant. *Science*, 224, 569–573.
- Chen, B. H., Peng, H. Y., & Chen, H. E. (1995). Changes of carotenoids, color and vitamin A contents during processing of carrot juices. *Journal of Agricultural and Food Chemistry*, 43, 1912–1918.
- Cui, Z. W., Xu, S. Y., & Sun, D. W. (2004). Effect of microwave-vacuum drying on the carotenoids retention of carrot slices and chlorophyll retention of Chinese chive leaves. *Drying Technology*, 22, 563–575.
- Devahastin, S., Suvarnakuta, P., Soponronnarit, S., & Mujumdar, A. S. (2004). A comparative study of low-pressure superheated steam and vacuum drying of a heat-sensitive material. *Drying Technology*, 22, 1845–1867.
- Dutta, D., Chaudhuri, U. R., & Chakraborty, R. (2005). Structure, health benefits, antioxidant property and processing and storage of carotenoids. *African Journal of Biotechnology*, 4, 1510–1520.
- Larson, R. A. (1988). The antioxidants of higher plants. *Phytochemistry*, 4, 969–978.
- Lessin, W. J., Catigani, G. L., & Schwartz, S. J. (1997). Quantification of *cis-trans* isomers of provitamin A carotenoids in fresh and processed fruits and vegetables. *Journal of Agricultural and Food Chemistry*, 45, 3728–3732.
- Marx, M., Stuparic, M., Schieber, A., & Carle, R. (2003). Effects of thermal processing on *trans-cis*-isomerization of β -carotene in carrot juices and carotene-containing preparations. *Food Chemistry*, 83, 609–617.
- Miller, N. J., Sampson, J., Candxias, L. P., Bramly, P. M., & Rice-Evans, C. A. (1996). Antioxidant activities of carotenes and xanthophylls. *FEBS Letters*, 384, 240–242.
- Patrick, L. (2000). β -Carotene: The controversy continues. *Alternative Medicine Review*, 5, 530–545.
- Rubatzky, V. E., Quiros, C. F., & Simon, P. W. (1999). *Carrots and related vegetable umbelliferae*. CABI: Oxon.
- Sergio, A. R. P., & Russell, M. R. (1999). β -carotene and other carotenoids as antioxidant. *Journal of the American College of Nutrition*, 18, 426–433.
- Stahl, W., & Sies, H. (2003). Antioxidant activity of carotenoids. *Molecular Aspects of Medicine*, 24, 345–351.
- Suvarnakuta, P., Devahastin, S., & Mujumdar, A. S. (2005). Drying kinetics and β -carotene degradation in carrot undergoing different drying processes. *Journal of Food Science*, 70, S520–S526.

Effects of drying methods and conditions on drying kinetics and quality of Indian gooseberry flake

Siporn Methakhup, Naphaporn Chiewchan*, Sakamon Devahastin

Department of Food Engineering, King Mongkut's University of Technology Thonburi, 91 Pracha u-tid Road, Bangkok 10140, Thailand

Received 10 June 2004; received in revised form 10 August 2004; accepted 11 August 2004

Abstract

Vacuum drying and low-pressure superheated steam drying (LPSSD) of Indian gooseberry flake (used to prepare Indian gooseberry tea) were carried out at various drying conditions to monitor the drying kinetics and quality degradation of the product during drying. In terms of drying kinetics, the vacuum drying took shorter time to dry the product than LPSSD at every drying condition. In terms of quality, it was found that only the product subjected to vacuum drying at 75 °C and absolute pressure of 7 kPa had similar level of ascorbic acid retention compared to those samples of LPSSD at every condition. The total color difference of this sample was, however, slightly higher than that of product dried by LPSSD. Nevertheless, since the color changes were not of much concern to the consumers of Indian gooseberry tea, vacuum drying at 75 °C and 7 kPa was proposed as the most favorable condition for drying of Indian gooseberry flake in terms of energy consumption.

© 2004 Swiss Society of Food Science and Technology. Published by Elsevier Ltd. All rights reserved.

Keywords: Ascorbic acid; Color; Low-pressure superheated steam drying; Page's equation; Vacuum drying

1. Introduction

Indian gooseberry (*Phyllanthus emblica* Linn.) or “Ma-khaam Pom” in Thai (Chatchavalchokchai, 1987) is indigenous in tropical Southeast Asia, including Thailand, and is known as a rich source of vitamin C. The fruit is commonly consumed as a health food in both fresh and various preserved forms such as pickles, dried fruits, and beverage products (Montri, 1998).

Indian gooseberry tea is an alternative product to instant beverage powder and pasteurized juice. It is usually consumed for thirst quenching. In Indian gooseberry tea processing, drying is the main thermal treatment, which affects the quality of the product such as its ascorbic acid content and color. This quality loss has an influence on the consumer satisfaction. Therefore, a suitable drying process, which involves an

identification of a suitable drying method and conditions, is important to minimize the quality loss of the product.

Vacuum drying has been applied widely to dry various heat-sensitive products in which qualities such as color, texture and various vitamins are deteriorated at elevated temperatures. Drouzas and Schubert (1996) studied drying of banana using microwave-vacuum drying at pressures of 15–300 mbar (1.5–30 kPa) and at magnetron levels of 150–850 W. The results showed no significant variations as far as the drying rates under different pressures were concerned. Moreover, better product quality (as examined by taste, aroma, smell and rehydration tests) was also obtained when using higher levels of vacuum. Markowski and Bialobrzewski (1997) studied the drying kinetics of celery slice (10 mm thick, 57 mm diameter) using vacuum drying. Experiments were carried out at temperatures in the range of 25–50 °C and the pressure inside the drying chamber was maintained at 10 ± 0.2 kPa. The results showed no

*Corresponding author. Tel.: +662-470-9243; fax: +662-470-9240.
E-mail address: naphaporn.rat@kmutt.ac.th (N. Chiewchan).

constant drying rate period in all cases. The samples dried at lower temperature level re-adsorbed more water than those dried at higher temperatures. The results also proved that vacuum drying could be used for preservation of high quality celery slices in terms of color and flavor. More recently, [Jaya and Das \(2003\)](#) studied the vacuum drying of mango pulp of various thicknesses (2, 3, and 4 mm) and temperatures (65, 70, and 75 °C) under 30–50 mm of mercury absolute pressure. A mathematical model based on the moisture diffusivity of the drying product was found to give close prediction of moisture content of the pulp at different times of drying. Color change of reconstituted pulp was found to depend more on the pulp thickness than the drying temperature.

Recently, a novel concept of low-pressure superheated steam drying (LPSSD) has been proposed as an alternative to drying heat-sensitive products since it can combine the advantages of drying at reduced temperature to those of conventional superheated steam drying ([Mujumdar & Devahastin, 2000](#)). [Elustondo, Elustondo, and Urbicain \(2001\)](#) studied sub-atmospheric pressure superheated steam drying of foodstuffs at pressures of 10,000–20,000 Pa, temperatures of 60–90 °C and steam circulating velocities of 2–6 m/s. A semi-empirical mathematical model was also developed and a simplified expression, which had two experimentally determined parameters, was derived and used to predict the drying rates of tested samples. A model proposed was found to predict the drying kinetics reasonably well. No mention about the dried product quality was given, however. [Devahastin, Suvarnakuta, Soponronnarit, and Mujumdar \(2004\)](#) studied the drying kinetics and various quality parameters of the dried carrot cubes undergoing both LPSSD and vacuum drying. Effects of pressure (absolute of 7–10 kPa) and temperature (60–80 °C) on the drying characteristics as well as quality attributes, i.e. volume, shrinkage, apparent density, color and rehydration behavior, of the dried product subjected to the two drying processes were also evaluated and compared. Although LPSSD required longer dwell time to achieve the same final moisture content than vacuum drying, some of the quality attributes were superior to those obtained in vacuum drying.

However, no data are available, either in terms of the drying kinetics and quality of Indian gooseberry undergoing either of these drying techniques. Therefore, the aim of this work was to study the drying kinetics as well as the quality degradation (in terms of ascorbic acid and color degradation) of Indian gooseberry flake undergoing both vacuum and LPSSD. The information obtained could be used to design an appropriate drying process to minimize the quality degradation of Indian gooseberry flake, which is used as the main ingredient of Indian gooseberry tea.

2. Material and methods

2.1. Experimental setup

A schematic diagram of the low-pressure superheated steam dryer and its accessories is shown in [Fig. 1](#). The dryer consists of a stainless steel drying chamber, insulated with rock wool; a steam reservoir, which received the steam from the boiler; and a liquid ring vacuum pump (Nash, ET32030, Germany), which was used to maintain the vacuum in the drying chamber. Steam trap was installed to reduce the excess steam condensation in the reservoir. An electric heater was controlled by a PID controller (Omron, E5CN, Japan). A variable-speed electric fan was used to disperse steam throughout the drying chamber. The steam inlet was made into a cone shape and was covered with a screen to help distributing the steam in the chamber. The change of the mass of the sample was detected continuously using a load cell (Minebea, Ucg-3 kg, Japan). The temperatures of the steam and of the drying sample were also measured continuously using type K thermocouples. Thermocouple signals were multiplexed to a data acquisition card (Omega Engineering, CIO-DAS16Jr., USA) installed in a PC. LABTECH NOTEBOOK software (version 12.1, Laboratory Technologies Corp., USA) was then used to read and record the temperature data. More detailed experimental setup could be referred in [Devahastin et al. \(2004\)](#). The same experimental setup was also used for vacuum drying experiments but without the application of steam to the drying chamber.

2.2. Experimental procedure

Fresh Indian gooseberry fruit was purchased from a local market and stored in a refrigerator at 5 °C. After rinsing the fruit, its seeds were removed using a stainless-steel knife. The flesh was cut into small pieces and blended for 1 min using a blender (Moulinex, AS184, France). Forty grams of the prepared sample was spread on a sample holder, which was made of an aluminum foil. The sample was then dried either by a vacuum or a low-pressure superheated steam dryer at temperatures of 65 and 75 °C and absolute pressures of 7, 10 and 13 kPa. During drying mass of samples was recorded at every 10 min interval. The dryer was operated until the mass of the sample reached its equilibrium value. The sample was then dried in a hot air oven (Mettler, ULM 600 II, Germany) at 105 °C until its mass, which was measured by a digital balance (Sartorius, RC 250S, Germany), was constant in order to obtain its bone-dry mass. Page's equation was used to fit the experimental data to calculate the drying time required for reducing the moisture content of Indian gooseberry flake to 7.5% (d.b.). This final moisture content was selected since it is

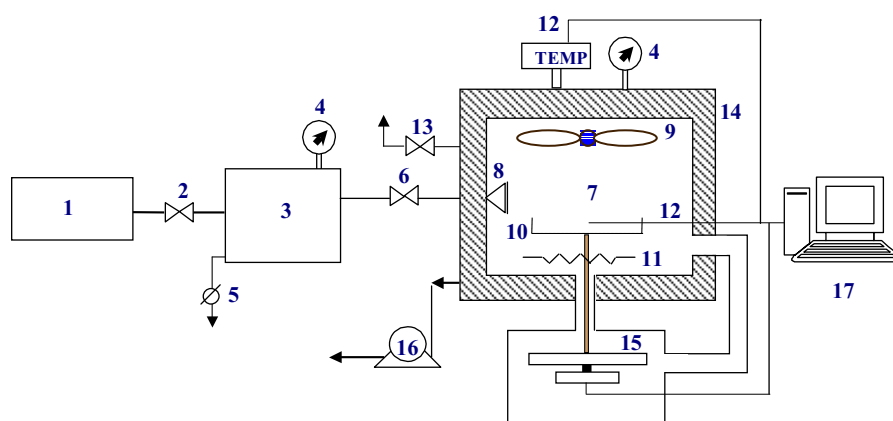


Fig. 1. Schematic diagram of low-pressure superheated steam dryer and associated units. 1, boiler; 2, steam valve; 3, steam reservoir; 4, pressure gauge; 5, steam trap; 6, steam regulator; 7, drying chamber; 8, steam inlet and distributor; 9, electric fan; 10, sample holder; 11, electric heater; 12, on-line temperature sensor and logger; 13, vacuum break-up valve; 14, insulator; 15, on-line mass indicator and logger; 16, vacuum pump; 17, PC with installed data acquisition card.

the maximum allowable final moisture content of a similar product, i.e., black tea (Thai Industrial Standard Institute (TISI), 1983). The new set of prepared sample, which had a pH value (measured by a pH meter, Tüv Rheinland, CG 841, Germany) in the range of 2.2–2.7, was dried again at the same conditions until its moisture content reached 7.5% (d.b.) using the time estimated from Page's equation. Moisture content (Association of Official Analytical Chemists, (AOAC), 1990), ascorbic acid and color of fresh and dried Indian gooseberry flake were measured. All experiments were performed in duplicate.

2.3. Total ascorbic acid (TAA) determination

TAA was measured by Roe and Kuther's method (Damrongnukool, 2000). The assay estimates the intensity of osazone formed by the coupling of 2,4-dinitrophenylhydrazine (DNPH) with the oxidative forms of ascorbic acid, which are dehydroascorbic acid (DHAA) and diketogulonic acid (DKGA), using a spectrophotometer (Shimadzu, UV-2101 PC, Japan).

2.4. Color measurement

The colors of fresh and dried Indian gooseberry flake were measured by a colorimeter (JUKI, JP7100, Japan) with 2° North skylight as the light source. The colorimeter was calibrated against a standard white plate for powder ($L = 91.78$, $a = -0.28$, $b = 0.07$) before each measurement. A glass cylinder containing fresh/dried Indian gooseberry flake was placed above the light source and covered with a lid. Three Hunter parameters, namely L (lightness), a (redness/greenness), and b (yellowness/blueness) were measured and the total color difference (ΔE) was calculated from ΔL , Δa and Δb values.

2.5. Statistical analysis

The data were analysed and presented as mean values with standard deviations. Differences between mean values were established using Duncan's-multiple range tests. Values were considered at 95% level of significance ($\alpha < 0.05$) and a statistical program SPSS was used to perform the calculation.

3. Results and discussion

3.1. Drying kinetics of Indian gooseberry flake

The drying curves of Indian gooseberry flake (initial moisture content of 380–470% d.b.) undergoing different drying techniques at various conditions are shown in Figs. 2–4. Moisture ratio (MR) of sample were fitted to Page's equation as follows:

$$MR = \frac{M_t - M_{eq}}{M_i - M_{eq}} = \exp(-Kt^N), \quad (1)$$

where MR is the moisture ratio; M_t is the moisture content at time t (kg/kg); M_{eq} is the equilibrium moisture content (kg/kg); M_i is the initial moisture content (kg/kg); K is the drying constant; N is the degree of nonlinearity of the drying curve.

Fig. 2 shows the drying curves of Indian gooseberry dried by vacuum drying. The dehydration times for reaching the equilibrium moisture contents (4.2–5.7% d.b.) were approximately 200, 210 and 230 min when using the drying temperature of 65 °C and absolute pressures of 7, 10 and 13 kPa, respectively. For drying at 75 °C at the same levels of absolute pressure, the drying times to reach the equilibrium moisture contents (2.4–3.8% d.b.) were reduced by roughly 20%, namely, 160, 170 and 190 min, respectively. This is due to the fact

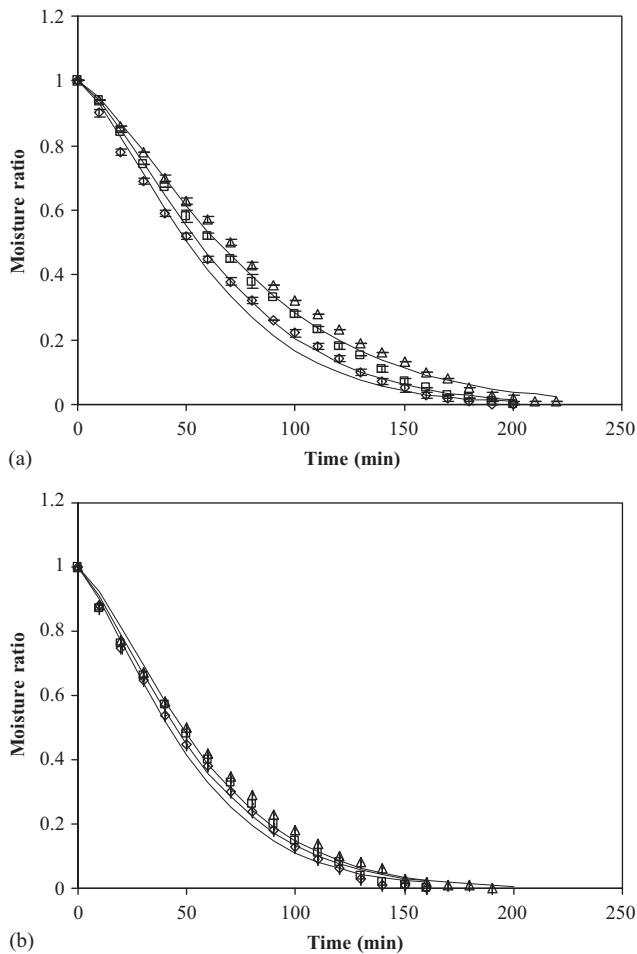


Fig. 2. Drying curves of Indian gooseberry flake undergoing vacuum drying at temperatures (a) 65 °C and (b) 75 °C; absolute pressures of 7 kPa (\diamond), 10 kPa (\square) and 13 kPa (\triangle). Solid line (—) represents curve fitting using Page's equation.

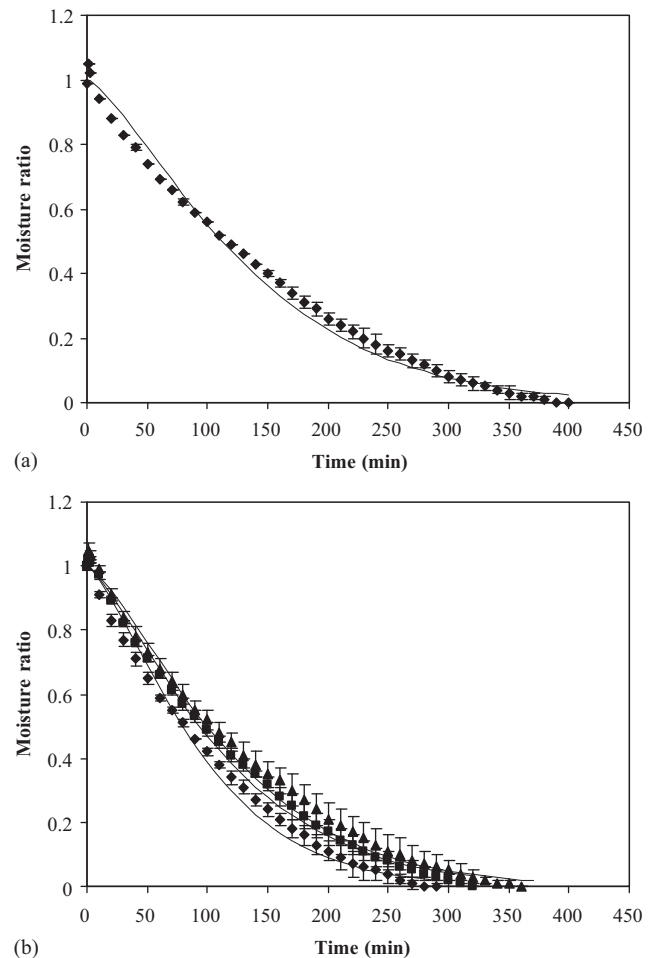


Fig. 3. Drying curves of Indian gooseberry flake undergoing LPSSD at temperatures (a) 65 °C and (b) 75 °C; absolute pressures of 7 kPa (\diamond), 10 kPa (\blacksquare) and 13 kPa (\blacktriangle). Solid line (—) represents curve fitting using Page's equation.

that drying at higher temperature implied a larger driving force for heat transfer, which was, in this case, the temperature difference between the drying medium and the temperature close to the wet-bulb temperature since the chamber was not at low-enough pressure and the effect of convection (due to the fan) was still significantly present. A higher drying temperature also led to a higher value of moisture diffusivity. In addition, it has also been reported by [Prabhanjan, Ramaswamy, and Raghavan \(1995\)](#) that the higher drying temperature provided a larger water vapor pressure deficit or the difference between the saturated water vapor pressure and partial pressure of water vapor in air at a given temperature, which is one of the driving forces for drying. Similar behavior was observed by [Jaya and Das \(2003\)](#).

It can also be seen in [Figs. 2\(a\) and \(b\)](#) that higher rates of drying were obtained when the absolute pressure of the dryer was decreased. This is because

decreasing of an absolute pressure resulted in a lower boiling point of water. The decrease of a boiling point of water resulted in an increase of the driving force for the outward moisture diffusion process. Hence, escaping of water molecules from the drying product became easier and faster.

[Fig. 3](#) shows the drying behavior of Indian gooseberry flake undergoing LPSSD at similar conditions to the vacuum drying reported earlier. It can be seen that during the first few minutes of superheated steam drying, there was an increase in moisture content of the sample due to the steam condensation on its surface. Such results are similar to the works reported by several investigators, e.g. [Tang and Cenkowski \(2000\)](#) and [Devahastin et al. \(2004\)](#).

Similar to drying in the vacuum system, the times needed to reach the equilibrium moisture content of Indian gooseberry flake dried at 65 °C were longer than those at 75 °C and lowering the absolute pressure could

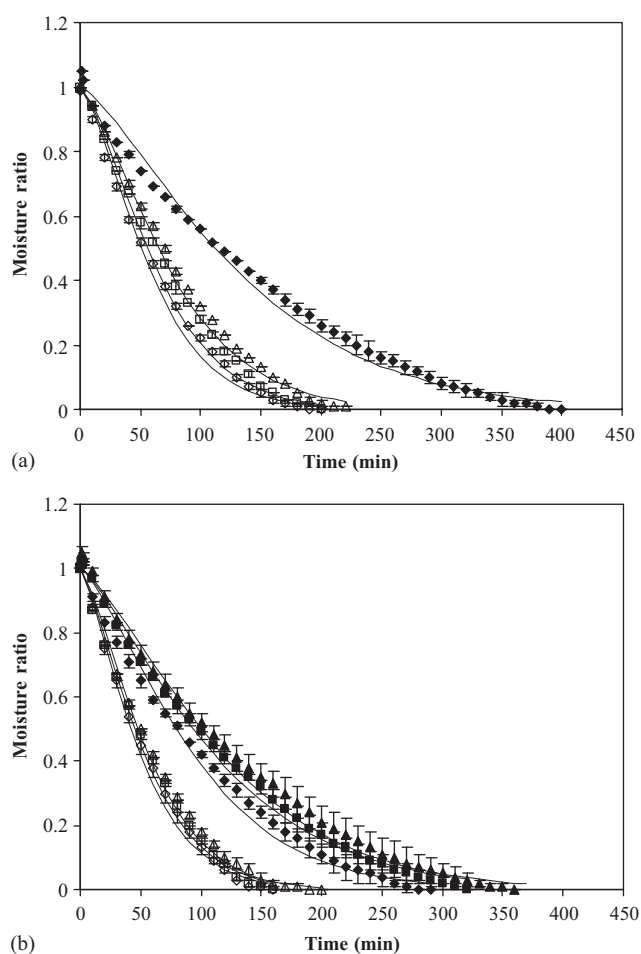


Fig. 4. Comparison of drying curves of Indian gooseberry flake at temperatures. (a) 65 °C and (b) 75 °C. Vacuum drying at 7 kPa (\diamond), 10 kPa (\square) and 13 kPa (\triangle). LPSSD at 7 kPa (\blacklozenge), 10 kPa (\blacksquare) and 13 kPa (\blacktriangle). Solid line (—) represents curve fitting using Page's equation.

reduce the moisture faster than doing so at higher absolute pressures. An increase of the absolute pressure caused the saturation temperature to increase and hence reduced the driving force for heat transfer and hence the reduced drying rates (Urbaniec & Malaczewski, 1997). From the experimental data, the time taken for the sample to reach its moisture content of 6.4% (d.b.) was approximately 400 min at 65 °C and at an absolute pressure of 7 kPa. For drying at 75 °C and absolute pressures of 7, 10 and 13 kPa, it took approximately 290, 330 and 370 min, respectively, to obtain the equilibrium moisture contents in the range of 4.4–6.1% (d.b.). Increasing the temperature from 65 to 75 °C at an absolute pressure of 7 kPa decreased the dehydration time by approximately 27.5%.

Fig. 4 compares the drying characteristics of Indian gooseberry flake undergoing vacuum drying and LPSSD at various conditions. It was found that after the condensation stage, the shape of the drying curves of LPSSD were very similar to those of vacuum drying.

However, the longer drying times were observed for the samples undergoing LPSSD. This is due to the existence of the condensation period and the lower evaporation rate of LPSSD than that of vacuum drying at these conditions.

As seen in Fig. 4(b), it was found that the impact of the operating pressure on the rate of moisture reduction was more pronounced in the case of LPSSD than in the case of vacuum drying.

3.2. Empirical modeling of the drying process

To describe the drying behavior of Indian gooseberry flake undergoing both types of drying processes a well-known Page's equation (Ramesh & Rao, 1996; Cronin & Kearney, 1998; Karathanos & Belessiotis, 1999) was used to fit the experimental data.

Table 1 lists the drying constants obtained by application of Page's equation to the experimental data. A good agreement was found between the experimental and fitted values with the R^2 -values of 0.9334–0.9862. It can be seen that K -values for vacuum drying were higher than LPSSD. This is because the moisture reduction rate of superheated steam drying was lower than that of vacuum drying at the conditions tested in this work.

Considering the two drying processes at the same temperature, parameter K of both LPSSD and vacuum drying decreased as the absolute pressure increased. This is due to the fact that a lower absolute pressure led to a lower boiling point of water. Thus, the evaporation of water from the sample was enhanced. At the same pressure, parameter K increased as temperature increased because an increase of the drying temperature increased the driving force of heat and mass transfer (through an increase of the value of moisture diffusivity). For parameter N , it did not possess a clear trend. The results for parameters K and N were similar as those found by Karathanos and Belessiotis (1999), Park, Vohnikova, and Brod (2002), and El-Aouar, Azoubel, and Murr (2003).

3.3. Quality degradation of Indian gooseberry flake

Table 2 shows the TAA content in fresh and dried Indian gooseberry flake samples. The average initial ascorbic acid content was about 1.04 g/100 g sample. The change of ascorbic acid was expressed as percentage of retention. The percentage of retention of TAA is calculated according to the following equation (Ramesh, Wolf, Tevini, & Jung, 2001):

$$\begin{aligned} \% \text{ Retention} &= \frac{(\text{mass of dried sample}) \times (\text{conc. of TAA in dried sample})}{(\text{mass of fresh sample}) \times (\text{conc. of TAA in fresh sample})} \quad (2) \end{aligned}$$

Table 1
Parameters of Page's equation and calculated drying times for various drying methods and conditions

Drying method	Condition		Page's parameter		R^2	Drying time to reach 7.5% (d.b.) (min)
	T (°C)	P_{abs} (kPa)	K ($\times 10^{-3} \text{ min}^{-1}$)	N		
VD ^a	65	7	2.86	1.4	0.9862	170
		10	2.4	1.41	0.9593	190
		13	2.29	1.37	0.9806	200
	75	7	5.02	1.32	0.9804	145
		10	4.24	1.36	0.9334	150
		13	3.33	1.38	0.9868	160
LPSSD ^b	65	7	1.3	1.33	0.9507	400
		10	—	—	—	—
		13	—	—	—	—
	75	7	1.89	1.35	0.9618	280
		10	1.59	1.35	0.9799	320
		13	1.45	1.34	0.9687	370

^aVD stands for vacuum drying.

^bLPSSD stands for low-pressure superheated steam drying.

All dried Indian gooseberry flake tended to lose some ascorbic acid as compared to the fresh one. The percentage of retention of ascorbic acid was in the range of 64–94% for vacuum drying and 93–96% for LPSSD. For vacuum drying, it was found that the ascorbic acid retention of the sample increased as the drying temperature increased. This may be due to the shorter drying time required to dry the samples to the desired moisture content (Jayaraman & Gupta, 1995; Maharaj & Sankat, 1996). However, the pressure had only a little effect on the ascorbic acid retention. This may be explained by the fact that the drying times were not much affected by the operating pressure and that the level of oxygen content (which caused the aerobic degradation of vitamin C) was not much different at different pressures.

For LPSSD, the ascorbic acid retention was not significantly different at different drying conditions even though the drying times were different. The results implied that no oxygen was available in the drying system and thus presented no effect on the ascorbic acid degradation during drying.

Generally, an increasing level of ascorbic acid degradation is resulted from slower drying methods (Nindo, Sun, Wang, Tang, & Powers, 2003). From the drying kinetics, it was found that drying by LPSSD took longer than vacuum drying at the same drying conditions. However, Table 2 shows that LPSSD could preserve ascorbic acid better than vacuum drying. This is because the level of ascorbic acid oxidation in the vacuum drying system was higher than in LPSSD. The ability to maintain vitamin C of the superheated steam drying system has, in fact, been reported earlier by other investigators (e.g. Moreira, 2001).

The effects of drying methods and conditions on the color of the sample were also determined. Table 3 shows the values of Hunter parameters (L, a, b) and the total color difference (ΔE) of Indian gooseberry flake. It was found that LPSSD and vacuum drying at every condition resulted in a decrease of an L-value and an increase of an a-value of dried sample compared with the fresh one. However, b-value of the dried sample was similar to that of fresh sample. These results implied that the browning reaction and pigment destruction occurred in the dried sample (Iyota, Nishimura, Nomura, Konishi, & Yoshida, 2002; Maskan, 2001; Maskan, Kaya, & Maskan, 2002). However, the overview of color changes of sample could be observed from the ΔE value, which is calculated using Eq. (3).

$$\Delta E = [(\Delta L)^2 + (\Delta a)^2 + (\Delta b)^2]^{1/2}. \quad (3)$$

In the vacuum drying system, drying at 65 °C and an absolute pressure of 7 kPa could preserve the color of the sample better than at other conditions. This is due to the fact that the main cause of color change in vacuum drying was chlorophyll degradation and nonenzymatic browning reaction, which is Maillard reaction and ascorbic acid oxidation since oxygen and light, which are the causes of these reactions existed at the lowest level in the system. Because Maillard reaction depends on temperature and duration of heat treatment (Chua, Hawlader, Chou, & Ho, 2002), drying at lower temperatures gave better color retention than drying at higher temperatures. However, there were no significant differences between drying at 65 °C, absolute pressures of 10 and 13 kPa and drying at 75 °C.

For LPSSD, it was found that there were no significant differences in terms of color between different drying conditions. In this case, the main cause of color change was the Maillard reaction. Other causes of color changes were the ascorbic acid and chlorophyll degradation. However, these degradations had negligible effect on the color of the sample when compared to Maillard reaction since the system had no oxygen.

When considering the color retention of the sample dried using two different methods, it was found that LPSSD could retain the color better than the vacuum

Table 2
Total ascorbic acid content of fresh and dried samples^a

Drying method	Conditions		Ascorbic acid (g/100 g)		% Retention
	<i>T</i> (°C)	<i>P</i> _{abs} (kPa)	Fresh	Dried	
VD ^b	65	7	1.08 _{±0.07}	3.67 _{±0.13}	71.52 ^{ab} _{±1.97}
		10	1.06 _{±0.09}	3.50 _{±0.25}	66.89 ^a _{±2.51}
		13	0.94 _{±0.05}	3.07 _{±0.30}	64.84 ^a _{±6.01}
	75	7	0.96 _{±0.02}	3.84 _{±0.18}	94.46 ^{cd} _{±2.57}
		10	0.99 _{±0.02}	3.72 _{±0.11}	89.46 ^c _{±2.78}
		13	0.98 _{±0.11}	3.34 _{±0.03}	78.13 ^b _{±2.83}
LPSSD ^c	65	7	1.05 _{±0.06}	3.99 _{±0.22}	93.46 ^{cd} _{±1.58}
		10	—	—	—
		13	—	—	—
	75	7	1.06 _{±0.04}	4.04 _{±0.08}	95.35 ^d _{±3.49}
		10	1.09 _{±0.08}	4.03 _{±0.11}	95.67 ^d _{±2.10}
		13	1.04 _{±0.08}	3.99 _{±0.11}	94.96 ^{cd} _{±2.14}

^aMean \pm SD ($n=2$). Means in the same column having the same letter are not significantly different ($\alpha < 0.05$).

^bVD stands for vacuum drying.

^cLPSSD stands for low-pressure superheated steam drying.

drying system. This is because the degree of ascorbic acid and chlorophyll degradation of LPSSD was much lower than that of the vacuum drying system.

The color results presented here are somewhat different from those studied in potato drying by [Iyota et al. \(2002\)](#) who reported that potato dried in superheated steam at temperatures ranging from 170 to 240 °C were glossier and reddish than that dried in hot air drying. This is due to the effect of high temperature used and also the effect of the amount of soluble polysaccharides available in potato.

Since for Indian gooseberry tea production, dried Indian gooseberry flake was filled in a tea bag before it was soaked into water by a consumer, the color of the dried product was not of much concern in this study. Therefore, it could be concluded that drying in the vacuum system at temperature of 75 °C and absolute pressure of 7 kPa was most suitable for Indian gooseberry flake. This is because these conditions gave the highest ascorbic acid retention while the color did not change much from the natural sample. Further, vacuum drying at 75 °C and absolute pressure 7 kPa also had the shortest drying time.

4. Conclusion

The effects of drying methods and conditions on the drying kinetics and quality degradation of Indian gooseberry flake were examined in this study. The drying temperature was found to have an effect on the moisture reduction rates of samples dried both by vacuum drying and LPSSD. However, pressure seemed to have an obvious effect only for LPSSD. Further, it was found that vacuum drying took shorter time to dry the product than that required by LPSSD at all drying conditions. The drying curves could be well fitted by Page's equation. For both LPSSD and vacuum drying, the drying constant *K* increased with an increase of temperature and a decrease of absolute pressure while the product constant *N* was not affected by these factors. Parameter *K* of vacuum drying was higher than that of LPSSD.

The quality studies showed that, except for vacuum drying at 75 °C and absolute pressures of 7 and 10 kPa, LPSSD could retain ascorbic acid better than the vacuum drying. In addition, LPSSD could preserve the color of the sample better than the vacuum drying at all

Table 3
Hunter parameters and total color difference (ΔE) of dried samples^a

Drying method	Conditions		$\Delta L/L_0$	$\Delta a/a_0$	$\Delta b/b_0$	ΔE
	T (°C)	P_{abs} (kPa)				
VD ^b	65	7	0.06 \pm 0.00	−0.91 \pm 0.01	0.01 \pm 0.01	3.83 ^b \pm 0.09
		10	0.08 \pm 0.00	−1.39 \pm 0.07	0.02 \pm 0.02	5.40 ^{cd} \pm 0.10
		13	0.07 \pm 0.01	−0.98 \pm 0.22	0.00 \pm 0.04	4.99 ^c \pm 1.04
	75	7	0.08 \pm 0.00	−0.71 \pm 0.01	−0.02 \pm 0.01	5.61 ^{cd} \pm 0.28
		10	0.09 \pm 0.00	−1.11 \pm 0.01	−0.02 \pm 0.00	6.42 ^d \pm 0.26
		13	0.07 \pm 0.01	−1.56 \pm 0.58	0.03 \pm 0.02	5.38 ^{cd} \pm 0.66
LPSSD ^c	65	7	0.04 \pm 0.00	−0.88 \pm 0.97	0.04 \pm 0.01	3.09 ^{ab} \pm 0.19
		10	—	—	—	—
		13	—	—	—	—
	75	7	0.03 \pm 0.01	−0.64 \pm 0.04	0.04 \pm 0.02	2.48 ^a \pm 0.44
		10	0.04 \pm 0.00	−0.49 \pm 0.18	0.04 \pm 0.01	2.88 ^{ab} \pm 0.18
		13	0.04 \pm 0.04	−0.64 \pm 0.23	0.02 \pm 0.04	2.93 ^{ab} \pm 0.39

^aMean \pm SD ($n=2$). Means in the same column having a same letter are not significantly different ($\alpha < 0.05$).

^bVD stands for vacuum drying.

^cLPSSD stands for low-pressure superheated steam drying.

drying conditions tested. For vacuum drying, temperature had a significant effect on ascorbic acid content and color of the product while absolute pressure did not significantly affect the quality. For LPSSD, on the other hand, the drying conditions did not affect the ascorbic acid and color of dried product.

It could be concluded that drying in a vacuum system at a temperature of 75 °C, absolute pressure of 7 kPa was the most suitable condition for drying Indian gooseberry flake since this condition gave highest ascorbic acid retention while the color did not change much from the natural sample and had shortest drying time. However, in the case where the importance of color could not be neglected, the conclusion would be different from that obtained in this study.

Acknowledgements

The authors would like to express their appreciation to the Thailand Research Fund (TRF), National Research Council of Thailand and the International

Foundation for Science (Sweden) for supporting this study financially.

References

- Association of Official Analytical Chemists (AOAC). 1990. *Official method of analysis* (15th ed.). Virginia: Association of Official Analytical Chemists.
- Chatchavalchokchai, N. (1987). *Effect of some ruminants on seed quality of Phyllanthus emblica Linn., Elaeocarpus madopetalous Pierre, Spondias pinnata Kurz and Terminalia chebula Retz*. M.Sc. Thesis. Botany Program. Faculty of Science. Kasetsart University, Thailand.
- Chua, K. J., Hawlader, M. N. A., Chou, S. K., & Ho, J. C. (2002). On the study of time-varying temperature drying—effect on drying kinetics and product quality. *Drying Technology*, 20, 1559–1577.
- Cronin, K., & Kearney, S. (1998). Monte Carlo modelling of a vegetable tray dryer. *Journal of Food Engineering*, 35, 233–250.
- Damrongnukool, J. (2000). *Determination of vitamin C contents in commercial fruit juice*. M.Sc. Thesis. Home Economics Program. Faculty of Home Economics. Kasetsart University, Thailand.
- Devahastin, S., Suvarnakuta, P., Soponronnarit, S., & Mujumdar, A. S. (2004). A comparative study of low-pressure superheated steam and vacuum drying of a heat-sensitive material. *Drying Technology*, in press.

- Drouzas, A. E., & Schubert, H. (1996). Microwave application in vacuum drying of fruits. *Journal of Food Engineering*, 28, 203–209.
- El-Aouar, A. A., Azoubel, P. M., & Murr, F. E. X. (2003). Drying kinetics of fresh and osmotically pre-treated papaya (*Carica papaya* L.). *Journal of Food Engineering*, 59, 85–91.
- Elustondo, D., Elustondo, M. P., & Urbicain, M. J. (2001). Mathematical modeling of moisture evaporation from foodstuffs exposed to subatmospheric pressure superheated steam. *Journal of Food Engineering*, 49, 15–24.
- Iyota, H., Nishimura, N., Nomura, T., Konishi, Y., & Yoshida, K. (2002). Effect of initial steam condensation on color changes of potatoes during drying in superheated steam. *Proceedings of the 13th international drying symposium, Part B*, pp. 1352–1359.
- Jaya, S., & Das, H. (2003). A vacuum drying model for mango pulp. *Drying Technology*, 21, 1215–1234.
- Jayaraman, K. S., & Gupta, D. K. (1995). Drying of fruits and vegetables. In A.S. Mujumdar (Ed.), *Handbook of industrial drying* 2nd ed (pp. 643–687). New York: Marcel Dekker.
- Karathanos, V. T., & Belessiotis, V. G. (1999). Application of a thin-layer equation to drying data of fresh and semi-dried fruits. *Journal of Agricultural Engineering Research*, 74, 355–361.
- Maharaj, V., & Sankat, C. K. (1996). Quality changes in dehydrated dasheen leaves: Effects of blanching pre-treatments and drying conditions. *Food Research International*, 29, 563–568.
- Markowski, M., & Bialobrzewski, I. (1997). Celery slice vacuum drying kinetics. In R. Jowitt (Ed.), *Engineering & food at ICEF 7 Part 2* (pp. 93–96). Boston: Sheffield Academic Press.
- Maskan, M. (2001). Kinetics of colour change of kiwifruits during hot air and microwave drying. *Journal of Food Engineering*, 48, 169–175.
- Maskan, A., Kaya, S., & Maskan, M. (2002). Effect of concentration and drying process on color change of grape juice and leather (pestil). *Journal of Food Engineering*, 54, 75–80.
- Montri, N. (1998). *In vitro propagation of Phyllanthus emblica* L. M.Sc. Thesis. Horticulture Program. Faculty of Science. Kasetsart University, Thailand.
- Moreira, R. G. (2001). Impingement drying of foods using hot air and superheated steam. *Journal of Food Engineering*, 49, 291–295.
- Mujumdar, A. S., & Devahastin, S. (2000). Fundamental principles of drying. In S. Devahastin (Ed.), *Mujumdar's practical guide to industrial drying* (pp. 1–22). Brossard: Exergex Corp.
- Nindo, C. I., Sun, T., Wang, S. W., Tang, J., & Powers, J. R. (2003). Evaluation of drying technologies for retention of physical quality and antioxidants in asparagus (*Asparagus officinalis* L.). *Lebensmittel-Wissenschaft und-Technologie*, 36, 507–516.
- Park, K. J., Vohnikova, Z., & Brod, F. P. R. (2002). Evaluation of drying parameters and desorption isotherms of garden mint leaves (*Mentha crispa* L.). *Journal of Food Engineering*, 51, 193–199.
- Prabhanjan, D. G., Ramaswamy, H. S., & Raghavan, G. S. V. (1995). Microwave-assisted convective air drying of thin layer carrots. *Journal of Food Engineering*, 25, 283–293.
- Ramesh, M. N., & Rao, P. N. S. (1996). Drying studies of cooked rice in a vibrofluidised bed drier. *Journal of Food Engineering*, 27, 389–396.
- Ramesh, M. N., Wolf, W., Tevini, D., & Jung, G. (2001). Influence of processing parameters on the drying of spice paprika. *Journal of Food Engineering*, 49, 63–72.
- Tang, Z., & Cenkowski, S. (2000). Dehydration dynamics of potatoes in superheated steam and hot air. *Canadian Agricultural Engineering*, 42(1), 43–49.
- Thai Industrial Standard Institute. (1983). *Black tea* (14p).
- Urbaniec, K., & Malaczewski, J. (1997). Experimental investigations of beet pulp drying in superheated steam under pressure. *Drying Technology*, 15, 2005–2013.

Drying and heat transfer behavior of banana undergoing combined low-pressure superheated steam and far-infrared radiation drying

Chatchai Nimmol^{a,*}, Sakamon Devahastin^b, Thanit Swasdisevi^a, Somchart Soponronnarit^a

^a School of Energy, Environment and Materials, King Mongkut's University of Technology Thonburi, 126 Pracha u-tid Road, Bangkok 10140, Thailand

^b Department of Food Engineering, King Mongkut's University of Technology Thonburi, 126 Pracha u-tid Road, Bangkok 10140, Thailand

Received 15 January 2007; accepted 20 February 2007

Available online 4 March 2007

Abstract

The present study aimed at investigating the use of a drying system combining the concept of already proven low-pressure superheated steam drying and far-infrared radiation (LPSSD–FIR) for banana. The effects of various operating parameters, i.e., drying medium temperature and pressure, on the drying kinetics and heat transfer behavior of banana as well as the energy consumption of the process were investigated and discussed. Comparison was also made with similar sets of data obtained from the system with combined far-infrared radiation and vacuum drying (VACUUM–FIR) and the system using only low-pressure superheated steam drying (LPSSD). The results showed that LPSSD–FIR and VACUUM–FIR took shorter drying time compared to LPSSD at all drying conditions. In terms of the specific energy consumption, it was observed that the specific energy consumption of the vacuum pump was much higher than that of the far-infrared radiator or electric heater. It was also found that the specific energy consumption of LPSSD–FIR and VACUUM–FIR were lower than that of LPSSD at all drying conditions. Based on the drying rates and the specific energy consumption of all tested processes, LPSSD–FIR at 90 °C and 7 kPa was suggested.

© 2007 Elsevier Ltd. All rights reserved.

Keywords: Banana; Drying kinetics; Drying rates; Specific energy consumption; Vacuum drying

1. Introduction

Fresh banana perishes rapidly after harvesting and appropriate technology is generally applied to prolong its shelf life. Drying is one of the possible means that can be used to preserve banana from being deteriorated and also to reduce the cost of transportation and storage as well as to produce products that would not be able to obtain otherwise. There are many drying techniques available to dry banana. Most common techniques for drying banana are hot air drying [1–3]. However, hot air drying is a very energy-intensive operation and leads to much degradation of product quality. Microwave drying is an alternative means that can be used to dry banana [4]. Although the

drying process is accelerated with the use of microwave, some product quality is poor if microwave is not properly applied [5–7].

Recently, low-pressure (or subatmospheric-pressure) superheated steam drying (LPSSD) has been proposed and applied to many food products [8–10]. Since superheated steam in the case of LPSSD can be produced at the temperature lower than 100 °C due to reduced pressure environment, quality degradation of the products due to elevated temperature is alleviated. Generally, it has been shown that products dried by LPSSD have superior quality than those dried by conventional hot air and even vacuum drying. However, LPSSD is a rather slow drying process resulting in higher energy requirement. In order to reduce the energy requirement of the process, it is necessary to add an extra source of energy to the system. Far-infrared radiation (FIR), which has received much attention recently, is one possible means for the above purpose

* Corresponding author. Tel.: +66 2 470 8695; fax: +66 2 470 8663.
E-mail address: ccnimmol@gmail.com (C. Nimmol).

[11–13]. During FIR drying, the energy in the form of electromagnetic wave is absorbed directly by the product without loss to the environment leading to considerable energy savings [14–16].

To attain the advantages of the above-mentioned drying techniques, the combination of low-pressure superheated steam and far-infrared radiation drying is proposed as a novel drying technology for food and other biomaterials. In this study, the effects of various operating parameters, i.e., drying medium temperature and pressure, on the drying kinetics and heat transfer behavior of banana used as a model material as well as the energy consumption of the process were investigated and discussed. Comparison was also made with similar sets of data obtained from the system with combined far-infrared radiation and vacuum drying and from the system using LPSSD alone.

2. Experimental set-up, materials and methods

2.1. Experimental set-up

A schematic diagram of the combined low-pressure superheated steam and far-infrared radiation drying system is shown in Fig. 1. The dryer consists of a stainless steel drying chamber, insulated with rock wool, with inner dimensions of $45 \times 45 \times 45 \text{ cm}^3$; a steam reservoir, which received the steam from a boiler and maintained the steam pressure at around 200 kPa; a liquid ring vacuum pump (Nash, ET32030, Trumbull, CT), which was used to maintain the vacuum in the drying chamber; a far-infrared radiator (Infrapara, A-2T-500, Malaysia) rated at 500 W with a surface area of $60 \times 120 \text{ mm}^2$, which was used to supply thermal radiation to the drying sample and the drying medium; and electric heater rated at 1500 W, which was used to maintain the superheated steam temperature in the case of low-pressure superheated steam drying experiments. The distance between the far-infrared radiator and the sample holder, made of a stainless steel screen with dimensions of $15 \times 15 \text{ cm}^2$, was set at 165 mm.

The operation of the far-infrared radiator was controlled through the temperature of the drying medium

(air or superheated steam) measured at 30 mm above the sample surface, via the use of a proportional-integral-derivative (PID) controller (Shinko, JCS-33A-R/M, Japan) with an accuracy of $\pm 0.1^\circ\text{C}$. Similar to the far-infrared radiator, the operation of the electric heater was also controlled by a PID controller (Omron, model E5CN, Japan) with an accuracy of $\pm 0.1^\circ\text{C}$. The change of the mass of the sample during drying was detected continuously (at 1 min interval) using a load cell (Minebea, Ucg-3 kg, Nagano, Japan) with an accuracy of $\pm 0.2 \text{ g}$. The temperatures of the drying medium and of the drying sample were measured continuously using type K thermocouples. The thermocouple used to measure the drying medium temperature was located at the same position as the thermocouple that was used for sending the signal to the PID controller to control the far-infrared radiator. The thermocouples were partly covered with an aluminum foil acting as a radiation shield. The average surface temperature of the far-infrared radiator was also measured using a type K thermocouple. Thermocouple signals were multiplexed to a data acquisition card (Omega Engineering, CIO-DAS16Jr., Stamford, CT) installed in a PC. LABTECH NOTEBOOK software (version 12.1, Laboratory Technologies Corp., MA) was then used to read and record the temperature data.

2.2. Materials

Gros Michel banana (*Musa Sapientum* L.) was used as the tested material in this study. Fresh banana with an initial moisture content [17] in the range of 2.65–3.10 kg/kg (d.b.) and selected ripeness level of green tip (color index no. 5) was obtained from a local supermarket and stored at 4°C . Prior to the start of each experiment banana was peeled and sliced by a slicing machine to 3 mm thick. The sliced samples were then cut into 30 mm diameter using a die.

2.3. Methods

To perform a drying experiment approximately 16 pieces of prepared banana slices were placed on the sample

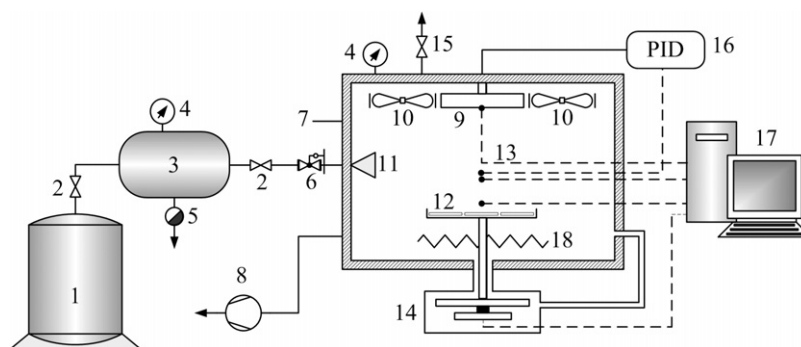


Fig. 1. A schematic diagram of the combined low-pressure superheated steam and far-infrared radiation drying system: (1) boiler, (2) steam valve, (3) steam reservoir, (4) pressure gauge, (5) steam trap, (6) steam regulator, (7) drying chamber, (8) vacuum pump, (9) far-infrared radiator, (10) electric fans, (11) steam inlet and distributor, (12) sample holder, (13) thermocouples, (14) load cell, (15) vacuum break-up valve, (16) PID controller, (17) PC with data acquisition card and (18) electric heater.

holder. To reduce the amount of steam condensation in the drying chamber during the start-up of a combined low-pressure superheated steam and far-infrared radiation drying (LPSSD–FIR) experiment, the far-infrared radiator was turned on to heat up the sample and to maintain the drying chamber temperature to the desired value without the application of steam to the drying chamber during the first 5 min of the drying process. The flow rate of steam into the drying chamber was maintained at about 26 kg/h and the speed of the electric fans was fixed at around 2100 rpm.

For a drying experiment using far-infrared radiation under vacuum (VACUUM–FIR) the same experimental set-up was used. Since the forced convection in the drying chamber led to lower temperatures of the far-infrared radiator and of the samples leading to lower drying rates, the electric fans were not used in this case.

For an experiment using LPSSD alone the same experimental set-up as that of LPSSD–FIR system was used. However, the electric heater located beneath the sample holder was used instead of the far-infrared radiator. Similar to LPSSD–FIR, preheating of the drying chamber was performed to reduce the initial condensation of steam.

The experiments were carried out at the drying medium (air or superheated steam) temperatures of 70, 80 and 90 °C and chamber absolute pressures of 7 and 10 kPa. Banana slices were dried until reaching their equilibrium moisture content at each operating condition. All experiments were performed in duplicate. It should be noted that the required final moisture content of banana slices should be lower than 0.035 kg/kg (d.b.).

2.4. Calculation of moisture ratio and drying rate

Because of the variation in initial moisture content of fresh banana, moisture ratio was used to describe the drying behavior of banana in this study. To calculate the drying rate, an appropriate empirical equation was fitted to the experimental moisture removal data (drying curve) and was then differentiated with respect to time. The moisture ratio and drying rate are defined as

$$MR = \frac{X - X_e}{X_i - X_e} \quad (1)$$

$$R = -\frac{dX}{dt} \quad (2)$$

where MR is the moisture ratio, R is the drying rate (kg kg^{-1} (d.b.) min^{-1}), X is the moisture content at any time (kg/kg (d.b.)), X_i is the initial moisture content (kg/kg (d.b.)), X_e is the equilibrium moisture content of sample (kg/kg (d.b.)) and t is time (min).

2.5. Evaluation of specific energy consumption and total steam consumption

In this study, the energy consumption of the drying processes, measured directly using a kilowatt-hour meter,

composed of the electric energy required to maintain the vacuum in the drying chamber and electric energy required to generate thermal energy. The former was the electric energy consumed by the vacuum pump and the latter was the energy consumed by the far-infrared radiator (for LPSSD–FIR and VACUUM–FIR) or the electric heater (for LPSSD), depending on the drying method employed. Since the electric fans consumed very small amount of electric energy, the energy consumption of the electric fans was neglected.

The efficiency of energy utilization during drying was evaluated through the specific energy consumption, which is the measure of the energy required during the process to remove 1 kg of water in the product being dried. The specific energy consumption of the vacuum pump and of the far-infrared radiator or electric heater was calculated by

$$SEC_{\text{vacuum}} = \frac{E_{\text{vacuum}}}{m_{\text{water}}} \quad (3)$$

$$SEC_{\text{radiator/heater}} = \frac{E_{\text{radiator/heater}}}{m_{\text{water}}} \quad (4)$$

where SEC_{vacuum} is the specific energy consumption of the vacuum pump (kWh/kg water), $SEC_{\text{radiator/heater}}$ is the specific energy consumption of the far-infrared radiator or electric heater (kWh/kg water), E_{vacuum} is the measured electric energy consumption of the vacuum pump (kWh), $E_{\text{radiator/heater}}$ is the measured electric energy consumption of the far-infrared radiator or electric heater (kWh) and m_{water} is the amount of water removed (kg), which could be estimated as the difference between the initial and final masses of the product.

Since the flow rate of steam into the drying chamber was maintained at about 26 kg/h, the total steam consumption during LPSSD–FIR and LPSSD experiments was estimated by multiplying the value of steam flow rate by the time required to attain the desired final product moisture content at each drying condition.

3. Results and discussion

Fig. 2 shows the drying curves of banana slices undergoing different drying methods at various conditions. In the case of LPSSD–FIR it is seen from Fig. 2a that the drying time decreased with an increase in the drying temperature, as expected. This is because the temperature difference between the sample and superheated steam at a higher drying temperature was greater than that at a lower temperature, hence a larger driving force for heat transfer, which is also related to the rate of mass transfer. The moisture diffusivity is also higher at a higher temperature. In addition, the drying time also decreased with a decrease in the drying pressure. This is due to the fact that water evaporated at lower temperature when drying was performed at a lower pressure. It can also be seen that the rates of moisture reduction were more affected by the drying temperature than by the drying pressure when drying was performed

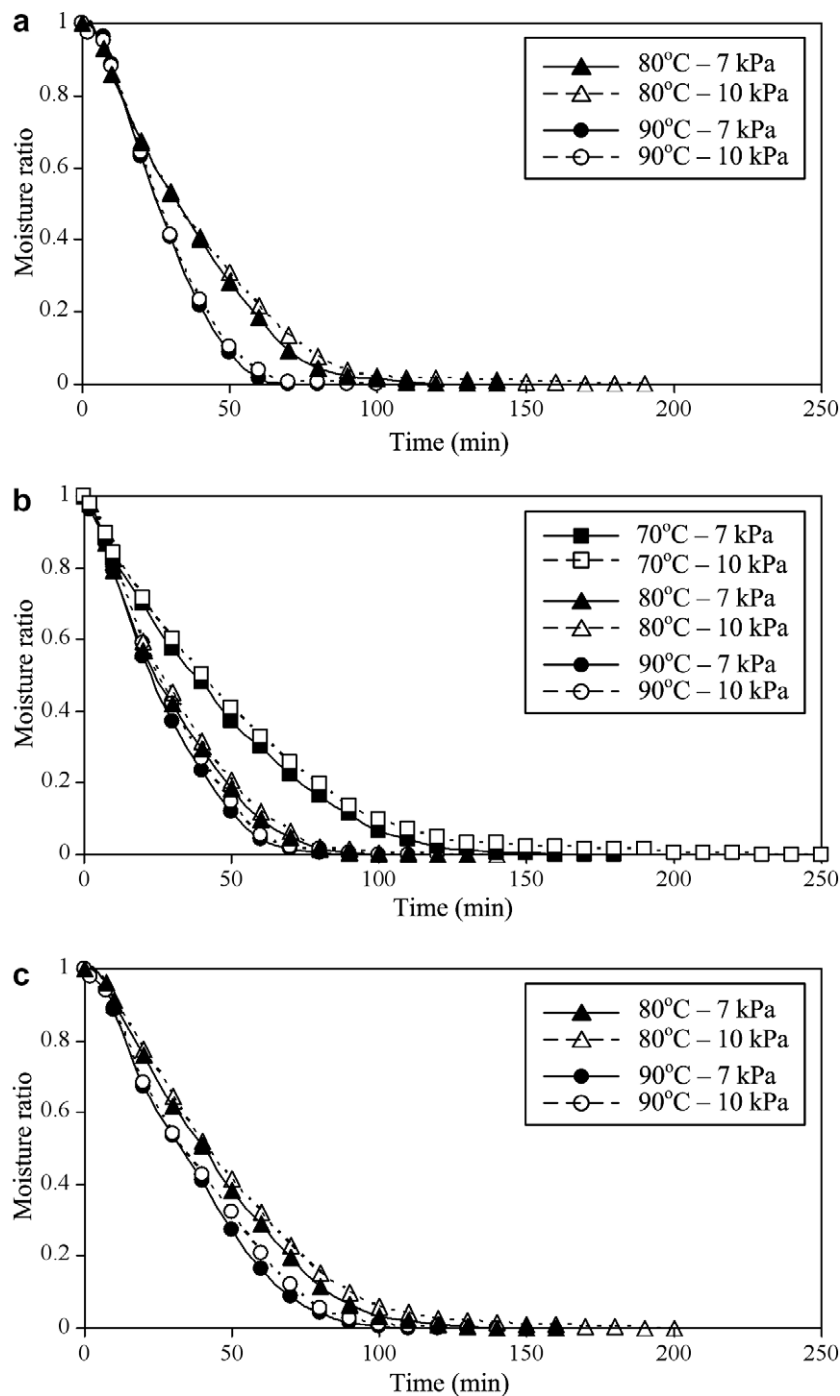


Fig. 2. Drying curves of banana slices undergoing (a) LPSSD-FIR, (b) VACUUM-FIR and (c) LPSSD.

at 80 and 90 °C. This may be due to the fact that temperature is the dominant factor influencing the superheated steam thermal properties, especially at higher drying temperatures.

It should be noted that, although the drying chamber was preheated via the use of the far-infrared radiator during the first 5 min of the process as mentioned earlier, small amount of steam condensation still occurred and could be observed over a short period; the results were not shown in Fig. 2a, however. Moreover, when drying was performed at

70 °C the sample could not reach the required final moisture content during the first 250 min of drying even at the lowest drying pressure tested (7 kPa). This is because of an excessive amount of steam condensation in the drying chamber. This phenomenon was also observed in the case of drying at 10 kPa (drying curves at 70 °C are not shown in Fig. 2a).

In the case of VACUUM-FIR (see Fig. 2b) the phenomenon was similar to that of LPSSD-FIR; drying at higher temperatures and lower pressures required shorter

drying time. Unlike LPSSD–FIR, however, the sample dried at the lowest drying temperature (70 °C) could reach the required final moisture content. This is because no steam condensation existed. It was also found that the effect of chamber pressure was not obvious at all drying temperatures. This may again be due to the fact that temperature is the main factor influencing the air thermal properties within the operating ranges tested.

In the case of LPSSD it was found from Fig. 2c that the drying time was shorter when drying was carried out at higher temperatures and lower pressures. Similar to LPSSD–FIR, the steam condensation still occurred during the initial stage of the process at all drying conditions and the sample could not reach the required final moisture content when drying was performed at 70 °C. The effect of the chamber pressure on the rate of moisture reduction was again not significant.

It is seen from Fig. 2a and c that the differences in the rates of moisture reduction of the samples dried at 80 and 90 °C during LPSSD–FIR were more clearly observed compared with those of the samples dried by LPSSD at 80 and 90 °C. This may be due to the fact that volumetric heating generated by the use of far-infrared radiation during LPSSD–FIR at 90 °C caused much larger temperature gradients within the sample than those within the sample dried by LPSSD at the same drying temperature resulting in a faster rate of moisture removal.

It was again found from Fig. 2 (see also Table 1) that the samples dried by LPSSD–FIR and VACUUM–FIR required less drying time than that of the samples dried by LPSSD at all drying conditions. This is because of the influences of volumetric heating caused by the use of far-infrared

radiation. In addition, it was observed that the samples dried by VACUUM–FIR required less drying time than that dried by LPSSD–FIR at lower drying temperatures (70 and 80 °C). However, LPSSD–FIR required shorter drying time (higher drying rates) when drying was conducted at 90 °C for all drying pressures tested. This is due to the sharp increase in the differences between the superheated steam temperature and the sample temperature in the case of LPSSD–FIR (see Figs. 4 and 5). On the other hand, the differences between the air temperature and the sample temperature in the case of VACUUM–FIR increased only slightly as the drying temperature increased. This suggested that the effective inversion temperature [18] calculated from the overall drying rates (the rates in both constant rate and falling rate periods) was somewhere between 80 and 90 °C. The details of the sample temperature evolution will be discussed again in subsequent sections.

Comparing with hot air drying [1–3], it was found that LPSSD–FIR and VACUUM–FIR required much less drying time (faster drying processes). This indicated that moisture transfer within the sample was rapid during the process applying far-infrared radiation.

Fig. 3 shows the plots of drying rates versus moisture content of banana slices undergoing different drying methods at various conditions. It can be seen from this figure that drying rates increased with an increase in the drying temperature and a decrease in the drying pressure in all cases.

In the case of LPSSD–FIR and VACUUM–FIR (see Fig. 3a and b) it was found that drying rates increased rapidly during an initial stage of drying (warming-up period). Since the radiation absorptivity of food products increased

Table 1
Specific energy consumption and total steam consumption of different drying methods

Drying method	Temp (°C)	Pressure (kPa)	Drying time (min)	Energy consumption (kWh)		Specific energy consumption (kWh/kg water)		Total steam consumption ^b (kg)
				E_{vacuum}	$E_{\text{radiator/heater}}$	$\text{SEC}_{\text{vacuum}}$	$\text{SEC}_{\text{radiator/heater}}$	
LPSSD–FIR	70	7	N/A ^a	N/A	N/A	N/A	N/A	N/A
		10	N/A	N/A	N/A	N/A	N/A	N/A
	80	7	140	3.50	0.49	128.57	18.00	60.67
		10	190	4.75	0.53	174.49	19.47	82.33
	90	7	90	2.25	0.41	82.65	15.06	39.00
		10	100	2.50	0.42	91.84	15.43	43.33
VACUUM–FIR	70	7	185	4.63	0.20	169.90	7.35	–
		10	255	6.38	0.23	234.19	8.45	–
	80	7	130	3.25	0.25	119.39	9.18	–
		10	145	3.63	0.27	133.16	9.92	–
	90	7	110	2.75	0.33	101.02	12.12	–
		10	120	3.00	0.34	110.21	12.49	–
LPSSD	70	7	N/A	N/A	N/A	N/A	N/A	N/A
		10	N/A	N/A	N/A	N/A	N/A	N/A
	80	7	160	4.00	0.54	146.90	19.84	69.33
		10	200	5.00	0.71	183.68	26.08	86.67
	90	7	115	2.88	0.61	105.61	22.41	49.83
		10	135	3.38	0.68	123.98	24.98	58.50

^a N/A implies that the final moisture content of 0.035 kg/kg (d.b.) was not obtainable at this condition.

^b The flow rate of steam into the drying chamber was maintained at about 26 kg/h.

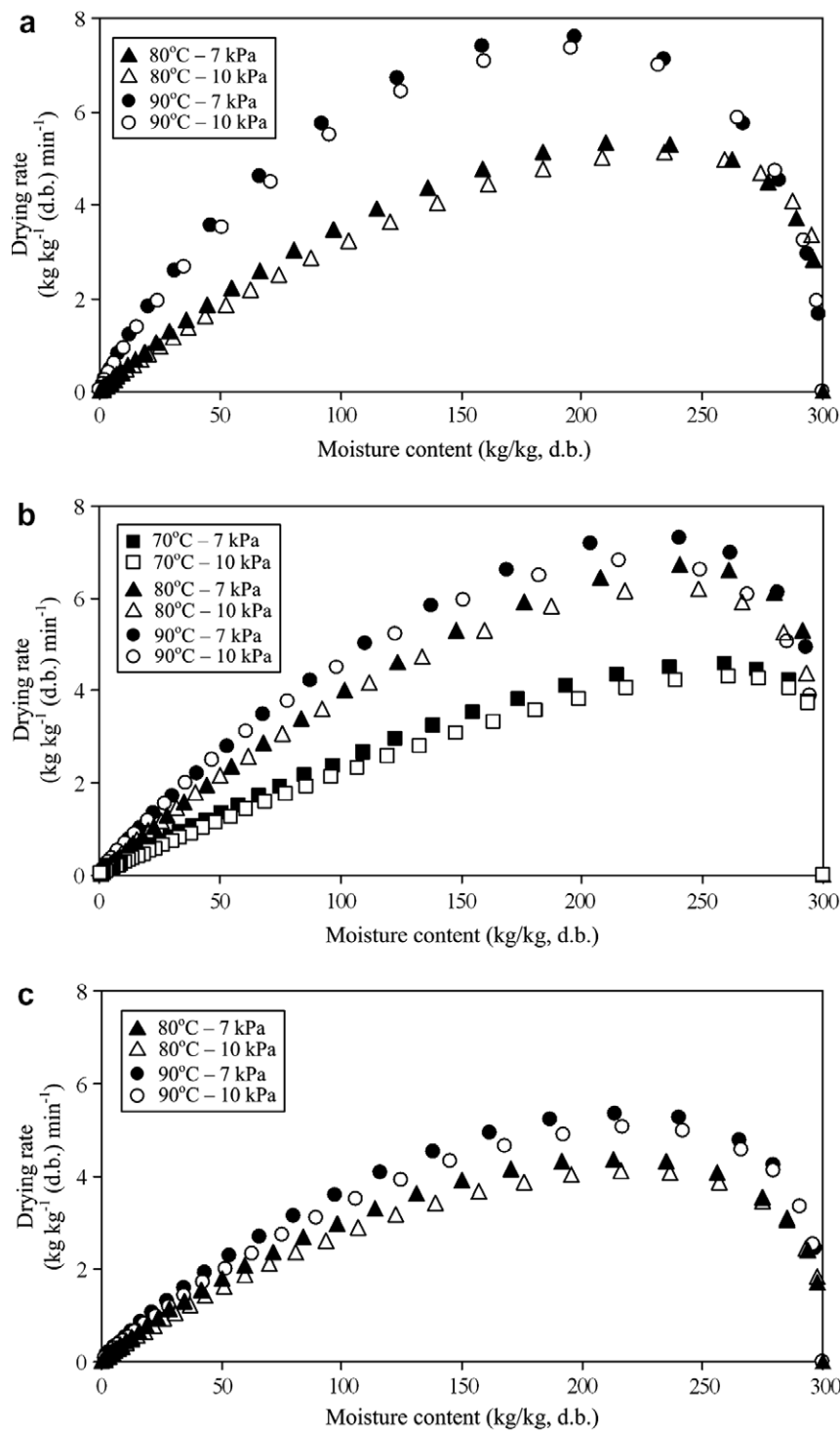


Fig. 3. Drying rates of banana slices undergoing (a) LPSSD-FIR, (b) VACUUM-FIR and (c) LPSSD.

with an increase in moisture content [15], thermal energy obtained from far-infrared radiation was more absorbed by banana slices during the initial stage of the process during which the sample moisture content was still high. This phenomenon is in agreement with that reported by Mongpraneet et al. [12,13] and Wang [19] who investigated the effect of far-infrared radiation on the drying characteristics of onion. However, Pathare and Sharma [20], who investi-

gated the use of infrared-convective drying for drying of onion, showed that the warming-up period was not observed. This is probably due to the fact that forced convection in the drying chamber accelerated the cooling effects, which reduced the temperature of the infrared heater and of the sample.

After the warming-up period the constant drying rate periods were observed; the duration of this period varied

with the drying techniques and conditions, however. In the case of LPSSD–FIR, it is seen that the period of constant drying rate was very short when drying was performed at the highest temperature (90 °C). For VACUUM–FIR the period of constant drying rate was almost not observed at all drying conditions even at the lowest drying temperature (70 °C). Drying process after this period took place in the falling rate period as indicated by a steady decrease in the drying rates. These results were contrary to those reported by many researchers such as Nguyen and Price [3] and Maskan [4] who found that drying of banana slices using hot air was in the falling rate period without the period of constant drying rate. Maskan [4] also reported that no period of constant drying rate was observed when microwave was applied. Although many researchers reported that the entire drying process took place in the falling rate period during hot air drying of some food products as mentioned above, the period of constant drying rate was clearly observed by Demirel and Turhan [1] during drying of banana slices using hot air at low drying temperature (40 °C). This implied that drying conditions employed are an important factor influencing the drying rate.

In the case of LPSSD (Fig. 3c) the characteristics of this drying process were also similar to those of LPSSD–FIR. However, the periods of constant drying rate were more obviously observed. The period of constant drying rate was longer, especially at lower drying temperature (80 °C in this case). It should be noted that at the same drying conditions drying rates of LPSSD–FIR and VACUUM–FIR were higher than that of LPSSD, especially when com-

paring with that of LPSSD–FIR at 90 °C. This is again because of the influence of volumetric heating caused by the application of far-infrared radiation.

The changes in moisture ratio and temperature of banana slices undergoing different drying methods at different conditions are shown in Figs. 4–6. As revealed by these figures the temperature evolution patterns were affected by both the drying methods and drying conditions. In the case of LPSSD–FIR, it can be seen from Fig. 4 that the temperature of the samples fell suddenly within the first 3 min of the process. This is due to the rapid reduction of the chamber pressure, which led to some flash evaporation of surface moisture [21]. After this period the temperature of the samples rose rapidly to the level close to the boiling point of water corresponding to the chamber pressure (not at the boiling point since far-infrared radiation was also present) and then remained unchanged at this level until the surface of the samples started to dry. In addition, it was observed that the period of constant sample temperature was longer when drying was conducted at lower temperatures and high pressures. This observation was in consistence with the period of constant drying rates (see Fig. 3a). Since heat transfer in the case of LPSSD–FIR simultaneously took place by radiation from the far-infrared radiator and by convection from superheated steam, the temperature of the samples rose steadily to the level higher than the pre-determined medium temperature. This is due to the fact that thermal radiation from the far-infrared radiator contributed additional energy to the drying medium and the samples. After this period the temperature of the samples remained almost unchanged. This is because

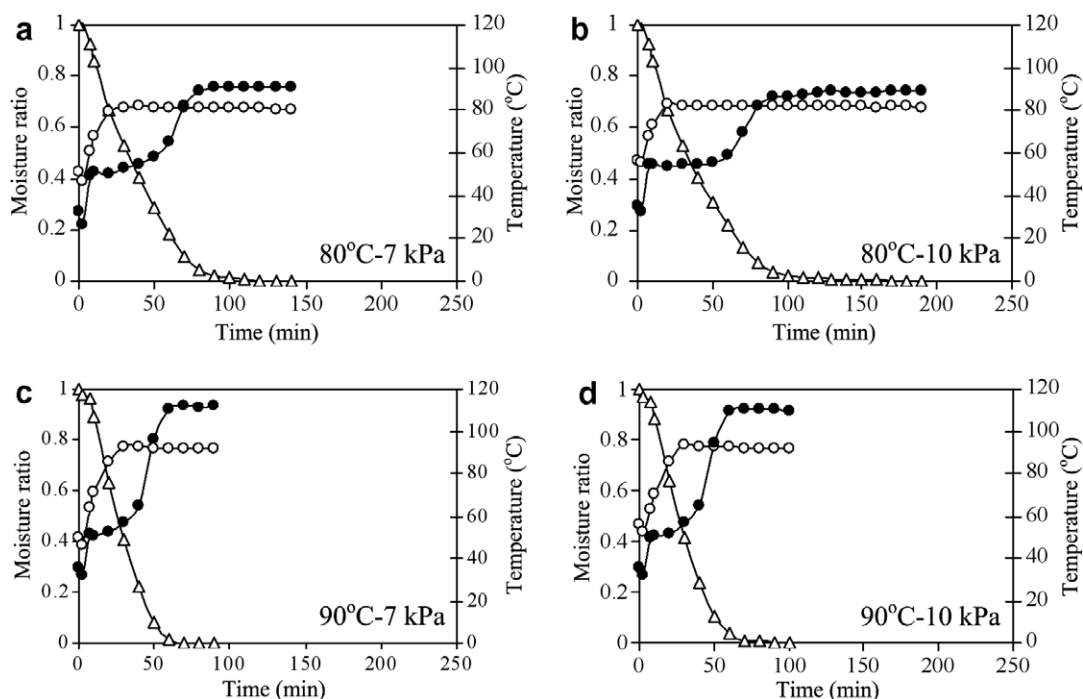


Fig. 4. Changes in moisture content and temperature of banana slices undergoing LPSSD–FIR at different drying conditions (–△– moisture ratio, –○– drying medium temperature, –●– sample temperature).

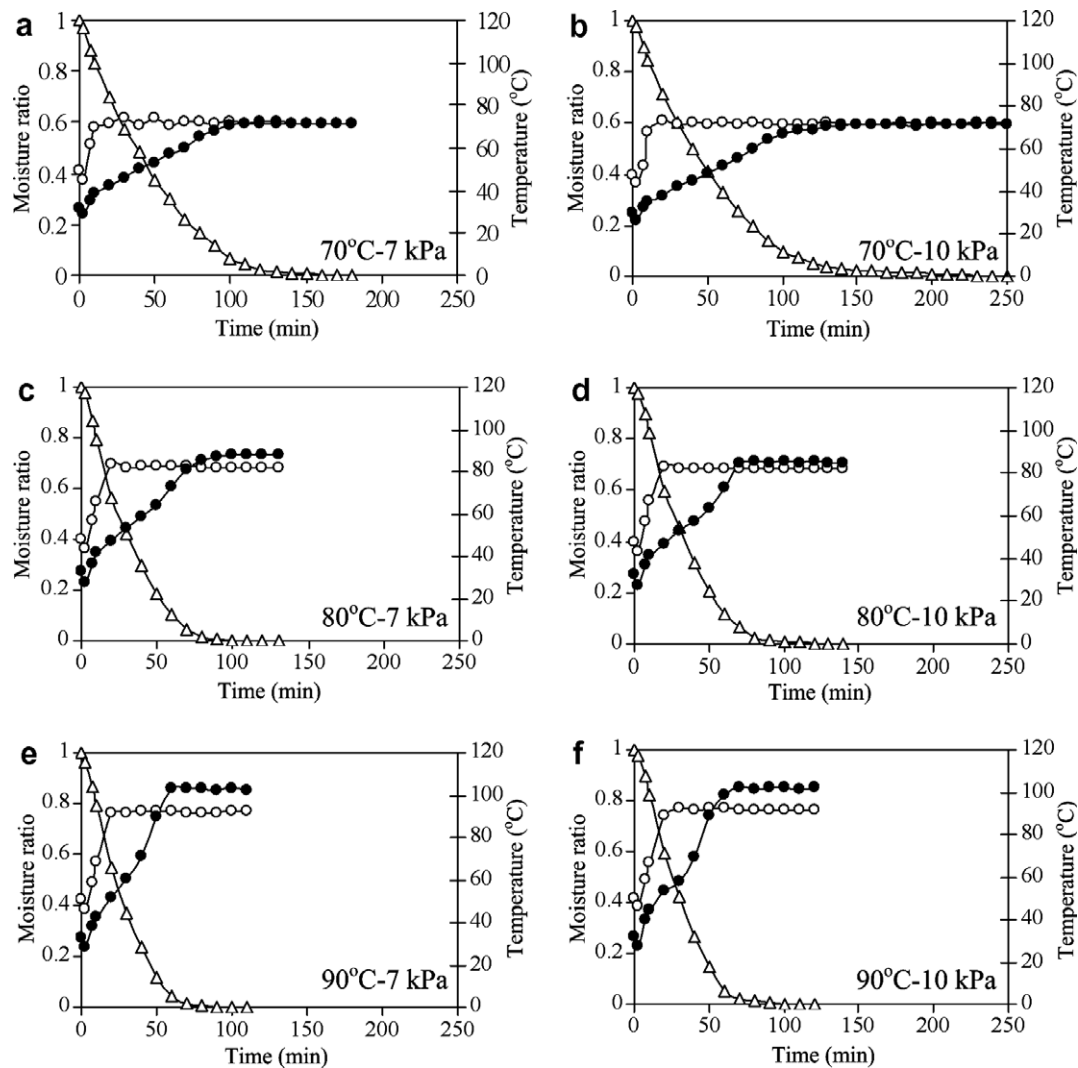


Fig. 5. Changes in moisture content and temperature of banana slices undergoing VACUUM-FIR at different drying conditions (- Δ - moisture ratio, - \circ - drying medium temperature, - \bullet - sample temperature).

during the later stage of the process moisture content within the samples was smaller leading to lower absorptivity of the samples [15].

In the case of VACUUM-FIR (see Fig. 5) it was found that the temperature of the samples also suddenly dropped during the initial period of the process. However, the temperature of the samples after this period steadily rose to the level higher than the pre-determined medium temperature, as noted earlier in the case of LPSSD-FIR, without the period of constant sample temperature. This result was in agreement with that of drying rates; no period of constant drying rate was observed (see Fig. 3b). After this period the temperature of the samples also remained almost unchanged as in the case of LPSSD-FIR.

For LPSSD the temperature evolution pattern of the samples after the initial stage of the process was different from those of the samples dried by LPSSD-FIR and VACUUM-FIR. It is seen from Fig. 6 that after the period of falling sample temperature the temperature of LPSSD sam-

ples rose rapidly to the boiling point of water corresponding to the chamber pressure and remained constant at this level for a certain period. Similar to LPSSD-FIR, longer constant sample temperature period was noted when drying was carried out at lower temperatures and higher pressures. This was also in consistence with the period of constant drying rates as can be seen in Fig. 3c. After this period the temperature of the samples rose steadily again and eventually approached the drying medium temperature. This temperature evolution pattern was similar to that reported by Devahastin et al. [8] and other investigators studying superheated steam drying at atmospheric pressure in which heat transfer took place only by convection from superheated steam.

To investigate the effect of radiation intensity on the temperature evolution of the samples the temperature of the samples dried by LPSSD-FIR and VACUUM-FIR were again compared. It is seen from Fig. 7 that, at the same pre-determined medium temperature, the sample

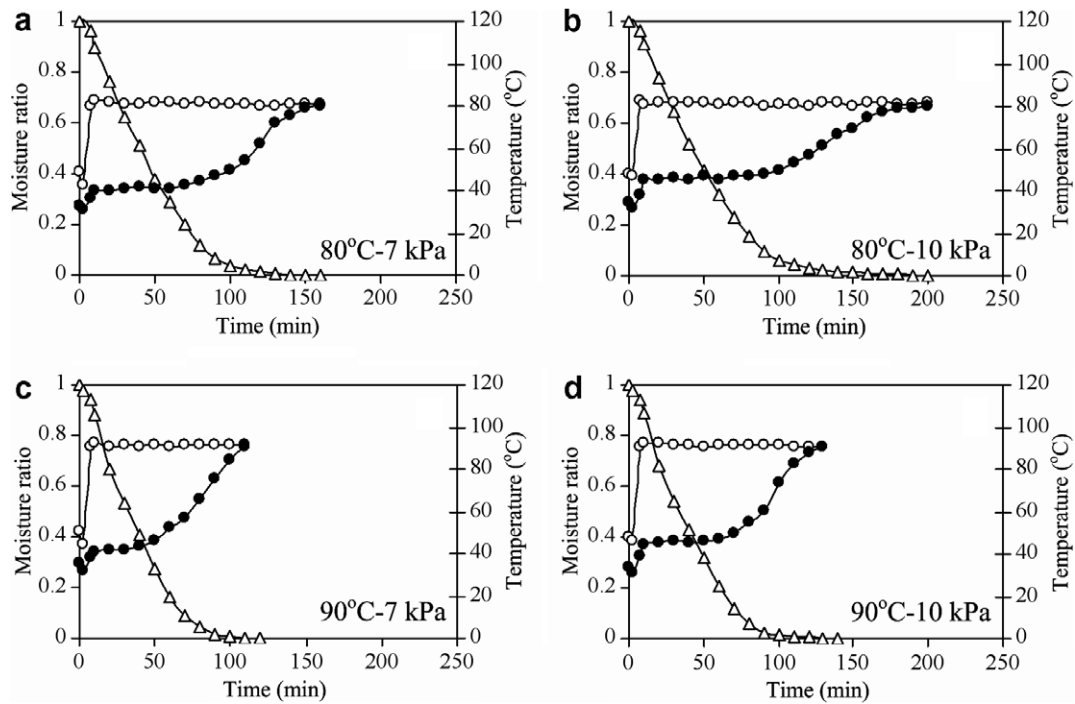


Fig. 6. Changes in moisture content and temperature of banana slices undergoing LPSSD at different drying conditions (-△- moisture ratio, -○- drying medium temperature, -●- sample temperature).

temperature during the later stage of LPSSD-FIR was higher than that in the case of VACUUM-FIR. This is due to the fact that in the case of LPSSD-FIR the radiation intensity at the position of the thermocouple used for sending the signal to the PID controller (30 mm above the sample surface) was less intense due to the higher absorptivity of superheated steam compared with that of air. Since the absorptivity of superheated steam is higher than that of air due to the presence of water vapor [22], the far-infrared radiator was used more often during LPSSD-FIR to maintain the desired level of the drying medium temperature leading to higher surface temperature of the far-infrared radiator as shown in Fig. 8. Consequently, the radiation intensity, which depended on the surface temperature of the far-infrared radiator, experienced by LPSSD-FIR samples was greater hence higher level of the sample temperature. It was also observed that in the case of VACUUM-FIR at the lowest temperature (70 °C) the sample temperature during the later stage of the process was much closer to the drying medium temperature (not much higher than the drying medium temperature) compared with that of samples dried at higher temperatures (see again Fig. 7). This is probably due to the fact that when drying was performed at lower temperature (70 °C in this case) the radiation intensity was lower as indicated by a lower surface temperature of the far-infrared radiator. Since the sample temperature was not dictated by the drying medium temperature but by the radiation intensity, very high sample temperature developed in the cases of drying at higher temperatures resulting in overheating and burning of the

product, especially in the case of LPSSD-FIR at the highest temperature tested (90 °C). It should be noted that the effect of drying pressure on the level of sample temperature during the later state of drying was not significant.

Table 1 lists the specific energy consumption and total steam consumption of different drying methods at different conditions. In the case of the specific energy consumption of the vacuum pump (SEC_{vacuum}) it was found from this table that SEC_{vacuum} decreased with a decrease in drying time, which related to both the drying methods and conditions. Since the vacuum pump used in this study consumed the same rate of electric energy (1.5 kWh) at all drying conditions, the shorter drying time led to lower energy consumption. Due to being the shortest drying process, LPSSD-FIR at 90 °C and 7 kPa led to the lowest value of SEC_{vacuum} . It should be noted from Table 1 that the vacuum pump consumed large amount of electric energy compared with that of the far-infrared radiator or electric heater, as will be discussed later.

Regarding the specific energy consumption of the far-infrared radiator or electric heater ($SEC_{\text{radiator/heater}}$), it was found that the values of $SEC_{\text{radiator/heater}}$ of LPSSD-FIR and VACUUM-FIR were lower than those of LPSSD at all drying conditions. This may probably be due to the fact that LPSSD-FIR and VACUUM-FIR took shorter drying time than LPSSD and the power rating of the far-infrared radiator used in the case of LPSSD-FIR and VACUUM-FIR was lower compared with that of the electric heater used in the case of LPSSD. In addition, $SEC_{\text{radiator/heater}}$ of LPSSD-FIR was higher than that of

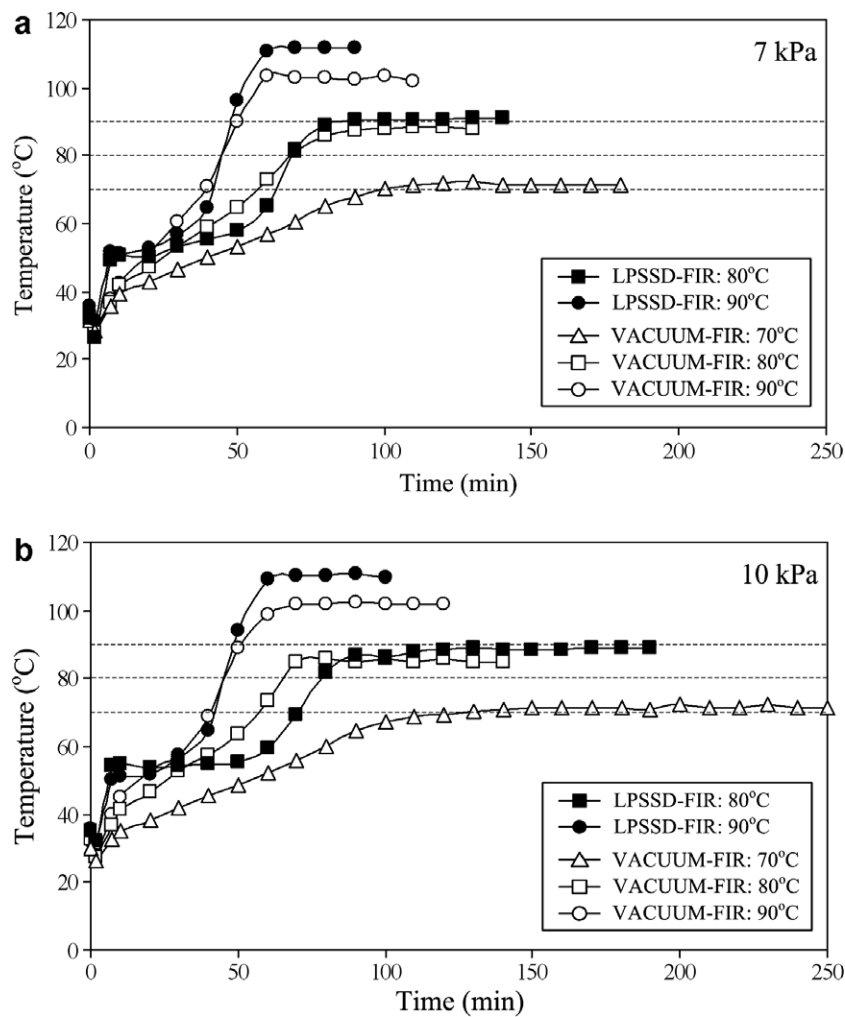


Fig. 7. Comparison of changes in temperature of banana slices undergoing LPSSD-FIR and VACUUM-FIR.

VACUUM-FIR. This is because the far-infrared radiator was used more often during LPSSD-FIR as noted earlier. It should be noted that although VACUUM-FIR at 70 °C and 7 kPa took longer drying time (185 min) than almost other drying methods and conditions except VACUUM-FIR at 70 °C and 10 kPa (255 min), $SEC_{\text{radiator/heater}}$ of VACUUM-FIR at this condition (70 °C and 7 kPa) was the lowest. This may probably be due to the fact that radiation intensity at this condition was much lower than that of other drying methods and conditions as indicated by a lower surface temperature of the far-infrared radiator (see Fig. 8a) resulting in a lower electric energy consumption of the far-infrared radiator. However, the electric energy consumption of the vacuum pump at this condition was rather high.

In the case of drying with the application of superheated steam to the drying chamber (LPSSD-FIR and LPSSD) it is seen from Table 1 that the total steam consumption increased with an increase in the drying time, as expected. Although superheated steam drying provided better products with higher quality [23], the cost of superheated steam should also be considered.

4. Conclusions

A drying system combining the concept of low-pressure superheated steam and far-infrared radiation (LPSSD-FIR) for drying banana was developed and studied. It was found that LPSSD-FIR and VACUUM-FIR took shorter drying time compared to LPSSD at all drying conditions. In addition, LPSSD-FIR required longer drying time than VACUUM-FIR at almost all drying conditions except at the temperature of 90 °C; this indicated that the inversion temperature calculated from the overall drying rates should be somewhere between 80 and 90 °C. It was also found that the temperatures of both LPSSD-FIR and VACUUM-FIR samples during the later stage of drying were higher than the pre-determined medium temperatures. In terms of the specific energy consumption the results showed that the specific energy consumption of LPSSD-FIR and VACUUM-FIR, both in terms of the electric energy required to maintain the vacuum in the drying chamber and electric energy required to generate thermal energy, was reduced with the use of far-infrared radiation. Although dried product quality is an important

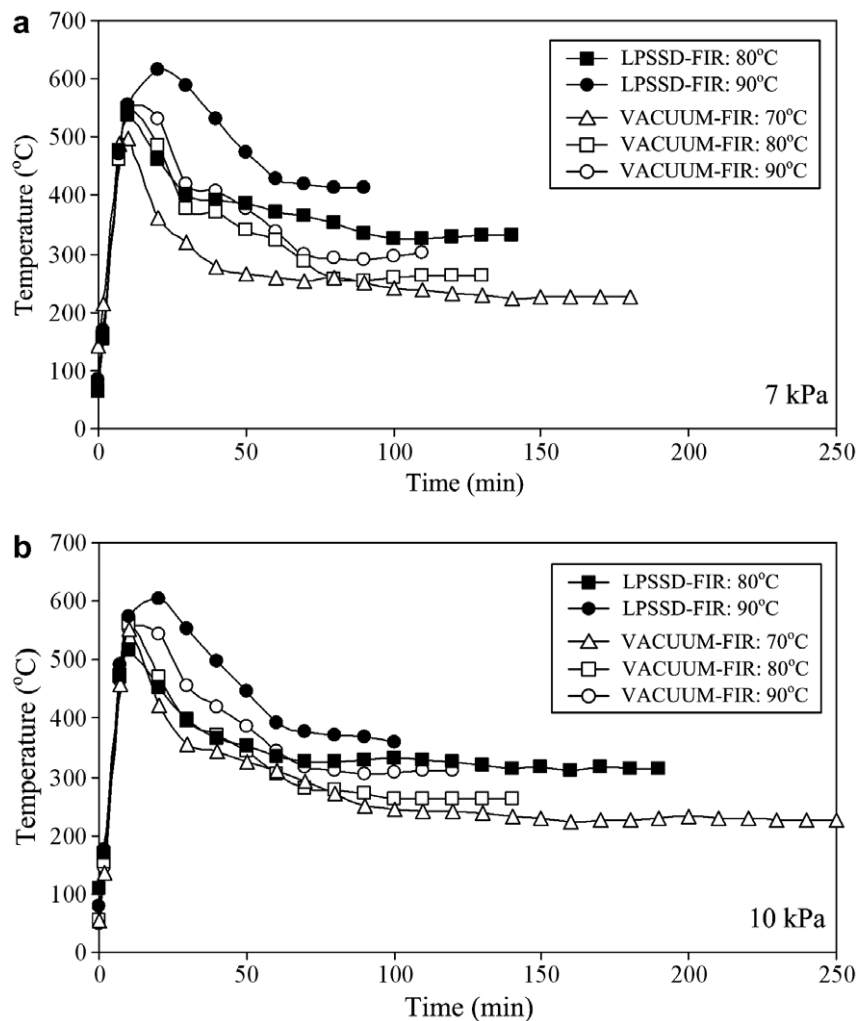


Fig. 8. Evolution of surface temperature of far-infrared radiator during LPSSD-FIR and VACUUM-FIR.

index for considering the drying efficiency, this is beyond the scope of this paper. Therefore, based only on the drying rates and the specific energy consumption of the process, LPSSD-FIR at 90 °C and 7 kPa was suggested in this study.

Acknowledgements

The authors express their sincere appreciation to the Commission on Higher Education, the Thailand Research Fund (TRF), the National Research Council of Thailand and the International Foundation for Science (IFS), Sweden for supporting the study financially.

References

- [1] D. Demirel, M. Turhan, Air-drying behavior of Dwarf Cavendish and Gros Michel banana slices, *Journal of Food Engineering* 59 (2003) 1–11.
- [2] M.A. Karim, M.N.A. Hawlader, Drying characteristics of banana: theoretical modeling and experimental validation, *Journal of Food Engineering* 70 (2005) 35–45.
- [3] M.H. Nguyen, W.E. Price, Air-drying of banana: influence of experimental parameters, slab thickness, banana maturity and harvesting season, *Journal of Food Engineering* 79 (2007) 200–207.
- [4] M. Maskan, Microwave/air and microwave finish drying of banana, *Journal of Food Engineering* 44 (2000) 71–78.
- [5] B. Adu, L. Otten, Effect of increasing hygroscopicity on the microwave heating of solid foods, *Journal of Food Engineering* 27 (1996) 35–44.
- [6] A.E. Drouzas, H. Schubert, Microwave application in vacuum drying of fruits, *Journal of Food Engineering* 28 (1996) 203–209.
- [7] J. Yongsawatdigul, S. Gunasekaran, Microwave-vacuum drying of cranberries: Part II. Quality evaluation, *Journal of Food Processing and Preservation* 20 (1996) 145–156.
- [8] S. Devahastin, P. Suvarnakuta, S. Soponronnarit, A.S. Mujumdar, A comparative study of low-pressure superheated steam and vacuum drying of a heat-sensitive material, *Drying Technology* 22 (2004) 1845–1867.
- [9] N. Leeratanarak, S. Devahastin, N. Chiewchan, Drying kinetics and quality of potato chips undergoing different drying techniques, *Journal of Food Engineering* 77 (2006) 635–643.
- [10] P. Suvarnakuta, S. Devahastin, A.S. Mujumdar, Drying kinetics and β -carotene degradation in carrot undergoing different drying processes, *Journal of Food Science* 70 (2005) S520–S526.
- [11] P. Glouannec, D. Lecharpentier, H. Noel, Experimental survey on the combination of radiating infrared and microwave sources for the

- drying of porous material, *Applied Thermal Engineering* 22 (2002) 1689–1703.
- [12] S. Mongpraneet, T. Abe, T. Tsurusaki, Accelerated drying of welsh onion by far infrared radiation under vacuum conditions, *Journal of Food Engineering* 55 (2002) 147–156.
- [13] S. Mongpraneet, T. Abe, T. Tsurusaki, Far infrared-vacuum and convection drying of welsh onion, *Transactions of the ASAE* 45 (2002) 1529–1535.
- [14] A.S. Ginzburg, *Application of Infrared Radiation in Food Processing*, Chemical and Process Engineering Series, Leonard Hill, London, 1969.
- [15] C. Sandu, Infrared radiative drying in food engineering: a process analysis, *Biotechnology Progress* 2 (1986) 109–119.
- [16] C. Ratti, A.S. Mujumdar, Infrared drying, in: A.S. Mujumdar (Ed.), *Handbook of Industrial Drying*, vol. 1, Marcel Dekker, New York, 1995, pp. 567–588.
- [17] AOAC, *Official Methods of Analysis*, 14th ed., Association of Official Agricultural Chemists, Washington DC, 1984.
- [18] P. Suvarnakuta, S. Devahastin, S. Soponronnarit, A.S. Mujumdar, Drying kinetics and inversion temperature in a low-pressure superheated steam-drying system, *Industrial and Engineering Chemistry Research* 44 (2005) 1934–1941.
- [19] J. Wang, A single-layer model for far-infrared radiation drying of onion slices, *Drying Technology* 20 (2002) 1941–1954.
- [20] P.B. Pathare, G.P. Sharma, Effective moisture diffusivity of onion slices undergoing infrared convective drying, *Biosystems Engineering* 93 (2006) 285–291.
- [21] D.W. Sun, L.J. Wang, Development of a mathematical model for vacuum cooling of cooked meats, *Journal of Food Engineering* 77 (2006) 379–385.
- [22] A.F. Mills, *Basic Heat and Mass Transfer*, second ed., Prentice-Hall, Upper Saddle River, 1999.
- [23] A.S. Mujumdar, Superheated steam drying-technology for the future, in: S. Devahastin (Ed.), *Mujumdar's Practical Guide to Industrial Drying*, Exergex, Brossard, Canada, 2000, pp. 115–138.



Effect of starch retrogradation on texture of potato chips produced by low-pressure superheated steam drying

Rungthip Kingcam, Sakamon Devahastin*, Naphaporn Chiewchan

Department of Food Engineering, King Mongkut's University of Technology Thonburi, 126 Pracha u-tid Road, Bangkok 10140, Thailand

ARTICLE INFO

Article history:

Received 19 January 2008

Received in revised form 8 April 2008

Accepted 8 April 2008

Available online 16 April 2008

Keywords:

Baking
Blanching
Crystallinity
Drying kinetics
Freezing
Health snack
Pretreatment
Texture
X-ray diffraction

ABSTRACT

The effects of the degree of starch retrogradation, initial slice thickness and final moisture content on the texture of potato chips dried by low-pressure superheated steam drying (LPSSD) were investigated in this study. Potato slices of different initial thicknesses (1.5, 2.5 and 3.5 mm) were pretreated with three different methods (blanching and then freezing for 24 h, blanching and then repeated freezing/thawing either for 3 or 5 cycles) to study the effects of these pretreatment methods on the degree of starch retrogradation. The potato slices were then dried by LPSSD at 90 °C and absolute pressure of 7 kPa to three levels of final moisture content (1.5%, 2.5% and 3.5% (d.b.)) to investigate the drying kinetics and the quality of dried potato chips in terms of hardness, toughness and crispness as well as degree of crystallinity by X-ray diffraction technique. The various pretreatment methods were found to have an obvious effect on the rates of moisture reduction of the samples. Higher degrees of starch retrogradation led to an increase in the hardness and toughness of dried chips, but did not show any significant effect on the crispness of the chips. An increase in the degree of starch retrogradation led to higher degree of crystallinity of dried potato chips.

© 2008 Elsevier Ltd. All rights reserved.

1. Introduction

Potato chips are generally dehydrated by deep fat frying to a moisture content of 0.02 kg/kg (d.b.) or less. Potato chips have oil content that ranges from 35% to 45% (w.b.) (Garayo and Moreira, 2002). Due to the high level of oil as well as to an increased demand of consumers for health snack, a technique to produce potato chips without oil is required. Drying may thus be an option for the production of fat-free potato chips with the desired color and texture characteristics.

Most of the research efforts have focused on hot air drying of potato pieces of various shapes (e.g., Wang and Brennan, 1995; McMinn and Magee, 1996; Krokida, Tsami and Maroulis, 1998). However, there are many problems with hot air drying such as slow drying rate, poor product color, product deformation and substantial degradation of nutrients. Therefore, a novel concept of low-pressure superheated steam drying (LPSSD) has been proposed as an alternative to dry heat-sensitive products (Devahastin et al., 2004) since it can combine the advantages of drying at reduced temperature and pressure with those of conventional atmospheric-pressure superheated steam drying such as the ability to

yield product with higher porosity, less shrinkage and better color (Mujumdar and Devahastin, 2000; Devahastin and Suvarnakuta, 2004).

Recently, LPSSD has also been applied to produce fat-free potato chips. Leeratanarak et al. (2006) studied the drying kinetics and quality of potato chips produced by LPSSD and hot air drying. It was found that LPSSD produced potato chips of better quality than did hot air drying by lowering the chips browning index. LPSSD at 90 °C was proposed as the most favorable condition for baking potato chips in their work. However, the best condition proposed still led to chips of much inferior quality compared with commercially available chips, especially in terms of texture (hardness).

To further improve the quality of potato chips, various pretreatment methods have been proposed and tested prior to LPSSD. Pimpaporn et al. (2007) studied the influences of various pretreatment methods on the low-pressure superheated steam drying kinetics and quality of dried potato chips in terms of color, texture and microstructure. The effects of blanching, combined blanching and freezing and blanching followed by immersion in chemical solutions, namely, glycerol and monoglyceride, at different concentrations and then freezing were investigated. Drying was performed at 70, 80 and 90 °C. It was found that combined blanching and freezing was the most appropriate method of pretreatment for producing good quality potato chips. This was probably due to the

* Corresponding author. Tel.: +66 2 470 9246; fax: +66 2 470 9240.

E-mail address: sakamon.dev@kmutt.ac.th (S. Devahastin).

effects of starch gelatinization and retrogradation that occurred during blanching and freezing, respectively. Potato slices pretreated by blanching and freezing, then dried by LPSSD, were found to have potential to compete with deep fat fried chips.

Many studies have indeed been conducted to study the effect of starch retrogradation on physical changes of various products including potato. Radley (1976) reported that repeated freezing/thawing cycles involving subjecting samples to repeated freezing and intermittent thawing to room temperature are known to accelerate retrogradation. This is due to the fact that when starch pastes are frozen, phase separation occurs with the formation of ice crystals. Upon thawing the pastes are composed of a starch-rich and a starch-deficient aqueous phase. The extent of phase separation increases with additional freezing/thawing cycles due to an increase in retrogradation in the starch-rich phase. O'Leary et al. (2000) studied the effect of freezing/chilling on the quality of ready-meal components such as instant mashed potato, steamed salmon and steamed broccoli. In the case of instant mashed potato, freezing/chilling was found to reduce the softness, adhesiveness, whiteness and vitamin C content of the samples. The fresh sample was the softest, while the samples that had been frozen and thawed were firmer. This is most probably due to the effect of freezing, which could lead to starch retrogradation and textural changes.

The aim of this work was to further investigate the effect of the degree of starch retrogradation on the texture of potato chips dried by LPSSD. In addition, the effects of initial slice thickness and final moisture content on the texture of the chips were also investigated.

2. Materials and methods

2.1. Experimental set-up

A schematic diagram of the low-pressure superheated steam dryer and its accessories is shown in Fig. 1. The dryer consists of a stainless steel drying chamber with inner dimensions of $45 \times 45 \times 45$ cm; a steam reservoir, which received steam from a boiler and maintained its pressure at around 200 kPa (gauge); and a liquid ring vacuum pump (Nash, model ET32030, Trumbull, CT), which was used to maintain vacuum in the drying chamber. Steam trap was installed to reduce excess steam condensation in the reservoir. An electric heater, rated at 1.5 kW, which was controlled by a proportional-integral-derivative (PID) controller (Omron, model E5CN, Tokyo, Japan) was installed in the drying chamber to control the steam temperature and to minimize condensation of steam in the drying chamber during the start-up

period. Two variable-speed electric fans were used to disperse the steam throughout the drying chamber. The sample holder was made of a stainless steel screen with dimensions of 16.5×16.5 cm. The change of the mass of the sample was detected continuously (at 60 s interval) using a load cell (Minebea, model Ucg-3 kg, Nagano, Japan), which was installed in a smaller chamber connected to the drying chamber by a flexible hose (in order to maintain the same vacuum pressure as that in the drying chamber), and also to an indicator and recorder (AND A&D Co., model AD4329, Tokyo, Japan). For detailed experimental set-up the reader is referred to Devahastin et al. (2004).

2.2. Materials

Fresh potato (*Solanum tuberosum*) was purchased from a local market and stored at 4 °C. Prior to each experiment, potato was washed with tap water to remove dirt and soil from its skin. After that potato was peeled and sliced to three levels of initial thickness (1.5, 2.5, and 3.5 mm) by an electric slicer. The potato slices were then shaped using a core borer to a diameter of 45 mm.

2.3. Methods

The sliced potato was blanched in hot water at 90 ± 2 °C for 5 min with the ratio of potato to water of 0.015 g/g (Leeratanarak et al., 2006). The samples were immediately cooled in cold water (4 °C) and placed on paper towel to remove excess water.

The samples were subjected to three different pretreatment methods to investigate the effect of starch retrogradation on the texture of dried potato chips. First, the samples were pretreated by blanching and then freezing at -20 °C in a chest freezer (Sanyo, Model SF-C-65, Tokyo, Japan) for 24 h (or 48 and 72 h in the preliminary experiments to determine the effect of freezing time on the degree of retrogradation of starch granules in potato). Second, blanched potato was frozen in the chest freezer at -20 °C for 24 h and then thawed at 30 °C for 1 h; the whole process was repeated for 3 cycles. Finally, blanched potato was frozen and thawed at the above-mentioned conditions for 5 cycles. The samples were then baked by LPSSD at 90 °C and absolute pressure of 7 kPa (Leeratanarak et al., 2006) to three levels of final moisture content (1.5%, 2.5% and 3.5%); 6 slices of potato were used in each drying experiment. The samples were placed horizontally on the tray. Since the drying chamber was heated prior to the start of each experiment, the effect of initial condensation was negligible (Devahastin et al., 2004). The moisture content of the samples was determined using the vacuum oven method (AOAC, 1984).

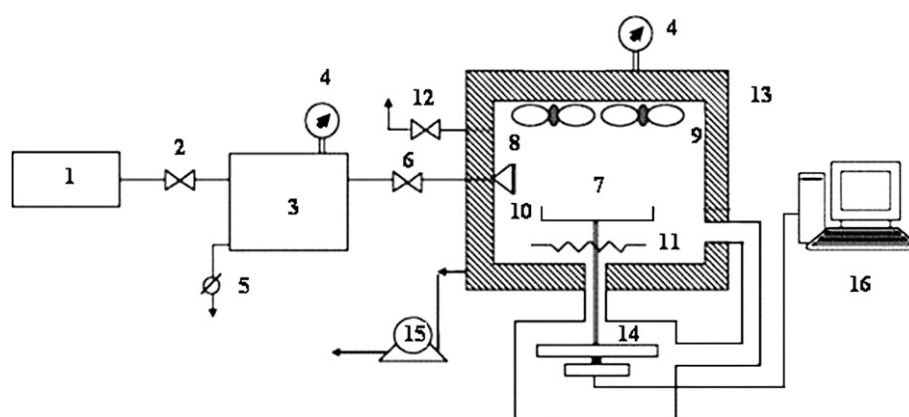


Fig. 1. A schematic diagram of low-pressure superheated steam dryer and associated units. (1) boiler; (2) steam valve; (3) steam reservoir; (4) pressure gauge; (5) steam trap; (6) steam regulator; (7) drying chamber; (8) steam inlet and distributor; (9) two electric fans; (10) sample holder; (11) electric heater; (12) vacuum break-up valve; (13) insulator; (14) on-line mass indicator and logger; (15) vacuum pump; (16) PC with installed data acquisition card.

2.3.1. Degree of starch retrogradation

The enthalpies of the samples with different degrees of starch retrogradation were determined by a differential scanning calorimeter (Mettler Toledo DSC 822^c, Schwerzenbach, Switzerland). Approximately 5 mg of sample was placed in an aluminum pan and was scanned from 25 to 90 °C at a heating rate of 10 °C/min. After heating to 90 °C, the sample was cooled to 4 °C. Once the temperature reached 4 °C, the sample was immediately removed and stored at 4 °C for 7 days. Then, the stored sample was heated from 25 to 90 °C at 10 °C/min again (Kim et al., 1995).

The degree of retrogradation (%R) was calculated using Eq. (1)

$$(\%R) = \frac{\Delta H_{\text{retrogradation}}}{\Delta H_{\text{gelatinization}}} \times 100 \quad (1)$$

where $\Delta H_{\text{retrogradation}}$ is the enthalpy of retrogradation of the sample (J/g) and $\Delta H_{\text{gelatinization}}$ is the enthalpy of gelatinization of the sample (J/g). All tests were performed in duplicate and the average values were reported.

2.3.2. Textural characteristics

A compression test was performed to analyze the texture of a dried sample. The test was performed using a texture analyzer (Stable Micro Systems, TA.XT. Plus, Surrey, UK). A chip was placed on a hollow planar base and the force was then applied to the sample by a 5-mm spherical probe at a constant speed of 2 mm/s until the sample was cracked (Moreno-Perez et al., 1996). Force-deformation data were recorded to determine the textural characteristics of the chip. The maximum force of break, area under the force-deformation curve (Rosenthal, 1999) and the number of peaks (van Loon et al., 2007) in the force-deformation curve of each sample were considered as an indication of hardness, toughness and crispness of the sample, respectively. All tests were performed in duplicate and the average values were reported.

2.3.3. X-ray diffraction pattern

X-ray diffraction (XRD) pattern of a dried potato chip was obtained using an X-ray diffractometer (Bruker AXS GmbH, Karlsruhe, Germany) under the following conditions: 40 kV and 40 mA with CuK α radiation at a wavelength of 0.1546 nm. The scanning region of 2 θ from 3° to 51° at 0.02° intervals and the counting time of 0.4 s/step were used in this study. The crystallinity (X_c) of dried potato sample was calculated by

$$X_c = \frac{A_c}{A_c + A_a} \times 100\% \quad (2)$$

where A_c and A_a are the areas of crystalline and non-crystalline regions, respectively. All tests were performed in duplicate and the average values were reported.

2.3.4. Statistical analysis

All experiments were performed in duplicate and the mean values with standard deviations were reported. The experimental data were analyzed using an analysis of variance (ANOVA). Duncan's multiple range test was used to establish the multiple comparisons of the mean values; mean values were considered at 95% confidence level. A statistical program SPSS (version 14) was used to perform all statistical calculations.

3. Results and discussion

3.1. Preliminary results

As mentioned earlier, a preliminary study was first performed to determine the effect of freezing time on the degree of retrogradation of starch granules in potato prior to drying. The degrees of

Table 1

Effect of freezing time on the degree of starch retrogradation

Freezing time (h)	Degree of retrogradation (%)
24	21.67 \pm 2.20 ^a
48	22.80 \pm 3.81 ^a
72	24.36 \pm 4.41 ^a

Different superscripts in the same column mean that the values are significantly different ($p \leq 0.05$).

starch retrogradation of the samples frozen for different durations are presented in Table 1.

Blanching the samples for 5 min at 90 °C yielded the degree of starch gelatinization of 100% (Leeratanarak et al., 2006). The results from the preliminary experiments revealed that the degrees of starch retrogradation were not significantly different when different freezing durations were used. Similar behavior has also been reported by other investigators who studied gelatinization and retrogradation of potato starch as assessed by differential scanning calorimetry (Karlsson and Eliasson, 2003). These authors reported that retrogradation of potato starch stored at 6 °C for 1, 2, 3 and 7 days was not significantly different. Additionally, these authors also found that recrystallization of starch occurred predominantly during the first 48 h of storage; retrogradation continued after this initial period, but slowed down with storage time.

The degree of starch retrogradation, as influenced by various pretreatment methods, was determined by differential scanning calorimetry and the results are presented in Table 2. The degree of starch retrogradation increased significantly when the number of freezing/thawing cycles increased. The increase in the degree of starch retrogradation with the number of freezing/thawing cycles might be due to the fact that freezing led to phase separation of starch into polymer-poor regions (ice crystals) and polymer-rich regions (starch network). Upon thawing these domains persisted, facilitating easier association of the polymer chains within the polymer-rich regions. Moreover, the extent of phase separation increased with additional freezing/thawing cycles due to an increase in amylopectin retrogradation in the polymer-rich regions (Yuan and Thompson, 1998). However, when comparing the degree of retrogradation reported in Tables 1 and 2, it was found that freezing alone appeared to be nearly as good as freezing/thawing pretreatment (when the same duration of treatment was considered). So, freezing/thawing process was not superior to freezing alone if only the degree of retrogradation was of concern.

Based on the preliminary results, combined blanching and freezing for 24 h, combined blanching and repeated freezing/thawing for 3 and 5 cycles were selected as the pretreatment methods in subsequent study. The effect of these pretreatment methods on the degree of starch retrogradation and subsequently on the degree of crystallinity and texture of dried potato chips were studied.

3.2. Drying kinetics of potato slices

As mentioned earlier, potato was sliced into initial thicknesses of 1.5, 2.5 and 3.5 mm and was pretreated with three different pre-

Table 2

Effects of pretreatments on the degree of starch retrogradation

Pretreatment method	Degree of retrogradation (%)
B + F 24 h	20.05 \pm 0.39 ^a
B + F + T (3 cycles)	25.24 \pm 0.78 ^b
B + F + T (5 cycles)	29.12 \pm 1.55 ^c

B, Blanching, F, freezing and T, thawing.

Different superscripts in the same column mean that the values are significant different ($p \leq 0.05$).

Table 3

Initial moisture content of potato slices exposed to different pretreatments

Thickness (mm)	Pretreatment method	Moisture content (% d.b.)
1.5	B + F 24 h	626 ± 19 ^e
	B + F + T (3 cycles)	533 ± 15 ^{bc}
	B + F + T (5 cycles)	479 ± 12 ^a
2.5	B + F 24 h	714 ± 12 ^{fg}
	B + F + T (3 cycles)	617 ± 8 ^e
	B + F + T (5 cycles)	560 ± 4 ^{cd}
3.5	B + F 24 h	686 ± 2 ^f
	B + F + T (3 cycles)	605 ± 2 ^e
	B + F + T (5 cycles)	526 ± 16 ^b
Raw potato		574 ± 8 ^d
Blanching		735 ± 23 ^g

B, Blanching, F, freezing and T, thawing.

Different superscripts in the same column mean that the values are significantly different ($p < 0.05$).

treatment methods. The initial moisture contents of all treated samples are as illustrated in Table 3. The decrease in the initial moisture content might be due to the fact that upon thawing water might be removed from potato due to syneresis (Karim et al., 2000) as well as drip loss (Redmond et al., 2004).

Pretreated potato slices were then dried in low-pressure superheated steam until their equilibrium moisture contents were reached as shown in Table 4. Generally, drying potato slices of larger thickness took longer time to reach the equilibrium moisture content (EMC). Potato with thicker slices also had higher values of equilibrium moisture content. This might be due to the effect of casehardening developed in the case of thick potato slices, which retards water removal and also leads to higher EMC of the samples. However, the influence of various pretreatment methods on the EMC of potato chips was not significant for all initial thicknesses.

Fig. 2 shows the drying kinetics of potato slices pretreated with different pretreatment methods. The results showed that the samples exposed to combined blanching and repeated freezing and thawing required shorter drying time to reach the desired final moisture content than those treated only by blanching and freezing for 24 h. This is due to the lower initial moisture content of the samples treated by repeated freezing and thawing.

Drying time of potato chips of various thicknesses treated by different pretreatment methods is shown in Table 5. As expected, chips with higher initial thicknesses required longer drying time to reach the desired final moisture content.

3.3. Quality of dried potato chips

3.3.1. Texture characteristics

The texture of dried potato chips is reported in terms of hardness, toughness and crispness, which were indicated from the

Table 4

Equilibrium moisture content of potato chips having various initial thicknesses when subjected to different pretreatment methods (the drying temperature was 90 °C and the absolute pressure was 7 kPa)

Thickness (mm)	Pretreatment method	EMC (% d.b.)
1.5	B + F 24 h	0.8 ± 0.2 ^{ab}
	B + F + T (3 cycles)	0.7 ± 0.1 ^a
	B + F + T (5 cycles)	0.7 ± 0.2 ^a
2.5	B + F 24 h	0.7 ± 0.1 ^{ab}
	B + F + T (3 cycles)	0.8 ± 0.1 ^{ab}
	B + F + T (5 cycles)	0.7 ± 0.1 ^{ab}
3.5	B + F 24 h	0.9 ± 0.1 ^{bc}
	B + F + T (3 cycles)	1.1 ± 0.1 ^c
	B + F + T (5 cycles)	1.1 ± 0.1 ^c

B, Blanching, F, freezing and T, thawing.

Different superscripts in the same column mean that the values are significantly different ($p < 0.05$).

maximum breaking force, area under the force-deformation curve (Rosenthal, 1999), and the number of peaks (van Loon et al., 2007), respectively. The results of these parameters are listed in Table 6 while a typical force-deformation curve of dried potato chip is illustrated in Fig. 3.

Regarding the hardness of dried potato chips, it was found that the initial thickness significantly affected the hardness of potato chips. This is due to the fact that as the thickness of the sample increased, the drying time required to reach the desired moisture content increased. The effect of casehardening developed during drying was more pronounced for longer drying time. The influence of the final moisture content was not significant on the value of hardness.

The degree of starch retrogradation also influenced the hardness of dried potato chips significantly. Higher degrees of starch retrogradation tended to increase the hardness of dried chips, especially in the case of samples having higher initial thickness (3.5 mm). It was found that in the case of chips with an initial thickness of 3.5 mm the hardness values of the samples pretreated by B + F, B + F + T 3 and B + F + T 5 were approximately 5.50, 6.52 and 7.24 N, respectively. The increase in the hardness might be due to an increase in the forces binding adjacent amylose molecules in potato cells, which were developed during the retrogradation process (Jankowski, 1992).

A preliminary examination of mouth feel revealed that higher degrees of starch retrogradation led to chips having better mouth feel and firmness. This result is consistent with the report by O'Leary et al. (2000) that freezing/chilling treatment of instant mashed potato led to the products of firmer texture compared with fresh samples. The firmness of starch gels, according to this study, seemed to reflect the extent of the network that was formed upon retrogradation. Amylose plays a key role in the formation of molecular networks in retrograded starch and this role is likely to be related to the ability of these molecules to link together through the formation of double helices (Tang and Copeland, 2007). However, a full sensory study is necessary to confirm this observation.

The same trends as those reported for hardness were also observed in the case of toughness. It was found that initial thickness significantly influenced the toughness of potato chips while the final moisture content was not a significant factor. The results also showed that higher degree of starch retrogradation led to significantly higher toughness of dried potato chips. The effect of the degree of retrogradation on the increase of toughness was more obvious when the initial thickness increased. It was found that in the case of chips with an initial thickness of 3.5 mm the toughness values of the samples pretreated by B + F, B + F + T 3 and B + F + T 5 were approximately 3.18, 4.42 and 5.54 N mm, respectively. The increase in toughness might be due to the higher strength of the internal bonds within the product. It was reported that freshly cooked potato had a loose texture, and upon storage, the cooked product got compacted and had waxy texture leading to lower fracturability and higher cohesiveness (Jankowski, 1992).

In terms of crispness, it was found that the initial slice thickness significantly affected the crispness of potato chips. As expected, an initial slice thickness of 1.5 mm yielded significantly crispier chips. This is due to the greater extent of puffing observed in the thinner samples. For the effect of the final moisture content, it was found that the final moisture content significantly influenced the crispness of dried chips except for the chips with an initial thickness of 3.5 mm. This might be due to the large variation of the final moisture content in the case of chips with an initial thickness of 3.5 mm (see Table 6). The results indicated that higher degrees of starch retrogradation led to some decrease in crispness of dried chips but the trend was not statistically significant.

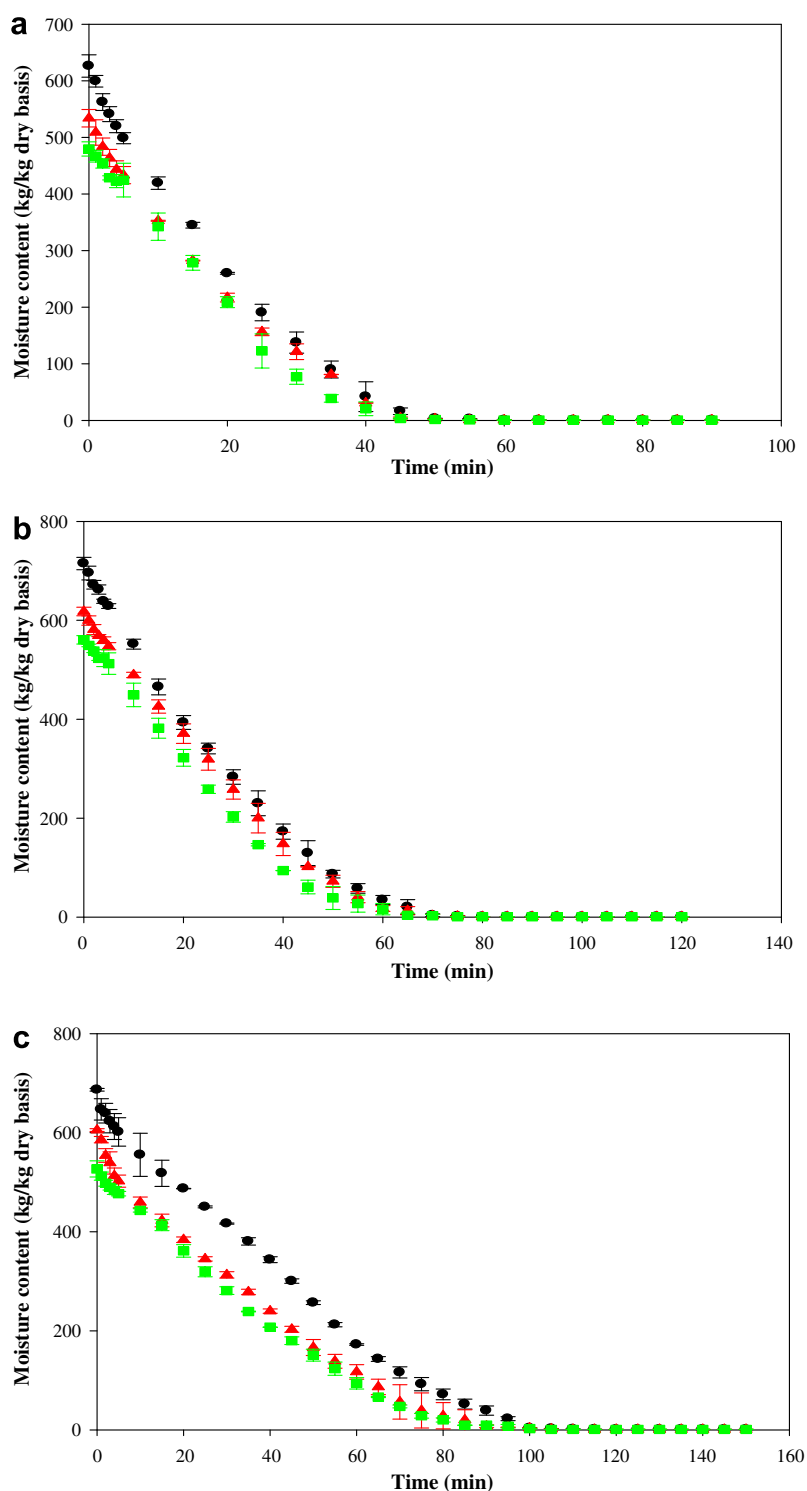


Fig. 2. Drying kinetics of potato chips with initial thickness of (a) 1.5 mm, (b) 2.5 mm, (c) 3.5 mm, subjected to different pretreatments (●) B + F, (▲) B + F + T (3 cycles), (■) B + F + T (5 cycles) (B, Blanching, F, Freezing and T, Thawing).

3.3.2. X-ray diffraction patterns

Fig. 4 shows the X-ray diffraction patterns of dried potato chips subjected to different pretreatment methods. It was observed that the diffraction patterns of all samples were almost the same. However, the relative height of the peak increased with the number of the freezing/thawing cycles indicating higher degrees of crystallinity, which was the result of starch retrogradation. Similar results

have also been reported by other researchers who studied the modification of granular potato starch by multiple deep-freezing and thawing (Szymonska et al., 2003). The degree of crystallinity of potato chips subjected to different pretreatments is listed in Table 7.

An increase in the degree of starch retrogradation led to higher degree of crystallinity due to the recrystallization of amylose

Table 5

Drying time of potato chips subjected to different pretreatment methods (the drying temperature was 90 °C and the absolute pressure was 7 kPa)

Initial thickness (mm)	Pretreatment method	Final moisture content (% d.b.)	Drying time (min)
1.5	B + F	1.6 ± 0.2	56 ± 4
	B + F + T (3 cycles)	1.6 ± 0.2	51 ± 2
	B + F + T (5 cycles)	1.6 ± 0.5	50 ± 3
2.5	B + F	1.7 ± 0.1	74 ± 2
	B + F + T (3 cycles)	1.6 ± 0.2	73 ± 4
	B + F + T (5 cycles)	1.5 ± 0.2	72 ± 3
3.5	B + F	1.6 ± 0.4	108 ± 3
	B + F + T (3 cycles)	1.6 ± 0.8	105 ± 3
	B + F + T (5 cycles)	1.6 ± 0.8	104 ± 2

B, Blanching, F, freezing and T, thawing.

and amylopectin within potato. Changing the degree of crystallinity, in turn, causes changes in the textural properties of starchy foods since it is known that aggregation and recrystallization of starch molecules during retrogradation can lead to increased rigidity and firmness (Liu et al., 2003). The results from present study indicated that higher degree of crystallinity led to an increase in hardness and toughness, while it did not show any significant effect on the crispness of dried potato chips. The formation of crystalline regions might increase the rigidity of the granules and reinforce the amylose matrix. This reorganization of retrograded starch imparted rigidity to both the swollen granules and the intergranular material by acting as physical cross-links in the overall gel structure (Ribotta et al., 2004). Therefore, higher crystallinity led to an increase in the hardness and toughness.

Table 6

Effects of initial slice thickness, pretreatment method and final moisture content on hardness, toughness, crispness and final thickness of LPSSD potato chips

Thickness (mm)	Pretreatment method	%MC (d.b.)	Hardness (N)	Toughness (N mm)	Crispness (number of peaks)	Final thickness (mm)
1.5	B + F	1.7 ± 0.2	1.6 ± 0.3 ^a	0.6 ± 0.2 ^a	8 ± 1 ^j	0.7 ± 0.1 ^a
		2.7 ± 0.2	1.7 ± 0.5 ^a	0.7 ± 0.3 ^{ab}	7 ± 1 ^{hi}	0.8 ± 0.1 ^a
		3.5 ± 0.3	1.7 ± 0.3 ^a	0.7 ± 0.3 ^{abc}	6 ± 1 ^{gh}	0.7 ± 0.16 ^a
	B + F + T 3	1.6 ± 0.2	1.7 ± 0.2 ^a	0.8 ± 0.3 ^{abcd}	7 ± 1 ^{ij}	0.8 ± 0.1 ^a
		2.6 ± 0.2	1.7 ± 0.4 ^a	0.9 ± 0.4 ^{abcd}	6 ± 1 ^{gh}	0.8 ± 0.1 ^a
		3.7 ± 0.5	1.7 ± 0.2 ^a	0.8 ± 0.3 ^{abcd}	6 ± 1 ^{gh}	0.8 ± 0.1 ^a
	B + F + T 5	1.6 ± 0.5	1.7 ± 0.2 ^a	0.9 ± 0.4 ^{abcd}	6 ± 1 ^{gh}	0.8 ± 0.1 ^a
		2.5 ± 0.2	1.8 ± 0.4 ^a	0.9 ± 0.4 ^{abcd}	6 ± 1 ^h	0.7 ± 0.1 ^a
		3.5 ± 0.8	1.7 ± 0.3 ^a	0.9 ± 0.5 ^{abcd}	5 ± 1 ^f	0.8 ± 0.1 ^a
	B + F	1.7 ± 0.1	2.8 ± 0.5 ^b	1.4 ± 0.3 ^{bcd}	6 ± 1 ^{fg}	1.3 ± 0.2 ^b
		2.6 ± 0.2	2.9 ± 0.5 ^{bc}	1.5 ± 0.6 ^d	5 ± 1 ^e	1.3 ± 0.1 ^b
		3.6 ± 0.2	2.8 ± 0.9 ^b	1.5 ± 0.7 ^{cd}	4 ± 1 ^{bcd}	1.3 ± 0.1 ^b
2.5	B + F + T 3	1.6 ± 0.2	2.9 ± 0.4 ^{bc}	2.4 ± 0.9 ^e	5 ± 1 ^e	1.3 ± 0.2 ^b
		2.5 ± 0.2	2.9 ± 0.5 ^{bc}	2.5 ± 0.8 ^{efg}	5 ± 1 ^e	1.3 ± 0.1 ^b
		3.7 ± 0.6	3.1 ± 0.3 ^{bcd}	2.4 ± 0.6 ^{ef}	4 ± 1 ^{de}	1.3 ± 0.2 ^b
	B + F + T 5	1.5 ± 0.2	3.4 ± 0.9 ^{cd}	2.7 ± 0.7 ^{efgh}	5 ± 1 ^e	1.4 ± 0.2 ^b
		2.6 ± 0.2	3.6 ± 0.8 ^d	2.7 ± 0.7 ^{efgh}	4 ± 1 ^{cde}	1.4 ± 0.2 ^b
		3.6 ± 0.2	3.4 ± 0.7 ^{cd}	2.8 ± 0.6 ^{efgh}	3 ± 1 ^a	1.4 ± 0.1 ^b
3.5	B + F	1.6 ± 0.7	5.6 ± 1.2 ^e	3.1 ± 0.9 ^{gh}	4 ± 1 ^{abc}	1.8 ± 0.1 ^c
		2.6 ± 0.7	5.3 ± 1.3 ^e	3.2 ± 0.9 ^h	4 ± 1 ^a	1.8 ± 0.1 ^c
		3.6 ± 0.7	5.6 ± 1.4 ^e	3.2 ± 0.9 ^{gh}	3 ± 1 ^a	1.8 ± 0.1 ^c
	B + F + T 3	1.6 ± 0.8	6.4 ± 0.8 ^f	4.4 ± 1.3 ⁱ	4 ± 1 ^{abcd}	1.8 ± 0.1 ^c
		2.7 ± 0.8	6.6 ± 0.9 ^{fg}	4.2 ± 1.6 ⁱ	3 ± 1 ^a	1.8 ± 0.1 ^c
		3.8 ± 0.9	6.5 ± 0.7 ^f	4.6 ± 1.3 ⁱ	3 ± 1 ^a	1.8 ± 0.1 ^c
	B + F + T 5	1.6 ± 0.8	7.1 ± 1.4 ^{gh}	5.6 ± 1.4 ^j	4 ± 1 ^{ab}	1.8 ± 0.1 ^c
		2.6 ± 0.6	7.3 ± 1.4 ^h	5.5 ± 1.0 ^j	4 ± 1 ^{cde}	1.8 ± 0.1 ^c
		3.7 ± 0.5	7.4 ± 1.2 ^h	5.5 ± 1.3 ^j	3 ± 1 ^a	1.8 ± 0.1 ^c

B, Blanching, F, freezing and T, thawing.

Different superscripts in the same column mean that the values are significantly different ($p < 0.5$).

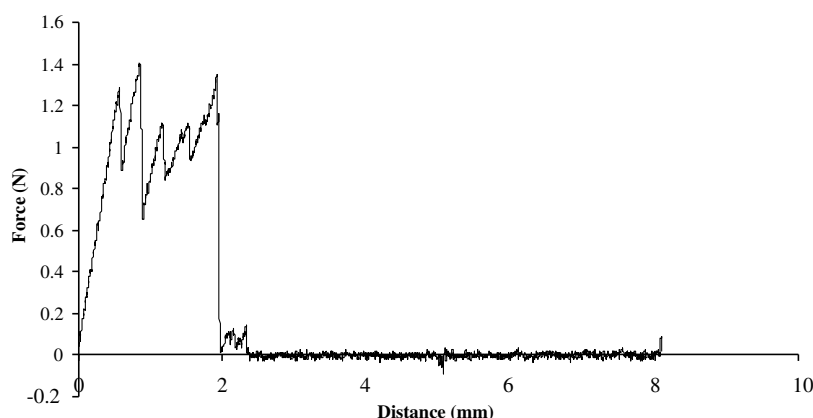


Fig. 3. A typical force-displacement curve of dried potato chips.

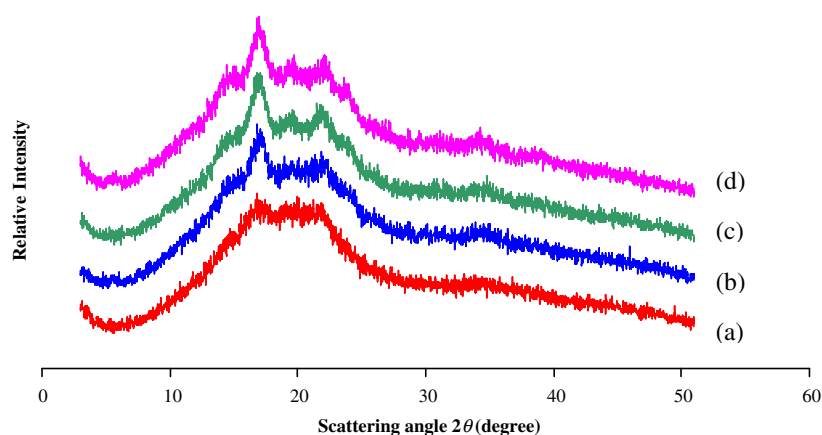


Fig. 4. X-ray diffraction patterns of dried potato chips (a) B, (b) B + F 24 h, (c) B + F + T (3 cycles), (d) B + F + T (5 cycles) (B, Blanching, F, Freezing and T, Thawing).

Table 7

Degree of crystallinity of potato chips subjected to different pretreatments

Pretreatment methods	Degree of crystallinity (%)
B	27.87 ± 2.12 ^a
B + F 24 h	35.90 ± 2.35 ^b
B + F + T (3 cycles)	40.57 ± 0.51 ^c
B + F + T (5 cycles)	45.94 ± 0.21 ^d

B, Blanching, F, freezing and T, thawing.

Different superscripts in the same column mean that the values are significantly different ($p < 0.05$).

4. Conclusion

The effects of initial slice thickness, degree of starch retrogradation and final moisture content on the texture and degree of crystallinity of potato chips dried by LPSSD were examined in this study. The various pretreatment methods were found to influence the rate of moisture reduction of the samples. The samples treated by repeated freezing/thawing required shorter drying time to reach the desired final moisture content due to the lower initial moisture content.

In terms of the product quality, it was found that initial thickness significantly influenced the hardness of potato chips. Higher degrees of starch retrogradation tended to increase the hardness of dried chips, especially in the case of chips with higher initial thicknesses. For example, in the case of chips with an initial thickness of 3.5 mm the hardness values of the samples pretreated by B + F, B + F + T 3 and B + F + T 5 were approximately 5.5, 6.5 and 7.2 N, respectively.

The same trend was also observed in terms of the toughness. In terms of crispness, chips with lower initial thickness were significantly crispier than those with higher initial thickness due probably to a greater extent of puffing. Higher degrees of starch retrogradation led to some decrease in crispness value but the trend was not statistically significant.

Increasing the degree of starch retrogradation yielded higher degree of crystallinity, which, in turn, led to an increase in the hardness and toughness, but had little effect on the crispness of dried potato chips. Nevertheless, a full sensory test is required before confirming this result. It is also important to note that, from an economic or commercial point of view, the pretreatment methods outlined in this study, especially the time scales used in freezing/thawing cycles, may not be entirely practical. A study is indeed underway to investigate how shorter freezing and/or thawing time might influence the degree of starch retrogradation.

Acknowledgements

The authors express their sincere appreciation to the Commission on Higher Education, the Thailand Research Fund (TRF) and the International Foundation for Science (IFS), Sweden for supporting this study financially.

References

- AOAC, 1984. Official methods of analysis, 14th ed. Association of Official Analytical Chemists, Washington, DC.
- Devahastin, S., Suvarnakuta, P., 2004. Superheated-steam-drying of food products. In: Mujumdar, A.S. (Ed.), *Dehydration of Products of Biological Origin*. Science Publishers, Enfield, NH, pp. 493–511.
- Devahastin, S., Suvarnakuta, P., Soponronnarit, S., Mujumdar, A.S., 2004. A comparative study of low-pressure superheated steam and vacuum drying of a heat-sensitive material. *Drying Technology* 22, 1845–1867.
- Garayo, J., Moreira, R., 2002. Vacuum frying of potato chips. *Journal of Food Engineering* 55, 181–191.
- Jankowski, T., 1992. Influence of starch retrogradation on the texture of cooked potato tuber. *International Journal of Food Science and Technology* 27, 637–642.
- Karim, A.A., Norziah, M.H., Seow, C.C., 2000. Methods for the study of starch retrogradation. *Food Chemistry* 71, 9–36.
- Karlsson, M.E., Eliasson, A., 2003. Gelatinization and retrogradation of potato (*Solanum tuberosum*) starch in situ as assessed by differential scanning calorimetry (DSC). *Lebensmittel-Wissenschaft und-Technologie* 36, 735–741.
- Kim, Y.S., Wiesenborn, D.P., Orr, P.H., Grant, L.A., 1995. Screening potato starch for novel properties using differential scanning calorimetry. *Journal of Food Science* 60, 1060–1065.
- Leeratanarak, N., Devahastin, S., Chiewchan, N., 2006. Drying kinetics and quality of potato chips undergoing different drying techniques. *Journal of Food Engineering* 77, 635–643.
- Liu, H., Eskin, M.N.A., Cui, S.W., 2003. Interaction of wheat and rice starches with yellow mustard mucilage. *Food Hydrocolloids* 17, 863–869.
- McMinn, W.A.M., Magee, T.R.A., 1996. Air drying kinetics of potato cylinders. *Drying Technology* 14, 2025–2040.
- Moreno-Perez, L.F., Gasson-Lara, J.H., Ortega-Rivas, E., 1996. Effect of low temperature-long time blanching on quality of dried sweet potato. *Drying Technology* 14, 1839–1857.
- Mujumdar, A.S., Devahastin, S., 2000. Fundamental principles of drying. In: Devahastin, S. (Ed.), *Mujumdar's Practical Guide to Industrial Drying*. Exergex, Brossard, Canada, pp. 1–22.
- O'Leary, E., Gormley, T.R., Butler, F., Shilton, N., 2000. The effect of freeze-chilling on the quality of ready-meal components. *LWT – Food Science and Technology* 33, 217–224.
- Pimpaporn, P., Devahastin, S., Chiewchan, N., 2007. Effects of combined pretreatment on drying kinetics and quality of potato chips undergoing low-pressure superheated steam drying. *Journal of Food Engineering* 81, 318–329.
- Radley, J.A., 1976. *Industrial Uses of Starch and Its Derivatives*. Applied Science, London.
- Redmond, G.A., Gormley, T.R., Butler, F., 2004. The effect of short- and long-term freeze-chilling on the quality of cooked green beans and carrots. *Innovative Food Science and Emerging Technologies* 5, 65–72.
- Ribotta, P.D., Cuffini, S., León, A.E., Añón, M.C., 2004. The staling of bread an X-ray diffraction study. *European Food Research and Technology* 218, 219–223.
- Rosenthal, A.J., 1999. *Food Texture: Measurement and Perception*. Aspen, Gaithersburg.

- Szymonska, J., Krok, F., Komorowska-Czepirska, E., Rebilas, K., 2003. Modification of granular potato starch by multiple deep-freezing and thawing. *Carbohydrate Polymers* 52, 1–10.
- Tang, M.C., Copeland, L., 2007. Investigation of starch retrogradation using atomic force microscopy. *Carbohydrate Polymers* 70, 1–7.
- van Loon, W.A.M., Visser, J.E., Linssen, F.P.H., Somsen, D.J., Jan Klok, H., Voragen, A.G.J., 2007. Effect of pre-drying and par-frying conditions on the crispness of French fries. *European Food Research and Technology* 225, 929–935.
- Wang, N., Brennan, J.G., 1995. Changes in structure, density and porosity of potato during dehydration. *Journal of Food Engineering* 24, 61–76.
- Yuan, R.C., Thompson, D.B., 1998. Freeze–thaw stability of three waxy maize starch pastes measured by centrifugation and calorimetry. *Cereal Chemistry* 75, 571–573.

Effects of combined pretreatments on drying kinetics and quality of potato chips undergoing low-pressure superheated steam drying

Phet Pimpaporn, Sakamon Devahastin^{*}, Naphaporn Chiewchan

Department of Food Engineering, King Mongkut's University of Technology Thonburi, 126 Pracha u-tid Road, Bangkok 10140, Thailand

Received 26 July 2006; received in revised form 3 November 2006; accepted 7 November 2006

Available online 17 January 2007

Abstract

Due to an increasing demand from health-conscious consumers more attention has been placed on investigating alternative techniques to replace conventional deep-fat frying to produce health-friendly snack products including potato chips. Recently, low-pressure superheated steam drying (LPSSD) has proved to have potential to produce fat-free potato chips if performed in combination with appropriate pre-drying treatments. In this study, the influences of various pretreatments and drying temperature on the LPSSD drying kinetics and quality parameters of dried potato chips were investigated. LPSSD of potato chips underwent various combined pretreatments, i.e., (a) blanching, (b) combined blanching and freezing, (c) blanching followed by immersion in glycerol solution and then freezing, and (d) combined blanching, immersion in monoglyceride solution and freezing, were carried out at different drying temperatures (70, 80, and 90 °C) at an absolute pressure of 7 kPa. The quality of the dried chips was then evaluated in terms of colors, texture (hardness, toughness and crispness) and microstructure. In terms of the drying behavior and the dried product quality, LPSSD at 90 °C with combined blanching and freezing pretreatments was proposed as the most favorable conditions for drying potato chips.

© 2006 Elsevier Ltd. All rights reserved.

Keywords: Blanching; Chemical pretreatments; Combined pretreatments; Colors; Freezing; Microstructure; Texture

1. Introduction

Potato chips are generally prepared by deep-fat frying thin potato slices to moisture content of 0.02 kg/kg (d.b.) or less; an oil content of chips generally range from 35% to 45% (w.b.) (Pedreschi & Moyano, 2005). This high level of oil content causes much concern to health-conscious consumers who are looking for snack products that are organic or all natural, low-calorie, low-fat, low-carbohydrate, low-sodium, or have health-promoting benefits. In particular, the elimination of fat is in greater demand by consumers. A technique to produce low-oil content chips, with high quality, is required. Drying is one of the techniques that could be used to prepare fat-free potato chips instead of the traditional deep-fat frying process. However, there are many problems encountered when performing

conventional hot air drying of potato slices including poor product color, dissatisfaction texture and much nutritional degradation (Leeratanarak, Devahastin, & Chiewchan, 2006).

Recently, superheated steam drying (SSD) has been applied to dry potato chips with various degrees of success. Caixeta, Moreira, and Castell-Perez (2002) studied the effects of impinging superheated steam temperature and convective heat transfer coefficient on the drying rates and some quality attributes of potato chips. These investigators found that the samples dried at higher steam temperatures and high convective heat transfer coefficients suffered less shrinkage, had higher porosity, darker color, and lower vitamin-C content. Hot air drying, on the other hand, resulted in less shrinkage because the air-dried samples developed hardened surfaces that increased the resistance to volume change. However, hot air drying produced lower porosity, darker color, and lower vitamin-C content potato chips. Iyota, Nishimura, Onuma,

^{*} Corresponding author. Tel.: +662 470 9246; fax: +662 470 9240.
E-mail address: sakamon.dev@kmutt.ac.th (S. Devahastin).

and Nomura (2001) determined the drying kinetics, surface conditions as well as color changes of dried raw potato slices undergoing SSD and hot air drying. It was found that the samples dried by superheated steam were glossier and there were no remaining starch granules on the surface. On the other hand, starch gelatinization of the samples dried by hot air occurred more slowly than in the case of SSD. Non-gelatinized starch granules still remained on the surface of the product after the hot air drying process was completed. Moreover, the second layer of crust on the chips dried by hot air could be seen. The redness of the product dried in superheated steam was found to be higher than that of the product dried in hot air.

Since most heat-sensitive foods and bioproducts deteriorate at elevated temperatures corresponding to the environment of atmospheric-pressure SSD, an alternative way to dry these heat-sensitive products has been proposed. Since it is known that water boils at lower temperature when the pressure is lowered, a concept of low-pressure superheated steam drying (LPSSD) has been proposed as an alternative to dry heat-sensitive foods and bioproducts (Devahastin, Suvarnakuta, Soponronnarit, & Mujumdar, 2004; Elustondo, Elustondo, & Urbician, 2001). This drying technique has also been tested with potato chips. Leera-tanarak et al. (2006) dried potato slices using both LPSSD and hot air drying. The effects of hot-water blanching as well as drying temperature on the drying kinetics and various quality attributes of potato chips viz. color, texture (in terms of hardness) and browning pigment accumulation were investigated. It was found that LPSSD took shorter drying time than hot air drying when the drying temperatures were higher than 80 °C. Longer blanching time and lower drying temperature resulted in better color retention and led to chips of lower browning index. Blanching also reduced the hardness and shrinkage of the product. However, the use of different blanching periods did not significantly affect the product hardness. Drying methods had no obvious effect on the product quality except on the browning index. However, the best condition proposed in their work still led to chips of inferior quality compared

with commercially available potato chips, especially in terms of texture, which is one of the important quality attributes of a snack product.

To improve the quality of a food product various pre-treatment methods have been proposed and suggested prior to drying. Much emphasis has indeed been laid on the application of pre-drying treatments as a means to improve the drying characteristics and minimize adverse structural and quality variations of the product (McMinn & Magee, 1999). In terms of the drying kinetics, physical pretreatments such as blanching (Maté, Quartaert, Meerdink, & van't Riet, 1998; Severini, Baidano, Pilli, Carbone, & Derossi, 2005) and freezing (Esh-tiaghi, Stute, & Knorr, 1994) change the physical properties of the sample cell structure, which in turn alter the rate of moisture removal. In terms of the product quality, many pretreatment methods are found to help retain or improve various quality attributes of many food products. Chemical pretreatments, which involve immersion of food materials in chemical solutions such as CaCl_2 and NaCl solutions, ionic and non-ionic surfactants, monoglyceride and glycerol solutions have also been investigated and applied successfully to many food products including potatoes (McMinn & Magee, 1999; Nargal & Ooraikul, 1996).

This research was aimed to improve the quality of LPSSD potato chips, especially in terms of their textural quality. The application of combined physical (blanching and/or freezing) and chemical (monoglyceride and glycerol) pretreatments and their effects on both the drying kinetics and some quality attributes of dried potato chips viz. colors, texture (hardness, crispness and toughness) and microstructure were investigated.

2. Materials and methods

2.1. Experimental set-up

A schematic diagram of the low-pressure superheated steam dryer and its accessories is shown in Fig. 1 (Devaha-

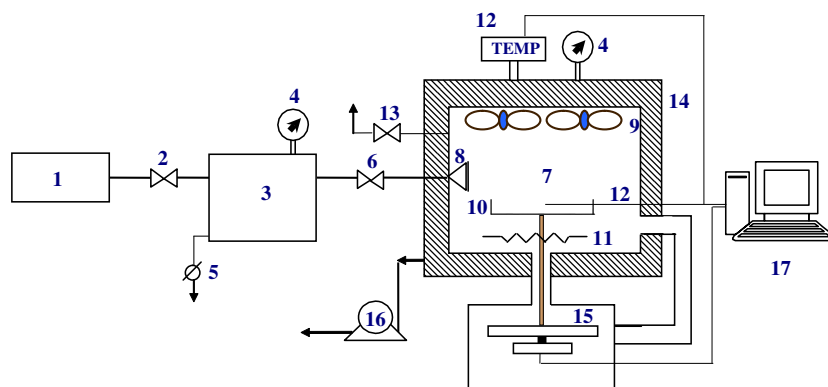


Fig. 1. A schematic diagram of low-pressure superheated steam dryer and associated units: (1) boiler; (2) steam valve; (3) steam reservoir; (4) pressure gauge; (5) steam trap; (6) steam regulator; (7) drying chamber; (8) steam inlet and distributor; (9) electric fans; (10) sample holder; (11) electric heater; (12) on-line temperature sensor and logger; (13) vacuum break-up valve; (14) insulator; (15) on-line weight indicator and logger; (16) vacuum pump; (17) PC with installed data acquisition card.

stin et al., 2004). The dryer consists of a stainless steel drying chamber; a steam reservoir, which received steam from a boiler and maintained its pressure at around 200 kPa (gage); and a liquid ring vacuum pump (Nash, model ET32030, Trumbull, CT), which was used to maintain vacuum in the drying chamber. An electric heater, rated at 1.5 kW, which was controlled by a Proportional-Integral-Derivative (PID) controller (Omron, model E5CN, Tokyo, Japan), was installed in the drying chamber to control the steam temperature and to minimize condensation of steam in the drying chamber during the start-up period. Variable-speed electric fans were used to disperse the steam throughout the drying chamber. The sample holder was made of a stainless steel screen with dimensions of $16.5 \times 16.5 \text{ cm}^2$. The change of the weight of the sample was detected continuously (at 60 s interval) using a load cell (Minebea, model Ucg-3 kg, Nagano, Japan), which was installed in a smaller chamber connected to the drying chamber by a flexible hose (in order to maintain the same vacuum pressure as that in the drying chamber). The signal from the load cell was transmitted to an indicator and a recorder (AND A& D Co., model AD 4329, Tokyo, Japan). The temperatures of the steam and of the drying sample were also measured continuously using type K thermocouples, which were connected to an expansion board (Omega Engineering, model no. EXP-32, Stamford, CT). Thermocouple signals were then multiplexed to a data acquisition card (Omega Engineering, model no. CIO-DAS16Jr., Stamford, CT) installed in a PC. Labtech Notebook software (version 12.1, Laboratory Technologies Corp., MA) was then used to read and record temperature data.

2.2. Material

White potato (*Solanum tuberosum*) was purchased from a local market and stored at 4 °C. Prior to an experiment potato was washed with tap water, peeled and sliced to a thickness of $3.5 \pm 0.3 \text{ mm}$ using an electric slicer. Potato slices were then shaped using a core borer to a diameter of 45 mm.

2.3. Methods

Prior to drying potato slices were pretreated with four different pretreatment methods, i.e., (a) blanching, (b) combined blanching and freezing, (c) blanching followed by immersion in glycerol solution (1%, 3% and 5% w/w) for 30 min and then freezing, and (d) combined blanching, immersion in monoglyceride solution (0.1%, 0.3% and 0.5% w/w) for 30 min and freezing. Blanching was performed in hot water at $90 \pm 2 \text{ °C}$ for 5 min with the ratio of potato to water of 0.015 g/g (Leeratanarak et al., 2006). The samples were immediately cooled afterwards in cold water at 4 °C. Freezing was performed at -20 °C overnight in a chest freezer (Sanyo, Model SF-C-65, Japan). Both glycerol and monoglyceride used in this study were of food grade.

After pretreatments, the samples were dried in the low-pressure superheated steam dryer at 70, 80 or 90 °C at an absolute pressure of 7 kPa. Six slices of potato were used in each drying experiment. The samples were dried until they reached the desired final moisture content of 3.5% (d.b.) (Caixeta et al., 2002). The equilibrium moisture contents of the samples were also determined by drying the samples until no changes in their weight were observed.

2.3.1. Color measurement

Colors of fresh, pretreated and dried potatoes were measured using a colorimeter (Juki, Model JP7100, Japan) with 2° North skylight as the light source. For each sample at least five measurements were made at different positions of the sample and the measured values were compared with those of the fresh sample. The data were reported as average values of two replications (each consisted of five measurements as mentioned earlier) with standard errors. Three Hunter parameters, namely, L (lightness), a (redness/greenness) and b (yellowness/blueness), were obtained from each color measurement. The normalized color differences of the samples were then calculated as

$$\Delta L = \frac{L - L_0}{L_0}, \quad \Delta a = \frac{a - a_0}{a_0}, \quad \text{and} \quad \Delta b = \frac{b - b_0}{b_0}$$

where L , a , b represent the lightness, redness and yellowness of the pretreated/dried samples, respectively, while L_0 , a_0 , b_0 represent the initial values of the lightness, redness and yellowness of the fresh sample, respectively.

2.3.2. Textural characteristics

Measurement of the texture of potato chips was carried out using a texture analyzer (Stable Micro System, TA.XT.Plus, UK). A chip was placed on a hollow planar base. The force was then applied to the sample by a 5-mm spherical probe at a constant speed of 2 mm/s until the sample was cracked (Moreno-Perez, Gasson-Lara, & Ortega-Rivas, 1996). Force–deformation data were recorded to determine the textural characteristics of the chip. The maximum force of break, initial slope of deformation and area under the force–deformation curve were indicated as hardness, crispness and toughness of the chip, respectively (Aguilera, Castro, & Cadoche, 2004). All tests were performed in duplicate and the average values were reported.

2.3.3. Microstructural evaluation

The microstructural changes of dried potato chips were observed by a scanning electron microscope (Leo 4551455, UK) at 100× magnification. The microstructure of dried potato chips was observed both on the surface and along the cross-section at the center of the chips.

2.4. Statistical analysis

All data were subjected to the analysis of variance (ANOVA) using SPSS® software and presented as mean

values with standard deviation. Differences between mean values were established using Tukey's multiple range tests at a confidence level of 95% ($p \leq 0.05$).

3. Results and discussion

3.1. Effects of pretreatments on initial moisture content of potato slices (prior to drying)

The initial moisture contents of all treated samples are listed in Table 1. Only the samples treated with the highest concentration of glycerol had significantly lower moisture contents compared with the controlled samples (B). It is important to note that blanching the samples for 5 min at 90 °C yielded the degree of starch gelatinization of 100%.

3.2. Drying kinetics of potato slices

Fig. 2 shows a typical phenomenon during LPSSD of potato slices. During the first few minutes of drying the sample gained a small amount of moisture (hence moisture ratio of higher than unity) due to steam condensation; this phenomenon is indeed typical of SSD and LPSSD (Devahastin et al., 2004; Iyota et al., 2001).

The temperature of the sample suddenly changed from around 0 °C to the boiling temperature of water of around

Table 1
Initial moisture contents of potato slices underwent different pretreatment methods

Pretreatment method	Moisture content (% d.b.)
B (control)	529.72 ± 3.09 ^{bc}
B + F	471.16 ± 15.66 ^b
B + I (0.1% monoglyceride) + F	510.30 ± 37.20 ^{bc}
B + I (0.3% monoglyceride) + F	510.87 ± 15.72 ^{bc}
B + I (0.5% monoglyceride) + F	476.23 ± 20.33 ^b
B + I (1% glycerol) + F	465.34 ± 20.39 ^b
B + I (3% glycerol) + F	467.06 ± 17.24 ^b
B + I (5% glycerol) + F	384.94 ± 18.43 ^a

B: blanching, I: immersion in solutions and F: freezing.

Different superscripts in the same column mean that the values are significantly different ($p \leq 0.05$).

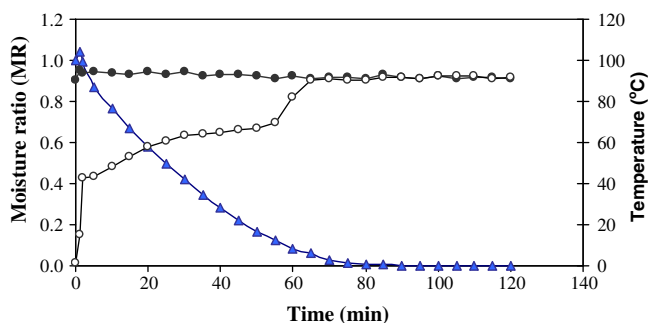


Fig. 2. Drying kinetics and temperature evolution of potato chips undergoing LPSSD at 90 °C (7 kPa): drying medium temperature (●), sample temperature (○), moisture ratio (▲).

40 °C (saturation temperature of water at 7 kPa) and remained briefly at this temperature indicating a short constant drying rate period. After this short period the sample temperature rose again and finally approached the steam temperature.

As expected, drying at higher steam temperatures led to higher rates of drying. This is due to the fact that higher degrees of superheat generate larger driving force for heat/mass transfer; in the case of superheated steam drying pressure gradient between the saturated vapor pressure of water at the sample surface and the partial pressure of water in the drying medium is the driving force for moisture transfer. Moreover, higher temperature leads to higher value of moisture diffusivity and hence higher rate of moisture removal.

3.2.1. Effects of combined blanching and freezing pretreatments on drying kinetics of potato slices

To examine the effects of combined blanching and freezing pretreatments on the drying kinetics of LPSSD potato slices, the drying kinetics of samples underwent combined pretreatments were compared with those of blanched-only and unblanched samples. Fig. 3 shows the comparison of the drying kinetics of different physically pretreated

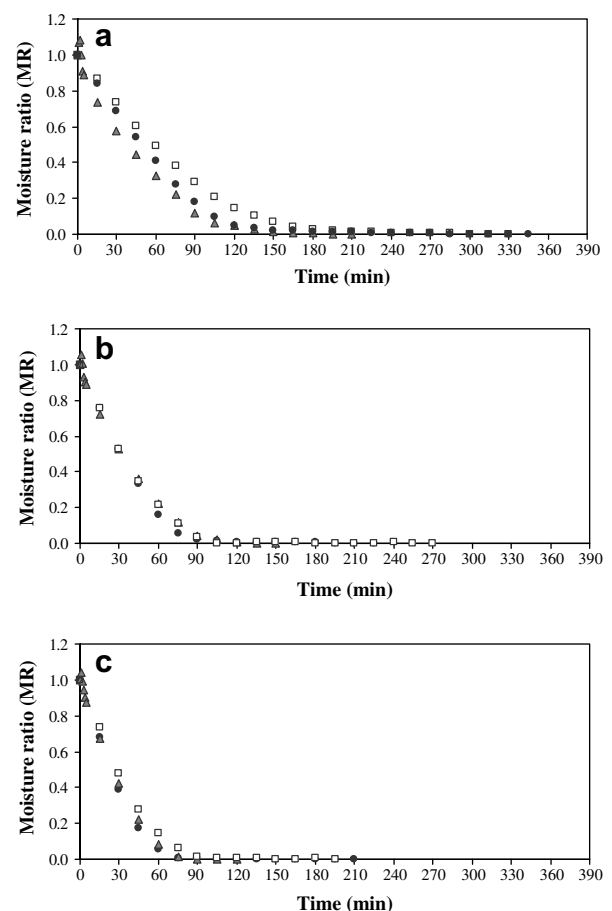


Fig. 3. Drying kinetics of unblanched (□), blanched (●) and blanched-frozen (▲) potato slices at (a) 70 °C, (b) 80 °C and (c) 90 °C.

samples undergoing LPSSD at different steam temperatures. At 70 °C the drying time to reach the equilibrium moisture content was approximately 180, 255 and 300 min for combined blanched-frozen, blanched and unblanched samples, respectively. For drying at 80 °C using the same pretreatment methods the drying time to reach the equilibrium moisture content was around 135, 165 and 255 min, respectively. For drying at 90 °C the corresponding drying time was 120, 120 and 195 min, respectively. Based on these comparisons it is seen that combination of blanching and freezing treatments prior to drying could improve the drying kinetics of potato slices at all drying temperatures. Nevertheless, the effect of combined pretreatment was more obvious at a lower drying temperature of 70 °C and less obvious at higher steam temperatures.

The combination of blanching and freezing pretreatments led to a shorter drying time than that of unblanched samples at all drying temperatures. This behavior was probably due to structure softening; blanching might modify the structure of potato tissue to promote water removal. In addition, freezing affected physical tissue of potato due to the large size of ice crystals formed during slow freezing. The ice crystals might cause openings of cell wall and semi-permeable membrane that could facilitate moisture transfer during drying. This improvement was also noted with many agricultural products, namely, green bean, carrots and potato (Eshtiaghi et al., 1994), avocado (Alzamora & Chirife, 1980) and banana (Dandamrongrak, Mason, & Young, 2003).

3.2.2. Effect of glycerol on drying kinetics of potato slices

The drying curves of glycerol-treated samples are shown in Fig. 4. It can be seen that glycerol had an influence on the drying kinetics of the samples at all drying conditions. All glycerol-treated samples needed longer time to reach their desired final moisture contents than those underwent blanching and freezing pretreatment. This is because glycerol has three hydroxyl groups that form hydrogen bonds with water in potato slices. Therefore, evaporation of free water on the surface of sliced potato becomes more difficult. However, the effect of glycerol was reduced at high drying temperatures, especially at 90 °C. The drying time of each case was nearly the same as that of combined blanched-frozen sample.

3.2.3. Effect of monoglyceride on drying kinetics of potato slices

Fig. 5 shows the drying curves of blanched potato slices with monoglyceride immersion at various concentrations (i.e., 0.1%, 0.3% and 0.5%). At 70 and 80 °C the drying time to reach the desired final moisture contents was longer than that of combined blanched-frozen samples. Since the degree of starch gelatinization of 100% was obtained after blanching and glycerol or monoglyceride was added only after blanching, not before, glycerol or monoglyceride might bind with leftover free water. This in turn led to lowering of the initial moisture contents of the samples and

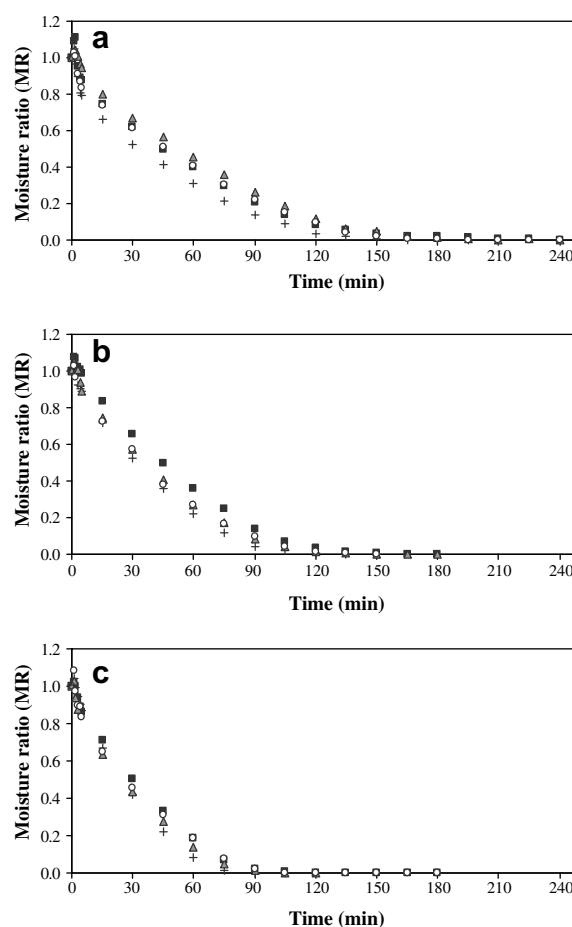


Fig. 4. Drying kinetics of blanched potato slices with glycerol immersion at concentrations of 0% (+), 1% (■), 3% (▲), and 5% (○) followed by freezing at drying temperature of (a) 70 °C, (b) 80 °C and (c) 90 °C.

affected the drying rates by retarding the water removal from the samples (Vittadini, Clubbs, Shellhammer, & Vodovotz, 2004).

However, the results showed an unclear effect of monoglyceride. For example, at the drying temperature of 70 °C the sample treated with 0.3% monoglyceride required shorter time to reach its equilibrium moisture content than samples treated at other concentrations. However, the sample treated with 0.5% monoglyceride required shorter time than the sample treated with 0.3% monoglyceride at the drying temperature of 80 °C.

3.3. Effects of pretreatments on equilibrium moisture content of potato slices

The equilibrium moisture contents of potato slices that underwent different pretreatments including blanching, immersion in solutions and freezing are listed in Table 2.

Glycerol had an effect on the equilibrium moisture contents of potato slices. All equilibrium moisture contents of samples containing glycerol were higher than those of both combined blanched-frozen and monoglyceride-treated samples. This is probably due to the formation of hydrogen

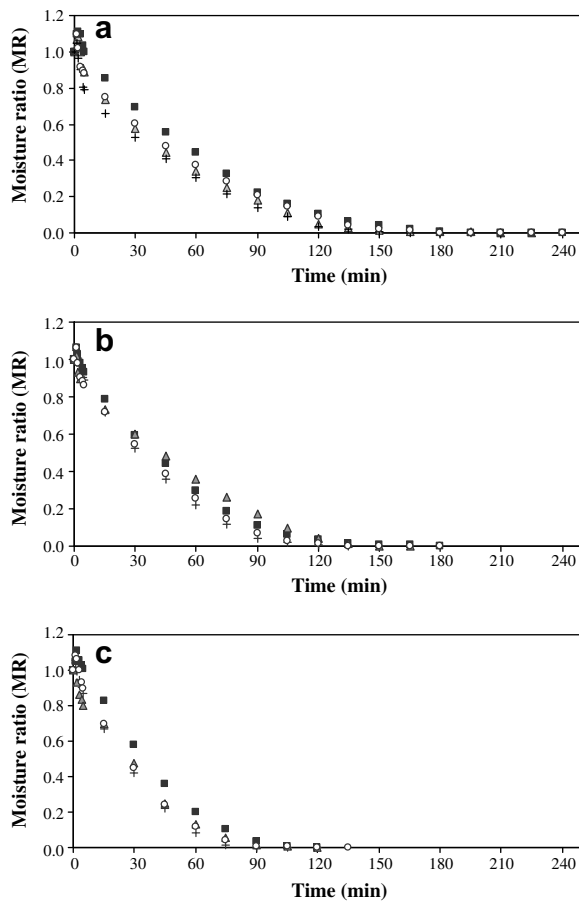


Fig. 5. Drying kinetics of blanched potato slices with monoglyceride immersion at concentrations of 0% (+), 0.1% (■), 0.3% (▲), and 0.5% (○) followed by freezing at drying temperature of (a) 70 °C, (b) 80 °C and (c) 90 °C.

Table 2
Equilibrium moisture contents of dried potato slices underwent various pretreatment methods

Pretreatment method	Equilibrium moisture content (% d.b.)		
	70 °C	80 °C	90 °C
B (control)	2.92 ± 0.55	2.57 ± 0.64	2.05 ± 0.34
B + F	3.06 ± 0.69	1.46 ± 0.20	0.84 ± 0.26
B + I (0.1% monoglyceride) + F	3.60 ± 0.34	2.02 ± 0.53	1.02 ± 0.59
B + I (0.3% monoglyceride) + F	3.15 ± 0.06	1.33 ± 0.11	0.78 ± 0.09
B + I (0.5% monoglyceride) + F	3.37 ± 0.05	1.61 ± 0.11	0.73 ± 0.36
B + I (1% glycerol) + F	3.35 ± 0.10	2.85 ± 0.11	1.23 ± 0.32
B + I (3% glycerol) + F	4.18 ± 0.02	2.68 ± 0.12	1.18 ± 0.27
B + I (5% glycerol) + F	5.15 ± 0.04	2.57 ± 0.06	1.29 ± 0.20

B: blanching, I: immersion in solutions and F: freezing.

bonds between the three hydroxyl groups of glycerol with moisture in potato slices.

Before the quality analysis of dried potato chips was performed the samples were dried until reaching the moisture content of approximately 3.5% (d.b.) in all cases (except for the samples treated with 3% and 5% glycerol and dried at 70 °C). The average drying time to reach the desired moisture content of 3.5% (d.b.) is listed in Table 3.

Table 3

Estimated drying time to reach the moisture content of 3.5% (d.b.)

Pretreatment method	Drying time (min)		
	70 °C	80 °C	90 °C
B (control)	261 ± 5 ^c	178 ± 6 ^b	84 ± 7 ^a
B + F	173 ± 15 ^a	128 ± 8 ^a	90 ± 4 ^{ab}
B + I (0.1% monoglyceride) + F	230 ± 11 ^b	157 ± 13 ^{ab}	109 ± 3 ^{ab}
B + I (0.3% monoglyceride) + F	175 ± 10 ^a	126 ± 12 ^a	81 ± 5 ^a
B + I (0.5% monoglyceride) + F	207 ± 8 ^{ab}	128 ± 10 ^a	98 ± 9 ^{ab}
B + I (1% glycerol) + F	228 ± 11 ^b	152 ± 9 ^{ab}	115 ± 4 ^b
B + I (3% glycerol) + F	235 ± 22 ^{bc*}	140 ± 10 ^{ab}	96 ± 13 ^{ab}
B + I (5% glycerol) + F	203 ± 12 ^{ab*}	116 ± 19 ^a	86 ± 6 ^a

B: blanching, I: immersion in solutions and F: freezing.

* Denotes the cases where the final moisture content of 3.5% (d.b.) was not achievable.

3.4. Quality of dried potato chips

3.4.1. Colors

The colors of the samples were measured in terms of Hunter parameters (*L*, *a* and *b*) in order to investigate the color changes of potato chips as affected by pretreatment methods and drying temperature. The results are presented in normalized color differences.

Regarding the lightness of potato samples (Table 4) it was found that after all samples were pretreated the lightness of all samples decreased because gelatinization of starch occurred during the blanching step. The lightness was reduced due to the clarity-like characteristic of gelatinized starch. When the samples were dried the lightness of blanched-only samples were significantly lower than those underwent combined blanching-freezing, combined blanching/immersion in monoglyceride or glycerol and freezing pretreatments. The lightness of dried sample obviously increased in almost all cases except for the blanched-only sample, which still had the light transparency characteristics. The lightness increased since the clarity-like characteristics of the sample became opaque; the opaque characteristics were noted only in the samples underwent freezing pretreatment. This phenomenon might be due to the fact that freezing might have an influence on the arrangement of gelatinized starch molecules during retrogradation. The drying temperature did not have any significant effect on the changes of lightness in all cases, however.

In terms of redness (Table 4) it was found that the redness of pretreated samples was not significantly different among all cases due probably to the leaching out of soluble pigments during blanching and immersion in solutions. After subsequent drying the changes of redness of dried potato were observed. All dried potato chips were obviously redder than fresh and pretreated potatoes. It was noted that the drying temperature had an influence on the redness, particularly at the highest drying temperature (90 °C). This is because Maillard reaction or other thermal damages occurred more at higher drying temperatures. The effect of high-temperature drying on the redness was obviously found in the monoglyceride-treated and glycerol-

Table 4
Effects of drying temperature and pretreatments on the changes of color of LPSSD potato chips

Pretreatment method	Drying temperature (°C)	Color		
		Fresh sample	Normalized color differences (fresh vs. pretreated samples)	Normalized color differences (fresh vs. dried samples)
Blanching	70	(L) 48.95 ± 0.70 ^{ab} (a) −2.95 ± 0.29 ^{ab} (b) 10.05 ± 1.16 ^{ab}	(L) −0.12 ± 0.02 ^d (a) 0.70 ± 0.26 ^b (b) −0.66 ± 0.04 ^{ab}	(L) −0.07 ± 0.04 ^a (a) 0.36 ± 0.05 ^{cde} (b) 0.46 ± 0.04 ^a
		(L) 48.93 ± 0.55 ^{ab} (a) −2.84 ± 0.59 ^{ab} (b) 9.22 ± 0.31 ^{ab}	(L) −0.15 ± 0.01 ^{cd} (a) 0.20 ± 0.22 ^{ab} (b) −0.64 ± 0.01 ^{abc}	(L) −0.11 ± 0.02 ^a (a) −0.06 ± 0.32 ^{abc} (b) 0.44 ± 0.11 ^a
		(L) 47.99 ± 1.36 ^a (a) −2.53 ± 0.05 ^b (b) 9.79 ± 0.05 ^{ab}	(L) −0.17 ± 0.01 ^{bcd} (a) 0.47 ± 0.10 ^{ab} (b) −0.62 ± 0.02 ^{abc}	(L) −0.10 ± 0.04 ^a (a) −0.02 ± 0.05 ^{bc} (b) 0.42 ± 0.04 ^a
	80	(L) 52.83 ± 0.64 ^b (a) −3.30 ± 0.01 ^{ab} (b) 11.21 ± 0.11 ^b	(L) −0.27 ± 0.01 ^a (a) 0.24 ± 0.03 ^{ab} (b) −0.69 ± 0.05 ^a	(L) 0.40 ± 0.04 ^c (a) 0.59 ± 0.05 ^{def} (b) 1.16 ± 0.13 ^{bc}
		(L) 51.38 ± 0.47 ^{ab} (a) −3.22 ± 0.04 ^{ab} (b) 10.93 ± 0.09 ^{ab}	(L) −0.27 ± 0.01 ^a (a) 0.17 ± 0.04 ^{ab} (b) −0.66 ± 0.04 ^{ab}	(L) 0.49 ± 0.06 ^b (a) 0.68 ± 0.16 ^{def} (b) 1.07 ± 0.06 ^b
		(L) 51.02 ± 1.03 ^{ab} (a) −3.08 ± 0.24 ^{ab} (b) 10.52 ± 0.55 ^{ab}	(L) −0.25 ± 0.02 ^{abc} (a) 0.29 ± 0.15 ^{ab} (b) −0.64 ± 0.03 ^{abc}	(L) 0.39 ± 0.01 ^{bc} (a) 0.18 ± 0.04 ^{cd} (b) 1.35 ± 0.06 ^{bcd}
	90	(L) 49.99 ± 0.34 ^{ab} (a) −2.90 ± 0.27 ^{ab} (b) 9.22 ± 0.68 ^{ab}	(L) −0.21 ± 0.01 ^{abcd} (a) 0.45 ± 0.18 ^{ab} (b) −0.61 ± 0.05 ^{abc}	(L) 0.38 ± 0.02 ^{bc} (a) 1.09 ± 0.06 ^f (b) 1.58 ± 0.06 ^{bcd}
		(L) 51.05 ± 0.79 ^{ab} (a) −3.52 ± 0.34 ^{ab} (b) 10.15 ± 1.19 ^{ab}	(L) −0.22 ± 0.02 ^{abc} (a) 0.18 ± 0.08 ^{ab} (b) −0.66 ± 0.03 ^{ab}	(L) 0.35 ± 0.01 ^{bc} (a) 0.26 ± 0.02 ^{cde} (b) 1.46 ± 0.31 ^{bcd}
		(L) 50.08 ± 1.13 ^{ab} (a) −3.10 ± 0.34 ^{ab} (b) 9.90 ± 1.39 ^{ab}	(L) −0.26 ± 0.02 ^{abcd} (a) 0.14 ± 0.15 ^a (b) −0.64 ± 0.01 ^{abc}	(L) 0.33 ± 0.02 ^{bc} (a) 0.01 ± 0.15 ^{bc} (b) 1.43 ± 0.37 ^{bcd}
B + I (0.1% monoglyceride) + F	70	(L) 49.50 ± 0.03 ^{ab} (a) −3.04 ± 0.40 ^{ab} (b) 9.80 ± 0.63 ^{ab}	(L) −0.23 ± 0.01 ^{abc} (a) 0.30 ± 0.30 ^{ab} (b) −0.60 ± 0.01 ^{abc}	(L) 0.40 ± 0.04 ^{bc} (a) 0.79 ± 0.30 ^{ef} (b) 1.57 ± 0.12 ^{bcd}
		(L) 47.50 ± 1.87 ^a (a) −3.06 ± 0.33 ^{ab} (b) 9.35 ± 0.07 ^{ab}	(L) −0.22 ± 0.02 ^{abc} (a) 0.11 ± 0.12 ^a (b) −0.60 ± 0.05 ^{abc}	(L) 0.39 ± 0.05 ^{bc} (a) 0.60 ± 0.17 ^{def} (b) 1.63 ± 0.04 ^{bcd}
		(L) 47.93 ± 0.92 ^a (a) −3.12 ± 0.15 ^{ab} (b) 10.62 ± 0.08 ^{ab}	(L) −0.20 ± 0.01 ^{abcd} (a) 0.29 ± 0.02 ^{ab} (b) −0.68 ± 0.02 ^a	(L) 0.35 ± 0.02 ^{bc} (a) −0.14 ± 0.07 ^{abc} (b) 1.30 ± 0.02 ^{bcd}
	80	(L) 48.31 ± 1.58 ^a (a) −3.14 ± 0.44 ^{ab} (b) 8.38 ± 0.29 ^a	(L) −0.23 ± 0.06 ^{abc} (a) 0.14 ± 0.12 ^a (b) −0.58 ± 0.07 ^{abc}	(L) 0.47 ± 0.01 ^b (a) 0.60 ± 0.31 ^{def} (b) 1.49 ± 0.03 ^{bcd}
		(L) 51.28 ± 0.91 ^{ab} (a) −2.99 ± 0.29 ^{ab} (b) 9.41 ± 0.29 ^{ab}	(L) −0.27 ± 0.02 ^a (a) 0.15 ± 0.16 ^a (b) −0.63 ± 0.04 ^{abc}	(L) 0.34 ± 0.04 ^{bc} (a) 0.71 ± 0.13 ^{def} (b) 1.41 ± 0.17 ^{bcd}
		(L) 48.11 ± 0.62 ^a (a) −2.71 ± 0.02 ^{ab} (b) 9.61 ± 0.09 ^{ab}	(L) −0.24 ± 0.02 ^{abc} (a) 0.24 ± 0.02 ^{ab} (b) −0.66 ± 0.02 ^{ab}	(L) 0.46 ± 0.07 ^c (a) 0.19 ± 0.17 ^{cd} (b) 1.12 ± 0.07 ^{bc}
	90	(L) 50.25 ± 0.31 ^{ab} (a) −3.37 ± 0.02 ^{ab} (b) 10.68 ± 0.05 ^{ab}	(L) −0.19 ± 0.01 ^{abcd} (a) 0.46 ± 0.02 ^{ab} (b) −0.64 ± 0.02 ^{abc}	(L) 0.40 ± 0.06 ^c (a) 0.31 ± 0.10 ^{cde} (b) 1.29 ± 0.03 ^{bcd}
		(L) 50.48 ± 0.37 ^{ab} (a) −3.23 ± 0.19 ^{ab} (b) 10.36 ± 0.35 ^{ab}	(L) −0.24 ± 0.02 ^{abc} (a) 0.30 ± 0.04 ^{ab} (b) −0.69 ± 0.02 ^a	(L) 0.37 ± 0.07 ^{bc} (a) 0.60 ± 0.07 ^{def} (b) 1.23 ± 0.09 ^{bc}
		(L) 50.82 ± 1.20 ^{ab} (a) −3.11 ± 0.07 ^{ab} (b) 10.78 ± 0.37 ^{ab}	(L) −0.20 ± 0.01 ^{abcd} (a) 0.29 ± 0.06 ^{ab} (b) −0.69 ± 0.01 ^a	(L) 0.37 ± 0.01 ^{bc} (a) 0.35 ± 0.05 ^{cde} (b) 1.12 ± 0.03 ^{bc}
B + I (3% glycerol) + F	70*	(L) 49.65 ± 0.69 ^{ab} (a) −2.74 ± 0.01 ^{ab} (b) 9.23 ± 0.42 ^{ab}	(L) −0.16 ± 0.03 ^{bcd} (a) 0.61 ± 0.16 ^{ab} (b) −0.64 ± 0.01 ^{abc}	(L) 0.46 ± 0.01 ^c (a) 1.10 ± 0.01 ^f (b) 1.60 ± 0.22 ^{cd}
		(L) 49.26 ± 0.31 ^{ab} (a) −2.83 ± 0.12 ^{ab} (b) 9.09 ± 0.16 ^{ab}	(L) −0.21 ± 0.02 ^{abcd} (a) 0.36 ± 0.04 ^{ab} (b) −0.66 ± 0.02 ^{ab}	(L) 0.44 ± 0.08 ^c (a) 1.08 ± 0.06 ^f (b) 1.52 ± 0.20 ^{bcd}

Table 4 (continued)

Pretreatment method	Drying temperature (°C)	Color		
		Fresh sample	Normalized color differences (fresh vs. pretreated samples)	Normalized color differences (fresh vs. dried samples)
B + I (5% glycerol) + F	90	(L) 47.99 ± 0.59^a	(L) -0.16 ± 0.01^{bcd}	(L) 0.30 ± 0.02^c
		(a) -2.68 ± 0.06^{ab}	(a) 0.59 ± 0.02^{ab}	(a) -0.43 ± 0.02^{ab}
		(b) 8.72 ± 0.02^a	(b) -0.60 ± 0.03^{abc}	(b) 1.39 ± 0.16^{bcd}
	70*	(L) 48.14 ± 2.65^a	(L) -0.20 ± 0.07^{abcd}	(L) 0.48 ± 0.04^c
		(a) -2.80 ± 0.11^{ab}	(a) 0.65 ± 0.03^{ab}	(a) 0.95 ± 0.07^f
		(b) 9.57 ± 0.07^{ab}	(b) -0.50 ± 0.02^c	(b) 1.82 ± 0.02^d
	80	(L) 51.11 ± 0.43^{ab}	(L) -0.23 ± 0.01^{abc}	(L) 0.40 ± 0.05^c
		(a) -3.53 ± 0.19^{ab}	(a) 0.38 ± 0.17^{ab}	(a) 0.63 ± 0.17^{def}
		(b) 10.70 ± 0.23^{ab}	(b) -0.53 ± 0.04^{bc}	(b) 1.50 ± 0.10^{bcd}
	90	(L) 51.12 ± 0.31^{ab}	(L) -0.16 ± 0.0^{cd}	(L) 0.20 ± 0.11^b
		(a) -3.64 ± 0.12^a	(a) 0.30 ± 0.02^{ab}	(a) -0.62 ± 0.02^a
		(b) 10.57 ± 0.51^{ab}	(b) -0.51 ± 0.02^c	(b) 1.25 ± 0.19^{bcd}

B: blanching, I: immersion in solutions and F: freezing.

Different superscripts in the same column mean that the values are significantly different ($p \leq 0.05$).

* Denotes the cases where the final moisture content of 3.5% (d.b.) was not achievable.

treated samples. Nevertheless, the effect of higher drying temperature on the redness was not significantly different among blanched-only and combined blanched-frozen samples.

Blanching pretreatment had more significant effect on the redness of the samples than combined pretreatments (blanching and freezing and treatments involving immersion in monoglyceride and glycerol, except at 5% glycerol).

Table 5

Effects of pretreatments and drying temperature on final thickness, hardness, crispness and toughness of LPSSD potato chips

Pretreatment method	Drying temperature (°C)	Thickness (mm)	Hardness (N)	Toughness (N mm)	Crispness (N/mm)
Blanching	70	1.58 ± 0.03^{bc}	12.75 ± 2.38^{efg}	18.81 ± 4.46^f	3.43 ± 1.65^{ab}
	80	1.55 ± 0.05^b	8.59 ± 2.30^{cdef}	17.59 ± 1.87^f	6.22 ± 0.94^{abcde}
	90	1.53 ± 0.03^b	8.21 ± 0.64^{bcdef}	16.22 ± 0.21^{ef}	5.07 ± 0.43^{abcd}
Blanching + freezing	70	1.65 ± 0.05^{bcd}	10.21 ± 0.58^{def}	9.13 ± 1.38^{bcde}	14.82 ± 2.86^{fghi}
	80	1.67 ± 0.06^{bcd}	8.00 ± 2.60^{bcdef}	4.14 ± 1.97^{ab}	13.00 ± 0.67^{fghi}
	90	1.90 ± 0.09^c	6.77 ± 0.25^{abcd}	3.35 ± 1.37^{ab}	15.98 ± 3.58^{fghi}
B + I (0.1% monoglyceride) + F	70	1.45 ± 0.09^b	9.94 ± 1.30^{fg}	14.28 ± 1.38^{def}	11.37 ± 0.84^{defgh}
	80	1.47 ± 0.06^b	9.60 ± 0.74^{cdef}	8.38 ± 0.92^{bcd}	12.54 ± 3.94^{efghi}
	90	1.62 ± 0.08^{bcd}	7.03 ± 0.67^{abcd}	3.59 ± 2.08^{ab}	14.96 ± 3.02^{fghi}
B + I (0.3% monoglyceride) + F	70	1.57 ± 0.03^b	10.34 ± 3.87^{def}	13.25 ± 1.02^{cdef}	9.26 ± 1.44^{bcdef}
	80	1.60 ± 0.17^{bcd}	8.73 ± 0.13^{cdef}	7.88 ± 1.70^{abcd}	10.55 ± 1.47^{cdefg}
	90	1.80 ± 0.03^{cde}	4.72 ± 0.48^{abc}	3.49 ± 2.05^{ab}	13.08 ± 2.68^{fghi}
B + I (0.5% monoglyceride) + F	70	1.53 ± 0.06^b	10.33 ± 0.39^{def}	16.34 ± 0.72^{ef}	11.00 ± 1.19^{defg}
	80	1.57 ± 0.06^b	9.47 ± 1.70^{cdef}	5.75 ± 2.49^{abc}	13.09 ± 2.34^{fghi}
	90	1.60 ± 0.03^{bcd}	7.54 ± 2.17^{abcde}	5.06 ± 2.41^{ab}	16.49 ± 1.15^{ghi}
B + I (1% glycerol) + F	70	1.55 ± 0.09^b	11.30 ± 2.10^{def}	18.95 ± 4.59^f	2.25 ± 0.18^a
	80	1.57 ± 0.06^b	9.40 ± 1.03^{cdef}	14.75 ± 1.68^{def}	13.10 ± 1.38^{fghi}
	90	1.60 ± 0.03^{bcd}	7.48 ± 1.25^{abcde}	3.28 ± 1.44^{ab}	14.47 ± 2.57^{fghi}
B + I (3% glycerol) + F	70*	1.52 ± 0.03^b	9.92 ± 0.51^h	18.63 ± 0.96^f	9.10 ± 2.97^{bcdef}
	80	1.63 ± 0.06^{bcd}	8.13 ± 1.87^{bcdef}	14.08 ± 1.61^{def}	12.39 ± 1.50^{efghi}
	90	1.62 ± 0.03^{bcd}	7.59 ± 0.76^{abcde}	3.07 ± 1.01^{ab}	18.34 ± 2.99^i
B + I (5% glycerol) + F	70*	1.57 ± 0.12^b	17.52 ± 0.59^g	34.09 ± 6.92^g	4.29 ± 0.64^{abc}
	80	1.62 ± 0.03^{bcd}	9.47 ± 2.06^{cdef}	13.35 ± 2.27^{cdef}	6.28 ± 2.42^{abcde}
	90	1.82 ± 0.08^{de}	7.41 ± 2.06^{abcde}	6.30 ± 2.12^{abc}	14.96 ± 1.41^{hi}

B: blanching, I: immersion in solution and F: freezing.

Different superscripts in the same column mean that the values are significantly different ($p \leq 0.05$).

* Denotes the cases where the final moisture content of 3.5% (d.b.) was not achievable.

This is probably due to the leaching out of reducing sugars, which are the substrates of Maillard reaction, during blanching. Thus, it minimized the non-enzymatic browning reaction and led to less red color of chips.

The yellowness changes of potato samples are shown in Table 4. For the samples that underwent various pretreatments it could be seen that the yellowness in all cases decreased compared with those of fresh samples. This is due to the leaching out of soluble pigments and entering of water during both steps of blanching and immersion as mentioned earlier.

In the case of dried samples it could be seen that the yellowness obviously increased compared with that of fresh and pretreated samples. This increase might be developed from an increase of carotenoid content per unit weight during drying (Park, 1987). For the effect of drying temperature on the yellowness it was found that drying temperature had no significant effect on yellowness in all cases. However, the yellowness of blanched-only samples was significantly lower than that of combined blanched-frozen, monoglyceride- and glycerol-treated samples. This is probably due to the effect of freezing on the optical characteristic of the samples mentioned earlier.

3.4.2. Texture

Regarding the hardness of dried potato chips it was noted that the influences of various pretreatments did not show any significant effect on the hardness of potato chips except when drying at 70 °C and using 3% and 5% concentrations of glycerol solution. This is because the final moisture content of 3.5% (d.b.) was not achievable in such cases, which resulted in higher values of hardness of chips as illustrated in Table 5.

For the effect of drying temperature it was found that drying temperature significantly affected the hardness, especially at higher temperatures. The hardness of the samples dried at 90 °C was lower than that dried at 70 °C but was not significantly different from that dried at 80 °C. This might be due to the effect of puffing that occurred more at higher temperatures and probably increased the porosity and resulted in a decrease of hardness and less shrinkage of the samples (indicated by the final thickness of the dried chips).

In terms of toughness combined blanching and freezing pretreatments led to significantly lower toughness of chips than only blanching pretreatment. However, blanching followed by immersion in glycerol or monoglyceride and freezing pretreatments did not lead to any statistically different results comparing with the combined pretreatments of blanching and freezing. The effect of freezing pretreatment on the reduction of toughness was more obvious when drying was performed at higher temperatures. It was found that the toughness significantly decreased as the drying temperature increased. The toughness of the sample dried at 90 °C was significantly lower than that dried at 70 °C but was not significantly different from that dried at 80 °C.

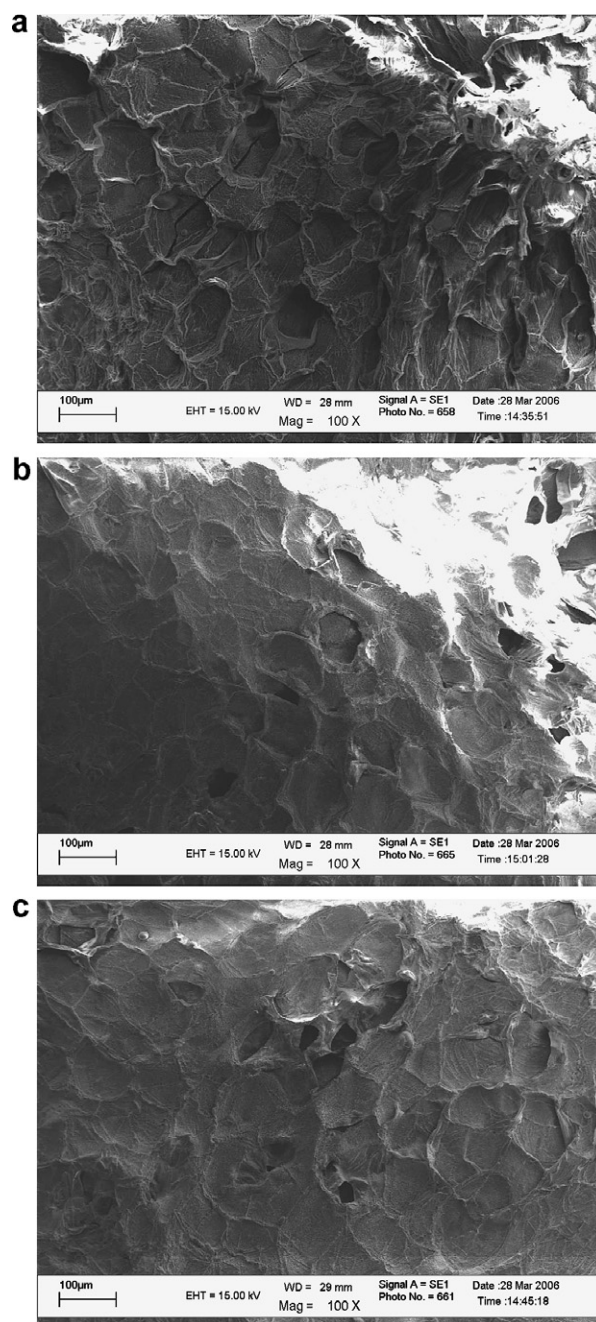


Fig. 6. Surface morphology of dried potato chips undergoing different drying temperatures: (a) 70 °C, (b) 80 °C, (c) 90 °C.

In terms of crispness higher drying temperature tended to increase the value of crispness of dried chips but the trend was not significantly obvious. For the effects of pretreatment methods on the crispness of dried samples the combined pretreatments of blanching and freezing did not show any significantly different result compared with the use of monoglyceride-immersing pretreatment at all drying temperatures. However, the combined blanched-frozen samples were significantly crispier than those underwent only blanching (at all drying temperatures) and glycerol-immersing pretreatments (drying at 70 °C).

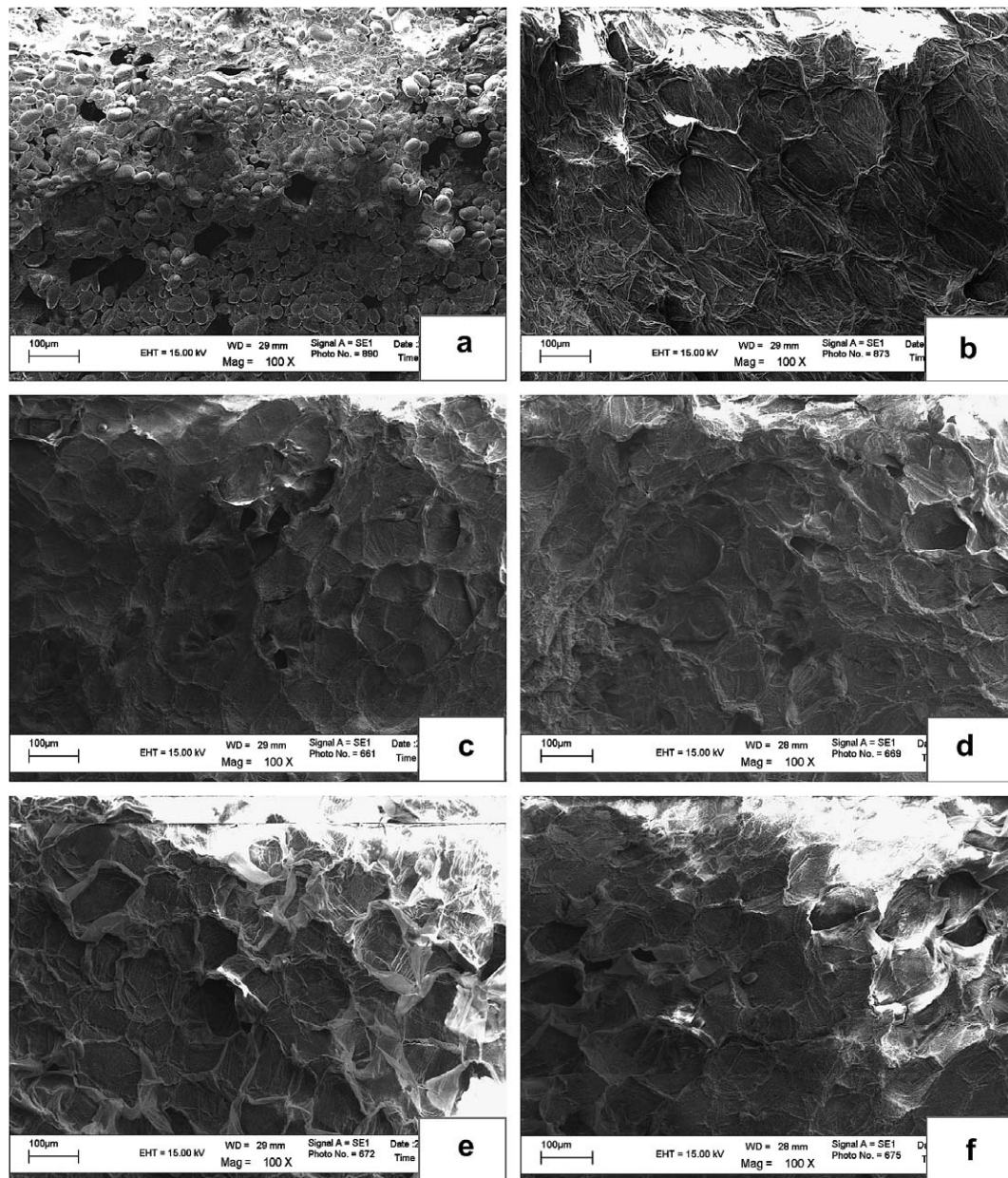


Fig. 7. SEM micrographs of surface of dried potato chips underwent different pretreatment methods (a) unblanched sample, (b) blanching, (c) blanching and freezing, (d) blanching + 0.1% MG + freezing, (e) blanching + 0.3% MG + freezing, (f) blanching + 0.5% MG + freezing, (g) blanching + 1% G + freezing, (h) blanching + 3% G + freezing, (i) blanching + 5% G + freezing.

The employment of freezing pretreatment yielded significantly crispier chips than those obtained using blanching only. This is because freezing might help improving the texture of dried potato chips. In general, starch-containing foods, likely potato chips, are cooked by heat in presence of water. In the present work, after the samples were blanched and cooled, the samples were frozen. Upon cooling the gel formed during blanching underwent transformation leading to a partially crystalline structure (Garcia-Alonso, Jimenez-Escrig, Martin-Carron, Bravo, & Saura-Calixto, 1999). This structure could in turn affect the texture of the dried chips.

3.4.3. Microstructure

Microstructural observation of the surface of dried potato chips was performed to explore the effects of pretreatment methods and drying temperature on the microstructural changes of the samples. SEM photographs (Fig. 6) shows the effect of the drying temperature on the surface morphology of dried potato chips. The chips dried at 80 and 90 °C (Figs. 6b and c) had more uniform pore size and pore distribution compared with the chips dried at 70 °C. Moreover, more extensive surface shrinkage was found on the samples dried at 70 °C.

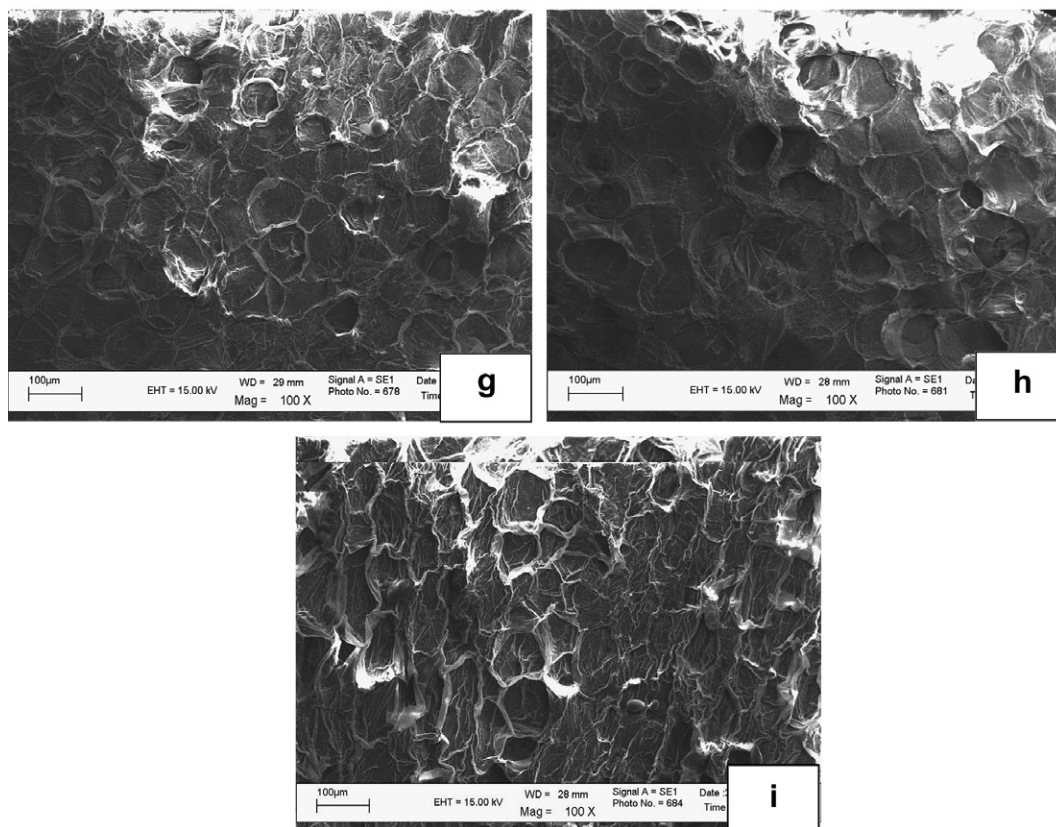


Fig. 7 (continued)

The effects of various pretreatments on the microstructure of dried chips are illustrated in Fig. 7. Fig. 7a shows the structure of dried potato chips without any pretreatment. It can be seen that the dried chips were distinguishable for they were fully covered with starch granules on the surface. Fig. 7b shows the microstructure of blanched-only sample. It is seen that there was poor uniformity of pore size and pore distribution. The extensive wrinkle on the surface was also seen.

On the other hand, the combined blanching and freezing pretreatments yielded more uniform pore size and pore distribution (Fig. 7c). This integrity of blanched-frozen microstructure led to the best textural quality of the dried potato chips in this work.

Monoglyceride pretreatment at 0.1% concentration (Fig. 7d) gave rather uniform pore size and pore distribution but the development of rigid dense layer was found on the surface of the dried samples. The rigid dense layer increased with an increase of monoglyceride concentration. In the cases of 0.3% and 0.5% concentrations (Figs. 7e and f) the pore size had more non-uniformity and their pore distribution was also non-uniform compared with the combined blanched-frozen samples. This adverse microstructure was due to more severe thermal damage due to longer drying time in the case of chemically treated samples.

For the influences of glycerol pretreatments on the microstructure it was found that the use of all concentrations (1%, 3% and 5%) of glycerol led to chips of smaller

pore size and deeper pore depth than those treated by combination of blanching and freezing as shown in Figs. 7g–i. In addition, rigid dense layer on the surface of dried chips was noted more clearly than combined blanched-frozen samples, especially at 5% concentration of glycerol. These attributes might be due to the thermal damage since glycerol delayed moisture removal during drying.

These results clearly indicated that the combined pretreatments of blanching and freezing gave the best products in terms of uniform pore size, pore distribution and the least formation of rigid dense layer. The superior integrity of the microstructure might lead to the favorable texture of dried potato chips.

4. Conclusion

The effects of pretreatments and drying temperature on the drying kinetics and quality of LPSSD potato chips were examined in this study. In terms of the drying kinetics the drying temperature was found to have an obvious effect on the rates of moisture reduction of the samples. In addition to the drying temperature pretreatments also possessed significant effects on the drying rates, especially at lower drying temperatures. However, the chemical pretreatments (both using glycerol and monoglyceride) did not improve the drying kinetics.

In terms of quality it was found that the lightness of dried potato chips was improved by the use of freezing pretreat-

ment; nevertheless, the lightness values were not significantly different among all freezing pretreated samples. Redness and yellowness of dried potato chips were not significantly affected by drying temperature but were significantly affected by the methods of pretreatment. Regarding the textural quality the hardness of dried potato chips was not significantly influenced by the pretreatment methods but was lower at higher drying temperature. However, in the cases of crispness and toughness these parameters were affected significantly by the drying temperature, especially at 90 °C. Moreover, the freezing pretreatment could improve the crispness and also reduce the toughness of dried chips. The crispness increased as the drying temperature increased but the toughness decreased with increased drying temperature. The microstructure of dried potato chips was significantly affected by the drying temperature. At 90 °C potato chips had more superior microstructure than those dried at lower drying temperatures. However, the effects of pretreatments on the microstructure were that only combined blanching and freezing pretreatments led to the best integrity of microstructure (in terms of pore size, pore distribution and also less formation of rigid dense layer).

Combined blanching and freezing pretreatment without any chemical pretreatments followed by drying in a low-pressure superheated steam dryer at a temperature of 90 °C and an absolute pressure of 7 kPa was proposed as the best conditions for producing potato chips in this study. These conditions gave better product quality, shorter total drying time and less thermal damage than other conditions. It is important to note, however, that a sensory study is needed prior to being able to make a definite conclusion on the validity of the results presented here.

Acknowledgements

The authors express their sincere appreciation to the Commission on Higher Education, the Thailand Research Fund (TRF) and the International Foundation for Science (IFS), Sweden for supporting this study financially. Special thanks are also extended to Berli Jucker Specialties Co., Ltd. for the generous supply of monoglyceride used in the study.

References

- Aguilera, J. M., Castro, L., & Cadoche, L. (2004). Structure property relationships in starch amorphous model. In *Proceedings of the 14th international drying symposium, Sao Paulo, Brazil* (pp.1468–1472).
- Alzamora, S. M., & Chirife, J. (1980). Some factors controlling the kinetics of moisture movement during avocado dehydration. *Journal of Food Science*, 45, 1649–1657.
- Caixeta, A. T., Moreira, R., & Castell-Perez, M. E. (2002). Impingement drying of potato chips. *Journal of Food Process Engineering*, 25, 63–90.
- Dandamrongrak, R., Mason, R., & Young, G. (2003). The effect of pretreatments on the drying rate and quality of dried bananas. *International Journal of Food Science and Technology*, 38, 877–882.
- Devahastin, S., Suvannakuta, P., Soponronnarit, S., & Mujumdar, A. S. (2004). A comparative study of low-pressure superheated steam and vacuum drying of a heat-sensitive material. *Drying Technology*, 22, 1845–1867.
- Elustondo, D., Elustondo, M. P., & Urbician, M. J. (2001). Mathematical modeling of moisture evaporation from foodstuffs exposed to subatmospheric pressure superheated steam. *Journal of Food Engineering*, 49, 15–24.
- Eshtiaghi, M. N., Stute, R., & Knorr, D. (1994). High-pressure and freezing pretreatment effects on drying, rehydration, texture and color of green beans, carrots and potatoes. *Journal of Food Science*, 59, 1168–1170.
- Garcia-Alonso, A., Jimenez-Escrig, A., Martin-Carron, N., Bravo, L., & Saura-Calixto, F. (1999). Assessment of some parameters involved in the gelatinization and retrogradation of starch. *Food Chemistry*, 66, 181–187.
- Iyota, H., Nishimura, N., Onuma, T., & Nomura, T. (2001). Drying of sliced raw potatoes in superheated steam and hot air. *Drying Technology*, 19, 1411–1424.
- Leeratanarak, N., Devahastin, S., & Chiewchan, N. (2006). Drying kinetics and quality of potato chips undergoing different drying techniques. *Journal of Food Engineering*, 77, 635–643.
- Maté, J. I., Quartaert, C., Meerdink, G., & van't Riet, K. (1998). Effect of blanching on structural quality of dried potato slices. *Journal of Agricultural and Food Chemistry*, 46, 676–681.
- McMinn, W. A. M., & Magee, T. R. A. (1999). Studies on the effect of surfactant, blanching, and osmotic pretreatments on the convective drying of potatoes. *Journal of Food Process Engineering*, 22, 419–433.
- Moreno-Perez, L. F., Gasson-Lara, J. H., & Ortega-Rivas, E. (1996). Effect of low temperature-long time blanching on quality of dried sweet potato. *Drying Technology*, 14, 1839–1857.
- Nargal, M. S., & Ooraikul, B. (1996). Effect of some physical and chemical pretreatments on improvement of drying characteristics of hash-brown potatoes. *Journal of Food Science and Technology*, 33, 436–439.
- Park, Y. W. (1987). Effect of freezing, thawing, drying, and cooking on carotene retention in carrots, broccoli and spinach. *Journal of Food Science*, 52, 1022–1025.
- Pedreschi, F., & Moyano, P. (2005). Effect of pre-drying on texture and oil uptake of potato chips. *Lebensmittel-Wissenschaft und-Technologie*, 38, 599–604.
- Severini, C., Baiano, A., Pilli, T. D., Carbone, B. F., & Derossi, A. (2005). Combined treatments of blanching and dehydration: study on potato cubes. *Journal of Food Engineering*, 68, 289–296.
- Vittadini, E., Clubbs, E., Shellhammer, T. H., & Vodovotz, Y. (2004). Effect of high pressure processing and addition of glycerol and salt on the properties of water in corn tortillas. *Journal of Cereal Science*, 39, 109–117.

Drying of banana slices using combined low-pressure superheated steam and far-infrared radiation

Chatchai Nimmol^{a,*}, Sakamon Devahastin^b, Thanit Swasdisevi^a, Somchart Soponronnarit^a

^a School of Energy, Environment and Materials, King Mongkut's University of Technology Thonburi, 126 Pracha u-tid Road, Bangkok 10140, Thailand

^b Department of Food Engineering, King Mongkut's University of Technology Thonburi, 126 Pracha u-tid Road, Bangkok 10140, Thailand

Received 18 October 2006; received in revised form 22 December 2006; accepted 24 December 2006

Available online 19 January 2007

Abstract

A concept of combining the already proven low-pressure superheated steam drying with far-infrared radiation (LPSSD–FIR) was proposed and studied as a novel drying technology for heat-sensitive products in the present study. The effects of various operating parameters, i.e., drying medium temperature and pressure, on the drying kinetics and dried product quality (in terms of color, shrinkage, rehydration behavior, microstructure and texture) of banana, which was used as a model heat-sensitive material, were investigated. Comparison was also made with similar sets of data obtained from the system with combined far-infrared radiation and vacuum drying (VACUUM–FIR) conducted in the same drying chamber. The results showed that the temperature of both LPSSD–FIR and VACUUM–FIR samples during the later stage of drying were higher than the pre-determined medium temperatures. It was also found that LPSSD–FIR took longer drying time than VACUUM–FIR at almost all drying conditions except at the highest drying temperature tested (90 °C). Although the drying time of LPSSD–FIR at the highest drying temperature studied was the shortest and dried banana slices obtained had more crispness, this condition gave dried banana slices with excessive changes of lightness and redness (darker color). Therefore, LPSSD–FIR at 80 °C was suggested as the best drying condition in this study.

© 2007 Elsevier Ltd. All rights reserved.

Keywords: Color; Hybrid drying technology; Microstructure; Rehydration; Shrinkage; Texture; Vacuum drying

1. Introduction

Banana is one of the most commonly consumed fruits and is abundantly available in Thailand as well as in other tropical countries. However, it deteriorates rapidly, especially in the case of ripe banana. Hot air drying is one technique performed to preserve banana and other agricultural products. However, hot air drying is a very energy-intensive operation and leads to much degradation of product quality due to elevated drying temperature and the presence of oxygen in the drying system (Krokida, Maroulis, & Saravacos, 2001; Khraisheh, McMinn, & Magee, 2004). An alternative drying means is therefore desired so

as to obtain dried products of higher quality at reduced energy consumption.

A concept of superheated steam drying (SSD) has been applied successfully to many food products during the past decade. The results obtained by several researchers clearly show that SSD is able to provide dried products with less quality deterioration compared with hot air drying. However, there still exist some limitations when applying SSD to drying heat-sensitive materials, e.g., fruits and vegetables. Because most fruits and vegetables are damaged at the temperature of superheated steam corresponding to the atmospheric pressure, it is desirable to operate the dryer at reduced pressure hence being able to obtain superheated steam at lower temperatures (Mujumdar, 2000; Elustondo, Elustondo, & Urbicain, 2001).

* Corresponding author. Tel.: +66 2 470 8695; fax: +66 2 470 8663.
E-mail address: ccnimmol@gmail.com (C. Nimmol).

Recently, low-pressure superheated steam drying (LPSSD) has been applied to several food products with various degrees of success. Elustondo et al. (2001) investigated the use of subatmospheric-pressure superheated steam to dry foodstuffs both experimentally and theoretically. A semi-empirical model that could be used to predict the drying characteristics of tested foodstuffs was also developed. It was found that the proposed model could predict the drying kinetics reasonably well. Devahastin, Suvarnakuta, Soponronnarit, and Mujumdar (2004) experimentally investigated drying of carrot cubes in both LPSSD and vacuum dryers. They found that, despite the longer required drying time in the operating ranges tested, carrot dried by LPSSD had superior quality (in terms of color and rehydration behavior) than that dried by vacuum drying. Leeratanarak, Devahastin, and Chiewchan (2006) also indicated that LPSSD gave better quality dried potato chips than did hot air drying, both in terms of the physical and nutritional qualities.

Despite the potential of LPSSD to produce high-quality dried products as mentioned above, LPSSD is a rather slow drying process. A means to accelerate this drying process is therefore desired. Application of an additional heat source, especially the one that can be absorbed directly by the drying material is among possible alternatives. Far-infrared radiation (FIR) is one possible alternative for the above purpose as it generates energy that is absorbed directly by the product without loss to the environment (Ginzburg, 1969; Sandu, 1986; Ratti & Mujumdar, 1995). Several researchers indeed successfully applied FIR to dry food products such as rice (Abe & Afzal, 1997), potato (Abe & Afzal, 1998), and barley (Afzal, Abe, & Hikida, 1999). The results obtained clearly indicated that the drying time could be considerably reduced with the use of FIR. More recently, Mongpraneet, Abe, and Tsurusaki (2002a), Mongpraneet, Abe, and Tsurusaki (2002b) proposed an idea of accelerating a drying process by using FIR under vacuum. Their results showed that the drying time of the product (welsh onion) dried by FIR under vacuum was much shorter than that of a system employing only combined convection and FIR and that of a system employing vacuum drying alone.

To combine the benefits of the above drying techniques, a combination of LPSSD and FIR was proposed and tested with banana slices, which was used as a model heat-sensitive material. In this study, FIR was used as the source of energy supplied to both the drying medium and drying product. The effects of various operating parameters, i.e., drying medium temperature and pressure, on the drying kinetics and dried product quality (in terms of color, shrinkage, rehydration behavior, microstructure and texture) were investigated. The results were also compared with the similar sets of data obtained from the system with combined FIR and vacuum drying. Moreover, the quality of dried banana slices were compared with that of banana slices undergoing LPSSD alone.

2. Experimental set-up, materials and methods

2.1. Experimental set-up

A schematic diagram of the combined low-pressure superheated steam and far-infrared radiation drying system is shown in Fig. 1. The dryer consists of a stainless steel drying chamber, insulated with rock wool, with inner dimensions of $45 \times 45 \times 45 \text{ cm}^3$; a steam reservoir, which received steam from a boiler and maintained the steam pressure at around 200 kPa; a liquid ring vacuum pump (Nash, ET32030, Trumbull, CT), which was used to maintain vacuum in the drying chamber; and a far-infrared radiator (Infrapara, A-2 T-500, Malaysia) rated at 500 W with a surface area of $60 \times 120 \text{ mm}^2$, which was used to supply thermal radiation to the drying sample and the drying medium. The distance between the far-infrared radiator and the sample holder, made of a stainless steel screen with dimensions of $15 \times 15 \text{ cm}^2$, was set at 165 mm.

The operation of the far-infrared radiator was controlled through the temperature of the drying medium (either air or superheated steam) measured at 30 mm above the sample surface via the use of a Proportional-Integral-Derivative (PID) controller (Shinko, JCS-33 A-R/M, Japan) with an accuracy of $\pm 0.1^\circ\text{C}$. The change of the mass of the sample during drying was detected continuously (at 1 min interval) using a load cell (Minebea, Ucg-3 kg, Nagano, Japan) with an accuracy of $\pm 0.2 \text{ g}$. The drying medium temperature was measured continuously using a type K thermocouple, which was located at the same position as the thermocouple that was used for sending the signal to the PID controller to control the far-infrared radiator. These thermocouples were partly covered with an aluminum foil acting as a radiation shield. The center temperature of two slices of banana, located at the middle of the sample holder, was also measured using type K thermocouples. The average surface temperature of the far-infrared radiator was also measured using a type K thermocouple. Thermocouple signals were multiplexed to a data acquisition card (Omega Engineering, CIO-DAS16Jr., Stamford, CT) installed in a PC. LABTECH NOTEBOOK software (version 12.1, Laboratory Technologies Corp., MA) was then used to read and record the temperature data.

2.2. Materials

Gros Michel banana (*Musa sapientum* L.), or 'kuauy-homtong' in Thai, was used as the tested material in this study. Fresh banana with an initial moisture content (AOAC, 1984) in the range of 2.65–3.10 kg/kg (d.b.) and selected ripeness level of green tip (color index no. 5) was obtained from a local supermarket and stored at 4°C . Prior to the start of each experiment banana was peeled and sliced by a slicing machine to 3 mm thick. The sliced samples were then cut into 30 mm diameter using a die.

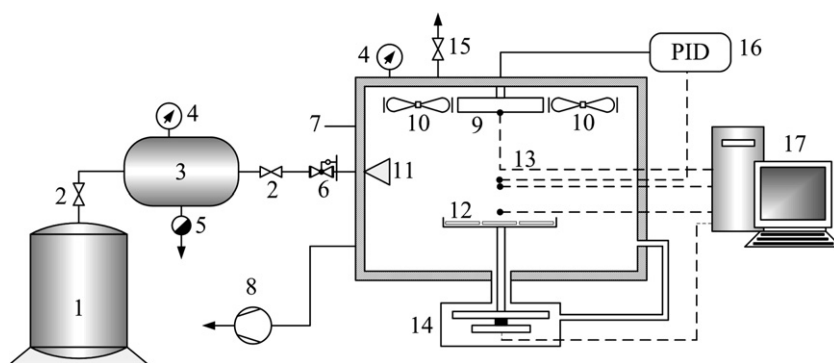


Fig. 1. A schematic diagram of the combined low-pressure superheated steam and far-infrared radiation drying system. 1: Boiler; 2: steam valve; 3: steam reservoir; 4: pressure gauge; 5: steam trap; 6: steam regulator; 7: drying chamber; 8: vacuum pump; 9: far-infrared radiator; 10: electric fans; 11: steam inlet and distributor; 12: sample holder; 13: thermocouples; 14: load cell; 15: vacuum break-up valve; 16: PID controller and 17: PC with data acquisition card.

2.3. Methods

To perform a drying experiment approximately 16 pieces of prepared banana slices (about 35 g) were placed on the sample holder. To reduce the amount of steam condensation in the drying chamber during the start-up of a combined low-pressure superheated steam and far-infrared radiation (LPSSD–FIR) experiment, the far-infrared radiator was turned on to heat up the sample and to maintain the drying chamber temperature to the desired value without the application of steam to the drying chamber during the first 5 min of the drying process. The flow rate of steam into the drying chamber was maintained at about 26 kg/h and the speed of the electric fans was fixed at around 2100 rpm.

For an experiment using far-infrared radiation under vacuum (VACUUM–FIR) the same experimental set-up was used. Since the forced convection in the drying chamber led to lower temperatures of the far-infrared radiator and of the samples leading to lower drying rates, the electric fans were not used in this case.

The experiments were carried out at the drying medium (air or superheated steam) temperatures of 70, 80, and 90 °C and absolute chamber pressures of 7 and 10 kPa. The drying experiments were performed until the sample moisture content of 0.035 kg/kg (d.b.) was obtained. All experiments were performed in duplicate.

2.3.1. Color measurement

The colors of a sample were analyzed using a colorimeter (JUKI, JP7100, Tokyo, Japan). 2° North skylight was used as the light source. The colorimeter was calibrated against a standard white plate before each actual color measurement. For each sample at least five measurements were performed at different positions and the measured values (mean values of the five measurements) were compared with those of the same sample prior to drying. Three hunter color parameters, namely, L (lightness), a (redness/greenness) and b (yellowness/blueness) were measured and the normalized color changes were then calculated by:

$$\Delta L/L_0 = \frac{L - L_0}{L_0}, \quad \Delta a/a_0 = \frac{a - a_0}{a_0}, \quad \text{and} \quad \Delta b/b_0 = \frac{b - b_0}{b_0} \quad (1)$$

where L , a , and b are the lightness, redness and yellowness of the dried sample, respectively, while L_0 , a_0 , and b_0 represent the initial values of the lightness, redness and yellowness of the sample prior to drying, respectively.

2.3.2. Shrinkage measurement

Since it was noted in a preliminary study that dried sample did not puff uniformly resulting in a difficulty to measure and analyze shrinkage in terms of the percentage change of the volume of the sample, shrinkage was evaluated in terms of the percentage change of the cross-sectional area of the sample in this study. Shrinkage of the dried sample was calculated in this case by:

$$\% \text{ Shrinkage} = \left(\frac{A_0 - A}{A_0} \right) \times 100 \quad (2)$$

where A_0 and A are, respectively, the initial and final cross-sectional area of a banana sample. The measurement of the area of a sample was performed using a digital planimeter (Ushikata, X-Plan360dII, Japan).

2.3.3. Rehydration ability

The ability of dried banana slices to reconstitute to its original state when immersing them in UHT milk is described by the rehydration ratio (R). The rehydration ratio, measured in terms of the mass ratio, was evaluated by immersing a dried banana sample in 600 ml of UHT milk, preconditioned to 30 °C by a water bath. After 10 min the sample was taken out and blotted with paper towel to eliminate excess milk on its surface. The masses of the dried and rehydrated samples were measured by an electric balance (Sartorius, CP323S, Germany) with an accuracy of ± 0.001 g. The rehydration ratio of the sample was then calculated by:

$$R = \frac{m_{\text{after}}}{m} \quad (3)$$

where m and m_{after} are, respectively, the masses of the dried and rehydrated samples.

2.3.4. Texture analysis

A compression test was used to analyze the texture of the dried sample. The test was performed using a texture analyzer (Stable Micro Systems, TA. XT. Plus, UK). The texture analyzer was fitted with a cutting probe (guillotine blade) connected to a 5 kg load cell. The test involved applying a direct force to the sample, which was placed on a hollow planar base. The cutting probe was set to travel at a crosshead speed of 2 mm/s until it cracked the sample. The maximum compression force and the number of peaks (over 50 g force threshold) in the force-deformation curve of each sample were considered as an indication of hardness and crispness of the sample, respectively.

2.3.5. Statistical analysis

All experiments were performed in duplicate and the mean values with standard deviations were reported. The experimental data were analyzed using an analysis of variance (ANOVA). Duncan's multiple range test was used to establish the multiple comparisons of the mean values; mean values were considered at 95% confidence level ($p = 0.05$). A statistical program SPSS (Version 12) was used to perform all statistical calculations.

3. Results and discussion

3.1. Drying characteristics of banana slices

Fig. 2 shows the drying curves of banana slices undergoing LPSSD–FIR at various conditions. It is seen that the drying time decreased with an increase in the drying temperature, as expected. This is because the temperature difference between the sample and superheated steam at a higher drying temperature was greater than that at a lower temperature, hence a larger driving force for heat transfer, which is also related to the rate of mass transfer. The moisture diffusivity is also higher at a higher temperature. In

addition, the drying time also decreased with a decrease in the drying pressure. This is due to the fact that water within the product evaporated at lower temperature when drying was performed at a lower pressure. It can also be seen that at higher drying temperatures (80 and 90 °C) the rates of moisture reduction were more affected by the drying temperature than by the drying pressure. This may be due to the fact that temperature is the dominant factor influencing the superheated steam thermal properties, especially at higher drying temperatures.

It should be noted that, although the drying chamber was preheated via the use of the far-infrared radiator during the first 5 min of the process as mentioned earlier, small amount of steam condensation still occurred and could be observed over a short period; the results were not shown in Fig. 2, however. Moreover, when drying was performed at 70 °C the sample could not reach the required final moisture content during the first 300 min of drying even at the lowest drying pressure tested (7 kPa). This is because of an excessive amount of steam condensation in the drying chamber. This phenomenon was also observed in the case of drying at 10 kPa (drying curve is not shown in Fig. 2).

Fig. 3 presents the drying curves of banana slices undergoing VACUUM–FIR at various conditions. The phenomenon was similar to that of LPSSD–FIR; drying at higher temperatures and lower pressures required shorter drying time. Unlike LPSSD–FIR, however, the sample dried at the lowest drying temperature (70 °C) could reach the required final moisture content because no steam condensation existed. It was also found that the effect of drying pressure was not obvious at all drying temperatures. This may again be due to the fact that temperature is the main factor influencing the air thermal properties within the operating ranges tested.

Table 1 compares the time to dry banana slices by LPSSD–FIR and VACUUM–FIR at various conditions. It was found that the samples dried by VACUUM–FIR required less drying time than that dried by LPSSD–FIR at lower drying temperatures (70 and 80 °C). However, LPSSD–FIR required shorter drying time (higher drying

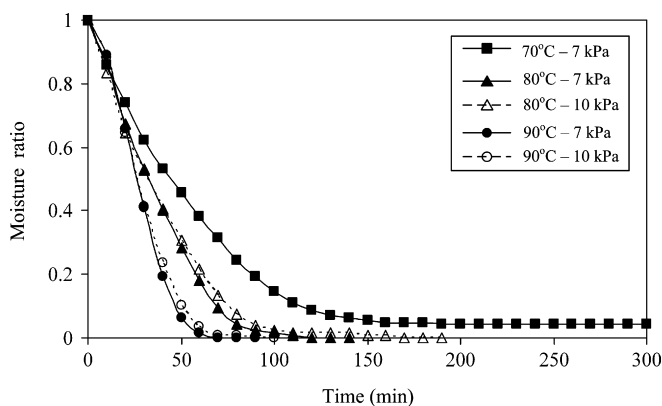


Fig. 2. Drying curves of banana slices undergoing LPSSD–FIR drying.

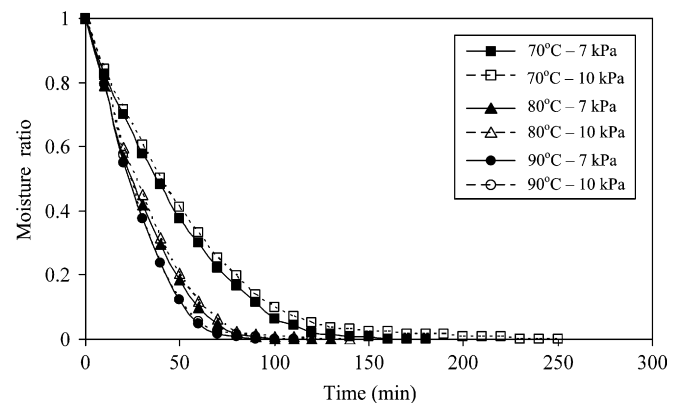


Fig. 3. Drying curves of banana slices undergoing VACUUM–FIR drying.

Table 1
Drying time of banana slices undergoing different drying methods and conditions

Drying method	Drying temperature (°C)	Drying pressure (kPa)	Drying time (min)
LPSSD–FIR	70	7	N/A
		10	N/A
	80	7	140
		10	190
	90	7	90
10		100	
VACUUM–FIR	70	7	185
		10	255
	80	7	130
		10	145
	90	7	110
		10	120

N/A implies that the final moisture content of 0.035 kg/kg (d.b.) was not obtainable at this condition.

rates) when drying was conducted at 90 °C for all drying pressures tested. This is due to the sharp increase in the differences between the superheated steam and the sample temperatures in the case of LPSSD–FIR (see Figs. 4 and 5). However, the differences between the air temperature and the sample temperature in the case of VACUUM–FIR increased only slightly as the drying temperature increased. This suggested that the effective inversion temperature calculated from the overall drying rates (the rates

in both constant rate and falling rate periods) was somewhere between 80 and 90 °C (Suvarnakuta, Devahastin, Soponronnarit, & Mujumdar, 2005). It is important to note again, however, that the fans were not used in the case of VACUUM–FIR experiments.

The changes in moisture ratio and temperature of banana slices undergoing LPSSD–FIR and VACUUM–FIR at some selected conditions are shown in Figs. 4 and 5, respectively. As revealed by these figures the temperature evolution patterns were affected by both the drying methods and conditions. In the case of LPSSD–FIR, it can be seen from Fig. 4 that the temperature of the samples fell suddenly within the first 3 min of the process. This is due to the rapid reduction of the chamber pressure, which led to some flash evaporation of surface moisture (Sun & Wang, 2006). After this period the temperature of the samples rose rapidly to the level close to the boiling point of water corresponding to the chamber pressure (not at the boiling point since far-infrared radiation was also present) and then remained unchanged at this level until the surface of the sample started to dry. In addition, it was also observed that the periods of constant sample temperature was longer when drying was conducted at lower temperatures and higher pressures as can be seen from Fig. 4a and b, respectively. Since heat transfer in the case of LPSSD–FIR simultaneously took place by radiation from the far-infrared radiator and by convection from superheated steam, the temperature of the samples rose steadily

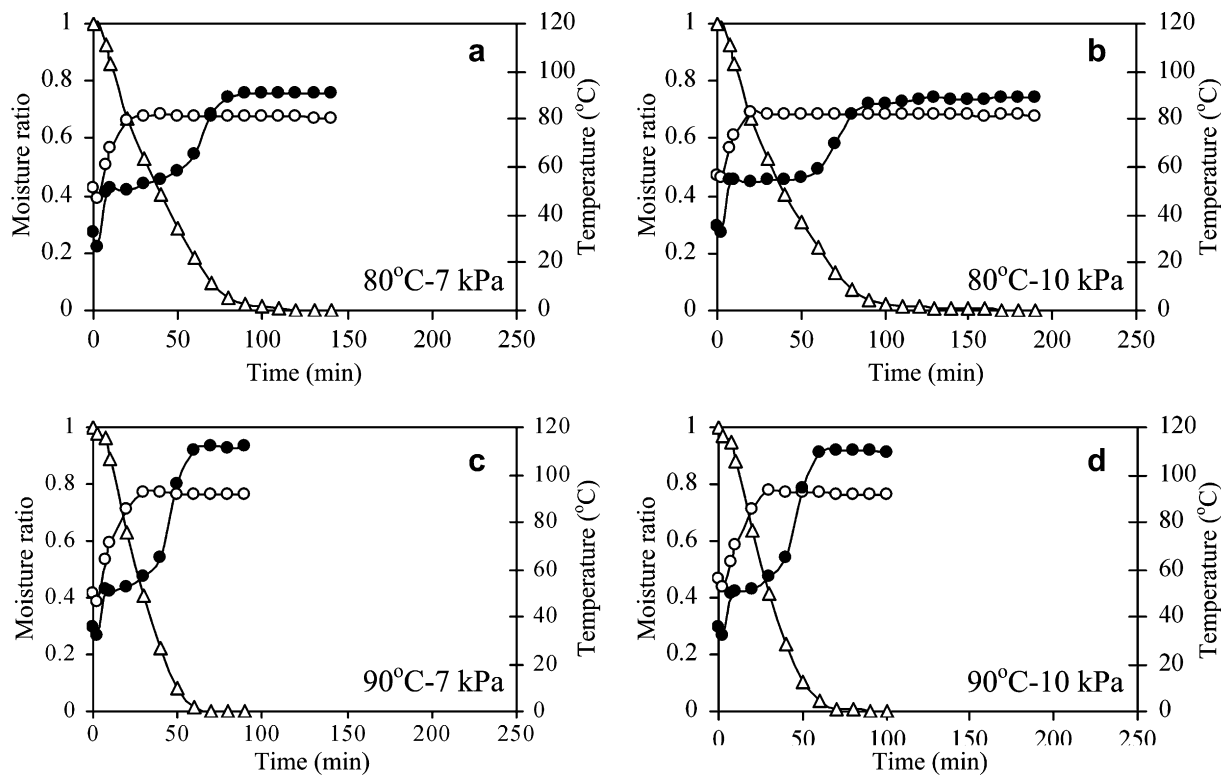


Fig. 4. Changes in moisture ratio and temperature of banana slices undergoing LPSSD–FIR. –○– drying medium temperature; –●– sample temperature; –△– moisture ratio.

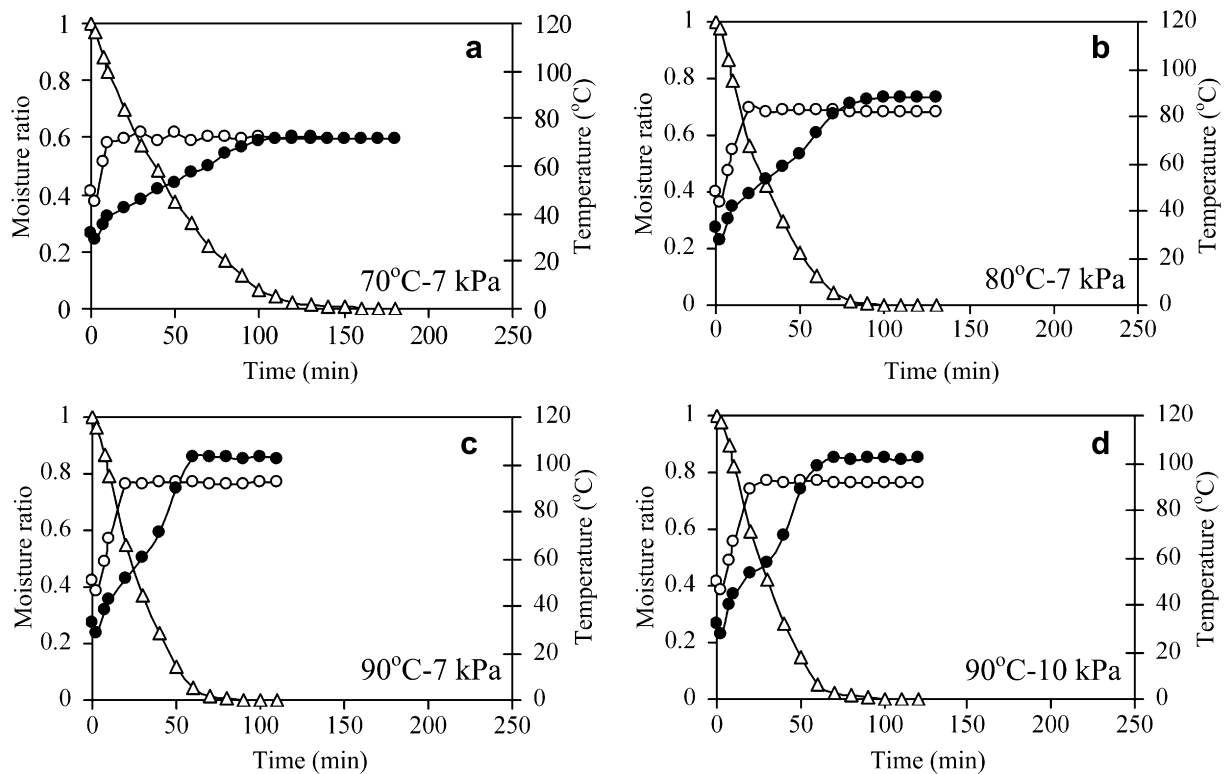


Fig. 5. Changes in moisture ratio and temperature of banana slices undergoing VACUUM-FIR. —○— drying medium temperature; —●— sample temperature; —Δ— moisture ratio.

to the level higher than the pre-determined medium temperature. This is due to the fact that thermal radiation from the far-infrared radiator contributed additional energy to the drying medium and the sample. After this period the temperature of the sample remained almost unchanged. This is because during the later stage of the process moisture content within the sample was smaller leading to lower absorptivity of the sample (Sandu, 1986).

In the case of VACUUM-FIR it was found from Fig. 5 that the temperature of the sample also dropped suddenly during the initial period of the process. However, the sample temperature after this period steadily rose to the level higher than the pre-determined medium temperature, as also noted earlier in the case of LPSSD-FIR, without the period of constant sample temperature. After this period the temperature of the samples also remained almost unchanged as in the case of LPSSD-FIR.

Comparison of the changes in the temperature of banana slices undergoing LPSSD-FIR and VACUUM-FIR at a selected drying pressure (7 kPa) is shown in Fig. 6a. It can be seen from this figure that, at the same pre-determined medium temperature, the sample temperature during the later stage of LPSSD-FIR was higher than that in the case of VACUUM-FIR. This is due to the fact that in the case of LPSSD-FIR, the radiation intensity at the position of the thermocouple used for sending the signal to the PID controller (30 mm above the sample surface) was less intense due to the higher absorptivity of super-

heated steam compared with that of air. Since the absorptivity of superheated steam is higher than that of air due to the presence of water vapor (Mills, 1999), the far-infrared radiator was used more often during LPSSD-FIR to maintain the desired level of the drying medium temperature leading to higher surface temperature of the far-infrared radiator as shown in Fig. 6b. Consequently, the radiation intensity, which depended on the surface temperature of the far-infrared radiator, experienced by LPSSD-FIR samples was greater hence higher levels of the sample temperature. It was also observed that in the case of VACUUM-FIR at the lowest temperature (70 °C) the sample temperature during the later stage of the process was much closer to the drying medium temperature (not much higher than the drying medium temperature) compared with that of samples dried at higher temperatures (see also Fig. 5a). This is due to the fact that when drying was performed at lower temperature (70 °C in this case) the radiation intensity was lower as indicated by a lower surface temperature of the far-infrared radiator (see Fig. 6b). Since the sample temperature was not dictated by the drying medium temperature but by the radiation intensity, very high sample temperature developed in the cases of drying at higher temperatures resulting in overheating and burning of the product, hence degradation of dried product quality, especially in the case of LPSSD-FIR at the highest temperature tested (90 °C). The results here will be discussed again in subsequent sections.

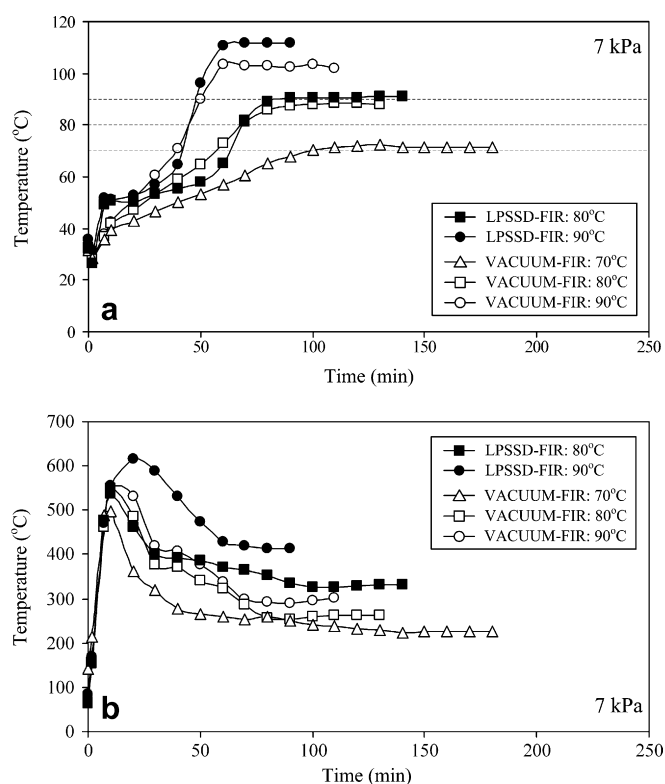


Fig. 6. Comparison of changes in (a) temperature of banana slices and (b) surface temperature of far-infrared radiator at 7 kPa.

3.2. Quality of dried banana slices

3.2.1. Colors

Table 2 lists the color changes of banana slices dried by LPSSD–FIR and VACUUM–FIR in terms of $\Delta L/L_0$, $\Delta a/a_0$, and $\Delta b/b_0$. The measured initial values of the lightness (L_0), redness (a_0), and yellowness (b_0) of fresh banana were in the ranges of 67.12–73.06, –3.75 to –4.49, and 18.42–22.20, respectively.

Since no oxygen was present in the case of LPSSD–FIR experiments, non-enzymatic browning reaction was considered as a main cause of color changes of dried banana slices. Since in the case of VACUUM–FIR, very small amount of oxygen was also available in the drying chamber due to very low level of drying chamber pressure, enzymatic browning was also negligible.

In the case of lightness it was found that drying temperature and drying methods were the significant factors influencing the changes of lightness. Drying at higher temperatures yielded darker dried banana than doing so at lower temperatures. In addition, banana dried by LPSSD–FIR was obviously darker than that dried by VACUUM–FIR at all drying conditions. This is because the temperature of banana slices undergoing LPSSD–FIR increased more rapidly and stayed at higher levels than that of samples dried by VACUUM–FIR as can be seen in Fig. 6a. The high temperatures led to higher levels of non-enzymatic browning reaction (Krokida, Karathanos, & Maroulis, 2000; Krokida et al., 2001; Chua, Hawlader,

Chou, & Ho, 2002). It was observed that the drying pressure had little effect on the lightness of dried banana samples, however.

The redness of dried banana slices was also significantly affected by both drying temperature and drying methods. It was observed that all dried banana slices were redder than the fresh ones. Also, drying at higher temperatures yielded redder dried banana than drying at lower temperatures. This is because non-enzymatic browning reactions were accelerated by temperature. Considering the effects of the drying methods it was found that LPSSD–FIR yielded dried banana slices with larger increase of the redness than the products obtained by VACUUM–FIR. This is due to the fact that in the case of LPSSD–FIR, the sample temperature increased more rapidly and stayed at higher levels than in the case of VACUUM–FIR, as described earlier. Consequently, banana dried by LPSSD–FIR subjected to the severe situation longer than that dried by VACUUM–FIR.

In the case of yellowness it was found that banana slices dried at higher temperatures tended to have higher values of yellowness than those dried at lower temperatures. The effects of the chamber pressure and drying methods on the changes of yellowness were not significant, however.

It is also seen in Table 2 that all dried banana slices of this study had higher values of color changes compared with those undergoing LPSSD alone (Thomkapanish, 2006), especially in the case of lightness and redness. This is due to the fact that banana slices undergoing LPSSD–FIR and VACUUM–FIR were subjected to the higher temperature for longer period than those dried by LPSSD, especially during the later stage of the process as noted earlier.

3.2.2. Shrinkage and rehydration behavior

Table 3 shows the results of shrinkage and rehydration behavior of banana slices dried by different methods and at different conditions. In the case of LPSSD–FIR it was found that the area shrinkage of banana slices dried at 80 °C was significantly higher than those dried at 90 °C. This is probably due to the fact that casehardening (rigid layers) on the sample perimeter, which retarded shrinkage (surface area change) of the samples, occurred least at this condition. This phenomenon is in agreement with that reported by Mongpraneet et al. (2002b) who observed that shrinkage of welsh onion was higher at a lower level of radiation intensity and hence lower sample temperature. The similar trend was observed in the case of VACUUM–FIR; drying at lower temperatures (70 and 80 °C in this case) yielded the dried products with lower degrees of shrinkage. It was also found that the drying methods and chamber pressure did not significantly affect the degree of shrinkage at the same drying temperature (80 and 90 °C). Comparing these results with those of the products obtained by LPSSD alone (Thomkapanish, 2006) it was found that the degrees of shrinkage of banana slices obtained in this study were lower. This is because casehar-

Table 2

Effects of drying methods, drying temperature and pressure on color changes of dried banana slices

Drying method	Drying temperature (°C)	Drying pressure (kPa)	$\Delta L/L_0$	$\Delta a/a_0$	$\Delta b/b_0$
LPSSD–FIR	70	7	N/A	N/A	N/A
		10	N/A	N/A	N/A
	80	7	-0.154 ± 0.026^d	-0.804 ± 0.172^c	0.255 ± 0.016^b
		10	-0.220 ± 0.023^c	-0.830 ± 0.144^c	0.257 ± 0.017^b
	90	7	-0.334 ± 0.022^a	-2.424 ± 0.202^a	0.335 ± 0.027^d
		10	-0.318 ± 0.023^b	-2.375 ± 0.217^a	0.327 ± 0.020^{cd}
VACUUM–FIR	70	7	-0.035 ± 0.005^f	-0.430 ± 0.036^d	0.213 ± 0.026^a
		10	-0.034 ± 0.004^f	-0.429 ± 0.031^d	0.210 ± 0.028^a
	80	7	-0.048 ± 0.005^f	-0.513 ± 0.039^d	0.253 ± 0.017^b
		10	-0.046 ± 0.004^f	-0.524 ± 0.038^d	0.251 ± 0.017^b
	90	7	-0.144 ± 0.016^{de}	-1.119 ± 0.195^b	0.313 ± 0.020^c
		10	-0.132 ± 0.015^e	-1.168 ± 0.157^b	0.309 ± 0.018^c
LPPSSD ^a	70	7	N/A	N/A	N/A
	80	7	-0.010 ± 0.002	-0.410 ± 0.100	0.070 ± 0.009
	90	7	-0.060 ± 0.003	-0.540 ± 0.010	0.080 ± 0.010

N/A implies that the final moisture content of 0.035 kg/kg (d.b.) was not obtainable at this condition. Values in the same column with different superscripts mean that the values are significantly different ($p < 0.05$).

^a Data obtained from Thomkapanish (2006).

Table 3

Effects of drying methods, drying temperature and pressure on shrinkage and rehydration ratio of dried banana slices

Drying method	Drying temperature (°C)	Drying pressure (kPa)	Area shrinkage (%)	Rehydration ratio
LPSSD–FIR	70	7	N/A	N/A
		10	N/A	N/A
	80	7	18.38 ± 1.34^b	1.55 ± 0.04^c
		10	18.81 ± 1.61^b	1.54 ± 0.04^c
	90	7	15.20 ± 1.01^a	1.54 ± 0.03^c
		10	14.14 ± 1.20^a	1.52 ± 0.04^c
VACUUM–FIR	70	7	18.07 ± 1.40^b	1.31 ± 0.06^a
		10	18.17 ± 0.86^b	1.31 ± 0.07^a
	80	7	18.04 ± 1.74^b	1.39 ± 0.07^b
		10	18.80 ± 1.23^b	1.40 ± 0.04^b
	90	7	14.50 ± 1.52^a	1.54 ± 0.06^c
		10	14.70 ± 1.07^a	1.54 ± 0.07^c
LPSSD ^a	70	7	N/A	–
	80	7	20.18 ± 1.70	–
	90	7	13.23 ± 0.61	–

N/A implies that the final moisture content of 0.035 kg/kg (d.b.) was not obtainable at this condition. Values in the same column with different superscripts mean that the values are significantly different ($p < 0.05$).

^a Data obtained from Thomkapanish (2006).

dening developed faster during LPSSD–FIR and VACUUM–FIR due to higher sample temperatures.

Regarding the rehydration behavior it can be clearly seen from Table 3 that banana slices dried at higher temperatures had higher rehydration ability than those dried at lower temperatures; the effect was more pronounced in the case of VACUUM–FIR. This is due to the fact that higher drying temperatures led to dried banana slices with more porous structure, thus facilitating rehydration ability. However, in general, banana slices dried by LPSSD–FIR had higher rehydration ability than those dried by VAC-

UUM–FIR. This is due to the fact that the temperature of banana dried by LPSSD–FIR suddenly rose to the level close to the boiling temperature (as can be seen in Fig. 4). Consequently, moisture in banana rapidly boiled leading to rigorous evolution of steam within the samples. Therefore, larger and more pores were developed compared with the samples dried by VACUUM–FIR. However, the rehydration ability of banana slices dried by LPSSD–FIR and VACUUM–FIR was not significantly different in the case of drying at 90 °C. This is probably due to the fact that moisture within the samples dried by VACUUM–FIR boiled as much rigorously as in the case of LPSSD–FIR at this higher temperature.

The above results were confirmed by SEM photographs shown in Fig. 7a–d, which illustrate cross section of banana slices dried by LPSSD–FIR and VACUUM–FIR at some selected conditions. It is clearly seen from these figures that when drying was performed at lower temperature (80 °C in this case) banana slices dried by LPSSD–FIR (see Fig. 7a) had larger and more pores compared with those dried by VACUUM–FIR as can be seen in Fig. 7b. This may be the reason why banana slices dried by LPSSD–FIR had higher rehydration ability than those dried by VACUUM–FIR when drying was performed at 80 °C. However, the structure of banana slices dried by both methods was similar in the case of drying at 90 °C (see Fig. 7c and d). Consequently, the rehydration ability of banana slices dried by LPSSD–FIR and VACUUM–FIR was not significantly different.

3.2.3. Texture

Because dried banana slices did not puff uniformly, the samples were cut through the part that was not the center to avoid the effect of dense structure at the core part. Table 4 shows the results of texture of dried banana slices in

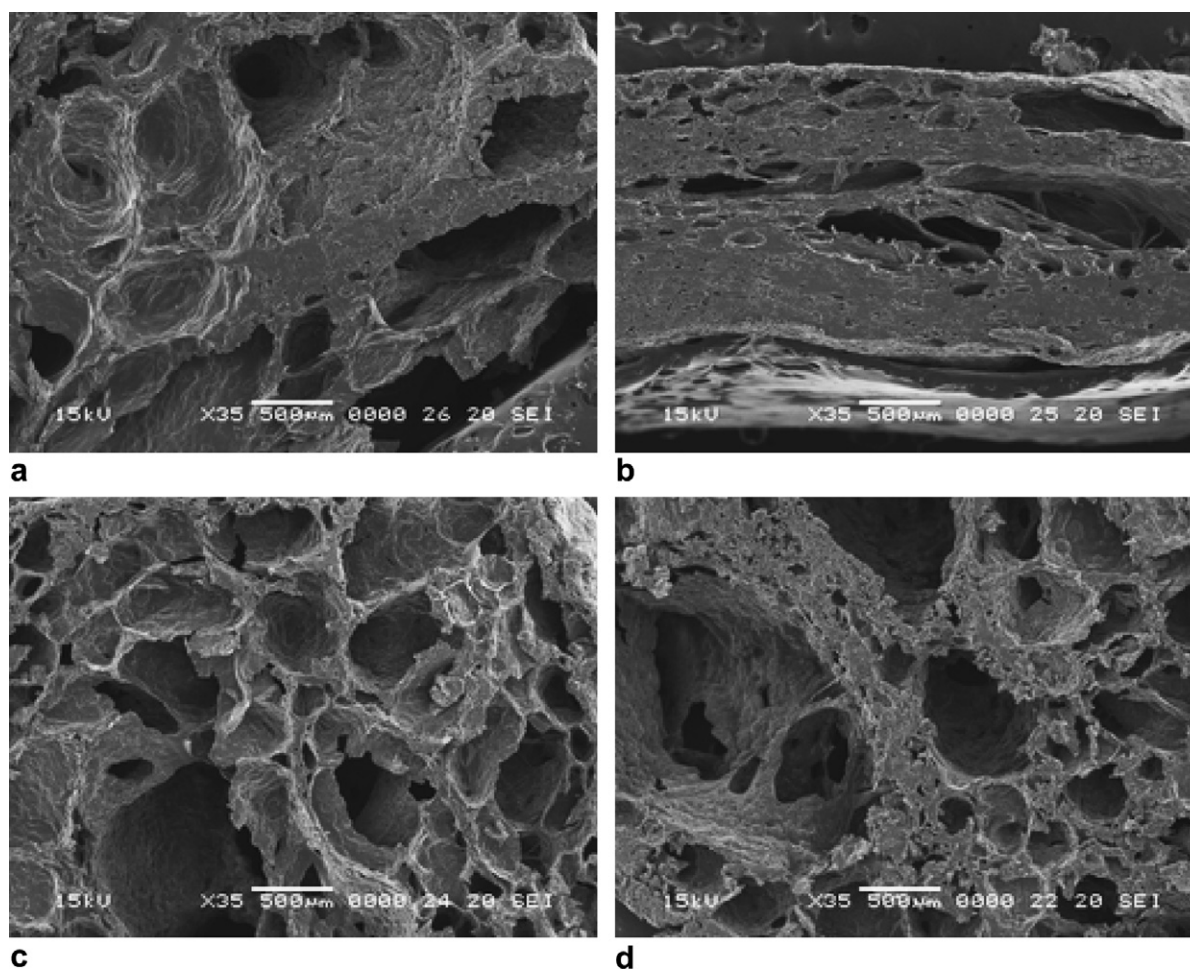


Fig. 7. SEM photographs showing cross section of banana slices dried by (a) LPSSD-FIR at 80 °C, 7 kPa; (b) VACUUM-FIR at 80 °C, 7 kPa; (c) LPSSD-FIR at 90 °C, 7 kPa and (d) VACUUM-FIR at 90 °C, 7 kPa.

terms of the maximum force (hardness) and the number of peaks in the force-deformation curve (crispness). In the case of hardness it was found that banana slices dried by VACUUM-FIR were harder than those dried by LPSSD-FIR, as indicated by the higher value of the maximum force. This may probably be due to the fact that VACUUM-FIR, especially at lower drying temperature (80 °C in this case), yielded dried banana slices with more dense structure (smaller and less pores), as can be clearly seen in Fig. 7a and b. However, the statistical analysis showed that the effects of drying temperature and drying pressure as well as drying methods on the hardness were not significant. It should be noted that, at the same drying temperature, the hardness of dried banana slices was lower than that of samples dried by LPSSD alone. This is probably due to the fact that LPSSD-FIR and VACUUM-FIR yielded dried banana slices with more porous structure than that of samples dried by LPSSD alone.

In terms of crispness it can be seen again from Table 4 that LPSSD-FIR yielded dried banana slices with a larger number of peaks (hence indicating that the products were crispier) compared with VACUUM-FIR, especially at 80 °C. This might be due to the larger and more pores that

Table 4
Effects of drying methods, drying temperature and pressure on maximum force and number of peaks of dried banana slices

Drying method	Drying temperature (°C)	Drying pressure (kPa)	Maximum force (N)	Number of peaks
LPSSD–FIR	70	7	N/A	N/A
		10	N/A	N/A
	80	7	17.09 ± 3.15 ^a	37 ± 3 ^d
		10	17.30 ± 3.60 ^a	36 ± 4 ^d
	90	7	16.39 ± 3.57 ^a	38 ± 4 ^d
		10	16.89 ± 4.58 ^a	38 ± 5 ^d
VACUUM–FIR	70	7	18.44 ± 3.80 ^a	22 ± 4 ^{ab}
		10	19.12 ± 4.07 ^a	21 ± 5 ^a
	80	7	19.95 ± 3.55 ^a	25 ± 5 ^{bc}
		10	18.16 ± 4.51 ^a	26 ± 5 ^c
	90	7	16.72 ± 3.19 ^a	36 ± 3 ^d
		10	17.81 ± 3.63 ^a	36 ± 4 ^d
LPSSD ^a	70	7	N/A	N/A
	80	7	21.52 ± 2.23	27 ± 3
	90	7	24.09 ± 1.26	28 ± 6

N/A implies that the final moisture content of 0.035 kg/kg (d.b.) was not obtainable at this condition. Values in the same column with different superscripts mean that the values are significantly different ($p < 0.05$).

^a Data obtained from Thomkapanish (2006).

occurred during LPSSD–FIR. However, the effects of drying methods on the number of peaks were not significant when drying was performed at 90 °C. These results were again compared with those of Thomkapanish (2006). It was found that LPSSD–FIR and VACUUM–FIR provided dried banana slices with slightly larger number of peaks compared with those dried only by LPSSD. This is again due to the larger and more pores presented during LPSSD–FIR and VACUUM–FIR.

The results of hardness and crispness of dried banana slices were also compared with those of commercially available banana chips (Fruit King™), which had the values of maximum force and number of peaks of 55.72 ± 5.48 N and 16 ± 3 , respectively. It was found that all dried banana slices in this study had lower values of maximum force (harder) and larger number of peaks (crispier) than the commercially available banana chips.

4. Conclusions

A novel drying system combining the advantages of low-pressure superheated steam drying and far-infrared radiation (LPSSD–FIR) has been developed for drying food products. The results showed that banana slices dried by LPSSD–FIR required longer drying time than those dried by VACUUM–FIR when drying was performed at lower temperatures. However, LPSSD–FIR required shorter drying time when the drying process was conducted at 90 °C; this indicated that the effective inversion temperature calculated from the overall drying rates should be somewhere between 80 and 90 °C. It was also found that the temperature of both LPSSD–FIR and VACUUM–FIR samples during the later stage of drying was higher than the predetermined medium temperature.

In terms of the dried product quality LPSSD–FIR yielded dried banana slices with more crispness than the products obtained by VACUUM–FIR, especially at higher drying temperatures. Although LPSSD–FIR at the highest temperature tested (90 °C) required shortest drying time to obtain the desired final moisture content and could produce dried banana with more crispness, this condition gave darker dried banana slices. Therefore, LPSSD–FIR at 80 °C was proposed as the best condition for drying banana slices in this study.

Acknowledgement

The authors express their sincere appreciation to the Commission on Higher Education, the Thailand Research Fund (TRF), the National Research Council of Thailand and the International Foundation for Science (IFS), Sweden for supporting the study financially.

References

- Abe, T., & Afzal, T. M. (1997). Thin-layer infrared radiation drying of rough rice. *Journal of Agricultural Engineering Research*, 67, 289–297.
- Abe, T., & Afzal, T. M. (1998). Diffusion in potato during far infrared radiation drying. *Journal of Food Engineering*, 37, 353–365.
- Afzal, T. M., Abe, T., & Hikida, Y. (1999). Energy and quality aspects during combined FIR-convection drying of barley. *Journal of Food Engineering*, 42, 117–182.
- AOAC (1984). *Official methods of analysis* (14th ed.). Washington DC: Association of Official Agricultural Chemists.
- Chua, K. J., Hawlader, M. N. A., Chou, S. K., & Ho, J. C. (2002). On the study of time-varying temperature drying-effect on drying kinetics and product quality. *Drying Technology*, 20, 1559–1577.
- Devahastin, S., Suvarnakuta, P., Soponronnarit, S., & Mujumdar, A. S. (2004). A comparative study of low-pressure superheated steam and vacuum drying of a heat-sensitive material. *Drying Technology*, 22, 1845–1867.
- Elustondo, D., Elustondo, M. P., & Urbicain, M. J. (2001). Mathematical modeling of moisture evaporation from foodstuffs exposed to sub-atmospheric pressure superheated steam. *Journal of Food Engineering*, 49, 15–24.
- Ginzburg, A. S. (1969). *Application of infrared radiation in food processing. Chemical and Process Engineering Series*. London: Leonard Hill.
- Khraisheh, M. A. M., McMinin, W. A. M., & Magee, T. R. A. (2004). Quality and structural changes in starchy foods during microwave and convective drying. *Food Research International*, 37, 497–503.
- Krokida, M. K., Karathanos, V. T., & Maroulis, Z. B. (2000). Effect of osmotic dehydration on color and sorption characteristics of apple and banana. *Drying Technology*, 18, 937–950.
- Krokida, M. K., Maroulis, Z. B., & Saravacos, G. D. (2001). The effect of the method of drying on the colour of dehydrated products. *International Journal of Food Science and Technology*, 36, 53–59.
- Leeratanarak, N., Devahastin, S., & Chiewchan, N. (2006). Drying kinetics and quality of potato chips undergoing different drying techniques. *Journal of Food Engineering*, 77, 635–643.
- Mills, A. F. (1999). *Basic heat and mass transfer* (2nd ed.). Upper Saddle River: Prentice-Hall.
- Mongpraneet, S., Abe, T., & Tsurusaki, T. (2002a). Accelerated drying of welsh onion by far infrared radiation under vacuum conditions. *Journal of Food Engineering*, 55, 147–156.
- Mongpraneet, S., Abe, T., & Tsurusaki, T. (2002b). Far infrared-vacuum and convection drying of welsh onion. *Transactions of the ASAE*, 45, 1529–1535.
- Mujumdar, A. S. (2000). Superheated steam drying—Technology for the future. In S. Devahastin (Ed.), *Mujumdar's practical guide to industrial drying* (pp. 115–138). Brossard: Exergex.
- Ratti, C., & Mujumdar, A. S. (1995). Infrared drying. In A. S. Mujumdar (Ed.) (2nd ed., *Handbook of industrial drying* (Vol. 1, pp. 567–588). New York: Marcel Dekker.
- Sandu, C. (1986). Infrared radiative drying in food engineering: A process analysis. *Biotechnology Progress*, 2, 109–119.
- Sun, D. W., & Wang, L. J. (2006). Development of a mathematical model for vacuum cooling of cooked meats. *Journal of Food Engineering*, 77, 379–385.
- Suvarnakuta, P., Devahastin, S., Soponronnarit, S., & Mujumdar, A. S. (2005). Drying kinetics and inversion temperature in a low-pressure superheated steam-drying system. *Industrial & Engineering Chemistry Research*, 44, 1934–1941.
- Thomkapanish, O. (2006). Study of intermittent low-pressure superheated steam and vacuum drying of banana. M.Eng thesis, Department of Food Engineering, King University of Technology Thonburi.

A mathematical model for low-pressure superheated steam drying of a biomaterial

Peamsuk Suvarnakuta^a, Sakamon Devahastin^{b,*}, Arun S. Mujumdar^c

^a Department of Food Science and Technology, Thammasat University, Pathum Thani 12121, Thailand

^b Department of Food Engineering, King Mongkut's University of Technology Thonburi, 126 Pracha u-tid Road, Bangkok 10140, Thailand

^c Department of Mechanical Engineering, National University of Singapore, 9 Engineering Drive 1, Singapore 117576, Singapore

Received 12 April 2006; received in revised form 4 September 2006; accepted 10 September 2006

Available online 15 September 2006

Abstract

Low-pressure superheated steam drying (LPSSD) has recently received much attention as an alternative drying technique for heat-sensitive biomaterials. Although there are a number of works that report studies of this drying technique experimentally, there are a very limited number of works that report attempts to model this drying process. The aim of the present study was therefore to propose the use of a simple three-dimensional liquid diffusion based model to predict the evolutions of the moisture content and temperature of a product undergoing LPSSD. The effect of the product shrinkage was also included directly in the model and the effect of this inclusion on the predictability of the model is shown. The model was found to be able to predict the heat and mass transfer behavior as well as the change of a selected chemical quality, i.e., β -carotene, of a model biomaterial viz., carrot cube reasonably well over some range of moisture content if accurate values of the heat transfer coefficient were used.

© 2006 Elsevier B.V. All rights reserved.

Keywords: β -Carotene evolution; Carrot; Deformation; Finite element method; Heat and mass transfer; Liquid diffusion model; Shrinkage

1. Introduction

During the past decade there has been considerable interest in applying superheated steam to dry various products with some success [1–3]. Despite the many advantages of near-atmospheric pressure superheated steam drying [4], there still exist some limitations, especially when applying it to drying heat-sensitive materials, e.g., foods and other biomaterials [5]. Since most foods or other heat-sensitive biomaterials are damaged at the saturation temperature of superheated steam corresponding to the atmospheric or higher pressures, one possible way to alleviate the above-mentioned problem is to operate the dryer at reduced pressure.

The concept of low-pressure (or sub-atmospheric pressure) superheated steam drying (LPSSD) has been applied to various types of heat-sensitive materials. Elustondo et al. [6] studied sub-atmospheric pressure superheated steam drying of shrimp, banana, apple, potato and cassava slices both experimentally and

theoretically. A semi-empirical mathematical model was developed based on a theoretical drying mechanism, which assumes that the water removal is carried out by evaporation in a moving boundary allowing the vapor to flow through the dry layer built as drying proceeds. Despite its simplicity, the model was found to predict the drying kinetics of the tested materials adequately.

Defo et al. [7] developed a two-dimensional mathematical model based on the combination of the mass conservation equation and Darcy's law with negligible temperature gradients to simulate superheated steam vacuum drying of sugar maple sapwood. The values of the convective mass and heat transfer coefficients were obtained by curve fitting the simulated results to the experimental data. The predicted and experimental drying curves were in good agreement when transfer coefficients were adjusted as a function of wood moisture content.

From an experimental side, Devahastin et al. [8] and Suvarnakuta et al. [9] studied experimentally LPSSD of a model heat-sensitive biomaterial, i.e., carrot. The effects of the operating pressure and temperature on the heat transfer and drying characteristics of the product as well as its various physical and chemical properties were evaluated. However, as mentioned earlier, no attempts were made to develop a mathematical model to

* Corresponding author. Tel.: +662 470 9246; fax: +662 470 9240.
E-mail address: sakamon.dev@kmutt.ac.th (S. Devahastin).

predict the temperature and moisture content evolutions of the sample during the process.

In addition to the above-mentioned works, which focus directly on modeling of LPSSD, there are also a number of other works that consider modeling of near-atmospheric pressure superheated steam drying (SSD). These include the use of various mathematical models to predict the heat and mass transfer of many products undergoing SSD and also to study the effects of various operating parameters on the temperature and moisture content profiles of those products [10,11]. A model that considers the effect of initial steam condensation, which is inevitable in SSD, is also available in literature [12].

Another aspect that is of great importance during drying of most biomaterials is product deformation. The degree of shrinkage and its variation with drying conditions as well as product moisture content influences the heat and mass transport within the product. There are a few numerical studies that investigated the effect of product deformation, which involves modeling of coupled heat and mass transfer and stress, on drying and heat transfer [13]. Mihoubi et al. [14] numerically studied and analyzed the distribution of temperature, moisture, strain, and stress of a shrinkable product during drying. A validation of the model was achieved by the comparison of the numerical and experimental data. The experimental temperature and moisture profiles compare well with the model predictions. They also found that the distribution of displacement was not necessarily uniform within the material (the stress variation is larger at the surface than in the sample body) and may cause some bending and cracking within the material.

Since the coupled mechanical and heat and mass transfer models are rather sophisticated and contain many parameters that must be known prior to the simulation, the need for a simple model that utilizes semi-empirical or empirical shrinkage information still exists. The objective of this work was therefore to develop a simple three-dimensional liquid diffusion based model to predict the evolutions of moisture and temperature of a model biomaterial viz., carrot cube during LPSSD. The model consists of coupled heat conduction and mass diffusion equations along with an empirical equation, which describes shrinkage of the product during drying. An empirical equation that expresses the β -carotene degradation in carrot was also included in the model so as to predict the evolution of β -carotene content in carrot during drying.

2. Experimental set-up, materials and methods

2.1. Experimental set-up

A schematic diagram of the low-pressure superheated steam dryer and its accessories [8] is shown in Fig. 1. The dryer consists of a drying chamber, a steam reservoir, which received steam from a boiler and maintained its pressure at around 200 kPa (gage); a liquid ring vacuum pump. An electric heater, rated at 1.5 kW, which was controlled by a PID controller, was installed in the drying chamber. Due to the use of the heater, the initial steam condensation during the start-up period

was reduced considerably. A variable-speed electric fan was used to disperse steam throughout the drying chamber. The change of the weight of the sample was detected continuously using a load cell (Minebea, model Ucg-3 kg, Japan) and an indicator and recorder (A&D Co., model AD 4329, Japan). The temperatures of the steam and of the drying sample were measured continuously using type K thermocouples, which were connected to an expansion board (Omega Engineering, model no. EXP-32, USA). Thermocouple signals were then multiplexed to a data acquisition card (Omega Engineering, model no. CIO-DAS16Jr., USA) installed in a PC. LABTECH NOTEBOOK software (Version 12.1, Laboratory Technologies Corp., USA) was then used to read and record the temperature data.

2.2. Materials and methods

Fresh carrot (*Daucus carota* var. *sativa*) was obtained from a supermarket and stored at 4 °C. Prior to the start of each drying experiment carrot was peeled and diced (only the cortex part) into 1 cm³ cubes.

To perform an LPSSD experiment approximately 35 cubes of carrot were placed as single layer on the sample holder. More detailed procedures of an LPSSD experiment could be found in Devahastin et al. [8]. The experiments were performed at the steam absolute pressure of 7 kPa and the steam temperatures of 60, 70 and 80 °C. The flow rate of steam into the drying chamber was maintained at about 26 kg/h and the speed of the fan was fixed at 1100 rpm.

3. Model development

A mathematical model was developed to predict the temperature and moisture content profiles of carrot cube of well-defined geometry undergoing LPSSD. This was accomplished by identifying the simplifying assumptions, defining the governing conservation equations for heat and mass transfer along with appropriate initial and boundary conditions. Since carrot shrinks significantly during drying, the shrinkage effect was also included empirically in the model to investigate the effect of shrinkage on the predictability of the model.

3.1. Assumptions

To formulate a mathematical description of the LPSSD process the following assumptions were made:

1. Since only the cortex part of carrot was used in the experiments, the sample was assumed to be isotropic and homogeneous.
2. Because of the pre-warming up of the drying chamber, initial condensation was neglected. Previous studies [8] also showed this to be a very short period in steam drying.
3. Mass transfer within carrot was controlled only by liquid diffusion. It was thus assumed that no vaporization occurred within the drying material.

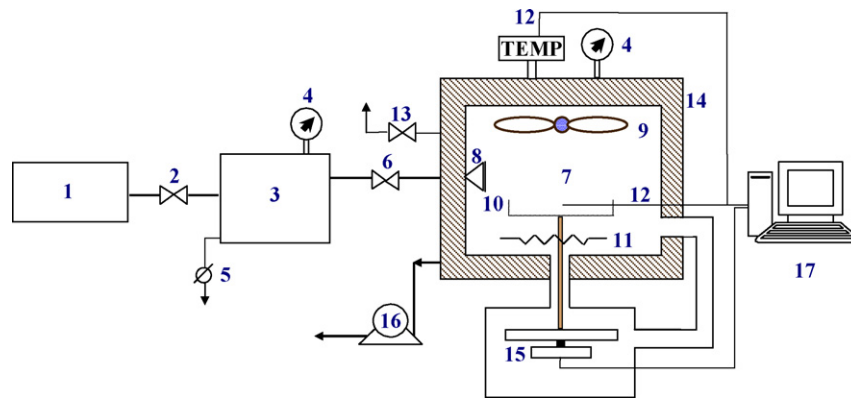


Fig. 1. A schematic diagram of the low-pressure superheated steam dryer and associated units [8]. 1, Boiler; 2, steam valve; 3, steam reservoir; 4, pressure gauge; 5, steam trap; 6, steam regulator; 7, drying chamber; 8, steam inlet and distributor; 9, electric fan; 10, sample holder; 11, electric heater; 12, on-line temperature sensor and logger; 13, vacuum break-up valve; 14, insulator; 15, on-line weight indicator and logger; 16, vacuum pump; 17, PC with installed data acquisition card.

- The density and thermal properties of carrot cube were considered as a function of the product moisture content. Mass diffusivity of carrot was considered as functions of both product temperature and moisture content.
- Shrinkage of material was significant that it was accounted for in all three directions (see Fig. 2). The volumetric shrinkage depends on the operating temperature and moisture content (as experimentally studied by Panyawong and Devahastin [15]).

3.2. Governing equations for heat and mass transfer

Heat transfer within carrot cube was driven by conduction as temperature gradients developed in all directions. The conduction equation to describe energy transfer is written as follows:

$$\rho C_p \frac{\partial T}{\partial t} = \frac{\partial}{\partial x} \left(k_x \frac{\partial T}{\partial x} \right) + \frac{\partial}{\partial y} \left(k_y \frac{\partial T}{\partial y} \right) + \frac{\partial}{\partial z} \left(k_z \frac{\partial T}{\partial z} \right) \quad (1)$$

where $k_x = k_y = k_z = k$ due to the product isotropy.

The moisture transfer within carrot cube was postulated to occur only by liquid diffusion. The three-dimensional form of the Fick's second law was therefore applied to simulate the moisture transfer. The equation to describe the mass transfer during LPSSD is then:

$$\frac{\partial X_f}{\partial t} = \frac{\partial}{\partial x} \left(D_{\text{eff}} \frac{\partial X_f}{\partial x} \right) + \frac{\partial}{\partial y} \left(D_{\text{eff}} \frac{\partial X_f}{\partial y} \right) + \frac{\partial}{\partial z} \left(D_{\text{eff}} \frac{\partial X_f}{\partial z} \right) \quad (2)$$

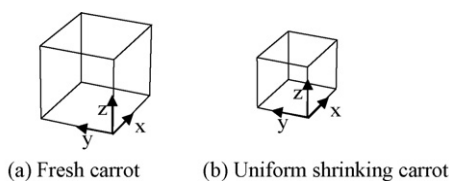


Fig. 2. Schematic diagram and directions of shrinking carrot cube undergoing LPSSD.

3.3. Initial and boundary conditions

At the onset of the LPSSD process the temperature and moisture content of carrot cube were uniform:

$$T = T_i \quad (3)$$

$$X = X_{f,i} \quad (4)$$

For carrot cube subjected to convective drying the boundary condition (Eq. (5)) at the surface was used:

$$-k(\nabla T \cdot n) = h(T_{\text{steam}} - T_s) - \rho L_v D_{\text{eff}}(\nabla X_f \cdot n) \quad (5)$$

where the term on the left hand side refers to heat conducted from the outer surface to the inside of the cube, the first term on the right hand side is heat penetrating from low-pressure superheated steam to the solid body by means of convection and the second term on the right hand side denotes latent heat of vaporization.

Mass transfer at the surface was modeled by assuming that there was no mass transfer resistance at the surface of carrot cube since water possessed no self-resistance in its own body. Therefore, the mass transfer boundary condition is as follows:

$$X_f = 0 \quad (6)$$

where X_f denotes free moisture content ($X_f = X - X_{\text{eq}}$). This condition simply implies that the moisture content at the surface was always at its equilibrium value at the corresponding operating condition.

4. Parameter estimation

4.1. Thermophysical properties of carrot

The physical and thermal properties of carrot used in the model are shown in Table 1.

Based on the correlation proposed by Mulet [18] the effective diffusion coefficient, D_{eff} , of carrot can be estimated by the

Table 1
Properties of carrot used in the model

Property	Source	Temperature range	Expression
Density ρ (kg m ⁻³)	[15]	25–80 °C	$\rho = 15.63X + 839$
Specific heat C_p (J kg ⁻¹ K ⁻¹)	[16]	Above freezing	$C_p = 837 + 4186X/1 + X$
Thermal conductivity k (W m ⁻¹ K ⁻¹)	[17]	Above freezing	$k = 0.148 + 0.641X/1 + X$

following form:

$$D_{\text{eff}} = \exp \left[-c_1 - \left(\frac{c_2}{T_{\text{abs}}} \right) + c_3 X \right] \quad (7)$$

where T_{abs} is the absolute product temperature (K) and c_1 , c_2 and c_3 are the constants. In this study, these constants were obtained by fitting the simulated results to the existing experimental results [8] at various drying conditions. As a result, D_{eff} was found (in terms of the absolute temperature and free moisture content) to be:

$$D_{\text{eff}} = \exp \left[-3 - \left(\frac{6420}{T_{\text{abs}}} \right) + 0.0005 X_f \right] \quad (8)$$

For the cases when the shrinking assumption was not used the values of D_{eff} were obviously different. In such cases, D_{eff} was found to be correlated by:

$$D_{\text{eff}} = \exp \left[-3 - \left(\frac{5880}{T_{\text{abs}}} \right) + 0.0005 X_f \right] \quad (9)$$

A simple empirical model that enables prediction of the β -carotene degradation as a function of carrot moisture content and temperature during LPSSD has been proposed in the following form [9]:

$$\frac{\beta_t}{\beta_i} = 1.104 + 0.261 \frac{X}{X_i} - 0.192 \frac{T_p}{T_i} - 0.561 \left(\frac{X}{X_i} \right)^2 - 6.61 \times 10^{-3} \left(\frac{T_p}{T_i} \right)^2 + 0.390 \left(\frac{X}{X_i} \right)^3 + 0.011 \left(\frac{T_p}{T_i} \right)^3 \quad (10)$$

where β_i and β_t are the initial and instantaneous β -carotene contents (mg/100 g solid), respectively. T_i and T_p are the initial and instantaneous temperatures of carrot (°C), respectively.

4.2. Shrinking correlation

The following relationship between the shrinkage and the moisture ratio of carrot undergoing LPSSD was reported by Panyawong and Devahastin [15] and used in this study:

$$\frac{V}{V_0} = a \left(\frac{X}{X_i} \right)^2 + b \left(\frac{X}{X_i} \right) + c \quad (11)$$

where a , b and c are the empirical constants, V_0 and V are the volumes of carrot cube before and after drying (cm³),

Table 2
Empirical constants of Eq. (11) at different temperatures [15]

Drying temperature (°C)	a	b	c
60	−0.8288	1.8170	0.0366
70	−0.9026	1.9663	−0.0433
80	−0.9492	1.9938	−0.0421

Table 3
Heat transfer coefficients (W m⁻² K⁻¹) of LPSSD at different operating pressures

7 kPa		10 kPa		13 kPa	
Mean	S.D.	Mean	S.D.	Mean	S.D.
7.661	0.61	8.353	0.44	9.168	0.33

respectively. The values of the empirical constants are listed in Table 2. Eq. (11) was implemented directly along with the Arbitrary Lagrange-Eulerian (ALE) formulation of *COMSOL Multiphysics*TM 3.2 (see Section 5).

4.3. Heat transfer coefficient

Based on the previous experimental data for molecular sieve beads undergoing LPSSD [19] the values of the heat transfer coefficient (h , W m⁻² K⁻¹) of LPSSD process could be estimated from the drying rates (evaporation rates) during the constant rate period as follows:

$$N = \frac{q}{L_v} = \frac{hA\Delta T}{L_v} \quad \text{or} \quad h = \frac{NL_v}{A(T_{\text{steam}} - T_s)} \quad (12)$$

where T_s is the surface temperature of the drying material, which is boiling point of water at the corresponding operating pressure, and T_{steam} is the temperature of the low-pressure superheated steam. L_v is the latent heat of vaporization at the operating pressure and A is the surface area of all molecular sieve particles used in each experiment [19]. The values of the heat transfer coefficient were then calculated and are listed in Table 3.

5. Model implementation

The above model was solved using *COMSOL Multiphysics*TM 3.2 (Comsol AB, Sweden) with the chemical engineering module extension. The package is based on the finite element method. The Arbitrary Lagrange-Eulerian (ALE) formulation was used to solve a problem with moving boundaries; this allowed consideration of a drying process of a shrinking body as is the case of the present study. The direct (UMFPACK) linear system solver was used in the simulation.

6. Results and discussion

6.1. Drying kinetics and heat transfer behavior

Selected experimental LPSSD results [8] were used to verify the present model. The experimental and simulated drying

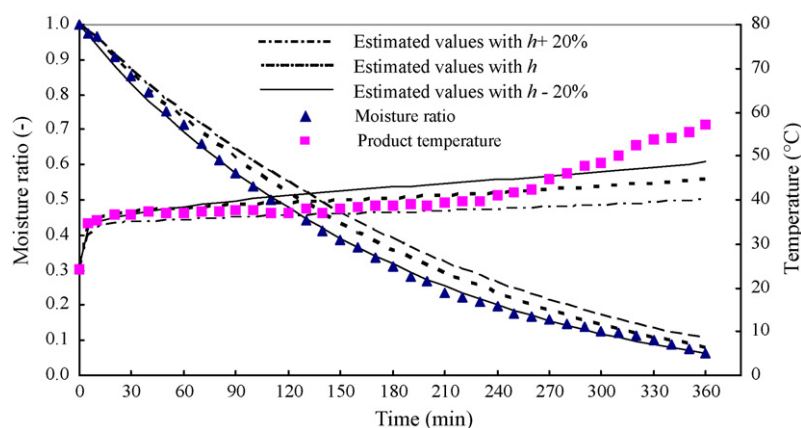


Fig. 3. Comparison between predicted (assuming shrinkage) and experimental moisture content and temperature variation with time of carrot cube at 60 °C and 7 kPa ($X_{eq} = 0.10$ kg/kg (d.b.)). Lines represent predicted data; symbols represent experimental data.

conditions are as follows: the drying temperatures of 60, 70 and 80 °C, the operating pressures of 7, 10 and 13 kPa. From the mesh independence test, it was found that a mesh size of 903 elements was enough to give mesh-independent results.

Since it was noted by Suvarnakuta et al. [19] that there existed noticeable variations in the weight measurement during molecular sieve beads drying experiments, the estimated values of the heat transfer coefficient were set in the range of $\pm 20\%$ to investigate the sensitivity of this parameter on the predictability of the product temperature and moisture content. This $\pm 20\%$ allowance was also due to the fact that the similarity principle requires that the same conditions of steam velocity and identical geometry of tested samples were employed. Since the molecular sieve beads and carrot cubes have different geometries, it was expected that the values of the heat transfer coefficient would be different.

Figs. 3–9 present the evolutions of the moisture ratio (MR) and the center temperature of carrot cube undergoing LPSSD at different operating conditions. The equilibrium moisture contents reported were obtained from Panyawong and Devahastin [15]. It was found that the trends of the moisture ratio prediction are in good agreement with the experimental data under

almost all conditions. However, at the highest operating pressure (13 kPa) the model was not able to predict the experimental data well (see Figs. 8 and 9). This is due to the fact that a larger amount of steam condensation occurred during the start-up period at a higher operating pressure (since steam at a lower degree of superheat tended to condense more easily) and this understandably led to under-prediction of the moisture ratio since the model, as mentioned earlier, did not take into account the effect of initial condensation. The same reason could also be used to explain a rather larger discrepancy between simulated and experimental results at lower drying steam temperature as well.

Representative product center temperature profiles over time are also presented in Figs. 3–9. The center temperature increased over time until it reached the boiling point of water at the corresponding operating pressure; after this point, the temperature slowly increased while latent heating prevented a temperature rise. It is seen from these figures that the simulated predictions did not quite agree with the experimental data. This is due to the fact that carrot undergoing LPSSD in fact shrank non-uniformly; this characteristic is indeed typical of most foods and biomaterials [20]. Thus, the assumption of uniform shrinkage used in this study was not quite correct. Another factor that contributed to the

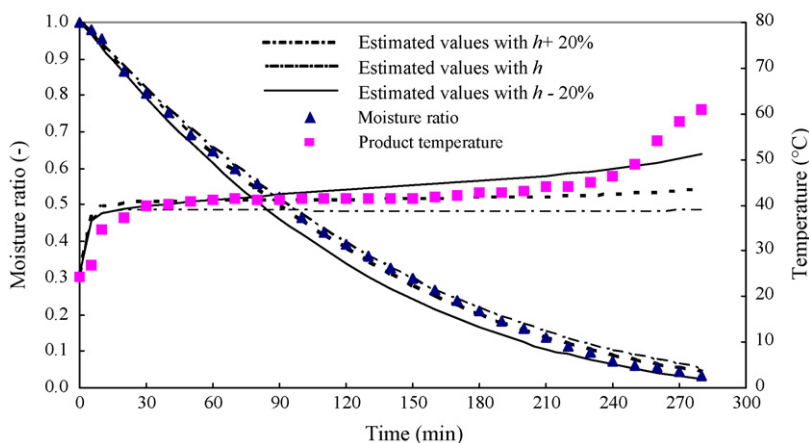


Fig. 4. Comparison between predicted (assuming shrinkage) and experimental moisture content and temperature of carrot cube at 70 °C and 7 kPa ($X_{eq} = 0.06$ kg/kg (d.b.)).

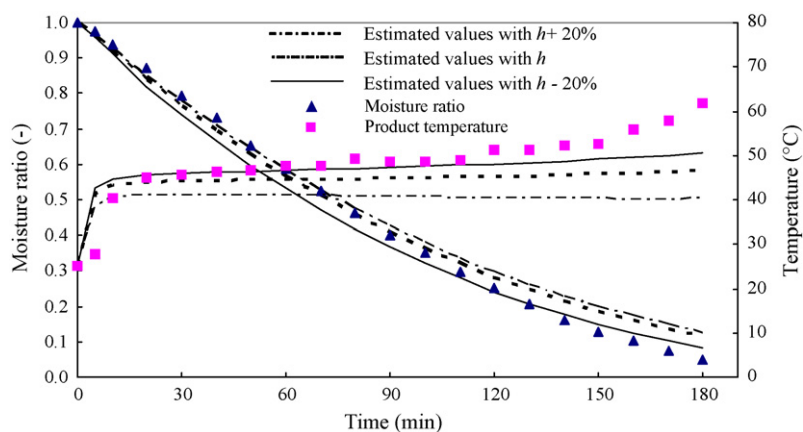


Fig. 5. Comparison between predicted (assuming shrinkage) and experimental moisture content and temperature of carrot cube at 80 °C and 7 kPa ($X_{eq} = 0.03$ kg/kg (d.b.)).

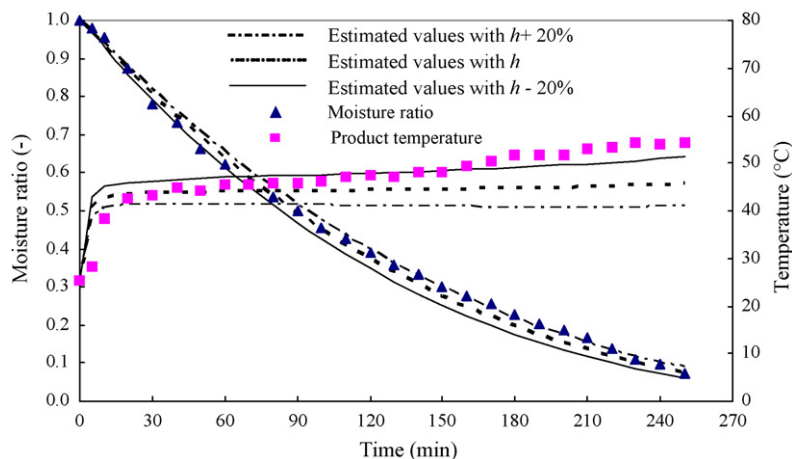


Fig. 6. Comparison between predicted (assuming shrinkage) and experimental moisture content and temperature of carrot cube at 70 °C and 10 kPa ($X_{eq} = 0.07$ kg/kg (d.b.)).

deviation of the simulated results from the experimental data is the fact that once the boiling point was reached there was vapor generation, which could give rise to an increase in the internal pressure in pores. Thus, it was possible that hydrostatic pressure

gradients were generated within the product, which could in turn drive the liquid-form moisture out of the product faster than what was permissible by liquid diffusion alone. Furthermore, the change in porosity and physical structure of carrot during

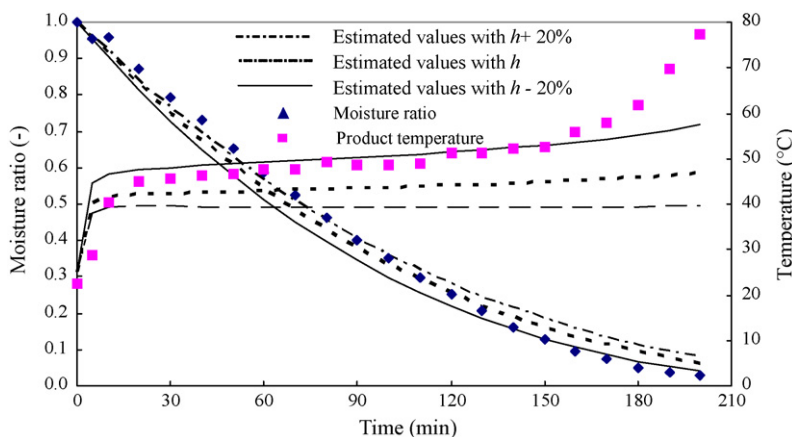


Fig. 7. Comparison between predicted (assuming shrinkage) and experimental moisture content and temperature of carrot cube at 80 °C and 10 kPa ($X_{eq} = 0.06$ kg/kg (d.b.)).

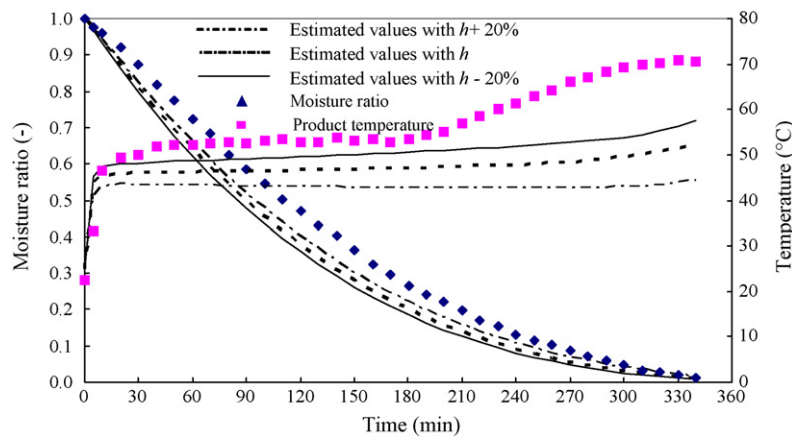


Fig. 8. Comparison between predicted (assuming shrinkage) and experimental moisture content and temperature of carrot cube at 70 °C and 13 kPa ($X_{eq} = 0.10$ kg/kg (d.b.)).

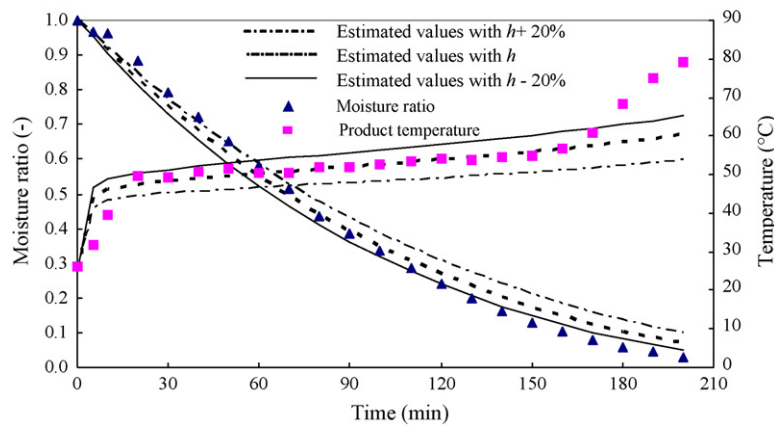


Fig. 9. Comparison between predicted (assuming shrinkage) and experimental moisture content and temperature of carrot cube at 80 °C and 13 kPa ($X_{eq} = 0.10$ kg/kg (d.b.)).

drying could, in principle, change the diffusivity from what was predicted by the empirical correlations used. Note that the correlations in the literature are based on original dimensions of the material, i.e., they do not account for changing geometry of the product. This effect has been shown by Islam and Mujumdar [21] via mathematical modeling and experiments conducted in a heat pump dryer using air as the drying medium.

6.2. Effect of shrinkage on predictability of the model

Fig. 10 illustrates the simulated product temperature and moisture content evolutions of carrot cube undergoing LPSSD without consideration of the product shrinkage. It is seen that the assuming non-shrinking model was not able to predict both the moisture content and, in particular, temperature of carrot

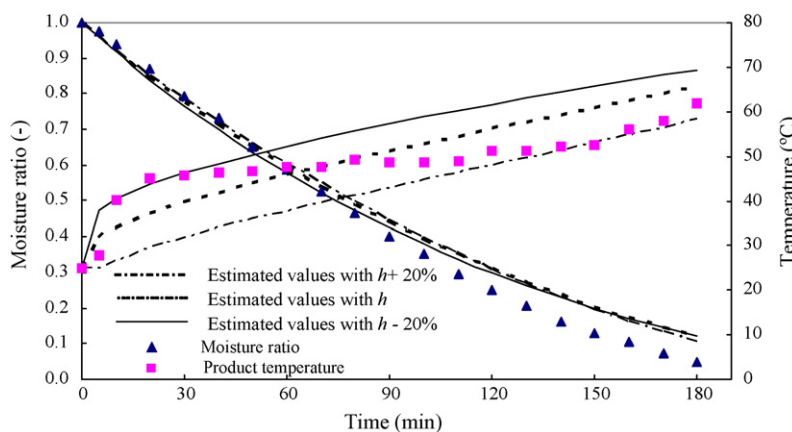


Fig. 10. Comparison between predicted (assuming non-shrinkage) and experimental moisture content and temperature of carrot cube at 80 °C and 7 kPa.

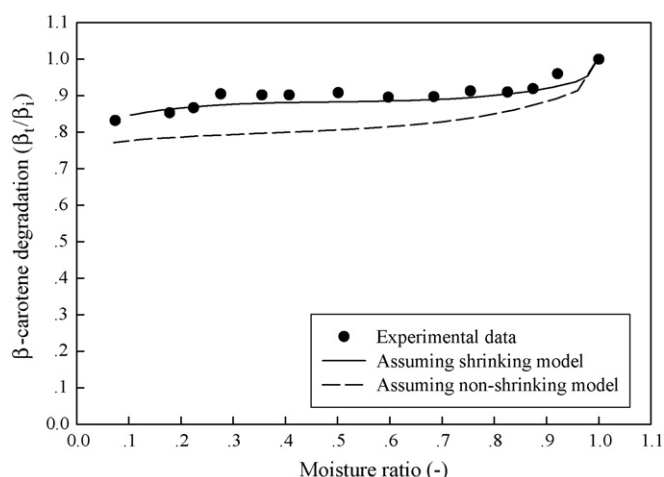


Fig. 11. Comparison between predicted and experimental β -carotene degradation of carrot at 60 °C.

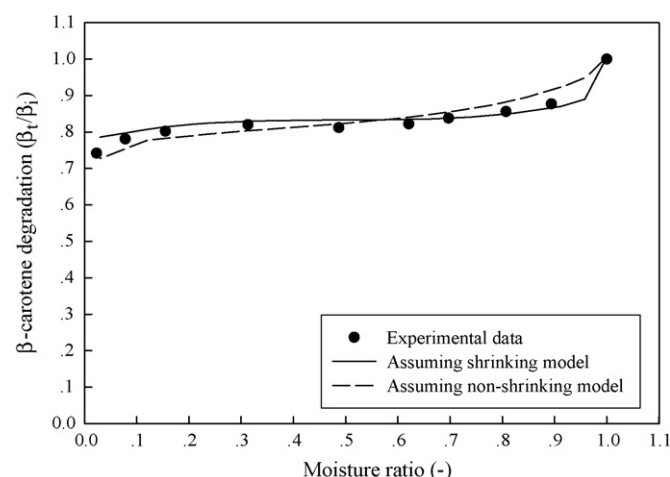


Fig. 13. Comparison between predicted and experimental β -carotene degradation of carrot at 80 °C.

undergoing LPSSD. Consideration of the product shrinkage is therefore very important to the success of the model.

It can be observed from Fig. 10 that when shrinkage effect was not considered the simulated moisture contents were higher than the experimental data, especially during the later stage of drying where internal diffusion controlled the drying process. This is due to the fact that the assuming non-shrinking model over predicted the diffusion path of moisture compared with that in the real situation. Therefore, at the same instant, predicted moisture content was higher than that of the experimental data and assuming shrinking predicted data. Also, the poor prediction is possibly due to vapor evolution within the product and possible generation of pressure gradients not accounted for by the model. A similar reason applies in the case of the product temperature. Non-shrinking assumption implies that the area for heat/mass transfer was constant, which was obviously not the case.

6.3. Prediction of β -carotene degradation

Figs. 11–13 show the predicted β -carotene degradation in carrot during LPSSD using the middle values of heat trans-

fer coefficients. The β -carotene degradation predictions, which followed from the simulated moisture content and temperature based on the assuming shrinking model, show good agreement with the experimental data under all conditions. Because assuming shrinking model could predict the product temperature and moisture content better, it is not surprising that it could also predict more precisely the β -carotene degradation than the assuming non-shrinking model.

7. Conclusions

A simple three-dimensional liquid diffusion based model was proposed to predict the evolutions of moisture and temperature of a biomaterial undergoing LPSSD. The model consists of the heat conduction and mass diffusion equations and utilizes an empirical equation, which describes shrinkage of the product. The model was found to predict the moisture content as well as product temperature reasonably well over some ranges of moisture content. The assumption of product deformation and the values of the heat transfer coefficient had effects on the shape of the moisture content and product temperature curves significantly.

The model was used in this study to show the effect of direct inclusion of uniform shrinkage of the product in the model on the shapes of drying and product temperature curves. However, a more realistic information on the deformation kinetics of the drying material should be used instead of the uniform shrinkage assumption employed in this study. The use of more realistic boundary conditions and the inclusion of terms that can take into account hydrostatic pressure gradients that may exist within the product during drying are also suggested.

Acknowledgments

The authors express their sincere appreciation to the Commission on Higher Education, the Thailand Research Fund (TRF), National Science and Technology Development Agency (NSTDA) and the International Foundation for Science (Sweden) for supporting this study financially.

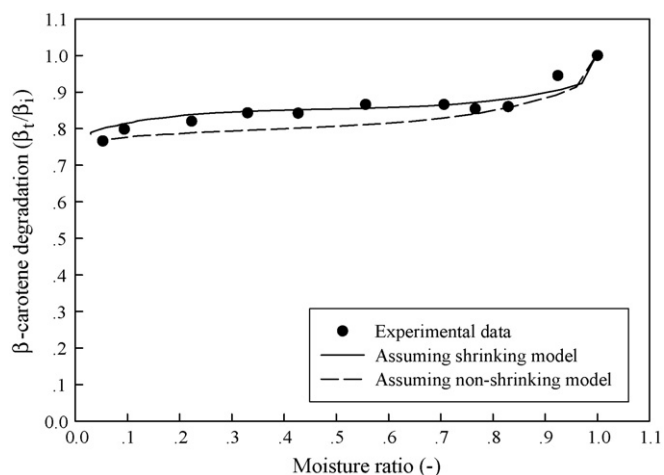


Fig. 12. Comparison between predicted and experimental β -carotene degradation of carrot at 70 °C.

List of symbols

A	surface area (m^2)
C_p	heat capacity ($\text{J kg}^{-1} \text{K}^{-1}$)
D_{eff}	effective diffusivity ($\text{m}^2 \text{s}^{-1}$)
h	heat transfer coefficient ($\text{W m}^{-2} \text{K}^{-1}$)
k	thermal conductivity ($\text{W m}^{-1} \text{K}^{-1}$)
L_v	latent heat of vaporization (J kg^{-1})
MR	moisture ratio, $X - X_{\text{eq}}/X_i - X_{\text{eq}}$
n	unit vector
N	evaporation rate (kg s^{-1})
q	heat transfer rate (W)
t	time (s)
T	temperature ($^{\circ}\text{C}$)
T_{abs}	absolute temperature (K)
T_i	initial temperature ($^{\circ}\text{C}$)
T_p	product temperature ($^{\circ}\text{C}$)
V	volume (cm^3)
V_i	volume of fresh carrot (cm^3)
X	total moisture content (kg water/kg dry solid (d.b.))
X_{eq}	equilibrium moisture content (kg water/kg dry solid (d.b.))
X_f	free moisture content (kg water/kg dry solid (d.b.))
X_i	total initial moisture content (kg water/kg dry solid (d.b.))

Greek letters

β	β -carotene content (mg/100 g solid)
ρ	density (kg m^{-3})

Subscripts

abs	absolute temperature
f	free
i	initial
s	surface of product
steam	superheated steam

References

- [1] J. Seyed-Yagoobi, Y.B. Li, R.G. Moreira, R. Yamsaengsung, Superheated steam impingement drying of tortilla chips, *Drying Technol.* 17 (1999) 191–213.
- [2] R.G. Moreira, Impingement drying of foods using hot air and superheated steam, *J. Food Eng.* 49 (2001) 291–295.
- [3] A.T. Caixeta, R. Moreira, M.E. Castell-Perez, Impingement drying of potato chips, *J. Food Proc. Eng.* 25 (2002) 63–90.
- [4] S. Devahastin, P. Suvarnakuta, Superheated steam drying of food products, in: A.S. Mujumdar (Ed.), *Dehydration of Products of Biological Origin*, Science Publishers, Enfield, NH, 2004, pp. 493–512.
- [5] A.S. Mujumdar, Superheated steam drying – technology of the future, in: S. Devahastin (Ed.), *Mujumdar's Practical Guide to Industrial Drying*, Exergex, Brossard, Canada, 2000, pp. 115–138.
- [6] D. Elustondo, M.P. Elustondo, M.J. Urbicain, Mathematical modeling of moisture evaporation from foodstuffs exposed to subatmospheric pressure superheated steam, *J. Food Eng.* 49 (2001) 15–24.
- [7] M. Defo, Y. Fortin, A. Cloutier, Modeling superheated steam vacuum drying of wood, *Drying Technol.* 22 (2004) 2231–2253.
- [8] S. Devahastin, P. Suvarnakuta, S. Soponronnarit, A.S. Mujumdar, A comparative study of low-pressure superheated steam and vacuum drying of a heat-sensitive material, *Drying Technol.* 22 (2004) 1845–1867.
- [9] P. Suvarnakuta, S. Devahastin, A.S. Mujumdar, Drying kinetics and β -carotene degradation in carrot undergoing different drying processes, *J. Food Sci.* 70 (2005) S520–S526.
- [10] L.M. Braud, R.G. Moreira, M.E. Castell-Perez, Mathematical modelling of impingement drying of corn tortillas, *J. Food Eng.* 50 (2001) 121–128.
- [11] O.E. Potter, C. Beeby, Steam drying, in: *Proceedings of the Fourth International Drying Symposium*, 1984, pp. 51–68.
- [12] H. Iyota, N. Nishimura, T. Onuma, T. Nomura, Simulation of superheated steam drying considering initial steam condensation, *Drying Technol.* 19 (2001) 1425–1440.
- [13] M. Hasatani, Y. Itaya, Drying-induced strain and stress: a review, *Drying Technol.* 14 (1996) 1011–1040.
- [14] D. Mihoubi, F. Zagrouba, J. Vaxelaire, A. Bellagi, M. Roques, Transfer phenomena during the drying of a shrinkable product: modeling and simulation, *Drying Technol.* 22 (2004) 91–109.
- [15] S. Panyawong, S. Devahastin, Determination of deformation of a food product undergoing different drying methods and conditions via evolution of a shape factor, *J. Food Eng.* 78 (2007) 151–161.
- [16] J.E. Siebel, Specific heat of various products, *Ice Refrig.* 2 (1982) 256–257.
- [17] V.E. Sweat, Experimental values of thermal conductivity of selected fruits and vegetables, *J. Food Sci.* 39 (1974) 1080–1083.
- [18] A. Mulet, Drying modelling and water diffusivity in carrots and potatoes, *J. Food Eng.* 22 (1994) 329–348.
- [19] P. Suvarnakuta, S. Devahastin, S. Soponronnarit, A.S. Mujumdar, Drying kinetics and inversion temperature in a low-pressure superheated steam drying system, *Ind. Eng. Chem. Res.* 44 (2005) 1934–1941.
- [20] N.N. Potter, J.H. Hotchkiss, *Food Science*, 5th ed., Chapman & Hall, New York, 1998, pp. 208–210.
- [21] M.R. Islam, A.S. Mujumdar, Role of product shrinkage in drying rate predictions using a liquid diffusion model, *Int. Comm. Heat Mass Trans.* 30 (2003) 391–400.

Study of Intermittent Low-Pressure Superheated Steam and Vacuum Drying of a Heat-Sensitive Material

Oearree Thomkapanich,¹ Peamsuk Suvarnakuta,² and Sakamon Devahastin¹

¹Department of Food Engineering, King Mongkut's University of Technology Thonburi, Bangkok, Thailand

²Department of Food Science and Technology, Thammasat University, Pathum Thani, Thailand

Low-pressure superheated steam drying (LPSSD) has recently been applied to drying of various heat-sensitive foods and bioproducts with success. Several studies have shown that the quality of LPSSD-dried products is superior to that obtained using conventional hot air or vacuum drying. However, drying time and energy consumption for LPSSD is generally greater than that for vacuum drying. Therefore, it is necessary to examine different methodologies to improve the energy efficiency of LPSSD. An intermittent drying scheme is one possible method to reduce the energy consumption of the process while maintaining the desired product quality. In this study, the effect of intermittent supply of energy (through an electric heater and steam injection to the dryer) and vacuum (through the use of a vacuum pump) at various intermittency values or on/off periods (10:5, 10:10 and 10:20 min in the case of intermittent supply of energy and 5:0, 5:5, and 5:10 min in the case of intermittent supply of vacuum) at the on-period setting temperatures of 70, 80, and 90°C on the drying kinetics and heat transfer behavior of the drying samples (banana chips) was studied. The effects of these intermittent drying schemes and conditions on the quality parameters of dried banana chips; i.e., color, shrinkage, texture, and ascorbic acid retention, were also studied. Finally, the energy consumption values for intermittent LPSSD and vacuum drying were monitored through the effective (or net) drying time at various intermittent drying conditions and compared with those using continuous LPSSD and vacuum drying.

Keywords Banana; Continuous drying; Intermittent temperature drying; Intermittent pressure drying; Low-pressure superheated steam drying; Quality; Tempering; Time-varying drying; Vacuum drying

INTRODUCTION

Low-pressure superheated steam drying (LPSSD) has recently received much attention as an alternative drying technique. It has been applied to drying various heat-sensitive foods and bioproducts with success since it combines the

advantages of drying at reduced temperature to those of conventional atmospheric-pressure superheated steam drying.^[1–3] Several studies have shown that the quality of dried products that underwent LPSSD was superior to that which underwent vacuum drying and hot air drying.^[3–6] However, drying time and, in particular, energy consumption of LPSSD is generally greater than that for vacuum drying due to the continuous use of an electric heater, vacuum pump, and steam generator. Therefore, it is desirable to examine different methodologies to improve the energy efficiency of LPSSD. An intermittent drying scheme is one possible method to reduce the energy consumption of the process while maintaining the desired product quality.

In general, intermittent drying is a process involving on/off pulsating of the three main process parameters: heat input, chamber pressure, and air velocity. Several experimental and modeling studies have appeared in the literature on intermittent or other time-varying drying schemes. For example, Ratti and Mujumdar^[7] conducted a numerical simulation to study batch drying of shrinking hygroscopic materials in a fixed bed under time-varying airflow rates. It was found that the total air consumption for time-varying drying was reduced with minor or no increase in drying time when compared with the case of continuous drying. This has an important economic implication in terms of reduced energy consumption for air handling, which would eventually impact the overall operating cost of the dryer. Jumah et al.^[8] studied the effect of intermittent drying on the drying kinetics of corn kernels in a rotating jet spouted bed (RJSB). By varying the rotational speed of the spouting jet of heated (or unheated) air, the magnitudes of “on” and “off” periods were varied. An intermittency ratio, α , which is a fraction of cycle time during which spouting gas was supplied for drying, was then defined as follows:

$$\alpha = \frac{\tau_{on}}{\tau} = \frac{\tau_{on}}{\tau_{on} + \tau_{off}} \quad (1)$$

Correspondence: Sakamon Devahastin, Department of Food Engineering, King Mongkut's University of Technology Thonburi, 126 Pracha u-tid Road, Bangkok 10140, Thailand; E-mail: sakamon.dev@kmutt.ac.th

where τ_{on} and τ_{off} are the on and off periods of each cycle, respectively. The drying conditions used in their study were $\alpha = 1$ (continuous), $\alpha = 2/3$, $\alpha = 1/2$, $\alpha = 1/3$ and $\alpha = 1/4$. It was shown that intermittent drying took longer time than the corresponding continuous one when the total elapsed time was considered but shorter time in terms of the effective drying time required to achieve the desired final moisture content of the product. The total drying time to reach 13% (d.b.) final moisture content increased by 19% relative to the continuous drying when $\alpha = 2/3$ was employed. However, the effective drying time decreased by 19%. Furthermore, the total drying time was less than doubled when decreasing α from $2/3$ to $1/4$. All these savings could be translated directly to energy savings. The maximum energy savings of 37% occurred with $\alpha = 1/4$.

Devahastin and Mujumdar^[9] studied numerically the effect of varying the inlet air temperature with time on the drying kinetics as well as on the surface temperature changes of wheat kernels in a rotating jet annular spouted-bed dryer. It was shown that either continuous reduction or a simple stepwise reduction of inlet air temperature from initially higher value, which was used to speed up drying at an initial stage of the process, to prevent the kernels from reaching their maximum permissible temperature, was adequate to reduce the batch drying time by up to 30%. A hybrid neuro-fuzzy system, adaptive network-based fuzzy inference system (ANFIS) was indeed illustrated to be capable of modeling periodic thermal drying of grains in a spouted bed.^[10] This model could thus be used along with the scheme of Devahastin and Mujumdar^[9] in practice.

Chua et al.^[11] studied time-varying drying (air temperature) in a heat pump dryer. It was observed that color degradation of banana slices was reduced up to 40% and drying time was saved up to 180 min when the air temperature was stepped up from an initial value of 20°C to finish drying at 35°C. It was also found that stepping down the air temperature from 35 to 20°C reduced the color degradation of banana slices by 23%.

Islam et al.^[12] employed a liquid diffusion model to examine the effect of time-varying air temperature, velocity, and relative humidity over different periods of time on the drying kinetics of potato slices in a heat pump dryer. The results showed that the step-down temperature and velocity profiles led to high drying performance; the energy consumption of an electric blower was reduced to almost 50%. The results also showed that one heat pump was sufficient to dehumidify the drying air and should be run only in an initial stage of drying.

A novel concept for drying heat-sensitive materials (such as yeast, biotech products, and enzymes) based on a succession of compression and decompression cycles was proposed by Rakotozafy et al.^[13] A drying material was subjected to pressures of 2–10 bar for a certain duration;

this was followed by evacuation to low pressures of the order of 100 mbar. The product was then maintained at the low-pressure level for a certain time interval. This process yielded better performance than a conventional freeze-drying process, both in terms of cost and drying time. The quality of the product (measured in terms of the viability of the yeast) was reported to be better compared with that freeze dried. This is likely due to the shortened duration of the total drying process.

In terms of drying using volumetric heating pulsed microwave-vacuum drying was studied in terms of power on/off time.^[14] The pulsing ratio, PR was indeed defined as:

$$PR = \frac{\text{Cycle Power on Time} + \text{Cycle Power off Time}}{\text{Cycle Power on Time}} \quad (2)$$

It was found that the method was very suitable for heat-sensitive materials as it yielded higher energy efficiency and better product quality than continuous drying, especially at larger pulsing ratios.

More recently, Xing et al.^[15] used NMR imaging to study both continuous and intermittent drying of pasta. Comparing continuous and intermittent drying, it was found that the wet layer near the surface of pasta was clearly observed in the case of intermittent drying and this caused a greater amount of moisture loss than that in the case of continuous drying. The energy consumption in the case of intermittent drying was less than that in the case of continuous drying as well.

The aim of this research was to study the drying kinetics of banana chips, which were used as a model heat-sensitive material, undergoing both LPSSD and vacuum drying at various intermittent drying schemes and conditions; various quality attributes of the chips that underwent LPSSD and vacuum drying at different conditions were also evaluated. The results were also compared with those of continuous drying.

EXPERIMENTAL SETUP, MATERIALS AND METHODS

Experimental Setup

A schematic diagram of the low-pressure superheated steam dryer and its accessories is shown in Fig. 1.^[3] The dryer consists of a stainless steel drying chamber with inner dimensions of $45 \times 45 \times 45 \text{ cm}^3$; a steam reservoir, which received steam from a boiler and maintained its pressure at around 200 kPa (gage); and a liquid ring vacuum pump (Nash, model ET32030, Trumbull, CT), which was used to maintain vacuum in the drying chamber. An electric heater, rated at 1.5 kW, which was controlled by a PID controller (Omron, model E5CN, Tokyo, Japan), was installed in the drying chamber to control the steam temperature and to minimize condensation of steam in the drying chamber

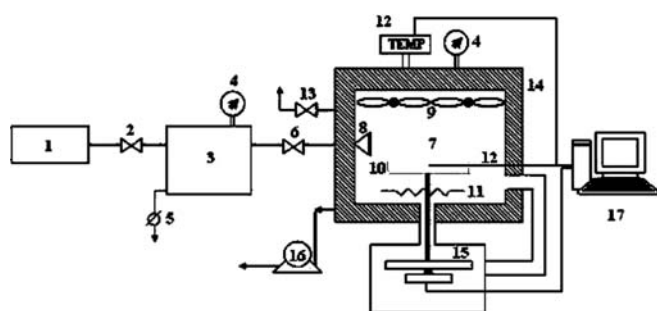


FIG. 1. A schematic diagram of low-pressure superheated steam dryer and associated units. 1, boiler; 2, steam valve; 3, steam reservoir; 4, pressure gauge; 5, steam trap; 6, steam regulator; 7, drying chamber; 8, steam inlet and distributor; 9, electric fans; 10, sample holder; 11, electric heater; 12, on-line temperature sensor and logger; 13, vacuum break-up valve; 14, insulator; 15, on-line weight indicator and logger; 16, vacuum pump; 17, PC with installed data acquisition card.

during the start-up period. Variable-speed electric fans were used to disperse the steam throughout the drying chamber. The sample holder was made of a stainless steel screen with dimensions of $16.5 \times 16.5 \text{ cm}^2$. The change of the weight of the sample was detected continuously (at 60-s interval) using a load cell (Minebea, model Ucg-3 kg, Nagano, Japan), which was installed in a smaller chamber connected to the drying chamber by a flexible hose (in order to maintain the same vacuum pressure as that in the drying chamber), and also to an indicator and recorder (AND A&D Co., model AD 4329, Tokyo, Japan). The temperatures of the steam and of the drying sample were also measured continuously using type-K thermocouples, which were connected to an expansion board (Omega Engineering, model no. EXP-32, Stamford, CT). Thermocouple signals were then multiplexed to a data acquisition card (Omega Engineering, model no. CIO-DAS16Jr., Stamford, CT) installed in a PC. Labtech Notebook software (version 12.1, Laboratory Technologies Corp., Andover, MA) was then used to read and record the temperature data. The same drying system was also used for vacuum drying experiments but without the application of steam to the drying chamber.

Material

Gros Michel banana (*Musa sapientum* L.), or “kuauy-homtong” in Thai, was purchased from a local supermarket with selected ripeness level of half green–half yellow (color index no. 4). The samples were skinned, peeled, sliced with an adjustable food-slicer to 3 mm thickness, and cut to a diameter of 30 mm.

Methods

Gros Michel banana pieces were dried until they reached the final moisture content of 0.025 kg/kg (d.b.) using two different drying methods, viz. low-pressure superheated steam drying and vacuum drying.

The drying chamber temperature and pressure were varied when intermittent drying was performed as on and off periods. For an intermittent temperature drying scheme, “on” refers to the use of all drying conditions in the same way as that in the case of continuous drying. On the other hand, “off” (or tempering) period implies turning off the steam and the heater. For an intermittent pressure drying scheme, “on” means the use of all drying conditions in the same way as that of continuous drying, while “off” means turning off the steam and the vacuum pump and opening of the vacuum break-up valve.

On:off period variation for intermittent temperature and pressure profiles is listed in Table 1; these values were specified as appropriate values (as assessed by the dried product external appearances) in the preliminary experiments. The chamber temperatures of 70, 80, and 90°C were used as the on-period setting temperature while the vacuum pressure was fixed at 7 kPa during an on period.

Quality Measurement

The quality of banana chips was investigated after drying with different schemes; the final moisture content of the product was set at 0.025 kg/kg (d.b.).

Color Measurement

Colors of fresh and dried samples were measured in a Hunter Lab color system using a colorimeter (Juki, model JP 7100, Tokyo, Japan). All experiments were performed in duplicate and the average values were then reported. The color changes were calculated by:

$$\frac{\Delta L}{L_0} = \frac{L - L_0}{L_0}, \quad \frac{\Delta a}{a_0} = \frac{a - a_0}{a_0}, \quad \text{and} \quad \frac{\Delta b}{b_0} = \frac{b - b_0}{b_0} \quad (3)$$

where L , a , b represent the lightness, redness, and yellowness of the dried samples, respectively. L_0 , a_0 , b_0 are, respectively, the lightness, redness, and yellowness of the fresh banana samples.

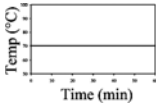
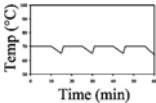
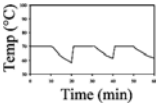
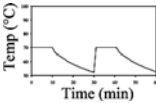
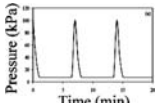
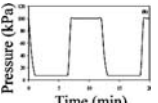
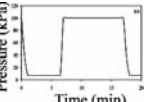
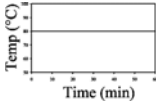
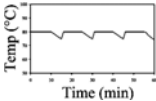
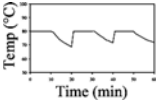
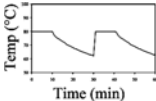
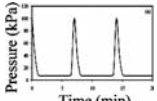
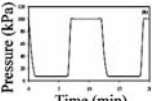
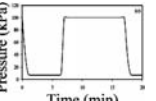
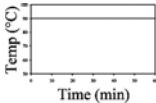
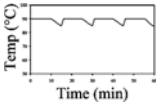
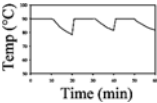
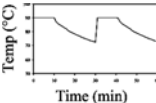
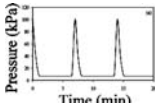
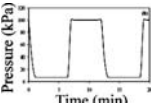
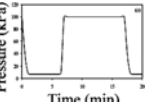
Texture Measurement

The texture of banana chips was evaluated by a compressive test using a texture analyzer (Stable Micro Systems, TA.XT. Plus, Surrey, UK). The test involved applying a direct force to the sample, which was placed on a hollow planar base. A blade probe moved at a constant rate of 2 mm/s until it cracked the sample. The maximum compression force was used to describe the hardness of the sample. The number of peaks in the force-deformation curves was also calculated and used to represent the crispness of the sample.

Shrinkage Measurement

Ten samples from each drying condition were used to determine the shrinkage in terms of the percentage change

TABLE 1
Conditions used for both LPSSD and vacuum drying experiments

Temp. (°C)	Continuous drying	Intermittent drying (temperature scheme)			Intermittent drying (pressure scheme)		
		On period:off period (min:min)			On period:off period (min:min)		
		10:5	10:10	10:20	5:0	5:5	5:10
70							
80							
90							

of the area compared with the original area of the sample. The projected area of the sample was determined by a planimeter (Ushikata, model X-plan360dII, Tokyo, Japan). The average values of ten samples were reported.

$$\% \text{ Shrinkage} = \frac{A_i - A}{A_i} \times 100 \quad (4)$$

where A_i and A are, respectively, initial and final area of banana chips.

Ascorbic Acid Analysis

The ascorbic acid content of the fresh and dried samples was determined using a high-performance liquid chromatography (HPLC) technique, as suggested by AOAC.^[16] The percentage retention of ascorbic acid (AA) was calculated using the following equation:

$$\begin{aligned} \% \text{ Retention} \\ = \frac{(\text{Conc. of AA in the sample after drying}) \times 100}{(\text{Conc. of AA in the sample before drying})} \end{aligned} \quad (5)$$

Statistical Analysis

The experiments were designed in complete randomness. The data were analyzed and presented as mean values with standard deviations. All data were analyzed using the analysis of variance (ANOVA). The Duncan's test was used to establish the multiple comparisons of mean values. Mean values were considered at 95% significance level ($\alpha = 0.05$). A statistical program Minitab (version 14) was used to perform all statistical calculations.

RESULTS AND DISCUSSION

Preliminary Study

In a preliminary study, suitable values of intermittency for both intermittent drying temperature and pressure profiles were first determined. In the case of an intermittent drying temperature scheme, the on period, which is the time that heat is supplied to the product, was investigated by fixing the intermittency ratio^[8] at $\alpha = 1/3$, $1/2$, and $2/3$. An actual time of the on period was, however, varied at 10, 20, and 30 min. It was found that the appearance of the dried banana chips that were dried with an on period of 10 min was the best.

In an off, or tempering, period of an intermittent pressure drying scheme, the vacuum pump and steam (in the case of LPSSD) were turned off. Hence, the oxygen content in the chamber increased, leading to poor product quality. Therefore, the off period was observed by varying the tempering time at 5, 10, and 15 min. It was observed that when the off period was more than 10 min, banana chips were too dark and not acceptable in quality. Hence, the off periods of 0, 5, and 10 min were selected to perform subsequent experiments.

Drying Kinetics of Banana Chips

Gros Michel banana pieces with initial moisture contents between 2.7 to 3.3 kg/kg (d.b.) were dried until their equilibrium moisture contents were reached in both LPSSD and vacuum dryer. To determine the quality of banana chips, the desired final moisture content was set at about 0.025 kg/kg (d.b.).

Time-Varying Temperature Drying

The drying curves of banana pieces undergoing LPSSD and vacuum drying are shown in Figs. 2 and 3, respectively. It can be seen in both figures that the rates of reduction of moisture at the same setting temperature during the first 10 min of drying were similar because the samples were still subjected to the same conditions; i.e., no off

period was activated yet. As expected, the rate of moisture removal at higher temperatures was higher than that at lower temperatures because the temperature differences between the sample and the drying medium and the moisture diffusivities at higher drying temperatures were greater than those at lower temperatures.

Comparing the drying time of continuous LPSSD and vacuum drying revealed that LPSSD took longer than

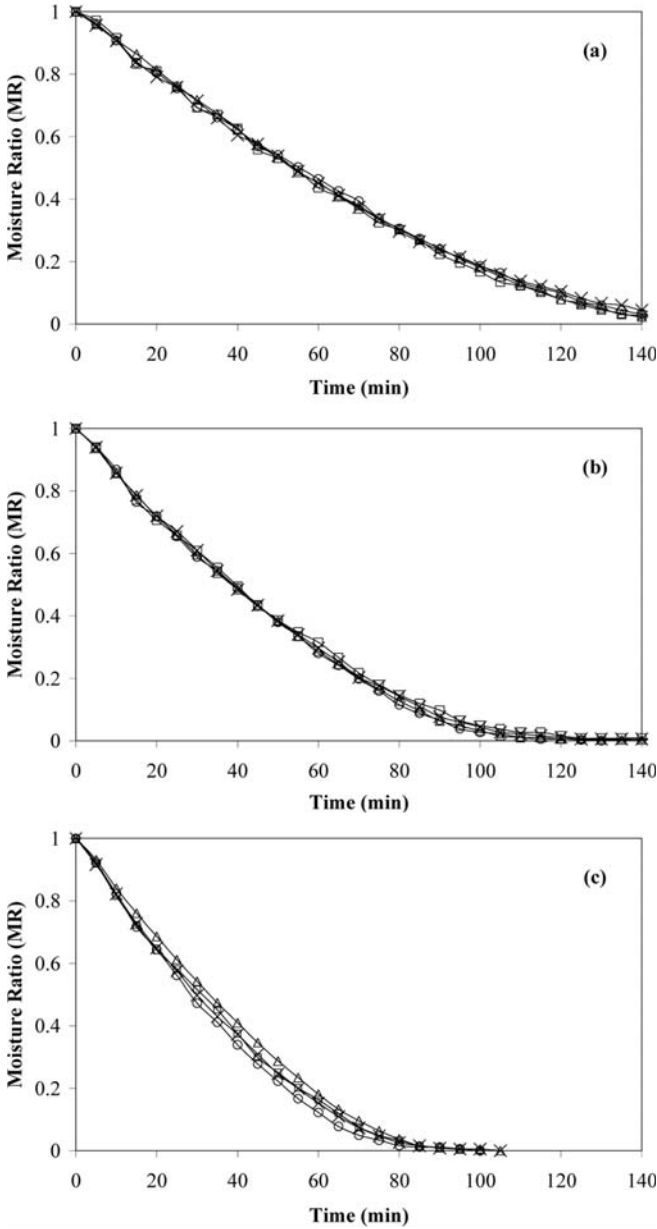


FIG. 2. Drying curves of banana chips undergoing intermittent temperature LPSSD at on:off period of 10:5 (○), 10:10 (×), 10:20 (◐), and continuous drying (Δ) at temperatures of (a) 70°C, (b) 80°C, and (c) 90°C. $MR = M_t - M_{eq} / M_i - M_{eq}$, where M_t is moisture content at any time, kg/kg (d.b.); M_{eq} is equilibrium moisture content, kg/kg (d.b.); and M_i is initial moisture content, kg/kg (d.b.).

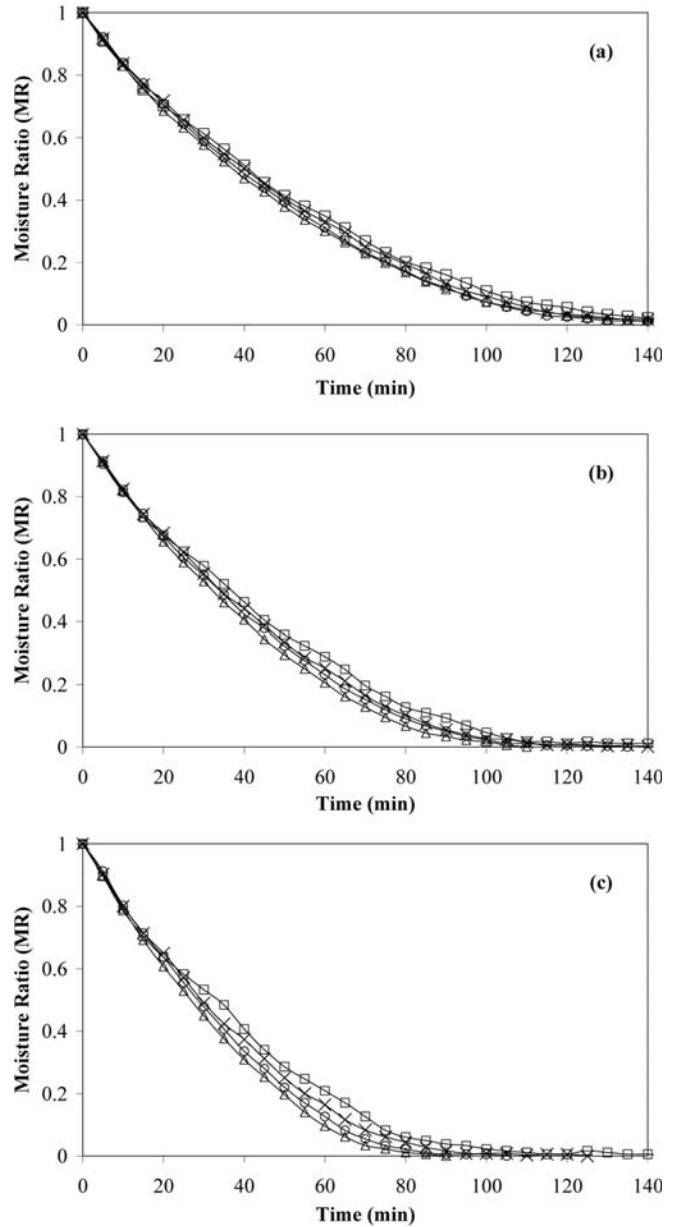


FIG. 3. Drying curves of banana chips undergoing intermittent temperature vacuum drying at on:off period of 10:5 (○), 10:10 (×), 10:20 (◐), and continuous drying (Δ) at temperatures of (a) 70°C, (b) 80°C, and (c) 90°C.

vacuum drying to reach the desired moisture content at the same temperature. However, the drying time at higher temperatures of LPSSD was closer to that of vacuum drying. Raising the drying temperature further would eventually lead to equal rates of drying at the inversion temperature due to increased temperature differences between steam and surface of sample.^[17] From the experimental data, the inversion temperature for the continuous cases

TABLE 2
Average total and net drying time of LPSSD and vacuum drying of banana chips at various conditions

Condition				Drying time (min)	
Drying scheme	Drying method	Temperature (°C)	Intermittency (on:off, min)	Total	Net
Continuous drying	LPSSD	70	—	N/A	N/A
		80	—	148	148
		90	—	93	93
	Vacuum drying	70	—	N/A	N/A
		80	—	105	105
		90	—	88	88
Intermittent temperature scheme	LPSSD	70	10:5	N/A	N/A
			10:10	N/A	N/A
			10:20	N/A	N/A
			10:5	140	95
		80	10:10	142	70
			10:20	151	51
			10:5	91	65
			10:10	93	50
		90	10:20	93	33
			10:5	N/A	N/A
			10:10	N/A	N/A
			10:20	N/A	N/A
	Vacuum drying	70	10:5	120	80
			10:10	140	70
			10:20	150	50
		80	10:5	104	70
			10:10	117	60
			10:20	135	45
		90	5:0	N/A	N/A
			5:5	N/A	N/A
			5:10	N/A	N/A
		80	5:0	151	110
			5:5	140	59
			5:10	155	49
Intermittent pressure scheme	LPSSD	70	5:0	87	61
			5:5	86	35
			5:10	125	39
		80	5:0	N/A	N/A
			5:5	N/A	N/A
			5:10	N/A	N/A
		90	5:0	111	80
			5:5	105	44
			5:10	143	42
		80	5:0	79	58
			5:5	80	34
			5:10	116	35
	Vacuum drying	70	5:0	N/A	N/A
			5:5	N/A	N/A
			5:10	N/A	N/A
		80	5:0	111	80
			5:5	105	44
			5:10	143	42

N/A implies that, at this condition, the final banana moisture content of 0.025 kg/kg (d.b.) was not achievable.

calculated from the overall drying rates was somewhere between 80 and 90°C.

In the case of LPSSD it can be seen that the overall drying rates of continuous LPSSD were slightly lower than those of intermittent drying. In the case of intermittent drying, steam was not injected into the drying chamber during the off period; therefore, the drying medium in the tempering (off) period was less humid. Thus, the mass transfer driving force between the sample surface and the drying medium in the case of intermittent drying was larger than in the case of continuous drying.

However, it was found that the effect of intermittent (time-varying) temperature LPSSD on the drying kinetics was not significant when the on-period setting temperatures were 70 and 80°C. During the tempering period, the energy in the case of intermittent drying at 90°C was accumulated within the sample more significantly than in the case of intermittent drying at lower temperatures. Therefore, when energy was supplied again in the effective drying period, the moisture removal was greater. Hence, the effect of intermittent drying on the drying behavior at 90°C was clearer than that at 70 and 80°C.

The average total and net drying times for banana chips under various conditions are listed in Table 2. It is seen from this table that the total drying time of intermittent LPSSD was similar to that for continuous LPSSD. Although the sample and chamber temperatures (shown here only for the case with the setting temperature of 70°C for the sake of brevity; see Fig. 4; the trends at other setting temperature were similar) in the case of intermittent drying were lower than those in the case of continuous drying, the drying system in the tempering period acted like vacuum drying, whose drying rates were greater than those of LPSSD, as mentioned earlier. This led to the steady decrease of moisture content in the case of intermittent drying. However, the effective or net drying time of intermittent drying was significantly shorter than that of continuous drying. These savings could be directly translated into the energy savings as discussed later.

In the case of vacuum drying it is observed from Fig. 3 that the effect of intermittency on the vacuum drying kinetics is again not significant when setting the on-period temperature at 70°C. However, the drying rates of intermittent drying were lower than those of continuous drying, especially at longer tempering (off) time, at the setting temperatures of 80 and 90°C. In the case of intermittent drying, an off period (heater turned off) led to reduced sample and chamber temperatures (Fig. 5; only results at the setting temperature of 70°C are shown). Thus, vapor pressure gradients, which are the driving force of the drying process, were reduced. At higher drying temperatures, the sample temperature, which was reduced during the tempering period, affected the vapor pressure even more significantly than at lower temperatures. Hence, the effect of intermit-

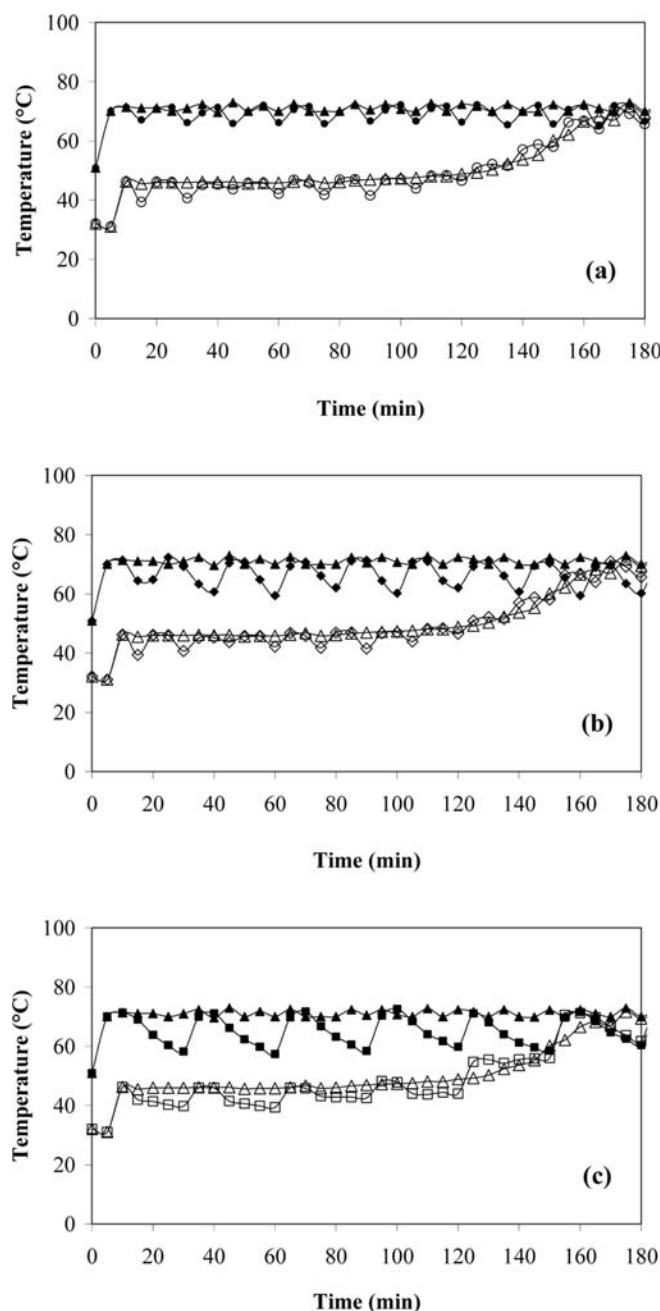


FIG. 4. Chamber (opaque sign) and sample (transparent sign) temperatures during continuous and intermittent temperature LPSSD at 70°C. Continuous drying (Δ) vs. intermittent drying at on:off period of (a) 10:5 (\circ), (b) 10:10 (\diamond), and (c) 10:20 (\square).

tency was more obvious at the setting temperature of 90°C. This behavior is shown in Fig. 6, which is the representative plots of the evolution of vapor pressure of continuous and intermittent drying at an on:off period of 10:20 min at various setting temperatures; only selected plots are again shown here for the sake of brevity as the

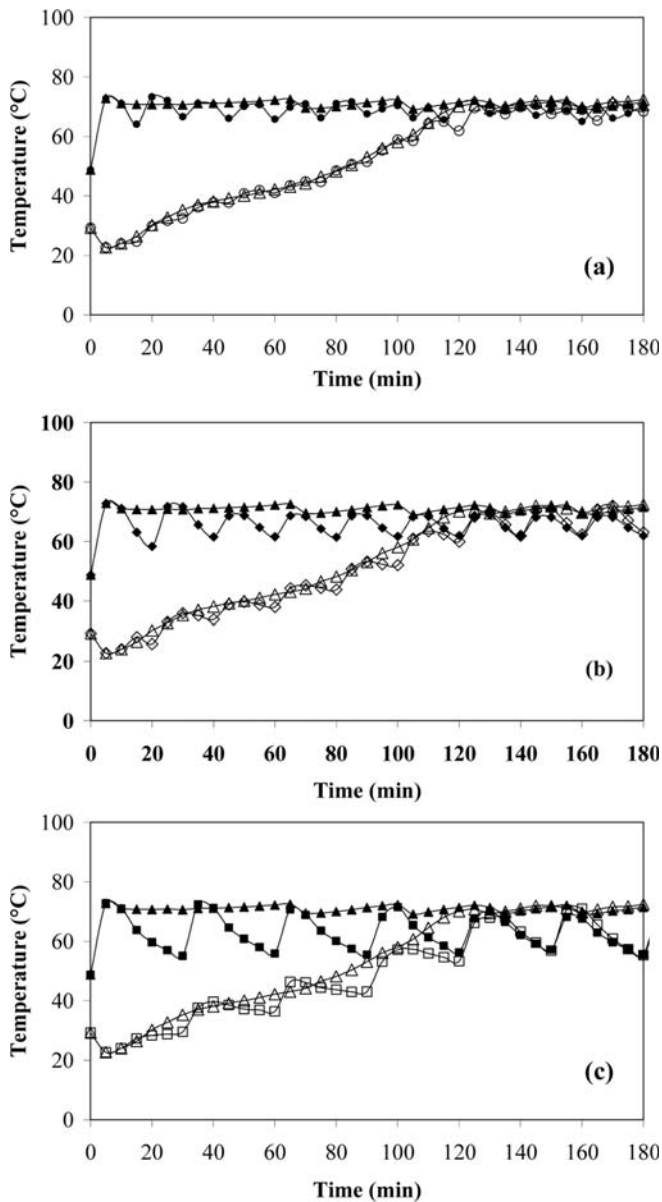


FIG. 5. Chamber (opaque sign) and sample (transparent sign) temperatures during continuous and intermittent temperature vacuum drying at 70°C. Continuous drying (Δ) vs. intermittent drying at on/off period of (a) 10:5 (\circ), (b) 10:10 (\diamond), and (c) 10:20 (ϵ).

trends of vapor pressure changes were the same at all tested conditions. Table 2 also shows that the total drying time of intermittent drying was significantly longer than that of continuous drying. However, the effective or net drying time was again significantly shorter than that of continuous drying.

Intermittent Pressure Drying

The drying curves of banana chips undergoing intermittent pressure LPSSD and vacuum drying are displayed in

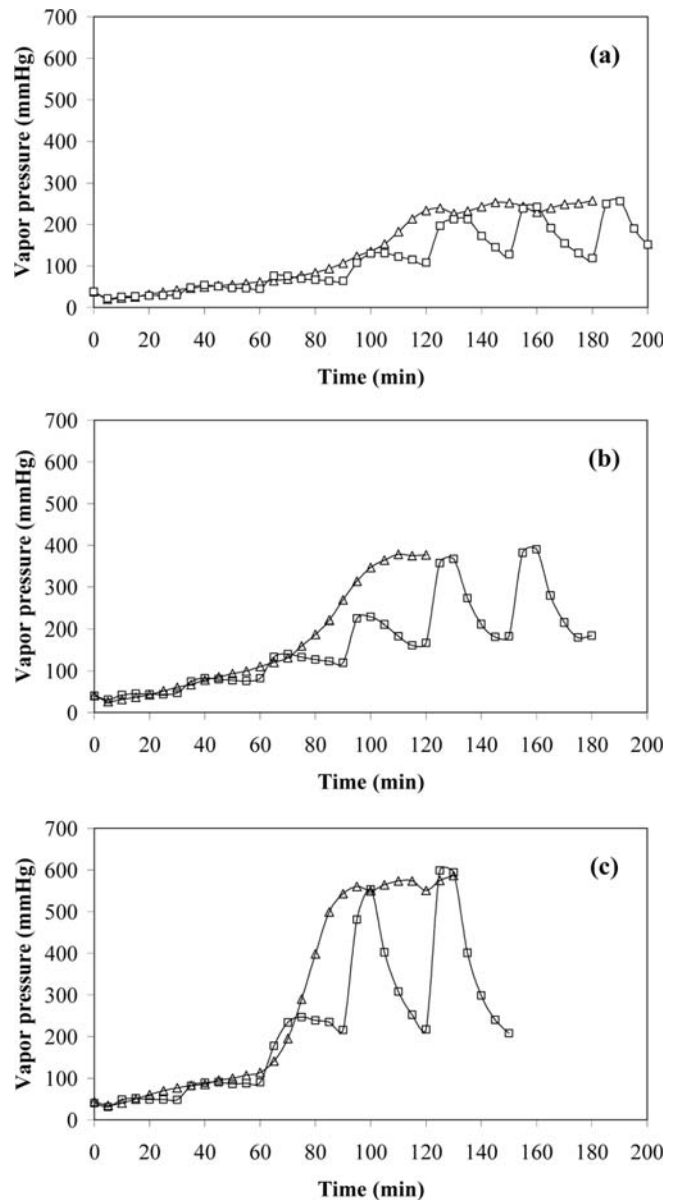


FIG. 6. Vapor pressure of continuous and intermittent vacuum drying at an on/off period of 10:20 min (ϵ) at temperatures of (a) 70°C, (b) 80°C, and (c) 90°C.

Figs. 7 and 8, respectively. The drying time of LPSSD at the setting temperature of 80°C was longer than that of vacuum drying. However, the drying time of LPSSD and vacuum drying at 90°C was similar. This may be due to the effect of an inversion phenomenon, as mentioned earlier.

It is seen that the drying rates of intermittent drying at all conditions were obviously higher than those of continuous drying. This is due to the higher sample surface temperatures in the case of intermittent drying. This behavior is shown in Figs. 9 and 10, which are the representative

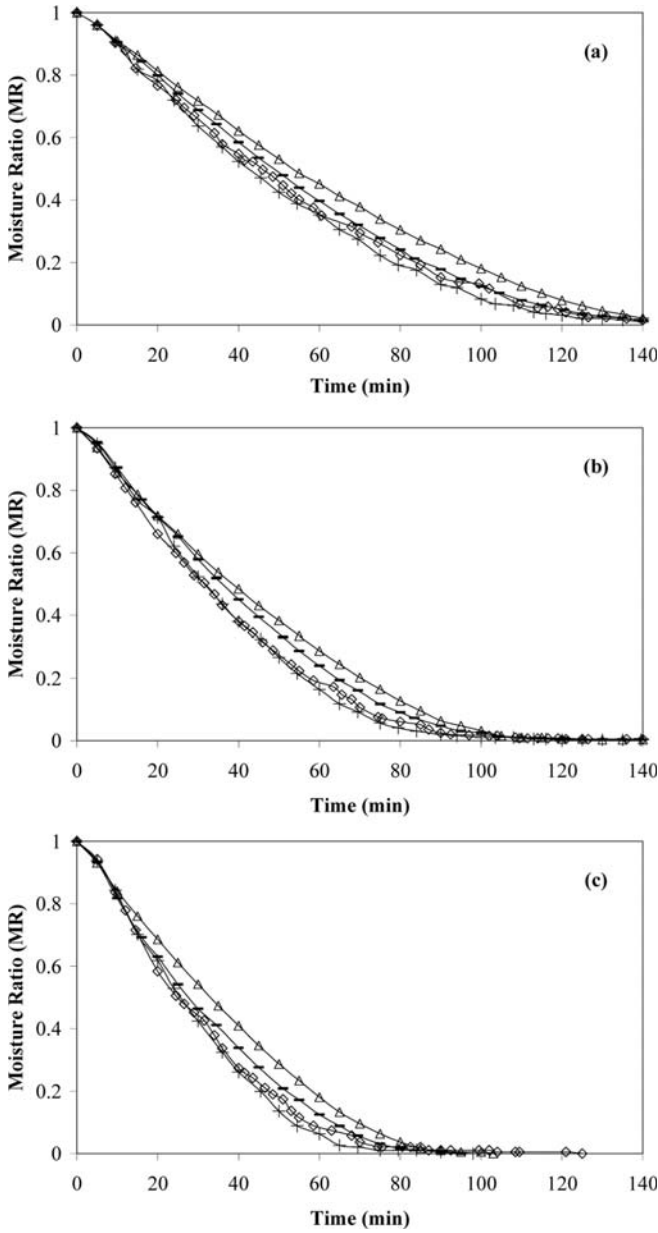


FIG. 7. Drying curves of banana chips undergoing intermittent pressure LPSSD at on/off period of 5:0 (—), 5:5 (+), 5:10 (◊), and continuous drying (Δ) at temperatures of (a) 70°C, (b) 80°C, and (c) 90°C.

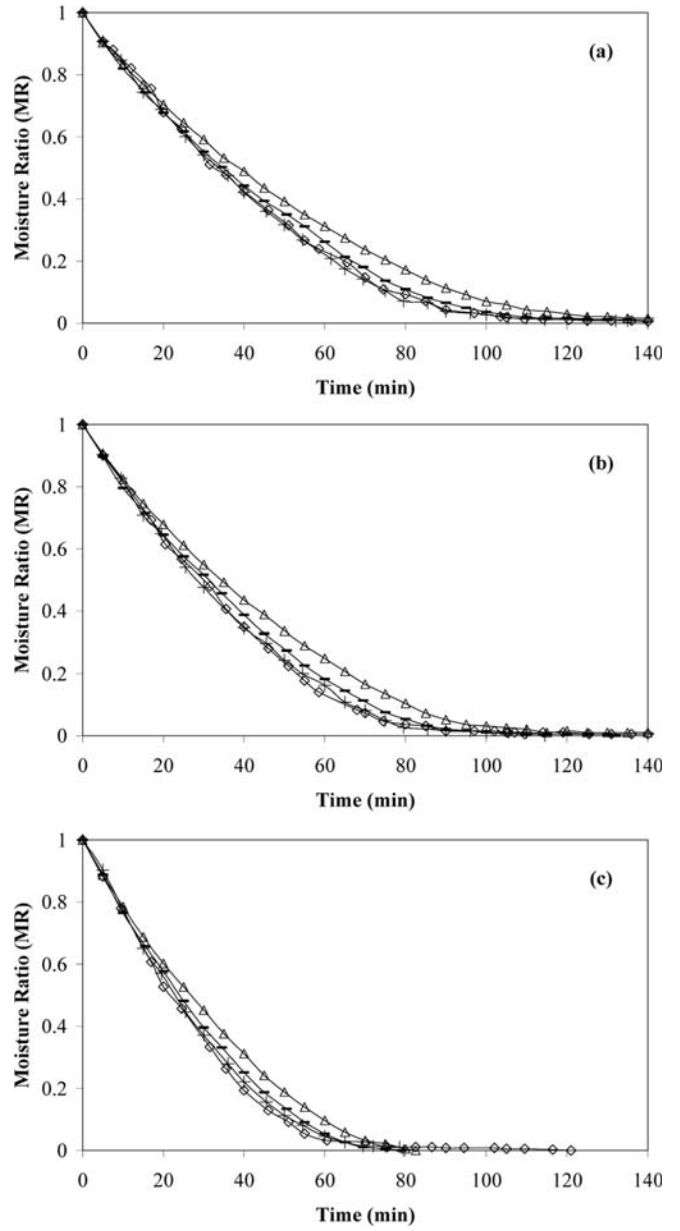


FIG. 8. Drying curves of banana chips undergoing intermittent pressure vacuum drying at on/off period of 5:0 (—), 5:5 (+), 5:10 (◊), and continuous drying (Δ) at temperatures of (a) 70°C, (b) 80°C, and (c) 90°C.

plots of the evolution of the chamber and sample temperatures; only selected plots are shown here for the sake of brevity, as the trends of temperature changes were the same at all tested conditions. In the case of intermittent pressure drying, the chamber absolute pressure was pulsed from 7 kPa during an on period to 100 kPa during an off or tempering period. This led to a higher boiling temperature of the water. In the case of LPSSD, the sample surface temperature corresponds to the saturation temperature of

water at the dryer operating pressure in the constant drying rate period. Hence, the sample temperature increased during an off period and then decreased back to the boiling temperature corresponding to the operating pressure of 7 kPa. On the other hand, the sample temperature in the case of continuous drying rose suddenly from its initial value and reached and remained rather constant at the boiling temperature of water corresponding to the operating pressure of 7 kPa until the constant drying

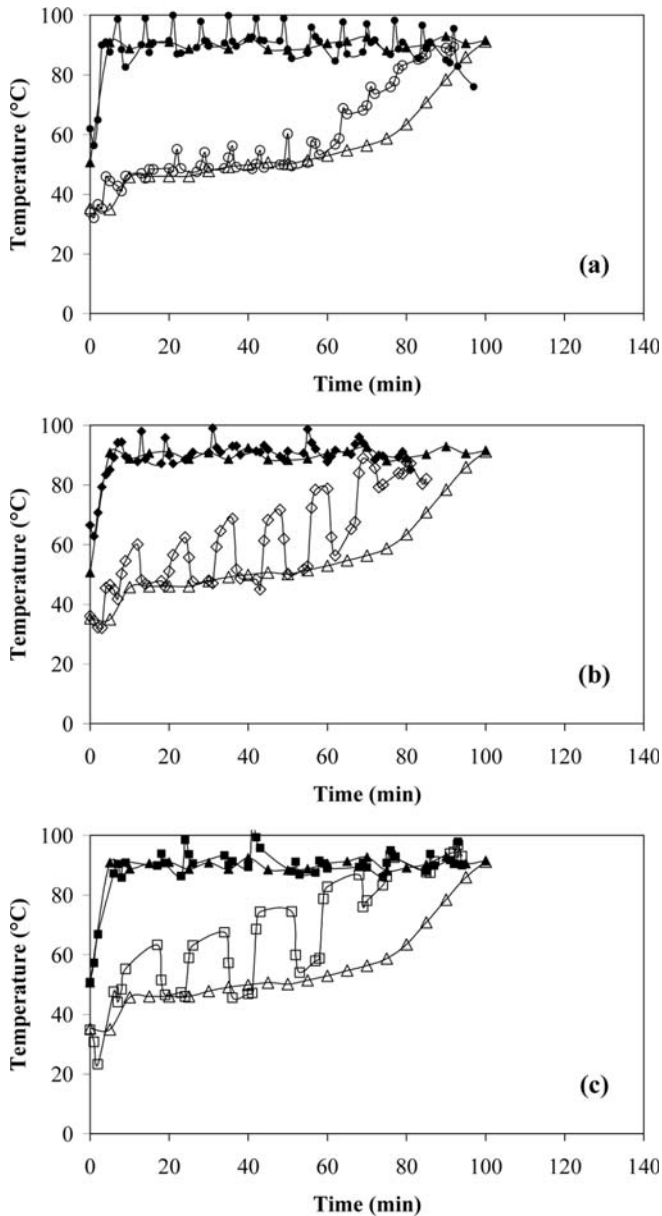


FIG. 9. Chamber (opaque sign) and sample (transparent sign) temperatures during continuous and intermittent pressure LPSSD at 90°C. Continuous drying (Δ) vs. intermittent drying at on:off period of (a) 5:0 (\circ), (b) 5:5 (\diamond), and (c) 5:10 (ϵ).

rate period ended. Then the sample temperature rose again to approach the drying medium temperature.

In the case of vacuum drying, the sample temperature in the case of continuous drying rose steadily from its initial value to the drying medium temperature. A similar behavior was also noted by Devahastin et al.^[3] The temperature of samples undergoing intermittent vacuum drying was also higher than that of continuous drying due to the effect of pressure variation. It was noted also that the sample

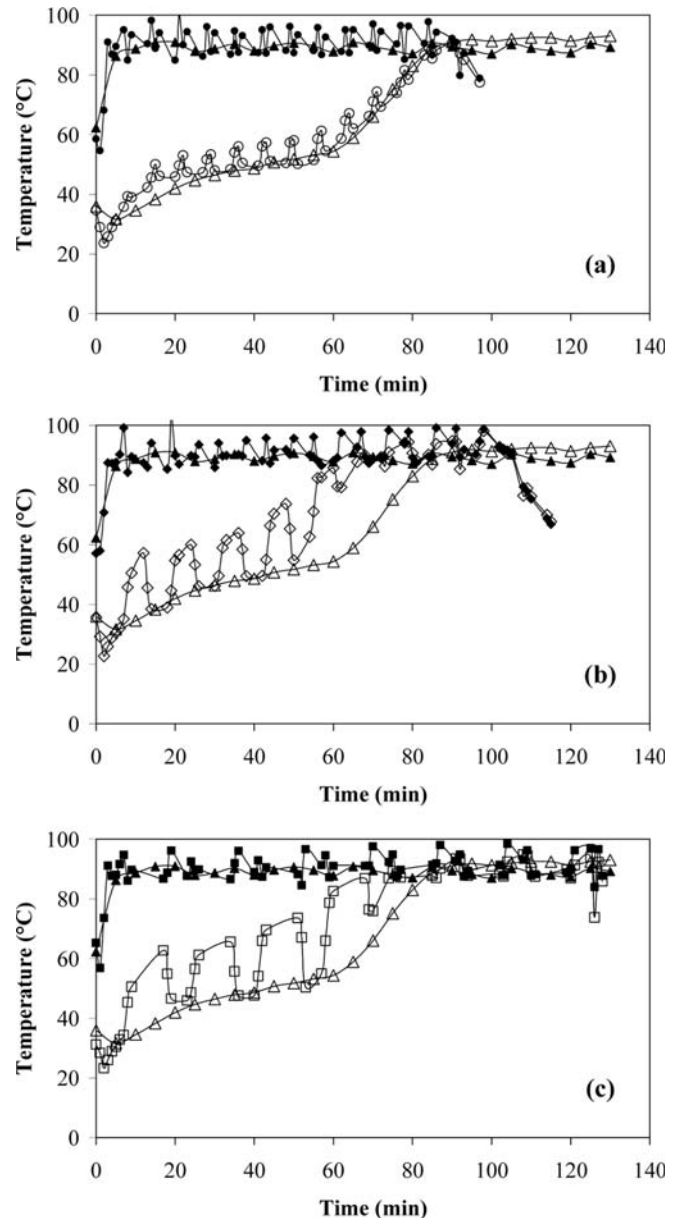


FIG. 10. Chamber (opaque sign) and sample (transparent sign) temperatures during continuous and intermittent pressure vacuum drying at 90°C. Continuous drying (Δ) vs. intermittent drying at on:off period of (a) 5:0 (\circ), (b) 5:5 (\diamond), and (c) 5:10 (ϵ).

temperature at longer tempering or off period was higher for longer duration. This phenomenon led to higher drying rates. Moreover, the decompression of pressure induced porous structure of the sample. This is the tunneling effect mentioned by Chua et al.^[18] after the drying process, the blind pores were observed to transform to interconnected pores. With the network of interconnected pores, the moisture diffusivity could be expected to improve significantly. The internal moisture was thus able to migrate

easily to the product surface.^[13] This result promoted moisture transport within the sample and therefore improved the drying rates.

It is seen in Table 2 that the total drying time at on:off periods of 5:0 and 5:5 min at all conditions was similar to that of continuous drying while at an on:off period of 5:10 min the total drying time of intermittent drying was longer. However, it is seen in Table 2 that the net (or

effective) drying time in the case of intermittent drying was shorter than the drying time of continuous drying.

Table 3 shows the energy savings of intermittent LPSSD and vacuum drying in comparison with continuous drying at various conditions. The savings in drying time were first calculated by subtracting the drying time of continuous drying with the net or effective drying time, which was the time that the drying process was actually on, and then

TABLE 3
Energy savings of intermittent LPSSD and vacuum drying at various conditions

Condition				Energy saving over continuous drying (%)		
Drying scheme	Drying method	Temp. (°C)	Intermittency (on:off, min)	Vacuum pump	Electric heater	Steam
Intermittent temperature scheme	LPSSD	70	10:5	—	N/A	N/A
			10:10	—	N/A	N/A
			10:20	—	N/A	N/A
		80	10:5	—	36	36
			10:10	—	53	53
			10:20	—	66	66
		90	10:5	—	30	30
			10:10	—	46	46
			10:20	—	65	65
	Vacuum drying	70	10:5	—	N/A	—
			10:10	—	N/A	—
			10:20	—	N/A	—
		80	10:5	—	24	—
			10:10	—	33	—
			10:20	—	52	—
		90	10:5	—	20	—
			10:10	—	32	—
			10:20	—	49	—
Intermittent pressure scheme	LPSSD	70	5:0	N/A	—	N/A
			5:5	N/A	—	N/A
			5:10	N/A	—	N/A
		80	5:0	11	—	26
			5:5	53	—	60
			5:10	61	—	67
		90	5:0	22	—	34
			5:5	55	—	62
			5:10	51	—	58
	Vacuum drying	70	5:0	N/A	—	—
			5:5	N/A	—	—
			5:10	N/A	—	—
		80	5:0	9	—	—
			5:5	50	—	—
			5:10	52	—	—
		90	5:0	22	—	—
			5:5	55	—	—
			5:10	53	—	—

N/A implies that, at this condition, the final banana moisture content of 0.025 kg/kg (d.b.) was not achievable.

dividing the result with the drying time of continuous drying. In the case of intermittent temperature drying, the vacuum pump was continuously used to maintain the pressure at 7 kPa. In the case of intermittent pressure drying, the heater was turned on continuously to maintain the temperature at the setting values. This information was used along with the time savings calculated above to determine the energy savings at each condition. Energy savings of steam in the case of intermittent vacuum drying was not calculated since steam was not injected into the chamber during vacuum drying.

It was found that intermittent temperature LPSSD at all temperatures could save the energy consumption of the electric heater more (up to about 65% at an on:off period of 10:20 min) than in the case of intermittent vacuum drying. Moreover, the power of the heater (in kWh) used in the case of LPSSD was lower than in the case of vacuum drying due to the fact that the electric heater was used more often during vacuum drying. Steam could also be saved up to about 65% in the case of intermittent LPSSD, both at 80 and 90°C, at an on:off period of 10:20 min.

In the case of intermittent pressure drying, it was observed that the energy savings of the vacuum pump in the case of LPSSD at fixed values of temperature and intermittency were similar to that of vacuum drying, which was around 50–60%. The energy savings of intermittent pressure LPSSD at 80°C and at an on:off period of 5:10 min was especially large due to a very long drying time of continuous drying at this condition. It is important to mention that, in the case of intermittent pressure LPSSD, steam was injected into the chamber during each vacuum cycle when the pressure was reduced to 7 kPa, which occurred after the vacuum pump was started for about 1.5 min. Therefore, the energy savings in terms of steam was larger than in terms of vacuum pump since the pump needed to be on longer than the on period of steam injection.

Considering the behavior of both drying processes at all conditions it was found that the drying rates in both intermittent pressure LPSSD and vacuum drying cases were higher than those in the cases of continuous drying and intermittent temperature drying. However, it was noted that the drying rates in the case of intermittent pressure

TABLE 4
Color changes of banana chips dried by intermittent temperature drying

Condition			Color changes		
Drying method	Temp. (°C)	Intermittency (on:off, min)	$\Delta L/L_0$	$\Delta a/a_0$	$\Delta b/b_0$
LPSSD	70	Continuous drying	N/A	N/A	N/A
		10:5	N/A	N/A	N/A
		10:10	N/A	N/A	N/A
		10:20	N/A	N/A	N/A
	80	Continuous drying	-0.01 ± 0.002^c	-0.41 ± 0.10^c	0.07 ± 0.009^{ab}
		10:5	-0.01 ± 0.006^c	-0.39 ± 0.02^c	0.05 ± 0.006^{ab}
		10:10	-0.01 ± 0.003^c	-0.33 ± 0.54^c	0.09 ± 0.009^{ab}
		10:20	-0.01 ± 0.007^c	-0.32 ± 0.01^c	0.10 ± 0.008^{ab}
	90	Continuous drying	-0.06 ± 0.003^{ab}	-0.54 ± 0.01^{bc}	0.08 ± 0.010^{ab}
		10:5	-0.05 ± 0.002^{bc}	-0.57 ± 0.02^{bc}	0.10 ± 0.001^b
		10:10	-0.03 ± 0.008^{bc}	-0.44 ± 0.04^{bc}	0.10 ± 0.003^b
		10:20	-0.02 ± 0.005^c	-0.66 ± 0.19^{bc}	0.07 ± 0.005^{ab}
Vacuum drying	70	Continuous drying	N/A	N/A	N/A
		10:5	N/A	N/A	N/A
		10:10	N/A	N/A	N/A
		10:20	N/A	N/A	N/A
	80	Continuous drying	-0.01 ± 0.003^c	-0.66 ± 0.01^{abc}	0.07 ± 0.005^{ab}
		10:5	-0.02 ± 0.005^c	-0.66 ± 0.02^{abc}	0.11 ± 0.011^b
		10:10	-0.02 ± 0.003^c	-0.64 ± 0.01^{bc}	0.10 ± 0.008^b
		10:20	-0.01 ± 0.005^c	-0.57 ± 0.02^{bc}	0.16 ± 0.001^c
	90	Continuous drying	-0.07 ± 0.008^{ab}	-0.89 ± 0.08^{ab}	0.07 ± 0.004^{ab}
		10:5	-0.08 ± 0.008^a	-0.91 ± 0.08^{ab}	0.09 ± 0.014^{ab}
		10:10	-0.06 ± 0.006^{ab}	-0.92 ± 0.05^{ab}	0.10 ± 0.014^{ab}
		10:20	-0.05 ± 0.007^{bc}	-0.66 ± 0.02^{abc}	0.17 ± 0.009^c

N/A implies that, at this condition, the final banana moisture content of 0.025 kg/kg (d.b.) was not achievable. Different letters in the same column indicate that values are significantly different ($\alpha < 0.05$).

LPSSD at fixed temperature and on/off period were similar to those in the case of intermittent pressure vacuum drying. However, the energy consumption of vacuum drying was lower than that of LPSSD due to the absence of steam injection.

Quality of Dried Banana Chips

The quality of banana chips was investigated after drying with different schemes as mentioned earlier; the final moisture content of the product was set at 0.025 kg/kg (d.b.). However, the equilibrium moisture content of banana chips dried either by LPSSD or vacuum drying at 70°C (approximately 0.04 kg/kg dry basis) was more than the desired final moisture content. Thus, the quality of banana chips dried at 70°C was not determined in this study.

Colors

Hunter color parameters (L , a , and b) were determined in order to investigate the color changes of banana chips. The normalized changes of lightness ($\Delta L/L_0$), redness ($\Delta a/a_0$), and yellowness ($\Delta b/b_0$) of banana underwent

intermittent temperature drying and intermittent pressure drying are shown in Tables 4 and 5, respectively.

It was observed that the drying methods (LPSSD and vacuum drying at the same temperature) did not significantly affect the color changes of banana chips when continuous drying was performed. However, the trend was that the color changes (especially lightness and redness) of banana chips dried by LPSSD were less than those dried by vacuum drying. This may be due to enzymatic browning reactions, which mainly depend on the level of oxygen and temperature of the product. Since LPSSD is an airless drying process and contains no oxygen in the system, the samples suffered less changes of color. Furthermore, it is seen in Figs. 4 and 5 that the temperature of samples undergoing LPSSD was lower than those undergoing vacuum drying.

The effect of drying temperature on the color changes was also observed. It is seen in Table 4 that at a high temperature of 90°C, colors changed more obviously than at lower temperatures of 70 and 80°C. This is because higher temperature leads to a higher rate of browning reaction.

TABLE 5
Color changes of banana chips dried by intermittent pressure drying

Condition			Color changes		
Drying method	Temp. (°C)	Intermittency (on:off, min)	$\Delta L/L_0$	$\Delta a/a_0$	$\Delta b/b_0$
LPSSD	70	Continuous drying	N/A	N/A	N/A
		5:0	N/A	N/A	N/A
		5:5	N/A	N/A	N/A
		5:10	N/A	N/A	N/A
	80	Continuous drying	-0.01 ± 0.002^d	-0.41 ± 0.10^c	0.07 ± 0.009^d
		5:0	-0.09 ± 0.01^c	-1.40 ± 0.53^{abc}	-0.01 ± 0.005^d
		5:5	-0.24 ± 0.02^a	-2.18 ± 0.91^{ab}	-0.14 ± 0.004^b
		5:10	-0.27 ± 0.01^a	-2.00 ± 0.77^{ab}	-0.15 ± 0.015^b
	90	Continuous drying	-0.06 ± 0.003^c	-0.54 ± 0.01^{bc}	0.08 ± 0.001^d
		5:0	-0.16 ± 0.01^b	-1.38 ± 0.80^{abc}	0.03 ± 0.011^{cd}
		5:5	-0.24 ± 0.01^a	-1.75 ± 0.55^{abc}	-0.18 ± 0.007^{ab}
		5:10	-0.24 ± 0.01^a	-2.49 ± 0.96^a	-0.17 ± 0.009^{ab}
Vacuum drying	70	Continuous drying	N/A	N/A	N/A
		5:0	N/A	N/A	N/A
		5:5	N/A	N/A	N/A
		5:10	N/A	N/A	N/A
	80	Continuous drying	-0.01 ± 0.003^d	-0.66 ± 0.01^c	0.07 ± 0.001^d
		5:0	-0.17 ± 0.01^b	-0.91 ± 0.20^{bc}	-0.05 ± 0.011^c
		5:5	-0.24 ± 0.01^a	-1.22 ± 0.17^{abc}	-0.12 ± 0.003^b
		5:10	-0.26 ± 0.01^a	-1.16 ± 0.19^{abc}	-0.16 ± 0.006^{ab}
	90	Continuous drying	-0.07 ± 0.008^c	-0.89 ± 0.08^c	0.07 ± 0.005^d
		5:0	-0.19 ± 0.01^b	-0.94 ± 0.01^{bc}	-0.03 ± 0.003^c
		5:5	-0.27 ± 0.01^a	-1.80 ± 0.03^{abc}	-0.16 ± 0.002^b
		5:10	-0.29 ± 0.01^a	-2.01 ± 0.02^{abc}	-0.16 ± 0.001^{ab}

N/A implies that, at this condition, the final banana moisture content of 0.025 kg/kg (d.b.) was not achievable. Different letters in the same column indicate that values are significantly different ($\alpha < 0.05$).

Nevertheless, temperature only significantly affected the lightness of the samples; this trend was also observed only in the case of vacuum drying as well.

In addition, the effect of the intermittency of time-varying temperature drying on color change was determined. It was found that, compared to continuous drying, intermittent drying significantly reduced the change of lightness only when LPSSD was performed at 90°C and at an on:off period of 10:20 min. At this condition, the time that the sample was subjected to a high-temperature environment during an effective (on) drying period was the shortest. In the case of redness it was observed that the redness of banana chips that underwent intermittent drying was insignificantly different from that obtained by continuous drying. In the case of intermittent LPSSD, steam was not injected into the drying chamber during the off period; therefore, the drying medium in the tempering (off) period was similar to that of vacuum drying. Thus, the level of oxygen was greater than in the case of continuous drying. However, the temperature of the product was

lower and therefore redness changes were not significantly different from those of continuous drying. In the case of yellowness, the changes of this color parameter in the case of intermittent drying were higher than those of continuous drying only when an on:off period of 10:20 min was used in the case of vacuum drying.

Overall, it was observed that, in almost all cases, the effect of intermittency or tempering period on the color changes was not significant when the same drying technique was used at the same setting temperature.

For the case of intermittent pressure drying the measured color changes are listed in Table 5. It was observed that the color changes of LPSSD samples were similar to those of vacuum drying. In the case of intermittent drying, the pressure increased from a vacuum condition to an atmospheric condition during the tempering period. The air with a high amount of oxygen was fed into the chamber to raise the chamber pressure, so the rates of browning reaction increased with the tempering time; this induced changes of colors of the samples. Therefore, at the same

TABLE 6
Texture of banana chips dried by intermittent temperature drying

Condition			Texture	
Drying method	Temp. (°C)	Intermittency (on:off, min)	Hardness (N)	Crispness (No. of peak)
LPSSD	70	Continuous drying	N/A	N/A
		10:5	N/A	N/A
		10:10	N/A	N/A
		10:20	N/A	N/A
	80	Continuous drying	21.52 ± 2.23 ^{ab}	27 ± 3 ^{abc}
		10:5	18.50 ± 2.97 ^a	27 ± 1 ^{ab}
		10:10	19.41 ± 1.12 ^a	31 ± 3 ^{abc}
		10:20	20.12 ± 2.90 ^a	32 ± 4 ^{abc}
	90	Continuous drying	24.09 ± 1.26 ^{ab}	28 ± 6 ^{abc}
		10:5	26.05 ± 2.47 ^b	33 ± 3 ^{abc}
		10:10	21.52 ± 5.43 ^{ab}	35 ± 2 ^{bc}
		10:20	20.49 ± 3.65 ^{ab}	36 ± 3 ^c
Vacuum drying	70	Continuous drying	N/A	N/A
		10:5	N/A	N/A
		10:10	N/A	N/A
		10:20	N/A	N/A
	80	Continuous drying	25.64 ± 7.21 ^{ab}	27 ± 1 ^{ab}
		10:5	22.79 ± 1.31 ^{ab}	23 ± 2 ^a
		10:10	20.46 ± 3.37 ^{ab}	30 ± 2 ^{abc}
		10:20	18.46 ± 2.12 ^a	31 ± 1 ^{abc}
	90	Continuous drying	26.44 ± 5.60 ^b	28 ± 7 ^{abc}
		10:5	20.99 ± 1.36 ^{ab}	28 ± 2 ^{abc}
		10:10	21.37 ± 4.49 ^{ab}	20 ± 4 ^{abc}
		10:20	16.81 ± 2.90 ^a	33 ± 6 ^{abc}

N/A implies that, at this condition, the final banana moisture content of 0.025 kg/kg (d.b.) was not achievable.

Different letters in the same column indicate that values are significantly different ($\alpha < 0.05$).

intermittency, the color changes of both drying methods were similar. However, it is seen in this table that the change of lightness of samples underwent LPSSD at 80°C with an on:off value of 5:0 min was significantly lower than for those that underwent vacuum drying. The same trends were observed for the change of yellowness. At an on:off period of 5:0 min, the time that the oxygen entered into the system was rather short. Hence, the effect of high oxygen content during the tempering period was small. It is seen that LPSSD yields lighter dried products due to the absence of oxygen during an on period.

Considering the effect of temperature (for the same drying method), it was found that the effect of temperature was only seen in change of lightness in the case of LPSSD at an on:off period of 5:0 min. The darker color at higher temperatures was due to the higher rates of browning reaction.

Regarding the effect of intermittency in each drying method and at each temperature, the lightness of samples that underwent intermittent drying significantly differed from those that underwent continuous drying. The

products were darker at longer tempering periods due to the higher amount of oxygen in the system. It was observed that on:off periods of 5:0 and 5:5 min, both in the case of LPSSD and vacuum drying, significantly affected the change of lightness of the samples. However, when an on:off period changed to 5:10 min, the results were not significantly different. The changes of redness of intermittently dried products were also larger than those in the case of continuous drying. The results, however, were more significant for longer tempering periods in the case of LPSSD since the difference in the amount of oxygen between an on period where the drying medium was steam and tempering period where the drying medium was moist air was larger.

It was observed that the yellowness changes in the case of intermittent vacuum drying were significantly higher than those in the case of continuous vacuum drying. It was found that, at both temperatures, when the tempering period was longer, the yellowness of the products was lower.

TABLE 7
Texture of banana chips dried by intermittent pressure drying

Condition			Texture	
Drying method	Temp. (°C)	Intermittency (on:off, min)	Hardness (N)	Crispness (No. of peak)
LPSSD	70	Continuous drying	N/A	N/A
		5:0	N/A	N/A
		5:5	N/A	N/A
		5:10	N/A	N/A
	80	Continuous drying	21.52 ± 2.23 ^{ab}	27 ± 3 ^a
		5:0	20.12 ± 2.90 ^{ab}	32 ± 1 ^a
		5:5	27.26 ± 2.12 ^{abc}	27 ± 1 ^a
		5:10	27.34 ± 6.48 ^{abcd}	30 ± 5 ^a
	90	Continuous drying	24.09 ± 1.26 ^{abc}	28 ± 6 ^a
		5:0	19.41 ± 1.12 ^{ab}	35 ± 4 ^a
		5:5	33.71 ± 2.52 ^{cd}	33 ± 8 ^a
		5:10	35.07 ± 1.04 ^d	32 ± 6 ^a
Vacuum drying	70	Continuous drying	N/A	N/A
		5:0	N/A	N/A
		5:5	N/A	N/A
		5:10	N/A	N/A
	80	Continuous drying	25.64 ± 7.21 ^{abcd}	27 ± 1 ^a
		5:0	18.50 ± 2.97 ^a	33 ± 5 ^a
		5:5	23.87 ± 4.91 ^{abc}	30 ± 5 ^a
		5:10	27.38 ± 4.49 ^{abcd}	31 ± 3 ^a
	90	Continuous drying	26.44 ± 5.60 ^{abcd}	28 ± 7 ^a
		5:0	17.71 ± 1.12 ^a	37 ± 6 ^a
		5:5	25.05 ± 2.47 ^{abcd}	33 ± 2 ^a
		5:10	30.91 ± 5.54 ^{bcd}	32 ± 5 ^a

N/A implies that, at this condition, the final banana moisture content of 0.025 kg/kg (d.b.) was not achievable. Different letters in the same column indicate that values are significantly different ($\alpha < 0.05$).

Texture

The texture (Tables 6 and 7) of dried banana chips is reported in terms of the hardness, which is the maximum breaking force, and crispness, which is the number of peaks in a force-deformation curve. A part of the samples with puffing (not core part) was cut to avoid the effect of dense structure at the core on the textural quality of the samples. This is because the samples were not puffed uniformly; less puffing was especially observed at the core. The blade-type probe was selected to cut the samples to represent the biting action of human front teeth.

Within the same drying method, the hardness and crispness of the products dried at a higher temperature (90°C) were higher than those obtained at a lower temperature (80°C). At higher temperature, water evaporated more intensely inside the sample and pushed open the cell structure, leading to high-porosity products. Hence, the products dried at higher temperature were crispier. However, more case hardening occurred at higher temperatures, leading to higher values of hardness. Nevertheless, the effect of temperature on these textural parameters was not significantly different. The effects of drying methods were not also significantly observed.

The effect of intermittency on the texture of the products was also determined. It was observed that generally the products that underwent intermittent temperature drying (Table 6) were less hard but crispier than those obtained with a continuous drying method. During a tempering period, in the case of intermittent temperature drying, heat was not supplied to the products. Therefore, moisture within the samples redistributed and moved to the surface. Hence, the samples were less stiff due to lower level of moisture gradient-induced stresses. Case hardening might occur to a lesser extent in the case of intermittent drying. However, the results were not significantly different among different conditions used.

In the case of intermittent pressure drying (Table 7), it is seen that the hardness at an on:off period of 5:0 min was not affected, whereas at on:off periods of 5:5 and 5:10 min the hardness was higher than in the case of continuous drying. During the tempering period in intermittent pressure drying, the sample temperature increased and approached the boiling point of water at higher pressure, as mentioned earlier. Rapid drying occurred in this period leading to case hardening. However, the period of high temperature when an on:off period of 5:0 min was used was rather short, so the effect on the hardness at this condition was negligible.

The results of hardness and crispness were also compared with those of commercially available freeze-dried banana chips. Hardness and crispness (number of peaks) of the commercially available vacuum-freeze-dried banana chips (Fruit King™) were 55.72 ± 5.48 N and 16 ± 3 ,

respectively. Thus, all samples in this study had lower values of hardness and were crispier than the commercially available banana chips.

Shrinkage

Since it was noticed that, although banana pieces puffed and hence their volume increased, the cross-sectional area of dried banana chips seemed to be smaller than that of fresh banana, shrinkage was determined in terms of the change of the cross-sectional area compared with the original area of the sample.

It is seen in Table 8 that shrinkage of banana chips in the case of LPSSD at 80°C was higher than at 90°C. This might be because case hardening occurred least at this condition; case hardening prevented shrinkage of the

TABLE 8
Shrinkage of banana chips dried by intermittent temperature drying

Condition			
Drying method	Temp. (°C)	Intermittency (on:off, min)	Shrinkage (%) ($\Delta A/A_0 \times 100$)
LPSSD	70	Continuous drying	N/A
		10:5	N/A
		10:10	N/A
		10:20	N/A
	80	Continuous drying	20.18 ± 1.70^{bc}
		10:5	22.23 ± 1.13^c
		10:10	21.23 ± 1.31^c
		10:20	22.19 ± 1.73^c
	90	Continuous drying	13.23 ± 0.61^a
		10:5	14.84 ± 0.57^{ab}
		10:10	14.90 ± 1.11^{ab}
		10:20	14.70 ± 1.85^{ab}
Vacuum drying	70	Continuous drying	N/A
		10:5	N/A
		10:10	N/A
		10:20	N/A
	80	Continuous drying	19.20 ± 0.81^{bc}
		10:5	19.14 ± 1.60^{bc}
		10:10	16.34 ± 0.29^{ab}
		10:20	16.72 ± 0.79^{abc}
	90	Continuous drying	16.05 ± 0.03^{ab}
		10:5	18.11 ± 1.41^{abc}
		10:10	16.34 ± 0.42^{ab}
		10:20	18.16 ± 1.64^{abc}

N/A implies that, at this condition, the final banana moisture content of 0.025 kg/kg (d.b.) was not achievable.

Different letters in the same column indicate that values are significantly different ($\alpha < 0.05$).

sample. The same trend was found for vacuum drying, for which shrinkage was less when a higher temperature was used. However, it was noted that the drying method did not significantly affect the shrinkage at the same drying temperature.

Shrinkage in the case of intermittent pressure drying was also observed (Table 9). It was found that shrinkage of the samples that underwent intermittent pressure drying was more obvious than in the case of continuous drying at all conditions. This may be due to the effect of pressure compression. In the case of intermittent drying, pressure was raised from 7 to 100 kPa during an off period. Therefore, the samples were pressed by the external pressure (force) and then collapsed. This collapse in turn led to more shrinkage of the samples.

TABLE 9

Shrinkage of banana chips dried by intermittent pressure drying

Condition			
Drying method	Temp. (°C)	Intermittency (on:off, min)	Shrinkage (%) ($\Delta A/A_0 \times 100$)
LPSSD	70	Continuous drying	N/A
		5:0	N/A
		5:5	N/A
		5:10	N/A
	80	Continuous drying	20.18 \pm 1.70 ^{cd}
		5:0	26.48 \pm 0.63 ^e
		5:5	28.52 \pm 0.20 ^e
		5:10	27.79 \pm 0.05 ^e
	90	Continuous drying	13.23 \pm 0.61 ^a
		5:0	18.86 \pm 0.75 ^{bc}
		5:5	21.48 \pm 1.01 ^d
		5:10	21.82 \pm 0.28 ^d
Vacuum drying	70	Continuous drying	N/A
		5:0	N/A
		5:5	N/A
		5:10	N/A
	80	Continuous drying	19.20 \pm 0.81 ^{cd}
		5:0	19.88 \pm 1.65 ^{bcd}
		5:5	20.76 \pm 0.77 ^{cd}
		5:10	20.83 \pm 0.81 ^d
	90	Continuous drying	16.05 \pm 0.03 ^{ab}
		5:0	16.48 \pm 1.50 ^{ab}
		5:5	21.37 \pm 0.83 ^d
		5:10	21.36 \pm 0.96 ^d

N/A implies that, at this condition, the final banana moisture content of 0.025 kg/kg (d.b.) was not achievable.

Different letters in the same column indicate that values are significantly different ($\alpha < 0.05$).

Ascorbic Acid Retention

The percentages of ascorbic acid retention in banana chips that underwent intermittent temperature and intermittent pressure drying are shown in Tables 10 and 11, respectively. It was observed that LPSSD prevents degradation of ascorbic acid better than vacuum drying. This is because the amount of oxygen, which causes aerobic degradation of ascorbic acid, in LPSSD was lower than in the case of vacuum drying.

Temperature was also found to affect the degradation of ascorbic acid. As expected, the ascorbic acid retention at a high temperature was less than at a low temperature in both LPSSD and vacuum drying. A similar result was found when drying gooseberry flake in LPSSD and vacuum drying.^[4]

TABLE 10

Ascorbic acid retention of banana chips dried by intermittent temperature drying

Condition			
Drying method	Temp. (°C)	Intermittency (on:off, min)	Ascorbic acid retention (%)
LPSSD	70	Continuous drying	N/A
		10:5	N/A
		10:10	N/A
		10:20	N/A
	80	Continuous drying	53.14 \pm 2.79 ^{bc}
		10:5	62.09 \pm 1.94 ^{cd}
		10:10	65.09 \pm 2.07 ^d
		10:20	63.99 \pm 0.52 ^d
	90	Continuous drying	41.33 \pm 2.76 ^a
		10:5	52.78 \pm 2.40 ^{bc}
		10:10	64.46 \pm 4.39 ^d
		10:20	55.78 \pm 2.55 ^d
Vacuum drying	70	Continuous drying	N/A
		10:5	N/A
		10:10	N/A
		10:20	N/A
	80	Continuous drying	40.75 \pm 2.73 ^a
		10:5	44.63 \pm 3.73 ^{ab}
		10:10	44.94 \pm 2.47 ^{ab}
		10:20	55.37 \pm 2.73 ^{cd}
	90	Continuous drying	37.76 \pm 2.63 ^a
		10:5	44.10 \pm 0.80 ^a
		10:10	54.04 \pm 1.53 ^{bcd}
		10:20	58.35 \pm 3.01 ^d

N/A implies that, at this condition, the final banana moisture content of 0.025 kg/kg (d.b.) was not achievable.

Different letters in the same column indicate that values are significantly different ($\alpha < 0.05$).

TABLE 11
Ascorbic acid retention of banana chips dried by
intermittent pressure drying

Condition			
Drying method	Temp. (°C)	Intermittency (on:off, min)	Ascorbic acid retention (%)
LPSSD	70	Continuous drying	N/A
		5:0	N/A
		5:5	N/A
		5:10	N/A
	80	Continuous drying	53.14 ± 2.79 ^g
		5:0	47.74 ± 2.21 ^{fg}
		5:5	41.60 ± 2.62 ^{ef}
		5:10	30.05 ± 2.42 ^{bc}
	90	Continuous drying	41.33 ± 2.76 ^{ef}
		5:0	37.04 ± 1.70 ^{de}
		5:5	31.20 ± 3.17 ^{bcd}
		5:10	25.76 ± 1.89 ^{ab}
Vacuum drying	70	Continuous drying	N/A
		5:0	N/A
		5:5	N/A
		5:10	N/A
	80	Continuous drying	40.75 ± 2.73 ^{ef}
		5:0	37.78 ± 0.41 ^{de}
		5:5	31.67 ± 0.89 ^{bcd}
		5:10	29.14 ± 2.53 ^{bc}
	90	Continuous drying	37.76 ± 2.63 ^{de}
		5:0	33.20 ± 1.42 ^{cde}
		5:5	30.47 ± 2.14 ^{bcd}
		5:10	21.82 ± 1.82 ^a

N/A implies that, at this condition, the final banana moisture content of 0.025 kg/kg (d.b.) was not achievable.

Different letters in the same column indicate that values are significantly different ($\alpha < 0.05$).

Intermittent temperature drying conditions led to a higher level of ascorbic acid retention, especially at longer tempering (off) period, because the samples were subjected less to high-temperature environment during drying. For long tempering period (10:20 min), the effect of the drying method was not observed, however; this may be because intermittent LPSSD system effectively became vacuum drying under this condition.

Regarding the effect of intermittent pressure drying on ascorbic acid retention, it was found that intermittent pressure drying led to more degradation of ascorbic acid. In the case of intermittent pressure drying, oxygen was fed into the chamber with air to raise the chamber pressure to atmosphere in tempering period. This caused more aerobic loss of ascorbic acid. Moreover, the temperatures of the samples during intermittent drying were higher than in the

case of continuous drying, leading to higher levels of ascorbic acid degradation.

CONCLUSIONS

The effects of intermittency and on-period setting drying temperature on the drying kinetics and quality of banana chips undergoing intermittent LPSSD and vacuum drying were investigated and compared with the results of continuous drying. In the case of intermittent temperature LPSSD, the overall drying rates of intermittent and continuous LPSSD were not significantly different. However, the effective or net drying time of intermittent drying was significantly shorter than that of continuous drying, especially at longer tempering periods, leading to high energy savings. Intermittent temperature LPSSD at 90°C and an on:off period of 10:20 min can reduce energy consumption by up to 65% compared with continuous drying. It was noted that the drying rates of intermittent pressure LPSSD and vacuum drying at all conditions were obviously higher than those of continuous drying. This implied energy savings of the vacuum pump of up to 51 and 53% in the cases of intermittent pressure LPSSD and vacuum drying, respectively; steam savings in the case of intermittent pressure LPSSD of up to 58% could be achieved.

The quality measurements showed that the effect of intermittency in intermittent temperature drying in almost all cases, when compared with continuous drying, was not significant except for changes in lightness, which was reduced only when LPSSD was performed at 90°C and at an on:off period of 10:20 min. Besides, it was observed that the colors of the products in the case of intermittent pressure drying were worse than that in the case of continuous drying. It was found that the product texture in almost all cases was not significantly different. Moreover, it was observed that intermittent temperature drying did not affect the shrinkage of the product, whereas the shrinkage of the samples that underwent intermittent pressure drying was more obvious than in the case of continuous drying at all conditions. Finally, intermittent temperature drying led to higher level of ascorbic acid retention, especially at longer tempering (off) periods. On the other hand, intermittent pressure drying led to greater degradation of ascorbic acid.

ACKNOWLEDGEMENTS

The authors express their sincere appreciation to the Commission on Higher Education, the Thailand Research Fund (TRF), and the International Foundation for Science (IFS), Sweden, for supporting this study financially.

REFERENCES

1. Elustondo, D.; Elustondo, M.P.; Urbicain, M.J. Mathematical modeling of moisture evaporation from foodstuffs exposed to subatmospheric pressure superheated steam. *Journal of Food Engineering* **2001**, *49*, 15–24.

2. Mujumdar, A.S. Superheated steam drying-technology of the future. In *Mujumdar's Practical Guide to Industrial Drying*, Devahastin, S., Ed.; Exergex: Brossard, Canada, 2000; 115–138.
3. Devahastin, S.; Suvarnakuta, P.; Soponronnarit, S.; Mujumdar, A.S. A comparative study of low-pressure superheated steam and vacuum drying of a heat-sensitive material. *Drying Technology* **2004**, *22*, 1845–1867.
4. Methakhup, S.; Chiewchan, N.; Devahastin, S. Effects of drying methods and conditions on drying kinetics and quality of Indian gooseberry flake. *Lebensmittel-Wissenschaft und-Technologie* **2005**, *38*, 579–587.
5. Suvarnakuta, P.; Devahastin, S.; Mujumdar, A.S. Drying kinetics and β -carotene degradation in carrot undergoing different drying processes. *Journal of Food Science* **2005**, *70*, S520–S526.
6. Leeratanarak, N.; Devahastin, S.; Chiewchan, N. Drying kinetics and quality of potato chips undergoing different drying techniques. *Journal of Food Engineering* **2006**, *77*, 635–643.
7. Ratti, C.; Mujumdar, A.S. Fixed-bed batch drying of shrinking particles with time varying drying air conditions. *Drying Technology* **1993**, *11*, 1311–1355.
8. Jumah, R.Y.; Mujumdar, A.S.; Raghavan, G.S.V. A mathematical model for constant and intermittent batch drying of grains in a novel rotating jet spouted bed. *Canadian Journal of Chemical Engineering* **1996**, *74*, 479–486.
9. Devahastin, S.; Mujumdar, A.S. Batch drying of grains in a well-mixed dryer—Effect of continuous and stepwise change in drying air temperature. *Transactions of the ASAE* **1999**, *42*, 421–425.
10. Jumah, R.Y.; Mujumdar, A.S. Modeling intermittent drying using an adaptive neuro-fuzzy inference system. *Drying Technology* **2005**, *23*, 1075–1092.
11. Chua, K.J.; Mujumdar, A.S.; Hawlader, M.N.A.; Chou, S.K.; Ho, J.C. Batch drying of banana pieces—Effect of stepwise change in drying air temperature on drying kinetics and product colour. *Food Research International* **2001**, *34*, 721–731.
12. Islam, M.R.; Ho, J.C.; Mujumdar, A.S. Convective drying with time-varying heat input: Simulation results. *Drying Technology* **2003**, *21*, 1333–1356.
13. Rakotozafy, H.; Louka, N.; Therisod, M.; Therisod, H.; Allaf, K. Drying of baker's yeast by a new method: Dehydration by successive pressure drops: Effect on cell survival and enzymatic activities. *Drying Technology* **2000**, *18*, 2253–2271.
14. Gunasekaran, S. Pulsed microwave-vacuum drying of food materials. *Drying Technology* **1999**, *17*, 395–412.
15. Xing, H.; Takhar, P.S.; Helms, G.; He, B. NMR imaging of continuous and intermittent drying of pasta. *Journal of Food Engineering* **2007**, *78*, 61–68.
16. Association of Official Analytical Chemists. *Official Methods of Analysis*, 15th Ed.; AOAC: Washington, D.C., 1995.
17. Suvarnakuta, P.; Devahastin, S.; Soponronnarit, S.; Mujumdar, A.S. Drying kinetics and inversion temperature in a low-pressure superheated steam drying system. *Industrial & Engineering Chemistry Research* **2005**, *44*, 1934–1941.
18. Chua, K.J.; Chou, S.K. On the experimental study of a pressure regulatory system for bioproducts dehydration. *Journal of Food Engineering* **2004**, *62*, 151–158.

Effects of Drying Methods and Tea Preparation Temperature on the Amount of Vitamin C in Indian Gooseberry Tea

Pao Kongsoontornkijkul, Prakaithip Ekwongsupasarn, Naphaporn Chiewchan, and Sakamon Devahastin

Department of Food Engineering, Faculty of Engineering, King Mongkut's University of Technology Thonburi, Bangkok, Thailand

Indian gooseberry is a rich source of vitamin C. The fruit can be consumed either fresh or after processing into different products including Indian gooseberry tea. Both drying and tea preparation steps affect quality of the gooseberry tea drink made using dried gooseberry. This study investigated the effects of different drying methods, i.e., hot air drying, vacuum drying, and low-pressure superheated steam drying, on the retention and degradation of vitamin C (in terms of the total ascorbic acid content, TAA) in dried gooseberry flakes. In addition, the effect of temperature of water used to prepare the tea on the release of TAA and on its later degradation was also investigated.

Keywords Ascorbic acid; Hot air drying; Leachability; Low-pressure superheated steam drying; Porosity; Release kinetics; Vacuum drying

INTRODUCTION

Indian gooseberry (*Phyllanthus emblica* Linn.), or “Ma-khaam Pom” in Thai and “Amla” in Hindi and several Indian languages, is a fruit native to the tropical Southeast Asian region.^[1] The fruit is known as a good source of natural vitamin C or ascorbic acid and its flesh is used as an ingredient in herbal medicine; it can also be processed into various forms such as pickles, marmalades, and beverage products, including herbal or fruit tea.

Indian gooseberry tea is an alternative drink to typical or fruit teas. The tea production simply starts from grinding Indian gooseberry flesh into small pieces, subjecting the ground product to a drying process, and then packing the dried product in a tea bag. Drying is one of the most important steps during the tea production as it affects directly the quality of the dried product, in terms of its physical and/or nutraceutical property, which is naturally related to the quality of the tea. Application of a suitable

drying technology and selection of appropriate drying conditions are therefore of great importance in the production of a good quality tea product.

Methakhup et al.^[2] studied the effects of drying methods, i.e., vacuum drying and low-pressure superheated steam drying, and conditions on the drying kinetics and quality of Indian gooseberry flakes. Their results showed that the product subjected to vacuum drying at 75°C and at an absolute pressure of 7 kPa contained similar level of ascorbic acid retention compared to those dried by low-pressure superheated steam drying at 65 and 75°C at absolute pressures of 7–13 kPa.

In addition to the loss during drying, vitamin C contained in the dried flake also degrades during the tea preparation step due to the use of high-temperature water to prepare tea. Moreover, the leachability of vitamin C from the solid structure of the flake is also of importance; this ability is again related directly to the choices of the drying process and conditions, which in turn affect the microstructure of the dried product.^[3–8]

This work aimed at a study of the effects of various drying methods, viz. hot air drying, vacuum drying, and low-pressure superheated steam drying, and the water temperature during Indian gooseberry tea preparation on the amount of ascorbic acid available in the final tea drink. Consideration was given on both the release of vitamin C (in terms of TAA) from the dried flakes and on the degradation of vitamin C during tea preparation.

MATERIALS AND METHODS

Materials

Fresh Indian gooseberry was obtained from a local market and stored in a refrigerator at 5°C until the time of experiment. After rinsing with tap water, the seeds of the fruit were removed. The flesh was then cut into small pieces and blended for one minute in an electric blender (Moulinex, AS184, France). Forty grams of the prepared sample

Correspondence: Naphaporn Chiewchan, Department of Food Engineering, Faculty of Engineering, King Mongkut's University of Technology Thonburi, 126 Pracha u-tid Road, Bangkok 10140, Thailand; E-mail: naphaporn.rat@kmutt.ac.th

was then spread on an aluminum foil sample holder ($9.5 \times 9.5 \text{ cm}^2$) and introduced to a drying process.

Experimental Setup

A schematic diagram of a low-pressure superheated steam dryer and its accessories is shown in Fig. 1.^[9] The dryer consists of a stainless steel drying chamber with inner dimensions of $45 \times 45 \times 45 \text{ cm}^3$; a steam reservoir, which received the steam from a boiler and maintained its pressure at around 200 kPa (gage); and a liquid ring vacuum pump (Nash, ET32030, Trumbull, Connecticut), which was used to maintain the vacuum in the drying chamber. A steam trap was installed to reduce the excess steam condensation in the reservoir. An electric heater, rated at 1.5 kW, which was controlled by a proportional-integral-derivative controller (Omron, E5CN, Tokyo, Japan), was installed in the drying chamber to control the steam temperature and to minimize the condensation of steam in the drying chamber during the startup period. A variable-speed electric fan was used to disperse steam throughout the drying chamber. The sample holder was made of stainless steel with dimensions of $12 \times 12 \text{ cm}^2$. The change of the mass of the sample was detected continuously (at 30-s intervals) using a load cell (Minibea, Ucg-3 kg, Nagano, Japan), which was installed in a smaller chamber connected to the drying chamber and also to an indicator and recorder (A & D Co., AD 4329, Tokyo, Japan). The temperatures of the steam and of the drying sample were measured continuously using type K thermocouples, which were connected to an expansion board (Omega Engineering, EXP-32, Stamford, Connecticut). Thermocouple signals were multiplexed to a data acquisition card (Omega Engineering, CIO-DAS16Jr.) installed on a PC. LAB-TECH NOTEBOOK software (version 12.1, Laboratory

Technologies Corp., Massachusetts) was used to read and record the temperature data.

For the vacuum drying experiments the same experimental set-up was used but without application of steam to the drying chamber. A hot air oven (Mettmert, ULM 600 II, Germany) was used for hot air drying experiments.

Production of Indian Gooseberry Flakes

Based on the previous study and our preliminary investigation, the sample was subjected to drying in a hot air oven at 75°C for 180 min while it was dried in a vacuum dryer at 75°C , 7 kPa for 145 min and a low-pressure superheated steam dryer, also at 75°C , 7 kPa, for 280 min.^[2] These conditions gave the final moisture content of Indian gooseberry flake of 0.07 kg/kg (d.b.), which is the standard moisture content recommended for tea.^[10] Two grams of dried flake were packed into a tea bag ($4 \times 5 \text{ cm}^2$). The tea bag was vacuum packed in a laminated aluminum packet to protect vitamin C from oxidative reaction prior to subsequent tea preparation.

Tea Preparation

Two hundred fifty milliliters of distilled water was heated and controlled at $70 \pm 1^\circ\text{C}$, $80 \pm 1^\circ\text{C}$, and $90 \pm 1^\circ\text{C}$, which are typical temperatures used to prepare tea, by a water bath. A tea bag containing dried gooseberry flake from each of the three drying processes was then soaked into 250 mL of hot water. The prepared tea was sampled at 0, 1, 2, 5, 8, 11, 14, 17, and 20 min for TAA analysis. All experiments were performed in duplicate.

Total Ascorbic Acid (TAA) Determination

In this study, vitamin C was determined in terms of TAA by Roe and Kuther's method.^[11] The assay estimates the intensity of osazone formed by the coupling of 2,4-dinitrophenylhydrazine (DNPH) with the oxidative forms of ascorbic acid, which are dehydroascorbic acid (DHAA) and diketogulonic acid (DKGA), using a spectrophotometer at 520 nm (Shimadzu, UV-2101 PC, Tokyo, Japan).

TAA in fresh fruits, dried flake, and tea samples at different sampling periods and gooseberry residues after tea preparation was determined and used for the determination of release and degradation of vitamin C during drying and tea preparation. The cumulative release of vitamin C during tea preparation is expressed by:

TAA Cumulative Release (%)

$$= \frac{(\text{Instantaneous amount of TAA in tea} \times 100)}{\text{Initial TAA in dried flake} - \text{TAA in gooseberry residue after 20min}} \quad (1)$$

The cumulative TAA release is the amount of TAA that was released and degraded during tea preparation

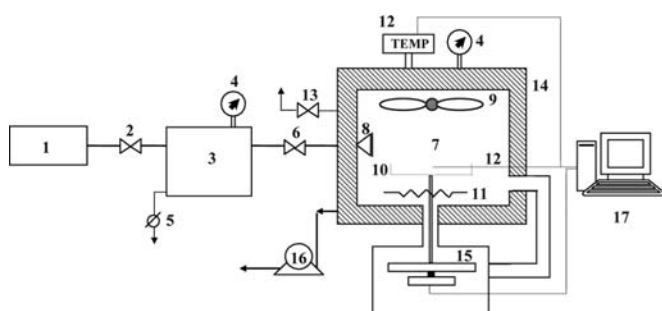


FIG. 1. schematic diagram of low-pressure superheated steam dryer and associated units. 1, boiler; 2, steam valve; 3, steam reservoir; 4, pressure gauge; 5, steam trap; 6, steam regulator; 7, drying chamber; 8, steam inlet and distributor; 9, electric fan; 10, sample holder; 11, electric heater; 12, on-line temperature sensor and logger; 13, vacuum break-up valve; 14, insulator; 15, on-line mass indicator and logger; 16, vacuum pump; 17, PC with installed data acquisition card.

TABLE 1
Degradation of TAA of Indian gooseberry flake underwent different drying processes

Drying method	TAA (g/100 g d.b.)		Drying time (min)	Degradation (%)
	Fresh	Dried		
Hot air drying at 75°C	5.8275 ± 0.0867	4.4845 ± 0.0452	180	23
Vacuum drying at 75°C, 7 kPa	5.1683 ± 0.1678	4.1558 ± 0.1357	145	20
LPSSD at 75°C, 7 kPa	4.8485 ± 0.0193	4.1696 ± 0.0313	280	14

compared with an ideal amount of TAA that would present in tea drink if there was no degradation.

Moreover, after tea preparation, the total degradation of TAA during tea preparation was calculated by Eq. (2), which represents the fraction of TAA which degraded to the initial TAA in dried flake.

$$\text{Total Degradation (\%)} = \frac{\text{Initial TAA in dried flake} - (\text{TAA in tea} + \text{TAA in residue})}{\text{Initial TAA in dried flake}} \quad (2)$$

Statistical Analysis

The experiments were designed complete randomly. The data were analyzed and presented as mean values with standard deviations. Differences between mean values were established using Duncan's multiple range tests. Values were considered at 95% confidence level ($p < 0.05$) and all experiments were performed in duplicate.

RESULTS AND DISCUSSION

Indian gooseberry flake was dried using different drying techniques and conditions as listed in Table 1; the selected conditions were based on the earlier study of Methakhup et al.^[2] Upon drying the amount of TAA in Indian gooseberry flakes expectedly decreased, as also shown in Table 1.

Based on the results summarized in Table 1 it can be seen that although hot air drying was the fastest drying process, it led to most TAA degradation. LPSSD, on the other hand, required the longest time to dry the product from an initial average moisture content of 4.60 kg/kg (d.b.) to 0.07 kg/kg (d.b.). However, LPSSD could best maintain the level of TAA compared with the other two drying methods. This is due to the oxygen-free environment of LPSSD, which prohibited aerobic degradation of ascorbic acid. This trend of results is similar to that reported by Methakhup et al.^[2]

Release of TAA from Dried Indian Gooseberry Flake

The release of TAA from the dried flake during tea preparation was determined by soaking the dried gooseberry flake in hot water at 70, 80, and 90°C for 20 min.

During tea preparation some TAA was released from the flake while some was still captured inside the flake and was destroyed by the high-temperature water used to prepare tea.^[12] Therefore, the experimental data are presented in terms of TAA cumulative release (%), which is shown in Table 2. Table 3, on the other hand, shows the TAA degradation during tea preparation. The use of flake obtained from LPSSD and water temperature at 90°C gave the highest total TAA degradation, while the lowest degradation was observed when using flake dried by hot air at 70°C and tea preparation temperature of 70°C.

Figures 2–4 show the percentage of cumulative release of TAA from flake at various tea preparation times and at different tea preparation temperatures. TAA in tea drink

TABLE 2
Average cumulative TAA release during tea preparation

Method used to prepare flake	Water temperature (°C)	Cumulative TAA release (%)
Hot air drying at 75°C	70	79.9 ± 1.0 ^c
	80	83.6 ± 1.0 ^b
	90	82.8 ± 1.0 ^b
Vacuum drying at 75°C, 7 kPa	70	86.9 ± 0.6 ^a
	80	78.0 ± 0.6 ^c
	90	72.8 ± 0.6 ^d
LPSSD at 75°C, 7 kPa	70	74.1 ± 0.6 ^d
	80	66.6 ± 0.6 ^e
	90	51.8 ± 0.6 ^f

Different letters in the same column indicate that values are significantly different ($p < 0.05$).

TABLE 3
TAA degradation of Indian gooseberry flake during tea preparation at various temperatures

Method used to prepare flake	Degradation (%)		
	70°C	80°C	90°C
Hot air drying at 75°C	5.0	3.0	2.0
Vacuum drying at 75°C, 7 kPa	6.0	11.0	15.0
LPSSD at 75°C, 7 kPa	12.0	16.0	38.0

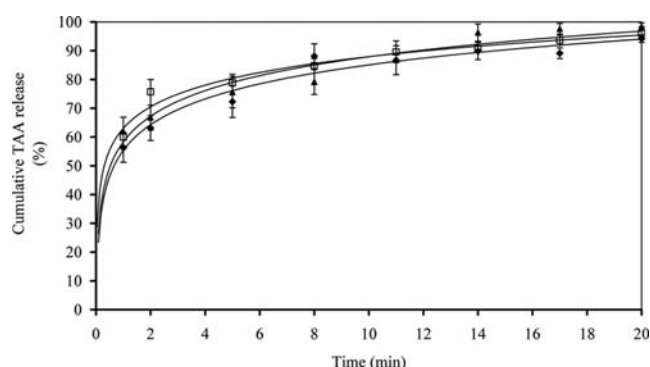


FIG. 2. TAA release of hot air dried (75°C) flake at water temperature of 70°C (◆), 80°C (□), and 90°C (▲).

rapidly increased during the first minutes of soaking and then increased steadily along with the soaking time. The effect of tea preparation temperature on the release rates of TAA from hot air dried flake was not as obvious as those from vacuum dried and LPSSD flakes. In general, degradation of TAA occurred both in tea drink and in flake and higher water temperatures naturally caused more destruction of ascorbic acid.^[13–15]

Considering the results at the same hot water temperature, the rates of TAA released from the flake to water were much higher than the rates of ascorbic acid degradation during the first minutes of tea preparation. After this initial period, the release of TAA occurred at slower rates as less TAA remained in the flake hence lower gradients for the release. However, the thermal degradation of TAA in tea drink still continued at constant rates. Therefore, the amount of TAA dissolved in the tea drink increased only slowly and finally approached constant values.

The structure of the flake also played an important role on the rate of release of TAA. High-porosity flake, which was obtained when subjecting the flake to LPSSD,^[2,9] facilitated hot water to transport into the flake. Thermal

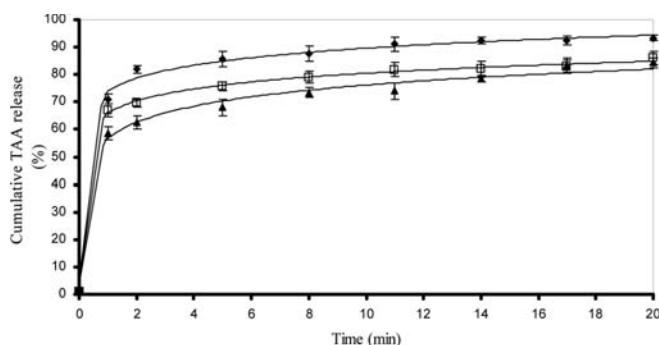


FIG. 3. TAA release of vacuum dried (75°C) flake at water temperature of 70°C (◆), 80°C (□), and 90°C (▲).

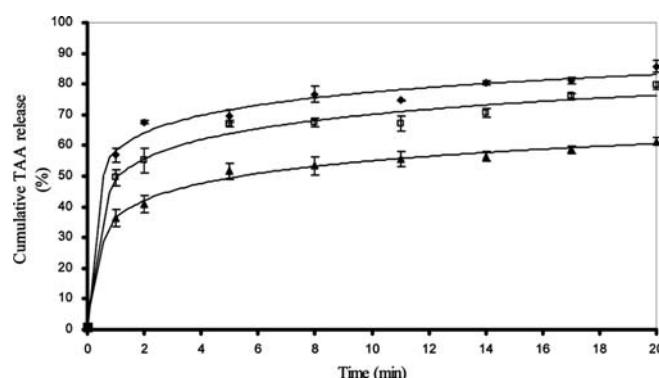


FIG. 4. TAA release of LPSSD (75°C) flake at water temperature of 70°C (◆), 80°C (□), and 90°C (▲).

degradation of ascorbic acid in the flake thus occurred at higher rates than that in the flakes obtained by hot air drying and vacuum drying.^[7,16] Therefore, the rates of release of TAA into tea drink were lowered in the case of LPSSD flake. It is important to note again, however, that the initial values of TAA in LPSSD flake were higher than those in hot air- and vacuum-dried flakes (see Table 1).

Combined Effects of Drying Techniques and Tea Preparation Methods on TAA Content

When considering the drying process it was found that the dried flake obtained from LPSSD had the highest TAA retention while the flake obtained from hot air drying had the lowest TAA retention. However, when these flakes were subjected to high-temperature water during the tea preparation process the situation was quite different. To aid understanding of the degradation of TAA during both drying and tea preparation processes a complete sketch of the processes is illustrated in Fig. 5. The total TAA degradation ranged between 24 and 47% as presented in Table 4.

Based on the results presented in Table 4, it is seen that at lower tea preparation temperature (70°C) the TAA degradation was similar, regardless of the type of dryer used to dry flake. However, at higher tea preparation temperatures, especially at 90°C, TAA degradation in tea prepared from LPSSD flake was the highest. This is probably due to the more porous structure of LPSSD flake, which facilitated movement of hot water into its structure; this hot water then had higher chance to be in contact with TAA and hence led to higher levels of degradation. In addition, since the initial level of TAA in LPSSD flake was high, more TAA was released and destroyed in the high-temperature environment; the level of degradation thus appeared higher than in the case of hot air or vacuum dried flake. Nevertheless, upon inspecting the data presented in Table 4, it could still be concluded that drying the flake by LPSSD led to the least TAA degradation, if a water temperature of 70°C was used to prepare tea.

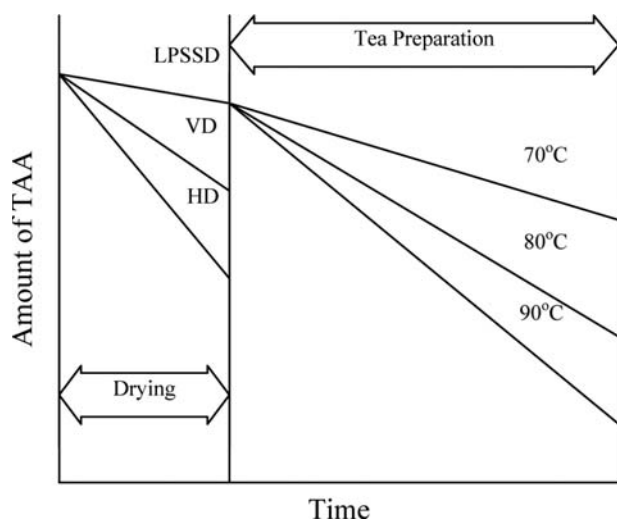


FIG. 5. Sketch of TAA evolution of Indian gooseberry during drying and tea preparation processes.

TABLE 4
Total TAA degradation

Method used to prepare flake	Total TAA degradation (%)		
	70°C	80°C	90°C
Hot air drying at 75°C	26.9	25.3	24.5
Vacuum drying at 75°C, 7 kPa	24.8	28.8	32.0
LPSSD at 75°C, 7 kPa	24.3	27.7	46.4

CONCLUSION

The present study demonstrated that the degradation of ascorbic acid, an antioxidant agent found in Indian gooseberry, could occur during drying and tea drink preparation. Furthermore, the release of ascorbic acid was dependent on both drying technique and hot water temperature for tea preparation. LPSSD helped retaining TAA in dried flake better than hot air and vacuum drying. Lower the hot water temperature during tea preparation was recommended to retard the ascorbic acid degradation. As Indian gooseberry contained various bioactive agents monitoring of such substances during processing and at the point of consumption should be conducted to optimize the suitable process conditions.

ACKNOWLEDGEMENTS

The authors express their sincere appreciation to the Commission on Higher Education, the Thailand Research Fund (TRF), the National Research Council of Thailand

and the International Foundation for Science (IFS, Sweden) for supporting the study financially.

REFERENCES

1. Chatchavalchokchai, N. Effect of some ruminants on seed quality of *Phyllanthus emblica* Linn., *Elaeocarpus madopetalous* Pierre, *Spondias pinnata* Kurz and *Terminalia chebula* Retz. M.Sc. Thesis, Botany Program, Kasetsart University, Thailand, 1987.
2. Methakhup, S.; Chiewchan, N.; Devahastin, S. Effects of drying methods and conditions on drying kinetics and quality of Indian gooseberry flake. *Lebensmittel-Wissenschaft und-Technologie* **2005**, *38*, 579–587.
3. Iyota, H.; Nishimura, N.; Onuma, T.; Nomura, T. Drying of sliced raw potatoes in superheated steam and hot air. *Drying Technology* **2001**, *19*, 1411–1424.
4. Mujumdar, A.S.; Devahastin, S. Fundamental principles of drying. In *Mujumdar's Practical Guide to Industrial Drying*; Devahastin, S., Ed.; Exergex: Brossard, Canada, 2000; 1–22.
5. Namsanguan, Y.; Tia, W.; Devahastin, S.; Soponronnarit, S. Drying kinetics and quality of shrimp undergoing different two-stage drying processes. *Drying Technology*, New Hampshire, **2004**, *22*, 759–778.
6. Devahastin, S.; Suvarnakuta, P. Superheated steam drying of food products. In *Dehydration of Products of Biological Origin*; Mujumdar, A.S., Ed.; Science Publishers: Enfield, New Hampshire, 2004; 493–512.
7. Siepmann, J.; Faisant, N.; Akiki, J.; Richard, J.; Benoit, J.P. Effect of the size of biodegradable microparticles on drug release: Experiment and theory. *Journal of Controlled Release* **2004**, *96*, 123–134.
8. Rahman, C.; Berkland, C.; Kim, K.; Pack, D.W. Modeling small-molecule release from PLG microspheres: Effects of polymer degradation and nonuniform drug distribution. *Journal of Controlled Release* **2004**, *103*, 149–158.
9. Devahastin, S.; Suvarnakuta, P.; Soponronnarit, S.; Mujumdar, A.S. A comparative study of low-pressure superheated steam and vacuum drying of a heat-sensitive material. *Drying Technology* **2004**, *22*, 1845–1867.
10. Thai Industrial Standard Institute (TISI). *Black Tea*, Ministry of Industry: Thailand, 1983.
11. Damrongnukool, J. *Determination of Vitamin C Contents in Commercial Fruit Juice*; M.Sc. Thesis, Home Economics Program, Kasetsart University, Thailand, 2000.
12. İpek, U.; Arslan, E.I.; Öbek, E.; Karataş, F.; Erulaş, F.A. Determination of vitamin losses and degradation kinetics during composting. *Process Biochemistry* **2005**, *40*, 621–624.
13. Margarida, C.V.; Teixeira, A.A.; Silva, C.L.M.. Mathematical modeling of the thermal degradation kinetics of vitamin C in cupuaçu (*Theobroma grandiflorum*) nectar. *Journal of Food Engineering* **2000**, *43*, 1–7.
14. Polydera, A.C.; Stoforos, N.G.; Taoukis P.S. Comparative shelf life study and vitamin C loss kinetics in pasteurised and high pressure processed reconstituted orange juice. *Journal of Food Engineering* **2003**, *60*, 21–29.
15. Ayranci, E.; Tunc, S. The effect of edible coatings on water and vitamin C loss of apricots (*Armeniaca vulgaris* Lam.) and green peppers (*Capsicum annuum* L.). *Food Chemistry* **2004**, *87*, 339–342.
16. Lee, T.H.; Wang, J.; Wang, C.H. Double-walled microspheres for the sustained release of a highly water soluble drug: Characterization and irradiation studies. *Journal of Controlled Release* **2002**, *83*, 437–452.

This article was downloaded by:[Devahastin, Sakamon]
On: 8 February 2008
Access Details: [subscription number 790481640]
Publisher: Taylor & Francis
Informa Ltd Registered in England and Wales Registered Number: 1072954
Registered office: Mortimer House, 37-41 Mortimer Street, London W1T 3JH, UK



Drying Technology An International Journal

Publication details, including instructions for authors and subscription information:
<http://www.informaworld.com/smpp/title~content=t713597247>

Comparative Evaluation of Physical Properties of Edible Chitosan Films Prepared by Different Drying Methods

Pornpimon Mayachiew^a; Sakamon Devahastin^a

^a Department of Food Engineering, King Mongkut's University of Technology Thonburi, Bangkok, Thailand

Online Publication Date: 01 February 2008

To cite this Article: Mayachiew, Pornpimon and Devahastin, Sakamon (2008) 'Comparative Evaluation of Physical Properties of Edible Chitosan Films Prepared by Different Drying Methods', Drying Technology, 26:2, 176 - 185

To link to this article: DOI: 10.1080/07373930701831309

URL: <http://dx.doi.org/10.1080/07373930701831309>

PLEASE SCROLL DOWN FOR ARTICLE

Full terms and conditions of use: <http://www.informaworld.com/terms-and-conditions-of-access.pdf>

This article maybe used for research, teaching and private study purposes. Any substantial or systematic reproduction, re-distribution, re-selling, loan or sub-licensing, systematic supply or distribution in any form to anyone is expressly forbidden.

The publisher does not give any warranty express or implied or make any representation that the contents will be complete or accurate or up to date. The accuracy of any instructions, formulae and drug doses should be independently verified with primary sources. The publisher shall not be liable for any loss, actions, claims, proceedings, demand or costs or damages whatsoever or howsoever caused arising directly or indirectly in connection with or arising out of the use of this material.

Comparative Evaluation of Physical Properties of Edible Chitosan Films Prepared by Different Drying Methods

Pornpimon Mayachiew and Sakamon Devahastin

Department of Food Engineering, King Mongkut's University of Technology Thonburi, Bangkok, Thailand

Edible films are alternative packaging, which have recently received much attention due mainly to environmental reasons. Edible films may be formed from edible biomaterials such as polysaccharides, proteins, or lipids. Among these biopolymers, chitosan is of interest because it has a good film-forming property and is biodegradable, biocompatible, and nontoxic. Several techniques have been used to prepare edible chitosan films with various degrees of success. However, it is always interesting to find an alternative technique to produce films of superior quality at shorter processing (drying) time. In this study, the influences of different drying methods and conditions on the drying kinetics and various properties of chitosan films were investigated. Drying at control conditions (ambient air drying and hot air drying at 40°C) as well as vacuum drying and low-pressure superheated steam drying (LPSSD) at an absolute pressure of 10 kPa were carried out at different drying temperatures (70, 80, and 90°C). The properties of chitosan films, in terms of color, tensile strength, percent elongation, water vapor permeability (WVP), glass transition temperature (T_g), and crystallinity, were also determined. Based on the results of both the drying behavior and film properties, LPSSD at 70°C was proposed as the most favorable conditions for drying chitosan films.

Keywords Biopolymers; Color; Crystallinity; Differential scanning calorimetry; Mechanical properties; Water vapor permeability; X-ray diffraction

INTRODUCTION

Food packaging provides barriers to conditions that could reduce the quality and shelf life of foods. Plastic is so far the most popular packaging but it causes environmental pollution since it does not degrade naturally. Biodegradable material, defined as a material that can be degraded completely by microorganisms into natural compounds, has been viewed as an alternative to plastic packaging.^[1] To further alleviate the problem, edible film, which is defined as a thin layer of edible, biodegradable material formed on a food as a coating or placed on or between

food components, may be an even better alternative for food applications because it does not have to be eliminated as solid wastes.^[1] Among various biodegradable materials, chitosan is of interest because it is an edible, biodegradable, biocompatible with living tissues, odorless, and nontoxic substance and has been widely used in the food industry.^[2]

Among the steps involved in the production of edible films, film formation is considered one of the most important. Chitosan can be easily formed into films by a casting/solvent evaporation technique. Drying is indeed an important step that affects the quality of chitosan and, in fact, any other polymeric films.^[3–6]

Numerous researchers prepared chitosan films by drying them at ambient temperature for 24–48 h.^[7–9] Some other researchers prepared chitosan films by oven drying^[10,11] or infrared drying.^[11] Srinivasa et al.^[11] prepared chitosan films by two methods of drying (oven drying and infrared drying) at 80, 90, and 100°C and compared film properties with those of films prepared by ambient temperature drying (~27°C). It was noted that tensile strength of infrared-dried films (49.58–52.34 MPa) was less than that of ambient-dried films (56.78–59.38 MPa). Water vapor and oxygen transmission rate values were slightly reduced for oven-dried and infrared-dried films compared with those of ambient-dried films.

During the past decade, the idea of using superheated steam to dry foods and other materials to preserve or even enhance the various properties of the products has been on the rise.^[12–14] Poirier,^[15] for example, reported that superheated steam drying (SSD) resulted in improved (20–30% better) strength of hand sheets compared with air-dried sheets. In addition, McCall and Douglas^[16] reported that filled papers containing 0–10% clay had around 23% higher tensile index when dried in superheated steam.

For heat-sensitive biomaterials, lowering the dryer operating pressure is a feasible option that not only preserves the quality of the dried product but may also enhance the drying rate as well. Recently, low-pressure superheated steam drying (LPSSD) has been tested and proved very

Correspondence: Sakamon Devahastin, Department of Food Engineering, King Mongkut's University of Technology Thonburi, 126 Pracha u-tid Road, Bangkok 10140, Thailand; E-mail: sakamon.dev@kmutt.ac.th

effective in drying a number of heat-sensitive materials, in terms of both the product physical and chemical properties.^[17,18] Devahastin et al.,^[17] for example, studied the drying kinetics and various quality parameters of carrot cubes undergoing both LPSSD and vacuum drying. Although LPSSD required longer drying time to achieve the same final moisture content, some of the quality attributes such as color, microstructure, shrinkage, and rehydration capability of the products were superior to those of products dried by vacuum drying. However, no report is so far available on the drying kinetics and properties of chitosan films prepared either by vacuum drying or LPSSD, which has potential for producing films of higher quality at shortened processing (drying) time.

The aim of this study was to determine and compare the drying kinetics of chitosan films undergoing different drying techniques, namely, ambient drying, hot air drying, vacuum drying, and LPSSD, at different conditions. In addition, the effects of drying methods and conditions on selected physical properties (color, water vapor permeability [WVP], tensile strength, and percent elongation), thermal properties (glass transition temperature), and crystallinity of chitosan films were also investigated. Finally, the effect of storage condition (%RH) on WVP, tensile strength, and percent elongation of the films was also determined.

MATERIALS AND METHODS

Materials

Chitosan (molecular weight of 900,000 Da and degree of deacetylation of 90.20%) was obtained from S.K. Profishery Co., Ltd. (Bangkok, Thailand). Glycerol was purchased from Carlo Erba (Val de Reuil, Italy), and acetic acid was obtained from Merck (Darmstadt, Germany).

Film Preparation

Chitosan solution (1.5% (w/v)) was prepared by dissolving chitosan in 1% (v/v) acetic acid under constant stirring at 300 rpm using a magnetic stirrer (Framo[®]-Gerätechnik, model M21/1, Eisenbach, Germany) at room temperature for 24 h. Twenty-five percent glycerol (w/w chitosan) was

then added into the chitosan solution; stirring was then continued at room temperature for 1 h. After mixing, the solution was centrifuged for 15 min at 12,400 rpm by a refrigerated centrifuge (Hitachi, model Himac CR21, Ibaragi, Japan) to remove undissolved impurities and bubbles in the solution. The solution (21 g) was then poured on an acrylic plate with dimensions of $13 \times 10 \text{ cm}^2$ to cast a chitosan film with a constant thickness of $20 \mu\text{m}$ for a drying experiment.

Film Drying

Ambient Temperature and Hot Air Drying

The cast films were dried at ambient temperature and at 40°C in a hot air dryer (Fig. 1); the air velocity across the drying chamber was fixed at 0.25 m/s. These films were used as control samples.

Low-Pressure Superheated Steam Drying

A schematic diagram of the low-pressure superheated steam dryer and its accessories is shown in Fig. 2. The dryer consists of a stainless steel drying chamber, insulated with rock wool, with inner dimensions of $45 \times 45 \times 45 \text{ cm}^3$; a steam reservoir, which received steam from a boiler and maintained its pressure at around 200 kPa (gauge); and a liquid ring vacuum pump (Nash, model ET32030, Trumbull, CT), which was used to maintain the vacuum in the drying chamber (fixed at 10 kPa in this study). A steam trap was installed to reduce the excess steam condensation in the reservoir. An electric heater, rated at 1.5 kW, which was controlled by a PID controller (Omron, model E5CN, Tokyo, Japan), was installed in the drying chamber to control the steam temperature and to minimize the condensation of steam in the drying chamber during the startup period. Two variable-speed electric fans were used to disperse steam throughout the drying chamber. The steam inlet was made into a cone shape and was covered with a screen to help distributing the steam in the chamber. The sample holder was made of a stainless steel screen with dimensions of $16.5 \times 16.5 \text{ cm}^2$. The change of the mass of the sample was detected continuously (at 60-s intervals) using a load cell with an accuracy of $\pm 0.2 \text{ g}$ (Minebea,

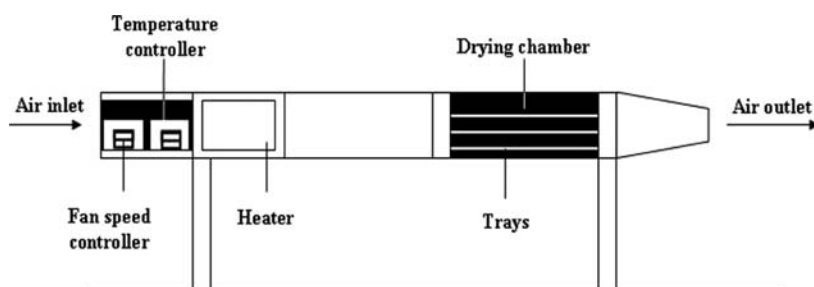


FIG. 1. A schematic diagram of hot air dryer and associated units.

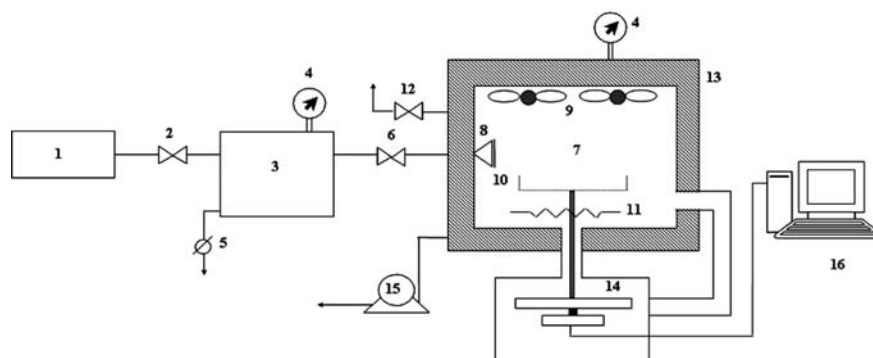


FIG. 2. A schematic diagram of the low-pressure superheated steam dryer and associated units. 1, boiler; 2, steam valve; 3, steam reservoir; 4, pressure gauge; 5, steam trap; 6, steam regulator; 7, drying chamber; 8, steam inlet and distributor; 9, electric fans; 10, sample holder; 11, electric heater; 12, vacuum break-up valve; 13, insulator; 14, on-line weight indicator and logger; 15, vacuum pump; 16, PC with installed data acquisition card.

model Ucg-3 kg, Nagano, Japan), which was installed in a smaller chamber connected to the drying chamber by a flexible hose (in order to maintain the same vacuum pressure as that in the drying chamber) and to an indicator and recorder (AND A&D Co., model AD 4329, Tokyo, Japan). The data were sent to a PC with installed data acquisition card.

Films were dried at 70, 80, and 90°C at 10 kPa in the LPSSD. The operating pressure was reduced in steps from an atmospheric pressure to 10 kPa to avoid the problem of solvent trapping in films following the pattern illustrated in Fig. 3.

Vacuum Drying

For vacuum drying experiments the same experimental setup as that used for the LPSSD experiments was used but without the application of steam to the drying chamber. Films were also dried at 70, 80, and 90°C at 10 kPa in the vacuum dryer. Again, the operating pressure was reduced in steps from an atmospheric pressure to 10 kPa following the pattern illustrated in Fig. 3.

Film Properties Determination

Chitosan films were dried at various conditions until their moisture content reached approximately 14% (d.b.).^[8,19]

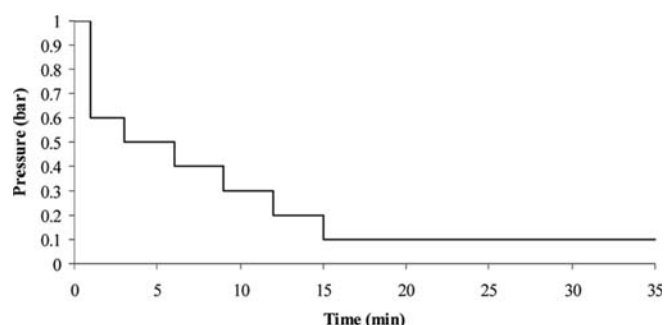


FIG. 3. Reduction of operating pressure from an atmospheric pressure to 10 kPa.

The films were then conditioned for at least 48 h either in a desiccator containing saturated salt solution of magnesium nitrate (Ajax Finechem, Seven Hills, NSW, Australia), which produced the relative humidity (RH) of 53%^[11,20] or in a desiccator containing saturated salt solution of sodium chloride (Ajax Finechem, Seven Hills, NSW, Australia), which produced an RH of 75%, before further analysis. The latter RH was selected because it is an average relative humidity of the environment in Thailand.

Film Thickness Measurement

The film thickness was measured using a micrometer (Mitutoyo, Model 102-309, Tokyo, Japan) with an accuracy of $\pm 2 \mu\text{m}$. Each film sample was measured at its center and four other positions along the edge in the case of WVP measurement and three other positions along the strips in the case of mechanical properties measurement. WVP and mechanical properties were calculated using the average thickness of each film sample.

Moisture Content Determination

The moisture content of films was determined using the standard vacuum oven method.^[21] Briefly, the film was dried in a vacuum oven (Sanyo, Model Gallenkamp/OM-09980, Loughborough, UK) at 70°C at the pressure of -900 mbar for 24 h. The mass of the dried sample (bone-dry mass) was then used to determine the film moisture content by:

$$\% \text{ Moisture content (d.b.)} = \frac{M_i - M_d}{M_d} \quad (1)$$

where M_i is the mass of the sample at any instant (g) and M_d is the bone-dry mass (g).

Mechanical Properties Determination

The measurement of mechanical properties of chitosan films was carried out using a texture analyzer (Stable Micro

System, TA.XT.Plus, Surrey, UK). After conditioning, chitosan films were cut into $10 \times 2.54 \text{ cm}^2$ strips and tested for tensile strength and percent elongation according to the ASTM Standard Method D882.^[22] Initial grip separation and crosshead speed were set at 50 mm and 50 mm/min, respectively. Tensile strength was calculated by dividing the maximum load for breaking the film by its cross-sectional area. Percent elongation was determined by dividing the film elongation at rupture by the initial grip separation. All tests were performed in triplicate and the average values were reported.

Water Vapor Permeability Determination

The water vapor permeability (WVP) of chitosan films was measured using a gravimetric method according to the ASTM E 96/E 96M-05 standard.^[23] The test cup was filled with 15 mL of distilled water to produce 100% RH below the film. Chitosan film was mounted to the top of the cup. The cup was placed in a desiccator containing magnesium nitrate solution at 25°C. Fans were operated in the chamber, thus circulating the air at 152 m/min over the surface of the film to remove the permeating water vapor. The mass of the cup was recorded 6 times at 2 h interval after steady state was reached. Mass loss was plotted versus time and a straight line was obtained in duplicate. Linear regression was then used to first estimate the slope of the line to calculate the water vapor transmission rate (WVTR) as follows:

$$\text{WVTR} = \frac{\text{Slope}}{A} \quad (2)$$

where WVTR is the water vapor transmission rate ($\text{g/m}^2 \text{ day}$), Slope is the slope of the mass loss versus time curve (g/day), and A is the test cup mouth area (m^2).

WVP was then determined using the WVP correction method.^[24] This method is necessary when dealing with films with low water vapor resistance since it accounts for the water vapor partial pressure gradient within the stagnant air layer of the test cup. Corrected water vapor permeability can be calculated using Eq. (3); the coefficient 1.157×10^{-5} in Eq. (3) satisfies unit conversion.

$$\text{WVP} = 1.157 \times 10^{-5} \frac{\text{WVTR } L}{p_1 - p_2} \quad (3)$$

where WVP is the water vapor permeability (g/s m Pa), L is the average film thickness (m), p_1 is the partial pressure of water vapor in air at surface of distilled water in the cup (Pa), and p_2 is the partial pressure of water vapor at the film surface outside the cup (Pa).

Color Measurement

The color of films was determined with a colorimeter (Juki, JP 7100, Tokyo, Japan). The color of the films after

conditioning at 53% RH for 2 days was investigated. The film specimen was covered with a standard white plate ($L = 97.75$, $a = -0.08$, and $b = -0.3$) and the values of L , a , b were evaluated by a reflectance measurement. For each sample at least three measurements were performed at different positions. The color changes (L , a , and b values) were calculated by:

$$\Delta L = L - L^*, \quad \Delta a = a - a^* \quad \text{and} \quad \Delta b = b - b^* \quad (4)$$

The total color difference (ΔE) was calculated as follows:

$$\Delta E = \sqrt{(L^* - L)^2 + (a^* - a)^2 + (b^* - b)^2} \quad (5)$$

where L^* , a^* , and b^* are the standard color values (lightness, redness/greenness, and yellowness/blueness, respectively) of the white plate and L , a , and b are the color values of the measured sample.^[25]

Differential Scanning Calorimetry (DSC)

The thermal characteristics of chitosan films were determined using a differential scanning calorimeter (DSC; Netzsch DSC 204 F1Phoenix[®], Selb, Germany). A small sample piece (10–12 mg) was cut from a film sample after conditioning at 53% RH and placed into an aluminum pan, which was then sealed. A small hole was made at the top of the pan in order to allow the release of moisture. An empty pan was used as the reference. The first scan was made from -30 to 190°C ; this was followed by 1-min holding at 190°C and a rapid cooling to -30°C and another holding at -30°C for 5 min. The second scan was then implemented by raising the temperature to 250°C . The scanning rate used was 10°C/min .^[26]

X-Ray Diffraction Analysis

X-ray diffraction (XRD) patterns of chitosan films after conditioning at 53% RH were obtained using a Bruker AXS D8 DISCOVER XRD (Bruker AXS GmbH, Karlsruhe, Germany) under the following conditions: 40 kV and 40 mA with $\text{CuK}\alpha$ radiation at a wavelength of 0.1546 nm with a scanning rate of $2^\circ 2\theta/\text{min}$.^[11] The relative intensity of the diffraction peak was recorded in the scattering range (2θ) of 4 – 40° and the crystallinity (X_c) of the film was calculated by:

$$X_c = [F_c / (F_c + F_a)] \times 100\% \quad (6)$$

where F_c and F_a are the areas of crystalline and noncrystalline regions, respectively.

Statistical Analysis

All data were subjected to the analysis of variance (ANOVA) using SPSS[®] software and are presented as mean values with standard deviations. Differences between

mean values were established using Duncan multiple range test at a confidence level of 95%. All experiments were performed in duplicate except when stated otherwise.

RESULTS AND DISCUSSION

Drying Kinetics of Chitosan Films

Chitosan films with initial moisture contents in the range of 51.51–58.79 kg/kg (d.b.) were first dried until their equilibrium moisture contents were reached in order to construct the drying curves at different conditions. The drying curves of chitosan films undergoing different drying methods and conditions are shown in Figs. 4 and 5. It was found that the film samples dried at control conditions required longer drying time, while vacuum drying required least drying time, even less than that required by LPSSD. This is due to the larger differences between the medium and sample surface temperature in the case of vacuum drying over the range of drying temperature used. Moreover, the electric heater was used more often during vacuum drying since it was the only source of energy for drying. This might increase the amount of radiation absorbed by the chitosan film surfaces, thus explaining the higher drying rates during vacuum drying.^[17]

The average drying time to reach the desired final moisture content of 14% (d.b.) is listed in Table 1. As expected, the usual trend of shorter drying time was found when the drying temperature increased. The moisture decreased faster at higher temperatures than at lower temperatures for both LPSSD and vacuum drying because the temperature differences between the medium and the samples at higher drying temperatures were greater than that at lower temperatures. Moisture diffusivity is also higher at a higher drying temperature.

The differences between the two sets of drying time (between vacuum drying and LPSSD), however, were smaller at higher drying temperatures (Table 1). Raising the drying temperature further would eventually lead to equal rates of drying at an inversion temperature (due to increased temperature difference between the steam and the sample).^[27]

The equilibrium moisture contents (EMC) of chitosan films undergoing different drying methods and conditions are listed in Table 2. It was found that EMC values of vacuum-dried chitosan films were lower than those of LPSSD films because the driving force for moisture transfer within the LPSSD system is generally lower than that in the vacuum drying system. Moreover, drying temperature has an influential effect on the moisture content at equilibrium; an increase in the drying temperature resulted in lower equilibrium moisture content for all drying methods.

Physical Properties of Chitosan Films

To determine the physical properties of chitosan films, the films were first dried to the final moisture content of approximately 14% (d.b.). This value is similar to that set by Wiles et al.^[8] and Nadarajah et al.,^[19] which is around 10–19% (d.b.); this is to allow the films to be peeled off easily from the casting surface. All chitosan films prepared by different drying methods and conditions showed smooth and uniform surface morphology without any cracks and pinholes as observed from the scanning electron micrographs (not shown).

Color

The changes of different color parameters of chitosan films dried by different drying methods and conditions

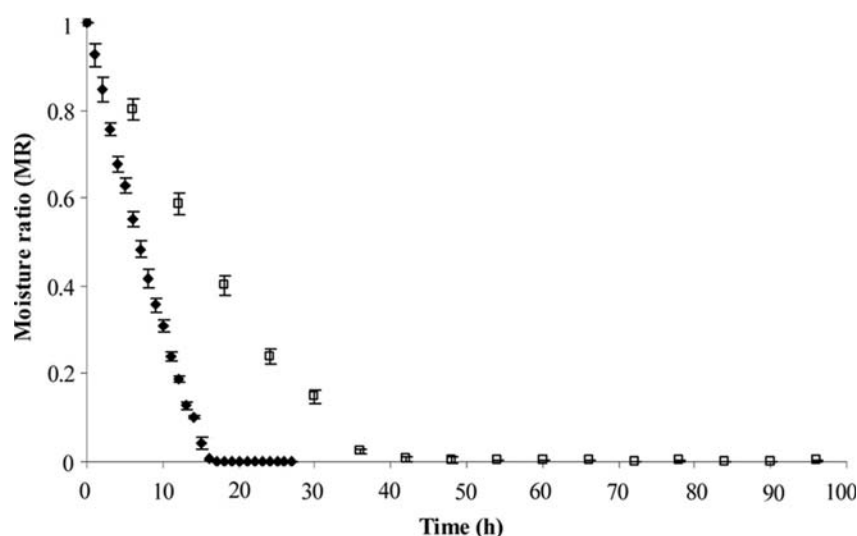


FIG. 4. Drying kinetics of chitosan films undergoing ambient drying (□) and hot air drying at 40°C (◆).

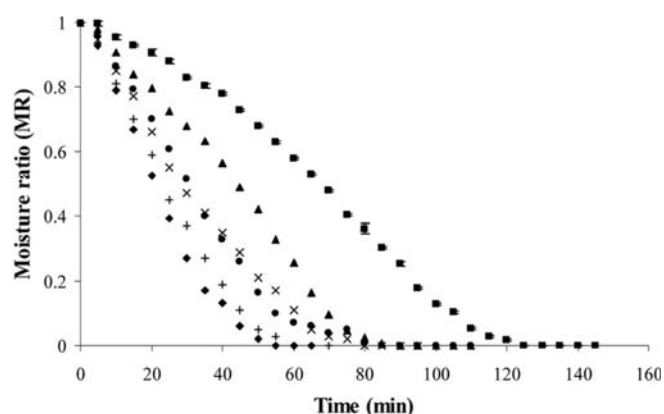


FIG. 5. Drying kinetics of chitosan films undergoing LPSSD of 70°C (■), 80°C (▲), 90°C (●); vacuum drying 70°C (×), 80°C (+), 90°C (◆) at 10 kPa.

are listed in Table 3. Regarding the effect of drying temperature on the lightness of the films, it is seen that higher drying temperatures led to slightly darker films, both in the cases of vacuum drying and LPSSD. This is because higher temperatures led to higher levels of Maillard browning reactions. It was also found that drying methods were significantly influencing the changes of lightness. Chitosan films dried by LPSSD were slightly lighter than the films dried by vacuum drying. This may be due to the fact that the film temperature increased more rapidly and stayed at higher levels in the case of vacuum drying compared with the case of LPSSD.

In terms of the redness (a value), it can be seen from Table 3 that the redness was also significantly affected by both the drying temperature and drying methods. Drying at higher temperatures yielded redder dried films than at lower temperatures. This is again because Maillard reactions are accelerated by temperature. The redness of films was obviously higher in the case of vacuum drying

TABLE 1

Drying time to reach final moisture content of 14% (d.b.)

Drying condition (°C)	Drying time
Control	
~30	54 h
40	18 h
Vacuum drying	
70	85 min
80	65 min
90	60 min
LPSSD	
70	130 min
80	95 min
90	90 min

TABLE 2

Equilibrium moisture content of chitosan films undergoing various drying methods and conditions

Drying condition (°C)	Equilibrium moisture content (% d.b.)
Control	
~30	17.9
40	12.0
Vacuum drying	
70	5.9
80	3.5
90	3.4
LPSSD	
70	13.7
80	10.1
90	9.9

compared with the case of ambient drying and LPSSD for the reasons mentioned earlier.

In the case of yellowness (b value) it was found that drying temperature had a significant effect on the change of yellowness, especially in the case of vacuum drying. This is again because of Maillard reactions that occurred at larger extents at higher drying temperatures. The yellowness was also significantly affected by the drying methods. The yellowness obviously increased during vacuum drying compared with the cases of ambient drying and LPSSD.

The overall changes of color of the films could be observed from the ΔE was also significantly affected by both the drying temperature and drying methods. Regarding the effect of the drying temperature it could be seen that higher drying temperatures led to larger changes of ΔE values, as expected. In addition, the ΔE value was also significantly affected by the drying methods. It was found that vacuum-dried films had significantly higher ΔE values than ambient-dried and LPSSD films for the reasons mentioned previously.

Mechanical Properties

Regarding the mechanical properties of chitosan films it was noted that different drying methods and conditions had significant effects on the tensile strength and percent elongation of the films (Table 4); the maximum value for tensile strength was observed in the case of LPSSD at 70°C and storage condition of 53% RH. This might be due to the effects of higher degree of crystallinity and thermal cross-linkage that occurred more at this condition.

From the result of the X-ray diffraction analysis (Fig. 6), chitosan films with higher degrees of crystallinity (LPSSD and ambient-dried films) exhibited higher tensile strength when only crystallinity of the films was considered. Rajendran and Marikani^[28] also stated that the mechanical

TABLE 3
Color of chitosan films

Drying condition	Temperature (°C)	ΔL	Δa	Δb	ΔE
Control	~30	-5.8 ± 0.1^d	-0.9 ± 0.1^d	2.0 ± 0.1^a	6.2 ± 0.1^a
	40	-5.8 ± 0.1^d	-1.0 ± 0.1^{cd}	2.2 ± 0.1^{ab}	6.3 ± 0.1^a
Vacuum drying	70	-6.0 ± 0.1^b	-1.4 ± 0.1^b	3.1 ± 0.1^d	6.9 ± 0.1^c
	80	-6.2 ± 0.1^a	-1.5 ± 0.1^b	3.4 ± 0.1^e	7.2 ± 0.1^d
	90	-6.2 ± 0.2^a	-1.7 ± 0.1^a	4.1 ± 0.2^f	7.6 ± 0.2^e
LPSSD	70	-5.9 ± 0.1^c	-1.0 ± 0.1^{cd}	2.1 ± 0.1^{ab}	6.4 ± 0.1^b
	80	-6.0 ± 0.1^b	-1.0 ± 0.1^{cd}	2.2 ± 0.1^b	6.5 ± 0.1^b
	90	-6.0 ± 0.1^b	-1.1 ± 0.2^c	2.5 ± 0.2^c	6.6 ± 0.2^b

Different superscripts within the same column mean that the values are significantly different ($p < 0.05$).

strength of polymer films normally increases with the degree of crystallinity. This observation agrees with that stated by Ogawa^[29] that chitosan films, which exhibited higher degree of crystallinity, had higher tensile strength.

The mechanical strength of polymer films also depends upon the method of preparation. The tensile strength of LPSSD films was higher than that of vacuum-dried films due probably to the fact that LPSSD required longer drying time than did vacuum drying. Ngui and Mallapragada^[30] stated that the degree of crystallinity of

semicrystalline polymer films was found to increase as a function of the drying time. Slower drying allows for the polymer chains to rearrange and form more crystals. However, the tensile strength of LPSSD films was higher than that of ambient dried films because the drying temperature of LPSSD was higher, thus inducing more thermal cross-linkage within the LPSSD films. The influence of the relative humidity during storage on the tensile strength was not significant but it was still observed that the strength was slightly lower at higher relative humidity in all cases.

TABLE 4
Mechanical properties of chitosan films

Drying condition (°C)	Relative humidity (%)	Tensile strength (MPa)	Percent elongation
Control			
	~30		
	53	40.2 ± 3.2^{cd}	23.5 ± 1.6^{de}
	75	38.7 ± 2.4^{cd}	24.6 ± 3.8^{de}
40	53	36.5 ± 2.5^{bcd}	23.1 ± 2.3^{de}
	75	34.9 ± 3.4^{bcd}	23.7 ± 2.8^{de}
Vacuum drying			
	70		
	53	32.8 ± 2.6^{ab}	19.2 ± 2.9^{abc}
	75	30.9 ± 3.8^{ab}	20.2 ± 4.4^{bcde}
	80		
	53	29.5 ± 3.0^{ab}	18.8 ± 2.4^{ab}
	75	27.0 ± 2.4^{ab}	19.8 ± 2.5^{abcd}
	90		
LPSSD	53	28.9 ± 3.5^{ab}	18.0 ± 2.5^{ab}
	75	27.2 ± 4.0^{ab}	19.7 ± 3.1^{abcd}
	70		
	53	69.1 ± 3.9^f	24.7 ± 4.6^e
	75	69.0 ± 2.8^f	24.9 ± 2.5^e
	80		
	53	68.4 ± 5.7^f	24.8 ± 4.0^e
	75	65.8 ± 3.4^f	25.1 ± 4.4^e
90	53	52.2 ± 5.6^e	24.2 ± 3.0^e
	75	50.2 ± 4.7^e	24.8 ± 3.5^e

Different superscripts within the same column mean that the values are significantly different ($p < 0.05$).

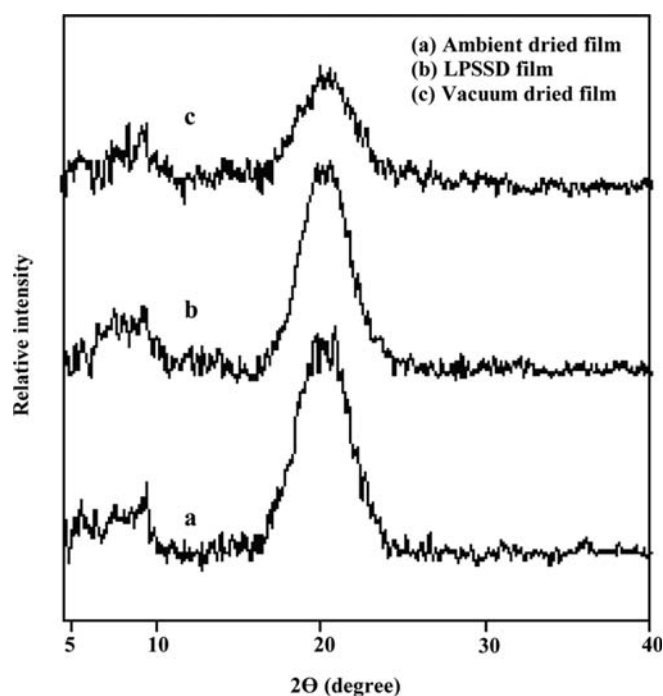


FIG. 6. X-ray diffraction patterns of chitosan films dried by ambient drying at $\sim 30^\circ\text{C}$, LPSSD at 70°C , and vacuum drying at 70°C .

In terms of the percent elongation, which is an indicator of the film extensibility, different drying methods and conditions led to films with significantly different values of percent elongation. The percent elongation of LPSSD films was higher than that of vacuum-dried films due probably to the higher degrees of crystallinity and thermal cross-linkage that occurred more in LPSSD films. The effect of the relative humidity during storage on the percent elongation of the films was again not significant. Drying temperature also did not significantly affect the percent elongation.

According to Krochta and Johnston,^[1] edible films with tensile strength of 10–100 MPa and percent elongation of 10–50% are considered to have moderate mechanical properties. Therefore, chitosan films obtained in this study, whose tensile strength was in the range of 27.04–69.12 MPa and percent elongation was in the range of 17.96–25.13, had moderate mechanical properties.

Water Vapor Permeability

WVP is an important property of films because most natural biopolymers are very likely to become plasticized when coming into contact with water. In this study, drying methods and drying temperature did not seem to have any significant effect on the WVP (Table 5). Phan The et al.^[31] also observed that the WVP of arabinoxylan and hydroxyl-propylmethyl cellulose films containing 15% glycerol was not affected by the drying temperature. For the effect of

TABLE 5
Water vapor permeability of chitosan films

Drying condition ($^\circ\text{C}$)	Relative humidity (%)	Water vapor permeability ($\times 10^{-10}$ g/m s Pa)
Control		
~ 30	53	2.1 ± 0.1^a
	75	2.1 ± 0.1^a
40	53	1.9 ± 0.2^a
	75	2.0 ± 0.2^a
Vacuum drying		
70	53	2.0 ± 0.3^a
	75	2.3 ± 0.2^a
80	53	2.2 ± 0.1^a
	75	2.3 ± 0.2^a
90	53	2.0 ± 0.2^a
	75	2.1 ± 0.2^a
LPSSD		
70	53	1.9 ± 0.1^a
	75	1.9 ± 0.1^a
80	53	1.9 ± 0.1^a
	75	1.9 ± 0.1^a
90	53	1.9 ± 0.2^a
	75	2.0 ± 0.2^a

Different superscripts within the same column indicate that the values are significantly different ($p < 0.05$).

RH during storage it was found that RH did not significantly affect WVP of the films as well.

WVP of chitosan films was in the range of 1.88×10^{-10} to 2.33×10^{-10} g/m s Pa. A high WVP value indicates poor barrier properties of chitosan films and WVP of most edible films is generally higher than that of common plastics. According to Krochta and Johnston,^[1] WVP values in the range of 1.15×10^{-12} to 1.15×10^{-10} g/m s Pa are considered moderate. Therefore, chitosan films in this study are moderate moisture barrier when comparing with other edible and biodegradable films. WVP of films obtained in this work are nearly comparable with that of the films of Caner et al.,^[7] who reported that WVP values of chitosan films with polyethylene glycol 400 as plasticizer were in the range of 1.03×10^{-10} to 1.09×10^{-10} g/m s Pa.

Glass Transition Temperature

Measurement of the glass transition temperature (T_g) of chitosan films was performed to understand the physical state of the samples. Only chitosan films dried by ambient temperature as well as by vacuum drying and LPSSD at 70°C and stored at 53% relative humidity were investigated because these conditions gave the best film properties for each drying method. To eliminate the effect of moisture on T_g measurement, the second heating run was performed.

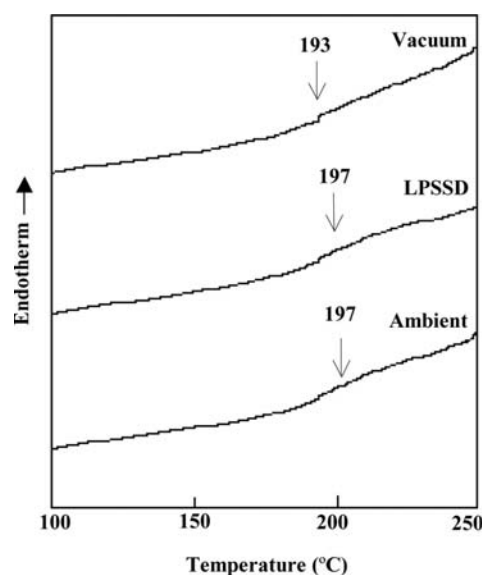


FIG. 7. DSC thermograms of chitosan films dried by ambient drying at $\sim 30^\circ\text{C}$, LPSSD at 70°C , and vacuum drying at 70°C .

The DSC thermograms of chitosan films (Fig. 7) from the second heating run showed that the T_g of ambient-dried and LPSSD chitosan films was around 197°C while vacuum drying led to films with slightly lower T_g of around 193°C . However, the change of the inclination of the baseline was small because chitosan is only a partially crystalline polymer and has small specific volume of rigid chain.^[32] Suyatma et al.^[20] also reported the values of T_g of chitosan films in the range of 194 to 196°C . A wider range of T_g of chitosan films, from 161 to 203°C , was also reported by other researchers.^[33]

Glass transition could be used to explain the discontinuous behavior of film properties in response to changes in temperature. Below glass transition temperature, films retain good mechanical and barrier properties. Ambient-dried and LPSSD films exhibited higher T_g than did vacuum-dried films, indicating that the former group had higher intensities of intermolecular forces.^[34] This phenomenon is probably related to the mechanical properties of chitosan films in which ambient-dried and LPSSD films had higher tensile strength and percent elongation than vacuum-dried films.

X-Ray Diffraction Patterns

Figure 6 shows the XRD patterns of chitosan films. Except for the relative intensity of diffractive peaks, it was observed that the diffraction patterns of all the films were almost the same. Chitosan films showed characteristic crystalline peaks at $2\theta = 20^\circ$, which represented the hydrated form of crystalline part of chitosan films.^[29] Urbanczyk and Lipp-Symonowicz^[35] indeed reported that

the peak at about 20° is a typical peak for an X-ray diffraction pattern of chitosan. The crystallinities of chitosan films dried by ambient, LPSSD, and vacuum drying were 15.3, 14.5, and 7.5%, respectively; the films prepared by vacuum drying had the lowest crystallinity. Overall, however, the intensities of all the crystal peaks at about 20° were not high, indicating that all the films had low crystallinity or were in amorphous state.

In addition to the reasons mentioned earlier, LPSSD led to films of higher crystallinity and hence better mechanical properties than did vacuum drying due probably to the different amounts and forms of crystal structure. Rittidej et al.^[36] observed that after moist heat treatment at 60°C and 75% RH, amide formation altered the lattice structure of chitosan salt films. This is possibly due to the intramolecular and intermolecular condensation of carboxylic acid in chitosan salt films. LPSSD, which provided relatively more humid drying environment compared with vacuum drying, might also lead to a similar effect. The altered lattice structure in turn led to the different properties and functionality of the film samples.^[29]

CONCLUSIONS

The effects of drying methods and drying temperature on the drying kinetics and selected properties of chitosan films were investigated in this study. In terms of the drying kinetics the drying method was found to have a significant effect on the rates of moisture reduction of the samples. Vacuum drying and LPSSD required much shorter drying time than did ambient and hot air drying at 40°C . However, LPSSD took a longer time to dry the product to the final desired moisture content than did vacuum drying.

In terms of properties, it was found that LPSSD produced chitosan films of less yellow color than did vacuum drying. LPSSD at 70°C led to films with higher tensile strength and percent elongation than at other drying conditions. Drying technique and drying temperature did not seem to have any significant effect on the water vapor permeability, however. T_g of ambient-dried and LPSSD films was 197°C , whereas vacuum-dried films exhibited lower T_g of 193°C . Ambient-dried and LPSSD films had more crystallinity than the films dried by vacuum drying.

LPSSD at 70°C was proposed as the best conditions for producing chitosan films in this study for it could enhance some physical properties of chitosan films, making them superior to films dried by other techniques or at other conditions. A future work will study the effects of different drying methods and conditions on physical and functional properties as well as controlled release characteristics of chitosan films incorporated with plant-based antimicrobial and antioxidant extracts.

ACKNOWLEDGEMENTS

The authors express their sincere appreciation to the Commission on Higher Education, the Thailand Research Fund (TRF), and the International Foundation for Science (IFS) in Sweden for supporting the study financially.

REFERENCES

- Krochta, J.M.; Johnston, C.M. Edible and biodegradable polymer films: Challenges and opportunities. *Food Technology* **1997**, *51*, 61–74.
- Shahidi, F.; Arachchi, J.K.V.; Jeon, Y. Food applications of chitin and chitosans. *Trends in Food Science and Technology* **1999**, *10*, 37–51.
- Sano, Y. Drying of polymer solution. *Drying Technology* **1992**, *10*, 591–622.
- Vinjamur, M.; Cairncross, R.A. A high airflow drying experimental set-up to study drying behavior of polymer solvent coatings. *Drying Technology* **2001**, *19*, 1591–1612.
- Etemad, S.G.; Etesami, N.; Bagheri, R.; Thibault, J. Drying of latex films of poly(vinyl acetate). *Drying Technology* **2002**, *20*, 1843–1854.
- Wong, S.; Altinkaya, S.A.; Mallapragada, S.K. Multi-zone drying schemes for lowering the residual solvent content during multi-component drying of semicrystalline polymers. *Drying Technology* **2007**, *25*, 995–1002.
- Caner, C.; Vergano, P.J.; Wiles, J.L. Chitosan film mechanical and permeation properties as affected by acid, plasticizer, and storage. *Journal of Food Science* **1998**, *63*, 1049–1053.
- Wiles, J.L.; Vergano, P.J.; Barron, F.H.; Bunn, J.M.; Testin, R.F. Water vapor transmission rates and sorption behavior of chitosan films. *Journal of Food Science* **2000**, *65*, 1175–1179.
- Hwang, K.T.; Kim, J.T.; Jung, S.T.; Cho, G.S.; Park, H.J. Properties of chitosan-based biopolymer films with various degrees of deacetylation and molecular weights. *Journal of Applied Polymer Science* **2003**, *89*, 3476–3484.
- Butler, B.L.; Vergano, P.J.; Testin, J.M.; Bunn, J.M.; Wiles, J.L. Mechanical and barrier properties of edible chitosan films as affected by composition and storage. *Journal of Food Science* **1996**, *61*, 953–955, 961.
- Srinivasa, P.C.; Ramesh, M.N.; Kumar, K.R.; Tharanathan, R.N. Properties of chitosan films prepared under different drying conditions. *Journal of Food Engineering* **2004**, *63*, 79–85.
- Mujumdar, A.S. CEA Report, 817 U 671: Montreal, Canada, 1990.
- Mujumdar, A.S. Superheated steam drying. In *Handbook of Industrial Drying*, 3rd ed.; Mujumdar, A.S., Ed. CRC Press: Boca Raton, 2007; 439–452.
- Devahastin, S.; Suvarnakuta, P. Superheated-steam-drying of food products. In *Dehydration of Products of Biological Origin*; Mujumdar, A.S., Ed.; Science Publishers: Enfield, MA, 2004; 493–512.
- Poirier, N.A. The effect of superheated steam drying on the properties of paper. *Drying Technology* **1994**, *12*, 2103–2105.
- McCall, J.M.; Douglas, W.J.M. Enhancement of properties of diverse grades of paper by superheated steam drying. *Drying Technology* **2005**, *23*, 397–406.
- Devahastin, S.; Suvarnakuta, P.; Soponronnarit, S.; Mujumdar, A.S. A comparative study of low-pressure superheated steam and vacuum drying of a heat-sensitive material. *Drying Technology* **2004**, *22*, 1845–1867.
- Suvarnakuta, P.; Devahastin, S.; Mujumdar, A.S. Drying kinetics and β -carotene degradation in carrot undergoing different drying processes. *Journal of Food Science* **2005**, *70*, S520–S526.
- Nadarajah, K.; Prinyawiwatukul, W.; Kyoong No, H.; Sathivel, S.; Xu, Z. Sorption behavior of crawfish chitosan films as affected by chitosan extraction processes and solvent types. *Journal of Food Science* **2006**, *71*, E33–E39.
- Suyatma, N.E.; Tighzert, L.; Copinet, A.; Coma, V. Effects of hydrophilic plasticizers on mechanical, thermal, and surface properties of chitosan films. *Journal of Agricultural and Food Chemistry* **2005**, *53*, 3950–3957.
- Association of Official Analytical Chemists. *Official Methods of Analysis*, 14th ed.; AOAC: Washington, DC, 1995.
- American Society for Testing and Materials. Standard test methods for tensile properties of thin plastic sheeting. In *Annual Book of ASTM Standards*; ASTM: Philadelphia, 1995, 182–190.
- American Society for Testing and Materials. Standard test methods for water vapor transmission of materials. In *Annual Book of ASTM Standards*; ASTM: Philadelphia, 1995, 697–704.
- Gennadios, A.; Weller, C.L.; Gooding, C.H. Measurement errors in water vapor permeability of highly permeable, hydrophilic edible films. *Journal of Food Engineering* **1994**, *21*, 395–409.
- Pranoto, Y.; Rakshit, S.K.; Salokhe, V.M. Enhancing antimicrobial activity of chitosan films by incorporating garlic oil, potassium sorbate and nisin. *LWT – Food Science and Technology* **2005**, *38*, 859–865.
- Suyatma, N.E.; Copinet, A.; Tighzert, L.; Coma, V. Mechanical and barrier properties of biodegradable films made from chitosan and poly(lactic acid) blends. *Journal of Polymers and the Environment* **2004**, *12*, 1–6.
- Suvarnakuta, P.; Devahastin, S.; Soponronnarit, S.; Mujumdar, A.S. Drying kinetics and inversion temperature in a low-pressure superheated steam-drying system. *Industrial & Engineering Chemistry Research* **2005**, *44*, 1934–1941.
- Rajendran, V.; Marikani, A. *Materials Science*; Tata McGraw-Hill: New Delhi, 2004.
- Ogawa, K. Effect of heating an aqueous suspension of chitosan on the crystallinity and polymorphs. *Agricultural Biological Chemistry* **1991**, *55*, 2375–2379.
- Ngui, M.O.; Mallapragada, S.K. Mechanistic investigation of drying regimes during solvent removal from poly(vinyl alcohol) films. *Journal of Applied Polymer Science* **1999**, *72*, 1913–1920.
- Phan The, D.; Debeaufort, F.; Péroval, C.; Despré, D.; Courthaudon, J.L.; Voilley, A. Arabinoxylan-lipid-based edible films and coatings. 3. Influence of drying temperature on film structure and functional properties. *Journal of Agricultural and Food Chemistry* **2002**, *50*, 2423–2428.
- Dong, Y.; Ruan, Y.; Wang, H.; Zhao, Y.; Bi, D. Studies on glass transition temperature of chitosan with four techniques. *Journal of Applied Polymer Science* **2004**, *93*, 1553–1558.
- Sakurai, K.; Maegawa, T.; Takahashi, T. Glass transition temperature of chitosan and miscibility of chitosan/poly(*N*-vinyl pyrrolidone) blends. *Polymer* **2000**, *41*, 7051–7056.
- Rudin, A. *The Elements of Polymer Science and Engineering: An Introductory Text and Reference for Engineers and Chemists*, 2nd ed.; Academic Press: London, 1999.
- Urbanczyk, G.W.; Lipp-Symonowicz, B. The influence of processing terms of chitosan membranes made of differently deacetylated chitin on the crystalline structure of membranes. *Journal of Applied Polymer Science* **1994**, *51*, 2191–2194.
- Ritthidej, G.C.; Phaechamud, T.; Koizumi, T. Moist heat treatment on physicochemical change of chitosan salt films. *International Journal of Pharmaceutics* **2002**, *232*, 11–22.

Drying Kinetics and β -Carotene Degradation in Carrot Undergoing Different Drying Processes

PEAMSUK SUVARNAKUTA, SAKAMON DEVAHASTIN, AND ARUN S. MUJUMDAR

ABSTRACT: Superheated steam drying, which is an airless drying technology, has recently received much attention as an alternative to conventional hot air drying, which is a relatively oxygen-rich drying process and causes much product quality degradation. However, because most food products are damaged when subjected to superheated steam at atmospheric or higher pressures, lowering the dryer operating pressure is preferred. In this study, the effects of a low-pressure superheated steam drying (LPSSD), vacuum drying, and hot air drying on the drying and degradation kinetics of β -carotene in carrot were investigated experimentally. LPSSD and vacuum drying led to less degradation of β -carotene in carrot than in the case of hot air drying. The empirical models, which can describe the experimental data of β -carotene degradation in carrot undergoing different drying techniques, were also proposed. β -Carotene degradation in carrot depended more on the carrot temperature than its moisture content in all cases.

Keywords: empirical correlations, hot air drying, low-pressure superheated steam drying, vacuum drying

Introduction

In recent years, the consumption of carrot and its related products has increased steadily due to the recognition of antioxidant and anticancer activities of β -carotene in carrot, which is also a precursor of vitamin A (Speizer and others 1999; Dreosti 1993). However, in food industry, especially instant food industry, carrot must usually be dried prior to its use. Several techniques have been used to dry carrot with the goal of maintaining its natural appearance as well as its nutritional values, including β -carotene, to the maximum level possible.

Many studies (Mulet and others 1989; Ratti 1994) were performed to study hot air drying of carrot of various shapes. It was found that hot air-dried carrot was characterized by the low porosity and the high apparent density nature (Krokida and Maroulis 1997). Khraisheh and others (1997) found that the increased density and shrinkage of carrot was dependent on the operating temperature of hot air drying. Significant color changes also occurred during hot air drying of carrot (Krokida and others 1998) and the change of its red color was attributed to the changing level of β -carotene (Lin and others 1998).

Vacuum drying is an alternative technique to improve the quality of dehydrated heat-sensitive products, including carrot. Krokida and others (1997) found that vacuum drying was able to yield higher porosity and redder carrot than that dried by hot air.

During the past decade, there has been considerable interest in applying superheated steam to dry various food products with some success (Seyed-Yagoobi and others 1999; Moreira 2001; Caixeta and others 2002). Despite the many advantages of near-atmospheric pressure superheated steam drying (Devahastin and Suvarnakuta 2004), there still exist some limitations, especially when applying it to drying heat-sensitive materials, for example, foods and bio-products (Mujumdar 2000). Because most foods or other

heat-sensitive products are damaged at the saturation temperature of superheated steam corresponding to the atmospheric or higher pressures, one possible way to alleviate the above-mentioned problems is to operate the dryer at reduced pressure.

Recently, the concept of low-pressure (or sub-atmospheric pressure) superheated steam drying (LPSSD) has been applied to various types of heat-sensitive materials. Elustondo and others (2001) studied sub-atmospheric pressure superheated steam drying of shrimp, banana, apple, potato, and cassava slices both experimentally and theoretically. A semi-empirical mathematical model was developed, and it was found to predict the drying kinetics reasonably well. However, no mention about the quality of dried food products was given. More recently, Devahastin and others (2004) studied experimentally drying of carrot cubes both in low-pressure superheated steam and vacuum dryers. The effects of operating pressure and temperature on the drying characteristics as well as various physical properties, i.e., volume, shrinkage, apparent density, color and rehydration behavior, of the dried carrot subjected to the 2 processes were evaluated. It was observed that steam drying provided better rehydration and redder dried carrot than that obtained in vacuum drying although the drying time in the former case was slightly longer. No mention about the chemical (nutritional) quality changes of carrot during drying was given, however.

The objective of this study was, therefore, to investigate experimentally the effects of a low-pressure superheated steam drying as well as other drying techniques, hot air and vacuum drying, on the drying kinetics and degradation of β -carotene in carrot undergoing these drying operations. Simple relationships between the amount of β -carotene and the product moisture content as well as temperature were also developed for all drying processes studied.

Material and Methods

Experimental setup

A schematic diagram of the low-pressure superheated steam dryer and its accessories is shown in Figure 1. The dryer consists of a stainless steel drying chamber, insulated with rock wool; a steam reservoir, which received steam from a boiler; and a liquid ring vac-

MS 20050213 Submitted 4/7/05, Revised 5/16/05, Accepted 6/16/05. Authors Suvarnakuta and Devahastin are with Dept. of Food Engineering, King Mongkut's Univ. of Technology Thonburi, 91 Pracha u-tid Rd., Bangkok 10140, Thailand. Author Mujumdar is with Dept. of Mechanical Engineering, Natl. Univ. of Singapore, Singapore. Direct inquiries to author Devahastin (E-mail: sakamon.dev@kmutt.ac.th).

uum pump (Nash, model ET32030, Nuremberg, Germany), which was used to maintain the vacuum in the drying chamber. A steam trap was installed to reduce the excess steam condensation in the reservoir. An electric heater, which was controlled by a Proportional-Integral-Derivative (PID) controller (Omron, model E5CN, Tokyo, Japan), was installed in the drying chamber to control the steam temperature and to minimize the condensation of steam in the drying chamber during the start-up period. With the use of a heater, the initial steam condensation during the start-up period was reduced considerably. An electric fan was used to disperse steam throughout the drying chamber. The change of the weight of the sample was detected continuously using a load cell (Minebea, model Ucg-3kg, Nagano, Japan). The temperatures of the steam and of the sample were measured continuously using type K thermocouples. Thermocouple signals were then multiplexed to a data acquisition card (Omega Engineering, model no. CIO-DAS16Jr., Stamford, Conn., U.S.A.) installed in a PC. Labtech Notebook Software (version 12.1, Laboratory Technologies Corp., Middleboro, Mass., U.S.A.) was used to read and record the temperature data. More detailed experimental setup can be found in Devahastin and others (2004). For vacuum-drying experiments, the same experimental set-up was used but without the application of steam to the drying chamber. Hot air-drying experiments were performed in a lab-scale tray dryer with an installed balance to monitor the weight change of the drying sample. The temperatures of the air and of the sample were measured continuously using the above-mentioned measuring equipment. The air velocity through the dryer was maintained at 0.8 m/s.

Sample preparation

Fresh carrot (*Daucus carota* var. *sativa*) was obtained from a supermarket and stored at 4 °C. Prior to the start of each drying experiment, carrot was peeled and diced (only the cortex part) into 1 cm³ cubes. The moisture content of the fresh carrot was determined by drying it at 105 °C for 12 h in a hot air oven (Memmert, model 800, Schwabach, Germany).

Drying experiments

Raw carrot cubes were dried using 3 different methods: LPSSD, vacuum drying, and hot air drying.

To perform an LPSSD experiment, approximately 35 cubes of carrot (about 40 g) were placed as singer layer on the sample holder.

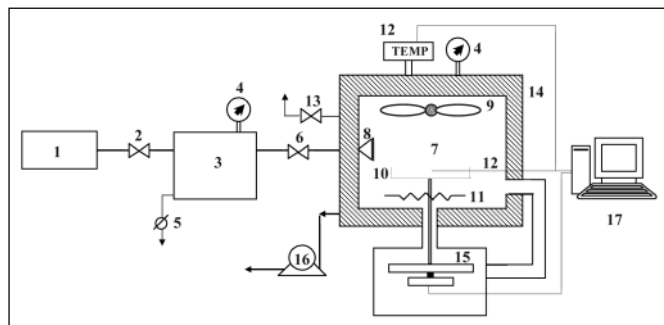


Figure 1—A schematic diagram of the low-pressure superheated steam dryer and associated units: 1, boiler; 2, steam valve; 3, steam reservoir; 4, pressure gauge; 5, steam trap; 6, steam regulator; 7, drying chamber; 8, steam inlet and distributor; 9, electric fan; 10, sample holder; 11, electric heater; 12, on-line temperature sensor and logger; 13, vacuum break-up valve; 14, insulator; 15, on-line weight indicator and logger; 16, vacuum pump; and 17, PC with installed data acquisition card.

More detailed procedures of an LPSSD experiment can be found in Devahastin and others (2004). Although only 40 g of the sample was used, the results reported here should be applicable to future commercial drying applications if care is made in maintaining the same drying conditions in an industrial dryer. The experiments were performed at the steam absolute pressure of 7 kPa and the steam temperatures of 60, 70, and 80 °C. The flow rate of steam into the drying chamber was maintained at about 26 kg/h and the speed of the fan was fixed at 1100 rpm.

For vacuum-drying experiments, the same operating conditions were used but without the application of steam to the chamber. For hot air drying, the experiments were performed at the drying temperatures of 60, 70, and 80 °C at an atmospheric pressure.

To determine the relationship between the β -carotene content of carrot and its moisture content as well as temperature, the drying carrot was sampled and its β -carotene content was measured at a predetermined sampling time; that particular experiment was ended at that time. A new experiment was then performed until the next predetermined sampling time was reached. The β -carotene content of the fresh sample was also measured, so a direct comparison could be made between the fresh and dried samples. The same procedure was repeated until the complete relationship, valid over the whole range of moisture content of interest, was obtained. All experiments were performed in duplicate.

β -Carotene analysis

Drying samples were sampled at different drying times and stored in sealed aluminum foil bags to protect them from light at –18 °C prior to the β -carotene analysis. The samples were thawed at room temperature before the analysis.

The β -carotene analysis method used was a modification of that suggested by AOAC (2000), and the high-performance liquid chromatography (HPLC) method described by Howard and others (1999). To extract β -carotene, dried carrot was prepared by grinding 5 to 8 g of the sample for 2 min using a stainless steel pulverizer (Waring, model SS110, Torrington, Conn., U.S.A.). The ground sample was then placed in a flask filled with 40 mL of ethanol. Forty milliliters of 2 N potassium hydroxide was added to saponify the solution at 70 °C for 30 min. The extract was then cooled to 0 °C. β -Carotene was then extracted twice with 5 mL diisopropyl ether and the aqueous layer was discarded. The extracted solution was diluted by a mobile phase and was filtered through a 0.45 μ m filter before injecting 10 μ L of the sample into the liquid chromatograph column.

Symmetry[®] C₁₈ 5 μ m (3.9 \times 150 mm) HPLC column (Waters, Milford, Mass., U.S.A.) was used for β -carotene analysis. The HPLC system consists of a pump and a controller (Waters, model 600), a tunable absorbance detector (Waters, model 486), and an auto sampler (Waters, model 717 plus). A mixture of methanol and acetonitrile (90:10) was used as the mobile phase, and its flow rate was set at 1.5 mL/min. A ultraviolet spectrophotometer detector at a wavelength of 450 nm was used for detecting β -carotene. The mobile phase was degassed using an ultrasonic generator. An HPLC β -carotene standard (Sigma, C4582, Steinheim, Germany) was run daily with the samples to accurately characterize the retention time of β -carotene. Quantification of β -carotene was carried out based on the β -carotene standard curve. The concentration of β -carotene was calculated from the relative peak area of the β -carotene standard curve. The standard curve was prepared daily by injecting solutions of HPLC β -carotene standard in diisopropyl ether at 6 concentrations (0, 2, 4, 6, 8, and 10 μ g/mL) and recording their respective absorbance values. All standard curves showed good linearity ($R^2 > 0.99$). A typical chromatogram of β -carotene is shown in Figure 2.

The measured total β -carotene content is expressed in this work

Table 1—Average drying times and losses of β-carotene of dried carrot (at moisture content of 0.1 kg/kg [d.b.]) that underwent different drying methods

Sample	Average drying time (min)	β-Carotene content ^a (mg/100 g)		β-Carotene Retention ratio (β _f /β _i)
		Wet basis	Dry basis	
Fresh carrot	—	4.86 ± 0.65	51.11 ± 6.89	—
LPSSD carrot				
T = 60 °C	420	54.92	43.94	0.83 ± 0.02a
T = 70 °C	330	50.32	41.24	0.76 ± 0.04b
T = 80 °C	210	38.81	31.55	0.74 ± 0.02b
Vacuum-dried carrot				
T = 60 °C	300	26.95	24.28	0.74 ± 0.03c
T = 70 °C	250	25.81	24.05	0.71 ± 0.03cd
T = 80 °C	180	31.61	27.85	0.68 ± 0.03d
Hot air-dried carrot				
T = 60 °C	420	22.56	21.46	0.62 ± 0.02e
T = 70 °C	300	35.66	23.3	0.62 ± 0.03e
T = 80 °C	240	36.26	22.05	0.58 ± 0.03e

^aMean ± SD. Different letters in the same column indicate that values are significantly different ($P < 0.05$).

in terms of the β-carotene retention ratio:

$$\beta\text{-carotene retention ratio} = \frac{\beta_f}{\beta_i} \quad (1)$$

where β_f and β_i are, respectively, the β-carotene contents of fresh carrot and dried carrot at the end of each drying experiment (mg/100 g dry solid). All β-carotene measurements were performed in duplicate, and the data presented are an average of the 2 measurements.

Statistical analysis

The data were analyzed and presented as mean values with standard deviations. Differences between mean values were established using Duncan's multiple range test. Values were considered at 95% level of significance ($P < 0.05$) and a statistical program SPSS (version 10.0, Chicago, Ill., U.S.A.) was used to perform the calculation.

Results and Discussion

Drying kinetics of carrot

The drying curves and temperature profiles of carrot (initial moisture contents of 9.5 to 10 kg/kg dry solid (dry basis) or 905 to 909 kg/kg sample (wet basis) undergoing different drying techniques at

drying temperatures of 60 to 80 °C are shown in Figure 3. The chosen operating conditions were those of Devahastin and others (2004). The drying times needed to dry carrot to the final moisture content of about 0.1 kg/kg (d.b.) are listed in Table 1.

As illustrated in Figure 3, although vacuum drying was a faster drying process than LPSSD and hot air drying, previous studies (Devahastin and others 2004; Suvarnakuta and others 2005) have shown that the differences between the drying times of LPSSD and vacuum drying were smaller at higher drying temperatures. Raising the drying temperature further would eventually lead to equal rates of drying at the so-called inversion temperature due to the increased temperature difference between the steam and the surface temperature of carrot as well as a reduction of the initial steam condensation, which is inevitable in any superheated steam drying applications (Mujumdar 2000). Although LPSSD generally required longer drying time than vacuum drying, LPSSD provided better product physical properties, i.e., better rehydrated and redder dried carrot, than that obtained by vacuum drying over the operating temperature range of 60 to 80 °C and operating pressure of 7 kPa used in this work (Devahastin and others 2004).

In the case of hot air drying, it can be seen in Figure 3 that the drying rates during the 1st 80 min were higher than those of LPSSD. Although the hot air drying rates (slope of the drying curves) in the constant rate period were higher than those of LPSSD, hot air drying

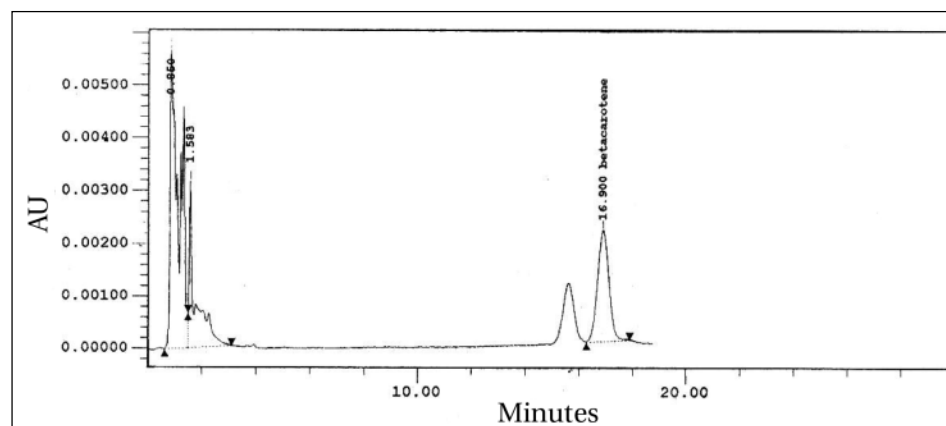


Figure 2—Chromatogram of β-carotene in dried carrot at a wavelength of 450 nm.

took as much time to dry carrot to the final desired moisture content as did LPSSD. This is because the falling rate period of hot air drying was longer than that of LPSSD. In the constant rate period, the water removal carried out by evaporation from the carrot surface in the case of LPSSD took longer time than in the case of hot air drying due to a smaller temperature difference between the drying medium (steam) and the carrot surface (if drying was carried out below the inversion temperature, as in this case). On the other hand, in the falling rate period, LPSSD was faster than hot air drying due to the more porous structure of carrot as well as the higher water diffusivity in the case of steam drying. Therefore, the 2 sets of overall drying times were not much different.

For more detailed information about the drying behavior of carrot cube undergoing LPSSD and vacuum drying the reader is referred to Devahastin and others (2004).

Degradation kinetics of β -carotene

The β -carotene retention in carrot during drying is presented in Table 1. The β -carotene content in fresh carrot on a dry solid basis (51.11 mg/100 g solid) was close to 54 mg/100 g solid documented by Chen and others (1993). The β -carotene content of fresh carrot varied slightly according to its maturity and initial moisture content. The ratio of the β -carotene content of fresh carrot and the dried one (β -carotene retention ratio) was then used to report the results in this study.

As seen in Table 1, all dried carrot cubes lost some β -carotene as compared with fresh ones. However, the loss of β -carotene in the case of hot air drying was significantly ($P < 0.05$) higher (about 21% to 25%) than those observed when drying carrot by other processes to a similar level of moisture content of 0.1 kg/kg (d.b.). LPSSD

and vacuum drying could, therefore, reduce the loss of β -carotene to some extent. The ability of LPSSD to conserve heat and oxygen-sensitive products (such as vitamin C) has indeed been shown earlier (Methakhup and others 2005).

It is known that carotene is degraded by free radical oxidation mechanism and that the degree of oxidation depends on the heating time, heating temperature, and oxygen content. In this case, hot air drying was the only non-airless process and, hence, caused more aerobic degradation of β -carotene compared with the other drying processes. These results were similar to those reported by Lin and others (1998) who compared β -carotene contents of carrot slices at a moisture content of 10% (d.b.) underwent vacuum microwave, air drying, and freeze drying. They reported that air drying resulted in the highest loss of β -carotene and the rapid heating and depletion of oxygen offered by vacuum microwave could reduce the loss of β -carotene.

Based on the experimental data, it was found that the total β -carotene retention in the cases of LPSSD and vacuum drying was higher than in the case of hot air drying. This is because of the oxygen-free environment of the LPSSD drying chamber. In the case of vacuum drying, however, because the level of vacuum pressure used in this study was not that low (7 kPa absolute), there still existed some oxygen that could participate in an oxidation reaction. The effect of aerobic degradation of β -carotene could not, therefore, be negligible, although its extent was still lower than in the case of hot air drying.

The relationships between the β -carotene content and the moisture content of carrot undergoing LPSSD, vacuum drying, and hot air drying are shown in Figure 4. As mentioned earlier, the level of oxidation, which is the major cause of carotene losses, depends in part on

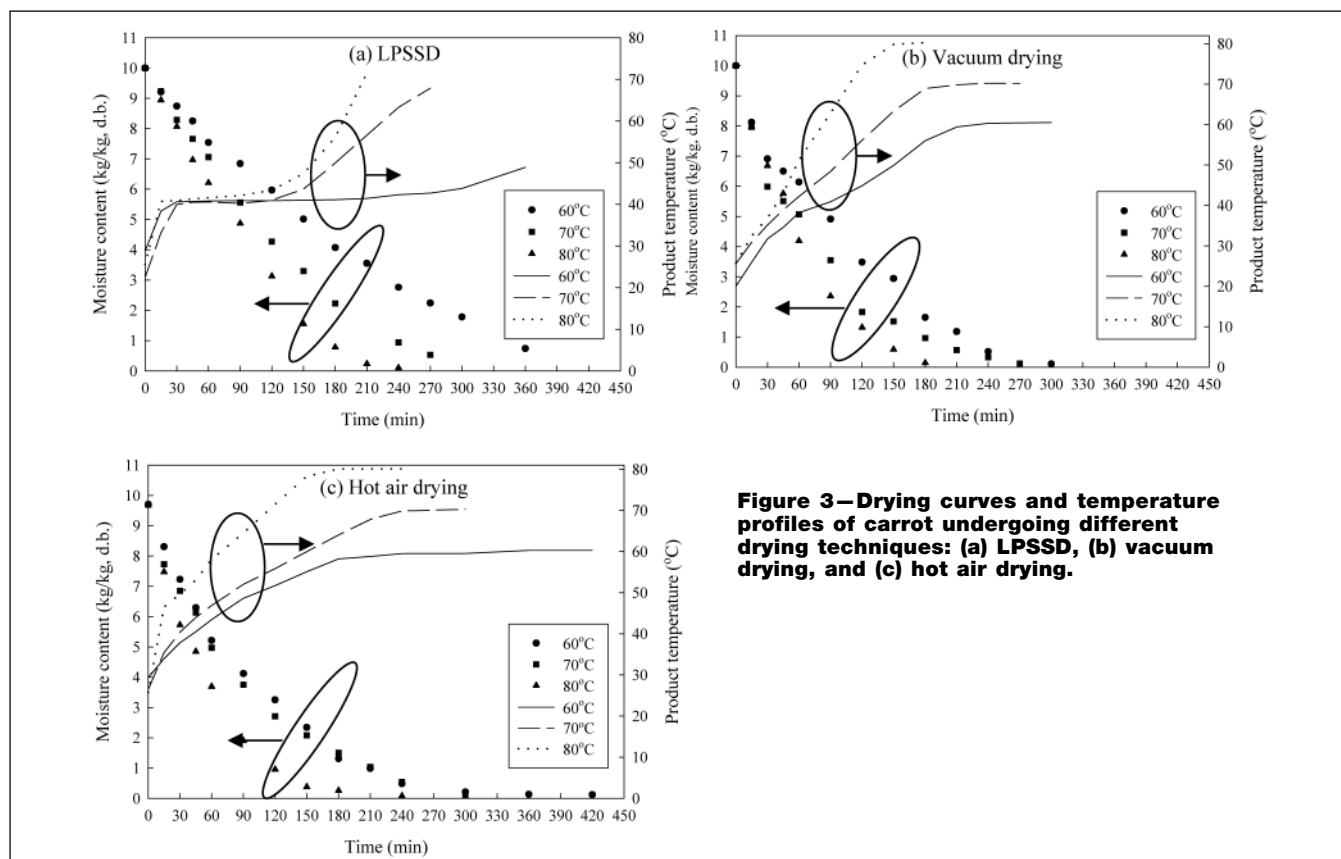


Figure 3—Drying curves and temperature profiles of carrot undergoing different drying techniques: (a) LPSSD, (b) vacuum drying, and (c) hot air drying.

the available oxygen content in the drying chamber. It can be seen from this figure that the level of β -carotene dropped rapidly during the start-up period of drying in all cases. This is due to the fact that moist carrot was immediately subjected to heat treatment, and there might still be some oxygen remained for oxidation initially.

It is seen from Figure 4c that the β -carotene content of carrot decreased continuously in the case of hot air drying while the levels of β -carotene in carrot undergoing LPSSD and vacuum drying remained relatively unchanged (Figures 4a and 4b) after the initial start-up period. This is due to the fact that in the case of hot air drying, lipoxygenase, and probably peroxidase, which are aerobic catalysts of an oxidation reaction, which are contained in unblanched carrot like the one used in this study, was activated significantly at temperatures in the range of 60 to 65 °C (Cui and others 2004). Therefore, it is seen that β -carotene degraded continuously in the case of hot air drying when product temperature increased to this range.

The negligible changes (until the moisture content of around 2 kg/kg [d.b.]) of β -carotene after the initial drop in the case of LPSSD might be explained by the fact that the activity of lipoxygenase and peroxidase, which are responsible for the oxidative degradation of β -carotene, was greatly reduced due to several possible effects, including the lower oxygen level in the drying chamber and the lower product temperature (see Figures 3a and 3c). After some period of time, the temperature of carrot undergoing LPSSD started to rise again. This rise induced additional degradation of β -carotene. At the drying temperature of 60 °C, for example, this rise of temperature occurred after 300 min of drying or at moisture contents of less than 2 kg/kg (d.b.). The corresponding degradation of β -carotene can be seen clearly in Figure 4.

Comparison between vacuum drying and LPSSD revealed that the β -carotene retention differed slightly between the 2 processes although vacuum drying took much shorter time than LPSSD to dry the sample to the desired moisture content (Figures 3 and 4). This is because the LPSSD chamber was fully contained with superheated steam; therefore, the oxygen content remaining in the LPSSD chamber was less (none indeed) than in the case of vacuum drying chamber. In addition, the product temperature of all vacuum drying cases was higher than LPSSD cases (Figure 3), thus thermal stability of β -carotene was decreased in the case of vacuum drying. Moreover, the change of the shape of carrot undergoing LPSSD was much more uniform than in the case of vacuum drying. This result was consistent with our previous findings (Devahastin and other 2004). Thus, the LPSSD product had less surface area for heat transfer and hence had higher β -carotene retention.

Empirical models

Figure 5 illustrates the relationship between the β -carotene content and the product temperature during different drying processes. It is seen that β -carotene degraded continuously as the product temperature increased, especially in the case of hot air drying. Because there was no period of constant carrot temperature that corresponded to the constant rate of β -carotene degradation, the use of a kinetic model of β -carotene degradation that refers to an elementary reaction expression and the Arrhenius equation was not appropriate. Therefore, in this study, simple empirical models that enable prediction of the β -carotene degradation as a function of carrot moisture content and temperature were instead proposed. Although, as can be seen in Figure 5c, there were periods of rather constant temperature, which corre-

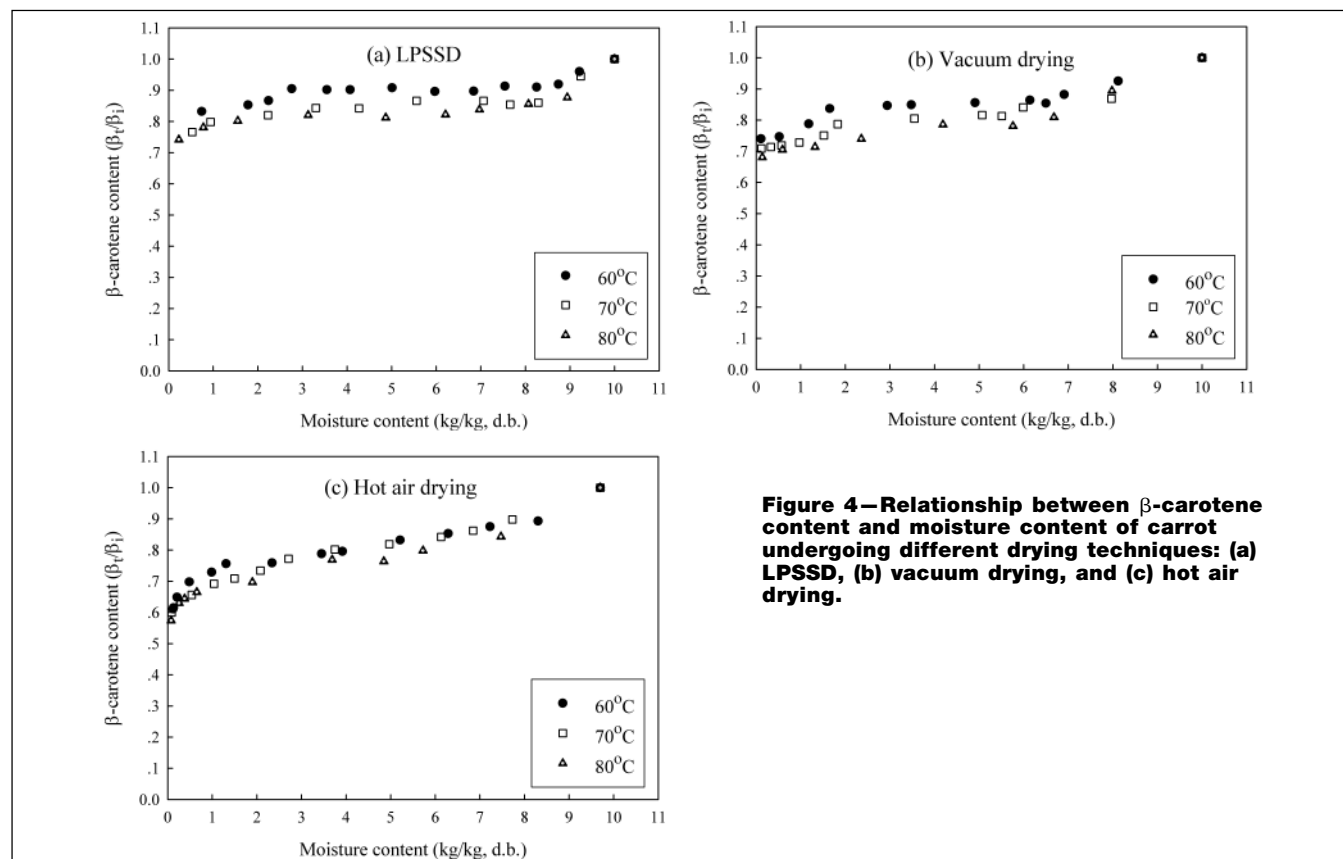


Figure 4—Relationship between β -carotene content and moisture content of carrot undergoing different drying techniques: (a) LPSSD, (b) vacuum drying, and (c) hot air drying.

sponded to the constant degradation rate of β-carotene toward the end of hot air drying, no attempt was made to consider only these rather short periods for a simple elementary reaction expression.

A simple empirical model that enables prediction of the β-carotene degradation as a function of carrot moisture content and temperature during LPSSD, vacuum and hot air drying was proposed in the following form:

$$\frac{\beta_t}{\beta_i} = a + b \frac{X_t}{X_i} + c \frac{T_p}{T_i} + d \left(\frac{X_t}{X_i} \right)^2 + e \left(\frac{T_p}{T_i} \right)^2 + f \left(\frac{X_t}{X_i} \right)^3 + g \left(\frac{T_p}{T_i} \right)^3 \quad (2)$$

where β_i and β_t are the initial and instantaneous β-carotene contents (mg/100 g solid), respectively. X_i and X_t are the initial and instantaneous moisture contents (kg/kg, d.b.), respectively. T_i and T_p are the initial and instantaneous temperatures of carrot (°C), respectively. a, b, c, d, e, f, g are empirical constants.

The following equations were fitted to the experimental data and the fitted equations were evaluated based on their R^2 and absolute mean error of estimation. The absolute mean error values are 0.015, 0.031, and 0.012 for the case of LPSSD, hot air drying, and vacuum drying, respectively.

For LPSSD:

$$\frac{\beta_t}{\beta_i} = 1.104 + 0.261 \frac{X_t}{X_i} - 0.192 \frac{T_p}{T_i} - 0.561 \left(\frac{X_t}{X_i} \right)^2 - 6.61 \times 10^{-3} \left(\frac{T_p}{T_i} \right)^2 + 0.390 \left(\frac{X_t}{X_i} \right)^3 + 0.011 \left(\frac{T_p}{T_i} \right)^3 \quad R^2 = 0.911 \quad (3)$$

For vacuum drying:

$$\frac{\beta_t}{\beta_i} = 0.754 + 0.596 \frac{X_t}{X_i} - 0.339 \frac{T_p}{T_i} - 0.708 \left(\frac{X_t}{X_i} \right)^2 + 0.221 \left(\frac{T_p}{T_i} \right)^2 + 0.517 \left(\frac{X_t}{X_i} \right)^3 - 0.038 \left(\frac{T_p}{T_i} \right)^3 \quad R^2 = 0.90 \quad (4)$$

For hot air drying:

$$\frac{\beta_t}{\beta_i} = 0.663 + 0.742 \frac{X_t}{X_i} + 0.165 \frac{T_p}{T_i} - 1.400 \left(\frac{X_t}{X_i} \right)^2 - 0.130 \left(\frac{T_p}{T_i} \right)^2 + 0.941 \left(\frac{X_t}{X_i} \right)^3 + 0.026 \left(\frac{T_p}{T_i} \right)^3 \quad R^2 = 0.982 \quad (5)$$

It can be seen from the above simple empirical relationships that the β-carotene retention depends on both the product moisture content and temperature. It should be noted that these empirical equations are based on the experimental results and conditions used in this study only. It can be seen also that the carrot temperature was the main contributor of β-carotene degradation. It is observed from the values of the main parameters of these equations (the terms of 3rd order and $0 < \frac{X_t}{X_i} \leq 1, 1 \leq \frac{T_p}{T_i} \leq 3.2$) that the effect of carrot temperature was larger than the effect of carrot moisture content on the β-carotene degradation of carrot during drying. This is because heat is the main reason for β-carotene degradation, especially in the low-oxygen system. Product temperature was,

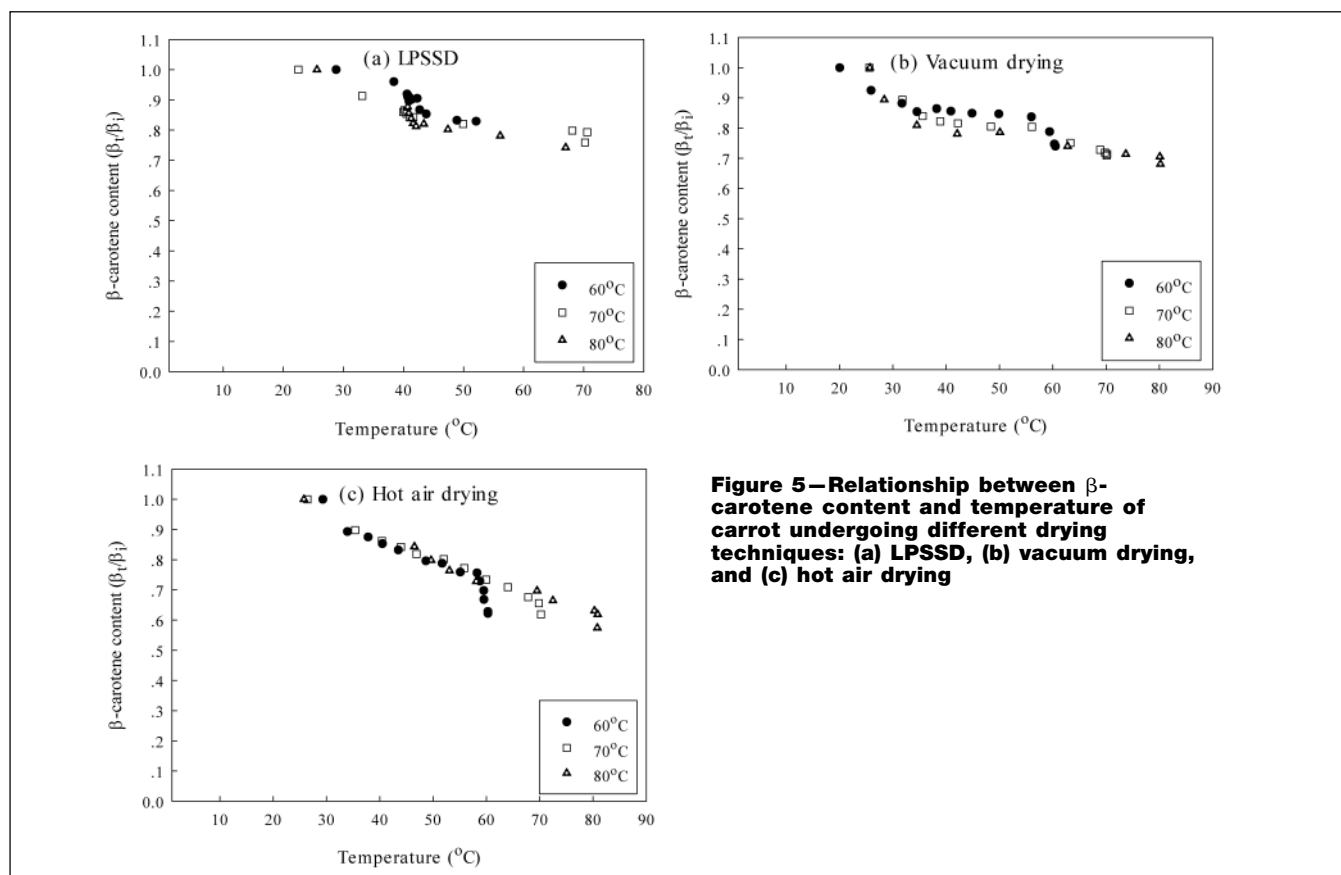


Figure 5—Relationship between β-carotene content and temperature of carrot undergoing different drying techniques: (a) LPSSD, (b) vacuum drying, and (c) hot air drying

therefore, the major player of the β -carotene degradation in the cases of LPSSD and vacuum. In the case of hot air drying, although the product temperature also affected more significantly the β -carotene degradation compared with the effect of moisture content, the effect of the product temperature was less obvious than in the cases of airless drying systems. This is due to the fact that for hot air drying the main cause of β -carotene degradation was the oxygen content available to an oxidative reaction of β -carotene in the drying chamber. Therefore, the effect of the product temperature was somehow overshadowed.

Conclusions

Comparison was made of the β -carotene degradation in carrot undergoing different drying techniques, such as LPSSD, vacuum drying, and conventional hot air drying. It was found that LPSSD and vacuum drying led to less degradation of β -carotene of carrot than in the case of hot air drying (up to 20% to 25% in the case of LPSSD). The empirical models, which can describe the experimental data of β -carotene degradation in carrot undergoing different drying techniques, were also proposed. The information obtained here can be used as a guideline in the design and operation of a system, which is suitable for drying heat- and/or oxygen-sensitive bio-products with the aim to minimize the quality losses of these products.

Acknowledgments

The authors express their sincere appreciation to Commission on Higher Education, the Thailand Research Fund (TRF), Natl. Science and Technology Development Agency (NSTDA), and the Intl. Foundation for Science (Sweden) for supporting this study financially.

References

[AOAC] Assn. of Official Analytical Chemists. 2000. Official methods of analysis. 17th ed., Gaithersburg, MD: AOAC.

Caixeta AT, Moreira R, Castell-Perez ME. 2002. Impingement drying of potato

chips. *J Food Process Eng* 25(1):63–90.

Chen BH, Chuang JR, Lin JH, Chiu CP. 1993. Quantification of provitamin A compounds in Chinese vegetables by high-performance liquid chromatography. *J Food Protect* 53(12):1076–8.

Cui ZW, Xu SY, Sun DW. 2004. Effect of microwave-vacuum drying on the carotenoids retention of carrot slices and chlorophyll retention of Chinese chive leaves. *Drying Technol* 22(3):563–75.

Devahastin S, Suvarnakuta P. 2004. Superheated steam drying of food products. In: Mujumdar AS, editor. *Dehydration of products of biological origin*. Enfield, NH: Science Publishers. p 493–512.

Devahastin S, Suvarnakuta P, Soponronnarit S, Mujumdar AS. 2004. A comparative study of low-pressure superheated steam and vacuum drying of a heat-sensitive material. *Drying Technol* 22(8):1845–67.

Dreosti IE. 1993. Vitamins A, C, E and β -carotene as protective factors for some cancers. *Asia Pacific J Clin Nutr* 2(1):21–5.

Elustondo D, Elustondo MP, Urbicain MJ. 2001. Mathematical modeling of moisture evaporation from foodstuffs exposed to subatmospheric pressure superheated steam. *J Food Eng* 49(1):15–24.

Howard LA, Wong AD, Perry AK, Klein BP. 1999. β -Carotene and ascorbic acid retention in fresh and processed vegetables. *J Food Sci* 64(5):929–36.

Khraisheh MAM, Cooper TJR, Magee TRA. 1997. Shrinkage characteristics of potatoes dehydrated under combined microwave and convective air conditions. *Drying Technol* 15(3–4):1003–21.

Krokida MK, Maroulis ZB. 1997. Effect of drying method on shrinkage and porosity. *Drying Technol* 15(10):1145–55.

Krokida MK, Tsami E, Maroulis ZB. 1998. Kinetics on color changes during drying of some fruits and vegetables. *Drying Technol* 16(3–5):667–85.

Krokida MK, Zogzas NP, Maroulis ZB. 1997. Modelling shrinkage and porosity during vacuum dehydration. *Int J Food Sci Tech* 32(6):445–58.

Lin TM, Durance TD, Scaman CH. 1998. Characterization of vacuum microwave, air and freeze dried carrot slices. *Food Res Int* 31(2):111–7.

Methakup S, Chiewchan N, Devahastin S. 2005. Effects of drying methods and conditions on drying kinetics and quality of Indian gooseberry flake. *Lebensm Wiss Technol* 38(6):579–87.

Moreira RG. 2001. Impingement drying of foods using hot air and superheated steam. *J Food Eng* 49(4):291–5.

Mujumdar AS. 2000. Superheated steam drying—technology of the future. In: Devahastin S, editor. *Mujumdar's practical guide to industrial drying*. Brossard, Canada: Exergex. p 115–38.

Mulet A, Berna A, Rosello C, Pinaga F. 1989. Drying carrots. II. Evaluation of drying models. *Drying Technol* 7(4):641–61.

Ratti C. 1994. Shrinkage during drying of foodstuffs. *J Food Eng* 23(1):91–5.

Seyed-Yagoobi J, Li YB, Moreira RG, Yamsaengsung R. 1999. Superheated steam impingement drying of tortilla chips. *Drying Technol* 17(1–2):191–213.

Speizer FE, Colditz GA, Hunter DJ, Rosner B, Hennekens C. 1999. Prospective study of smoking, antioxidant intake, and lung cancer in middle-aged women. *Cancer Cause Control* 10(5):475–82.

Suvarnakuta P, Devahastin S, Soponronnarit S, Mujumdar AS. 2005. Drying kinetics and inversion temperature in a low-pressure superheated steam drying system. *Ind Eng Chem Res* 44(6):1934–41.

Effect of far-infrared radiation assisted drying on microstructure of banana slices: An illustrative use of X-ray microtomography in microstructural evaluation of a food product

Angélique Léonard^{a,*}, Silvia Blacher^a, Chatchai Nimmol^b, Sakamon Devahastin^c

^a *Laboratory of Chemical Engineering, Department of Applied Chemistry, University of Liège, FNRS, B6c, Sart Tilman, 4000 Liège, Belgium*

^b *School of Energy, Environment and Materials, King Mongkut's University of Technology Thonburi, 126 Pracha u-tid Road, Bangkok 10140, Thailand*

^c *Department of Food Engineering, King Mongkut's University of Technology Thonburi, 126 Pracha u-tid Road, Bangkok 10140, Thailand*

Received 22 May 2007; received in revised form 11 July 2007; accepted 20 July 2007

Available online 3 August 2007

Abstract

X-ray microtomography coupled with image analysis represents a non-destructive technique, which allows scanning an entire sample to obtain such information as total pore volume and pore size distribution without the need of serial cuts as in the case of scanning electron microscopy (SEM). The technique has been applied successfully to obtain reliable microstructural information of many products undergoing different physical and chemical processes. However, the technique has still found limited use in food processing. To illustrate the use of X-ray microtomography the technique was applied to investigate the effect of far-infrared radiation (FIR) assisted drying on microstructure of a food product viz. banana. Two representative drying techniques, i.e., low-pressure superheated steam drying (LPSSD) and vacuum drying (VACUUM) were tested. Banana slices were dried by LPSSD–FIR at two different temperatures (80 and 90 °C) at a fixed pressure of 7 kPa. The total pore volume and pore size distribution of dried banana slices were then determined using X-ray microtomography. The results were also compared with those of products dried by LPSSD without FIR. Far-infrared radiation was found to modify the structure of the dried bananas by increasing their final porosity. The same effect of FIR was also observed in the case of vacuum drying with FIR (VACUUM–FIR). An increase of the drying temperature was also found to globally lead to an increase in the final porosity of the products.

© 2007 Elsevier Ltd. All rights reserved.

Keywords: Image analysis; Low-pressure superheated steam drying; Microstructure; Porosity; X-ray microtomography; Vacuum drying

1. Introduction

Although scanning electron microscopy (SEM) is a significant means to analyse the microstructure of a sample, SEM does not give reliable information on the total pore volume and pore size distribution of the sample. Indeed, due to the small parts that can be investigated with this method, measurements must be largely repeated in order to give statistically relevant results. Moreover, this technique fails to describe the whole 3D morphology as only

2D information is obtained. X-ray microtomography, on the other hand, is a powerful technique that can be used to obtain the above information. The main advantage of X-ray microtomography lies in its non-destructive character, as opposed to SEM that requires cutting of the sample. With its large field of view, X-ray microtomography also allows scanning of the entire sample. This technique is quite new in the field of food engineering (Babin et al., 2006; Haedelt, Pyle, Beckett, & Niranjana, 2005; Lim & Barigou, 2004; van Dalen, Blonk, van Haalts, & Hendriks, 2003) but it has been successfully applied for the characterization of highly porous materials (Blacher et al., 2006; Blacher et al., 2004; Léonard et al., 2007), the follow-up

* Corresponding author. Tel.: +32 4 366 47 22; fax: +32 4 366 28 18.
E-mail address: a.leonard@ulg.ac.be (A. Léonard).

of shrinkage and crack formation (Job, Sabatier, Pirard, Crine, & Léonard, 2006; Léonard, Blacher, Marchot, Pirard, & Crine, 2004) as well as internal moisture profiles during drying (Léonard, Blacher, Marchot, Pirard, & Crine, 2005).

Porosity is one of the important properties of dried foods and is generally related to their texture. To obtain dried products with higher degree of porosity, several novel drying methods have been proposed and tested. Low-pressure superheated steam drying (LPSSD) is one of the drying techniques that has recently been applied to various products for the above-mentioned purpose. Due to the low-pressure environment and evolution of evaporated moisture within the products during LPSSD, high-pressure gradients within the products occur, leading to an expansion of the cells of the products. Consequently, LPSSD dried products have more porous structure than those obtained by conventional hot air drying or vacuum drying (Devahastin, Suvarnakuta, Soponronnarit, & Mujumdar, 2004). Despite the potential of LPSSD to provide dried products with higher degree of porosity, the process is rather slow. To accelerate the drying process, a drying system combining LPSSD and far-infrared radiation (FIR) has been developed and applied successfully to a heat-sensitive food material (Nimmol, Devahastin, Swasdisevi, & Soponronnarit, 2007). It was found in this latter work that when FIR was applied to the process as an additional heat source, not only the drying time was reduced but the dried product quality, as assessed by texture analysis and SEM, was also improved.

As an illustrative example of the use of X-ray microtomography to evaluate the microstructure of a food product undergoing drying, the effect of FIR on the microstructure of banana slices dried by the system combining LPSSD and FIR (or LPSSD–FIR) was analysed. The results were also compared with those obtained by only low-pressure superheated steam drying (LPSSD), vacuum drying (VACUUM), and combination of FIR with vacuum drying (VACUUM–FIR). Two drying temperatures, 80 and 90 °C, were investigated in this work.

2. Experimental set-up, materials and methods

2.1. Experimental set-up

Fig. 1 shows a schematic diagram of the far-infrared radiation assisted drying system (Nimmol et al., 2007). Depending on whether the steam injection was switched on or off, two operating modes were respectively realized, i.e., low-pressure superheated steam drying or vacuum drying. The dryer consists mainly of a stainless steel drying chamber with inner dimensions of $45 \times 45 \times 45$ cm³; a boiler for steam production; a steam reservoir, which maintained a steam pressure at around 200 kPa; a liquid ring vacuum pump (Nash, ET32030, Trumbull, CT), which was used to maintain vacuum in the drying chamber; a sample holder; a load cell (Minebea, Ucg-3 kg, Nagano, Japan) with an accuracy of ± 0.2 g, which was used to record continuously the mass of the sample (at 1 min interval); a far-infrared radiator (Infrapara, A-2T-500, Selangor, Malaysia) rated at 500 W with a surface area of 60×120 mm², which was used to supply thermal radiation to the drying sample and the drying medium in the case of LPSSD–FIR and VACUUM–FIR experiments; and an electric heater rated at 1500 W, which was used to maintain the superheated steam and air temperature in the case of LPSSD and VACUUM experiments.

The operation of the far-infrared radiator was controlled through the temperature of the drying medium (air or superheated steam) measured at 30 mm above the sample surface via the use of a Proportional–Integral–Derivative (PID) controller (Shinko, JCS-33A-R/M, Osaka, Japan) with an accuracy of ± 0.1 °C. Similar to the far-infrared radiator, the operation of the electric heater was also controlled by a PID controller (Omron, E5CN, Tokyo, Japan) with an accuracy of ± 0.1 °C. The temperatures of the drying medium and of the drying sample were measured continuously using type K thermocouples. Thermocouple signals were multiplexed to a data acquisition card (Omega Engineering, CIO-DAS16Jr., Stamford, CT) installed in a PC. Labtech Notebook software (version

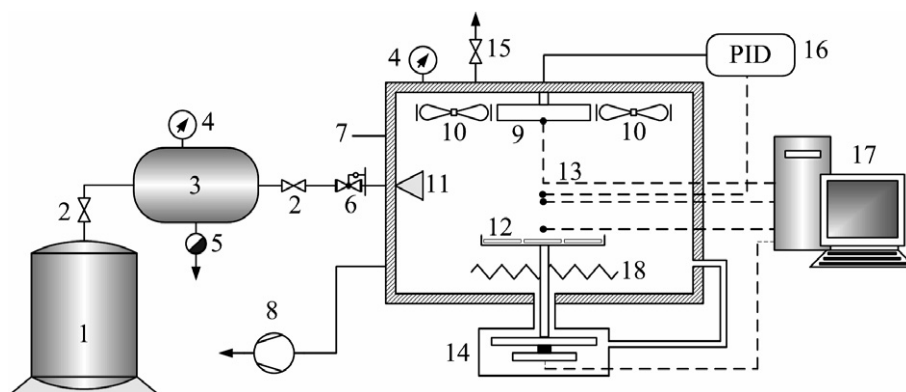


Fig. 1. A schematic diagram of the far-infrared radiation assisted drying system: (1) boiler; (2) steam valve; (3) steam reservoir; (4) pressure gauge; (5) steam trap; (6) steam regulator; (7) drying chamber; (8) vacuum pump; (9) far-infrared radiator; (10) electric fans; (11) steam inlet and distributor; (12) sample holder; (13) thermocouples; (14) load cell; (15) vacuum break-up valve; (16) PID controller; (17) PC with data acquisition card; (18) electric heater.

12.1, Laboratory Technologies Corp., Wilmington, MA) was then used to read and record the temperature data.

2.2. Material

Gros Michel banana (*Musa Sapientum* L.) was used as the tested material in this study. Fresh banana with initial moisture content (AOAC, 1984) in the range of 2.65–3.10 kg/kg (d.b.) and selected ripeness level of green tip (color index no. 5) was obtained from a local supermarket in Bangkok, Thailand and stored at 4 °C. Before each drying experiment, banana was peeled and sliced by an electric food slicer (Chef's Choice, 667 S, Aurora, NE) to 3 mm thick. The sliced samples were then cut into 30 mm diameter using a die.

2.3. Methods

In this study, approximately 16 pieces of prepared banana slices were used in each drying experiment. The experiments were carried out at the drying medium temperatures of 80 and 90 °C and absolute chamber pressure of 7 kPa. It should be noted that low-pressure superheated steam was the drying medium in the case of LPSSD–FIR and LPSSD experiments, while low-pressure air was the drying medium in the case of VACUUM–FIR and VACUUM experiments. Since the forced convection in the drying chamber led to lower temperatures of the far-infrared radiator and of the samples leading to lower drying rates, the electric fans were not used in the case of VACUUM–FIR experiments. Detailed methods of LPSSD–FIR and VACUUM–FIR experiments can be found in Nimmol et al. (2007), while detailed methods of LPSSD and VACUUM experiments are available in Devahastin et al. (2004). The drying experiments were performed until a moisture content of 0.035 kg/kg (d.b.) was obtained. This final moisture content was estimated from both the knowledge of the initial water content and the loss of mass, obtained through the drying curve. All experiments were performed in duplicate.

2.4. X-ray microtomography

X-ray microtomography is a powerful non-invasive technique allowing the visualization of the internal structure of a sample based upon local variation of the X-ray attenuation coefficient. During tomographic investigation an X-ray beam is sent to the sample and the transmitted beam is recorded by a detector. According to the Beer–Lambert's law the transmitted intensity is related to the integral of the X-ray attenuation coefficient (μ) along the path of the beam. This coefficient depends on the density (ρ), the atomic number (Z) of the material and on the energy of the incident beam (E) according to

$$\mu = \rho \left(a + \frac{bZ^{3.8}}{E^{3.2}} \right), \quad (1)$$

where a is a quantity with a relatively small energy dependence and b is a constant (Vinegar & Wellington, 1987).

Projections (assembling of transmitted beams) are recorded for several angular positions by rotating the sample between 0° and 180°. Then, a back-projection algorithm is used to reconstruct 2D or 3D images, depending on the method used. In the case of 2D images each pixel has a grey level value corresponding to the local attenuation coefficient.

The “Skyscan-1172 high-resolution desk-top micro-CT system” (Skyscan, Kontich, Belgium) was used in this study. A banana slice was placed vertically in a polystyrene holder, the latter being almost transparent to X-rays. In contrast to a classical medical scanner, the source and the detector were fixed, while the sample was rotated during the measurement. The cone beam source operated at 60 kV and 167 μ A. The detector was a 2 D, 1048 \times 2000 pixels, 16-bit X-ray camera. The distance source-object-camera was adjusted to produce images with a pixel size of 15 μ m. Because of the sample height, three successive sub-scans, each corresponding to one third of the slice height, had to be performed. The rotation step was fixed at 0.4°. For each angular position, a radiograph of the sample, instead of a 1D-projection of a cross-section, was recorded by a 2D camera.

Fig. 2 shows a typical radiograph obtained after the three sub-scans were linked together. The acquisition time required for each of the three segments was close to 50 min. The Feldcamp back-projection algorithm was used to reconstruct 2D images of the cross-sections. For each banana slice about 200 cross-sections, separated by 150 μ m, were reconstructed. Fig. 3a and b shows typical grey level cross-sections obtained for two vertical positions in the sample.

2.5. Image analysis and measurement

3D images of the samples were built by stacking ca. 200 cross-sections obtained by X-ray microtomography. The

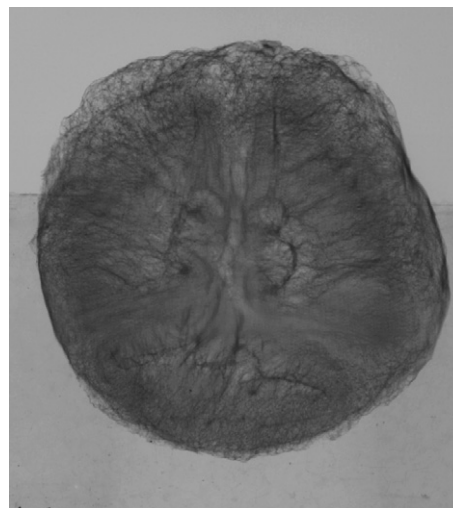


Fig. 2. Typical radiograph of a dried banana slice.

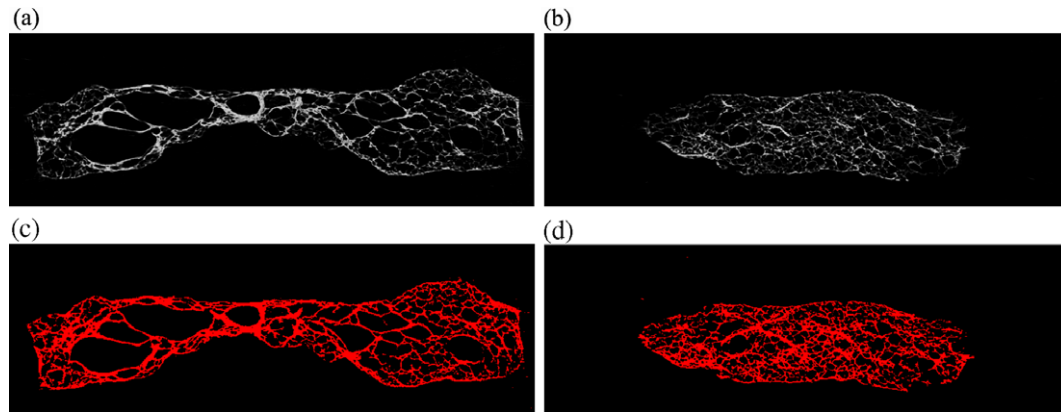


Fig. 3. Grey level cross-sections (a–b) and the corresponding binary images after thresholding (c–d).

resulting 3D grey level images were formed by two phases: the pore space at low grey levels (dark voxels), and the banana skeleton at high grey levels (bright voxels) (see Fig. 3a and b). To perform a measurement, the 3D image was preliminary segmented by assigning the value 1 to all pixels whose intensity was below a given grey tone value and 0 to the others, which implies fixing a threshold on the 3D grey level image. This threshold was determined as follows: an automatic threshold based on the entropy of the histogram (Sahoo, Soltani, Wong, & Chen, 1988) was calculated for each 2D cross-section. In this method, the inter-class entropy (S), defined by Eq. (2), was maximized.

$$S = - \sum p_i \times \log(p_i), \quad (2)$$

where p_i is the probability of a pixel grey scale value in the image.

Fig. 3c and d show the result of the segmentation process applied to Fig. 3a and b, respectively. The threshold values obtained from the entropy method for the set of cross-sections, which formed each 3D image, were very close indicating that skeleton tomograms had an homogeneous contrast. Then, a single threshold value for the 3D images was determined as an average of the cross-section thresholds. After this thresholding step, some small black holes were still present in the image and were removed by applying a closing filter (Soille, 1999).

From the 3D processed binary images the porosity (δ), defined as the fraction of voxels of the image that belong to the pores, was first measured. As the 3D images of banana slices presented a continuous and rather disordered pore structure in which it was not possible to assign to each pore a precise geometry, a standard granulometry measurement could not be applied. Therefore, to quantify the larger pore sizes, the opening size distribution (Soille, 1999), which allows assigning a size to both continuous and individual particles, was calculated. When an opening transformation was performed on a binary image with a structuring element (SE) of size λ , the image was replaced by an envelope of all SEs inscribed in its objects. For the sake of simplicity spheres of increasing radii λ (approximated by octahedra) were used. When an image was opened by a sphere whose

diameter was smaller than the smallest features of its objects it remains unchanged. As the size of the sphere increased, larger parts of the objects were removed by the opening transformation. Therefore, opening could be considered as equivalent to a physical sieving process. This procedure was applied to the reversed 3D images of the foams, i.e., to the 3D images in which pores correspond to white measurable voxels and the matrix to black voxels. Image processing and measurements were performed with software Aphelion 3.2 (Adsis, Meythet, France) on a PC.

3. Results and discussion

3.1. Temperature evolution of banana slices during drying

Because the temperature of the samples during drying is an important factor influencing their pore structure, the temperature of banana slices undergoing different drying methods and conditions is first discussed. As revealed by Fig. 4a and b the temperature of the samples undergoing the process applying FIR (LPSSD–FIR and VACUUM–FIR) was much higher than that of samples undergoing LPSSD and VACUUM. This is due to an extra heating. In the cases of LPSSD and LPSSD–FIR, the periods of constant sample temperature, which were consistent with the period of constant drying rates, were observed after a rapid increase of the sample temperature during the first 10 min of drying. For LPSSD the level of constant sample temperature was the boiling point of water corresponding to the chamber pressure. However, for LPSSD–FIR the level of constant sample temperature was higher than the boiling point of water because FIR was present. For the processes without the application of superheated steam (VACUUM and VACUUM–FIR) no periods of constant sample temperature were observed because no constant drying rate periods were observed (Nimmol et al., 2007). It should also be noted from Fig. 4 that the temperatures of LPSSD–FIR and VACUUM–FIR samples during the later stages of drying rose to levels higher than the set medium temperatures and remained rather constant until the end of the processes. This is again due to the influence of

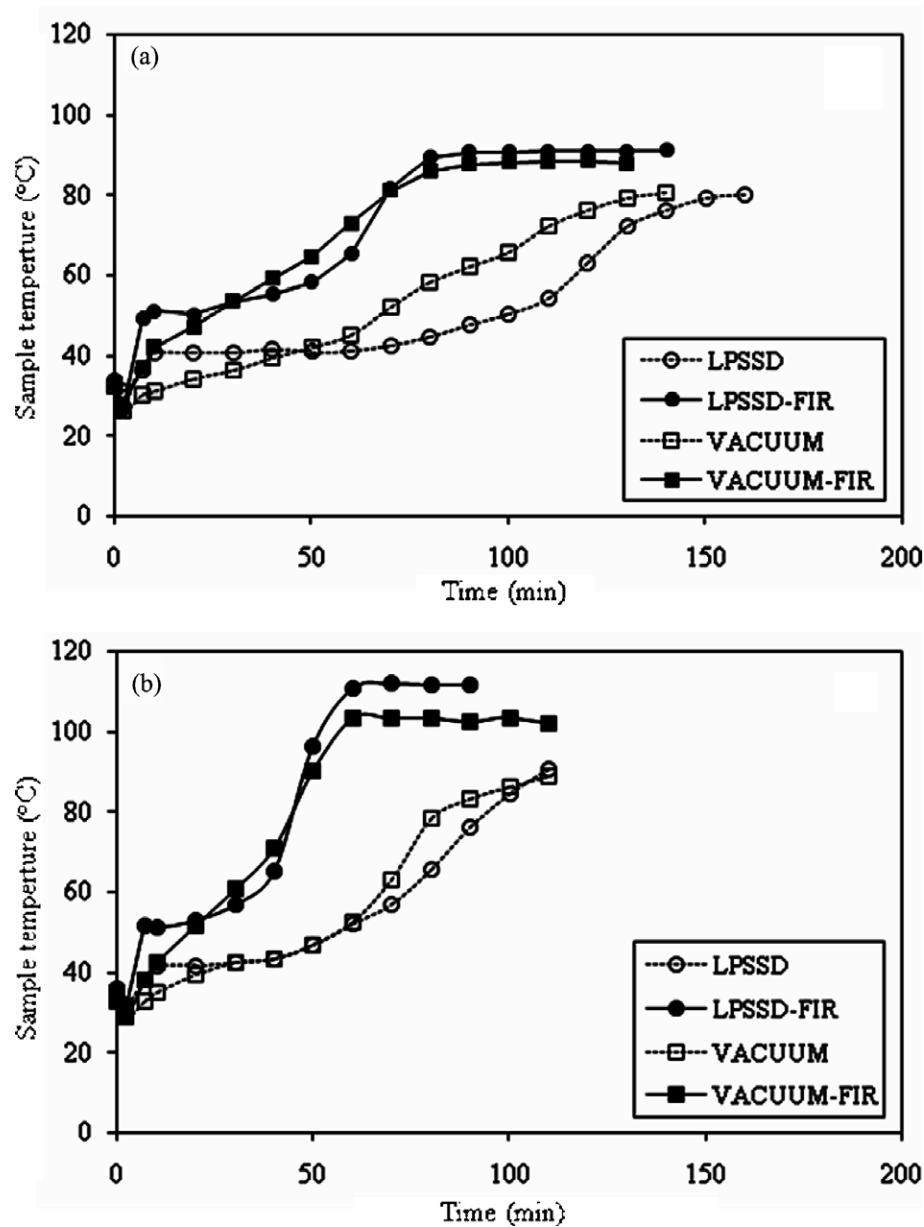


Fig. 4. Temperature evolution of banana slices dried at (a) 80 °C and (b) 90 °C.

additional energy obtained from FIR. These results are in contrast to those of LPSSD and VACUUM for which the sample temperature approached the drying medium

Table 1
Total porosity of banana slices undergoing various drying methods at different drying conditions

Drying method	Drying temperature (°C)	Porosity
LPSSD	80	0.42 ± 0.05
	90	0.53 ± 0.06
LPSSD-FIR	80	0.55 ± 0.06
	90	0.70 ± 0.08
VACUUM	80	0.54 ± 0.05
	90	0.46 ± 0.05
VACUUM-FIR	80	0.57 ± 0.06
	90	0.63 ± 0.07

temperature toward the end of drying. It was also observed that the sample temperature during the later stage of LPSSD-FIR was higher than that in the case of VACUUM-FIR. This is because in the case of LPSSD-FIR the far-infrared absorptivity of superheated steam is higher than that of air (Nimmol et al., 2007). More detailed explanation of the temperature evolutions during drying using methods employed in this study is available in Nimmol et al. (2007) and Thomkapanish, Suvarnakuta, and Devahastin (2007).

3.2. Pore structure characterization

The total porosity obtained from the 3D reconstructed images of banana slices are listed in Table 1. The porosity

values indicated that an increase in the drying temperature generally led to an increase in the porosity of the samples. This is because drying at a higher temperature resulted in a higher sample temperature and hence higher pressure gradients within the sample. These gradients in turn led to stronger evolution of moisture within the sample during drying resulting in higher values of the sample porosity.

At the same drying temperature, the use of FIR clearly resulted in an increase of the sample porosity in all cases. For example, at 90 °C a relative augmentation of about 32% and 37% was observed in the case of LPSSD and VACUUM, respectively, when FIR was used. This is due to the fact that during the processes applying FIR higher sample temperature was developed (see again Fig. 4). Consequently, the internal pressure gradients increased more

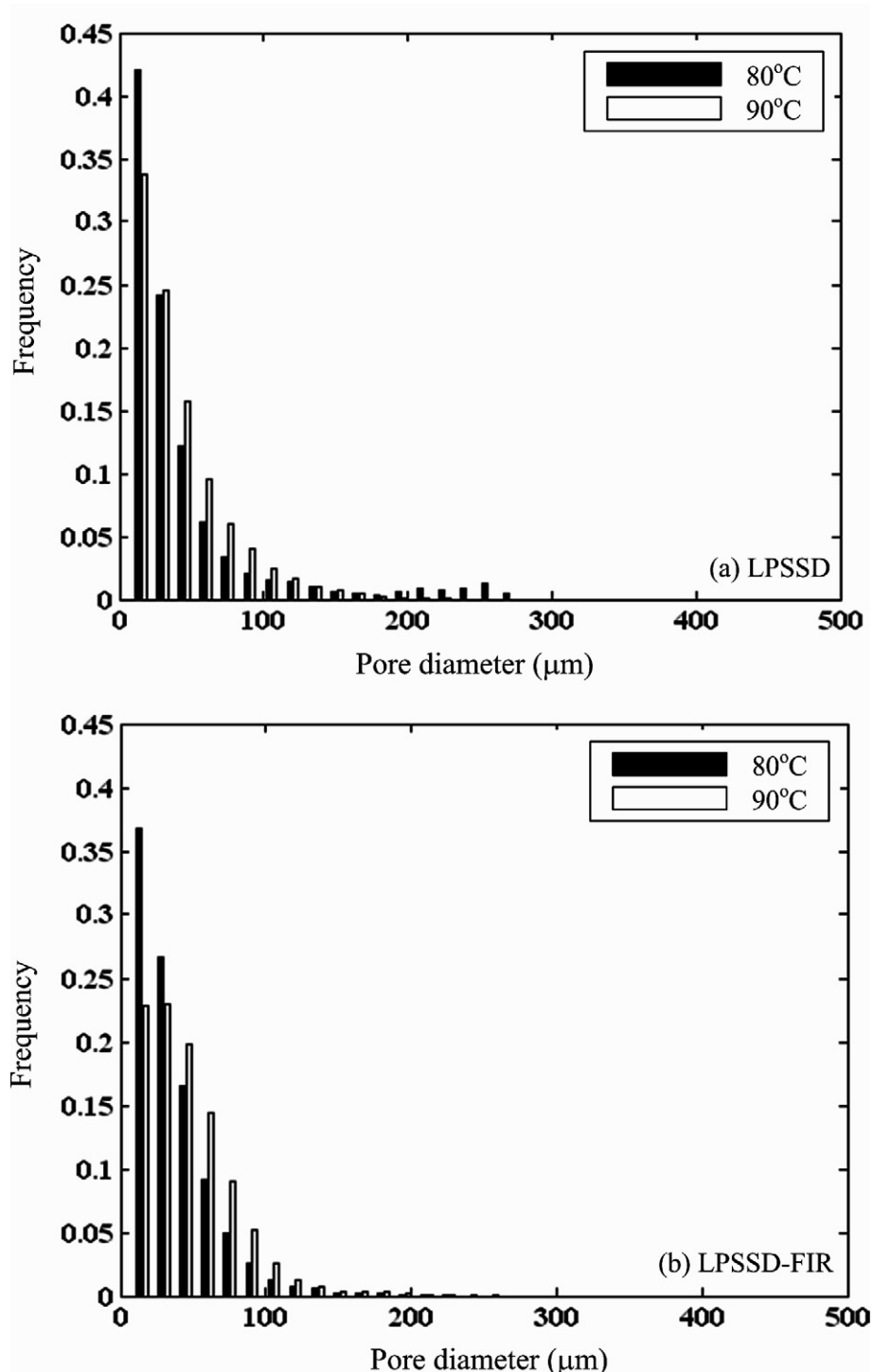


Fig. 5. Pore size distributions of the samples dried at 80 and 90 °C with (a) LPSSD and (b) LPSSD-FIR.

intensely leading to high-porosity products. It is also found from Table 1 that drying at a higher temperature led to the dried products with higher porosity in almost all cases, except for VACUUM. This may probably be due to the fact that, in the case of VACUUM, the stresses developed during drying at a higher temperature were larger and this led to a higher degree of microstructural deformation and collapse of structure leading to denser structure of the

product (Devahastin et al., 2004). No additional effect of FIR was also present to help expanding the sample structure as well in the case of VACUUM.

It should be noted from Table 1 that when drying was performed at a higher temperature (90 °C) the porosity values of LPSSD and LPSSD–FIR samples were higher than those of VACUUM and VACUUM–FIR samples, respectively. This is due to a rapid increase of the sample temper-

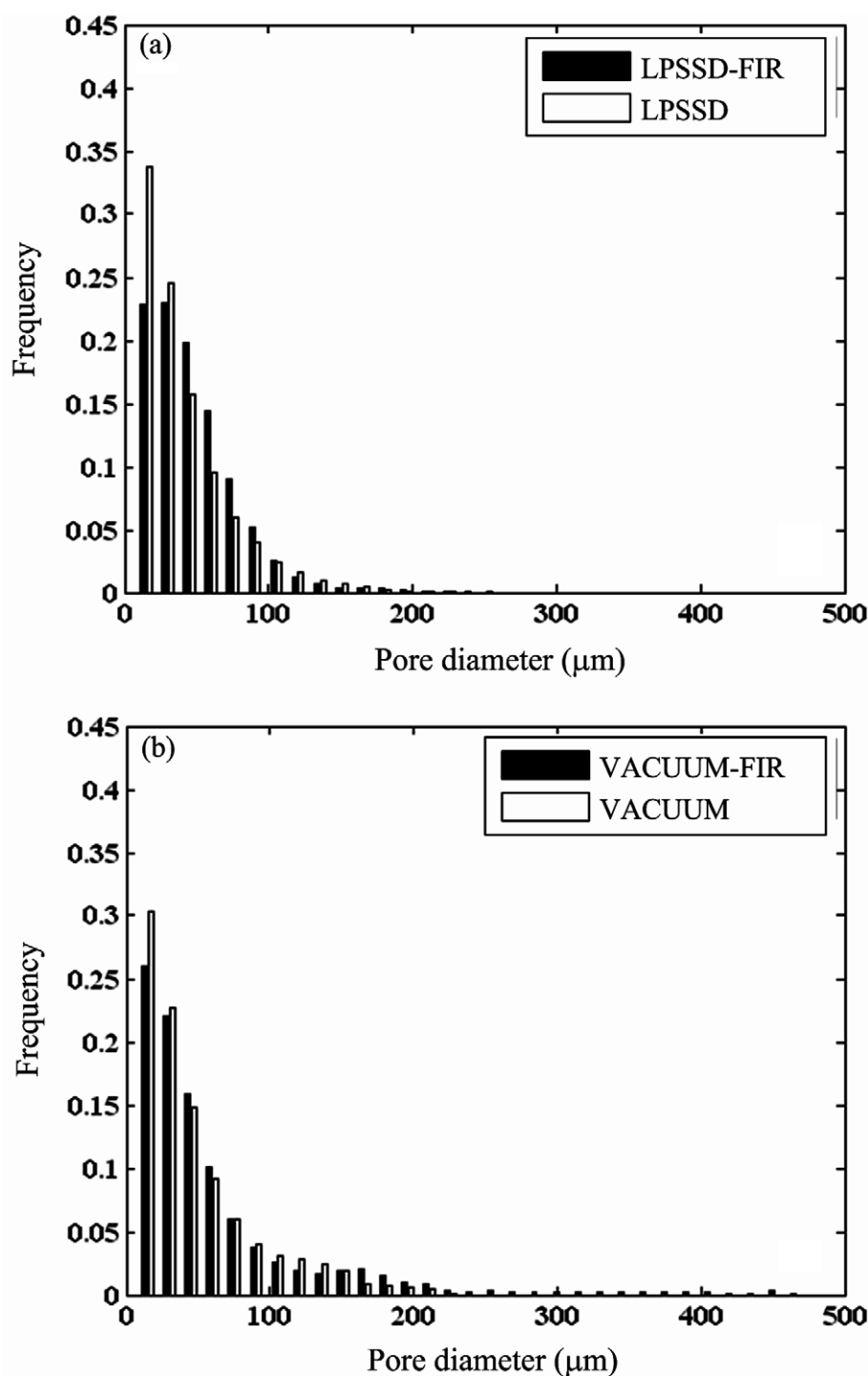


Fig. 6. Pore size distributions of the samples dried at 90 °C: (a) comparison between LPSSD–FIR and LPSSD dried samples and (b) comparison between VACUUM–FIR and VACUUM dried samples.

ature during initial stages of LPSSD and LPSSD–FIR (see Fig. 4b) resulting in rigorous boiling of moisture within the samples. However, the results were opposite when drying was performed at a lower temperature (80 °C). This may probably be due to the effect of an inversion phenomenon (Suvarnakuta, Devahastin, Soponronnarit, & Mujumdar, 2005), which happened somewhere between 80 and 90 °C in this case (Nimmol et al., 2007; Thomkapanish, et al., 2007). This effect could also be viewed from the evolution of the sample temperature. Although a rapid increase of the sample temperature during an initial stage was also observed in the cases of LPSSD and LPSSD–FIR at 80 °C, the period of constant sample temperature occurring afterwards was clearly found to be longer than that at 90 °C (see Fig. 4a). Consequently, moisture within the samples had less chance to boil rigorously leading to lower degrees of porosity.

The observed changes of porosity could be attributed to a modification of the pore size distribution. Fig. 5a and b show the histograms comparing the pore size distribution of the samples obtained at 80 and 90 °C with LPSSD and LPSSD–FIR, respectively. Fig. 6a and b show the histograms representing the pore size distribution of the samples obtained at 90 °C with LPSSD–FIR and LPSSD as well as VACUUM–FIR and VACUUM, respectively. These four figures clearly show that the pore sizes were non-normally distributed but that pores with sizes lower than 100 µm prevailed. The use of FIR as well as a higher drying temperature resulted in a shift of the distribution towards larger pore sizes for both drying techniques; the frequency of pores whose sizes were smaller than 50 µm clearly decreased. Moreover, for LPSSD experiments, there was a frequency increase of pores with sizes between 50 and 150 µm when the drying conditions were more intense, while for VACUUM experiments large pores appeared, especially in the case of VACUUM–FIR for which pores with diameters up to 450 µm were created.

4. Conclusions

X-ray microtomography coupled with 3D image analysis was used to study the effect of a combination of far-infrared radiation (FIR) with low-pressure superheated steam drying or vacuum drying. The results clearly showed that FIR and higher drying temperature led to an increase in the total porosity and the displacement of pore size towards larger sizes. The knowledge of the pore structure is essential in order to relate the quality of the product (e.g., shrinkage, rehydration and texture) to the drying conditions and hence the ability to optimize the drying processes better.

Regarding its possibilities and advantages in comparison with classical characterization techniques, X-ray microtomography will surely find a lot of applications in food engineering research. It is important to note here, however, that this measurement was limited to micron-size

pores although submicron and even nano-size pores can be as important.

Acknowledgements

A. Léonard is grateful to the FRS-FNRS (Fund for Scientific Research, Belgium) for a Postdoctoral Researcher position. S. Devahastin and C. Nimmol express their appreciation to the Commission on Higher Education, the Thailand Research Fund (TRF), the National Research Council of Thailand and the International Foundation for Science (IFS) in Sweden for their financial support.

References

- AOAC (1984). *Official methods of analysis* (14th ed.). Washington, DC, USA: Association of Official Analytical Chemists.
- Babin, P., Della Valle, G., Chiron, H., Cloetens, P., Hoszowska, J., Pernot, P., et al. (2006). Fast X-ray tomography analysis of bubble growth and foam setting during breadmaking. *Journal of Cereal Science*, 43, 393–397.
- Blacher, S., Calberg, C., Kerckhofs, G., Léonard, A., Wevers, M., Jérôme, R., et al. (2006). The porous structure of biodegradable scaffolds obtained with supercritical CO₂ as foaming agent. *Studies in Surface Science and Catalysis*, 160, 681–688.
- Blacher, S., Léonard, A., Heinrichs, B., Tcherkassova, N., Ferauche, F., Crine, M., et al. (2004). Image analysis of X-ray microtomograms of Pd–Ag/SiO₂ xerogel catalysts supported on Al₂O₃ foams. *Colloids and Surfaces A: Physicochemical and Engineering Aspects*, 241, 201–206.
- Devahastin, S., Suvarnakuta, P., Soponronnarit, S., & Mujumdar, A. S. (2004). A comparative study of low-pressure superheated steam and vacuum drying of a heat-sensitive material. *Drying Technology*, 22, 1845–1867.
- Haedelt, J., Pyle, D. L., Beckett, S. T., & Niranjana, K. (2005). Vacuum-induced bubble formation in liquid-tempered chocolate. *Journal of Food Science*, 70, E159–E164.
- Job, N., Sabatier, F., Pirard, J. P., Crine, M., & Léonard, A. (2006). Towards the production of carbon xerogel monoliths by optimizing convective drying conditions. *Carbon*, 44, 2534–2542.
- Léonard, A., Blacher, S., Marchot, P., Pirard, J. P., & Crine, M. (2004). Measurement of shrinkage and cracks associated to convective drying of soft materials by X-ray microtomography. *Drying Technology*, 22, 1695–1708.
- Léonard, A., Blacher, S., Marchot, P., Pirard, J. P., & Crine, M. (2005). Moisture profiles determination during convective drying using X-ray microtomography. *Canadian Journal of Chemical Engineering*, 83, 127–131.
- Léonard, A., Guiot, L., Pirard, J. P., Crine, M., Balligand, M., & Blacher, S. (2007). Non-destructive characterization of deer antlers by X-ray microtomography coupled with image analysis. *Journal of Microscopy*, 225, 258–263.
- Lim, K. S., & Barigou, M. (2004). X-ray micro-computed tomography of cellular food products. *Food Research International*, 37, 1001–1012.
- Nimmol, C., Devahastin, S., Swasdisevi, T., & Soponronnarit, S. (2007). Drying of banana slices using combined low-pressure superheated steam and far-infrared radiation. *Journal of Food Engineering*, 81, 624–633.
- Sahoo, P. K., Soltani, S., Wong, K. C., & Chen, Y. C. (1988). A survey of thresholding techniques. *Computer Vision, Graphics, and Image Processing*, 41, 233–260.
- Soille, P. (1999). *Morphological Image Analysis – Principles and Applications*. New York: Springer-Verlag.
- Suvarnakuta, P., Devahastin, S., Soponronnarit, S., & Mujumdar, A. S. (2005). Drying kinetics and inversion temperature in a low-pressure

- superheated steam-drying system. *Industrial and Engineering Chemistry Research*, 44, 1934–1941.
- Thomkapanish, O., Suvarnakuta, P., & Devahastin, S. (2007). Study of intermittent low-pressure superheated steam and vacuum drying of banana. *Drying Technology*, 25, 205–223.
- van Dalen, G., Blonk, H., van Haalts, H., & Hendriks, C. L. (2003). 3-D imaging of foods using X-ray microtomography. *G.I.T. Imaging and Microscopy*, 3, 18–21.
- Vinegar, H. J., & Wellington, S. L. (1987). Tomographic imaging of three-phase flow experiments. *Review of Scientific Instruments*, 58, 96–107.

Drying kinetics and quality of potato chips undergoing different drying techniques

Namtip Leeratanarak, Sakamon Devahastin *, Naphaporn Chiewchan

Department of Food Engineering, King Mongkut's University of Technology Thonburi, 91 Pracha u-tid Road, Bangkok 10140, Thailand

Received 1 May 2005; accepted 4 July 2005

Available online 26 August 2005

Abstract

Potato slices were dried using both low-pressure superheated steam drying (LPSSD) and hot air drying in this study. The effects of blanching as well as the drying temperature on the drying kinetics as well as various quality attributes of potato slices viz. color, texture, and brown pigment accumulation were also investigated. It was found that LPSSD took shorter time to dry the product to the final desired moisture content than that required by hot air drying when the drying temperatures were higher than 80 °C. Longer blanching time and lower drying temperature resulted in better color retention and led to chips of lower browning index. Blanching also reduced the hardness and shrinkage of the product; however, the use of different blanching periods did not significantly affect the product hardness. Drying methods had no obvious effect on the product quality except the browning index.

© 2005 Elsevier Ltd. All rights reserved.

Keywords: Blanching; Browning index; Color; Hardness; Hot air drying; Low-pressure superheated steam drying

1. Introduction

Potato chips have been popular snacks for more than a century (Pedreschi, Moyano, Kaack, & Granby, 2005) and its production is indeed a more competitive industry than other snack products (Garayo & Moreira, 2002). Currently, there are demands for low-fat or fat-free snack products, which have been the driving force of the snack food industry (Moreira, 2001). Drying as one of the most common preservation methods could therefore be a feasible alternative for production of low-fat or fat-free potato chips with desirable color and textural characteristics.

Many works have been performed to study hot air drying of potato pieces of various shapes (e.g., Krokida, Tsami, & Maroulis, 1998; McMinin & Magee, 1996; Wang & Brennan, 1995). Generally, it is found that hot air drying causes much quality degradation (in terms

of nutritional values, color, shrinkage and other organoleptic properties). Krokida, Maroulis, and Saravacos (2001) investigated the effects of drying methods on the color of dried potato and found that the conventional air drying caused extensive browning with a significant drop of the lightness and an increase in the redness and yellowness of dried potato. Khraisheh, McMinin, and Magee (2004) studied the quality and structural changes (in terms of vitamin C destruction, shrinkage and rehydration) of potato during microwave and convective drying. They reported that air drying led to higher vitamin C destruction than in the case of microwave drying. The rehydration potential of the air-dried sample was also lower than that of microwave-dried sample. Moreover, case hardening of the surface developed in the case of air-dried sample at higher temperatures and thus reduced the degree of shrinkage.

During the past decade the idea of using superheated steam to dry foods has been derived from other industries, e.g., paper and wood industries (Mujumdar,

* Corresponding author. Tel.: +662 470 9246; fax: +662 470 9240.
E-mail address: sakamon.dev@kmutt.ac.th (S. Devahastin).

1995), and has been applied as well to drying of potato. Caixeta, Moreira, and Castell-Perez (2002) studied the effects of impinging superheated steam temperature and convective heat transfer coefficient on the drying rate and quality attributes of potato chips. They found that the samples dried at higher steam temperatures and high convective heat transfer coefficients had less shrinkage, higher porosity, darker color, and lower vitamin C content. Unlike superheated steam drying (SSD) hot air drying produced less shrinkage because the air-dried samples developed hardened surfaces that increased the resistance to volume change. However, hot air drying led to chips of lower porosity, darker color, and lower vitamin C content. Moreira (2001) studied the use of superheated steam and hot air impingement drying for tortilla and potato chips. It was found that impingement drying with superheated steam could produce potato chips with less color deterioration and less vitamin C losses than drying with hot air. Iyota, Nishimura, Onuma, and Nomura (2001) experimentally determined the drying kinetics, surface conditions as well as color changes of potato slices using atmospheric-pressure SSD and hot air drying. They found that the samples dried by superheated steam were more glossy and there were no starch granules remain on the surface. On the other hand, starch gelatinization of the samples dried by hot air occurred more slowly than in the case of SSD. Non-gelatinized starch granules still remained on the surface of the product after the hot air drying process was completed.

Recently, a concept of using low-pressure superheated steam drying has been proposed as an alternative to dry heat-sensitive products (Chen, Chen, & Mujumdar, 1992; Devahastin, Suvarnakuta, Soponronnarit, & Mujumdar, 2004; Elustondo, Elustondo, & Urbicain, 2001) since it can combine the advantages of drying at reduced temperature to those of conventional atmospheric-pressure superheated steam drying (Mujumdar & Devahastin, 2000). Elustondo et al. (2001) studied sub-atmospheric pressure superheated steam drying of foodstuffs both experimentally and theoretically. Wood slab, shrimp, banana, apple, potato and cassava slice were dried using the steam pressures of 10,000–20,000 Pa, the steam temperatures of 60–90°C and the steam circulating velocities of 2–6 m/s. However, no mention about the dried product quality is given.

Prior to drying most food products are usually subjected to one form of pretreatments; among other methods hot water blanching is one of the most common techniques. Potato blanching helps inactivate enzymes that lead to some quality degradations (Moreno-Perez, Gasson-Lara, & Ortega-Rivas, 1996). Blanching also facilitates starch gelatinization that leads to the change of internal structure and influences the drying rate and quality of the dried product (Senadeera, Bhandari, Young, & Wijesinghe, 2000). The combined effects of

blanching and drying on the drying behavior and quality of the dried product are thus the interesting issues.

The present work is aimed at studying the effects of pretreatment (i.e., hot water blanching), drying methods and conditions on the drying kinetics and quality of potato chips in terms of color, texture, and browning index, which can be used as an indicator of quality deterioration causing from excessive heat treatment (Cohen, Birk, Mannheim, & Saguy, 1998). Low-pressure superheated steam drying (LPSSD) and the conventional hot air drying were selected for this comparative purpose.

2. Materials and methods

2.1. Materials

Fresh potato was obtained from a local supermarket and stored at 4°C. Prior to starting of each experiment it was washed, peeled, and sliced into chips of 3.5 ± 0.3 mm thickness. The sliced potato chips were blanched in hot water at $90 \pm 2^\circ\text{C}$ for 0, 1, 3, and 5 min with the ratio of potato to water of 0.015 g/g. Chips were then immediately cooled down in cold water (4°C) and placed on a paper towel to remove excess water prior to drying.

2.2. Experimental set-up and methods

A schematic diagram of the hot air dryer used is illustrated in Fig. 1. It consists of a stainless steel drying chamber, which is connected to an electric heater rated at 6.6 kW, which was used to heat up the air to the desired drying temperature; the heater was controlled by a PID temperature controller. The air velocity was controlled by a fan speed controller. In each experiment approximately 28 slices of potato were placed on the tray with a dimension of $30 \times 40 \text{ cm}^2$. Samples from the tray were collected at every 15 min interval for moisture content determination. Drying temperatures used were 70, 80, and 90°C while the constant inlet air velocity of 0.8 m/s was used.

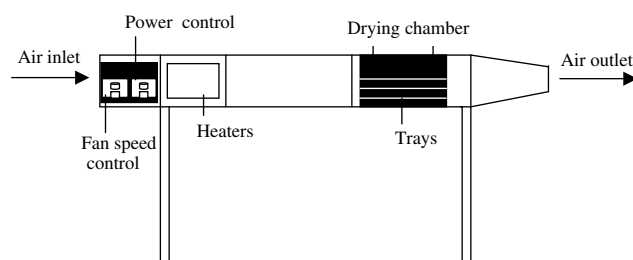


Fig. 1. A schematic diagram of hot air dryer and associated units.

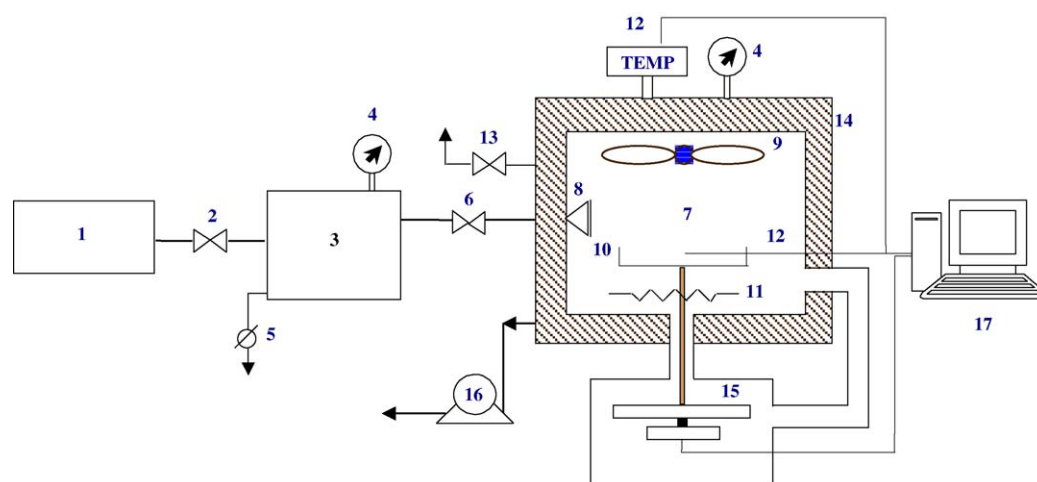


Fig. 2. A schematic diagram of the low-pressure superheated steam dryer and associated units: (1) boiler; (2) steam valve; (3) steam reservoir; (4) pressure gauge; (5) steam trap; (6) steam regulator; (7) drying chamber; (8) steam inlet and distributor; (9) electric fan; (10) sample holder; (11) electric heater; (12) on-line temperature sensor and logger; (13) vacuum break-up valve; (14) insulator; (15) on-line weight indicator and logger; (16) vacuum pump and (17) PC with installed data acquisition card.

A schematic diagram of the low-pressure superheated steam dryer and its accessories is shown in Fig. 2. The dryer consists of a stainless steel drying chamber, insulated with rock wool; a steam reservoir, which received steam from the boiler; and a liquid ring vacuum pump (Nash, ET32030, Trumbull, CT), which was used to maintain the vacuum in the drying chamber. Steam trap was installed to reduce the excess steam condensation in the reservoir. The steam inlet was made into a cone shape and was covered with a screen to help distributing the steam in the chamber. An electric fan was used to disperse steam throughout the drying chamber. An electric heater, rated at 1.5 kW, which was controlled by a PID controller (Omron, E5CN, Tokyo, Japan), was installed in the drying chamber to control the steam temperature and reduce steam condensation during the start-up period. The change of the mass of the sample was detected continuously using a load cell (Minebea, Ucg-3 kg, Nagano, Japan). The temperatures of the steam and of the drying sample were measured continuously using type K thermocouples. Thermocouple signals were multiplexed to a data acquisition card (Omega Engineering, CIO-DAS16Jr., Stamford, CT) installed in a PC. LABTECH NOTEBOOK software (version 12.1, Laboratory Technologies Corp., MA) was then used to read and record the temperature data. More detailed experimental set-up could be referred in Devahastin et al. (2004).

To perform a drying experiment approximately seven slices of potato were placed on the sample holder. Drying experiments were performed at the drying temperatures of 70, 80, and 90 °C and at an absolute pressure of 7 kPa. During drying mass of samples was recorded at every 1 min interval. The samples were dried until reaching the final moisture content of around 3.5%

(d.b.) (Caixeta et al., 2002), which is similar to that of commercially available potato chips (Pringle™ and Lay™) of 2–3% (d.b.).

Moisture content (AOAC, 1984), color, browning index, and hardness of the samples were measured. Preliminary test was also performed to evaluate the peroxidase activity and the degree of starch gelatinization of chips after blanching. The qualitative method described by Raganna (1982) was used to determine peroxidase activities of raw and blanched potato slices. All experiments were performed in duplicate and the mean values with standard deviations are reported.

2.3. Degree of starch gelatinization

Degree of starch gelatinization was evaluated using the differential scanning calorimetry method. Approximately 15 mg of sample was placed in an aluminum pan. The sample was then scanned from 25 to 160 °C at a heating rate of 10 °C/min by a differential scanning calorimeter (DSC) (Mettler Toledo DSC 822^e, Schwerzenbach, Switzerland). The degree of starch gelatinization was calculated using Eq. (1).

$$DG = \left(1 - \frac{\Delta H_g}{\Delta H_{\text{raw}}} \right) \times 100 \quad (1)$$

where DG is the degree of starch gelatinization (%), ΔH_g is the enthalpy of gelatinization of the sample (J/g), ΔH_{raw} is the enthalpy of gelatinization of the raw sample (J/g).

2.4. Color measurement

The color of samples were analyzed by measuring the reflectance using a colorimeter (JUKI, model JP7100,

Tokyo, Japan). Two degree North skylight was used as the light source. The colorimeter was calibrated against a standard white plate before each actual color measurement. For each sample at least five measurements were performed at different positions and the measured values (mean values) were compared with those of the same sample prior to drying. Three Hunter parameters, namely, L (lightness), a (redness/greenness), and b (yellowness/blueness) were measured and color changes were calculated by

$$\Delta L = \frac{L - L_0}{L_0}, \quad \Delta a = \frac{a - a_0}{a_0}, \quad \text{and} \quad \Delta b = \frac{b - b_0}{b_0} \quad (2)$$

where L , a , b represent the lightness, redness and yellowness of the dried samples, respectively, while L_0 , a_0 , b_0 represent the initial values of the lightness, redness and yellowness of the sample prior to drying, respectively.

2.5. Browning index

The browning index was determined using the procedure described by Hendel, Silveira, and Harrington (1955). The samples were ground and 2 g portion was extracted with 20 ml of 2% acetic acid solution (Carlo Erba, Val de Reuil, Italy) and then filtered through a filter paper (Whatman No. 3, Maidstone, England). An aliquot of the filtrate was mixed with an equal volume of acetone (Carlo Erba, Val de Reuil, Italy) and filtered again. The absorbance of the extracted color solution was measured at 420 nm using a spectrophotometer (Shimadzu, Model UV 2101 PC, Tokyo, Japan) using a 1 cm cell. The results are expressed in terms of the optical density.

2.6. Texture analysis

The texture of potato chips was evaluated by a compressive test using a texture analyzer (Instron 4301, Buckinghamshire, England). The test involved applying a direct force to the sample, which was placed on the hollow planar base. A 3 mm cylindrical probe was inserted at a constant rate of 2 mm/s until it cracked the sample (Moreno-Perez et al., 1996). The maximum compression force of a rupture test of each sample was used to describe the sample texture (in terms of hardness).

2.7. Statistical analysis

All data were analyzed using the analysis of variance (ANOVA). The Duncan's test was used to establish the multiple comparisons of mean values. Mean values were considered at 95% significance level ($\alpha = 0.05$). A statistical program SPSS was used to perform all statistical calculations.

3. Results and discussion

3.1. Effect of blanching on potato slices

From peroxidase activity determination the results showed that peroxidase did not exist after blanching, even for 1 min. Thus, the effect of enzymatic browning during subsequent drying could be neglected in the case of blanched samples. Potato slices blanched at various periods also had different degrees of starch gelatinization, which are shown in Table 1.

3.2. Drying kinetics of potato chips

Raw and blanched potato slices with initial moisture contents in the range of 445.41–599.3% (d.b.) (or 81.67–85.7% (w.b.)) were dried until reaching their equilibrium moisture contents. Fig. 3 shows the drying curves of potato chips undergoing hot air drying at various conditions. It was found that drying at higher temperature took shorter time to reach the desired moisture content because of a larger driving force for heat transfer. Moisture diffusivity is also higher at higher drying temperature. Similar results were observed for chips underwent any blanching conditions. However, it was found that the blanched samples dried faster than the unblanched one. This behavior was probably due to structure softening due to blanching that might facilitate water removal (Severini, Baiano, Pilli, Carbone, & Derossi, 2005; Potter & Hotchkiss, 1998). When the tissue was blanched or cooked the cells might become more permeable to moisture. However, excessive blanching time decreased the rate of moisture removal. This might be due to the effect of starch gelatinization, structural changes, and water content absorbed during blanching. Higher degree of starch gelatinization might affect the cell structure and increase the internal resistance to moisture movement, which resulted in lower diffusivity (Maté, Quartaert, Meerdink, & van't Riet, 1998). Therefore, the samples blanched for 1 min resulted in the highest drying rates followed by those blanched for 3 and 5 min, respectively; unblanched potato chips had the lowest drying rates for all drying conditions. However, it was found that, at higher drying temperatures, the drying rates of samples treated with different

Table 1
Degree of starch gelatinization of potato slices blanched for various periods

Blanching time (min)	Enthalpy (J/g)	Degree of starch gelatinization (%)
0	5.48	0.00
1	1.98	63.96
3	1.87	65.88
5	0.99	81.93

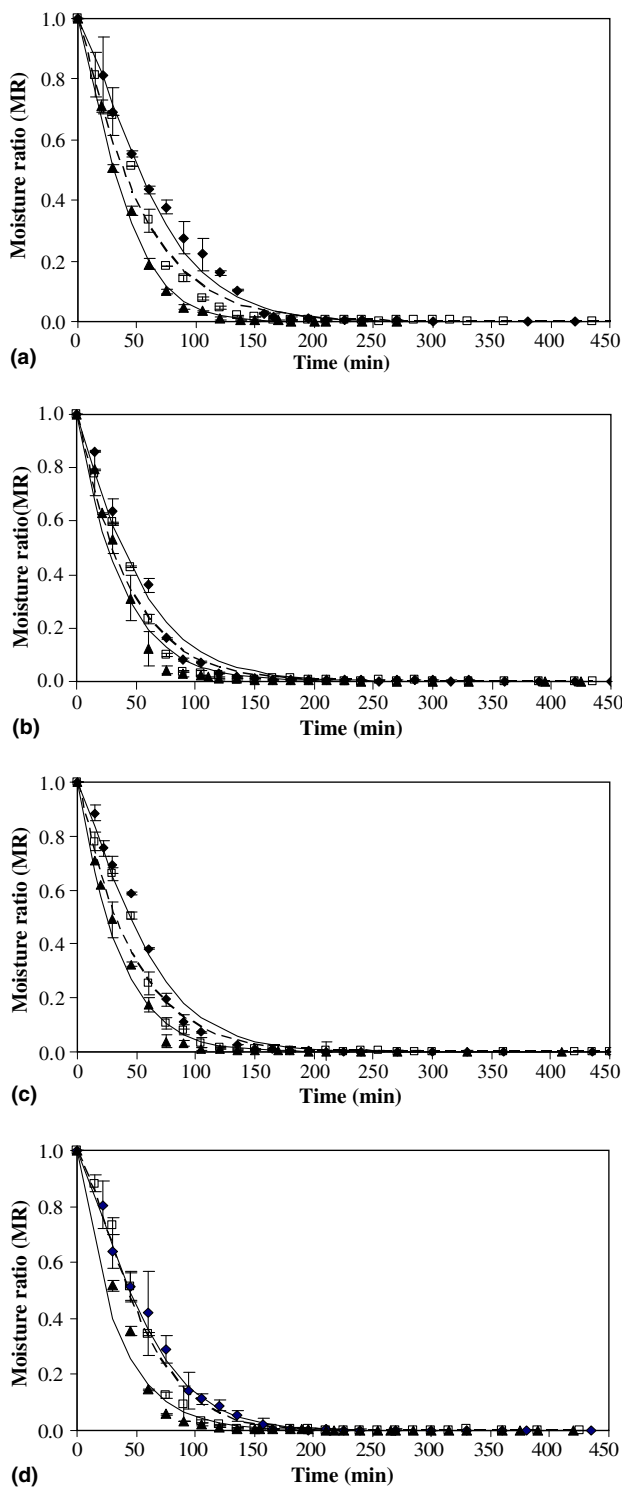


Fig. 3. Drying curves of potato chips underwent blanching at (a) 0, (b) 1, (c) 3, and (d) 5 min in a hot air dryer at 70°C (◆), 80°C (□), 90°C (▲).

blanching periods were not obviously different. So, the effect of drying temperature was greater than the effect of blanching time at higher drying temperatures.

Fig. 4 shows the drying curves of potato slices undergoing low-pressure superheated steam drying at various

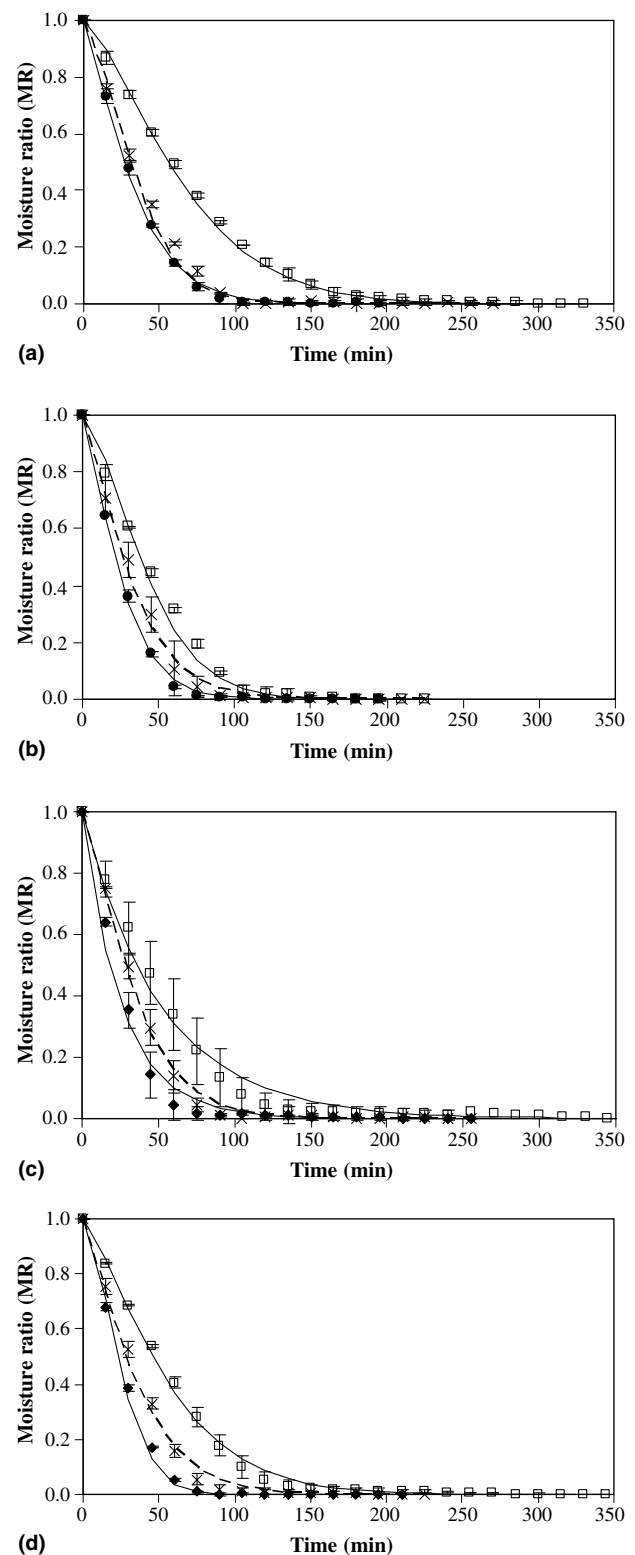


Fig. 4. Drying curves of potato chips underwent blanching at (a) 0, (b) 1, (c) 3, and (d) 5 min in a low-pressure superheated steam dryer at 70°C (□), 80°C (×), 90°C (◆).

conditions. Similar to hot air drying higher drying temperature resulted in a faster reduction of moisture

content. Blanching time also had an effect on the drying rates at all drying temperatures as observed in the case of hot air drying. The blanched sample again dried faster than the unblanched one; the effect of blanching time was again smaller at higher drying temperatures.

Considering the drying rates of hot air drying and LPSSD it was found that the drying rates of the two drying methods were not different at a low drying temperature (70 °C). However, LPSSD yielded higher drying rates when the drying temperature was higher than 80 °C for all blanching conditions. This suggests that the effective inversion temperature calculated from the overall drying rates is somewhere between 70 and 80 °C (Suvarnakuta, Devahastin, Soponronnarit, & Mujumdar, 2005). Fig. 5 illustrates the drying curves of the samples blanched for 5 min undergoing both dry-

ing methods. The results of samples treated with different blanching periods (e.g., 0, 1, and 3 min) were similar to that of 5 min.

4. Quality of dried potato chips

4.1. Color

Table 2 illustrates the color changes of potato chips in terms of color differences, $\Delta L/L_0$, $\Delta a/a_0$, and $\Delta b/b_0$. Since the enzymes that caused the quality degradation were destroyed during blanching, the non-enzymatic browning was considered a major cause of color changes of dried potato chips. In the case of lightness it was found that the drying method and drying temperature did not as significantly affect the change of lightness as blanching time did. However, the reduction of lightness ($\Delta L/L_0$) was greater at higher drying temperatures for both drying methods although the results were not significantly different.

Regarding the change of redness of dried potato chips the drying temperature, blanching time and their interaction had significant influences on this color parameter under certain conditions. It was observed that all dried potato chips were redder than the fresh potato, however, LPSSD led to smaller increase of a value than hot air drying but the results were again not significantly different. Regarding the effect of the drying temperature higher drying temperature led to an increase of a value for both drying methods at all blanching conditions. The above results were due to Maillard reaction or heat damage that occurred more at higher drying temperatures. The changes of redness of blanched chips treated at 90 °C were significantly higher than those at 70 °C but did not statistically differ from those at 80 °C for both drying methods.

For the effect of blanching unblanched chips had higher a values than those of blanched samples and thus resulted in greater changes of $\Delta a/a_0$ values at all drying temperatures. Blanching reduced the a value of potato chips due to the leaching out of reducing sugars, which are the substrates of Maillard reaction, prior to drying and thus minimized the non-enzymatic browning reaction and led to less red chips. These results are similar to those reported by Pedreschi et al. (2005).

The yellowness (b value) of dried potato chips was affected by blanching while the drying method and drying temperature did not show any significant influence on the b value. The unblanched potato chips showed an obvious reduction of the yellowness (lower $\Delta b/b_0$ values) after drying. In other words, blanched potato chips showed relative stability of yellowness. Potato chips dried at lower temperatures tended to have higher values of yellowness than those dried at higher temperatures. It was also observed that shorter blanching time led to

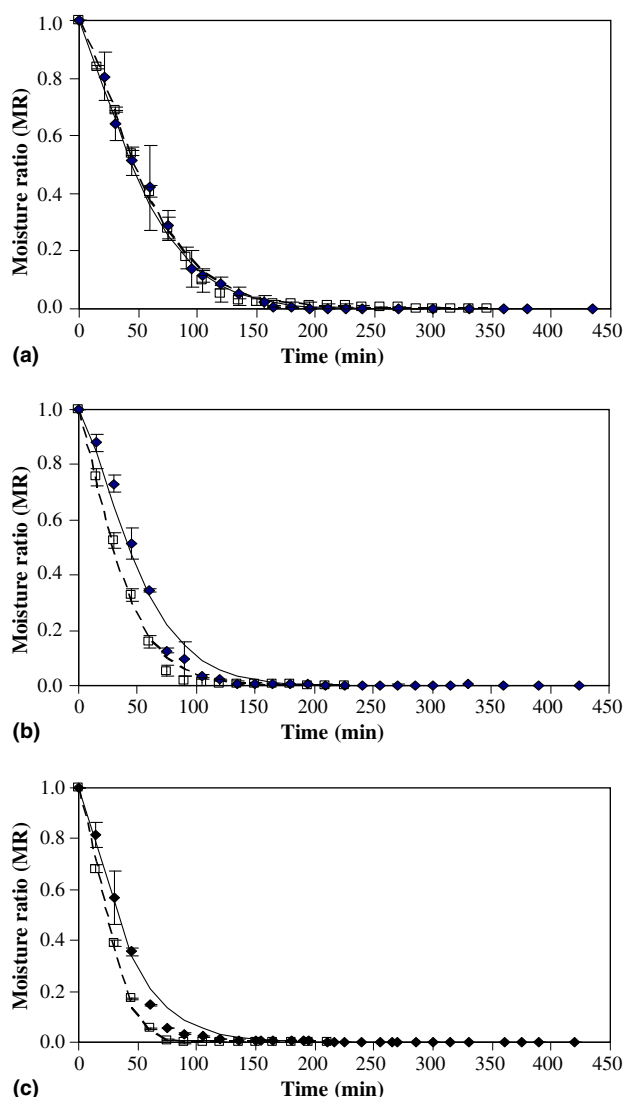


Fig. 5. Drying curves of potato chips undergoing hot air drying (♦), and LPSSD (□) at drying temperatures of (a) 70 °C, (b) 80 °C, and (c) 90 °C.

Table 2

Effects of drying method, drying temperature, and blanching time on color changes and browning index of dried potato chips

Drying method	Drying temp (°C)	Blanching time (min)	$\Delta L/L_0$	$\Delta a/a_0$	$\Delta b/b_0$	Browning index
Hot air drying	70	0	-0.769 ± 0.004^a	1.305 ± 0.067^{abcde}	-0.797 ± 0.085^d	0.076 ± 0.019^{ab}
		1	-0.085 ± 0.047^{cd}	0.483 ± 0.087^f	0.603 ± 0.097^{ab}	0.071 ± 0.008^{ab}
		3	-0.037 ± 0.002^d	0.536 ± 0.076^f	0.542 ± 0.033^{abc}	0.063 ± 0.003^a
		5	-0.146 ± 0.066^{cd}	0.556 ± 0.003^f	0.546 ± 0.072^{abc}	0.039 ± 0.005^a
	80	0	-0.792 ± 0.048^a	1.336 ± 0.048^{abcde}	-0.810 ± 0.045^d	0.256 ± 0.058^g
		1	-0.143 ± 0.014^{cd}	0.845 ± 0.053^{def}	0.563 ± 0.037^{abc}	0.207 ± 0.017^{efg}
		3	-0.113 ± 0.047^{cd}	0.998 ± 0.076^{cdef}	0.435 ± 0.030^{abc}	0.184 ± 0.005^{de}
		5	-0.145 ± 0.078^{cd}	1.028 ± 0.022^{bcdef}	0.697 ± 0.069^{ab}	0.14 ± 0.007^{cd}
	90	0	-0.812 ± 0.073^a	1.897 ± 0.020^a	-0.826 ± 0.023^d	0.755 ± 0.043^m
		1	-0.221 ± 0.020^{bcd}	1.471 ± 0.025^{abcd}	0.259 ± 0.027^{bc}	0.557 ± 0.041^l
		3	-0.197 ± 0.013^{bcd}	1.573 ± 0.073^{abc}	0.179 ± 0.063^{bc}	0.436 ± 0.028^k
		5	-0.223 ± 0.033^{bcd}	1.448 ± 0.070^{abcd}	0.239 ± 0.028^{bc}	0.360 ± 0.023^{hi}
LPSSD	70	0	-0.655 ± 0.073^a	1.220 ± 0.010^{bcde}	-0.604 ± 0.020^d	0.075 ± 0.001^{ab}
		1	-0.021 ± 0.063^d	0.722 ± 0.062^{ef}	1.069 ± 0.098^a	0.070 ± 0.001^{ab}
		3	0.005 ± 0.058^d	0.497 ± 0.016^f	0.710 ± 0.006^{ab}	0.062 ± 0.006^a
		5	-0.117 ± 0.006^{cd}	0.540 ± 0.044^f	0.903 ± 0.014^{ab}	0.045 ± 0.008^a
	80	0	-0.707 ± 0.021^a	1.283 ± 0.012^{abcde}	-0.669 ± 0.077^d	0.246 ± 0.008^{fg}
		1	-0.214 ± 0.094^{bcd}	1.261 ± 0.012^{abcde}	0.631 ± 0.089^{ab}	0.193 ± 0.012^{def}
		3	-0.211 ± 0.068^{bcd}	0.960 ± 0.043^{cdef}	0.484 ± 0.067^{abc}	0.166 ± 0.043^{cde}
		5	-0.101 ± 0.025^{cd}	0.971 ± 0.090^{cdef}	0.769 ± 0.054^{ab}	0.124 ± 0.007^{bc}
	90	0	-0.726 ± 0.088^a	1.676 ± 0.029^{ab}	-0.679 ± 0.032^d	0.564 ± 0.011^l
		1	-0.427 ± 0.007^b	1.417 ± 0.047^{abcd}	-0.149 ± 0.02^{cd}	0.429 ± 0.025^{jk}
		3	-0.292 ± 0.047^{bc}	1.472 ± 0.089^{abcd}	0.245 ± 0.048^{bc}	0.381 ± 0.040^{ji}
		5	-0.303 ± 0.028^{bc}	1.486 ± 0.051^{abcd}	0.294 ± 0.038^{bc}	0.322 ± 0.038^h

Different superscripts in the same column mean that the values are significantly different at 95% confidence level ($\alpha = 0.05$).

higher b values but the results were again not significantly different.

4.2. Browning index

The effects of blanching, drying method and drying temperature on the browning index of potato chips are shown in Table 2. The results were significantly different between the two drying methods at high drying temperatures. Hot air drying resulted in higher browning index than did LPSSD at higher drying temperatures but there was no difference between the two methods at low temperatures. This is due to the difference in surface temperature of potato during drying. In the constant drying rate period the surface temperature of potato chips undergoing hot air drying at 70, 80, and 90°C were equal to the wet-bulb temperature, which was 41, 44, and 48°C, respectively. In the case of LPSSD the surface temperature of potato chips was equal to the saturation temperature at the operating pressure (i.e., 7 kPa) or about 40°C. As the drying temperature increased, of course, the wet-bulb temperature also increased. This increase in turn led to larger differences in browning index between the chips treated with different drying methods at higher drying temperatures. The highest value of browning index was obtained in the case of air-dried sample at 90°C. A higher degree of non-enzymatic browning occurring during hot air drying might be due to both Maillard reaction and ascorbic acid oxida-

tion. In the case of LPSSD there was no oxygen left in the drying chamber and the main cause of non-enzymatic browning could be only Maillard reaction.

The results of the browning index were also related to the color changes, especially the change of redness. The results showed similar trends for both physical and chemical changes. From the results of color changes and browning index it might be concluded that hot air drying resulted in more severe chemical damage of potato chips than did LPSSD. Browning occurring in hot air drying was due to Maillard reaction and ascorbic acid oxidation while LPSSD possible led to only Maillard reaction. It might be implied that LPSSD could better preserve quality, especially nutrients, than hot air drying at the same drying temperature.

4.3. Texture

The texture of dried potato chips is reported in terms of hardness, which is the maximum breaking force, and the results are shown in Table 3. It was found that blanching and drying temperature significantly affected the hardness of potato chips under certain conditions while the drying method did not show any significant influence on the hardness. Generally, blanching caused starch gelatinization, softening of structure and led to less hardness of dried starchy products. It was observed in this work that unblanched chips had the maximum hardness in all cases; blanching only led to significantly

Table 3
Effects of drying method, drying temperature, and blanching time on hardness of dried potato chips

Drying method	Drying temp (°C)	Blanching time (min)	Maximum force (N)
Hot air drying	70	0	6.256 ± 0.914 ^{ab}
		1	4.890 ± 0.671 ^{bcd}
		3	4.843 ± 0.417 ^{bcd}
		5	4.537 ± 1.267 ^{bcd}
	80	0	6.283 ± 1.163 ^{ab}
		1	4.633 ± 0.257 ^{bcd}
		3	4.769 ± 0.632 ^{bcd}
		5	4.810 ± 0.743 ^{bcd}
	90	0	5.446 ± 0.263 ^{bcd}
		1	3.191 ± 0.474 ^{cde}
		3	3.136 ± 0.067 ^{de}
		5	3.121 ± 0.244 ^{de}
LPSSD	70	0	7.956 ± 0.600 ^a
		1	5.520 ± 0.215 ^{bc}
		3	5.670 ± 0.503 ^b
		5	5.518 ± 0.155 ^{bc}
	80	0	5.859 ± 0.124 ^{ab}
		1	4.721 ± 1.682 ^{bcd}
		3	4.588 ± 0.484 ^{bcd}
		5	4.603 ± 1.086 ^{bcd}
	90	0	4.796 ± 0.578 ^{bcd}
		1	2.991 ± 0.349 ^e
		3	2.834 ± 0.413 ^e
		5	2.814 ± 0.163 ^e

Different superscripts in the same column mean that the values are significantly different at 95% confidence level ($\alpha = 0.05$).

less hard chips only in the case of LPSSD at low temperature (70°C), however. This might be due to the effect of casehardening developed during moisture removal. In the case of hot air drying casehardened skin occurred in all cases and overshadowed the effect of blanching on the hardness of the chips. As a result, no statistical difference between blanched and unblanched air-dried chips was observed. On the other hand, LPSSD tended to protect the integrity of the surface better and casehardening seemed to occur only at higher drying temperatures (i.e., 80 and 90°C). This similar behavior has also been reported by other workers who studied superheated steam in general (Mujumdar, 1995). Different blanching periods did not seem to alter the hardness of the chips in all cases.

Although potato chips underwent LPSSD, which led to puffing at higher drying temperatures, were obviously less hard than those treated with hot air drying based on human perception, the results were not statistically different between the two drying methods. This could be due to a large variation of the experimental results caused by the non-uniform or heterogeneous nature of raw potato.

Fig. 6 illustrated the maximum breaking force of steam-dried chips treated with different blanching periods and drying temperatures in comparison with those of commercial products. The maximum breaking forces

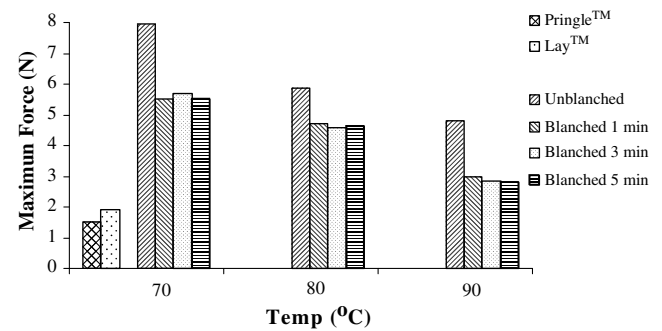


Fig. 6. Hardness of potato chips blanched for different periods and underwent LPSSD at different drying temperatures compared with the commercial products.

of the commercially available potato chips, which are Lay™ and Pringle™, are 1.919 ± 0.248 and 1.517 ± 0.338 N, respectively. It was found that potato chips treated with LPSSD at 90°C (with 5 min blanching time), which puffed more than those treated with other conditions and consequently required the lowest force of compression (Table 3), were still harder than the commercial products.

5. Conclusions

The effects of blanching time, drying methods and conditions on the drying kinetics and quality of potato chips were examined in this study. In terms of drying kinetics blanching time as well as drying temperature were found to have effects on the moisture reduction rate of samples, both in cases of hot air drying and LPSSD. It was found that blanching could increase the drying rates of both hot air drying and LPSSD. Moreover, LPSSD took shorter time to dry the product to the final desired moisture content than that of hot air drying when the drying temperatures were higher than 80°C.

The quality study showed that blanching led to better color retention, less hardness and lower degree of browning of chips. Regarding the drying method, LPSSD provided better quality chips than hot air drying in terms of the browning index, especially at high drying temperatures. No significant effect of the drying method on the hardness was observed, however. Casehardening seemed to overshadow the effect of blanching on the hardness of the chips at all drying conditions except in the case of LPSSD at low temperature.

A blanching time of 5 min followed by LPSSD at 90°C at an absolute pressure of 7 kPa was proposed as the best condition for drying potato chips in this study. These conditions gave puffed product, less hard with moderate browning index, which corresponded to less nutrients and other heat damages. These conditions

also provided potato chips that had small changes of colors from their natural values and required shortest drying time. However, the best condition proposed still led to chips of inferior quality compared with the commercially available potato chips, especially in terms of hardness. The study of the combined effects of blanching and/or freezing pretreatments with higher drying temperature is recommended for future work.

Acknowledgement

The authors express their sincere appreciation to the Commission on Higher Education, the Thailand Research Fund (TRF) and the International Foundation for Science (IFS), Sweden for supporting this study financially.

References

- AOAC (1984). *Official method of analysis* (14th ed.). Washington DC: Association of Official Agricultural Chemists.
- Caixeta, A. T., Moreira, R., & Castell-Perez, M. E. (2002). Impingement drying of potato chips. *Journal of Food Process Engineering*, 25, 63–90.
- Chen, S. R., Chen, J. Y., & Mujumdar, A. S. (1992). Preliminary study of steam drying of silkworm cocoons. *Drying Technology*, 10, 251–260.
- Cohen, E., Birk, Y., Mannheim, C. H., & Saguy, I. S. (1998). A rapid method to monitor quality of apple juice during thermal processing. *Lebensmittel-Wissenschaft und-Technologie*, 31, 612–616.
- Devahastin, S., Suvarnakuta, P., Soponronnarit, S., & Mujumdar, A. S. (2004). A comparative study of low-pressure superheated steam and vacuum drying of a heat-sensitive material. *Drying Technology*, 22, 1845–1867.
- Elustondo, D., Elustondo, M. P., & Urbicain, M. J. (2001). Mathematical modeling of moisture evaporation from foodstuffs exposed to sub-atmospheric pressure superheated steam. *Journal of Food Engineering*, 49, 15–24.
- Garayo, J., & Moreira, R. (2002). Vacuum frying of potato chips. *Journal of Food Engineering*, 55, 181–191.
- Hendel, C. E., Silveira, V. G., & Harrington, W. O. (1955). Rates of non-enzymatic browning of white potato during dehydration. *Food Technology*, 9, 433–438.
- Khraisheh, M. A. M., McMin, W. A. M., & Magee, T. R. A. (2004). Quality and structural changes in starchy foods during microwave and convective drying. *Food Research International*, 37, 497–503.
- Krokida, M. K., Maroulis, Z. B., & Saravacos, G. D. (2001). The effect of the method of drying on the colour of dehydrated products. *International Journal of Food Science and Technology*, 36, 53–59.
- Krokida, M. K., Tsami, E., & Maroulis, Z. B. (1998). Kinetics on color changes during drying of some fruits and vegetables. *Drying Technology*, 16, 667–685.
- Iyota, H., Nishimura, N., Onuma, T., & Nomura, T. (2001). Drying of sliced raw potatoes in superheated steam and hot air. *Drying Technology*, 19, 1411–1424.
- McMin, W. A. M., & Magee, T. R. A. (1996). Air drying kinetics of potato cylinders. *Drying Technology*, 14, 2025–2040.
- Maté, J. I., Quartaert, C., Meerdink, G., & van't Riet, K. (1998). Effect of blanching on structural quality of dried potato slices. *Journal of Agricultural and Food Chemistry*, 46, 676–681.
- Moreira, R. G. (2001). Impingement drying of food using hot air and superheated steam. *Journal of Food Engineering*, 49, 291–295.
- Moreno-Perez, L. F., Gasson-Lara, J. H., & Ortega-Rivas, E. (1996). Effect of low temperature-long time blanching on quality of dried sweet potato. *Drying Technology*, 14, 1839–1857.
- Mujumdar, A. S. (1995). Superheated steam drying (Second ed.). In A. S. Mujumdar (Ed.). *Handbook of industrial drying* (Vol. 2, pp. 1071–1086). New York: Marcel Dekker.
- Mujumdar, A. S., & Devahastin, S. (2000). Fundamental principles of drying. In S. Devahastin (Ed.), *Mujumdar's practical guide to industrial drying* (pp. 1–22). Brossard: Exergex.
- Pedreschi, F., Moyano, P., Kaack, K., & Granby, K. (2005). Color changes and acrylamide formation in fried potato slices. *Food Research International*, 38, 1–9.
- Potter, N. M., & Hotchkiss, J. H. (1998). In *Food science* (5th ed., pp. 207–211). Gaithersburg: Aspen Publisher.
- Raganna, S. (1982). *Manual of analysis of fruit and vegetable products*. New Delhi: Tata McGraw-Hill.
- Senadeera, W., Bhandari, B., Young, G., & Wijesinghe, B. (2000). Physical property changes of fruits and vegetables during hot air drying. In A. S. Mujumdar (Ed.), *Drying technology in agriculture and food sciences* (pp. 159–161). Enfield: Science Publishers.
- Severini, C., Baiano, A., Pilli, T. D., Carbone, B. F., & Derossi, A. (2005). Combined treatments of blanching and dehydration: Study on potato cubes. *Journal of Food Engineering*, 68, 289–296.
- Suvarnakuta, P., Devahastin, S., Soponronnarit, S., & Mujumdar, A. S. (2005). Drying kinetics and inversion temperature in a low-pressure superheated steam drying system. *Industrial & Engineering Chemistry Research*, 44, 1934–1941.
- Wang, N., & Brennan, J. G. (1995). Changes in structure, density and porosity of potato during dehydration. *Journal of Food Engineering*, 24, 61–76.

This article was downloaded by: [2007 King Mongkut's University of Technology Thonburi]
[2007 King Mongkut's University of Technology Thonburi]

On: 12 July 2007

Access Details: [subscription number 780012218]

Publisher: Taylor & Francis

Informa Ltd Registered in England and Wales Registered Number: 1072954

Registered office: Mortimer House, 37-41 Mortimer Street, London W1T 3JH, UK



Drying Technology An International Journal

Publication details, including instructions for authors and subscription information:

<http://www.informaworld.com/smpp/title-content=t713597247>

Errata

Online Publication Date: 01 June 2007

To cite this Article: , (2007) 'Errata', Drying Technology, 25:6, 1127

To link to this article: DOI: 10.1080/07373930701402622

URL: <http://dx.doi.org/10.1080/07373930701402622>

PLEASE SCROLL DOWN FOR ARTICLE

Full terms and conditions of use: <http://www.informaworld.com/terms-and-conditions-of-access.pdf>

This article maybe used for research, teaching and private study purposes. Any substantial or systematic reproduction, re-distribution, re-selling, loan or sub-licensing, systematic supply or distribution in any form to anyone is expressly forbidden.

The publisher does not give any warranty express or implied or make any representation that the contents will be complete or accurate or up to date. The accuracy of any instructions, formulae and drug doses should be independently verified with primary sources. The publisher shall not be liable for any loss, actions, claims, proceedings, demand or costs or damages whatsoever or howsoever caused arising directly or indirectly in connection with or arising out of the use of this material.

© Taylor and Francis 2007

Errata

The following text provides errata for the publication noted below.

Kerdpi boon, S.; Devahastin, S. Fractal characterization of some physical properties of a food product under various drying conditions. *Drying Technology* **2007**, 25, 135–146.

The authors regret any inconvenience caused.

On page 145, right column:

The normalized change of fractal dimension could be used to monitor the physical property changes of carrot during drying. For example, at $\Delta FD/FD_o$ of around 0.06, the percentage of shrinkage was around 70–80% in all HAD and LPSSD cases (Figs. 12 and 13). This kind of relationship was also observed at other $\Delta FD/FD_o$ and percentage of shrinkage values. These results are supported by results presented in Fig. 14, which illustrates the microstructure of the samples at $\Delta FD/FD_o$ of 0.06 when drying

with HAD at 60°C, 1 m/s, 150 min; 70°C, 1 m/s, 120 min; 80°C, 1 m/s, 90 min; LPSSD at 60°C, 7 kPa, 210 min; 70°C, 7 kPa, 150 min; and 80°C, 7 kPa, 90 min. All of the samples had similar levels of shrinkage although they had different microstructure. However, they all had the same $\Delta FD/FD_o$ values. The deviations in the percentage of shrinkage might arise from the errors that occurred during the collection of the experimental data.

On the other hand, values of the rehydration ratio at the same $\Delta FD/FD_o$ were quite different. For instance, at $\Delta FD/FD_o$ of around 0.06, the rehydration ratio was around 2.8–3.0 at all conditions of HAD while the rehydration ratio was around 2.0–2.2 at all conditions of LPSSD (Figs. 12 and 13). However, $\Delta FD/FD_o$ could be used to correlate the rehydration behavior of samples dried using the same type of dryer.

5 Low-pressure superheated steam drying of food products

Sakamon Devahastin and Peamsuk Suvarnakuta

5.1 INTRODUCTION

Although the concept of superheated steam drying (SSD) was originally proposed over a century ago and the first industrial applications were reported some 60 years ago (Mujumdar, 2000, 2007), SSD has only recently re-emerged as an alternative drying technology for a wider array of products including woods (Pang, 1997; Pang and Dakin, 1999), paper (Douglas, 1994) as well as foods and biomaterials (Devahastin and Suvarnakuta, 2004). SSD involves the use of superheated steam in a direct (convective) dryer in place of hot air, combustion, or flue gases as the drying medium to supply heat for drying and to carry away the evaporated moisture. Any direct or direct/indirect (e.g. combined convection/conduction) dryer can be, in principle, operated as a superheated steam dryer although, in practice, this conversion may not always be straightforward.

In addition to the energy-related advantages reported by many researchers (Mujumdar, 2000; Devahastin and Suvarnakuta, 2004), SSD also possesses many other advantages that are of special interest to processors of foods and biomaterials. Generally, no oxidative reactions, e.g. enzymatic browning (Nimmol *et al.*, 2007; Thomkapanish *et al.*, 2007), lipid oxidation or aerobic degradation of vitamins (Suvarnakuta *et al.*, 2005a), are possible in SSD due to lack of oxygen.

SSD can also help decontaminate micro-organisms, toxins and spores due to its normally high-temperature environment, even during an early stage of drying (Pronyk *et al.*, 2006; Cenkowski *et al.*, 2007). A combination of drying with other thermal treatments, for example, blanching (Iyota *et al.*, 2001; Prachayawarakorn *et al.*, 2002; Namsanguan *et al.*, 2004; Sotome *et al.*, 2006), deodorization (Furukawa and Akao, 1983), parboiling (Soponronnarit *et al.*, 2006), pasteurization and sterilization (Abe and Miyashita, 2006) as well as popping (Iyota *et al.*, 2005) is also possible.

Another advantage of SSD is that, for certain foods or vegetables, the porosity of the products dried in superheated steam is higher than that dried in hot air. This is due to the evolution of steam within the product, which decreases the bulk density of the product while enhancing its rehydration characteristics. This feature is especially attractive for the instant food as well as confectionary industries (Devahastin *et al.*, 2004).

Higher drying rates (comparing with hot air drying or in the case of the low-pressure superheated steam drying, vacuum drying) are possible in both constant and falling rate periods of SSD, depending on the steam temperature. The higher thermal conductivity and heat capacity of superheated steam leads to higher rates of surface moisture removal above the so-called inversion temperature (Schwartz and Bocker, 2002; Suvarnakuta *et al.*, 2005b). Below the inversion temperature drying in air is faster. In the falling rate period the higher

product temperature in SSD (over 100°C at 1 bar) and lack of diffusional resistance to water vapor lead to faster drying rates.

On the other hand, since most foods and biomaterials are damaged or degraded at the saturation temperature of superheated steam corresponding to atmospheric or higher pressures, these products cannot suitably be dried in SSD even if they contain only surface moisture. Lowering the dryer operating pressure is clearly a feasible option that could lead to preservation of the quality of dried products and additionally, in some cases, to enhanced drying rates as well.

In the following section a short description of the basic principles of SSD and low-pressure superheated steam drying (LPSSD) is first illustrated. This is followed by a review of the recent advances in LPSSD of foods and biomaterials. For superheated steam drying of foods at near-atmospheric pressure the reader is referred to Devahastin and Suvarnakuta (2004).

5.2 BASIC PRINCIPLES OF SUPERHEATED STEAM DRYING

A simple schematic sketch of a superheated steam drying system is shown in Figure 5.1. Saturated steam from a boiler or a steam generator is heated up in a heater (steam superheater) and becomes superheated steam. Drying takes place through direct contact between superheated steam and the product to be dried. As mentioned earlier, the exhaust of the dryer is also steam, albeit at lower specific enthalpy. Steam may be recirculated and reheated in a closed loop; only the amount of steam that corresponds to the amount of evaporated water is removed from the closed loop and used either directly or indirectly after its energy is recovered via a heat exchanger. The closed loop of SSD implies that emissions coming from the drying product are not emitted to the environment but are included in the condensate; toxic or expensive organic liquids can therefore be recovered more easily than in the case of hot air drying.

In the case of LPSSD the same basic concept applies except for the fact that an external steam superheater may not be required. As the saturated steam is introduced to

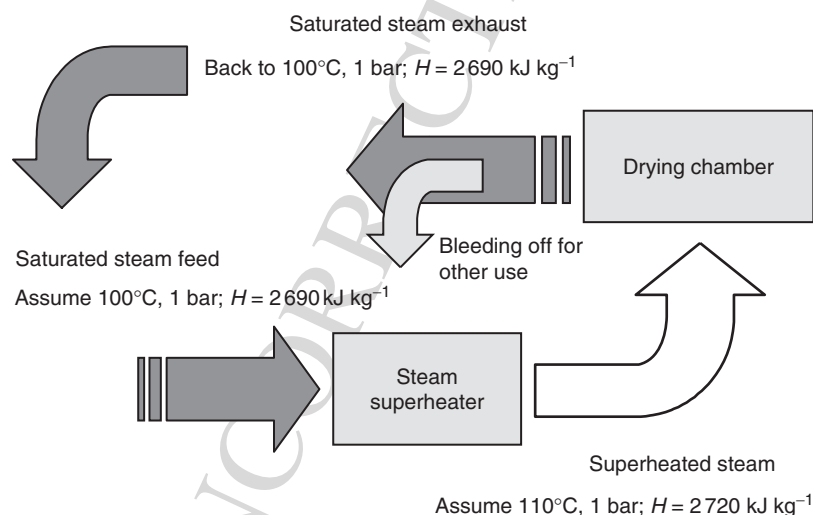


Fig. 5.1 A schematic sketch of a superheated steam drying system.

the low-pressure drying chamber, saturated steam becomes low-pressure superheated steam since its temperature is already well above the saturation temperature at the reduced pressure of the drying chamber. To minimize the effect of adiabatic expansion of steam that may occur in the low-pressure drying chamber, a heater is generally installed in the drying chamber to help control the low-pressure superheated steam temperature at a desired value (Devahastin *et al.*, 2004).

Since there is no resistance to diffusion of the evaporated water in its own vapor, the drying rate in the constant rate period is dependent only on the heat transfer rate q . If sensible heat effects, heat losses and other modes of heat transfer are neglected, the rate at which surface moisture evaporates in steam is given simply by:

$$N = \frac{q}{\lambda} = \frac{h(T_{steam} - T_s)}{\lambda} \quad (5.1)$$

where N is the evaporation rate, h is the convective heat transfer coefficient, T_s is the drying surface temperature which corresponds to the saturation temperature at the dryer operating pressure, T_{steam} is the temperature of the superheated steam and λ is the latent heat of vaporization. In hot air drying, $T_s = T_{wet-bulb}$ and hence at lower drying temperatures, ΔT is higher in air drying but h is lower since air has heat transfer properties inferior to superheated steam at the same temperature. It turns out that these counter-acting effects lead to the phenomenon of inversion; a temperature beyond which the superheated steam drying rate is greater than hot air drying rate (see Figure 5.2). This is confirmed experimentally as well as numerically for water as well as several organic solvent systems (superheated vapor drying). It is observed that the inversion temperature is in the order of 160–200°C for evaporation of water in superheated steam for various flow configurations and flow regimes, for example, laminar/turbulent boundary layer flows, impinging jet flows, free convective flow over complex geometries (Chow and Chung, 1983; Wu *et al.*, 1987, 1989; Haji and Chow, 1988; Sheikholeslami and Watkinson, 1992; Bond *et al.*, 1994).

Strictly speaking, the inversion temperature is defined only for surface moisture evaporation and not for internal moisture removal, although some researchers do not make this distinction

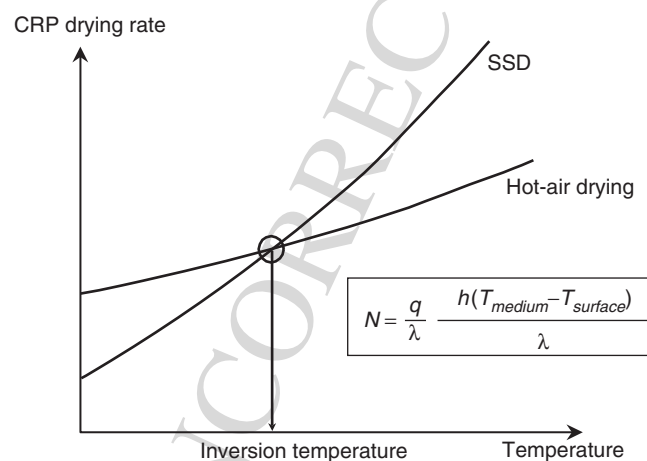


Fig. 5.2 An inversion phenomenon.

clear when reporting their results. However, the values of the inversion temperature calculated only from the surface moisture evaporation rates are obviously not the same as those calculated from the combined constant rate and falling rate drying rates (Suvarnakuta *et al.*, 2005b).

The convective heat transfer coefficient, h , between steam and the solid material surface can either be estimated using standard correlations for inter-phase heat transfer (Incropera and Dewitt, 2002) or from the experimental drying rates data. The following example illustrates how the values of the convective heat transfer coefficient are calculated from the experimental low-pressure superheated steam drying rates.

Example 1: Based on the data of Suvarnakuta *et al.* (2005b) who experimentally determined the drying rates of molecular sieve beads undergoing LPSSD at various operating pressures (see Figure 5.3), it is possible, through the use of equation (5.1), to determine the values of the convective heat transfer coefficient. First of all, it is recognized that equation (5.1) can be rewritten as:

$$h = \frac{N\lambda}{A(T_{\text{steam}} - T_{\text{surface}})} \quad (5.2)$$

As an illustrative case, consider the case at the drying temperature of 80°C and absolute pressure of 7 kPa (Figure 5.3a). Since the drying rates reported by Suvarnakuta *et al.* (2005b) are in $\text{kg kg}^{-1} \text{ (d.b.) min}^{-1}$, it is necessary to multiply the reported drying rates by the bone-dry mass of the sample (approximately 24 g). Hence, $N = 1.4 \times 10^{-2} \text{ kg kg}^{-1} \text{ (d.b.) min}^{-1} \times 0.024 \text{ kg} = 3.36 \times 10^{-4} \text{ kg min}^{-1}$. In this case, A is the surface area of all molecular sieve particles used in each experiment and is equal to 0.044 m^2 .

At the pressure of 7 kPa the surface temperature is around 40°C, which corresponds to the saturation temperature at 7 kPa. Also at this pressure $\lambda = 2406.0 \text{ kJ kg}^{-1}$. Hence, $h = [3.36 \times 10^{-4} \text{ kg min}^{-1} \times 2406.0 \text{ kJ kg}^{-1}] / [0.044 \text{ m}^2 \times (80 - 40) \text{ K}] = 0.4593 \text{ kJ min}^{-1} \text{ m}^{-2} \text{ K}^{-1}$ or $7.66 \text{ W m}^{-2} \text{ K}^{-1}$.

The values of the heat transfer coefficient at other conditions are listed in Table 5.1. As expected, the values of the heat transfer coefficient increase with the operating pressure of the dryer as there is more mass (steam) available for convection heat transfer in the dryer.

5.3 LOW-PRESSURE SUPERHEATED STEAM DRYING OF FOODS AND BIOMATERIALS

Although there exist a number of publications on low-pressure superheated steam drying of other products, both from the fundamental (e.g. Shibata *et al.*, 1988, 1990; Sano *et al.*, 2005; Shibata, 2006; Tatemoto *et al.*, 2007) and application-oriented points of view (e.g. Chen *et al.*, 1992; Pang and Dakin, 1999; Defo *et al.*, 2004), this section is focused only on a more limited pool of information on LPSSD of foods and biomaterials. Near-atmospheric pressure superheated steam drying is not included either; the reader is referred to Devahastin and Suvarnakuta (2004) for a review on near-atmospheric pressure superheated steam drying and also to the literature for some recent advances of this drying technique applied to foods and biomaterials (e.g. Taechapairoj *et al.*, 2004; Rordprapat *et al.*, 2005; Prachayawarakorn *et al.*, 2006; Nathakaranakule *et al.*, 2007; Jamradloedluk *et al.*, 2007).

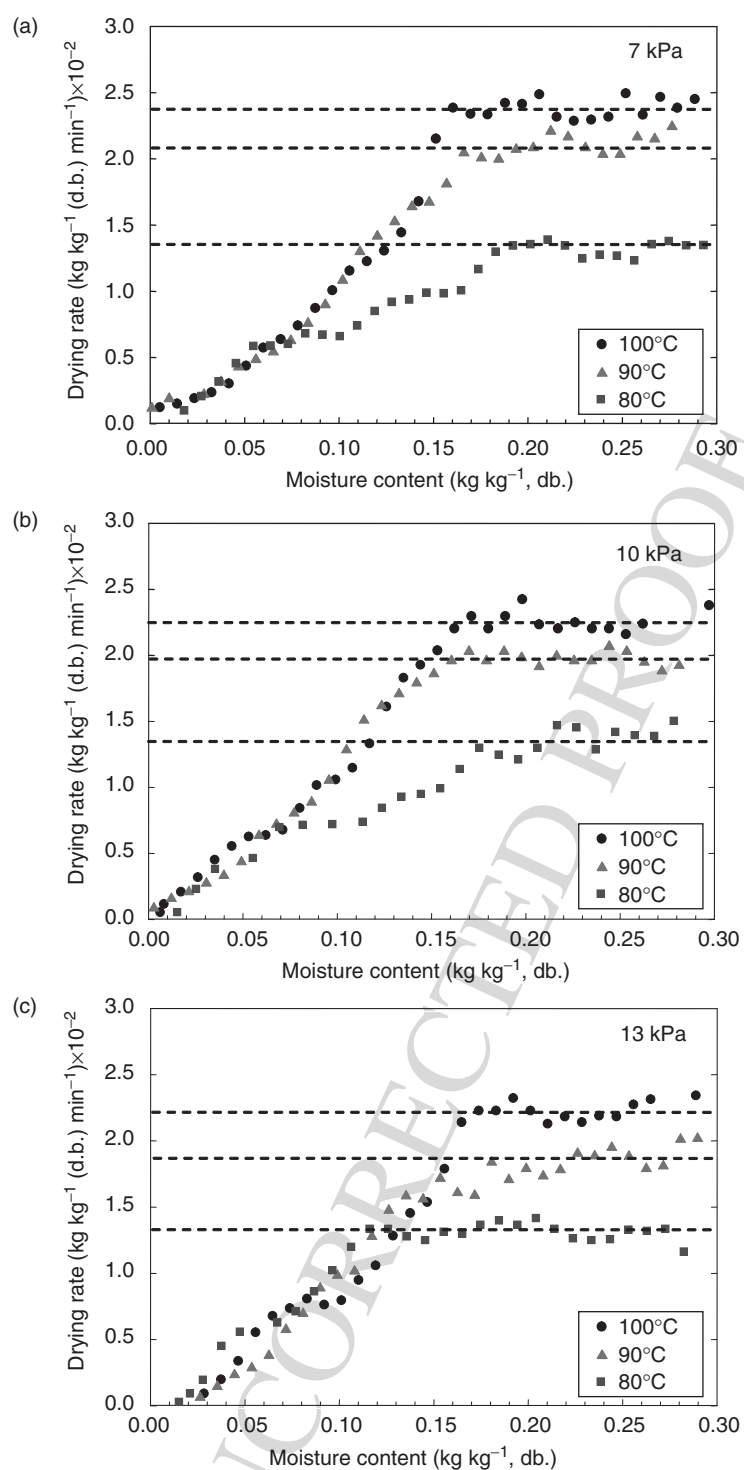
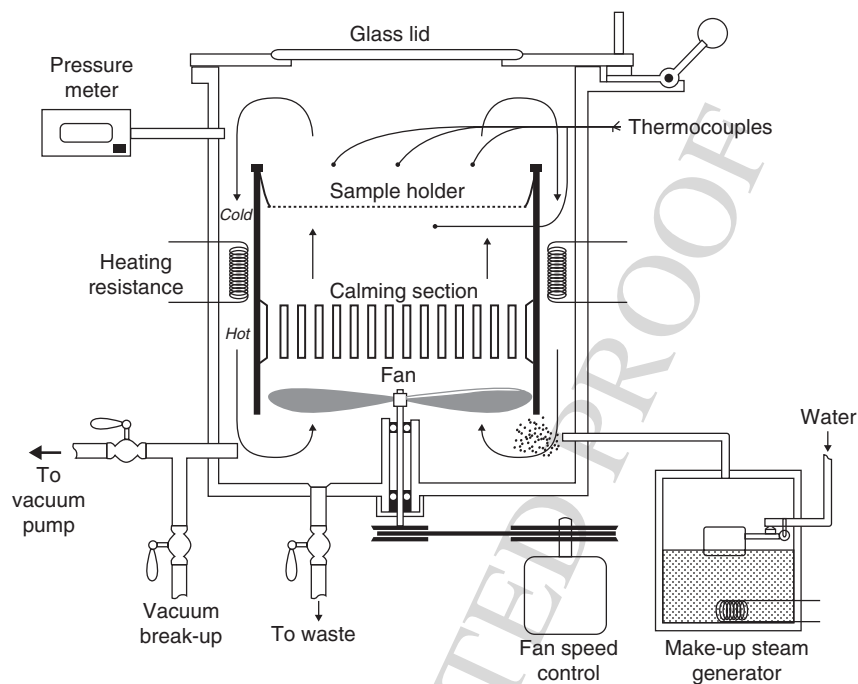


Fig. 5.3 Drying rate curves of molecular sieve beads undergoing LPSSD at various operating pressures. Reproduced with permission from Suvarnakuta *et al.* (2005b). Copyright 2005 American Chemical Society.

Table 5.1 Values of heat transfer coefficient ($\text{W m}^{-2} \text{K}^{-1}$) calculated from equation (5.2).

Absolute pressure					
7 kPa		10 kPa		13 kPa	
Mean	SD	Mean	SD	Mean	SD
7.661	0.61	8.353	0.44	9.168	0.33

**Fig. 5.4** Schematic of the experimental set up of Elustondo *et al.* (2001). Copyright 2001, reproduced with permission from Elsevier.

Among the first reported works on LPSSD of foods and biomaterials is the work of Elustondo *et al.* (2001) who studied LPSSD of foodstuffs both experimentally and theoretically. Wood slabs, shrimp, banana, apple, potato and cassava were dried using the steam pressures of 10 000–20 000 Pa, the steam temperatures of 60–90°C and the steam circulating velocities of 2–6 m s^{-1} in a set up shown schematically in Figure 5.4. A mathematical model was also developed based on a theoretical drying mechanism, which assumes that the water removal is carried out by evaporation in a moving boundary allowing the vapor to flow through the dry layer built as drying proceeds to predict the drying characteristics of foodstuffs undergoing this drying operation. A simplified expression, which has two experimentally determined parameters, was derived and used to predict the drying rate of test samples.

An example of the dimensionless drying rate curve is shown in Figure 5.5. The constant drying rate period cannot be observed in this figure (and all other experiments conducted).

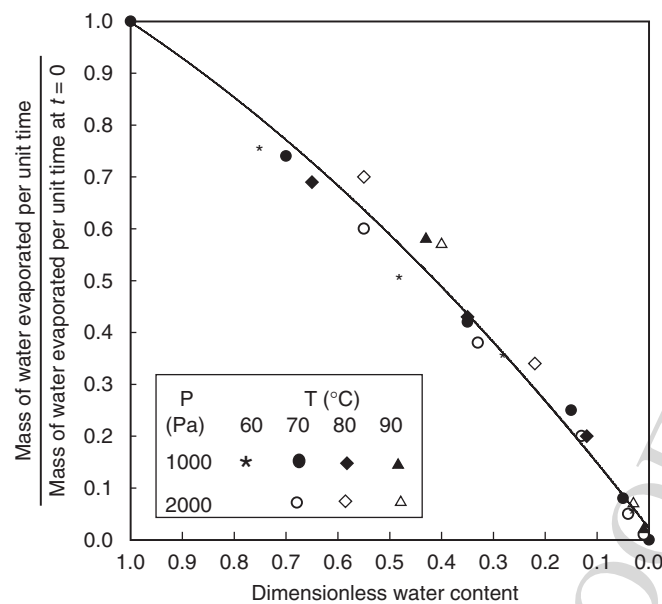


Fig. 5.5 Dimensionless drying rate of banana slices as a function of the instantaneous moisture content (Elustondo *et al.*, 2001). Copyright 2001, reproduced with permission from Elsevier.

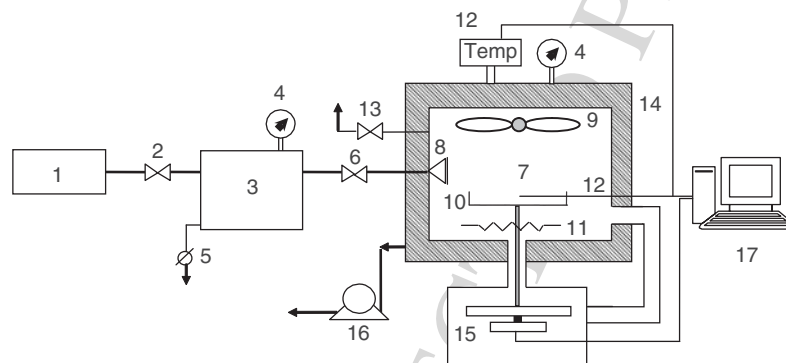


Fig. 5.6 A schematic diagram of the low-pressure superheated steam dryer and associated units (Devahastin *et al.*, 2004). 1, boiler; 2, steam valve; 3, steam reservoir; 4, pressure gauge; 5, steam trap; 6, steam regulator; 7, drying chamber; 8, steam inlet and distributor; 9, electric fan; 10, sample holder; 11, electric heater; 12, on-line temperature sensor and logger; 13, vacuum break-up valve; 14, insulator; 15, on-line weight indicator and logger; 16, vacuum pump; 17, PC with installed data acquisition card.

An approximately linear relationship between the dimensionless drying rate and moisture content could be observed during an early stage of drying, whereas the slope of the curve increased toward the end of the drying process. A model proposed was found to predict the drying kinetics reasonably well. No mention about product quality was given, however.

Devahastin *et al.* (2004) developed another version of a low-pressure superheated steam dryer, which can be operated by using steam supplied from a typical boiler available in a food plant. A schematic diagram of this dryer is shown in Figure 5.6.

AQ: Please check the labelling of y-axis if any change is required for figure 5.5.

By using carrot as a model heat-sensitive material, experiments were conducted to examine the drying kinetics and various quality parameters of the product undergoing LPSSD. For comparison experiments were also performed under a vacuum condition (by using the same set-up but without the application of steam to the dryer) at the same operating conditions, that is, absolute pressures of 7, 10 and 13 kPa and temperatures of 60, 70 and 80°C. Based on the experimental drying data it was observed that all samples undergoing LPSSD gained a small amount of moisture during the first few minutes of drying. Nevertheless, the condensation of steam was rather negligible if the operating pressure was low. It was also observed that the effect of temperature on the drying rates was greater than the effect of pressure in the case of LPSSD, especially at higher drying temperatures. The effect of operating pressure was less clear even at lower temperature (60°C) for the case of vacuum drying, however. This is probably due to the fact that the steam thermal properties were affected by temperature to a larger extent than those of air, especially at lower drying temperatures. No initial condensation was also observed, as expected, in the case of vacuum drying. It was also reported that the moisture content decreased faster, especially in the case of LPSSD at lower drying temperatures, at lower pressures since water boiled and evaporated at lower temperatures. It was found that the drying times of vacuum drying were shorter than those of LPSSD (at the same pressure) for all conditions tested. This is probably due to the fact that the electric heater was used more often during vacuum drying since it was the only source of energy for drying. This might increase the amount of radiation absorbed by the carrot surfaces, thus explaining the higher drying rate during vacuum drying. The initial steam condensation on the product surface might also contribute to the longer drying times for the case of LPSSD. The differences between the two sets of drying times, however, were smaller at higher drying temperatures. Raising the drying temperature further would eventually lead to equal rates of drying at an inversion temperature (due to increased temperature difference between the steam and the product as well as a reduction of the initial steam condensation).

Figure 5.7 illustrates changes of moisture content and temperature of carrot undergoing LPSSD at some selected conditions. It can be seen in this figure that the shapes of the drying and temperature curves were affected by both the drying temperature and pressure. At lower drying temperatures the temperature of carrot changed suddenly from its initial value and remained rather constant at the boiling temperature of water corresponding to the operating pressure until the first falling rate period drying ended (drying rate data are not shown here for the sake of brevity). Beyond this point, the carrot temperature rose again and finally approached the temperature of the drying medium. As the medium temperature increased (at the same operating pressure) it can be seen (for example, from Figure 5.7c) that the period of constant product temperature was shorter; the product temperature rose almost steadily from its initial value to the medium temperature. At the same drying temperature, however, increasing the operating pressure led to a lower rate of drying but a longer period of constant product temperature (as can be seen from Figures 5.7c and 5.7d). It may depend both on the characteristics of the drying product and on these effects to determine the optimum operating conditions of an LPSSD.

Figure 5.8 shows the evolutions of moisture content and temperature of carrot undergoing vacuum drying at the same operating as those used for LPSSD shown in Figure 5.7. It can be seen from this figure that the drying and heat transfer behavior of carrot undergoing vacuum drying was quite different from that of LPSSD; the product temperature, in this case, rose almost steadily from its initial value to the medium temperature. However, the rates of moisture reduction in the case of vacuum drying were higher than those belonged to LPSSD, especially at lower drying temperatures as mentioned earlier.

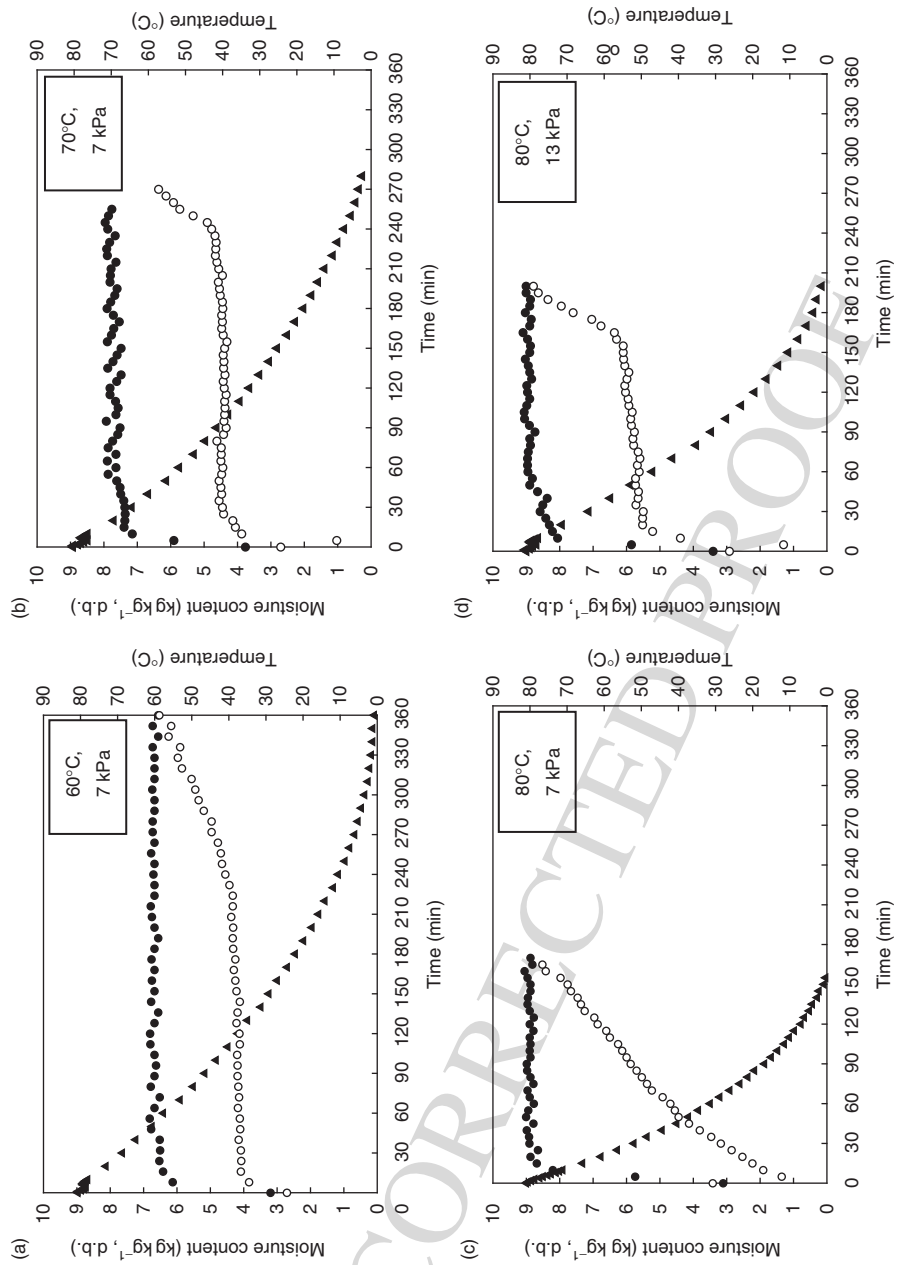


Fig. 5.7 Changes in moisture content and temperature of carrot undergoing LPSSD at different operating conditions. (▲), Moisture content; (●), steam temperature; (○), simple temperature.

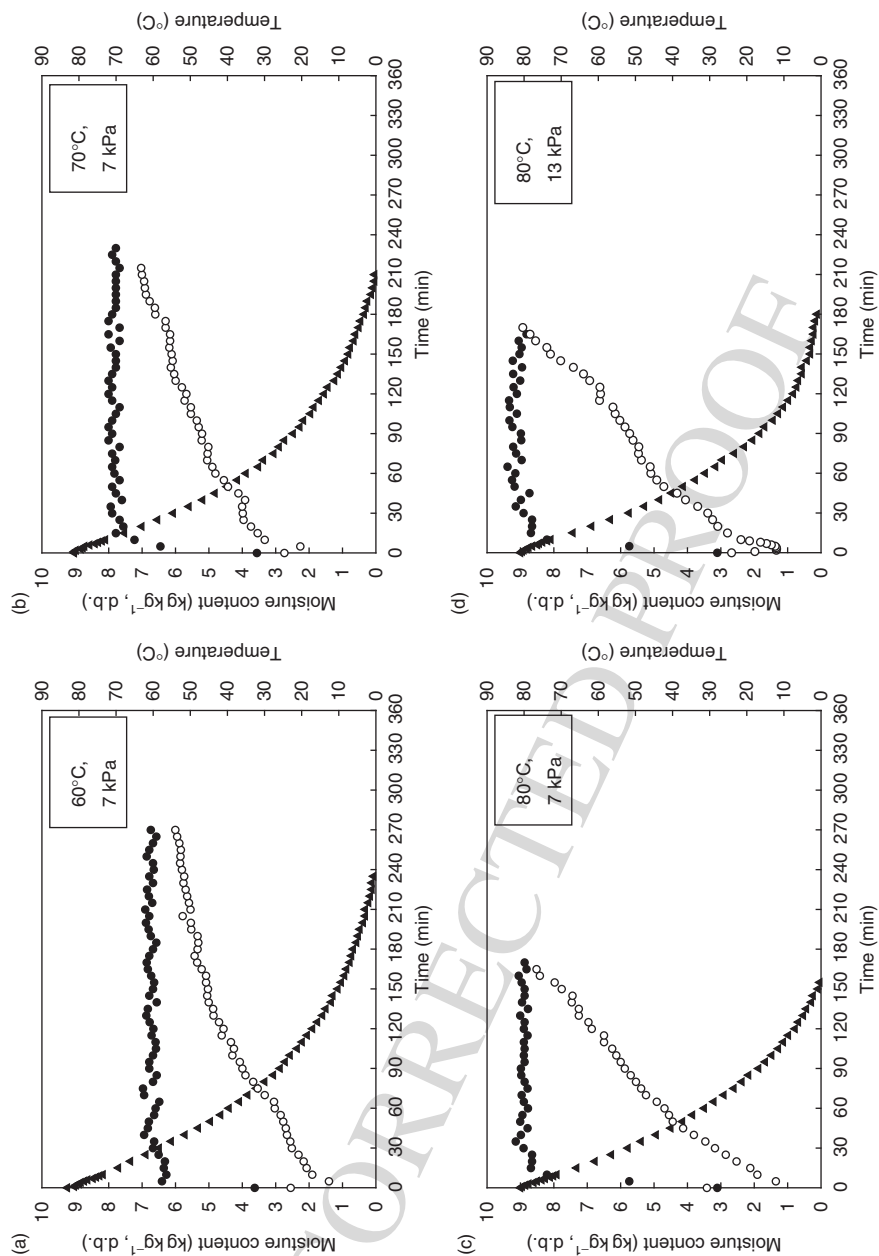


Fig. 5.8 Changes in moisture content and temperature of carrot undergoing vacuum drying at different operating conditions. (▲), moisture content; (●), steam temperature; (○), sample temperature.

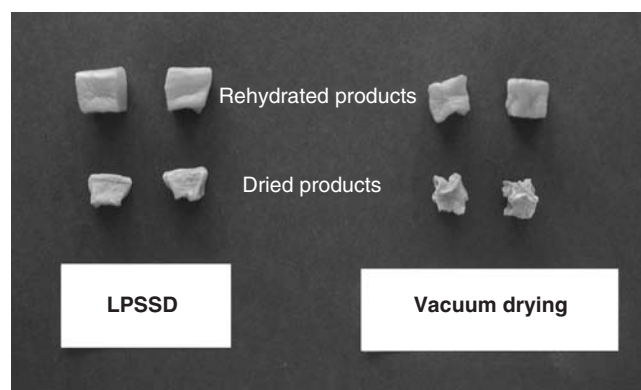


Fig. 5.9 Photographs of carrot cubes both after drying and after rehydration.

In terms of quality it was reported that the volume and apparent density of dried carrot undergoing both drying techniques slightly decreased and increased, respectively, as the operating pressure increased; both properties changed only slightly in this case, however, because of the narrow range of operating pressures tested. It was noted, however, that although the values of shrinkage of carrot that underwent LPSSD and vacuum drying were similar, the shrinkage patterns resulting from the two different drying processes were quite different. Carrot that underwent vacuum drying tended to shrink non-uniformly. In a more rapid drying (as in the case of vacuum drying when compared with LPSSD) the surface of the drying product became dry and rigid long before the center had dried out; the center dried and shrank much later than the outer surface did and hence pulled away from the rigid surface layers and caused a non-uniform shrinkage. Drying carrot in LPSSD, however, led to a more uniform shrinkage; in this case shrinkage seemed to occur because the carrot structure could not support its own weight and hence collapsed under gravitational force in the absence of moisture (Achanta and Okos, 2000). This is because LPSSD offered a milder drying condition (since the drying chamber was moister than in the case of vacuum drying). Dense or rigid large formations might not be formed as much in the case of LPSSD as in the case of vacuum drying. The photographs of carrot cubes both after drying and after rehydration are shown in Figure 5.9. These results are supported by the SEM photographs of Figures 5.10a and 5.10b, which show the micro-structure of LPSSD and vacuum dried carrot, respectively. It is seen from these figures that carrot that underwent vacuum drying developed a rather dense layer and its pore distribution was rather non-uniform compared to carrot that underwent LPSSD.

A simple technique has indeed been proposed to monitor deformation of a food product undergoing different drying techniques and conditions (Panyawong and Devahastin, 2007). The use of such a technique has confirmed the above-mentioned argument that the product undergoing LPSSD suffered less irregular deformation than the product undergoing vacuum drying although the percentage of the volumetric shrinkage of the two products was not significantly different.

Many studies were also performed to study the capability of LPSSD to retain some heat-sensitive chemical properties (e.g. various vitamins, flavors and aromas) of food products. Barbieri *et al.* (2004) compared the effects of hot air drying (40–60°C) and LPSSD (at a temperature of 50°C and pressure of around 5 kPa) on the retention of some volatile compounds in basil (*Ocimum basilicum*). It was found that the original aroma profiles were

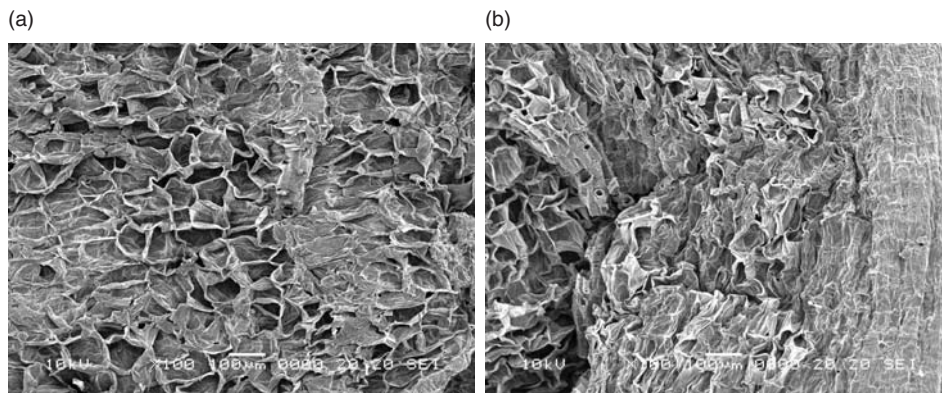


Fig. 5.10 SEM photographs of carrot undergoing (a) LPSSD and (b) vacuum drying.

kept almost constant in the case of basil dried by LPSSD. On the other hand, air-dried basil suffered significant variations in the relative proportions of aroma compounds.

Methakhup *et al.* (2005) dried Indian gooseberry (*Phyllanthus emblica* L.) flakes in both LPSSD and vacuum conditions using the same set-up as that used by Devahastin *et al.* (2004). Although vacuum drying took a shorter time to dry the product than did LPSSD at all drying conditions tested (temperatures in the range of 65–75°C and absolute pressures in the range of 7–13 kPa), it was found that LPSSD could retain ascorbic acid better than vacuum drying in almost all cases studied. In addition, LPSSD could preserve the colors of the sample better than vacuum drying at all drying conditions tested. In vacuum drying, temperature had a significant effect on ascorbic acid content and colors of the product while absolute pressure did not significantly affect the quality. In low-pressure superheated steam drying, on the other hand, the drying conditions did not affect the ascorbic acid and colors of the dried product. The quality results of their study are summarized in Tables 5.2 and 5.3.

From Table 5.2 it is seen that all dried Indian gooseberry flakes tended to lose some ascorbic acid as compared to fresh. The ascorbic acid retention was in the ranges of 64–94% for vacuum drying and 93–96% for LPSSD. For vacuum drying it was found that the ascorbic acid retention of the sample increased as the drying temperature increased. This may be due to the shorter drying time required to dry the samples to the desired moisture content. However, the pressure had only a little effect on the ascorbic acid retention. This may be explained by the fact that the drying time was not much affected by the operating pressure and that the level of oxygen content (which caused the aerobic degradation of vitamin C) was not much different at different pressures.

In LPSSD the ascorbic acid retention was not significantly different at different drying conditions even though the drying time was different. The results implied that no oxygen was available in the drying system and thus presented no effect on the ascorbic acid degradation during drying. The ability of the superheated steam drying system to maintain vitamin C has, in fact, been reported earlier by other investigators (e.g. Moreira, 2001)

From Table 5.3 it was found that LPSSD and vacuum drying at every condition resulted in a decrease of an *L* value and an increase of an *a* value of the dried sample compared with the fresh. However, *b* value of the dried sample was similar to that of the fresh sample. These results implied that the browning reaction and pigment destruction occurred in the dried sample. When considering the color retention of samples between two different drying

Table 5.2 Total ascorbic acid content of fresh and dried Indian gooseberry samples.

Drying method	Condition		Ascorbic acid (g per 100 g)		% Retention
	T (°C)	P _{ab} (kPa)	Fresh	Dried	
VD ¹	65	7	1.08 ± 0.07	3.67 ± 0.13	71.52 ^{ab} ± 1.97
		10	1.06 ± 0.09	3.50 ± 0.25	66.89 ^a ± 2.51
		13	0.94 ± 0.05	3.07 ± 0.30	64.84 ^a ± 6.01
	75	7	0.96 ± 0.02	3.84 ± 0.18	94.46 ^{cd} ± 2.57
		10	0.99 ± 0.02	3.72 ± 0.11	89.46 ^c ± 2.78
		13	0.98 ± 0.11	3.34 ± 0.03	78.13 ^b ± 2.83
LPSSD ²	65	7	1.05 ± 0.06	3.99 ± 0.22	93.46 ^{cd} ± 1.58
		10	—	—	—
		13	—	—	—
	75	7	1.06 ± 0.04	4.04 ± 0.08	95.35 ^d ± 3.49
		10	1.09 ± 0.08	4.03 ± 0.11	95.67 ^d ± 2.10
		13	1.04 ± 0.08	3.99 ± 0.11	94.96 ^{cd} ± 2.14

Means in the same column having the same letter are not significantly different ($\alpha < 0.05$).

¹ VD stands for vacuum drying.

² LPSSD stands for low-pressure superheated steam drying.

Table 5.3 Hunter parameters and total color difference (ΔE) of dried samples.

Drying method	Conditions		$\Delta L/L_0$	$\Delta a/a_0$	$\Delta b/b_0$	ΔE
	T (°C)	P _{ab} (kPa)				
VD ¹	65	7	0.06 ± 0.00	-0.91 ± 0.01	0.01 ± 0.01	3.83 ^b ± 0.09
		10	0.08 ± 0.00	-1.39 ± 0.07	0.02 ± 0.02	5.40 ^{cd} ± 0.10
		13	0.07 ± 0.01	-0.98 ± 0.22	0.00 ± 0.04	4.99 ^c ± 1.04
	75	7	0.08 ± 0.00	-0.71 ± 0.01	-0.02 ± 0.01	5.61 ^{cd} ± 0.28
		10	0.09 ± 0.00	-1.11 ± 0.01	-0.02 ± 0.00	6.42 ^d ± 0.26
		13	0.07 ± 0.01	-1.56 ± 0.58	0.03 ± 0.02	5.38 ^{cd} ± 0.66
LPSSD ²	65	7	0.04 ± 0.00	-0.88 ± 0.97	0.04 ± 0.01	3.09 ^{ab} ± 0.19
		10	—	—	—	—
		13	—	—	—	—
	75	7	0.03 ± 0.01	-0.64 ± 0.04	0.04 ± 0.02	2.48 ^a ± 0.44
		10	0.04 ± 0.00	-0.49 ± 0.18	0.04 ± 0.01	2.88 ^{ab} ± 0.18
		13	0.04 ± 0.04	-0.64 ± 0.23	0.02 ± 0.04	2.93 ^{ab} ± 0.39

Means in the same column having the same letter are not significantly different ($\alpha < 0.05$).

¹ VD stands for vacuum drying.

² LPSSD stands for low-pressure superheated steam drying.

methods it was found that LPSSD could retain the colors better than the vacuum drying system. This is because the degree of ascorbic acid and, probably, chlorophyll degradation of LPSSD was much lower than that of the vacuum drying system.

The drying methods were also found to affect the degradation and release of vitamin C (evaluated in terms of the total ascorbic acid, TAA) from Indian gooseberry flakes during preparation of Indian gooseberry tea (Kongsoontornkijkul *et al.*, 2006). LPSSD was indeed found to help retain TAA in dried gooseberry flakes better than hot air and vacuum drying.

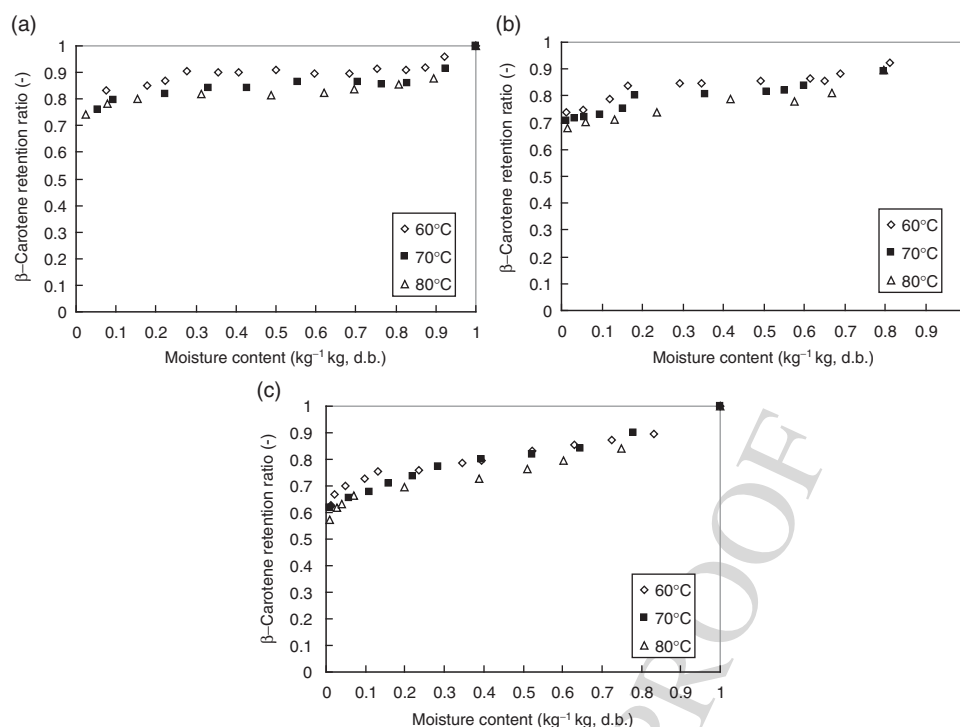


Fig. 5.11 Relationship between β -carotene content and moisture content of carrot undergoing different drying techniques: (a) LPSSD; (b) vacuum drying; (c) hot air drying.

Suvarnakuta *et al.* (2005a) experimentally studied the effects of LPSSD, vacuum and hot air drying on the drying and degradation kinetics of β -carotene in carrot. It was found that LPSSD and vacuum drying led to less degradation of β -carotene in carrot than in the case of hot air drying (see Figure 5.11 and Table 5.4). This is again due to the oxygen-free environment of LPSSD.

In terms of the texture of dried products (e.g. snacks) Leeratanarak *et al.* (2006) reported that the drying methods, in their case hot air drying (70–90°C) and LPSSD (at temperatures of 70–90°C and pressure of 7 kPa), had no significant effect on the texture (in terms of hardness) of dried potato chips. Hot-water blanching (95°C) of potato slices prior to drying, on the other hand, led to improved drying kinetics (due to structural softening leading to easier migration of moisture), colors (due to lower extents of browning reactions) and texture of the products. The degree of browning was also lowered. However, the use of different blanching periods (1–5 min) did not significantly affect the hardness of the chips.

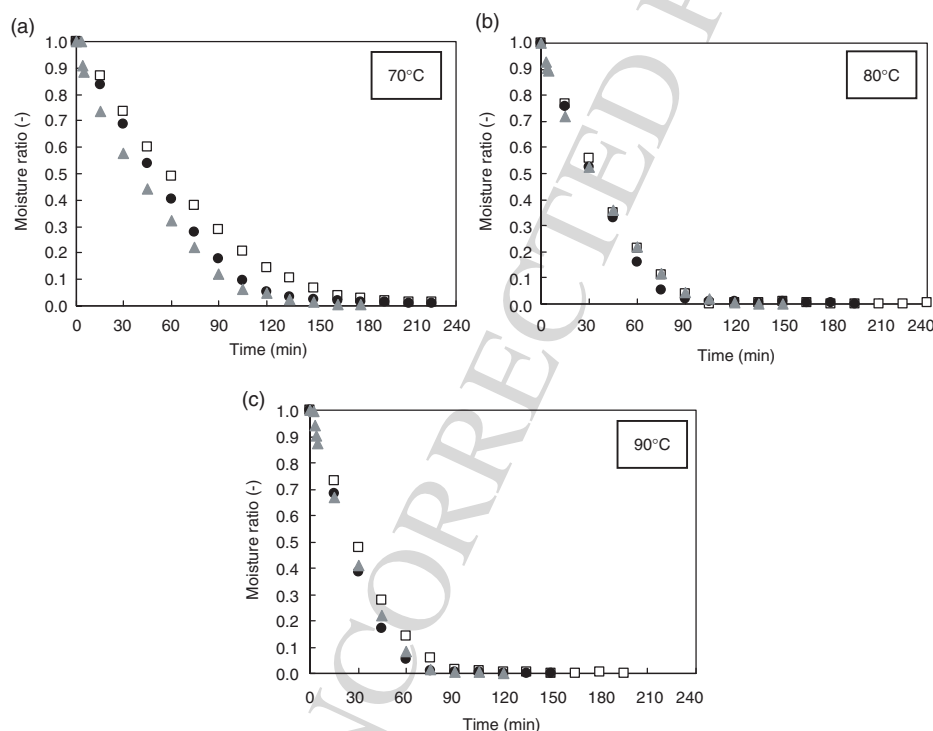
Although blanching has been proved to enhance the quality of potato chips, the chips of Leeratanarak *et al.* (2006) were still observed to be of inferior quality to those available commercially. Pimpaporn *et al.* (2007) therefore investigated the use of different combined pretreatments prior to LPSSD (at temperatures of 70–90°C and pressure of 7 kPa) to improve the quality of potato chips, especially in terms of their texture. Both physical pre-treatments, such as blanching, combined blanching and freezing, as well as chemical pre-treatments, such as dipping raw potato slices in several chemicals including glycerol and monoglyceride, were evaluated. In terms of the drying kinetics it was noted (see Figure 5.12) that the combination

Table 5.4 Average drying times and losses of β -carotene of dried carrot (at moisture content of 0.1 kg kg^{-1} d.b.) undergoing different drying methods.

Sample	Average drying time (min)	β -Carotene content* (mg per 100)		β -Carotene retention ratio (β_t/β_i)
		Wet basis	Dry basis	
Fresh carrot	—	4.86 ± 0.65	51.11 ± 6.89	—
LPSSD carrot				
$T = 60^\circ\text{C}$	420	54.92	43.94	0.83 ± 0.02^a
$T = 70^\circ\text{C}$	330	50.32	41.24	0.76 ± 0.04^b
$T = 80^\circ\text{C}$	210	38.81	31.55	0.74 ± 0.02^b
Vacuum-dried carrot				
$T = 60^\circ\text{C}$	300	26.95	24.28	0.74 ± 0.03^c
$T = 70^\circ\text{C}$	250	25.81	24.05	0.71 ± 0.03^{cd}
$T = 80^\circ\text{C}$	180	31.61	27.85	0.68 ± 0.03^d
Hot air-dried carrot				
$T = 60^\circ\text{C}$	420	22.56	21.46	0.62 ± 0.02^e
$T = 70^\circ\text{C}$	300	35.66	23.30	0.62 ± 0.03^e
$T = 80^\circ\text{C}$	240	36.26	22.05	0.58 ± 0.03^e

Means in the same column having the same letter are not significantly different ($\alpha < 0.05$).

AQ:Please provide explanation for '*' which is appearing in Table 5.4 column head.

**Fig. 5.12** Drying kinetics of unblanched (\square), blanched (\bullet) and blanched-frozen (\blacktriangle) potato slices.

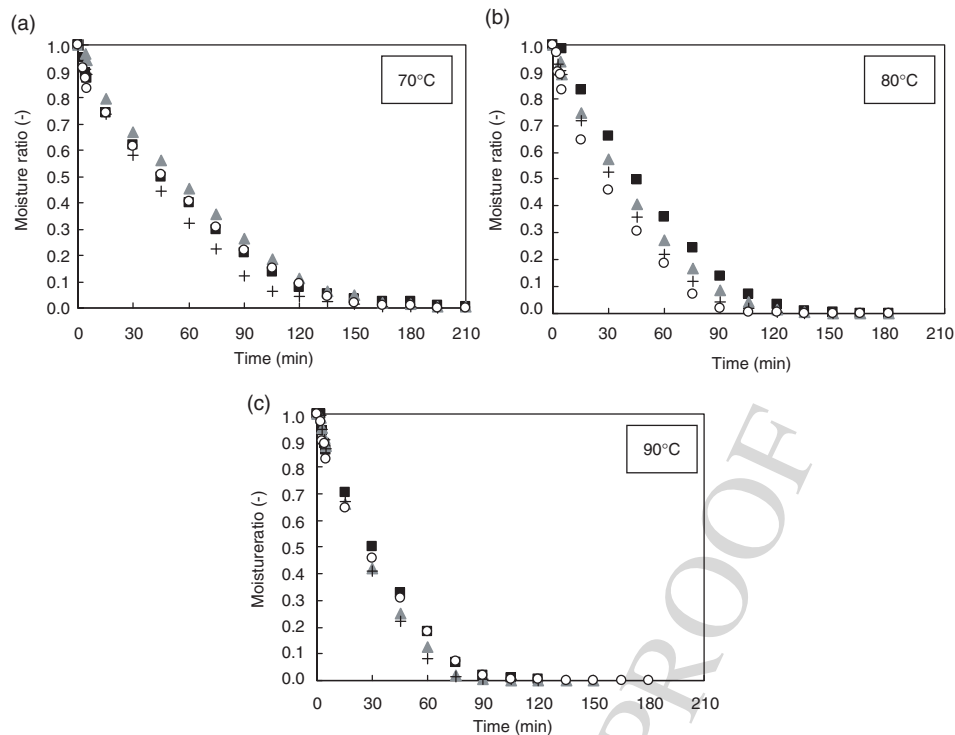


Fig. 5.13 Drying kinetics of blanched potato slices with glycerol immersion at concentrations of 0% (+), 1% (■), 3% (▲), and 5% (○) followed by freezing at different drying temperatures.

of blanching and freezing led to a shorter drying time compared to that of unblanched samples at all drying temperatures. This is probably due to structure softening during blanching. In addition, freezing affects the physical tissue of potato due to the large size of ice crystals formed during slow freezing. The ice crystals might cause openings of the cell wall and semi-permeable membrane that could facilitate moisture transfer during drying. Chemically treated samples showed different drying behavior, however. As can be seen in Figure 5.13, which shows the drying curves of glycerol-treated samples, all glycerol-treated samples needed a longer time to reach their desired final moisture contents than those that underwent blanching and freezing pre-treatment. This is because glycerol has three hydroxyl groups that form hydrogen bonds with water in potato slices. Therefore, evaporation of free water on the surface of sliced potato becomes more difficult. However, the effect of glycerol was reduced at high drying temperatures, especially at 90°C. The drying time of each case was nearly the same as that of combined blanched-frozen samples. However, the results showed an unclear effect of monoglyceride on the drying kinetics of the samples.

In terms of quality it was found that the lightness of dried potato chips was improved by the use of freezing pre-treatment; nevertheless, the lightness values were not significantly different among all freezing pre-treated samples. Redness and yellowness of dried potato chips were not significantly affected by drying temperature but were significantly affected by the methods of pre-treatment.

The hardness of dried potato chips was not significantly influenced by the pre-treatment methods but was better at higher drying temperatures. However, in the cases of crispness

Table 5.5 Effects of pre-treatments and drying temperature on final thickness, hardness, crispness and toughness of LPSSD potato chips.

Pretreatment method	Drying temperature (°C)	Hardness (N)	Toughness (N mm ⁻¹)	Crispness (N mm ⁻¹)
Blanching	70	12.75 ± 2.38 ^{efg}	18.81 ± 4.46 ^f	3.43 ± 1.65 ^{ab}
	80	8.59 ± 2.30 ^{cdef}	17.59 ± 1.87 ^f	6.22 ± 0.94 ^{abcde}
	90	8.21 ± 0.64 ^{bcdef}	16.22 ± 0.21 ^{ef}	5.07 ± 0.43 ^{abcd}
Blanching + freezing	70	10.21 ± 0.58 ^{def}	9.13 ± 1.38 ^{bcde}	14.82 ± 2.86 ^{fghi}
	80	8.00 ± 2.60 ^{bcdef}	4.14 ± 1.97 ^{ab}	13.00 ± 0.67 ^{fghi}
	90	6.77 ± 0.25 ^{abcd}	3.35 ± 1.37 ^{ab}	15.98 ± 3.58 ^{fghi}
B + I (0.1% monoglyceride) + F	70	9.94 ± 1.30 ^{fg}	14.28 ± 1.38 ^{def}	11.37 ± 0.84 ^{defgh}
	80	9.60 ± 0.74 ^{cdef}	8.38 ± 0.92 ^{bcd}	12.54 ± 3.94 ^{efghi}
	90	7.03 ± 0.67 ^{abcd}	3.59 ± 2.08 ^{ab}	14.96 ± 3.02 ^{fghi}
B + I (0.3% monoglyceride) + F	70	10.34 ± 3.87 ^{def}	13.25 ± 1.02 ^{cdef}	9.26 ± 1.44 ^{bcdefg}
	80	8.73 ± 0.13 ^{cdef}	7.88 ± 1.70 ^{abcd}	10.55 ± 1.47 ^{cdefg}
	90	4.72 ± 0.48 ^{abc}	3.49 ± 2.05 ^{ab}	13.08 ± 2.68 ^{fghi}
B + I (0.5% monoglyceride) + F	70	10.33 ± 0.39 ^{def}	16.34 ± 0.72 ^{ef}	11.00 ± 1.19 ^{defg}
	80	9.47 ± 1.70 ^{cdef}	5.75 ± 2.49 ^{abc}	13.09 ± 2.34 ^{fghi}
	90	7.54 ± 2.17 ^{abcde}	5.06 ± 2.41 ^{ab}	16.49 ± 1.15 ^{ghi}
B + I (1% glycerol) + F	70	11.30 ± 2.10 ^{def}	18.95 ± 4.59 ^f	2.25 ± 0.18 ^a
	80	9.40 ± 1.03 ^{cdef}	14.75 ± 1.68 ^{def}	13.10 ± 1.38 ^{fghi}
	90	7.48 ± 1.25 ^{abcde}	3.28 ± 1.44 ^{ab}	14.47 ± 2.57 ^{fghi}
B + I (3% glycerol) + F	70*	9.92 ± 0.51 ^h	18.63 ± 0.96 ^f	9.10 ± 2.97 ^{bcdefg}
	80	8.13 ± 1.87 ^{bcdef}	14.08 ± 1.61 ^{def}	12.39 ± 1.50 ^{efghi}
	90	7.59 ± 0.76 ^{abcde}	3.07 ± 1.01 ^{ab}	18.34 ± 2.99 ⁱ
B + I (5% glycerol) + F	70*	17.52 ± 0.59 ^g	34.09 ± 6.92 ^g	4.29 ± 0.64 ^{abc}
	80	9.47 ± 2.06 ^{cdef}	13.35 ± 2.27 ^{cdef}	6.28 ± 2.42 ^{abcde}
	90	7.41 ± 2.06 ^{abcde}	6.30 ± 2.12 ^{abc}	14.96 ± 1.41 ^{hi}

B: blanching, I: immersion in solution and F: freezing

Different superscripts in the same column mean that the values are significantly different ($p \leq 0.05$).

*Denotes the cases where the final moisture content of 3.5% (d.b.) was not achievable.

and toughness, the drying temperature affected these parameters significantly, especially at 90°C. More importantly, freezing pre-treatment could improve the crispness and also toughness of dried chips. The crispness increased as the drying temperature increased but the toughness decreased with increased drying temperature. The textural results are summarized in Table 5.5.

A micro-structural evaluation of the potato chips was also performed. It was noted that the drying temperature significantly affected the micro-structure of dried potato chips. On the other hand, the effects of pre-treatments on the micro-structure were only that combined blanching and freezing pre-treatments led to the best integrity of micro-structure (in terms of pore size, pore distribution and also less formation of rigid dense layer). This superior integrity of the micro-structure might lead to the favorable texture of dried potato chips as summarized earlier.

Based on the aforementioned arguments, combined blanching and freezing without any chemical pre-treatments, followed by drying in LPSSD at a higher temperature (90°C in this

case) was recommended. It is important to note, however, that a sensory study is needed prior to being able to make a definitive conclusion on the validity of the results.

5.4 SOME ADVANCES IN LPSSD OF FOODS AND BIOMATERIALS

In addition to drying foods and biomaterials in LPSSD tray dryers, some researchers have applied LPSSD to other types of dryers. It should be noted that the concept of combining different modes of drying by itself is obviously not new.

Kozanoglu *et al.* (2006) dried coriander and pepper seeds in a low-pressure (in the range of 40–66 kPa) superheated steam fluidized-bed dryer over the temperature range of 90–110°C. General trends of drying kinetics were observed. At a given temperature lowering the operating pressure led to a higher degree of steam superheat and higher fluidizing air velocity. The degree of steam superheat was found to have the most important effect on the drying behavior of both types of seeds.

Nimmol *et al.* (2007) combined LPSSD and far-infrared radiation (FIR) as an external heat source to enhance the rates of the drying process. The combined process (LPSSD-FIR) was also compared with combined vacuum drying and FIR (VACUUM-FIR) for banana slices, both in terms of the drying kinetics and quality of the dried chips (in terms of color, shrinkage, rehydration behavior, texture and micro-structure), over the temperature range of 70–90°C and pressures of 7 and 10 kPa. Moreover, the quality of dried banana chips was compared with that of banana slices undergoing LPSSD alone.

The changes in moisture ratio and temperature of banana slices undergoing LPSSD-FIR and VACUUM-FIR at some selected conditions are shown in Figures 5.14 and 5.15, respectively. After a slight drop of the sample temperature due to the rapid reduction of the chamber pressure, which led to some flash evaporation of surface moisture, the temperature of the sample (in the case of LPSSD-FIR) rose rapidly to a level close to the boiling point of water corresponding to the chamber pressure (not at the boiling point, as is seen in Figure 5.7, since far-infrared radiation was also present in this case) and then remained unchanged at this level until the surface of the sample started to dry. Another important aspect is that the temperature of the sample rose steadily to a level higher than the pre-determined medium temperature because heat transfer, in the case of LPSSD-FIR, simultaneously took place by radiation from the far-infrared radiator and by convection from superheated steam. After this period the temperature of the sample remained almost unchanged because during the later stage of the process moisture content within the sample was smaller leading to lower absorptivity of the sample.

Comparing the changes in the temperature of banana slices undergoing LPSSD-FIR and VACUUM-FIR reveals that, at the same pre-determined medium temperature, the sample temperature during the later stage of LPSSD-FIR was higher than that in the case of VACUUM-FIR. This is due to the fact that in the case of LPSSD-FIR, radiation intensity at the position of the thermocouple used for sending the signal to the temperature controller (30 mm above the sample surface) was less intense due to the higher absorptivity of superheated steam compared to that of air. The far-infrared radiator was thus used more often during LPSSD-FIR to maintain the desired level of drying medium temperature, leading to a higher surface temperature of the far-infrared radiator. Consequently, the radiation intensity, which depends on the surface temperature of the far-infrared radiator, experienced by LPSSD-FIR samples was greater, hence higher levels of the sample temperature.

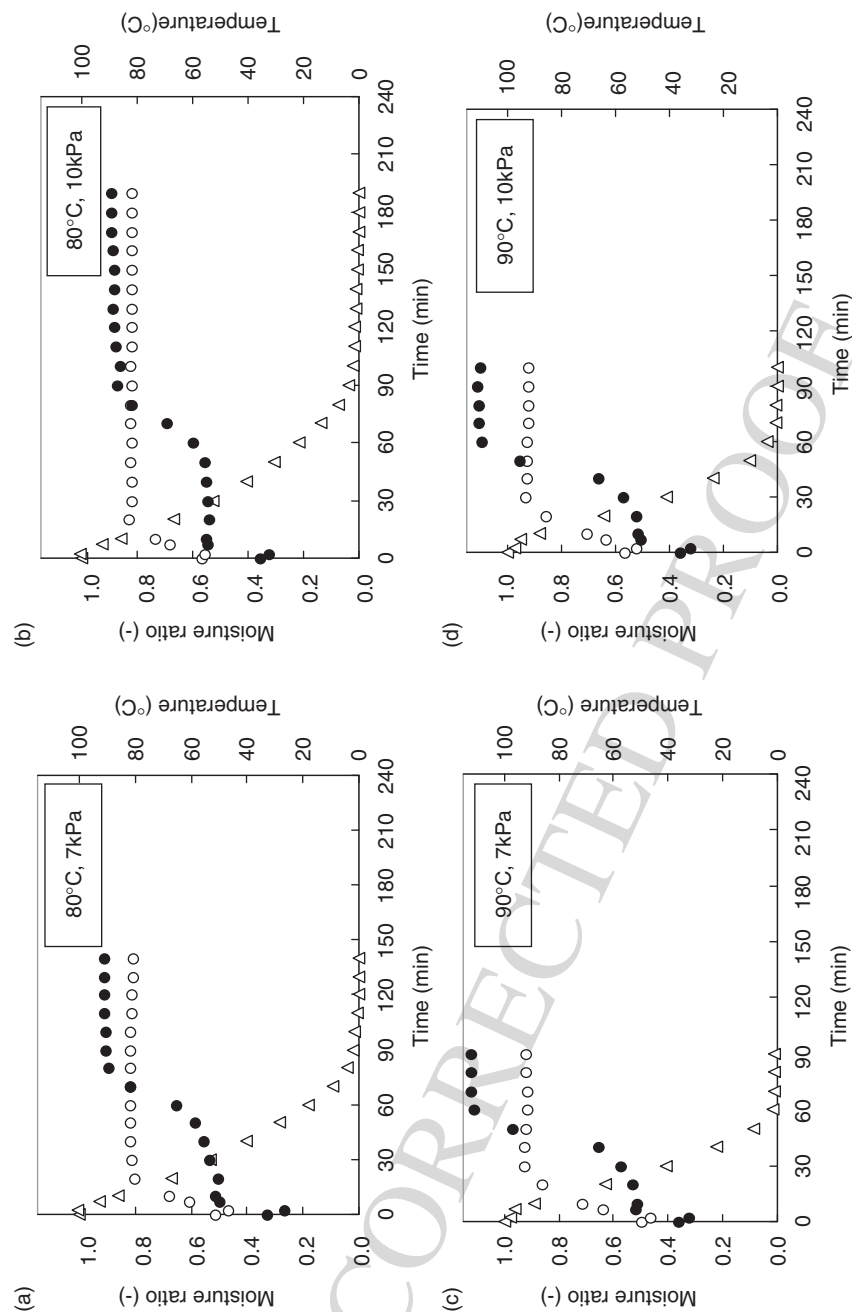


Fig. 5.14 Changes in moisture ratio and temperature of banana slices undergoing LPSSD-FIR. (○), Drying medium temperature; (●), sample temperature; (△), moisture ratio.

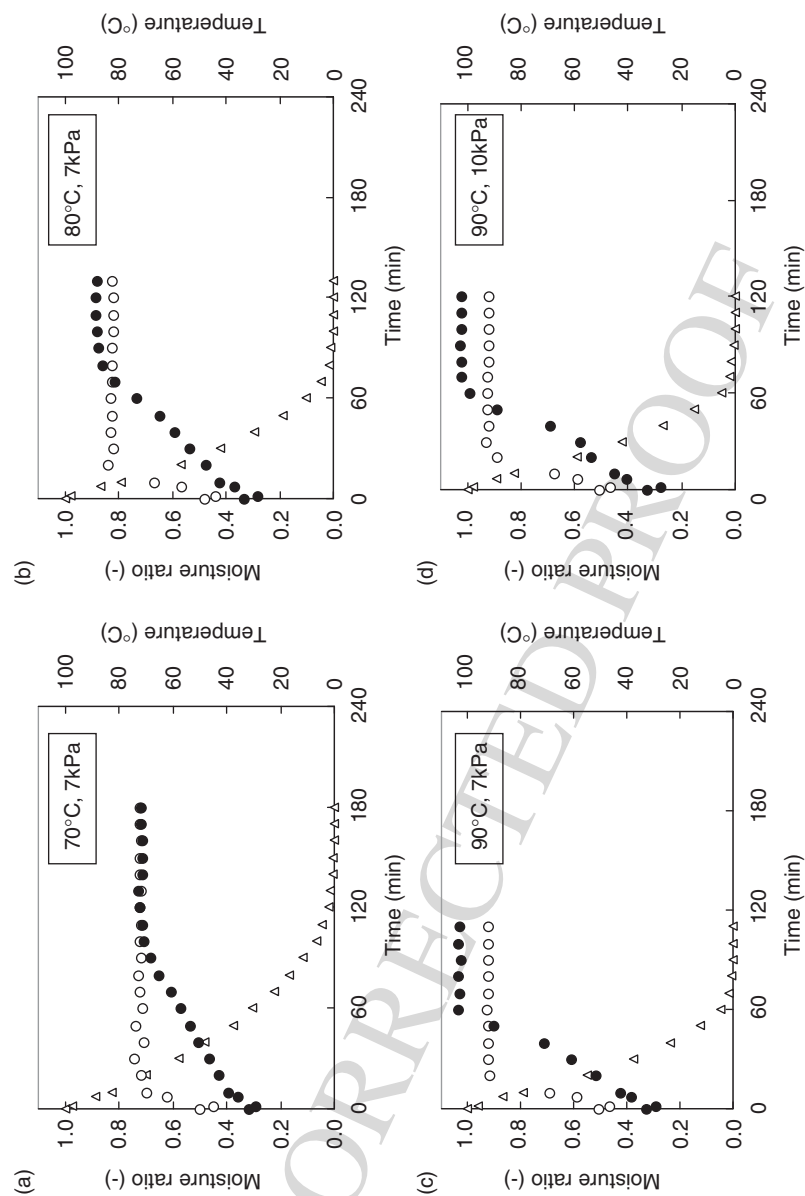


Fig. 5.15 Changes in moisture ratio and temperature of banana slices undergoing VACUUM-FIR. (○), drying medium temperature; (●), sample temperature; (△), moisture ratio.

In terms of quality it was observed that banana dried by LPSSD-FIR was significantly darker and redder than that dried by VACUUM-FIR at all drying conditions. This is because the temperature of banana slices undergoing LPSSD-FIR increased more rapidly and stayed at higher levels than that of samples dried by VACUUM-FIR as mentioned earlier.

When comparing the colors of banana chips dried either by LPSSD-FIR or VACUUM-FIR with those of banana chips dried only by LPSSD (Thomkapanish *et al.*, 2007) it is noted that bananas dried by FIR-assisted processes had higher values of color changes, especially in the case of lightness and redness. This is due to the fact that banana slices undergoing LPSSD-FIR and VACUUM-FIR were subjected to the higher temperature for a longer period than those dried by LPSSD, especially during the later stage of the process.

In terms of shrinkage it was noted that drying at lower temperatures (70° and 80°C in this case) yielded dried products with lower degrees of area shrinkage because case hardening (rigid layers) on the sample perimeter, which retarded shrinkage (surface area change) of the samples, occurred less at these conditions. Case hardening also developed faster during LPSSD-FIR and VACUUM-FIR compared with the case of LPSSD alone due to the higher sample temperatures mentioned earlier. Regarding the rehydration behavior, it was noted that banana slices dried at higher temperatures had higher rehydration ability than those dried at lower temperatures. This is because higher drying temperatures led to dried banana slices with a more porous structure, thus facilitating rehydration ability. It was also noted that banana slices dried by LPSSD-FIR generally had higher rehydration ability than those dried by VACUUM-FIR. This is due to the fact that the temperature of bananas dried by LPSSD-FIR suddenly rose to a level close to boiling temperature (as can be seen in Figure 5.14). Consequently, moisture in the banana rapidly boiled leading to rigorous evolution of steam within the samples. Larger and more pores were developed compared with the samples dried by VACUUM-FIR (see Figure 5.16, which clearly shows that when drying was performed at lower temperature banana slices dried by LPSSD-FIR had larger and more pores compared with those dried by VACUUM-FIR). However, the rehydration ability of banana slices dried by LPSSD-FIR and VACUUM-FIR was not significantly different in the case of drying at 90°C. This is probably due to the fact that moisture within the samples dried by VACUUM-FIR boiled as rigorously as in the case of LPSSD-FIR at this higher temperature. This hypothesis was confirmed by the fact that the micro-structure of banana slices dried by both methods was similar in the case of drying at 90°C (see Figures 5.16c and 5.16d).

Table 5.6 shows the results of the texture of banana chips in terms of the maximum force (hardness) and the number of peaks in the force-deformation curve (crispness). In the case of hardness it was found that banana slices dried by VACUUM-FIR were harder than those dried by LPSSD-FIR, as indicated by the higher value of the maximum force. This is probably due to the fact that VACUUM-FIR, especially at a lower drying temperature (80°C in this case), yielded dried banana slices with a more dense structure (smaller and less pores), as can be seen in Figures 5.16a and 5.16b. However, the statistical analysis showed that the effects of drying temperature and drying pressure as well as drying methods on the hardness were not significant. It should be noted that, at the same drying temperature, the hardness of banana chips was lower than that of samples dried by LPSSD alone.

In terms of crispness it can be seen again from Table 5.6 that LPSSD-FIR yielded banana chips with a larger number of peaks (hence indicating that the products were crispier) compared with VACUUM-FIR, especially at 80°C. This might be due to the larger and more numerous pores that occurred during LPSSD-FIR. Comparing these results with those obtained using LPSSD it was found that LPSSD-FIR and VACUUM-FIR provided banana

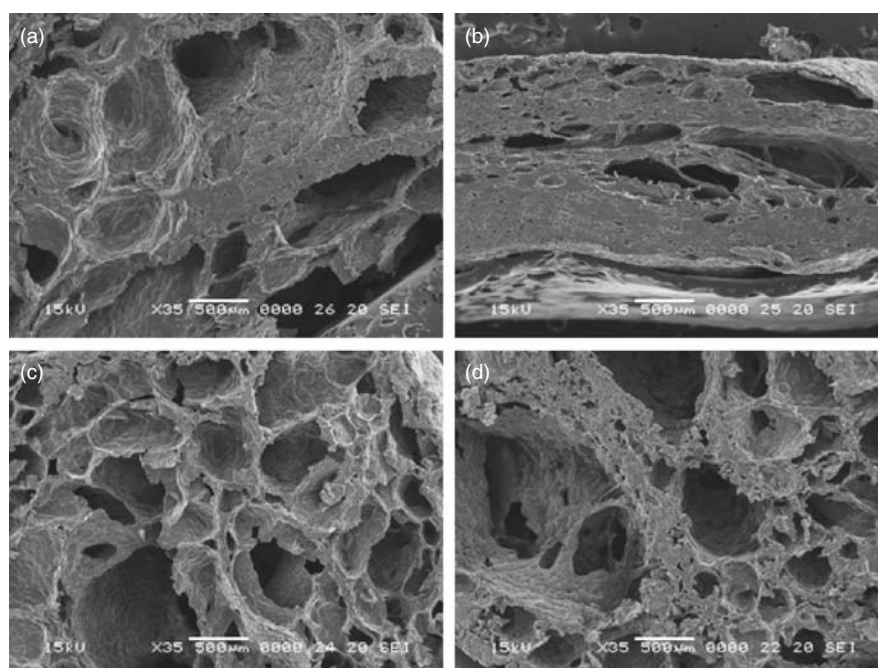


Fig. 5.16 SEM photographs showing cross section of banana slices dried by (a) LPSSD-FIR at 80°C–7 kPa, (b) VACUUM-FIR at 80°C–7 kPa, (c) LPSSD-FIR at 90°C–7 kPa, (d) VACUUM-FIR at 90°C–7 kPa.

Table 5.6 Effects of drying methods, drying temperature and pressure on maximum force and number of peaks of dried banana slices.

Drying method	Drying temperature (°C)	Drying pressure (kPa)	Maximum force (N)	Number of peaks
LPSSD-FIR	70	7	N/A	N/A
		10	N/A	N/A
	80	7	17.09 ± 3.15^a	37 ± 3^d
		10	17.30 ± 3.60^a	36 ± 4^d
	90	7	16.39 ± 3.57^a	38 ± 4^d
		10	16.89 ± 4.58^a	38 ± 5^d
VACUUM-FIR	70	7	18.44 ± 3.80^a	22 ± 4^{ab}
		10	19.12 ± 4.07^a	21 ± 5^a
	80	7	19.95 ± 3.55^a	25 ± 5^{bc}
		10	18.16 ± 4.51^a	26 ± 5^c
	90	7	16.72 ± 3.19^a	36 ± 3^d
		10	17.81 ± 3.63^a	36 ± 4^d
LPSSD ^a	70	7	N/A	N/A
	80	7	21.52 ± 2.23	27 ± 3
	90	7	24.09 ± 1.26	28 ± 6

^a Data obtained from Thomkapanish *et al.* (2007).

N/A implies that the final moisture content of 0.035 kg kg^{-1} (d.b.) was not obtainable at this condition.

Values in the same column with different superscripts mean that the values are significantly different ($p < 0.05$).

chips with a slightly larger number of peaks. This is again due to the larger and more numerous pores presented during LPSSD-FIR and VACUUM-FIR.

Instead of supplying thermal energy (via the application of low-pressure superheated steam or via the use of an electric heater) and vacuum condition continuously, Thomkapanish *et al.* (2007) implemented intermittent LPSSD of a food product (banana slices). Two intermittent modes, namely, intermittent temperature and intermittent pressure LPSSD, were tested. The effects of intermittent drying schemes, along with the other drying parameters viz. drying temperature (70–90°C) and pressure as well as the intermittency (on/off) period (10:5, 10:10 and 10:20 min in the case of intermittent supply of energy and 5:0, 5:5 and 5:10 min in the case of intermittent supply of vacuum) on the drying kinetics and various quality attributes (color, shrinkage, texture and ascorbic acid retention) of the dried banana chips were evaluated. The energy consumption values for intermittent LPSSD were also monitored through the effective (or net) drying time at various intermittent drying conditions and the results compared to those using continuous LPSSD.

In the case of intermittent temperature LPSSD the overall drying rates of intermittent and continuous LPSSD were not significantly different. However, the effective or net drying time of intermittent drying was significantly shorter than that of continuous drying, especially with a longer tempering period leading to high energy savings (up to 65%). It was also noted that the drying rates of intermittent pressure LPSSD were higher than those of continuous drying (in the range of 50–58%).

In terms of the quality of the dried chips it was found that the effect of intermittency in intermittent temperature drying in almost all cases, when compared with continuous drying, was not significant. However, intermittent temperature drying led to higher level of ascorbic acid retention, especially at longer tempering (off) periods.

On the other hand, it was noted that the colors of the products in the case of intermittent pressure drying were worse than those in the case of continuous drying. Shrinkage of the samples dried by intermittent pressure drying was also more obvious than in the case of continuous drying at all conditions. In addition, intermittent pressure drying led to greater degradation of ascorbic acid. This drying scheme is therefore not appropriate for heat- and, in particular, oxygen-sensitive products, as oxygen (air) is necessarily introduced to the drying chamber during the off period.

5.5 MATHEMATICAL MODELING OF LPSSD OF FOODS AND BIOMATERIALS

Several models with different degrees of complexity and predictability have been proposed for LPSSD. In this section only selected models applied to LPSSD of foods and biomaterials are reviewed, however. Mathematical models for LPSSD of other products are available in the literature (e.g. Shibata *et al.*, 1990; Pang, 1997; Elustondo *et al.*, 2002; Defo *et al.*, 2004; Suvarnakuta *et al.*, 2005b).

Elustondo *et al.* (2001) developed a mathematical model based on a theoretical drying mechanism, which assumes that the water removal is carried out by evaporation in a moving boundary allowing the vapor to flow through the dry layer built as drying proceeds to predict the drying characteristics of foodstuffs undergoing LPSSD. A simplified expression, which has two experimentally determined parameters, was derived and used to predict the drying rate of test samples. Despite its simplicity it was noted that the model could predict the drying kinetics of the tested materials adequately.

Suvarnakuta *et al.* (2007) proposed the use of a simple three-dimensional liquid diffusion based model to predict the evolutions of the moisture content and temperature of a biomaterial (carrot cube) undergoing LPSSD. The model consists of coupled heat conduction and mass diffusion equations along with an empirical equation, which describes shrinkage of the product during drying. An empirical equation that expresses the β -carotene degradation in carrot is also included in the model so as to predict the evolution of β -carotene content in carrot during drying.

The model assumes that the sample is isotropic and homogenous. Initial condensation of steam is also neglected in the model. In addition, mass transfer within the material is controlled only by liquid diffusion; it is thus assumed that no vaporization occurs within the drying material. Finally, it is assumed that shrinkage of the material is significant, and that it is accounted for in all three directions. The volumetric shrinkage depends on the operating temperature and moisture content and is described by an empirically determined correlation.

The conduction equation to describe energy transfer is written as follows:

$$\rho C_p \frac{\partial T}{\partial t} = \frac{\partial}{\partial x} \left(k_x \frac{\partial T}{\partial x} \right) + \frac{\partial}{\partial y} \left(k_y \frac{\partial T}{\partial y} \right) + \frac{\partial}{\partial z} \left(k_z \frac{\partial T}{\partial z} \right) \quad (5.3)$$

where $k_x = k_y = k_z = k$ due to the product isotropy.

The equation to describe the mass transfer during LPSSD is:

$$\frac{\partial X_f}{\partial t} = \frac{\partial}{\partial x} \left(D_{eff} \frac{\partial X_f}{\partial x} \right) + \frac{\partial}{\partial y} \left(D_{eff} \frac{\partial X_f}{\partial y} \right) + \frac{\partial}{\partial z} \left(D_{eff} \frac{\partial X_f}{\partial z} \right) \quad (5.4)$$

At the onset of the LPSSD process the temperature and moisture content of the material are uniform.

$$T = T_i \quad (5.5)$$

$$X = X_{fi} \quad (5.6)$$

For the material subjected to convective drying the boundary condition (equation (5.7)) at the surface is used:

$$-k(\nabla T \cdot n) = h(T_{steam} - T_s) - \rho \lambda D_{eff}(\nabla X_f \cdot n) \quad (5.7)$$

where the term on the left-hand side refers to heat conducted from the outer surface to the inside of the cube, the first term on the right-hand side is heat penetrating from low-pressure superheated steam to the solid body by means of convection and the second term on the right-hand side denotes the latent heat of vaporization.

Mass transfer at the surface is modeled by assuming that there is no mass transfer resistance at the surface of the material since water possesses no self-resistance in its own body. This is certainly not a very realistic assumption and a model should be developed in future to better represent the phenomenon (by, for example, recognizing that the driving force for mass transfer from the surface is the difference between the vapor pressure of moisture at the surface temperature and the steam pressure in the bulk phase).

$$X_f = 0 \quad (5.8)$$

where X_f denotes free moisture content ($X_f = X - X_{eq}$). This condition simply implies that the moisture content at the surface was always at its equilibrium value at the corresponding operating condition.

The detailed estimation of the parameters required in the model is described in Suvarnakuta *et al.* (2007). It is only important to note here that the values of the effective diffusion coefficient (D_{eff}) obtained, assuming that the material suffers no shrinkage, are different from those obtained assuming that the material suffers uniform shrinkage.

The above-mentioned model was validated by the available experimental data. The estimated values of the heat transfer coefficient were set in the range of $\pm 20\%$ (see Table 5.1) to investigate the sensitivity of this parameter on the predictability of the product temperature and moisture content.

Figure 5.17 illustrates the sample evolutions of the moisture ratio and the center temperature of carrot cube undergoing LPSSD. It was found that the trends of moisture ratio prediction are in good agreement with the experimental data. However, at the highest operating pressure (13 kPa) the model was not able to predict the experimental data well (see Figures 5.18 and 5.19). This is due to the fact that a larger amount of steam condensation occurred during the start-up period at a higher operating pressure (since steam at a lower degree of superheat tended to condense more easily) and this led to under-prediction of the moisture ratio since the model, as mentioned earlier, did not take into account the effect of initial condensation. The same reason could also be used to explain a rather larger discrepancy between simulated and experimental results at lower drying steam temperatures as well.

Representative product center temperature profiles over time are also presented in Figures 5.17–5.19. The center temperature increased over time until it reached the boiling point of water at the corresponding operating pressure; after this point, the temperature slowly increased while latent heating prevented a temperature rise. It is seen from these figures that the simulated predictions did not quite agree with the experimental data. This is due to the fact that carrots undergoing LPSSD in fact shrank non-uniformly. Thus, the assumption of

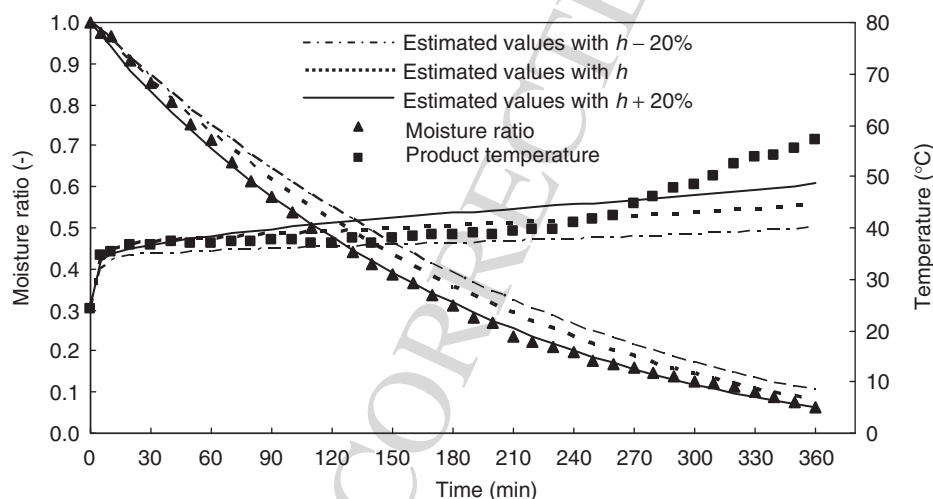


Fig. 5.17 Comparison between predicted (assuming shrinkage) and experimental moisture content and temperature variation with time of carrot cube at 60°C and 7 kPa ($X_{eq} = 0.10 \text{ kg kg}^{-1}$ (d.b.)). Lines represent predicted data; symbols represent experimental data.

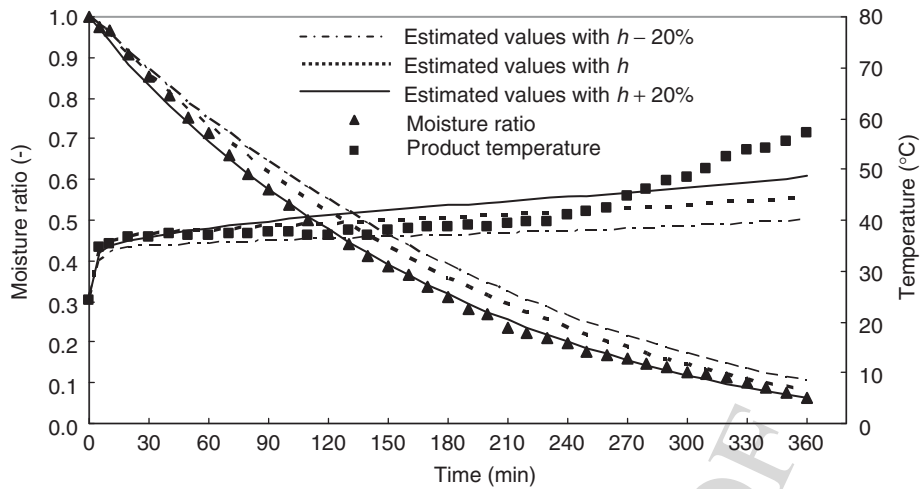


Fig. 5.18 Comparison between predicted (assuming shrinkage) and experimental moisture content and temperature of carrot cube at 70°C and 13 kPa ($X_{eq} = 0.10 \text{ kg kg}^{-1}$ (d.b.)).

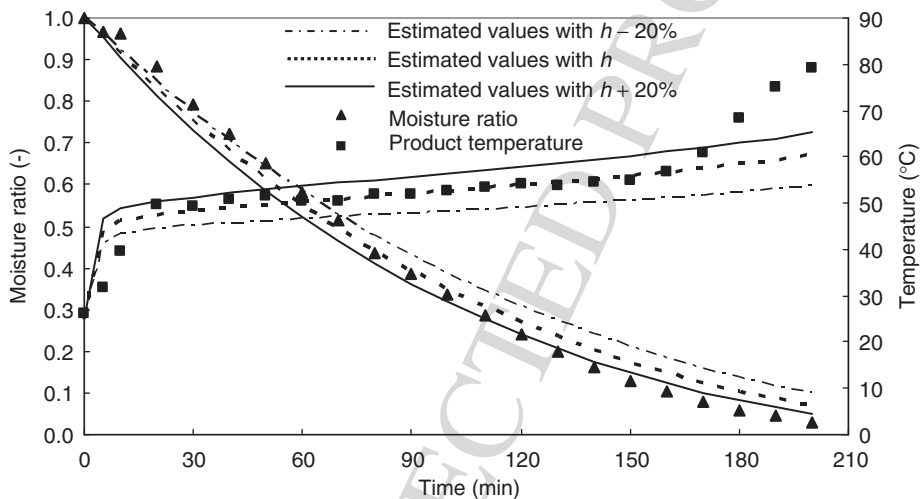


Fig. 5.19 Comparison between predicted (assuming shrinkage) and experimental moisture content and temperature of carrot cube at 80°C and 13 kPa ($X_{eq} = 0.10 \text{ kg kg}^{-1}$ (d.b.)).

uniform shrinkage used in this study was not quite correct. Another factor that contributed to the deviation of the simulated results from the experimental data is the fact that once the boiling point was reached there was vapor generation, which could give rise to an increase in the internal pressure in pores. Thus, it was possible that hydrostatic pressure gradients were generated within the product, which could in turn drive the liquid-form moisture out of the product faster than that permissible by liquid diffusion alone. Furthermore, the change in porosity and physical structure of carrot during drying could, in principle, change the diffusivity from what was predicted by the empirical correlations used.

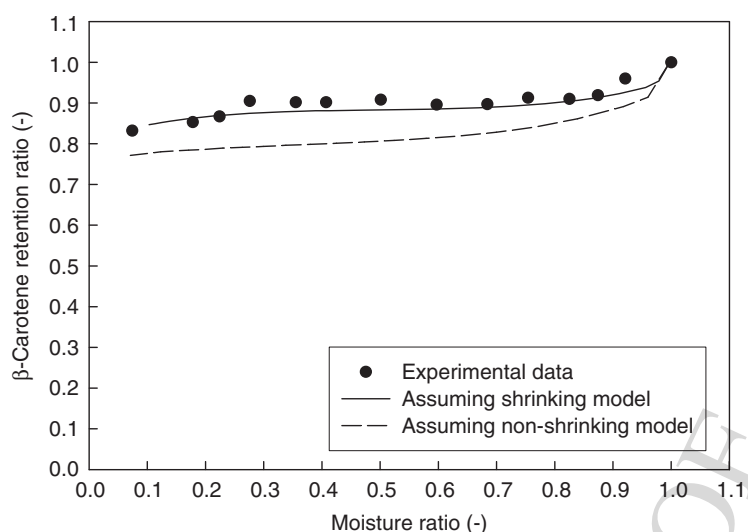


Fig. 5.20 Comparison between predicted and experimental β -carotene degradation of carrot at 60°C.

Figure 5.20 shows a sample predicted β -carotene degradation in carrot during LPSSD using the middle values of heat transfer coefficients. The β -carotene degradation predictions, which follow from the simulated moisture content and temperature based on the assuming shrinking model, show good agreement with the experimental data under all conditions.

The next step for model development should be directed towards the use of more realistic assumptions, boundary conditions and inclusion of phenomena that really occur during LPSSD, for example, vaporization of moisture within the drying material.

5.6 CONCLUDING REMARKS

Owing to several limitations of near-atmospheric pressure superheated steam drying, low-pressure superheated steam drying (LPSSD) has emerged as an alternative for drying heat- and/or oxygen-sensitive food products. Over the past several years, many attempts have been made to apply this technology to a wide array of foods and it has been shown that LPSSD could produce dried products with superior quality, either in terms of physical or chemical (nutritional) quality, compared with products dried by conventional hot air drying or vacuum drying. In addition to applying this technology to drying foods *per se*, LPSSD also has the potential to produce engineered biomaterials for different applications in food engineering, for example, production of antioxidant/antimicrobial edible films for active packaging applications. Preliminary results have indeed shown that LPSSD could yield edible films with higher strength, compared with films obtained from vacuum drying, due to its ability to enhance crystallinity of the film structure.

Future developments in this area should aim towards developing a more realistic mathematical model that enables predictions of moisture content and temperature evolutions within the drying material. Further use of the technology for the production of advanced materials should also be investigated.

5.7 NOTATION

C_p	heat capacity, $\text{J kg}^{-1} \text{K}^{-1}$
D_{eff}	effective diffusivity, $\text{m}^2 \text{s}^{-1}$
h	heat transfer coefficient, $\text{W m}^{-2} \text{K}^{-1}$
k	thermal conductivity, $\text{W m}^{-1} \text{K}^{-1}$
MR	moisture ratio, $\frac{X - X_{eq}}{X_i - X_{eq}}$
n	unit vector
N	evaporation rate, kg s^{-1}
q	heat transfer rate, W
t	time, s
T	temperature, $^{\circ}\text{C}$
T_i	initial temperature, $^{\circ}\text{C}$
X	total moisture content, $\text{kg water per kg dry solid (d.b.)}$
X_{eq}	equilibrium moisture content, $\text{kg water per kg dry solid (d.b.)}$
X_f	free moisture content, $\text{kg water per kg dry solid (d.b.)}$

Greek letters

λ	latent heat of vaporization, J kg^{-1}
ρ	density, kg m^{-3}

Subscripts

f	free
i	initial
s	surface of product
<i>steam</i>	superheated steam

REFERENCES

- Abe, T. and Miyashita, K. (2006) Surface sterilization of dried fishery products in superheated steam and hot air. *Nippon Shokuhin Kagaku Kogaku Kaishi*, **53**, 373–379.
- Achanta, S. and Okos, M.R. (2000) Quality changes during drying of food polymers. In: *Drying Technology in Agriculture and Food Science* (ed. A.S. Mujumdar). Science Publishers, Enfield, NH, pp. 133–147.
- Barbieri, S., Elustondo, M. and Urbicain, M. (2004) Retention of aroma compounds in basil dried with low pressure superheated steam. *Journal of Food Engineering*, **65**, 109–115.
- Bond, J.F., Mujumdar, A.S., van Heiningen, A.R.P. and Douglas, W.J.M. (1994) Drying paper by impinging jets of superheated steam. Part 2: Comparison of steam and air as drying fluids. *Canadian Journal of Chemical Engineering*, **72**, 452–456.
- Cenkowski, S., Pronyk, C., Zmidzinska, D. and Muir, W.E. (2007) Decontamination of food products with superheated steam. *Journal of Food Engineering*, **83**, 68–75.
- Chen, S.R., Chen, J.Y. and Mujumdar, A.S. (1992) Preliminary study of steam drying of silkworm cocoons. *Drying Technology*, **10**, 251–260.
- Chow, L.C. and Chung, J.N. (1983) Evaporation of water into a laminar stream of air and superheated steam. *International Journal of Heat and Mass Transfer*, **26**, 373–380.
- Defo, M., Fortin, Y. and Cloutier, A. (2004) Modeling superheated steam vacuum drying of wood. *Drying Technology*, **22**, 2231–2253.

- Devahastin, S. and Suvarnakuta, P. (2004) Superheated-steam-drying of food products. In: *Dehydration of Products of Biological Origin* (ed. A.S. Mujumdar). Science Publishers, Enfield, NH, pp. 493–512.
- Devahastin, S., Suvarnakuta, P., Soponronnarit, S. and Mujumdar, A.S. (2004) A comparative study of low-pressure superheated steam and vacuum drying of a heat-sensitive material. *Drying Technology*, **22**, 1845–1867.
- Douglas, W.J.M. (1994) Drying paper in superheated steam. *Drying Technology*, **12**, 1341–1355.
- Elustondo, D., Elustondo, M.P. and Urbicain, M.J. (2001) Mathematical modeling of moisture evaporation from foodstuffs exposed to subatmospheric pressure superheated steam. *Journal of Food Engineering*, **49**, 15–24.
- Elustondo, D.M., Mujumdar, A.S. and Urbicain, M.J. (2002) Optimum operating conditions in drying of foodstuffs with superheated steam. *Drying Technology*, **20**, 381–402.
- Furukawa, T. and Akao, T. (1983) Deodorization by superheated steam drying. *Drying Technology*, **2**, 407–418.
- Haji, M. and Chow, L.C. (1988) Experimental measurement of water evaporation rates into air and superheated steam. *Journal of Heat Transfer*, **110**, 237–242.
- Incropera, F.P. and DeWitt, D.P. (2002) *Fundamentals of Heat and Mass Transfer*, 5th edn. Wiley, New York.
- Iyota, H., Konishi, Y., Inoue, T., Yoshida, K., Nishimura, N. and Nomura, T. (2005) Popping of Amaranth seeds in hot air and superheated steam. *Drying Technology*, **23**, 1273–1287.
- Iyota, H., Nishimura, N., and Nomura, T. (2001) Drying of sliced raw potatoes in superheated steam and hot air. *Drying Technology*, **19**, 1411–1424.
- Jamradloedluk, J., Nathakaranakule, A., Soponronnarit, S. and Prachayawarakorn, S. (2007) Influences of drying medium and temperature on drying kinetics and quality attributes of durian chips. *Journal of Food Engineering*, **78**, 198–205.
- Kongsoontornkijkul, P., Ekwongsupasarn, P., Chiewchan, N. and Devahastin, S. (2006) Effects of drying methods and tea preparation temperature on the amount of vitamin C in Indian gooseberry tea. *Drying Technology*, **24**, 1509–1513.
- Kozanoglu, B., Vazquez, A.C., Chanes, J.W. and Patino, J.L. (2006) Drying of seeds in a superheated steam vacuum fluidized bed. *Journal of Food Engineering*, **75**, 383–387.
- Leeratanarak, N., Devahastin, S. and Chiewchan, N. (2006) Drying kinetics and quality of potato chips undergoing different drying techniques. *Journal of Food Engineering*, **77**, 635–643.
- Methakhup, S., Chiewchan, N. Devahastin, S. (2005) Effects of drying methods and conditions on drying kinetics and quality of Indian gooseberry flake. *LWT – Food Science and Technology*, **38**, 579–587.
- Moreira, R.G. (2001) Impingement drying of foods using hot air and superheated steam. *Journal of Food Engineering*, **49**, 291–295.
- Mujumdar, A.S. (2000) Superheated steam drying – Technology of the future. In: *Mujumdar's Practical Guide to Industrial Drying* (ed. S. Devahastin). Exergex Corp., Brossard, Canada, pp. 115–138.
- Mujumdar, A.S. (2007) Superheated steam drying. In: *Handbook of Industrial Drying*, 3rd edn. (ed. A.S. Mujumdar). CRC Press, Boca Raton, FL, pp. 439–452.
- Namsanguan, Y., Tia, W., Devahastin, S. and Soponronnarit, S. (2004) Drying kinetics and quality of shrimp undergoing different two-stage drying processes. *Drying Technology*, **22**, 759–778.
- Nathakaranakule, A., Kraiwanichkul, W. and Soponronnarit, S. (2007) Comparative study of different combined superheated-steam drying techniques for chicken meat. *Journal of Food Engineering*, **80**, 1023–1030.
- Nimmol, C., Devahastin, S., Swasdisevi, T. and Soponronnarit, S. (2007) Drying of banana slices using combined low-pressure superheated steam and far-infrared radiation. *Journal of Food Engineering*, **81**, 624–633.
- Pang, S. (1997) Some considerations in simulation of superheated steam drying of softwood lumber. *Drying Technology*, **15**, 651–670.
- Pang, S. and Dakin, M. (1999) Drying rate and temperature profile for superheated steam vacuum drying and moist air drying of softwood lumber. *Drying Technology*, **17**, 1135–1147.
- Panyawong, S. and Devahastin, S. (2007) Determination of deformation of a food product undergoing different drying methods and conditions via evolution of a shape factor. *Journal of Food Engineering*, **78**, 151–161.

- Pimpaporn, P., Devahastin, S. and Chiewchan, N. (2007) Effects of combined pretreatments on drying kinetics and quality of potato chips undergoing low-pressure superheated steam drying. *Journal of Food Engineering*, **81**, 318–329.
- Prachayawarakorn, S., Soponronnarit, S., Wetchacama, S. and Jaisut, D. (2002) Desorption isotherms and drying characteristics of shrimp in superheated steam and hot air. *Drying Technology*, **20**, 669–684.
- Prachayawarakorn, S., Prachayawasin, P. and Soponronnarit, S. (2006) Heating process of soybean using hot-air and superheated-steam fluidized-bed dryers. *LWT – Food Science and Technology*, **39**, 770–778.
- Pronyk, C., Cenkowski, S. and Abramson, D. (2006) Superheated steam reduction of deoxynivalenol in naturally contaminated wheat kernels. *Food Control*, **17**, 789–796.
- Rordprapat, W., Nathakaranakule, A., Tia, W. and Soponronnarit, S. (2005) Comparative study of fluidized bed paddy drying using hot air and superheated steam. *Journal of Food Engineering*, **71**, 28–36.
- Sano, A., Senda, Y., Oyama, K., Tanigawara, R., Bando, Y., Nakamura, M., Sugimura, Y. and Shibata, M. (2005) Drying characteristics in superheated steam drying at reduced pressure. *Drying Technology*, **23**, 2437–2447.
- Schwartz, J.P. and Brocker, S. (2002) A theoretical explanation for the inversion temperature. *Chemical Engineering Journal*, **86**, 61–67.
- Sheikholeslami, R. and Watkinson, A.P. (1992) Rate of evaporation of water into superheated steam and humidified air. *International Journal of Heat and Mass Transfer*, **35**, 1743–1751.
- Shibata, H., Mada, J. and Shinohara, H. (1988) Steam drying of sintered glass bead spheres under vacuum. *Industrial & Engineering Chemistry Research*, **27**, 2385–2387.
- Shibata, H., Mada, J. and Funatsu, K. (1990) Prediction of drying rate curves on sintered spheres of glass beads in superheated steam under vacuum. *Industrial & Engineering Chemistry Research*, **29**, 614–617.
- Shibata, H. (2006) Drying rate curves of porous solids in steam and in air under low-pressure conditions. *Drying Technology*, **24**, 37–43.
- Soponronnarit, S., Nathakaranakule, A., Jirajindalert, A. and Taechapairoj, C. (2006) Parboiling brown rice using superheated steam fluidization technique. *Journal of Food Engineering*, **75**, 423–432.
- Sotome, I., Suzuki, K., Koseki, S., *et al.* (2006) Blanching of potato with superheated steam containing micro-droplets of hot water. *Nippon Shokuhin Kagaku Kogaku Kaishi*, **53**, 451–458.
- Suvarnakuta, S., Devahastin, S. and Mujumdar, A.S. (2005a) Drying kinetics and β -carotene degradation in carrot undergoing different drying processes. *Journal of Food Science*, **70**, S520–S526.
- Suvarnakuta, S., Devahastin, S. and Mujumdar, A.S. (2007) A mathematical model for low-pressure superheated steam drying of a biomaterial. *Chemical Engineering and Processing*, **46**, 675–683.
- Suvarnakuta, S., Devahastin, S., Soponronnarit, S. and Mujumdar, A.S. (2005b) Drying kinetics and inversion temperature in a low-pressure superheated steam-drying system. *Industrial & Engineering Chemistry Research*, **44**, 1934–1941.
- Taechapairoj, C., Prachayawarakorn, S. and Soponronnarit, S. (2004) Characteristics of rice dried in superheated-steam fluidized-bed. *Drying Technology*, **22**, 719–743.
- Tatemoto, Y., Yano, S., Mawatari, Y., Noda, K. and Komatsu, N. (2007) Drying characteristics of porous material immersed in a bed of glass beads fluidized by superheated steam under reduced pressure. *Chemical Engineering Science*, **62**, 471–480.
- Thomkapanish, O., Suvarnakuta, S. and Devahastin, S. (2007). Study of intermittent low-pressure superheated steam and vacuum drying of a heat-sensitive material. *Drying Technology*, **25**, 205–223.
- Wu, C.-H., Davis, D.C. and Chung, J.N. (1989) Simulated dehydration of wedge-shaped specimens in turbulent flow of superheated steam and air. *Drying Technology*, **7**, 761–782.
- Wu, C.-H., Davis, D.C., Chung, J.N. and Chow, L.C. (1987) Simulation of wedge-shaped product dehydration using mixture of superheated steam and air in laminar flow. *Numerical Heat Transfer*, **11**, 109–123.

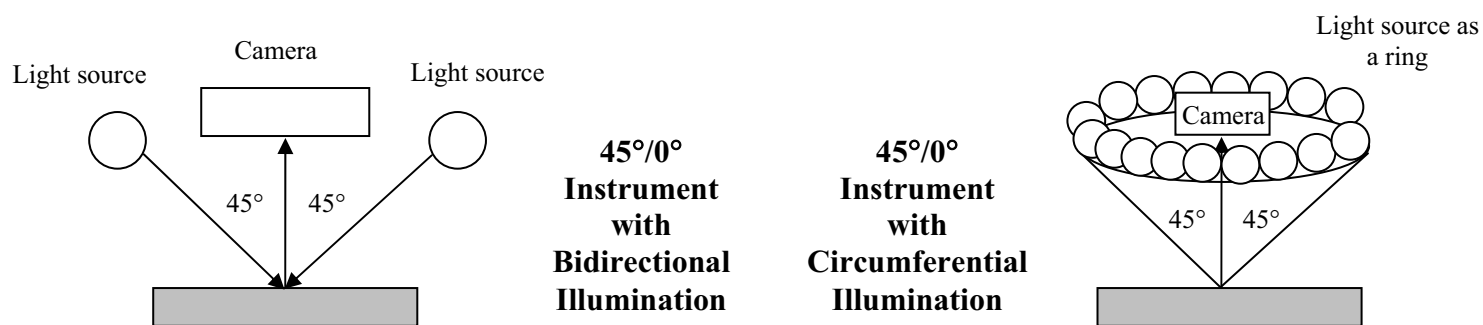


Figure 1. Set-up of a camera and illuminant with 45° reflection

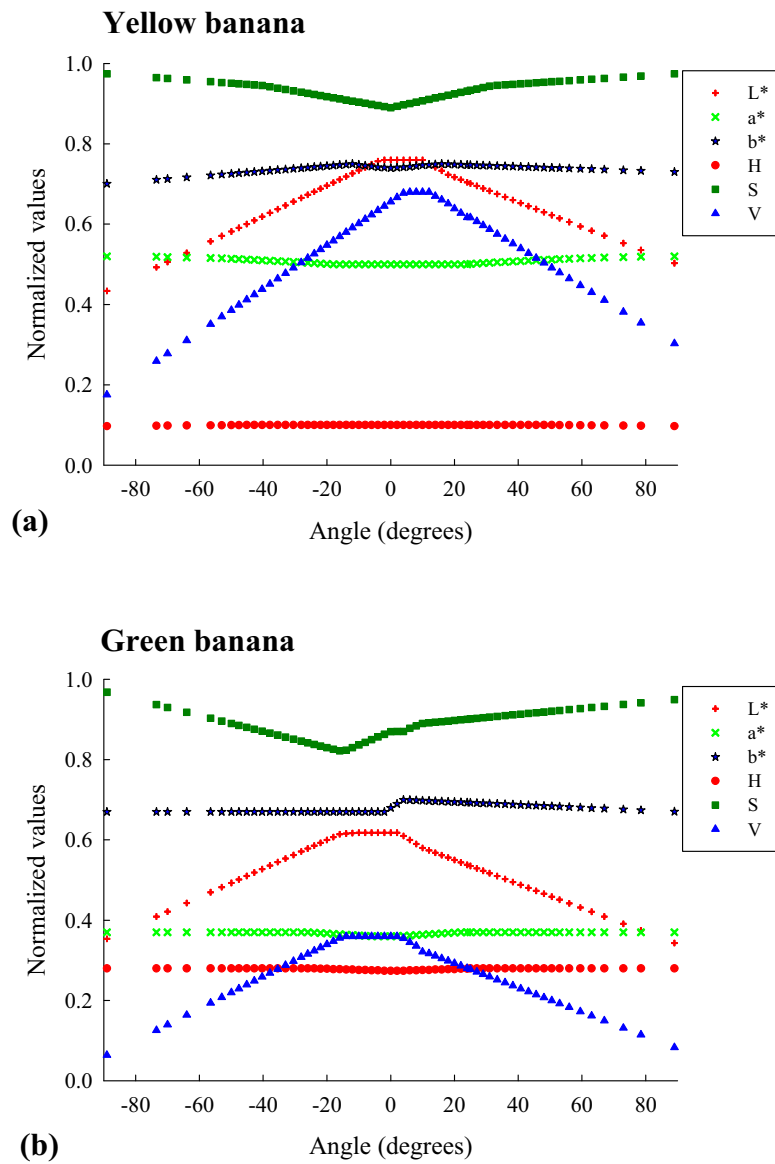


Figure 2. Color profiles expressed in $L^*a^*b^*$ and HSV color scales for: (a) yellow banana; (b) green banana (Mendoza et al., 2006)

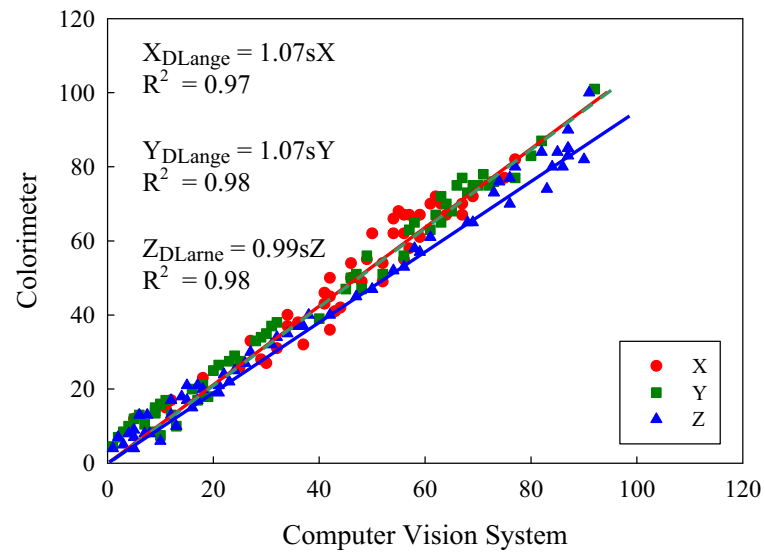


Figure 3. Plots of color scale values acquired by Computer Vision System against values measured by a colorimeter on 125 Pantone® color sheets (Mendoza et al., 2006)

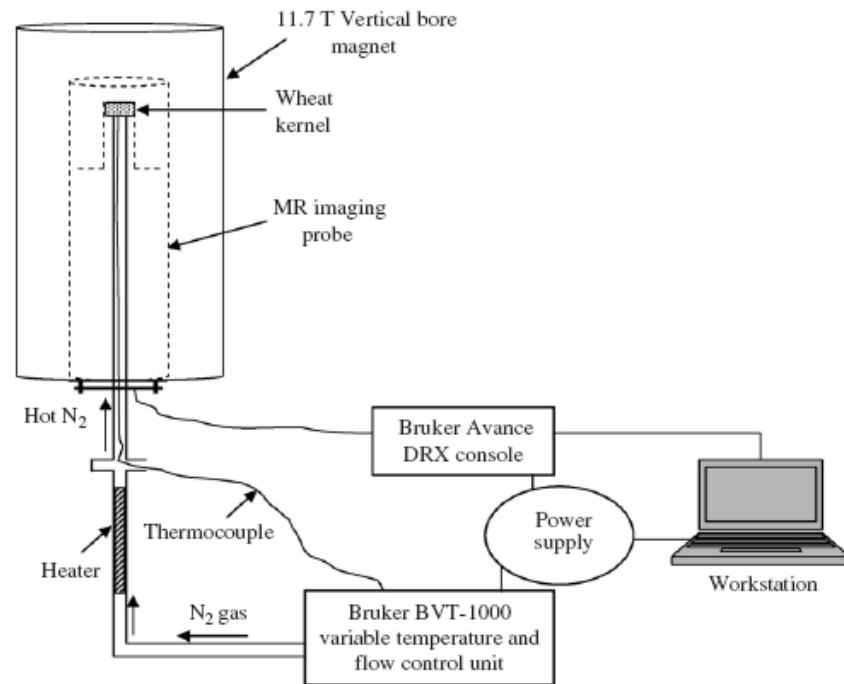


Figure 4. A schematic diagram of MRI experimental set up with the dryer assembly (Ghosh et al., 2007)

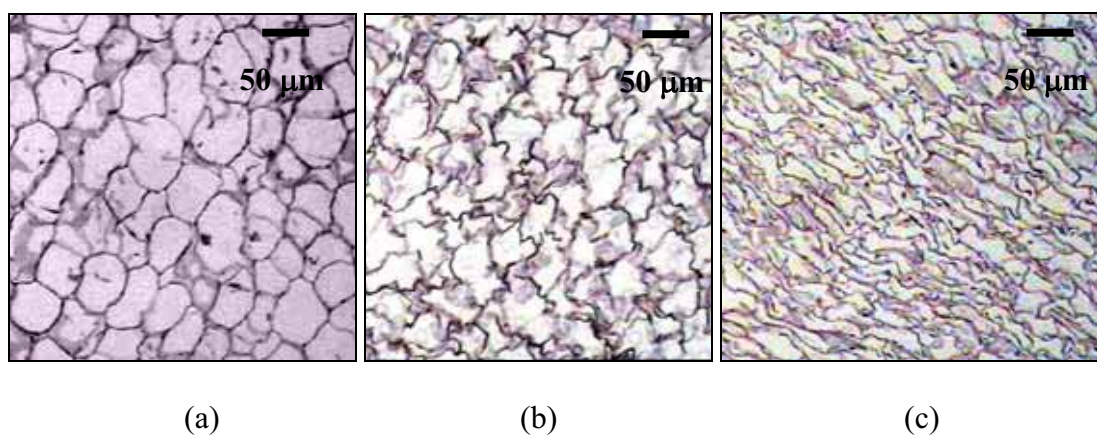


Figure 5. Microstructure of carrot cube undergoing hot air drying at 60°C, 0.5 m/s after (a) 0 min, (b) 150 min and (c) 300 min

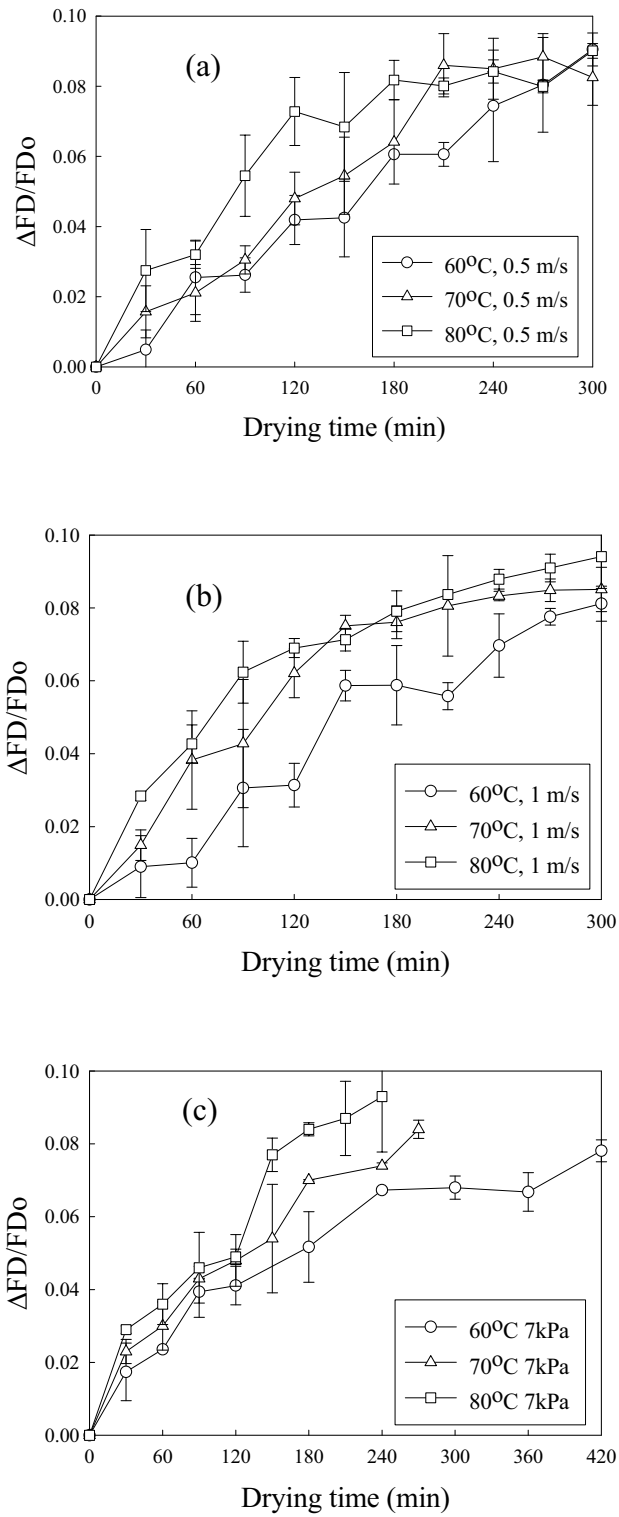


Figure 6. $\Delta FD/FD_0$ of carrot cube undergoing hot air drying (a) velocities of 0.5 m/s and (b) 1 m/s) and (c) LPSSD at 7 kPa

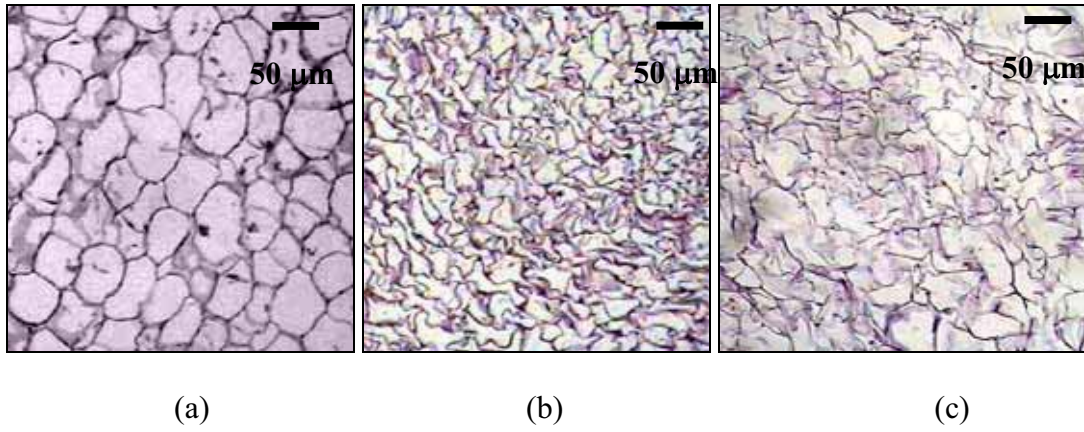


Figure 7. Microstructure of (a) fresh carrot cube and of carrot cube dried until reaching equilibrium moisture content using (b) hot air drying and (c) LPSSD

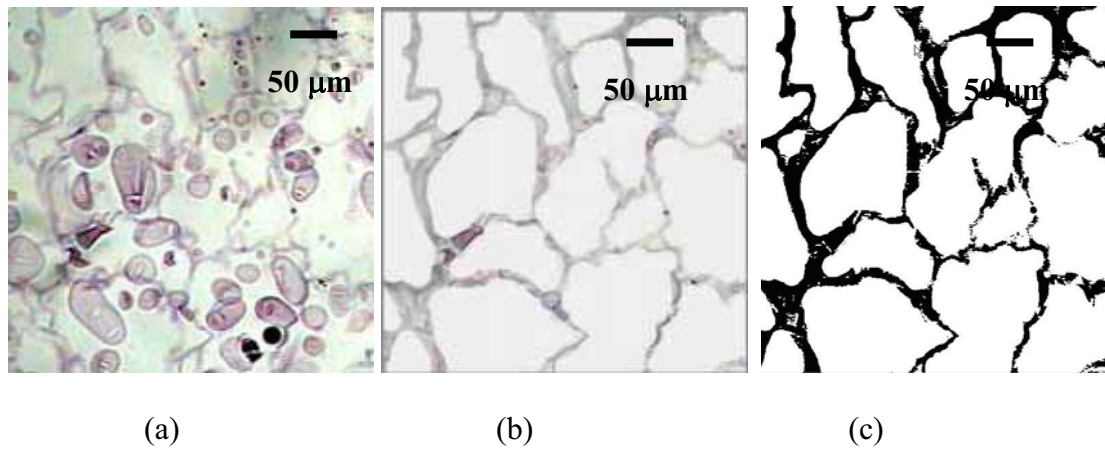


Figure 8. Image processing of potato cube (a) original image, (b) image after deleting of starch granules and (c) black and white image

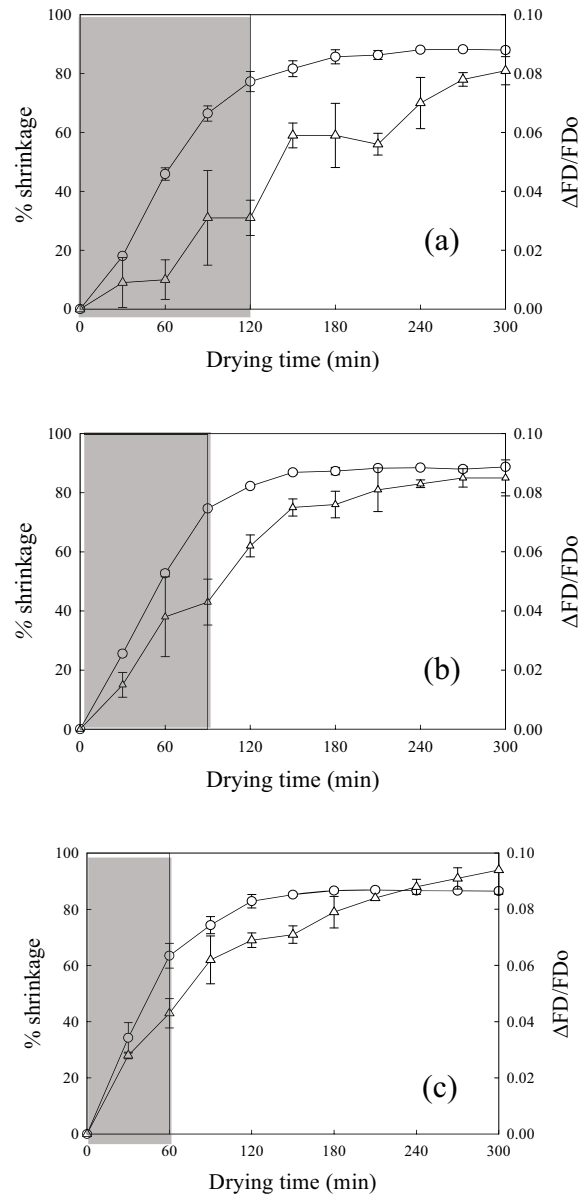


Figure 9. Relationship between % shrinkage (o) and $\Delta FD/FD_0$ (Δ) of carrot cube undergoing hot air drying at velocity of 1 m/s and temperatures of (a) 60°C, (b) 70°C and (c) 80°C

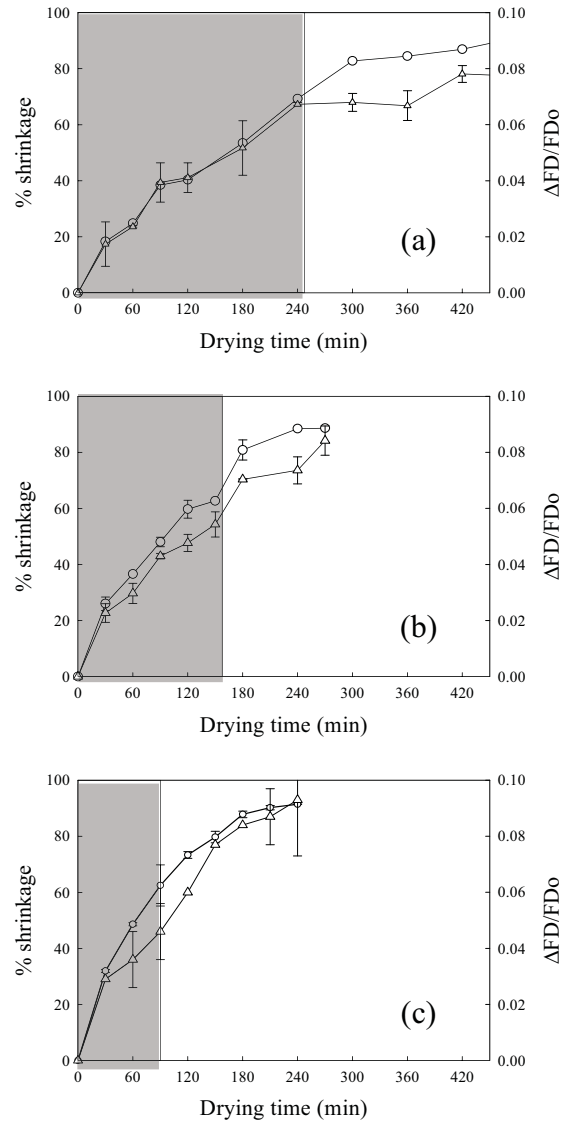
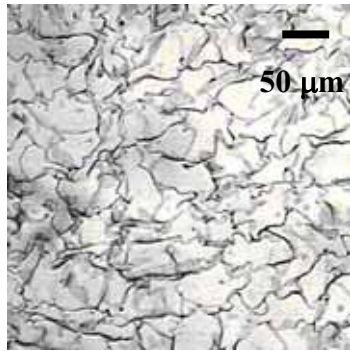
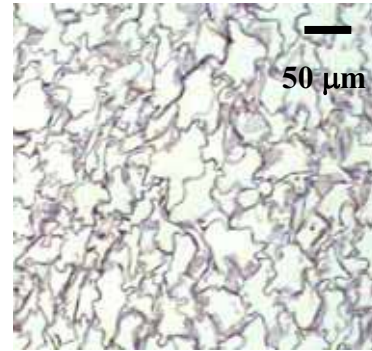


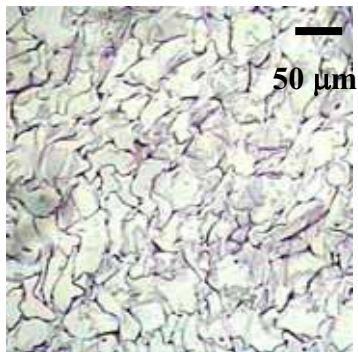
Figure 10. Relationship between % shrinkage (○) and $\Delta FD/FD_0$ (Δ) of carrot cube undergoing LPSSD at temperatures of (a) 60°C, (b) 70°C and (c) 80°C



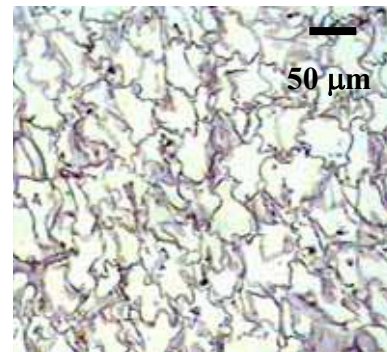
LPSSD, 60°C, 210 min



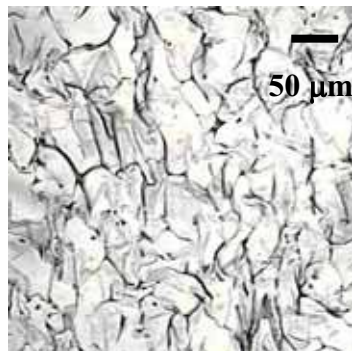
HAD, 60°C, 1 m/s, 150 min



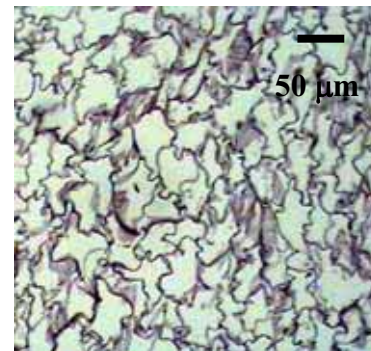
LPSSD, 70°C, 150 min



HAD, 70°C, 1m/s, 120 min

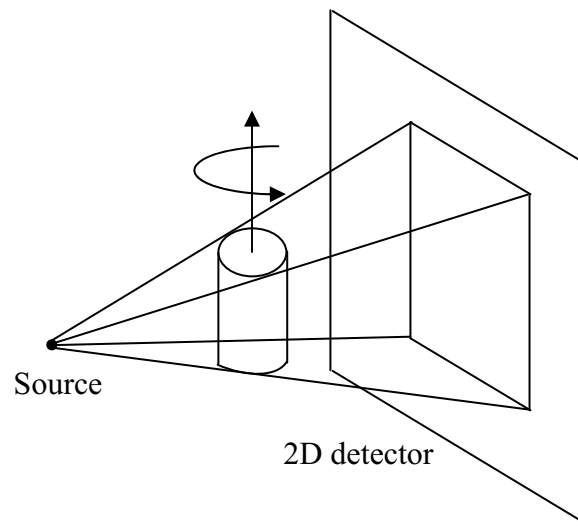


LPSSD, 80°C, 120 min

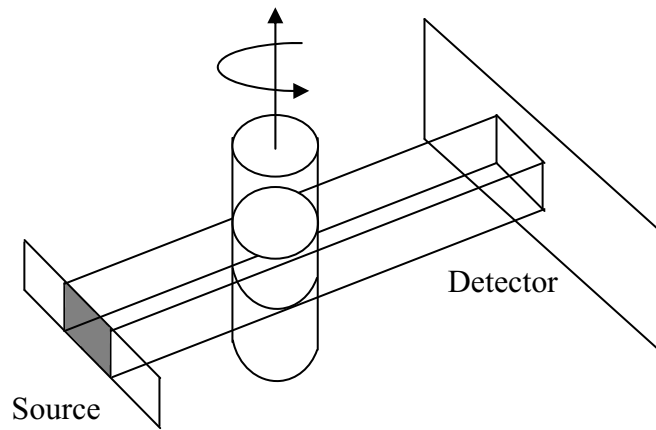


HAD, 80°C, 1m/s, 90 min

Figure 11. Microstructural images of carrot cube at $\Delta FD/FD_0 = 0.06$



(a)



(b)

Figure 12. (a) A schematic view of an X-ray microtomograph with cone-beam geometry; (b) A schematic view of a synchrotron microtomography

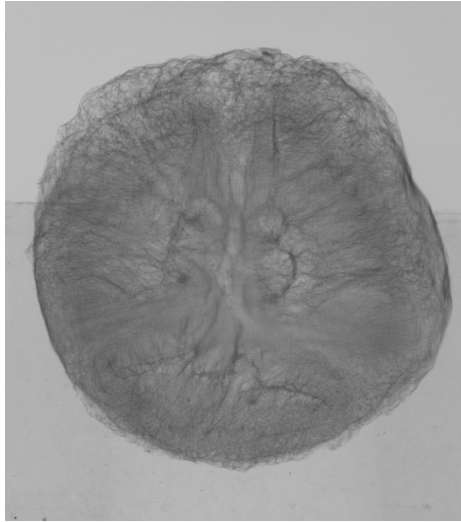
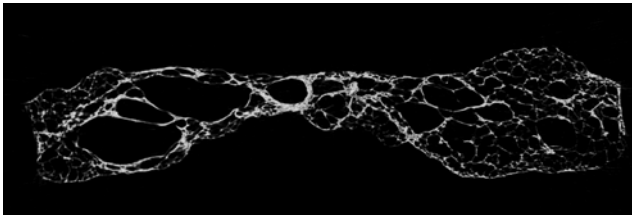
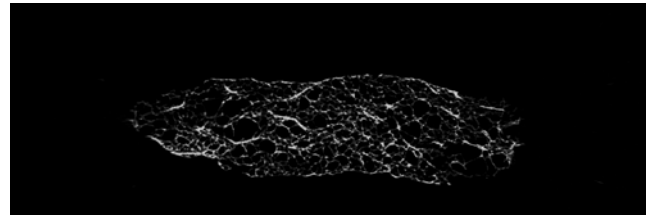


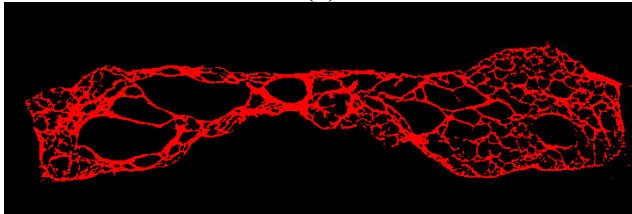
Figure 13. Radiograph of a dried banana slice



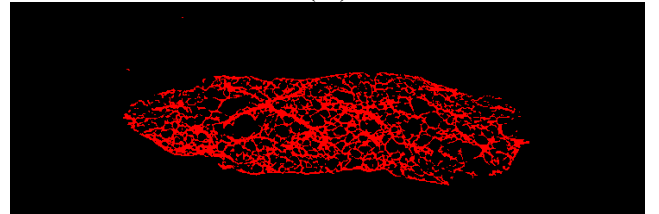
(a)



(b)



(c)



(d)

Figure 14. Grey level cross sections (a-b) and the corresponding binary images after thresholding (c-d)

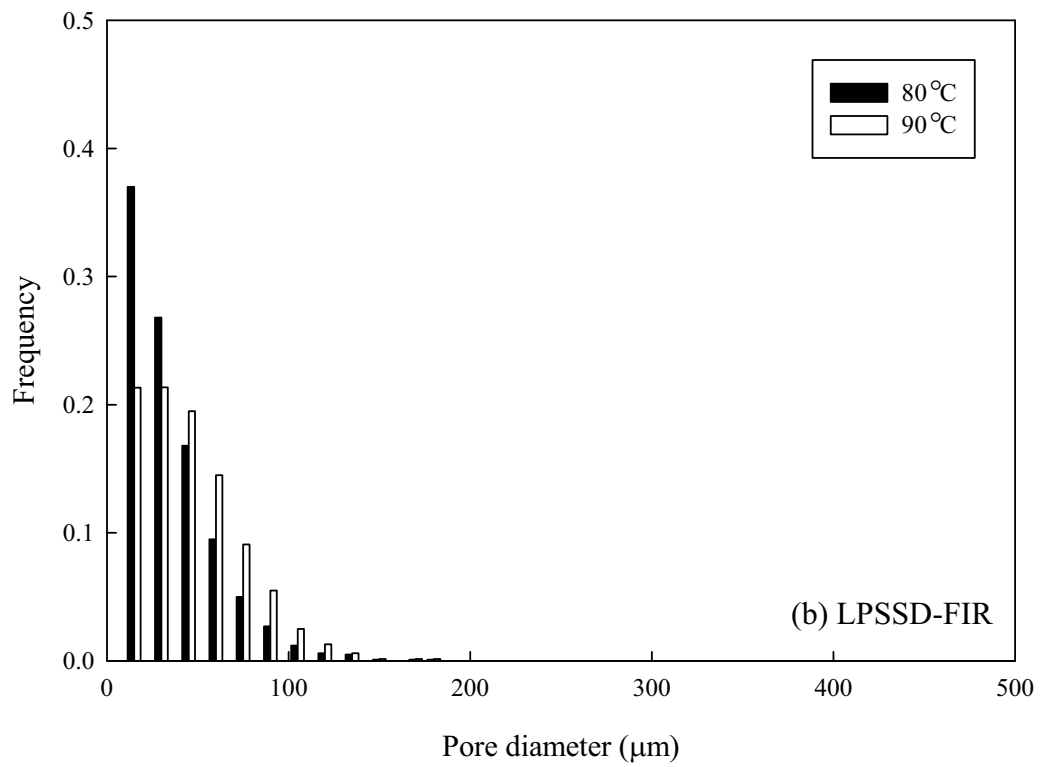
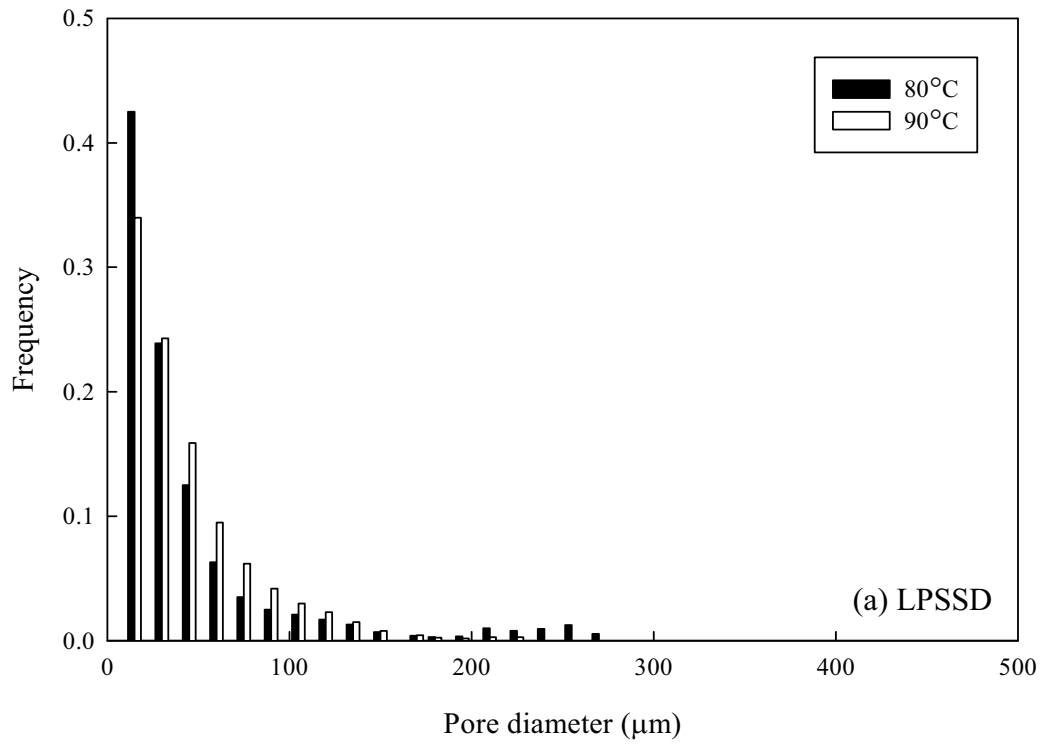


Figure 15. Pore size distributions of the samples dried at 80 and 90°C with (a) LPSSD and (b) LPSSD-FIR